

Edited by  
Klaus Wanner, Georg Höfner

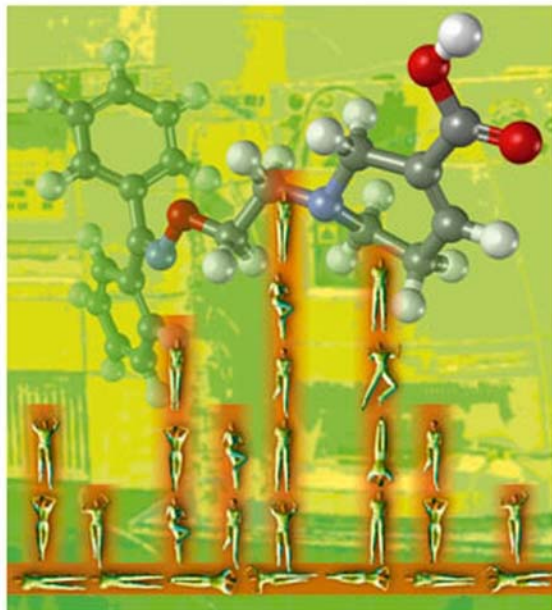
 WILEY-VCH

# Mass Spectrometry in Medicinal Chemistry

Applications in Drug Discovery

**Volume 36**

Series Editors:  
R. Mannhold,  
H. Kubinyi,  
G. Folkers



# Mass Spectrometry in Medicinal Chemistry

*Edited by*

*Klaus T. Wanner and Georg Höfner*



WILEY-VCH Verlag GmbH & Co. KGaA



**Mass Spectrometry in  
Medicinal Chemistry**

*Edited by*

*Klaus T. Wanner and Georg Höfner*

## 1807–2007 Knowledge for Generations

Each generation has its unique needs and aspirations. When Charles Wiley first opened his small printing shop in lower Manhattan in 1807, it was a generation of boundless potential searching for an identity. And we were there, helping to define a new American literary tradition. Over half a century later, in the midst of the Second Industrial Revolution, it was a generation focused on building the future. Once again, we were there, supplying the critical scientific, technical, and engineering knowledge that helped frame the world. Throughout the 20th Century, and into the new millennium, nations began to reach out beyond their own borders and a new international community was born. Wiley was there, expanding its operations around the world to enable a global exchange of ideas, opinions, and know-how.

For 200 years, Wiley has been an integral part of each generation's journey, enabling the flow of information and understanding necessary to meet their needs and fulfill their aspirations. Today, bold new technologies are changing the way we live and learn. Wiley will be there, providing you the must-have knowledge you need to imagine new worlds, new possibilities, and new opportunities.

Generations come and go, but you can always count on Wiley to provide you the knowledge you need, when and where you need it!



William J. Pesce  
President and Chief Executive Officer



Peter Booth Wiley  
Chairman of the Board

# Mass Spectrometry in Medicinal Chemistry

*Edited by*

*Klaus T. Wanner and Georg Höfner*



WILEY-VCH Verlag GmbH & Co. KGaA

#### Series Editors

**Prof. Dr. Raimund Mannhold**

Molecular Drug Research Group  
Heinrich-Heine-Universität  
Universitätsstrasse 1  
40225 Düsseldorf  
Germany  
mannhold@uni-duesseldorf.de

**Prof. Dr. Hugo Kubinyi**

Donnersbergerstrasse 9  
67256 Weisenheim am Sand  
Germany  
kubinyi@t-online.de

**Prof. Dr. Gerd Folkers**

Collegium Helveticum  
STW/ETH Zurich  
8092 Zurich  
Switzerland  
folkers@collegium.ethz.ch

#### Volume Editors

**Prof. Dr. Klaus T. Wanner**

Ludwig-Maximilians-University Munich  
Department of Pharmacy  
Center of Drug Research  
Butenandstr. 7  
81377 Munich  
Germany  
klaus.wanner@cup.uni-muenchen.de

**Dr. Georg Höfner**

Ludwig-Maximilians-University Munich  
Department of Pharmacy  
Center of Drug Research  
Butenandstr. 7  
81377 Munich  
Germany  
georg.hoefner@cup.uni-muenchen.de

■ All books published by Wiley-VCH are carefully produced. Nevertheless, authors, editors, and publisher do not warrant the information contained in these books, including this book, to be free of errors. Readers are advised to keep in mind that statements, data, illustrations, procedural details or other items may inadvertently be inaccurate.

**Library of Congress Card No.:** applied for  
**British Library Cataloguing-in-Publication Data**

A catalogue record for this book is available from the British Library.

**Bibliographic information published by the Deutsche Nationalbibliothek**

Die Deutsche Nationalbibliothek lists this publication in the Deutsche Nationalbibliografie; detailed bibliographic data are available in the Internet at <http://dnb.d-nb.de>.

© 2007 WILEY-VCH Verlag GmbH & Co. KGaA, Weinheim

All rights reserved (including those of translation into other languages). No part of this book may be reproduced in any form – by photoprinting, microfilm, or any other means – nor transmitted or translated into a machine language without written permission from the publishers. Registered names, trademarks, etc. used in this book, even when not specifically marked as such, are not to be considered unprotected by law.

Printed in the Federal Republic of Germany  
Printed on acid-free paper

**Typesetting** Asco Typesetter, Hong Kong  
**Printing** betz-druck GmbH, Darmstadt  
**Binding** Litges & Dopf GmbH, Heppenheim  
**Cover Design** Grafik-Design Schulz, Fußgönheim  
**Wiley Bicentennial Logo** Richard J. Pacifico

ISBN 978-3-527-31456-0

## Contents

**Preface** XV

**A Personal Foreword** XVII

**List of Contributors** XIX

### **I Introduction to MS in bioanalysis** 1

#### **1 Mass Spectrometry in Bioanalysis – Methods, Principles and Instrumentation** 3

*Gérard Hopfgartner*

- 1.1 Introduction 3
- 1.2 Fundamentals 4
- 1.3 Ionization Techniques 10
  - 1.3.1 Electron Impact and Chemical Ionization 10
  - 1.3.2 Atmospheric Pressure Ionization 12
    - 1.3.2.1 Electrospray 14
    - 1.3.2.2 Atmospheric Pressure Chemical Ionization 17
    - 1.3.2.3 Photoionization 19
    - 1.3.2.4 Multiple Ionization Source 19
    - 1.3.2.5 Desorption Electrospray and Direct Analysis in Real Time 20
  - 1.3.3 Matrix Assisted Laser Desorption Ionization 21
- 1.4 Mass Analyzers 23
  - 1.4.1 Quadrupole Analyzers 23
  - 1.4.2 Triple Quadrupole Mass Analyzer 24
  - 1.4.3 Ion Trap Mass Spectrometry 27
  - 1.4.4 Triple Quadrupole Linear Ion Trap 30
  - 1.4.5 Time of Flight Mass Spectrometry 33
  - 1.4.6 Fourier Transform Mass Spectrometry 36
    - 1.4.6.1 Fourier Transform–Ion Cyclotron Resonance Mass Spectrometry 36
    - 1.4.6.2 Orbitrap Mass Spectrometer 37
- 1.5 Ion Detectors 38
- 1.6 Practical Aspects and Applications in Bioanalysis 41



1.6.1	Introduction	41
1.6.2	Quantitative Analysis in Biological Matrices	42
1.6.3	Drug Metabolism	45
1.6.4	Analysis of Proteins	49
1.7	Perspectives	54
1.8	Common Definitions and Abbreviations	58
	<i>References</i>	58

## II Studying target-ligand interactions analyzing the ligand by MS 63

### 2 Drug Screening Using Gel Permeation Chromatography Spin Columns Coupled with ESI-MS 65

*Marshall M. Siegel*

2.1	Introduction	65
2.1.1	Preface	65
2.1.2	Direct and Indirect ESI-MS Analysis of Non-covalent Drug–Protein Complexes	65
2.1.3	Advantages of GPC Spin Columns	66
2.1.4	Application of Equilibrium and Non-equilibrium Theory for the Analysis of GPC Spin Column Eluates	68
2.1.4.1	Sample Prepared Under Equilibrium Conditions Prior to Spin Column Treatment	69
2.1.4.2	Calculation for Predicting the Concentration of Sample Complex Eluted From the Spin Column	69
2.1.4.3	Estimation of Relative Binding Affinities from GPC Spin-Column/ESI-MS Data	72
2.1.4.4	Experimental Determination of the $K_d$ Value from GPC Spin-Column/ESI-MS Data	72
2.2	Experimental	73
2.2.1	Spin Columns	73
2.2.2	Spin Column Media: Advantages and Disadvantages, Volatile vs Non-volatile Buffers	74
2.2.3	Preparing Non-covalent Complexes in Protein Buffer; Protein Concentration, Ligand Concentration, Incubation Time	75
2.2.4	Sample Organization: Single Samples vs Mixtures, Mixture Set-up: Compatibility of Components, Plate Set-up	79
2.2.5	Pooling Spin Column Eluates for Higher Throughput	80
2.2.6	Manual vs Robotic Instrumentation for Sample Preparation and Acquiring Spin Column Eluates	80
2.2.7	ESI Mass Spectrometer: ESI, APCI, Photodissociation, Positive/Negative Ionization	81
2.2.8	ESI Multi-sprayer (MUX) Technology; Sample Throughput; Protein Consumption	82
2.2.9	Reversed Phase (RP) HPLC ESI-MS Considerations	83
2.2.10	Protein Removal for Optimum Sensitivity	84

2.2.11	Data Reduction and Automated Interpretation of GPC Spin Column/ESI-MS Data	84
2.3	Results	89
2.3.1	Secondary Screens	89
2.3.1.1	GPC Spin Column/ESI-MS Drug Screening Demonstration Papers	89
2.3.1.2	Estrogen Receptor Target	89
2.3.1.3	Non-covalent Binding of Drugs to RNA/DNA Targets	90
2.3.1.4	Amgen Secondary Screens	94
2.3.1.5	Novartis Secondary Screens	94
2.3.2	Primary Screens	94
2.3.2.1	RGS4 Protein Target	94
2.3.2.2	Amgen Primary Screens	98
2.3.2.3	Novartis Primary Screens	98
2.3.3	Additional Spin Column Methods	99
2.3.3.1	Competition Experiments of Inhibitor Mixture with Protein Target	99
2.3.3.2	GPC Spin Column/ESI-MS Determination of Binding Sites	101
2.3.3.3	Obtaining MS EC <sub>50</sub> s and K <sub>d</sub> s for Ligands Non-covalently Bound to Protein Active Sites	112
2.3.3.4	Multiple Passes Through Spin Columns – Finding Strongest Binders	113
2.3.3.5	Reverse Screening with GPC Spin Columns	113
2.4	Conclusions	113
2.4.1	GPC Spin Column/ESI-MS: Ease of Use, Mixture Analysis, High Speed, Reliability, Uncoupling of GPC from ESI-MS and HPLC ESI-MS	113
2.4.2	Comparison of GPC Spin Column/HPLC ESI-MS with Tandem Chromatographic Method of GPC/HPLC ESI-MS	114
2.4.3	Future Developments	115
2.4.3.1	MS and HPLC Improvements	115
2.4.3.2	Use of Automated Nanospray for Greater Sensitivity and Smaller Sample Size (Less Protein/Drug)	115
2.4.3.3	Microfluidic Systems: Sensitivity, High Speed	116
2.4.3.4	GPC Spin Column Eluates Analyzed by ESI/Ion Mobility/Mass Spectrometry	116
2.4.3.5	GPC Spin Columns with Matrixless MALDI-MS and Gyros GPC Microfluidic ESI/MALDI-MS System	116
	References	117
<b>3</b>	<b>ALIS: An Affinity Selection–Mass Spectrometry System for the Discovery and Characterization of Protein–Ligand Interactions</b>	<b>121</b>
	<i>Allen Annis, Cheng-Chi Chuang, and Naim Nazef</i>	
3.1	Introduction	121
3.1.1	State of the Art	122

3.1.1.1	Spectroscopic and Biophysical Methods	122
3.1.1.2	Mass Spectrometry-based Methods	123
3.2	ALIS: An Affinity Selection–Mass Spectrometry System based on Continuous SEC	124
3.2.1	ALIS System Design	126
3.3	Discovery of Ligands from Combinatorial Libraries	127
3.4	Quantitative Binding Affinity Measurement	130
3.4.1	Theory	131
3.4.2	Simulations and Experimental Results	134
3.5	Competition-based Binding Site Determination and Affinity Ranking in Mixtures	135
3.5.1	Binding Site Classification	136
3.5.2	Affinity Ranking in Compound Mixtures	140
3.6	Protein–Ligand Dissociation Rate Measurement	142
3.6.1	Theory	143
3.6.2	Simulations	145
3.6.3	Experimental Results	147
3.7	Conclusions	150
3.8	Future Directions	151
	<i>References</i>	152

#### **4 Library Screening Using Ultrafiltration and Mass Spectrometry 157**

*Timothy E. Cloutier and Kenneth M. Comess*

4.1	Introduction	157
4.2	Ultra-high Throughput Filtration-based Affinity Screening as a Discovery Tool	163
4.2.1	Affinity Selection/Mass Spectrometry	163
4.2.2	Primary Screening Strategy	164
4.2.3	Retesting and Deconvolution Strategy	167
4.2.4	Promiscuous Compound Filter	168
4.2.5	MurF Lead Discovery	171
4.3	Additional Affinity Screening Methodology That Includes Mass Spectrometry-based Readout	177
4.3.1	Pulsed Ultrafiltration MS	177
4.4	Conclusions and Future Directions	180
	<i>References</i>	181

#### **5 Continuous-flow Systems for Ligand Binding and Enzyme Inhibition Assays Based on Mass Spectrometry 185**

*Hubertus Irth*

5.1	Introduction	185
5.2	Continuous-flow Enzyme Assays Based on Mass Spectrometry	186

5.2.1	Assay Principle	186
5.2.2	ESI-MS Assay of Cathepsin B	188
5.2.2.1	MS Assay Development for Cathepsin B	188
5.2.2.2	Compatibility of Cathepsin B Assay with MS Detection	188
5.2.2.3	On-line Coupling of MS-based Cathepsin B Assay to HPLC	190
5.2.2.4	Screening of Natural Products for Cathepsin B Activity	192
5.2.3	ESI-MS Assay of Acetylcholinesterase	194
5.2.3.1	MS Assay Development for Acetylcholinesterase	194
5.2.3.2	Assay Validation and Stability	197
5.2.3.3	Screening of Natural Products for Acetylcholinesterase Activity	197
5.2.4	Miniaturization of Electrospray MS Assays	198
5.2.4.1	Chip-based Electrospray MS Assays	198
5.2.4.2	Chip Performance	199
5.2.4.3	Sensitivity of the Chip-based MS Screening System	200
5.3	Continuous-flow Ligand Binding Assays Based on Mass Spectrometry	200
5.3.1	Assay Principle	200
5.3.2	Optimization of MS Conditions	201
5.3.3	On-line Continuous-flow Biochemical Interaction	202
5.3.4	Monitoring Bioactive Compounds	204
5.3.5	Antibody–Antigen Interactions	205
5.3.6	Continuous-flow Multi-protein Binding Assays Using Electrospray MS	205
5.4	MS Assay Based on Dissociation of Isolated Protein–Ligand Complexes	207
5.4.1	Assay Set-up	207
5.4.2	Flow Injection Label-free MS Assay	209
5.4.3	Flow Injection Label-free MS Assay Screening of Natural Extracts	211
5.5	Future Prospects	211
	<i>References</i>	213

## **6 Frontal Affinity Chromatography – Mass Spectrometry for Ligand Discovery and Characterization** 217

*Nora Chan, Darren Lewis, Michele Kelly, Ella S.M. Ng, and David C. Schriemer*

6.1	Introduction	217
6.1.1	The Basic Frontal Method	218
6.1.2	FAC – Basic Theory	220
6.1.3	FAC Advantages	221
6.1.4	FAC Disadvantages	223
6.2	Enabling FAC with MS Detection	224
6.2.1	Direct FAC-MS Methods for Compound Binding Data	224
6.2.2	Direct Method for Discovering and Ranking Multiple Ligands	226
6.2.3	Indirect Methods	232

6.3	System Advancements – Fluidics, Immobilization, Detection	235
6.3.1	Column	235
6.3.2	System	239
6.3.3	Breakthrough Curve Detection and Data Analysis	241
6.4	Select Applications	242
6.5	Summary and Evaluation	243
	<i>References</i>	244
<b>7</b>	<b>MS Binding Assays – An Alternative to Radioligand Binding</b>	<b>247</b>
	<i>Georg Höfner, Christine Zepperitz, and Klaus T. Wanner</i>	
7.1	Introduction	247
7.2	Radioligand Binding Assays	248
7.2.1	General Principle	248
7.2.1.1	Saturation Assays	248
7.2.1.2	Competition Assays	249
7.2.1.3	Kinetic Assays	250
7.2.2	Application	251
7.2.3	Disadvantages and Alternatives	252
7.3	MS Binding Assays	254
7.3.1	MS Binding Assays Quantifying the Nonbound Marker	255
7.3.1.1	Competition Assays for D <sub>1</sub> and D <sub>2</sub> Dopamine Receptors	257
7.3.1.2	Library Screening and Competition Assays for $\mu$ -Opioid Receptors	263
7.3.2	MS Binding Assays Quantifying the Bound Marker	267
7.3.2.1	Saturation Assays for mGAT1	268
7.3.2.2	Competition Assays for mGAT1	272
7.3.2.3	Kinetic Assays for mGAT1	272
7.4	Summary and Perspectives	276
	<i>References</i>	278
<b>8</b>	<b>Laser Desorption Assays – MALDI-MS, DIOS-MS, and SAMDI-MS</b>	<b>285</b>
	<i>Martin Vogel, Andy Scheffer, André Liesener, and Uwe Karst</i>	
8.1	MALDI-MS Assays	285
8.1.1	Principles of MALDI	285
8.1.2	Application of MALDI-MS in Bioanalysis	287
8.2	DIOS: Desorption/Ionization on Silicon	289
8.2.1	Principles of DIOS	289
8.2.2	Application of DIOS in Bioanalysis	292
8.3	SAMDI: Self-assembled Monolayers for MALDI-MS	295
8.3.1	Principles of SAMDI-MS	295
8.3.2	Application of SAMDI in Bioanalysis	297
8.4	Conclusion	299
	<i>References</i>	300

### III     **Studying target-ligand interactions analyzing intact target-ligand complexes by MS**    303

#### 9        **Tethering: Fragment-based Drug Discovery by Mass Spectrometry**    305

*Mark T. Cancilla and Daniel A. Erlanson*

##### 9.1      Introduction    305

##### 9.2      Reduction to Practice    307

##### 9.2.1    Technique    307

##### 9.2.2    Advantages    310

##### 9.3      Finding Fragments: Thymidylate Synthase Proof of Principle    310

##### 9.4      Finding and Linking Fragments in One Step: Tethering with Extenders    312

##### 9.4.1    Caspase-3    312

##### 9.4.2    Caspase-1    316

##### 9.5      Conclusions    316

*References*    318

#### 10      **Interrogation of Noncovalent Complexes by ESI-MS: A Powerful Platform for High Throughput Drug Discovery**    321

*Steven A. Hofstadler and Kristin A. Sannes-Lowery*

##### 10.1     Analysis of Noncovalent Complexes by ESI-MS    321

##### 10.1.1   Solution Conditions    321

##### 10.1.2   Proteins    322

##### 10.1.3   Oligonucleotides    323

##### 10.2     Multitarget Affinity/Specificity Screening    328

##### 10.3     Multitarget Affinity/Specificity Screening in a High Throughput Format    329

##### 10.4     Affinity/Specificity    330

##### 10.5     SAR by MS    332

##### 10.6     Future Directions    333

*References*    335

### IV      **Studying target-ligand interactions analyzing the target binding site by MS**    339

#### 11      **Quantification of Protein–Ligand Interactions in Solution by Hydrogen/Deuterium Exchange (PLIMSTEX)**    341

*Mei M. Zhu, David Hambly, and Michael L. Gross*

##### 11.1     Introduction    341

##### 11.2     The PLIMSTEX Method    342

##### 11.2.1   A General Protocol of H/D Exchange and LC/MS Analysis for PLIMSTEX    342

11.2.2	Determination and Interpretation of the Titration Curves	343
11.3	Applications of PLIMSTEX	345
11.3.1	Determination of Association Constant ( $K_a$ ), Stoichiometry ( $n$ ), and Protection ( $\Delta D_i$ )	345
11.3.2	Ras-GDP Interacting with $Mg^{2+}$ : A 1:1 Protein:Metal Ion Interaction	347
11.3.2.1	Kinetic Study of Forward H/D Exchange Ras-GDP with Different [ $Mg^{2+}$ ]	347
11.3.2.2	PLIMSTEX Results for Ras-GDP Titrated with $Mg^{2+}$	348
11.3.2.3	Interpretation of PLIMSTEX Results with H/D Exchange Kinetics	349
11.3.2.4	Application of PLIMSTEX to Relatively Weak Protein–Ligand Binding	350
11.3.2.5	Experimental Issues Regarding Using Metal Chelators	350
11.3.3	Apo-CaM Interacting with $Ca^{2+}$ : A 1:4 Protein:Metal Ion Interaction	351
11.3.3.1	PLIMSTEX Results for CaM and Intermediate Protein–Ligand Binding Species	351
11.3.3.2	PLIMSTEX in Biologically Relevant Media and High Ionic Strength	352
11.3.4	Apo-IFABP and Oleate: A Protein–Small Organic Molecule Interaction	353
11.3.5	Holo-CaM and Melittin: A Protein–Peptide Interaction	354
11.3.5.1	PLIMSTEX Curves Under Different Holo-CaM Concentrations	355
11.3.6	Self-association of Insulin: A Protein–Protein Interaction	356
11.3.6.1	Modified Version of PLIMSTEX for Insulin Self-association	356
11.4	Features of PLIMSTEX	357
11.4.1	Determines $K_i$ , Stoichiometry, and Protection ( $\Delta D_i$ )	357
11.4.2	Requires Low Quantities of Protein	357
11.4.3	Relies Only on MS to Measure $m/z$ And Not Solution Concentration	358
11.4.4	Works in Biologically Relevant Media at High Ionic Strength	359
11.4.5	Does Not Need Specially Labeled Protein or Ligand	359
11.4.6	Avoids Perturbation of the Binding Equilibrium	360
11.4.7	Has Potential for Peptide Resolution	360
11.4.8	Current Challenges and Future Directions	360
11.5	Fast Radical Footprinting for Protein–Ligand Interaction Analysis	361
11.5.1	Rationale for Hydroxyl Radicals as a Probe	362
11.5.2	Methods for Generating Hydroxyl Radicals	362
11.5.3	Fast Photochemical Oxidation of Proteins	363
11.5.4	Locating the Sites of Oxidation	364
11.5.5	Application of FPOP to Apomyoglobin	364
11.5.6	Advantages of FPOP	366

11.6	Potential Applications in Drug Discovery	367
	<i>References</i>	368
<b>12</b>	<b>Protein-targeting Drug Discovery Guided by Hydrogen/Deuterium Exchange Mass Spectrometry (DXMS)</b>	<b>377</b>
	<i>Yoshitomo Hamuro, Stephen J. Coales, and Virgil L. Woods Jr</i>	
12.1	Introduction	377
12.2	Theory of H/D Exchange	378
12.2.1	Amide H/D Exchange	378
12.2.2	Protection Factor	378
12.2.3	Backbone Amide Hydrogens as Thermodynamic Sensors	379
12.3	Overview of H/D Exchange Technologies	380
12.3.1	On Exchange Reaction	380
12.3.2	Quench of Exchange Reaction	380
12.3.3	Protein Fragmentation by Proteolysis	381
12.3.4	Digestion Optimization	381
12.3.5	HPLC Separation	381
12.3.6	Mass Analysis	381
12.3.7	Automation of H/D Exchange by MS	382
12.3.8	Automated Data Analysis	383
12.4	DXMS-guided Design of Well Crystallizing Proteins	383
12.4.1	Disordered Regions and Protein Crystallography	383
12.4.2	Poorly Crystallizing Proteins Contain Substantial Disordered Regions	384
12.4.3	Disorder-depleted Mutant Preserved Ordered Structure	384
12.4.4	Disorder-depleted Mutant Improved Crystallization Efficiency and Produced High Resolution Structure	384
12.5	Rapid Characterization of Protein Conformational Change with DXMS	385
12.5.1	Human Growth Hormone	386
12.5.2	H/D Exchange of hGH	386
12.5.3	Free Energy Change upon Folding of hGH	386
12.6	Application of H/D Exchange to Protein–Small Molecule Ligand Interactions	388
12.6.1	p38 Mitogen-activated Protein Kinase	388
12.6.2	H/D Exchange of p38 MAP Kinase	389
12.6.3	Peroxisome Proliferator-activated Receptor $\gamma$	390
12.6.4	H/D Exchange of PPAR $\gamma$	390
12.7	DXMS-guided Design of Small Molecules that Target Protein–Protein Interaction Surfaces	391
12.8	Optimal Formulation and Quality Control of Whole-protein Therapeutics with DXMS	393
12.9	Conclusions	394
	<i>References</i>	394



<b>V</b>	<b>MS in early pharmacokinetics</b>	<b>399</b>
<b>13</b>	<b>Mass Spectrometry in Early Pharmacokinetic Investigations</b>	<b>401</b>
	<i>Walter A. Korfmacher</i>	
13.1	Introduction	401
13.2	HPLC-MS/MS Overview	402
13.3	<i>In Vitro</i> Applications	405
13.4	<i>In Vivo</i> Applications	406
13.5	Rapid Method Development	408
13.6	Increasing Throughput in HPLC-MS/MS	410
13.7	Matrix Effects	411
13.8	Discovery PK Assay Rules	413
13.9	New Technology in LC-MS	415
13.10	Conclusion	419
	<i>References</i>	419
	<b>Index</b>	<b>429</b>

## Preface

For a long time, mass spectrometry in organic chemistry was just used for the “fingerprint” identification of different compounds. Initiated by F.W. McLafferty and K. Biemann, and largely extended by C. Djerassi, H. Budzikiewicz and D.H. Williams, sets of structure-specific fragmentation rules were established, which enabled organic chemists to interpret the chemical structures of their compounds, even highly complex natural products and drugs. Within a few years, between 1962 and 1964, five books on mass spectrometry of organic compounds were published, three of them by the Djerassi group. In this manner, Carl Djerassi made another significant contribution to medicinal chemistry, besides his research results on optical rotation dispersion and his role in the development of the “pill”. Nowadays, mass spectrometry is well established in drug research, for the characterization of new compounds, their structure elucidation and structural confirmation, the identification of drugs and their metabolites in body fluids, and in anti-doping campaigns.

Largely unperceived by medicinal chemists, in the past two decades mass spectrometry developed into a powerful tool in drug discovery, by the detection and analysis of ligand–protein interactions. One of the major breakthroughs to enable such applications was the development of new desorption – ionisation techniques for large-sized, non-volatile molecules, i.e. proteins, RNA, and DNA fragments. The importance of these new tools was honored in 2002, by the Nobel prize in Chemistry for John B. Fenn, Professor at the Virginia Commonwealth University, for his contributions to electrospray ionisation (ESI), and to Koichi Tanaka, an engineer at Shimadzu Corp., Japan, for the development of matrix-assisted laser desorption ionisation (MALDI), sharing the prize with Kurt Wüthrich at ETH Zurich, Switzerland, for his contributions to protein 3D structure elucidation by NMR. In parallel, progress in instrumentation, for better mass (more correctly, mass/charge:  $m/z$ ) separation and ion detection, and coupling with HPLC separation broadened the field of potential applications.

Whereas mass spectrometry in proteomics was discussed in an earlier volume of this series (Volume 28, M. Hamacher et al. 2006, *Proteomics in Drug Research*, Wiley–VCH, Weinheim), the current monograph focuses on mass spectrometry applications in lead discovery and optimization. As discussed in more detail in the foreword of the volume editors, the chapters provide a comprehensive over-

view on all current and potential, “non-classic” applications of mass spectrometry in various areas of drug research, especially small molecule screening, fragment-based drug discovery, ligand–protein interactions, protein 3D structure characterization, and the study of pharmacokinetics.

The series editors would like to thank Klaus T. Wanner and Georg Höfner, as well as all chapter authors, for compiling and structuring this comprehensive monograph on mass spectrometry techniques. In addition, we want to thank the publisher Wiley–VCH, especially Dr. Frank Weinreich and Renate Dötzer, for their ongoing support of our series “*Methods and Principles in Medicinal Chemistry*”.

Raimund Mannhold, Düsseldorf  
Hugo Kubinyi, Weisenheim am Sand  
Gerd Folkers, Zürich

November 2006

## A Personal Foreword

Mass spectrometry has been a well established technique in analytical chemistry for more than five decades, but its use to characterize target–ligand interactions is comparatively new. Only the availability of modern mass spectrometers achieving sufficient accuracy and sensitivity as well as the advent of soft ionization techniques such as ESI or MALDI has paved the way for successful studies in this field. From the first investigations in the early 1990s until now a great variety of mass spectrometry-based approaches covering target–ligand interactions have been implemented in the drug discovery process, so that drug–ligand interactions can be explored from almost every perspective: it is possible to focus on the ligand, the target–ligand complex or the target (i.e. its binding site). Among the numerous advantages that qualify mass spectrometry for this purpose are two that should be emphasized: First, mass spectrometry offers the possibility to monitor the interacting partners without labelling either the ligand or the target. Second, mass spectrometry has the capability to identify structurally unknown hits, i.e. compounds binding to the target, from huge combinatorial compound libraries. Conversely, mass spectrometry can also provide an insight into the molecular structure of the binding domains on macromolecular targets.

It is the intention of this book to give an overview of the opportunities that mass spectrometry provides in medicinal chemistry, focusing primarily on the early drug discovery process. Therefore, particular emphasis is put on screening procedures for low relative molecular mass drug candidates supplemented by other approaches suitable to elucidate target–ligand interactions and the field of pharmacokinetic investigations. Instead of giving a complete summary of this topic, which would be clearly beyond the scope of a single book, selected approaches are presented reflecting the diversity of possible strategies.

For those readers who are not yet familiar with mass spectrometry, the introduction provides an explanation of the basics of mass spectrometry and its instrumentation as well as practical aspects and applications in bioanalysis. Next, a block of three chapters shows different affinity selection procedures suitable to identify hits from combinatorial compound libraries. This subject, being metaphorically speaking a search for a needle in a haystack, is of outstanding relevance for “big pharma”. The techniques described here offer real high throughput capabilities and are implemented already in the routine industrial screening

process. The next three chapters present more techniques also dealing with small molecule screening. One approach combines the biological assay directly with the analytical method using microcoil reactors integrated in a HPLC system to study target–ligand interactions. Another is based on the unique features of frontal affinity chromatography and has already proved its potential in several screening projects. The last one is a very simple but also very effective approach that enables binding assays with native, i.e. nonlabelled markers in analogy to conventional radioligand binding assays. Although ESI clearly dominates mass spectrometric screening procedures, MALDI and other ionization techniques based on laser desorption can also be utilized for this purpose. This is documented in the following chapter summing up recent advances in this field. In a further chapter the challenging concept of fragment-based drug discovery is presented which makes use of dynamic equilibrium processes in order to accumulate fragments with rather moderate affinity to a target binding site by forming a covalent bond to a linker. Even though this concept is basically a synthetic approach, its success is unambiguously connected to the use of mass spectrometry. The topic of target–ligand interactions presented in the preceding chapters is rounded off by two chapters showing mass spectrometric strategies benefiting from hydrogen deuterium exchange at the target. In one approach the deuterium uptake by the target as a function of the test compound is quantified in order to deduce binding affinity or stoichiometry. The other approach describes the possibility to characterize protein structure and conformational changes of proteins as well as how to localize the physical interactions between target and ligand, based on the exact assignment of target incorporated deuterium atoms in proteolytically generated peptide fragments. The last chapter touches on the issue of pharmacokinetics where mass spectrometry traditionally plays a prominent role. The fact that these mass spectrometric investigations can help to avoid failures in later clinical trials further illustrates the immense value of mass spectrometry for the drug discovery process.

As editors we would also like to take the opportunity to cordially thank all authors for their contributions. We hope that the applications collected in this book will give the reader an idea of the capabilities of mass spectrometry when used in the early stages of drug discovery. Considering that mass spectrometry only began to have an impact on early drug discovery in the past decade, we can expect that this process will be further accelerated in the near future by the rapidly proceeding evolution of mass spectrometry as an analytical tool to screen bioactivity.

Munich, November 2006

Klaus T. Wanner

Georg Höfner

## List of Contributors

**Allen Annis**

Schering–Plough Research  
Institute  
320 Bent Street  
Cambridge, MA 02141  
USA

**Mark T. Cancilla**

Sunesis Pharmaceuticals, Inc.  
341 Oyster Point Boulevard  
South San Francisco, CA 94080  
USA

**Nora Chan**

Defence R & D Canada – Suffield  
Box 4000, Stn Main  
Medicine Hat, Alberta T1A 8K6  
Canada

**Cheng-Chi Chuang**

Schering–Plough Research  
Institute  
840 Memorial Drive  
Cambridge, MA 02139  
USA

**Timothy E. Cloutier**

Target and Lead Discovery  
Global Pharmaceutical R&D  
100 Abbott Park  
Abbott Park, IL 60064  
USA

**Stephen J. Coales**

ExSAR Corporation  
11 Deer Park Drive, Suite 103  
Monmouth Junction, NJ 08852  
USA

**Kenneth M. Comess**

Abbott Labs PPD R&D  
100 Abbott Park  
Abbott Park, IL 60064  
USA

**Daniel A. Erlanson**

Sunesis Pharmaceuticals, Inc.  
341 Oyster Point Boulevard  
South San Francisco, CA 94080  
USA

**Michael L. Gross**

Center for Biomedical and Bioorganic  
Mass Spectrometry  
Department of Chemistry  
Washington University  
Campus Box 1134, One Brookings  
Drive  
St. Louis, MO 63130  
USA

**David Hambly**

1201 Amgen Court West  
Seattle, WA 98119  
USA

**Yoshitomo Hamuro**

ExSAR Corporation  
11 Deer Park Drive, Suite 103  
Monmouth Junction, NJ 08852  
USA

**Georg Höfner**

Ludwig-Maximilians-University  
Munich  
Department of Pharmacy  
Center of Drug Research  
Butenandtstrasse  
81377 Munich  
Germany

**Steven A. Hofstadler**

Ibis BioSciences  
ISIS Pharmaceuticals  
1891 Rutherford Road  
Carlsbad, CA 92008  
USA

**Gérard Hopfgartner**

Life Sciences Mass Spectrometry,  
School of Pharmaceutical  
Sciences  
University of Geneva  
University of Lausanne  
20 Boulevard d'Yvoy  
CH-1211 Geneva 4  
Switzerland

**Hubertus Irth**

Department of Analytical  
Chemistry & Applied  
Spectroscopy  
Vrije Universiteit Amsterdam  
De Boelelaan 1083  
1081 HV Amsterdam  
The Netherlands

**Uwe Karst**

Institute of Inorganic and Analytical  
Chemistry  
University of Münster  
Corrensstrasse 30  
48149 Münster  
Germany

**Michele Kelly**

Groton/New London Laboratories  
Pfizer Inc.  
Eastern Point Road  
Groton, CT 06340  
USA

**Walter A. Korfmacher**

Exploratory Drug Metabolism  
Department of Drug Metabolism and  
Pharmacokinetics  
Schering-Plough Research Institute  
Kenilworth, NJ 07033  
USA

**Darren Lewis**

Upchurch Scientific Inc.  
619 Oak Street  
Oak Harbor, WA 98277  
USA

**André Liesener**

Boehringer Ingelheim Pharma GmbH  
& Co. KG  
Birkendorfer Strasse 65  
88397 Biberach/Riss  
Germany

**Naim Nazef**

Schering-Plough Research Institute  
840 Memorial Drive  
Cambridge, MA 02139  
USA

***Ella S.M. Ng***

Department of Biochemistry and  
Molecular Biology  
University of Calgary  
Calgary, Alberta T2N 4N1  
Canada

***Kristin A. Sannes-Lowery***

Ibis Therapeutics  
ISIS Pharmaceuticals  
1891 Rutherford Road  
Carlsbad, CA 92008  
USA

***Andy Scheffer***

Institute of Inorganic and  
Analytical Chemistry  
University of Münster  
Corrensstrasse 30  
48149 Münster  
Germany

***David C. Schriemer***

Department of Biochemistry and  
Molecular Biology  
University of Calgary  
Calgary, Alberta T2N 4N1  
Canada

***Marshall M. Siegel***

Wyeth Research  
401 N. Middletown Rd.  
Bldg. 222/Room 1043  
Pearl River, NY 10965  
USA

***Martin Vogel***

Institute of Inorganic and Analytical  
Chemistry  
University of Münster  
Corrensstrasse 30  
48149 Münster  
Germany

***Klaus T. Wanner***

Ludwig-Maximilians-University Munich  
Department of Pharmacy  
Center of Drug Research  
Butenandtstrasse  
81377 Munich  
Germany

***Virgil L. Woods Jr.***

Department of Medicine and  
Biomedical Sciences Graduate Program  
University of California San Diego  
Basic Science Building  
9500 Gilman Drive, Dept 0656  
La Jolla, CA 92093-0656  
USA

***Christine Zepperitz***

Ludwig-Maximilians-University Munich  
Department of Pharmacy  
Center of Drug Research  
Butenandtstrasse  
81377 Munich  
Germany

***Mei M. Zhu***

Millennium Pharmaceuticals, Inc.  
40 Landsdowne Street  
Cambridge, MA 02139  
USA





## **Part I**

### **Introduction to MS in bioanalysis**



## 1

## Mass Spectrometry in Bioanalysis – Methods, Principles and Instrumentation

*G rard Hopfgartner*

## 1.1

### Introduction

Mass spectrometry started about 100 years ago with the work of Sir J.J. Thomson. His interest was the quantitative measurement of the mass and charge of the cathode rays (electrons). For that purpose he constructed the first mass spectrometer (parabola mass spectrograph) and he received in 1906 the Nobel Prize for Physics in recognition of his work [1]. In the next decades the major focus in the development and application of mass spectrometry was dedicated to the studies of isotopes [2]. In 1918 Dempster [3] developed an instrument in which a strong magnetic field was produced, between two semicircular iron plates, to separate positive ion rays with great resolving power. He also described the bombardment of chemical compounds with electrons forming positive ions. This technique is known today as electron impact ionization and is still widely used in modern mass spectrometry. In the early 1940s the first commercial instruments based on magnetic deflection and electron impact ionization became available. These instruments were mostly applied for the analysis of hydrocarbons in petroleum products. Beyond instrumental development the end of the 1950s saw the application of mass spectrometry for structure elucidation of natural products and the studies of fragmentation patterns. At the same time the concept of several mass analyzers was described, such as time of flight or ion cyclotron resonance.

While the first coupling of gas chromatography and mass spectrometry had been reported in the late fifties [4] one had to wait for almost another 20 years before the direct interfacing of liquid chromatography with mass spectrometry (LC-MS) was described by Arpino et al. [5]. With the direct liquid interface (DLI) the effluent of the chromatographic column was directly introduced in the electron impact source. Contrarily to gas chromatography coupled to mass spectrometry (GC-MS), LC-MS did not catch on as rapidly. One of the reasons was that the MS interface could only handle LC flow rates of a few microliters per minute. Another limitation was that electron impact or chemical ionization was not suit-

able for very thermolabile and high molecular weight compounds. It took almost ten years before the LC-MS analysis of larger molecules, using continuous flow fast atom bombardment (FAB), was first reported [6, 7]. For small molecules it was thermospray (TSP) [8] and particle beam (PB) [9] which allowed the routine use of LC-MS. Thermospray formed in most cases ammonium adducts, while particle beam yielded electron impact spectra. Within a few years thermospray was rapidly replaced by atmospheric pressure ionization techniques.

Quadrupole mass spectrometers [10] or quadrupole ion traps are today the most widely used mass spectrometers. The physical bases were described in the early 1950s by Paul and Steinwedel. For his work Paul received the Nobel Prize in 1989 [11]. Triple quadrupole mass spectrometers have become very popular instruments for qualitative and quantitative analysis. Yost et al. [12] built in 1978 the first instrument and it took four years before this type of instrument was commercialized. The coupling with liquid chromatography or gas chromatography is well established and benchtop ion traps or quadrupoles are nowadays part of the standard equipment of many analytical laboratories.

For the analysis of macromolecules and in particular for proteins a major milestone was achieved with the development in 1987 of matrix assisted laser desorption ionization by Karas and Hillenkamp [13] and in 1988 of electrospray ionization by J. Fenn (Nobel Prize in 2002) [14].

Over the past decade progress in mass spectrometry and its hyphenation with separation techniques has made these tools essential in life sciences. The present chapter will describe current ionization techniques as well as mass analyzers.

## 1.2

### Fundamentals

Mass spectrometry is a sensitive analytical technique which is able to quantify known analytes and to identify unknown molecules at the picomoles or femtomoles level. A fundamental requirement is that atoms or molecules are ionized and analyzed as gas phase ions which are characterized by their mass ( $m$ ) and charge ( $z$ ). A mass spectrometer is an instrument which measures precisely the abundance of molecules which have been converted to ions. In a mass spectrum  $m/z$  is used as the dimensionless quantity that is an independent variable. There is still some ambiguity how the  $x$ -axis of the mass spectrum should be defined. Mass to charge ratio should not longer be used because the quantity measured is not the quotient of the ion's mass to its electric charge. Also, the use of the Thomson unit (Th) is considered obsolete [15, 16]. Typically, a mass spectrometer is formed by the following components: (i) a sample introduction device (direct probe inlet, liquid interface), (ii) a source to produce ions, (iii) one or several mass analyzers, (iv) a detector to measure the abundance of ions, (v) a computerized system for data treatment (Fig. 1.1).

Most mass analyzers operate under high vacuum or at low pressure, so that the charged particles do not deviate from their trajectories due to collision with resid-

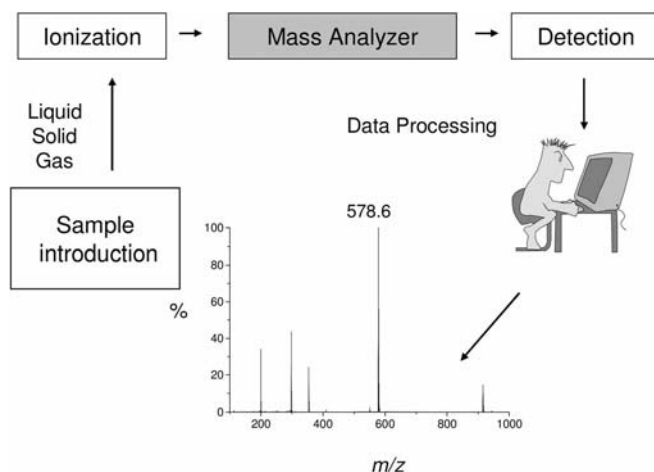


**Fig. 1.1** Principle of a mass spectrometer, the outcome of an analysis is a mass spectrum with  $m/z$  in the x-axis and ion intensities in the y-axis. The ion intensities can be given in percentages (relative intensity) or in counts or in counts per second (absolute intensity). The most abundant peak at  $m/z$  578.6 is called the base peak.

ual gas and thus never reach the detector. Mass spectrometers can be grouped into different types of operation mode: continuous mode (magnetic sector, quadrupole), pulsed mode (time of flight), and ion trapping mode (quadrupole traps, Fourier transform ion cyclotron, orbitrap). In the source, positive or negative ions are produced either under vacuum or at atmospheric pressure. Depending on the ionization technique either molecular ions ( $M^+$ ) with an odd electron number or protonated ions ( $[M+H]^+$ ) with an even electron number are formed. In the mass spectrum when no fragmentation occurs, in general the most intense peak represents the molecular ion, the protonated molecule or a molecule with an adduct ion followed by ions containing the heavier isotopes.  $M_r$  is the mass of one molecule of a compound, with a specified isotopic composition, relative to one-twelfth of the mass of one atom of  $^{12}\text{C}$ . An important aspect is that many atoms have naturally occurring isotopes which can be differentiated by mass spectrometry. Molecules analyzed by organic mass spectrometry contain in general carbon, hydrogen, nitrogen, oxygen and sulfur. These elements have stable isotopes (Table 1.1) which have different atomic mass. Therefore, under certain conditions and for a given molecule, the isotopic contribution can be measured by mass spectrometry.

For example, carbon is composed of two naturally occurring isotopes:  $^{12}\text{C}$  for 98.9% and  $^{13}\text{C}$  for 1.1% abundance, respectively. For cyclohexane ( $\text{C}_6\text{H}_{12}$ ) the  $M^+$  ion composed exclusively of  $^{12}\text{C}$  and  $^1\text{H}$  atoms is observed at a nominal mass of  $m/z$  84. The nominal mass is the integer of the sum of the masses calculated from the most abundant naturally occurring isotopes. The monoisotopic

**Table 1.1** Isotopic abundance of common elements. Interesting to note is that chlorine and bromine have two naturally intense isotopes.

Element	Atomic mass	Symbol	Isotopic mass	Abundance (%)
Carbon	12.0110	$^{12}\text{C}$	12.000000	98.9
		$^{13}\text{C}$	13.003354	1.1
Hydrogen	1.0080	H	1.007825	99.985
		D	2.013999	0.015
Oxygen	15.993	$^{16}\text{O}$	15.994915	99.76
		$^{17}\text{O}$	16.999133	0.04
		$^{18}\text{O}$	17.999160	0.20
Nitrogen	14.0067	$^{14}\text{N}$	14.0030698	99.64
		$^{15}\text{N}$	15.00010	0.36
Chlorine	35.4610	$^{35}\text{Cl}$	34.968849	75.77
		$^{37}\text{Cl}$	36.999988	24.23
Bromine	79.9035	$^{79}\text{Br}$	78.918348	50.5
		$^{81}\text{Br}$	80.916344	49.5
Sulfur	32.066	$^{32}\text{S}$	31.97207	95.02
		$^{33}\text{S}$	32.971456	0.75
		$^{34}\text{S}$	33.96787	4.21
		$^{36}\text{S}$	35.96708	0.02

peak represents the exact mass of an ion or a molecule calculated from the most abundant isotope of each element. The relative intensity of this ion compared to the others ions is 100%. A weaker isotopic peak ( $M^+ + 1$ ) is observed at  $m/z$  85 with an abundance of 6.5% corresponding to one  $^{13}\text{C}$ , five  $^{12}\text{C}$  and 12  $^1\text{H}$  atoms. An even weaker peak (0.2% abundance) is visible at  $m/z$  86 ( $M^+ + 2$ ) corresponding to two  $^{13}\text{C}$ , four  $^{12}\text{C}$  and 12  $^1\text{H}$  atoms. In this example, the contribution of deuterium can be neglected. For large molecules with increasing the number of carbon atoms, a shift of the maximum of the isotopic distribution towards higher masses can be observed, as depicted in Fig. 1.2. Above several hundred atoms of carbons, mostly a Gaussian distribution is observed. The consequence is that, in particular for protein analysis, only the relative molecular mass and not the monoisotopic mass is observed since either the monoisotopic masses can no longer be resolved or the intensity of the peak is too weak. The average mass is the calculated mass of an ion based on the relative atomic mass of each atom.

The isotopic contribution of various atoms is additive. For low molecular weight compounds, the isotopic contribution originates mainly from the carbon atom as long as no other element with a second isotope of significant abundance is present. For a molecule of  $M_r$  192 the intensity of the  $m/z$  194 ion represents 12% of the  $[\text{M}+\text{H}]^+$  peak ( $m/z$  193; Fig. 1.3A). Chlorine (Cl) has two intense isotopes:  $^{35}\text{Cl}$  and  $^{37}\text{Cl}$  (76% and 24% abundance, respectively). Replacing one H by a Cl atom results in a change of the isotopic distribution of the molecule

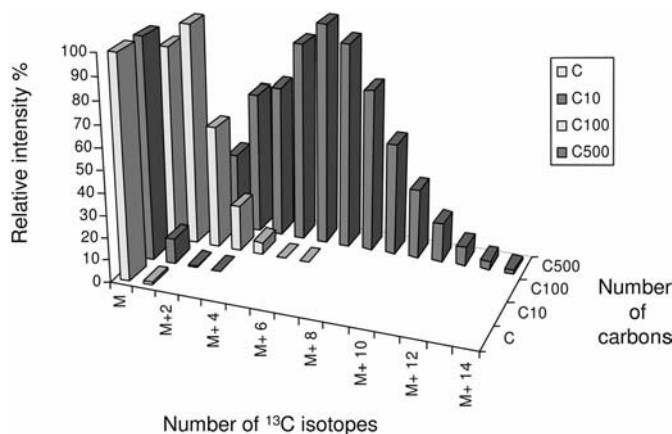


**Fig. 1.2** Isotopic distribution as function of the number of carbon atoms. It can be observed that with increasing numbers of carbon atoms the maximum of the isotopic distribution shifts towards higher masses. M represents the molecular ion with only <sup>12</sup>C isotope; M+1 represents the molecular ion with only one <sup>13</sup>C isotope; M+2 represents the molecular ion with only two <sup>13</sup>C isotope; and so on.

(Fig. 1.3B). The  $[M+H]^+ + 1$  peak is not affected, while the  $[M+H]^+ + 2$  is increased to about 25%. The replacement of the F by a second Cl results in an increase of the  $[M+H]^+ + 2$  and  $[M+H]^+ + 4$  peaks (Fig. 1.3c). Chlorine and bromine have typical isotopic patterns therefore their presence in a molecule can be easily confirmed.

Mass analyzers are characterized by their mass range in  $m/z$  and their resolving power. The mass range is the  $m/z$  range where ions can be detected. The mass resolving power (R) is the ability of a mass analyzer to separate ions of different  $m/z$  with similar intensities. It is basically the  $m/z$  ( $m$ ) at which the measurement was made divided by the difference ( $\Delta m_a$ ) between the two peaks overlapping at a defined height (2  $\sigma$ %; Fig. 1.4). Because it is difficult to find two ions of equal intensities, the measure of the resolving power is often performed on a single peak. In general, the peak width is measured at 50% of its height. It is often referred to as full width at half maximum (FWHM). There is often confusion with the terms mass resolving power and mass resolution. Basically mass resolution is the smallest difference ( $\Delta m$ ) between two equal magnitude peaks such as the valley between them is a specified fraction of the peak height. M1 and M2 are considered resolved when the valley between the two peaks represents 10% (2  $\sigma$ %) of their heights. In practice the definition of the resolution is often determined upon  $\Delta m$  of the a single peak at its full width at half maximum (Fig. 1.4,  $\Delta m_b$ ).

For example for an ion measured at  $m/z$  552 with a peak width of 0.5  $m/z$  units (FWHM) the mass resolution would be 0.5, while the mass resolving power



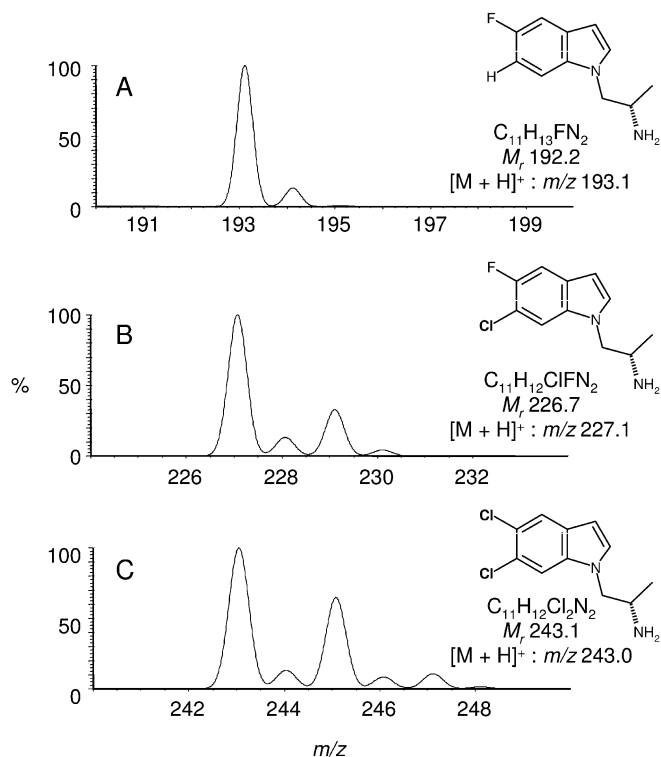


**Fig. 1.3** The influence of chlorine on the isotopic distribution. (A) No chlorine atom, (B) one chlorine atom, (C) two chlorine atoms.

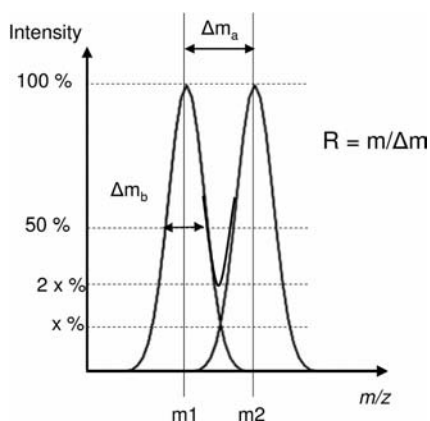


**Fig. 1.4** Illustration of the mass resolution using two peaks of equal intensities ( $\Delta m_a$ ) and a single peak ( $\Delta m_b$ ).

would be 1104. With quadrupole and ion trap instruments the mass resolution is tuned to be constant over a defined mass range. With these instruments the term unit mass resolution is often employed to mention that the mass spectrometer is able to differentiate two ions distant by one  $m/z$  unit bearing a single charge.

While the relative molecular mass is calculated using the relative atomic mass considering all isotopes, the observed mass in mass spectrometry depends on the mass resolving power of the instrument; and various definitions are used. The exact mass represents the calculated mass of an ion or a molecule containing a single isotope of each atom. In general the lightest isotope of each atom is considered. The monoisotopic mass represents the calculated exact mass of an ion or molecule considering the most abundant naturally occurring isotopes. The accurate mass of an ion is the experimentally measured mass that is used to determine an elemental formula. The accurate mass is generally measured with at least three significant figures. The accuracy of the measure, corresponding to the difference between the measured mass and the calculated mass divided by the mass of the molecule, is indicated in parts per million (ppm).

Figure 5A, B shows the isotopic distribution, of protonated bosentan ( $C_{27}H_{30}N_5O_6S$ ,  $M_r$  552.6) with a mass resolution of 0.5 and 0.1 at FWHM, respectively. It is worthwhile to observe the mass shift of the most abundant ion from  $m/z$  552.2006 to  $m/z$  552.1911. This value does not change with a mass resolving power of 15 000 (Fig. 1.5C) or even 500 000 (Fig. 1.5D). Accurate mass measurements are essential to obtain the elemental composition of unknown compounds or for confirmatory analysis. An important aspect in the calculation of the exact mass of a charged ion is to count for the loss of the electron for the protonated molecule  $[M+H]^+$ . The mass of the electron is about 2000 times lower than of the proton and corresponds to  $9.10956 \times 10^{-31}$  kg. The exact mass of protonated bosentan without counting the electron loss is 552.1917 units, while it is 552.1911 units with counting the loss of the electron. This represents an error of about 1 ppm.

With time of flight instruments, a mass accuracy better than 5 ppm can be achieved, while with Fourier transform ion cyclotron resonance or orbitrap mass spectrometers mass accuracies better than 1 ppm have been reported. It is obvious that, for good mass accuracies, the peaks must be baseline resolved and resolution plays an essential role. For the present example, a mass resolving power of 5000 seems to be quite acceptable. In the case of the  $[M+H]^+ + 1$  isotope peak, the situation becomes somewhat more complex for molecules containing nitrogen, sulfur or carbon. Figure 1.5D illustrates at a mass resolving power of 500 000 the contribution of  $^{15}N$ ,  $^{33}S$ .

In qualitative analysis, the isotopic distribution remains an important information. For example in the case the parent drug contains Br or Cl, metabolites or decomposition products can be easily identified by considering the isotopic distribution. With accurate mass measurements a list of elemental compositions can be proposed for a compound for a given accuracy range. Because the intensity of the isotopic distribution is also dependent on the elemental composition of the molecule it can be used to reduce the list of possible elemental formulas [17].

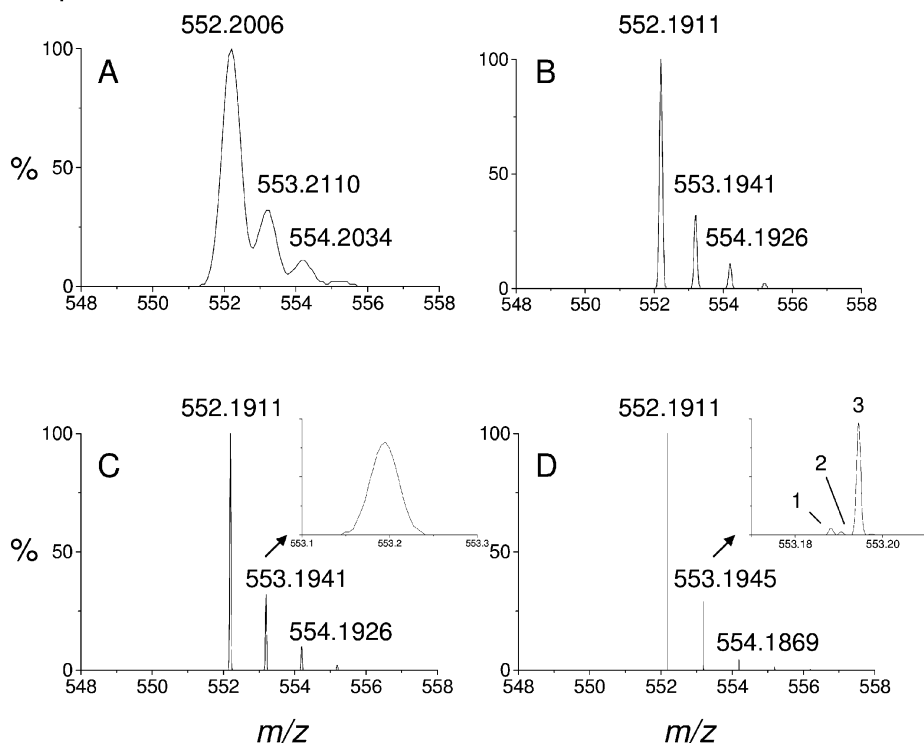


**Fig. 1.5** Simulated isotopic distribution of the protonated bosentan ( $C_{27}H_{30}N_5O_6S$ ) at mass resolving power: **(A)**  $R = 1104$ , with a peak full width at half maximum (FWHM) of 0.5 u. **(B)**  $R = 5520$ , FWHM = 0.1 u. **(C)**  $R = 15\,000$ . **(D)**  $R = 500\,000$  with isotopic contribution of  $^{15}N$  (peak 1),  $^{33}S$  (peak 2) and  $^{13}C$  (peak 3).

### 1.3

#### Ionization Techniques

##### 1.3.1

##### Electron Impact and Chemical Ionization

Electron impact (EI) ionization is one of the most classic ionization techniques used in mass spectrometry. A glowing filament produces electrons, which are then accelerated to an energy of 70 eV. The sample is vaporized into the vacuum where gas phase molecules are bombarded with electrons. One or more electrons are removed from the molecules to form odd electron ions ( $M^+$ ) or multiply charged ions. Solids, liquids and gases can be analyzed by EI, if they endure vaporization without decomposition. Therefore the range of compounds which can be analyzed by EI is somewhat limited to thermally stable and volatile compounds. The coupling with gas chromatography has been well established for

decades. The ionization energy of most organic compounds to form a radical cation is below 15–20 eV. The excess of energy transferred to the molecules causes reproducible fragmentation. Fragmentation of odd electron ions has been extensively studied but remains still a challenging task for non-experts. Under standard conditions at 70 eV, EI spectra are reproducible and instrument independent. Large commercial libraries are available to rapidly identify compounds present in a sample [18]. A limitation of the use of EI is that similar spectra can be obtained for isomers. Most analytical applications use EI in the positive mode but negative mode operation is also possible. EI is mostly combined with single quadrupole mass analyzers because often in the same spectrum, the molecular ions as well as fragment ions are present. Figure 1.6A shows the electron impact spectrum of a compound with a relative molecular mass of 355. The radical cation ion at  $m/z$  355 as well as many fragments can be observed. Chemical ionization would generate the protonated molecule ion at  $m/z$  356 (see Fig. 1.6B). To obtain structural information requires tandem mass spectrometry. Interestingly, odd and even electron ions undergo different fragmentation pathways, as observed in Fig. 1.6. This information is complementary, underlining that electron ionization remains an important technique for structural elucidation.

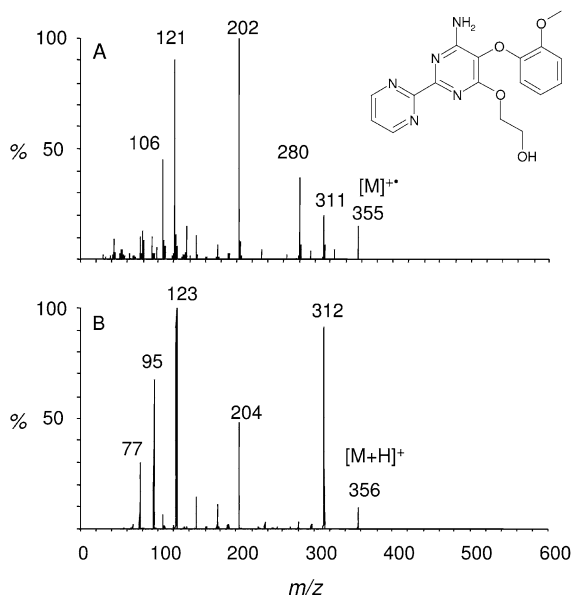


**Fig. 1.6** (A) Electron impact spectrum obtained on a single quadrupole mass spectrometer of a compound with  $M_r = 355$ . (B) Product ion spectrum after atmospheric pressure ionization obtained on a triple quadrupole instrument. Chemical ionization and atmospheric pressure ionization give in both cases protonated precursor ions, which is ideal for tandem mass spectrometry.

Protonated or deprotonated molecules can be generated by chemical ionization (CI) sources with similar design to the classic EI sources [19]. The principal difference between CI and EI mode is the presence of a reagent gas which is typically methane, isobutane or ammonia. The electrons ionize the gas to form the radical cations (in the case of methane,  $\text{CH}_4 + \text{e}^- \rightarrow \text{CH}_4^+ + 2\text{e}^-$ ). In positive chemical ionization (PCI) the radical cations undergo various ion–molecule reactions to form “ $\text{CH}_5^+$ ” and finally lead to the formation, after proton transfer ( $\text{CH}_5^+ + \text{M} \rightarrow [\text{M}+\text{H}]^+$ ), of protonated molecules. Negative chemical ionization (NCI), after proton abstraction, leads to deprotonated molecules  $[\text{M}-\text{H}]^-$ . Negative ions can be produced by different processes, such as by capture of low energy electrons present in the chemical ionization plasma. The major advantages of negative CI over positive EI or CI are higher sensitivity, the occurrence of the molecular ion and less fragmentation. Due to its high sensitivity NCI is mainly used in quantitative analysis after derivatization of the analyte [20].

### 1.3.2

#### Atmospheric Pressure Ionization

In atmospheric pressure ionization sources (API) the ions are first formed at atmospheric pressure and then transferred into the vacuum. In addition, some API sources are capable of ionizing neutral molecules in solution or in the gas phase prior to ion transfer to the mass spectrometer. Because no liquid is introduced into the mass spectrometer these sources are particularly attractive for the coupling of liquid chromatography with mass spectrometry. Pneumatically assisted electrospray (ESI), atmospheric pressure chemical ionization (APCI) or atmospheric pressure photoionization (APPI) are the most widely used techniques.

API offers unique opportunities for the implementation of new sources or to develop new applications. Atmospheric pressure matrix assisted laser desorption (AP-MALDI) [21] can be mounted on instruments such as ion traps which were originally designed only for electrospray and LC-MS. New API desorption techniques such as desorption electrospray (DESI) [22] or direct analysis in real time (DART) [23] have been described and offer unique opportunities for the analysis of surfaces or of solid samples.

The sampling of ions from atmospheric pressure into the high vacuum region of the mass analyzer requires significant pressure reduction. A gas stream introduced into a vacuum system expands and cools down. When this gas stream contains ions and solvent vapors the formation of ion–solvent clusters is observed. To obtain good sensitivities and high quality spectra one of the key roles of the interface is to prevent cluster formation. Different instrument designs have been proposed, including single stage pumping or differential stage pumping. Figure 1.7 depicts a typical single stage interface with curtain gas. The space between the orifice and the curtain plate is flushed with heated pure nitrogen. Ions are moved through the curtain gas into the mass analyzer with the help of an electric field formed between the curtain plate and the orifice. In this way, neutral solvent molecules cannot penetrate into the high vacuum region, which prevents

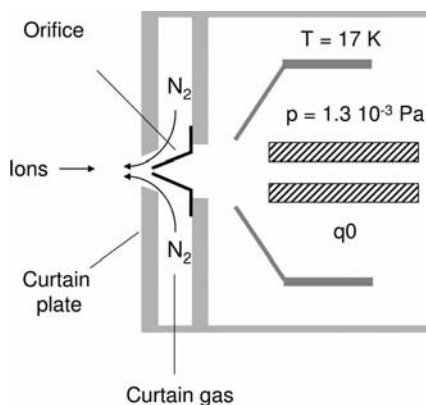


**Fig. 1.7** Single stage pumping atmospheric pressure ionization interface with curtain gas. The size of the orifice is ca. 100  $\mu\text{m}$ ,  $q_0$  acts as a focusing quadrupole and the nitrogen curtain gas prevents neutral molecules being introduced into the mass spectrometer.  $T$  = Temperature of the cryoshells (in Kelvin);  $p$  = pressure.

the formation of cluster ions. In a single-stage pumping interface, as described in Fig. 1.7, the size of the orifice is ca. 100  $\mu\text{m}$  and to maintain a high vacuum cryogenic pumps are mandatory. Declustering can also be performed by applying a potential difference between the orifice and quadrupole  $q_0$  [24]. If the value of

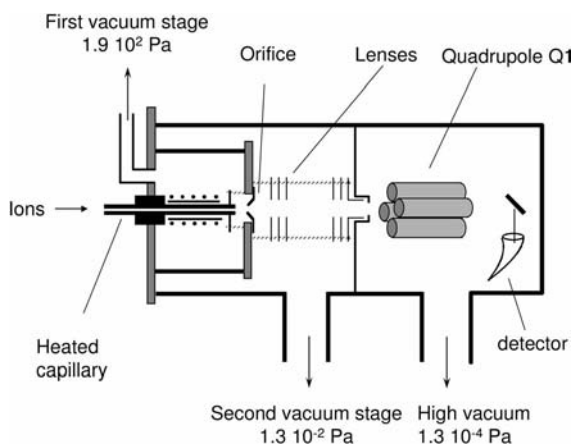


**Fig. 1.8** Differential pumping design with heated capillary. This configuration requires a dual stage pumping system before the ions are introduced into the quadrupole mass analyzer which needs to be operated at high vacuum. The role of the lenses is to focus ions. In some systems the lenses are replaced by hexapoles or octapoles.

the declustering potential is set too high “in source” or “up front” collision-induced dissociation can be observed. Cryogenic pumps have high pumping capacity ( $10\,000\text{ L s}^{-1}$  and more) but they need to be recycled every 48 h, which jeopardizes automated use of the instrument. Turbomolecular or diffusion pumps have much lower pumping capacities ( $50\text{--}800\text{ L s}^{-1}$ ). To achieve the desired vacuum in the mass analyzer, differential pumping designs were developed. An instrument design using differential pumping with a heated capillary interface is illustrated in Fig. 1.8. In a first step ions flow through a heated capillary ( $T = 150\text{--}300\text{ }^{\circ}\text{C}$ ) which helps desolvation. The internal diameter of the capillary is typically 0.5 mm. A reduced vacuum is achieved in the first pumping region with the help of a rotary pump. Ions are then pushed through a skimmer or an orifice into a second vacuum chamber where the vacuum is produced by a turbomolecular pump and then analyzed in the mass analyzer. Most modern instruments use differential pumping either with capillary skimmer or with an orifice skimmer setup with or without curtain gas.

#### 1.3.2.1 Electrospray

A spray of small droplets at atmospheric pressure can be generated by: (i) a nebulizing gas, (ii) the application of heat, (iii) the application of ultrasounds iv) the application of an electric field. Electrospray ionization (ESI) is a process where charged droplets result from the nebulization of a solution in an electric field. The liquid flows through a stainless steel or a fused silica capillary while the potential (typically 3–6 kV in positive mode) is applied directly on the capillary or on a counter electrode. In negative mode to avoid discharge, the range is somewhat lower (typically 3–4 kV). After nebulization the charged droplets reduce their size and subdivide, up to a point where gas phase ions escape from the droplets. A stable spray can be obtained at flow rates of  $1\text{--}10\text{ }\mu\text{L min}^{-1}$ . When performing LC-MS with standard bore LC columns (4.6 mm i.d.) the LC effluent must be split. To overcome this limitation, the spray process can be assisted by a nebulizing gas such as nitrogen or air [25] (Fig. 1.9). This way of operation was originally named ionspray but the term is less and less used. With liquid chromatography most sources use air or nitrogen to assist the electrospray process (pneumatically assisted electrospray). Stable sprays can be observed with flow rates above  $1\text{ mL min}^{-1}$ , allowing direct interfacing of LC with MS. Most modern commercial instruments operate with pneumatically assisted electrospray placed orthogonally to the entrance of the MS. The nebulizing process can be further assisted with the use of heat, where either the sprayer is heated or a hot stream of nitrogen is directed orthogonally towards the formed droplets.

Very low flow electrospray is called nanoelectrospray [26] where the samples are infused into the mass spectrometer at the nanoliter flow rate range. The infusion of a few microliters will result in a stable signal for more than 30 min, using pulled capillaries or chip-based emitters [27]. With infusion, signal averaging allows to improve the limit of detection in tandem mass spectrometry. Nanoelectrospray is particularly important in combination with nanoflow liquid chromatography or chip-based infusion for the analysis of peptides and proteins.

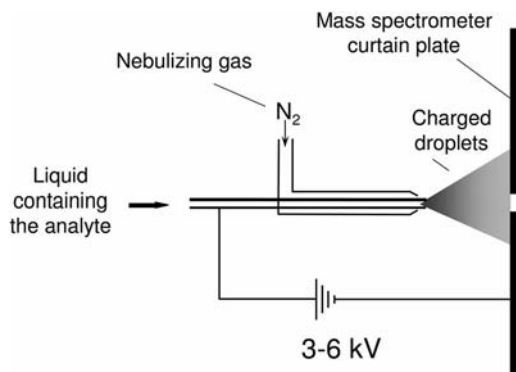


**Fig. 1.9** Pneumatically assisted electrospray. The coaxial nitrogen gas assists the electrospray process allowing to operate at flow rates of several hundred microliters.

ESI is a condensed phase ionization process and the ions have to be already present in solution. To generate ions, the pH has to be adjusted in such a way that ionizable groups are either protonated or deprotonated. In some cases neutral molecules can be analyzed by the formation of adducts with ions such as ammonium, sodium, potassium, acetate or silver.

Peptides and proteins have several ionizable sites, resulting in the formation of multiply charged ions [14]. Figure 1.10 shows the ESI spectrum of human gamma interferon ( $M_r = 16\,908.50$ ). The mass spectrum of the protein corresponds to a distribution of multiply charged ions obtained through protonation ( $[M+zH]^{z+}$ ). The ion at  $(m/z)_1$  846.4 corresponds to human gamma interferon protonated 20 times [ $z_1 \cdot (m/z)_1 = M_r + z_1 \cdot m_p$ ],  $M_r$  being the relative molecular mass of the protein,  $z_1$  the number of charges and  $m_p$  the mass of the proton. Because each pair of ions differs by one proton [ $(m/z)_2$  806.1 bears 21 protons] the charge state ( $z_i$ ) of any ion and therefore the relative molecular mass of an unknown protein can be determined with the following equations:

$$z_2 = \frac{(m/z)_1 - m_p}{(m/z)_1 - (m/z)_2} \quad (1)$$

$$M_r = z_2 \cdot [(m/z)_2 - m_p] \quad (2)$$

where  $z$  is charge,  $m$  is mass and  $m_p$  is proton mass.

The relative molecular mass determination of an unknown protein is generally performed automatically using various deconvolution algorithms, but the procedure is limited to relatively simple mixtures.

Electrospray ionization can be considered as an electrolysis cell (Fig. 1.11) where, in the positive mode, cations are enriched at the surface of the solution and negative ions move inside the capillary. Oxidation of the analyte has been observed at certain occasions, in particular at very low flow rates. Also in the case of



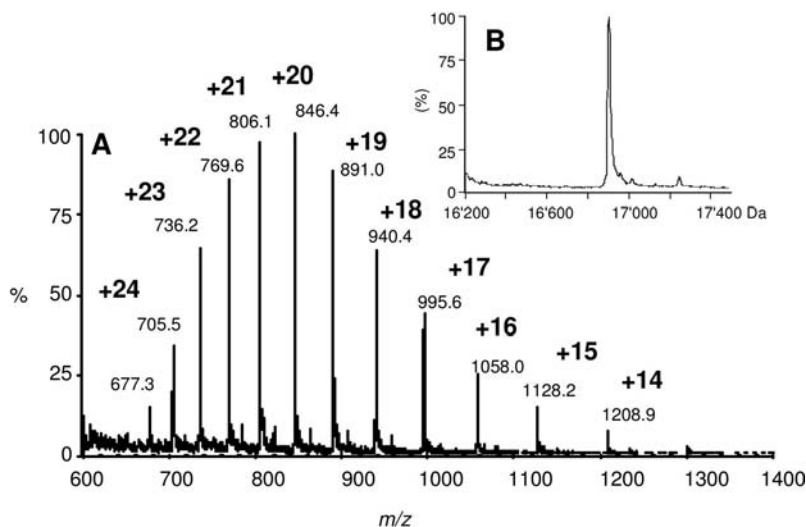


**Fig. 1.10** (A) Positive mode electrospray spectrum of human gamma interferon on a quadrupole mass analyzer. (B) Deconvoluted spectrum of human gamma interferon. The molecular mass was measured at  $16\,908 \pm 2$  Da.

stainless steel sprayers nickel or iron ions can be released and form positively charged complexes with certain types of analytes.

The mechanisms for the formation of gas phase ions from droplets are not fully understood and two theories have been proposed: the ion evaporation model (IEV) and the charge residue model (CR) [28]. The IEV model proposes that the ions are directly emitted into the gas phase when, after evaporation and

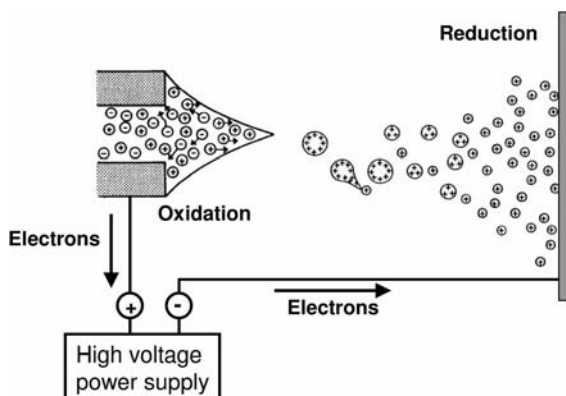


**Fig. 1.11** Electrospray as an electrophoretic cell. Adapted with permission from reference [28].

coulomb droplet fission, the droplets reach a certain radius. In the case of the CR model it is assumed that gas phase ions are produced when no further solvent evaporation is possible. In the case of small molecules it is believed that the IEV model predominates while for the proteins the CR model is assumed to occur.

A very interesting characteristic of electrospray MS is that it behaves, under controlled settings, like a concentration-sensitive detector [29]. This means that the MS response is directly proportional to the concentration of the analyte. A direct consequence is that LC post-column splitting does not affect the intensity of the MS signal. Another important point is that the reduction of the internal diameter of the column results in an increase in the MS response proportional to the squared ratio between the internal diameters of the greater i.d. column to the smaller i.d. column. Assuming that the same amount of analyte is injected onto a 0.3 mm i.d. column instead of a 2.0 mm i.d. column, a 44-fold increase in response is observed. Or the same response is obtained using a 44 times smaller sample volume. The use of smaller sample volumes is attractive for qualitative analysis where sample consumption can be critical. Because the injection volumes have also to be much lower with smaller i.d. columns, column-switching approaches become mandatory to really benefit from the gain of sensitivity in quantitative analysis [30]. Generally the trapping column is of a larger i.d. than the analytical column, allowing the rapid injection of 50–100  $\mu\text{L}$  of sample.

### 1.3.2.2 Atmospheric Pressure Chemical Ionization

Atmospheric pressure chemical ionization (APCI) is a gas phase ionization process based on ion–molecule reactions between a neutral molecule and reactant ions [31]. The method is very similar to chemical ionization with the difference that ionization occurs at atmospheric pressure. APCI requires that the liquid sample is completely evaporated (Fig. 1.12). Typical flow rates are in the range 200–1000  $\mu\text{L min}^{-1}$ , but low flow APCI has also been described. First, an aerosol is formed with the help of a pneumatic nebulizer using nitrogen. The aerosol is directly formed in a heated quartz or ceramic tube (typical temperatures 200–500  $^{\circ}\text{C}$ ) where the mobile phase and the analytes are evaporated. The temperature of the nebulized mobile phase itself remains in the range 120–150  $^{\circ}\text{C}$  due to evapo-

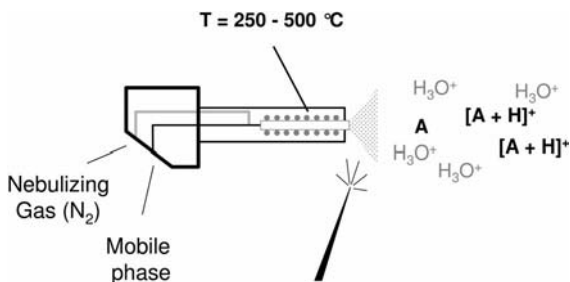
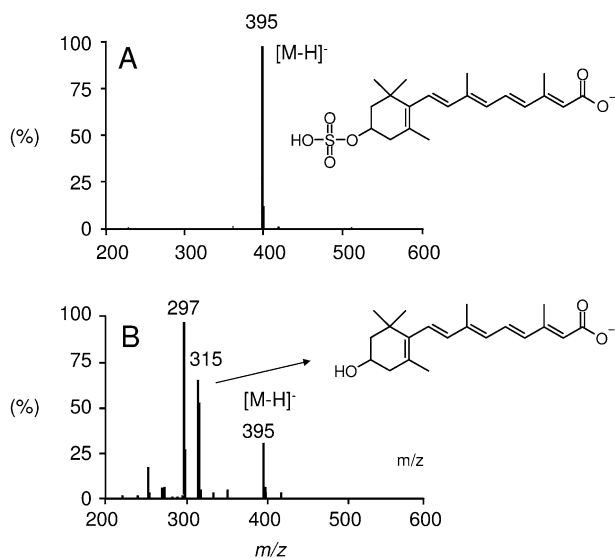


Fig. 1.12 Atmospheric pressure chemical ionization source. A Analyte.

ration enthalpy. In a second step, the evaporated liquid is bombarded with electrons formed by corona discharge. In positive mode primary ions such as  $\text{N}_2^+$  are formed by electron impact. These ions react further with water in several steps by charge transfer to form  $\text{H}_3\text{O}^+$ . Ionization of the analyte A occurs then by proton transfer. In negative mode ions are formed either by: (i) resonance capture ( $\text{AB} \rightarrow \text{AB}^-$ ), (ii) dissociative capture ( $\text{AB} \rightarrow \text{B}^-$ ) or (iii) ion–molecule reaction ( $\text{BH} \rightarrow \text{B}^-$ ). Generally APCI is limited to compounds with  $M_r < 2000$  which do not undergo thermal decomposition. Singly charged ions  $[\text{M}+\text{H}]^+$  or  $[\text{M}-\text{H}]^-$  are predominantly observed. While electrospray is a condensed phase ionization process, APCI is a gas phase ionization process where the analyte ionization efficiency depends on its gas phase proton affinity. APCI ionization has become very popular for liquid chromatography coupled with mass spectrometry because it can handle very easily liquid flow rates from  $200 \mu\text{L min}^{-1}$  to  $1 \text{ mL min}^{-1}$ . In contrast to electrospray, the application of heat may generate thermal decomposition of the analyte. At atmospheric pressure, ionization occurs with the high collision frequency of the ambient gas and rapid desolvation and vaporization limits the thermal decomposition of the analyte. Figure 1.13A shows the electrospray full-scan spectrum of the sulfuric acid monoester of 3-hydroxy retinoic acid, which is a phase II metabolite of 3-hydroxy retinoic acid without any degradation. In the APCI spectrum of the same analyte (Fig. 1.13B) several intense ions at  $m/z$  315 and  $m/z$  297 can be observed. These ions are not generated by collision-



**Fig. 1.13** Negative mode single quadrupole MS spectra of sulfuric acid monoester of 3-hydroxy retinoic acid: (A) electrospray, (B) atmospheric pressure chemical ionization.

induced dissociation but by thermal degradation. The product ion spectrum of the precursor ion at  $m/z$  395 shows only a strong ion at  $m/z$  97, corresponding to the  $\text{HSO}_4^-$  ion (data not shown). The ion at  $m/z$  315 corresponds to 3-hydroxy retinoic acid generated in the source by the loss of  $\text{SO}_3$ . The second ion at  $m/z$  297 corresponds to the loss of an additional 18 units ( $\text{H}_2\text{O}$ ). At a first glance thermal degradation in APCI sounds detrimental, but because it is quite reproducible it can provide further structural information in qualitative analysis.

#### 1.3.2.3 Photoionization

The setup for atmospheric pressure photoionization (APPI) [32–34] is very similar to that for APCI. Only the corona discharge is replaced by a gas discharge lamp (krypton, 10.0 eV) that generates vacuum ultraviolet photons. The liquid phase is also vaporized by a pneumatic nebulizer. Most analytes have ionization potentials below 10 eV while HPLC solvents have higher ionization potentials (water 12.6 eV, methanol 10.8 eV, acetonitrile 12.2 eV). The absorption of a photon by the molecule and the ejection of an electron forms a radical cation. Better sensitivities have been reported with the addition of dopants such as toluene or acetone. The mechanism of ionization is not fully understood but two different mechanisms can occur: (i) dopant radical cations react with the analyte by charge transfer or (ii) the dopant radical cation ionize the solvent molecules by proton transfer which can then ionize the analyte. APPI can also be performed in the negative mode. Like APCI, APPI can handle a large range of analytes. The performance of APPI is flow rate-dependent; and better sensitivities, compared to APCI, have been reported at lower flow rates. It appears also that APPI is less sensitive to matrix suppression and source contamination. Atmospheric pressure photoionization proves to be particularly attractive for the analysis of steroids and quinones.

#### 1.3.2.4 Multiple Ionization Source

With atmospheric pressure ionization the signal response is strongly analyte-dependent. To combine more than one ionization source (ESI, APCI, APPI) is particularly attractive to extend the range of compounds that can be analyzed simultaneously. Most pharmaceutical compounds can be analyzed automatically with positive or negative ESI mode using standard conditions [35]. Those compounds which give no signal require special attention, such as optimized solvent conditions or a change in ionization method resulting in a significant loss in time. Gallagher et al. [35] have developed a combined ESI-APCI (ESCi) source for high speed online LC-MS analysis. The combined source allows alternate online ESI and APCI scans with polarity switching within a single analysis. During the LC-MS run the high voltage power supply can be switched within 100 ms from the electrospray capillary to the APCI discharge needle. Figure 1.14 shows the LC-MS analysis of a mixture of daidzein and acetophenone with the ESCi source. In this case daidzein shows the best response with ESI while acetophenone gives a strong signal with APCI.

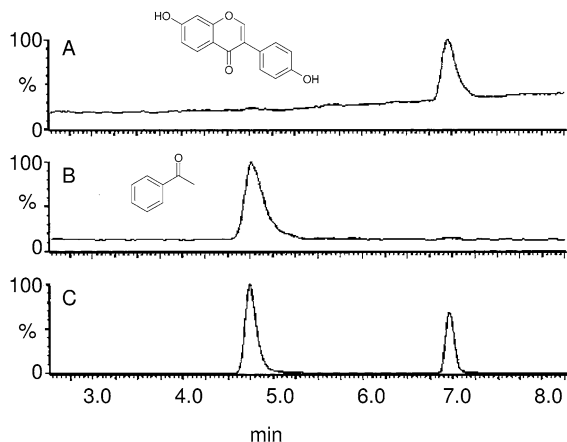


**Fig. 1.14** LC-MS analysis of a mixture of daidzein and acetophenone with a ESI source: (A) ESI, (B) APCI, (C) photo diode array detection. Adapted with permission from reference [35].

An other approach has been described by Syage et al. [36], who investigated the potential of various ionization sources (ESI, APCI, APPI) either in simultaneous or in switching mode. They suggest that ESI/APPI is the best combination because APPI covers a broad range of analytes while ESI covers the larger molecules.

#### 1.3.2.5 Desorption Electrospray and Direct Analysis in Real Time

Direct analysis of solid samples or analytes present on solid surfaces without any sample preparation has always been a topic of interest. Desorption electrospray ionization (DESI) is an atmospheric pressure desorption ionization method introduced by Cooks et al., producing ions directly from the surface to be analyzed, which are then sampled with the mass spectrometer [22, 37]. DESI is based on charged liquid droplets that are directed by a high velocity gas jet (in the order of  $300 \text{ m s}^{-1}$ ) to the surface to be analyzed. Analytes are desorbed from the surface and analyzed by mass spectrometer (Fig. 1.15).

Compared to atmospheric pressure MALDI (see Section 1.3.3.), no matrix is needed to perform the experiment. Direct analysis in real time (DART), a method related to DESI, has been reported by Cody et al. [23]. This technique is based on the reactions of metastable helium atoms generated by corona discharge with oxygen/water (negative mode) or water clusters (positive mode). The formed reactant ions ionize the analytes either by cluster assisted desorption or proton exchange. Both methods generate mostly protonated or deprotonated molecular ions. Various applications of both techniques for the analysis of the mass spectrometric profiling of intact biological tissue nicely demonstrated the characterization of the active ingredients in pharmaceutical samples formulated as tablets, ointments, or the sampling of plant material [38].

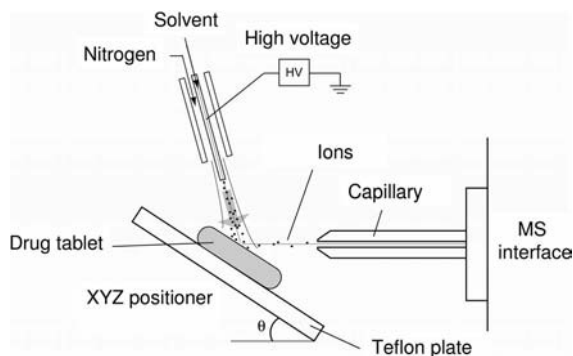


**Fig. 1.15** Desorption electrospray ionization interface. The sample, in this case a pharmaceutical pill, is placed in front of the orifice and is hit by nebulized droplets. Desorbed ions are then sampled into the mass spectrometer.

### 1.3.3

#### Matrix Assisted Laser Desorption Ionization

Matrix assisted laser desorption ionization (MALDI) has grown from the efforts to analyze macromolecules by mass spectrometry. Two groups were able, in the late 1980s, to obtain mass spectra of proteins. The first group was led by T. Tanaka [39] (Nobel Prize 2002) and developed MALDI where the analyte is mixed in a matrix of glycerol and cobalt and ionized with a laser. The second group formed by M. Karas and F. Hillenkamp [13] developed MALDI where the analyte is mixed with a matrix solution containing UV-absorbing molecules (Table 1.2). A few microliters of solution are spotted onto a MALDI target where the sample crystallizes.

After introduction of the target into the vacuum, an UV laser pulse is used to desorb and ionize the sample. Nitrogen laser emitting at 337 nm and Nd:YAG laser emitting at 355 nm are the most widely used. MALDI is a very powerful technique for the analysis of synthetics and natural biopolymers. It has completely replaced former techniques such as fast atom bombardment (FAB). In

**Table 1.2** Commonly used matrices for matrix assisted laser desorption ionization.

Sinapinic acid Proteins, imaging	$\alpha$ -Cyano-4-hydroxycinnamic acid Peptides, small molecules	2,5-Dihydroxybenzoic acid Proteins
<chem>COc1cc(C(=O)O)cc(OC)c1</chem>	<chem>N#CC(=O)C=Cc1ccc(O)cc1</chem>	<chem>O=C(O)c1cc(O)cc(O)c1</chem>

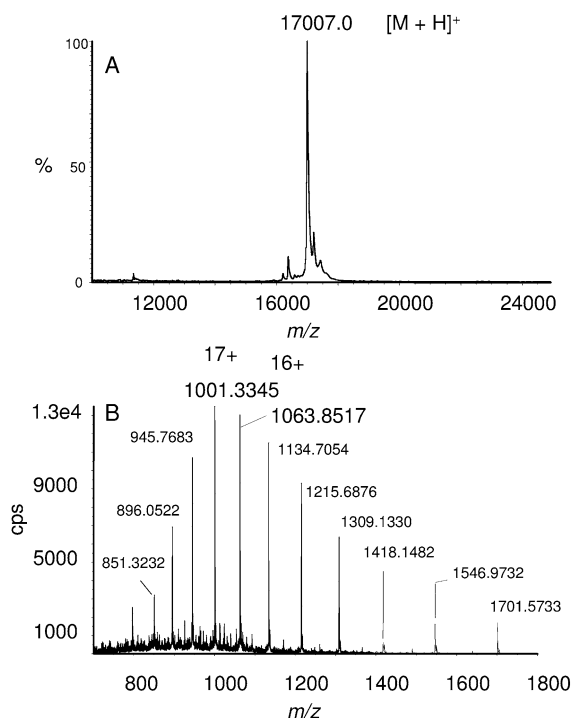


**Fig. 1.16** Mass spectra of a recombinant protein obtained by: (A) matrix assisted laser desorption ionization–time of flight, (B) electrospray–quadrupole time of flight. *cps* Counts per second.

most cases singly charged ions are predominantly detected while very little fragmentation or multiply charged ions are observed. MALDI is commonly used for the analysis of high molecular weight compounds such as peptides and proteins [40], synthetic polymers [41], DNA [42] and lipids [43].

MALDI has the intrinsic advantage over ESI-LC-MS in that it can achieve a high sample throughput. Sample preparation and separation can also be decoupled from the mass spectrometric analysis. The MALDI target plate can be easily archived, which allows simple reanalysis of selected samples. MALDI or ESI are suitable for the analysis of proteins, as depicted in Fig. 1.16. One of the key advantages of ESI over MALDI is the formation of multiply charged ions which allows the analysis of proteins on almost any type of mass analyzer while MALDI requires a time of flight mass analyzer in the linear mode to cover the high mass range.

The high throughput capability of MALDI and the different ionization mechanisms make this technique also an attractive alternative to electrospray ionization for the analysis of low relative molecular mass compounds (LRMM) [44]. However, interferences of matrix ions and the ionization of the low relative molecular mass compounds are the challenges of this technique [45, 46].

Desorption/ionization on porous silicon (DIOS) without any matrix has been described for the analysis of LRMM compounds with no chemical background [47, 48]. The use of MALDI for the analysis of small molecules was recently reported. Particularly attractive is the coupling of a MALDI source with a triple quadrupole mass analyzer for quantitative analysis in the selected reaction monitoring (SRM) mode due to very high analysis speed.

Surface enhanced laser desorption/ionization (SELDI) is a distinctive form of laser desorption ionization where the target plays an active role in the sample preparation procedure and ionization process [49]. Depending on the chemical or biochemical treatment, the SELDI surface acts as solid phase extraction or an affinity probe. Chromatographic surface is used for sample fractionation and purification of biological samples prior to direct analysis by laser desorption/ionization. SELDI is mainly applied for protein profiling and in biomarker discovery by comparing protein profiles from control and patient groups.

Because MALDI is a desorption technique, it is particularly suited for the analysis of surfaces such as biological tissues [50]. In this application, the matrix is applied on the complete surface of the tissue. The laser resolution is about 100  $\mu\text{m}$  and complete analyte distribution images (low molecular weight compounds, peptides, proteins) can be recorded [51, 52].

## 1.4 Mass Analyzers

### 1.4.1 Quadrupole Analyzers

A quadrupole mass analyzer is made of four hyperbolic or circular rods placed in parallel with identical diagonal distances from each other. The rods are electrically connected in diagonal. In addition to an alternating radiofrequency (RF) potential ( $V$ ), a positive direct current (DC) potential ( $U$ ) is applied on one pair of rods while a negative potential is applied to the other pair (Fig. 1.17). The ion trajectory is affected in  $x$  and  $y$  directions by the total electric field composed by a quadrupolar alternating field and a constant field. Because there is only a two-dimensional quadrupole field the ions, accelerated after ionization, maintain their velocity along the  $z$  axis.

The motion of ions in the quadrupole ( $x, y$ ) is quite complex and can be described by the Mathieu equations. The solution of the Mathieu equations generate two terms,  $a$  and  $q$ , which are proportional to the RF and DC potentials, respectively. For a detailed description of Mathieu equations, please see reference [53]. The trajectories of ions are stable when the ions never reach the rods of the quadrupole. To reach the detector an ion must have a stable trajectory in the  $x$  and  $y$  directions. With a quadrupole mass analyzer a mass spectrum is obtained by increasing the magnitude of  $U$  (DC) and  $V$  (RF) at a constant ratio. In a quadrupole mass analyzer when the DC voltage of a quadrupole is set to zero and



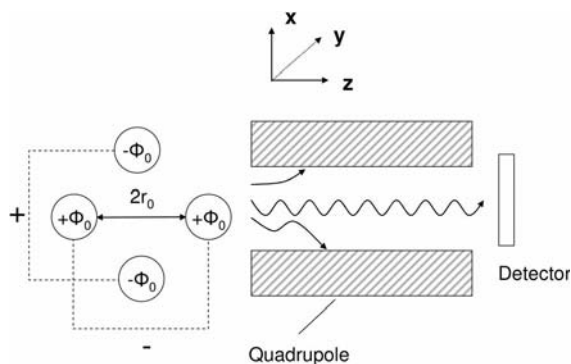


**Fig. 1.17** The quadrupole mass analyzer is formed by four circular or hyperbolic rods placed in parallel.  $\Phi$  Quadrupolar potential.

the RF voltage is maintained, the ions remain focused with no mass selectivity. Therefore, RF quadrupoles are ideal as ion guides or as a collision cell. Typically, quadrupole mass analyzers operate at unit mass resolution (FWHM 0.6–0.7  $m/z$  units). There is a strong relation between resolution and transmission. In general higher mass resolution results in a decrease of transmission, but mass resolution corresponding to peak width of 0.1  $m/z$  units without significant loss in sensitivity have also been reported. The mass range of quadrupoles is typically between  $m/z$  5 and  $m/z$  4000. Most common ionization sources are available on quadrupole instruments, including EI, ESI, APCI, APPI and MALDI.

#### 1.4.2

##### Triple Quadrupole Mass Analyzer

A triple quadrupole instrument (QqQ) is a combination of two mass quadrupole mass filters (tandem mass spectrometry) separated by a collision cell which is also a quadrupole operating in RF-only mode (Fig. 1.18). A common nomencla-

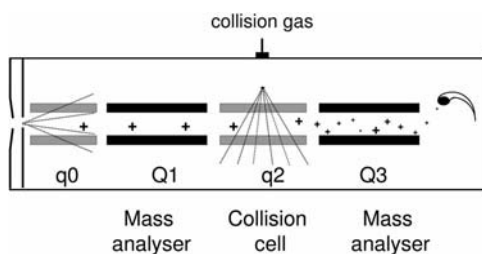


**Fig. 1.18** Schematic of a triple quadrupole instrument. Stage  $q_0$ : focusing quadrupole;  $Q_1$ ,  $Q_3$ : mass analyzing quadrupoles;  $q_2$ : collision cell. In the present configuration the collision energy (CE) is determined by the potential difference between  $q_0$  and  $q_2$ .

ture is to use (Q) to describe a quadrupole which is operated in RF/DC mode and (q) for a quadrupole which is operated in RF only mode. Tandem mass spectrometry is particularly attractive to obtain additional mass spectral information. In a first step, a specific  $m/z$  ion (precursor ion) is selected in the first mass analyzer (Q1). Collision induced dissociation (CID) occurs in the collision cell (q2) which is filled with a neutral gas such as argon or nitrogen. The fragment ions (product ions) are then sorted according to their mass to charge ratio in the second mass analyzer (Q3) and recorded by the detector. This way to obtain MS/MS data is called MS/MS in space, contrasting with quadrupole ion traps where MS/MS experiments are performed in time. On triple quadrupole mass spectrometers the potentials used to carry out collision induced dissociation are in the range 0–250 V. The collision energy is defined in electrons volts (eV) and is therefore dependent on the charge of the ions. For a potential difference of 30 volts the collision energy for a singly charge precursor ion would be 30 eV, and 60 eV for a doubly charged precursor ion. The nature of the collision gas ( $N_2$  or Ar) does not affect the product ion spectrum. The gas pressure in the collision cell mainly influences the sensitivity while collision energy influences the nature of the spectrum.

Depending on how the mass analyzers are operated, various types of MS and MS/MS experiments can be performed on a QqQ and these are summarized in Table 1.3. To normalize the description of various MS/MS or multi-stage MS<sup>n</sup> experiments a symbolism has also been described [54, 55].

A product ion scan can obtain structural information of a given precursor ion while a precursor ion scan is more suited to find structural homologues in a complex mixture. Bosentan ( $M_r = 551$ , Fig. 1.19) has two metabolites corresponding to the tert-butyl hydroxylation product ( $M_r = 567$ ) and the dealkylation of the methoxy group to form the phenol ( $M_r = 537$ ). Bosentan (Tracleer, Actelion Pharmaceuticals) is an oral dual endothelin receptor antagonist approved for the use in arterial hypertension [56]. Selection of the fragment at  $m/z$  280 can fish out precursor ions corresponding only to bosentan and these two metabolites (Fig. 1.19C). A similar result is obtained with the constant-neutral loss scan mode (Fig. 1.19D) which is based on neutral loss of 44 units.

**Table 1.3** Settings of the Q1 and Q3 quadrupoles for the various scan modes of a triple quadrupole mass spectrometer.

Mode	Q1 quadrupole	Q3 quadrupole
Full scan Q1/single ion monitoring (SIM) Q1	Scan/fixed	Rf mode
Full scan Q3/single ion monitoring (SIM) Q3	Rf mode	Scan/fixed
Product ion scan (PIS)	Fixed	Scan
Precursor ion scan (PC)	Scan	Fixed
Neutral loss (NL)	Scan	Scan: neutral loss offset
Selected reaction monitoring (SRM)	Fixed	Fixed

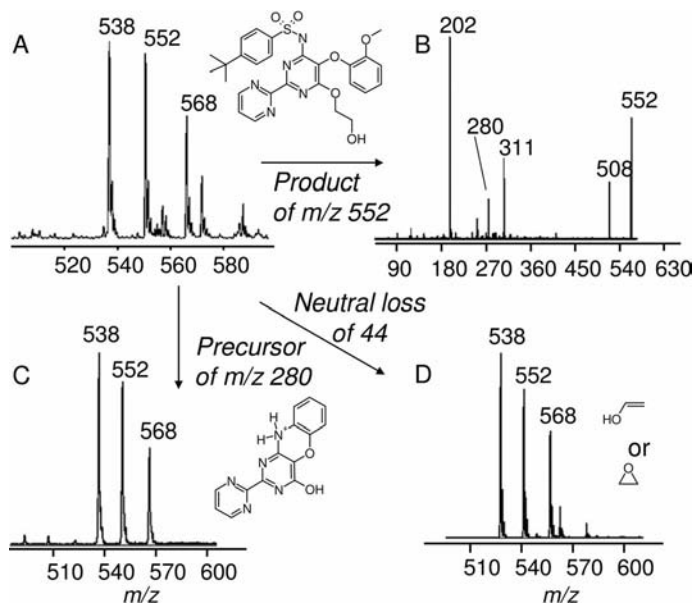


**Fig. 1.19** (A) Q1 full-scan spectrum of bosentan  $[(M+H)^+]$ ,  $m/z$  552], its demethylated metabolite  $[(M+H)^+]$ ,  $m/z$  538] and its hydroxylated metabolite  $[(M+H)^+]$ ,  $m/z$  568], (B) product ion spectrum of bosentan, (C) precursor ion spectrum, (D) neutral loss spectrum. Electrospray ionization is in positive ion mode.

Precursor ion and neutral loss scans are efficient on QqQ to identify structurally related compounds in a mixture, using either a common fragment with the parent compound or the specific neutral loss such as glucuronid or sulfate for phase II metabolites. These selective scan modes do not require any knowledge of the molecular weight or the structure of the compounds. In the selected reaction monitoring (SRM) mode, Q1 is set at the mass of the precursor  $[M+H]^+$  ( $m/z$  552) and Q3 at  $m/z$  202, which is the most important fragment of bosentan. Because in SRM mode both quadrupoles are not scanning, better detection limits can be achieved compared to full-scan acquisition. Therefore, this mode has become the working horse for quantitative analysis. Typical dwell times are in the range 5–250 ms. Because with quadrupole mass analyzers transmission is dependent on the mass resolution, it is always mandatory, in SRM mode, to indicate the mass resolution of quadrupole Q1 and Q3. In general, full width of the peak at half maximum (FWHM) is indicated. Analysis in single ion monitoring mode can also be performed on a QqQ either using Q1 and Q3. Generally when performing a SIM analysis in Q3 mode, the collision cell is filled with collision gas and serves as a further declustering device to improve signal-to-noise.

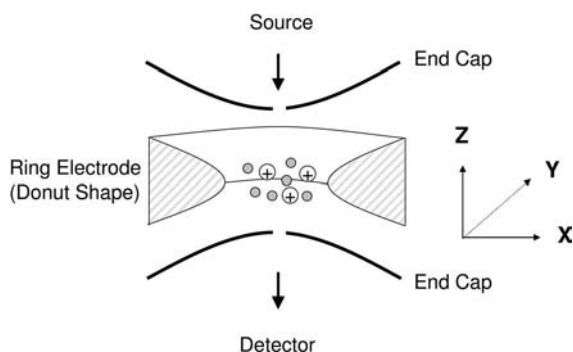


**Fig. 1.20** The quadrupole ion trap. A fundamental RF potential is applied onto the ring electrode to trap ions. The gray circles represent helium gas.

### 1.4.3

#### Ion Trap Mass Spectrometry

The ion trap is a device that utilizes ion path stability of ions for separating them by their  $m/z$  [53]. The quadrupole ion trap and the related quadrupole mass filter were invented by Paul and Steinwedel [57]. A quadrupole ion trap (QIT or 3D-IT) mass spectrometer operates with a three-dimensional quadrupole field. The QIT is formed by three electrodes: a ring electrode with a donut shape placed symmetrically between two end cap electrodes (Fig. 1.20).

By applying a fundamental RF potential, the QIT can be described as a small ion storage device where ions are focused toward the center of the trap by collision with helium gas. In the QIT, because of the cylindrical symmetry of the trap, the  $x$  and  $y$  components of the field are combined to a single radial  $r$  component, where  $r^2 = x^2 + y^2$ . The motion of ions in the trap is characterized by one radial and one axial frequency (secular frequencies). Like quadrupoles, the motion of ions can be described by the solutions of Mathieu's equations ( $a, q$ ). Ions with various  $m/z$  can be stored in the trap with the condition that trajectories are stable in  $r$ - and  $z$ - directions. Each ion of a certain  $m/z$  will be trapped at a certain  $q_z$  value. The higher  $m/z$  ions will be located at lower  $q$  values while the lower  $m/z$  will be located at the higher  $q_z$  values. The quadrupole ion trap can store only a limited number of ions before space charging occurs. To circumvent this effect, most instruments have an automatic gain control procedure (AGC). This procedure exactly determines the adequate fill time of the trap to maximize sensitivity and minimize resolution losses due to space charge. A mass spectrum can be obtained by mass-selective ejection where the amplitude of the RF potential is continuously increased at a certain rate. Ions with the lowest  $m/z$  are ejected first. The mass-selective axial instability mode requires that the ions are confined at the center of the trap and at a limited mass range. Resonant mass

ejection is another procedure which can generate a mass spectrum with a higher mass range. Ion motion can be modified either by exciting the radial or the axial frequencies by applying a small oscillating potential at the end cap electrodes during the RF ramp. In both mass-analyzing modes, the resolution of the spectrum is strongly dependent on the speed at which the RF amplitude is increased. Higher resolution can be obtained with slower scan speed. Compared to quadrupole instruments with the quadrupole ion trap, high sensitivity can be obtained in full-scan mode due to the ability of ion accumulation in the trap before mass analysis. Rapid mass analysis with the mass instability scan allows scanning at a speed of several thousand  $m/z$  units per second. There are several important components which affect the time necessary to obtain a mass spectrum (duty cycle): (i) the injection time (within 0.5–500.0 ms), (ii) the scan speed (in the range 5000–20 000  $m/z$  units  $s^{-1}$ ), (iii) isolation of the precursor ion and fragmentation in tandem MS or  $MS^n$ . Contrarily to the triple quadrupole, MS/MS is not performed in *space* but in *time*. Another significant difference is the use of helium as collision gas. Because the trap is permanently filled with gas, the instrument can switch very rapidly from single MS to MS/MS mode. High sensitivity can be achieved in the QIT because of ion selective accumulation of the precursor. Another advantage compared to the triple quadrupole is the short duty cycle for an MS/MS experiment. A typical  $MS^n$  ( $MS^3$ ) sequence is illustrated in Fig. 1.21. To obtain a  $MS^2$  spectrum the precursor ion is isolated and then excited while fragments are trapped. The next step to obtain an  $MS^3$  spectrum is to isolate a fragment ion again and to perform CID fragmentation. Because MS/MS is performed in time in the same physical device, the operation can be repeated several times. Most commercial instruments can perform  $MS^n$  to the tenth or 11th level. A difficulty is to excite the precursor ions efficiently and trap the product ions in the same device. Generally, solely the precursor is excited in a specific window corresponding to 1–4  $m/z$  units. The consequence is that fragment ions are not further excited and cannot produce second generation fragments. In many cases,

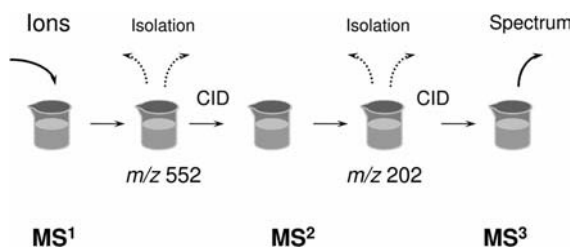


**Fig. 1.21** Typical  $MS^3$  scheme  $m/z$  552  $\rightarrow$   $m/z$  202  $\rightarrow$ . In a first step the protonated bosentan molecule at  $m/z$  552 is isolated and fragmented ( $MS^2$ ). The fragments are trapped. In a second step the fragment at  $m/z$  202 is isolated and fragmented and the spectrum is recorded.

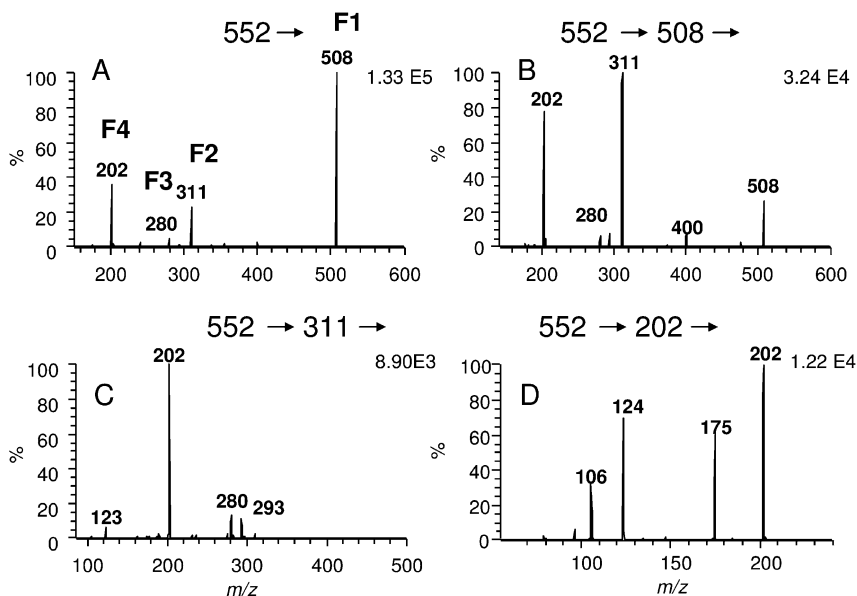


**Fig. 1.22** Various  $MS^2$  and  $MS^3$  spectra of bosentan: (A)  $MS^2$ , (B)  $MS^3$ , (C)  $MS^3$ , (D)  $MS^3$ . F1 to F4 correspond to the main fragments of bosentan obtained also on the QqQ.

$MS^2$  trap CID generates similar spectra than quadrupole CID, but there are cases where the spectra differ significantly.

For molecules which can easily lose water or ammonia, the most abundant fragment observed in  $MS^2$  is M-18 or M-17, which is not very informative. To overcome this limitation, wide band excitation (range 20  $m/z$  units) can be applied. Another difference compared to QqQ is that QIT have a low mass cutoff of about one-third of the mass of the precursor ion. However QIT is particularly attractive to follow fragmentation cascades as illustrated for bosentan in Fig. 1.22. It can clearly be concluded that the fragment at  $m/z$  175 originated from the precursor at 202 and not from the precursor at  $m/z$  311.

Due to the high sensitivity in  $MS^n$  mode, ion traps are particularly attractive for qualitative analysis in drug metabolism and proteomics studies. Compared to QqQ, similar sensitivities can be achieved for quantitative analysis but at the cost of precision and accuracy. A major difference is the number of transitions which can be monitored at the same time. While more than 100 SRM transitions can be recorded within one second on a QqQ, this number is much lower with the QIT (generally four to eight transitions). Ion traps have larger mass ranges (up to 50 000) than quadrupole instruments but smaller ranges than time of flight mass analyzers. Most commercial instruments use two mass ranges: (i) from  $m/z$  50 to  $m/z$  2000–3000 with a mass resolution of 0.7  $m/z$  units or better and (ii) from  $m/z$  200 to  $m/z$  4000–6000 with a mass resolution of 2–4  $m/z$  units.

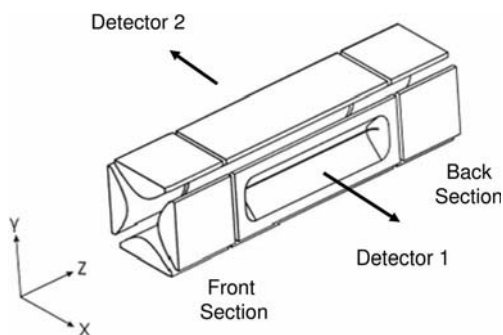


**Fig. 1.23** Standalone linear ion trap. Because the ions are ejected radially two detectors are required for best sensitivity. Adapted with permission from reference [59].

Very recently linear ion traps (LIT) or two-dimensional ion traps (2D IT) have gained interest for various applications, either as standalone mass analyzers or coupled with Fourier transform ion cyclotron, three-dimensional ion trap (3D IT), TOF or orbitrap mass analyzers [58]. Physically, a linear ion trap is like a quadrupole formed by four hyperbolic or circular rods placed symmetrically. In a linear ion trap the ions are confined radially by a two-dimensional radio frequency field. To prevent ions from escaping axially, a DC potential is applied to the end electrodes. The same type of experiments which can be performed on 2D or 3D ion traps are basically the same but there are several advantages to trap ions in a 2D trap compared to 3D traps: (i) no quadrupole field along the  $z$ -axis, (ii) enhanced trapping efficiencies, (iii) more ions can be stored before observing space charging effects and (iv) strong focusing along the center line instead of focusing ions to a point.

Schwartz et al. [59] described a standalone linear ion trap where mass analysis is performed by ejecting the ions radially through slits of the rods using the mass instability mode. To maximize sensitivity the detection is performed by two detectors placed axially on either side of the rods (see Fig. 1.23).

#### 1.4.4

##### **Triple Quadrupole Linear Ion Trap**

In a linear ion trap one of the most efficient ways to perform mass analysis is to eject ions radially. Hager [60] demonstrated that, by using fringe field effects, ions can also be mass-selectively ejected in the axial direction. There are several benefits for axial ejection: (i) it does not require open slits in the quadrupole, (ii) the device can be operated either as a regular quadrupole or a LIT using one detector. A commercial hybrid mass spectrometer was developed based on a triple quadrupole platform where Q3 can be operated either in normal RF/DC mode or in the LIT ion trap mode (Fig. 1.24).

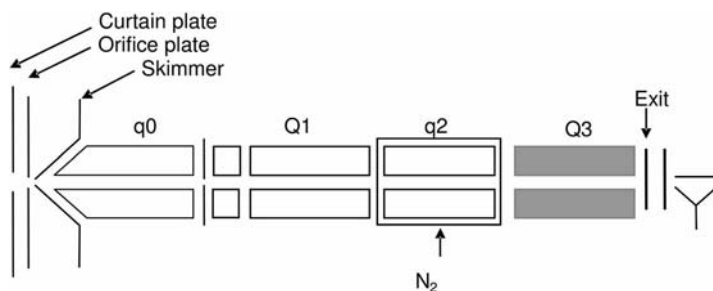


**Fig. 1.24** Schematic of the triple quadrupole linear ion trap (AB/MDS Sciex). Q3 can be operated in quadrupole or trap mode. In both modes ions are detected in the axial direction.

In the triple quadrupole linear ion trap, tandem  $MS^2$  is performed in space where the LIT serves only as a trapping and mass-analyzing device. Figure 1.25 illustrates the difference between quadrupole CID spectra and trap CID spectra for trocade.

With quadrupole CID all fragments are recorded in one experiment, while in the case of the 3D ion trap  $MS^2$ ,  $MS^3$  and  $MS^4$  experiments are required to ob-

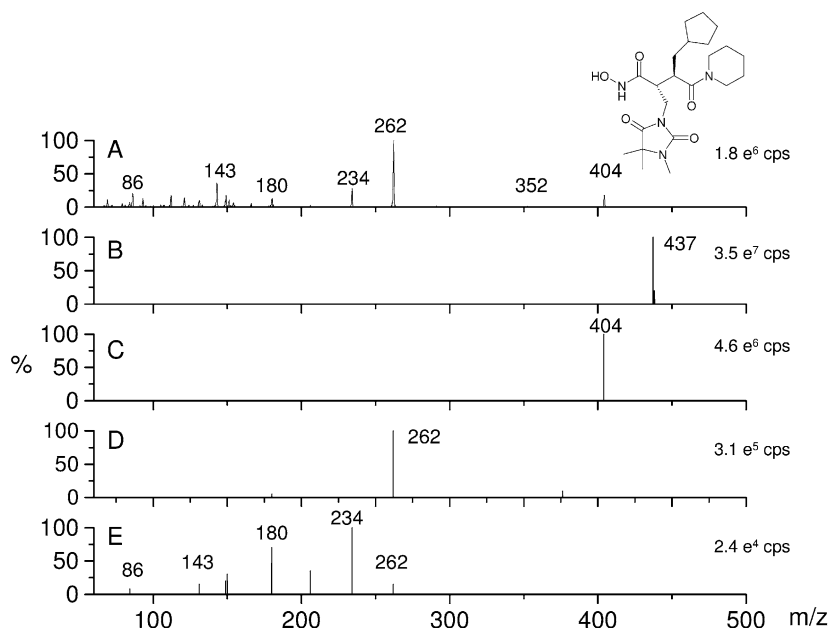


**Fig. 1.25** Quadrupole CID spectra and ion trap CID spectra for trocade ( $M_r$  403): (A) MS/MS on QqQ-LIT, (B) MS, (C)  $MS^2$ , (D)  $MS^3$ , (E)  $MS^4$ . Spectra B–E were recorded on a 3D ion trap).



tain the low mass fragments. In the triple quadrupole linear ion trap  $MS^3$  is performed in the following manner. The first stage of fragmentation is accomplished by accelerating the precursor ions chosen by Q1 into the pressurized collision cell, q2. The fragments and residual precursor ions are transmitted into the Q3 linear ion trap mass spectrometer and are cooled for approximately 10 ms. The next generation precursor ion is isolated within the linear ion trap by application of resolving DC near the apex of the stability diagram. The ions are then excited by a single frequency of 85 kHz auxiliary signal and fragmented. The particularity of the QqQ<sub>LIT</sub> is that the instrument can be operated in various ways, as described in Table 1.4 [61, 62].  $MS^2$  spectra are obtained in the quadrupole CID mode while  $MS^3$  spectra are obtained in the trap CID mode.

The major advantage of this instrument is that qualitative and quantitative analysis can be performed in the same LC-MS run. As an example in a data-dependent experiment, the selected reaction monitoring mode can be used as a survey scan and the enhanced product ion mode (EPI) as a dependent scan. The consequence is that for each quantified analyte a confirmatory MS/MS spectrum can be obtained.

**Table 1.4** Mode of operation of the triple quadrupole linear ion trap (QqQ<sub>LIT</sub>).

Mode of operation	Q1	q2	Q3
Q1 scan	Resolving (scan)	RF only	RF only
Q3 scan	RF only	RF only	Resolving (scan)
Product ion scan (PIS)	Resolving (fixed)	Fragment	Resolving (scan)
Precursor ion scan (PC)	Resolving (scan)	Fragment	Resolving (fixed)
Neutral loss scan (NL)	Resolving (scan)	Fragment	Resolving (scan offset)
Selected reaction monitoring mode (SRM)	Resolving (fixed)	Fragment	Resolving (fixed)
Enhanced Q3 single MS (EMS)	RF only	No fragment	Trap/scan
Enhanced product ion (EPI)	Resolving (fixed)	Fragment	Trap/scan
$MS^3$	Resolving (fixed)	Fragment	Isolation/fragment trap/scan
Time delayed fragmentation (TDF)	Resolving (fixed)	Trap/no fragment	Fragment/trap/scan
Enhanced resolution Q3 single MS (ER)	RF only	No fragment	Trap/scan
Enhanced multiply charged (EMC)	RF only	No fragment	Trap/scan

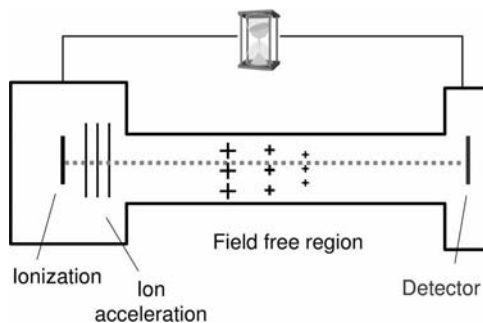


**Fig. 1.26** Schematic of the simplest form of a time of flight mass spectrometer. After ionization the ions are accelerated with a strong electric field.

#### 1.4.5

#### Time of Flight Mass Spectrometry

From the physical principle time of flight (TOF) may be the simplest way to perform mass spectrometric analysis (Fig. 1.26). TOF is the measure of the time that ions need to cross in a field free tube of about 1 m length [63, 64]. It is a pulsed technique and requires a starting point. The motion of an ion is characterized by its kinetic energy  $E_c = 0.5m \times v^2$  ( $m$  = mass,  $v$  = speed). Therefore, the speed of ions or the time to fly through the tube is proportional to their  $\sqrt{m/z}$  value. The velocity of the ions formed is generally low and they are accelerated by strong electric fields (2–30 kV) in the direction of the detector. Low mass ions reach the detector more rapidly than high mass ions. Due to the short flight time (50–100  $\mu$ sec) and the good transmission, a spectrum can be generated within 100 ms over an almost unlimited mass range. Detection of the ions is performed with a multi-channel plate detector (MCP, see Section 1.5) which has a relatively small dynamic range (generally two to three orders of magnitude).

With soft ionization techniques such as MALDI, ions of  $m/z$  200 000 can be routinely detected. The mass range is mainly limited by the fact that with the detector the response decreases with increasing  $m/z$  of the ions. The mass resolution of a TOF mass analyzer is relatively poor (unit mass resolution and less) and is affected by factors that create a distribution in the flight time of ions with the same  $m/z$ . The simplest way to increase the mass resolution is to increase the length of flight tube or to reduce the kinetic energy spread of the ions leaving the source.

One way to reduce the kinetic energy spread is to introduce a time delay between ion formation and acceleration, referred to as delayed pulsed extraction. After a certain time delay ranging from nanoseconds to microseconds a voltage pulse is applied to accelerate the ions out of the source.

The second way to improve the mass resolution significantly is to use an electrostatic mirror (mass reflectron) placed in the drift region of ions (Fig. 1.27).

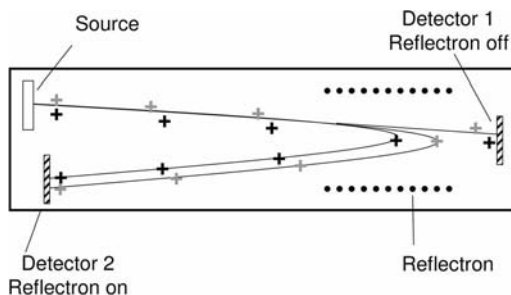


**Fig. 1.27** Schematic of a time of flight mass spectrometer equipped with a reflectron. The instrument can be operated in the linear mode (reflectron off) or in the reflectron mode (reflectron on).

Briefly, the ions with high energy penetrate deeper into the ion mirror region than those with the same  $m/z$  at a lower energy. Because of the different trajectories, all ions of the same  $m/z$  reach the detector at the same time. Thus, all ions of the same  $m/z$  have then a much lower energy dispersion. With the reflectron the flight path is increased without changing the physical size of the instrument. In reflectron mode a mass resolving power of 15 000 is standard but the mass range is limited to several thousand  $m/z$  units. TOF instruments are non-scanning mass spectrometers resulting in an increased sensitivity compared to quadrupole mass spectrometers.

In general the commercial TOF instruments have two detectors; one for the linear mode and one for the reflectron mode. The combination of MALDI with TOF is ideal because both techniques are pulsed techniques. However, it is also possible to arrange a continuous beam as generated by electrospray ionization. For that purpose orthogonal acceleration was developed [65]. The ion beam is introduced perpendicularly to the TOF and packets are accelerated orthogonally (oa-TOF) at similar frequencies improving the sensitivity. While a packet of ions is analyzed, a new beam is formed in the orthogonal acceleration.

Time of flight instruments are mainly used for qualitative analysis with MALDI or atmospheric pressure ionization. With MALDI ionization one of the main applications is the identification of proteins by analyzing their peptides after trypsin digestion (peptide mass finger print; PMF). Further structural information of the peptides can be obtained from metastable transitions or collision-induced dissociations generated in the drift tube prior to entering the reflectron. This technique is called post-source decay (PSD). A metastable ion is an ion which dissociates in the free field region of the mass spectrometer. For TOF instruments the acquisition rate is in the range 10–20 Hz, making these mass analyzers best suited for the interfacing of fast liquid chromatographic separations or capillary electrophoresis using electrospray ionization.

Due to their fast acquisition rate and high resolution capabilities TOF mass analyzers are often used as the last mass analyzing stage in hybrid tandem mass

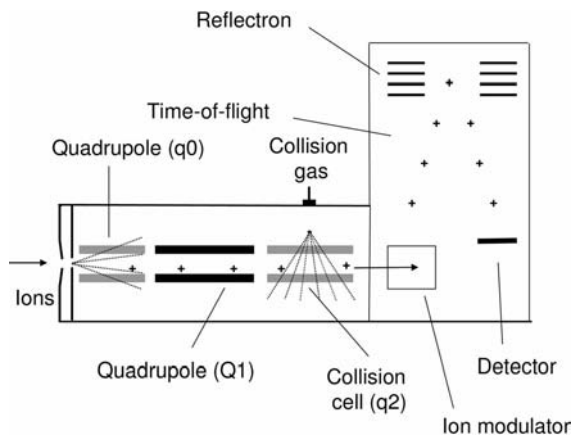


**Fig. 1.28** Schematic of a quadrupole–time of flight instrument. Quadrupole  $q_0$  is used for collisional cooling and ion focusing. Nitrogen or argon is generally used as collision gas. The ion modulator pushes the ions orthogonally to their initial direction into the TOF analyzer.

spectrometers such as quadrupole–time of flight instruments. A quadrupole–time of flight instrument (QqTOF) is the result of the replacement of the last quadrupole section (Q3) of a triple quadrupole instrument by a time of flight analyzer (Fig. 1.28), a powerful combination in regards of mass range ( $m/z$  5 to  $m/z$  40 000), mass resolving power of 10 000 and sensitivity [66, 67]. In single MS mode the quadrupoles ( $q_0$ , Q1,  $q_2$ ) serve as RF ion guides and the mass analysis is performed in the TOF. To accommodate ion injection a pulsed field is applied in the ion modulator to push the ions orthogonally to their initial direction into the TOF analyzer.

In tandem MS mode, because the product ions are recorded with the same TOF mass analyzers as in full scan mode, the same high resolution and mass accuracy is obtained. Isolation of the precursor ion can be performed either at unit mass resolution or at 2–3  $m/z$  units for multiply charged ions. Accurate mass measurements of the elemental composition of product ions greatly facilitate spectra interpretation and the main applications are peptide analysis and metabolite identification using electrospray ionization [68]. In TOF mass analyzers accurate mass determination can be affected by various parameters such as: (i) ion intensities, (ii) room temperature or (iii) detector dead time. Interestingly, the mass spectrum can be recalibrated post-acquisition using the mass of a known ion (lock mass). The lock mass can be a cluster ion in full scan mode or the residual precursor ion in the product ion mode. For LC-MS analysis a dual spray (LockSpray) source has been described, which allows the continuous introduction of a reference analyte into the mass spectrometer for improved accurate mass measurements [69]. The versatile precursor ion scan, another specific feature of the triple quadrupole, is maintained in the QqTOF instrument. However, in pre-

cursor scan mode the sensitivity is lower in QqTOF than in QqQ instruments. The lack of good quality product ion spectra on conventional MALDI-TOF instruments made the use of MALDI on QqTOF instruments an interesting alternative for the sequencing of peptides. As in electrospray TOF, in the case of QqTOF the MALDI ion production needs to be decoupled from mass measurements. The technique to interface MALDI with QqTOF is named orthogonal MALDI (o-MALDI) TOF with collisional cooling. With o-MALDI the pulse is almost converted in a continuous beam equivalent to that originated from an electrospray source.

The TOF mass analyzer has a low duty cycle, and the combination with an ion accumulation device such as an ion trap is therefore very advantageous. It offers also  $MS^n$  capabilities with accurate mass measurement. In all acquisition modes, the ions are accelerated into the time of flight for mass analysis. Various other hybrid mass spectrometers with TOF have been described, including quadrupole ion trap [70] and linear ion trap [58]. High energy tandem mass spectrometry can be performed on TOF-TOF mass spectrometers [71, 72].

#### 1.4.6

#### Fourier Transform Mass Spectrometry

##### 1.4.6.1 Fourier Transform–Ion Cyclotron Resonance Mass Spectrometry

The main components of a Fourier transform ion cyclotron resonance mass spectrometer are a superconducting magnet and a cubic or cylindrical cell (Fig. 1.29). Typically, the magnet field strengths ( $B$ ) are in the range 3.0–9.4 Tesla. Ions are stored in the cell according to their cyclotronic motion arising from the interaction of an ion with the unidirectional constant homogenous magnetic field. A static magnetic field applied on the  $z$  direction confines ions in the  $x$ - and  $y$ -directions according to the cyclotronic motion. To avoid the escape of ions along the  $z$  axis, a low electrostatic potential is applied to the end cap electrodes [73].

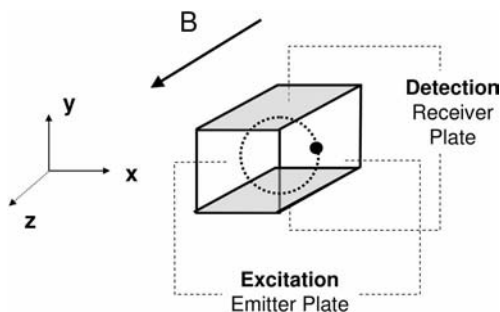


**Fig. 1.29** Diagram of an ion cyclotron resonance instrument. The magnetic field is oriented along the  $z$ -axis and ions (●) are trapped according to the same axis. Due to the cyclotronic motion the ions rotate around the  $z$ -axis in the  $x$ - $y$  plane.

Cyclotron motion is characterized by its cyclotron frequency ( $f$ ; from 5 kHz to 5 MHz) which depends on: (i) the magnetic field ( $B$ ), (ii) the charge on the ion ( $z$ ) and (iii) the mass of the ion ( $m$ ). In contrast to other types of mass spectrometers, detection is performed in a non-destructive way. The ions are detected by excitation applying a coherent broadband excitation. The ions undergo cyclotron motion as a packet with a larger radius. When the ion packet approaches the detection plates it generates an alternating current named image current. The resulting signal is generally called the transient free induction decay (FID). Ions of any mass can be detected simultaneously with Fourier transform mass spectrometry (FTMS). The image current is composed of different frequencies and amplitudes which are converted by applying a Fourier transformation to frequency components and further to a mass spectrum. Mass resolution is best with high field strength, decreases when the mass increases and is dependent on acquisition time. The mass resolution is strongly dependent on the length of the transient time. Typical transient times are in the range 0.1–2.0 s. With commercial instruments a mass resolving power of 100 000 or more can be routinely achieved. Collision induced dissociation can also be performed in the FT-ICR cell. The transient signal decreases with collision of ions and neutral gas molecules. It is therefore essential to work at very high vacuum ( $1.3 \times 10^{-8}$  Pa). The dynamic range of a FT-ICR mass spectrometer is relatively poor because the instrument suffers from the fact that the number of ions in the trap must be in a specified range. Over- and underfilling of the trap results in mass shifts towards high and low values, respectively. To have a better control of the ion population in the cell, a commercial hybrid instrument (LTQ-FTMS, Thermo) was developed by combining a linear ion trap (LIT) with a FT-ICR mass spectrometer [74]. Because the LIT is equipped with two detectors data can be recorded simultaneously in the ion trap and in the FT-ICR mass spectrometer. In this way the FT-ICR operates only as a high resolution detector for MS or MS<sup>n</sup> experiments performed in the linear ion trap.

#### 1.4.6.2 Orbitrap Mass Spectrometer

Makarov [75] invented a novel type of mass spectrometer based on the orbital trapping of ions around a central electrode using electrostatic fields named orbitrap. Kingdon had already described the orbiting of ions around a central electrode using electrostatic fields in 1923, but the device had been only used for ion capturing and not as a mass analyzing device. The orbitrap (Fig. 1.30) is formed by a central spindle-like electrode surrounded by an electrode with a barrel-like shape to create an electrostatic potential. The  $m/z$  is a reciprocal proportionate to the frequency ( $\omega$ ) of the ions oscillating along the  $z$ -axis. There is no collisional cooling inside the orbitrap, which operates at very high vacuum ( $2 \times 10^{-8}$  Pa). Detection is performed by measuring the current image of the axial motion of the ions around the inner electrode. The mass spectrum is obtained after Fourier transformation of the image current. The mass resolving power depends on the time constant of the decay transient. The orbitrap provides a mass resolving power exceeding 100 000 (FWHM) and a mass accuracy  $\leq 3$  ppm. To be opera-

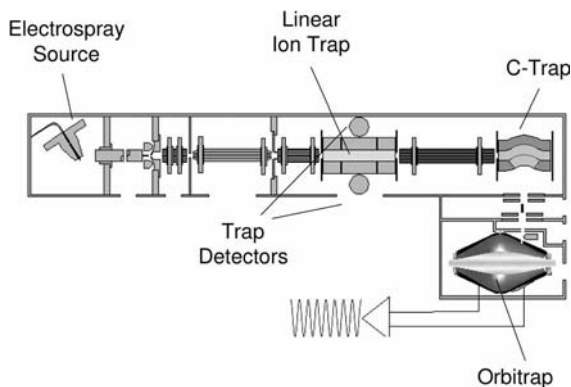


**Fig. 1.30** Schematic of the linear ion trap (LIT)–orbitrap (LITQ orbitrap, Thermo). One of the specificities of the system is that the LIT has two detectors. Therefore the LIT can perform various experiments at the same time. Adapted with permission from reference [76].

tional as a mass spectrometer the orbitrap requires external ion accumulation, cooling and fragmentation. The setup of the LIT–orbitrap from Thermo is depicted in Fig. 1.30. The instrument consists of a linear ion trap with two detectors connected to the orbitrap via a C-trap. With the LIT various MS or MS<sup>n</sup> experiments can be performed. When the orbitrap is used as a detector the ions are transferred into the C-trap where they are collisionally damped by nitrogen at low pressure. The C-trap acts as a trapping and focusing device. Injection from the C-Trap into the orbitrap is then performed with short pulses of high voltages.

The particularity of the LIT–orbitrap instrument is the independent operation of the orbitrap and the LIT. Because high resolution requires longer transient time, further data can already be collected in the LIT at the same time. As an example accurate mass measurements of the precursor ion can be performed in the orbitrap while MS<sup>2</sup> and MS<sup>3</sup> spectra are recorded with the linear ion trap. The LIT–orbitrap has less resolution than a FT-ICR instrument with similar duty cycle, but its maintenance costs are far lower than for the FT-ICR. Both instruments will have a major impact in mainly qualitative analysis of low molecular weight compounds and macromolecules.

## 1.5

### Ion Detectors

To obtain a mass spectrum, ions need to be converted into a usable signal by a detector. The simplest form of ion detection is a photographic plate or a Faraday cup for the direct measurement of the charge. In a Faraday cup the induced current is generated by an ion which hits the surface of a dynode and emits

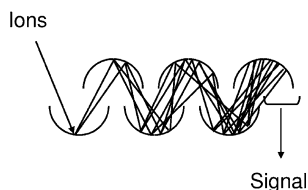


**Fig. 1.31** Discrete-dynode electron multiplier. When the ions hit the surface of the detector electrons are emitted to form an avalanche of electrons which generates the signal.

electrons. This type of detector is generally insensitive and mounted in isotopic ratio mass spectrometers. The first electron multipliers mounted in mass spectrometers were discrete-dynode multipliers fabricated from beryllium copper alloy. When a positively or a negatively charged ion reaches the detector electrons are produced (Fig. 1.31).

In this type of detector the electrons are accelerated down the channel producing additional electrons to the output signal. The created cascade of electrons results in a measurable current at the end of the detector [77].

Channel electron multipliers (CEM) are fabricated from lead-silica glass (Fig. 1.32) and can have curved or straight forms. In a channel electron multiplier, when the charged particles (positive or negative) hit the surface of the electrode, electrons are produced from the surface which then generate the current.

Channel electron multipliers can be operated either in analog or pulse counting mode. The difference between the two modes of operation is that pulse counting produces output pulses with a certain amplitude while analog detectors produce a wide distribution of output pulses. Therefore, the pulse counting mode is more suitable for high sensitivity mode while analog mode is best suited for intense signals. In modern mass spectrometers, autotune procedures optimize the analog multipliers based on signal-to-noise. The tuning of pulse counting detectors is somewhat different because they operate in a different mode. The sensitivity of a detector decreases almost exponentially with the mass of the ions. One way to improve the signal in the channel electron multiplier detector sensitivity at higher mass is to use a conversion dynode (Fig. 1.33). A conversion dynode is a metal surface which is held at high potential ( $>3$  kV). The role of the dynode

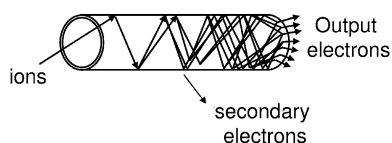


**Fig. 1.32** Straight channel electron multipliers (CEM) are typically used in quadrupole-type mass spectrometers.



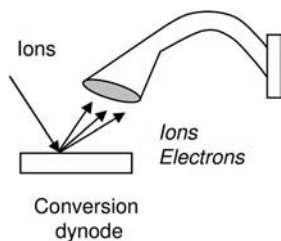


**Fig. 1.33** Curved channel electron multiplier with conversion dynode. The conversion dynode acts as a post acceleration device of the ions before they hit the surface of the channel electron multiplier.

potential is to accelerate ions to a point where good conversion in secondary ions or electrons occurs.

The lifetime of channel electron multipliers is ca. 1–2 years. Neutrals or photons hitting the detector also increase the noise of the detection.

A further widely used multiplier is the photon multiplier. In this case the ions (positive or negative) elicit secondary ions formed by a conversion dynode, which are further accelerated towards a phosphorescent screen where they undergo conversion into photons detected by a photomultiplier (Fig. 1.34).

The advantage of the photomultiplier compared to the electron multiplier is the longer lifetime (several years). Channel electron multiplier and photomultiplier are mostly used in quadrupole instruments or ion traps.

Array detectors, such as the multichannel plate (MCP) detector are best suited for mass analyzers where ions are spatially dispersed like in time of flight instruments. Array detectors are detectors [78] which allow simultaneous multichannel detection. The advantages of such detectors are high sensitivity and the possibility to eliminate the accompanying noise. Array detectors are largely used with TOF mass analyzers. Generally, the array consists generally of  $10^6$  microscopic glass channels, ca. 5–50  $\mu\text{M}$  in diameter, bound together and electrically connected with each other. Each channel operates as a continuous dynode electron multiplier (Fig. 1.35).

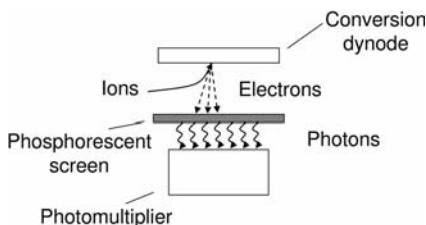


**Fig. 1.34** In the photon multiplier detector ions are transformed into photons which are detected by a photomultiplier.

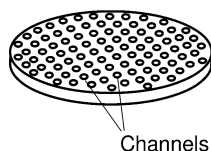


**Fig. 1.35** Multi-channel plate multiplier. Each hole corresponds to a single channel detector.

## 1.6

### Practical Aspects and Applications in Bioanalysis

#### 1.6.1

##### Introduction

Mass spectrometry plays currently a major role in the qualitative and quantitative analysis of low molecular weight compounds and macromolecules in life sciences. Quantitation of pharmaceutical compounds, their metabolites and endogenous metabolites in biological matrices, such as plasma and urine, is nowadays mostly done with liquid chromatography coupled with atmospheric pressure tandem mass spectrometry (LC-MS/MS) [79]. Gas chromatography coupled with electron impact ionization mass spectrometry (GC-MS) remains an important analytical tool in forensic sciences, doping control and toxicology. For this purpose quadrupole or ion trap mass analyzers are typically used. In contrast, triple quadrupole instruments have become more the working horse for quantitative pharmaceutical bioanalysis. While quantitative analysis is already well established, many of the new developments in the field of mass spectrometry will contribute to improve metabolites identification, metabolomics and proteomics analysis. Automated computerized data handling (bioinformatics) has become mandatory to cope with the large amount of data generated by the various systems. Mass spectrometers are, from a software point of view, becoming more user friendly while the expanding analysis capabilities of hybrid systems may require more fundamental user training. Due to the enhanced scan possibilities of MS, data dependent acquisition (DDA) has become state of the art for qualitative analysis. A DDA experiment includes a survey scan, a dependent scan and a selection criterion. Typically a survey scan is a full-scan MS and the dependent scan is a MS/MS scan. The selection criterion requires to record a MS/MS spectrum of the most abundant ion in the survey scan which is above a certain threshold and taking into account the inclusion of ions of interest and exclusion of background ions.

One critical feature of mass spectrometry when combined with chromatographic or electrophoretic separation techniques remains the duty cycle of the mass analyzer. A conventional LC chromatographic peak lasts about 10 s, which is sufficient to perform various MS and MS/MS experiments on various types of instruments. In the case of fast LC, the peak width can be in the range 1–2 s which is too fast for most mass analyzers except for TOF mass spectrometers.

## 1.6.2

**Quantitative Analysis in Biological Matrices**

Due to its high selectivity and sensitivity LC-MS with quadrupole mass analyzers has almost completely replaced traditional UV detection in many bioanalytical laboratories. ESI, APCI and APPI have become the ionization techniques of choice, covering a large variety of analytes. One limitation with API techniques is that the ionization response factor is compound-dependent and thus requires the use of an internal standard. Isotopically labeled ( $^2\text{H}$  or  $^{13}\text{C}$ ) internal standards have become very popular because they are capable of compensating for losses during sample preparation, HPLC and ion evaporation due to co-elution with the analyte. In the early days of LC-MS, analysis was mostly performed on QQQ instruments. Quantitative LC-MS analysis can also be performed on single quadrupole instruments, in particular when the  $M_r$  of the analyte is higher than 400 and when the limit of quantification is not below the  $\text{ng ml}^{-1}$  level. Figure 1.36 shows the total ion current (TIC) chromatogram of the LC-MS analysis of a cyclohexanediol derivative analyzed in human plasma after liquid–liquid extraction. It demonstrates clearly the selectivity of triple quadrupole compared to single quadrupole MS. Because this analyte does not have an appropriate chromophore, UV detection would not have been suitable. In contrast to GC, LC is not a high resolution separation technique and co-elution with endogenous compounds may require longer analysis time or improved sample preparation.

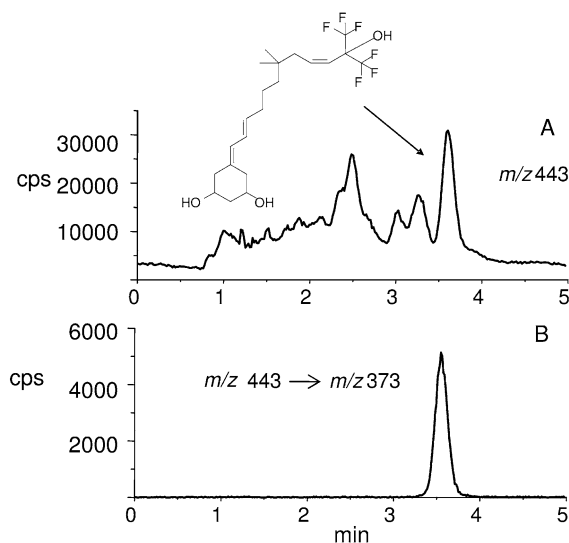


**Fig. 1.36** Comparison of the LC-MS and LC-MS/MS analysis of a cyclohexanediol derivative in human plasma. (A) Selected ion monitoring mode  $m/z$  443. (B) Selected reaction monitoring  $m/z$  443  $\rightarrow$   $m/z$  373. Ions were detected in the negative mode.

An important issue with quantitative LC-MS analysis concerns the matrix effects which need to be addressed during method development and validation. Matrix effects are caused by the co-elution of endogenous analytes which either enhance or suppress the analyte signal [80]. The major concern is that matrix effects are sample-dependent and may vary from one sample to another. It is also believed that ESI is more prone to matrix effects than APCI. Various approaches were devised and applied to investigate matrix effects. However, adequate sample preparation and selection of an appropriate internal standard generally provide the key to success. For multicomponent assays it is also important to use the internal standards most appropriate for the respective analyte. Offline and online solid phase extraction, column switching and automated liquid-liquid extractions are the most used sample preparation techniques. Online SPE combined with column switching are particularly attractive because they allow direct analysis of plasma in an automated and high throughput setup. With the high sensitivity of modern triple quadrupole instruments, protein precipitation of plasma in 96-well plate format followed by dilution and direct injection of the eluent has also become a viable approach. Shortterm matrix effects due to different samples may be relatively simple to monitor while longterm matrix effects are very difficult to monitor. Table 1.5 shows the calibration and quality control (QC) results obtained in human plasma of a cyclohexanediol derivative analyzed by LC-MS/MS. At a first glance the calibration seems to be very good. However, when the 10 ng mL<sup>-1</sup> calibration sample is reanalyzed ( $n = 35$ ) and declared as a quality control sample the accuracy becomes disastrous.

The explanation of this result is illustrated in Fig. 1.37, which shows selected reaction-monitoring traces of the sample at 10 ng mL<sup>-1</sup>. It becomes obvious that the response ratio between the analyte and the IS has dramatically changed. On one side there is enhancement of the analyte's response and on the other side suppression of the internal standard (IS) signal. These effects are mainly caused

**Table 1.5** Calibration and QC data for a cyclohexanediol derivative in human plasma.

Sample	n	spiked ng/ml	found ng/ml	Accuracy %
00 Plasma	5	0	0	—
C01	6	1	0.994	99.4
C02	7	2	1.991	99.6
C03	8	4	4.124	103.1
<b>C04</b>	<b>9</b>	<b>10</b>	<b>10.19</b>	<b>101.9</b>
C05	10	20	19.93	99.7
C06	11	50	46.44	92.9
C07	12	100	102.1	102.1
C08	13	200	203	101.5
<b>QC04</b>	<b>35</b>	<b>10</b>	<b>5.925</b>	<b>59.3</b>

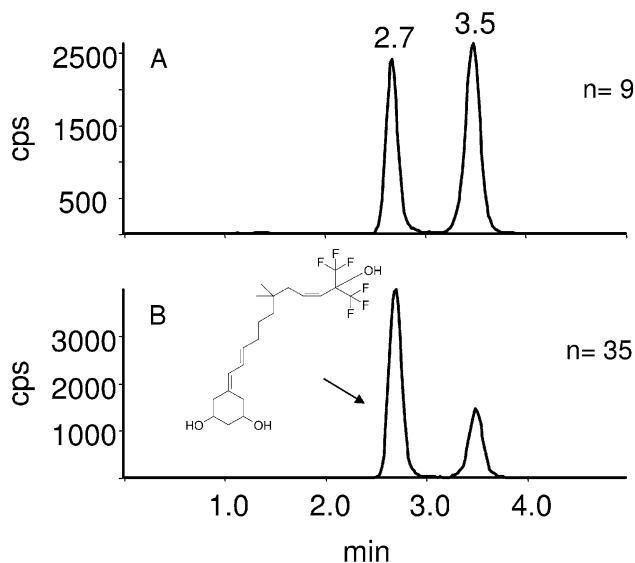


**Fig. 1.37** Selected reaction monitoring mode LC-MS/MS analysis of the same human plasma sample standard at  $10 \text{ ng mL}^{-1}$  placed at different positions in the analytical sequence: (A) at position 9, (B) at position 35. The peak at  $\text{RT} = 2.7 \text{ min}$  corresponds to the analyte and the peak at  $\text{RT} = 3.5 \text{ min}$  to the internal standard. Detection was performed in the negative mode.

by the accumulation of endogenous compounds on the HPLC column after each run, and therefore an increasing bleed of these endogenous sample components to the effluent of the column directed to the API interface. In this case the gradient elution was obviously not effective enough to remove efficiently endogenous compounds after each analysis. The IS, a structural analogue, was not capable of compensating the matrix effect. The solution to the problem was to replace the IS by an isotopically labeled structural analogue which co-eluted with the analyte. This example exemplifies how critical appropriate method development and validation is before running real study samples.

LC-MS/MS has dramatically changed the way bioanalysis is conducted. Accurate and precise quantitation in the  $\text{pg mL}^{-1}$  scale is nowadays possible; however one has to be aware of certain issues which are specific to mass spectrometric detection such as matrix effects and metabolite crosstalk. With the current growing interest in the analysis of endogenous biomarkers in biological matrices, quantitative bioanalysis with MS has certainly the potential to contribute further in this field with the development of multicomponent assays. Modern triple quadrupole instruments have the feature to use very short dwell times (5–10 ms), allowing the simultaneous determination of more than 100 analytes within the timescale of an HPLC peak. Due to the selectivity of the MS detection the various analytes

do not need to be chromatographically baseline resolved. This is only true for analytes with different precursor and product ions.

### 1.6.3

#### Drug Metabolism

During drug discovery and drug development, it is important to establish how the body metabolizes a drug; therefore rapid identification of metabolites from *in vitro* or *in vivo* samples becomes essential [81]. The classic way to perform metabolic studies is to use  $^{14}\text{C}$  or  $^3\text{H}$  radiolabeled drugs. Liquid chromatography with online radioactivity detection is applied to collect the metabolites, which after further purification are identified by mass spectrometry and nuclear magnetic resonance spectroscopy (Fig. 1.38). One of the advantages of the radiolabeled parent drug is that the response of the radioactivity detector is directly proportional to the amount of metabolite. Also due to the high specificity of the radioactivity detector urine or plasma can be directly injected onto the LC system.

Metabolic stability of drugs has become an important parameter in drug discovery and hundreds of samples can be rapidly generated using *in vitro* systems such as hepatocytes and microsomes. For structural elucidation, nuclear magnetic resonance spectroscopy is the technique of choice, but it does not allow high throughput analysis and sensitivity is still in the microgram range. LC-MS has therefore become the technique of choice. Ideally one would require a mass spectrometer with fast acquisition capabilities in positive and negative mode, selective scan modes, multiple stage MS and accurate mass measurements. Such an ideal instrument is currently not available and therefore drug metabolism studies require multi-instrument strategies.

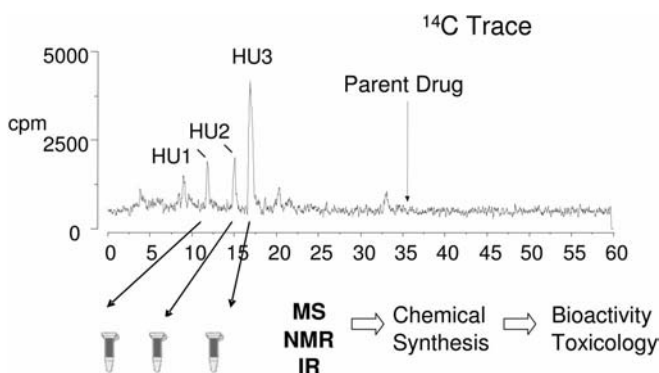


**Fig. 1.38** LC separation with radioactivity detection of an urine sample. The response of the various peaks is directly proportional to the amount of metabolites present in the sample. Peaks HU1–HU3: human urine metabolites.

When working with non-radiolabeled drugs the major challenge is to find metabolites in the biological matrices. Because the enzymes responsible for metabolism are quite well characterized metabolic changes can partially be predicted. For example hydroxylation of the parent drug is in many cases the principal metabolic pathway. From a mass spectrometric point of view it results in an increase of 16 units in the mass spectrum. In the full-scan mode an extracted ion current profile can be used to screen for potential metabolites. In a second step a product ion spectrum is recorded for structural interpretation. Ideally, one would like to obtain relative molecular mass information and the corresponding product ion spectrum in the same LC-MS run. This information can be obtained by data dependant acquisition (DDA), as illustrated in Fig. 1.39.

In this case the survey scan was set as a full scan and the dependent scan as a product ion scan. The problem with data dependent acquisition is to determine the selection criteria. In most cases the system picks up the most abundant ion in the full scan spectrum. An inclusion list with masses of potential metabolites or exclusion list of known interferences significantly improves the procedure. In the example shown in Fig. 1.39, a procedure called dynamic background subtraction (DBS) was applied. This procedure considers chromatographic peak shapes and monitors not the most abundant signal in the spectrum but the largest increase of an ion in a spectrum. The advantage is that once a signal of a peak has

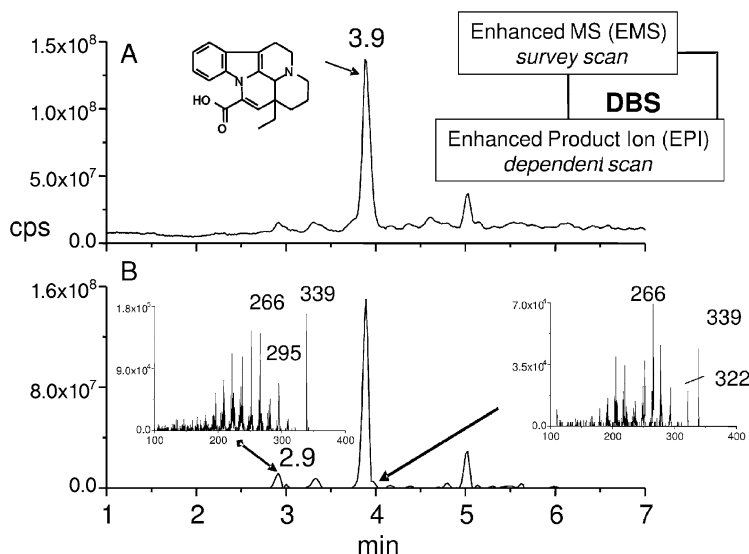


**Fig. 1.39** LC-MS data dependent analysis of vinpocetin in rat urine using dynamic background subtraction (DBS) on a triple quadrupole linear ion trap. (A) Full scan MS (survey scan) trace. (B) Enhanced product ion scan (dependent scan). The major peak at 3.9 min corresponds to apovinpocetin, the minor one at 2.9 min to the hydroxylation product of apovinpocetin ( $m/z$  339).

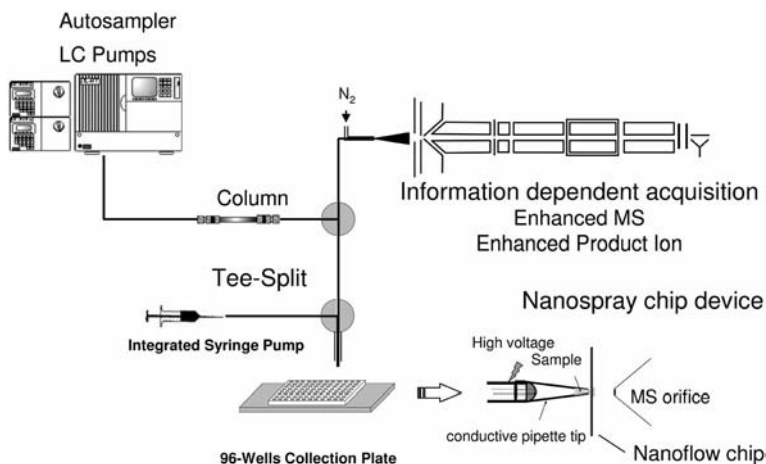


**Fig. 1.40** Schematic of online LC-MS analysis combined with fraction collection into 96-well plate. Depending on the online MS data, further MS experiments are performed with chip-based infusion at  $200 \text{ nL min}^{-1}$ .

reached its maximum it switches automatically to the next mass. This is particularly important with co-eluting peaks of different intensities, as illustrated in Fig. 1.39B. It is then possible to obtain a good product ion spectrum of the small peak eluting at 4.0 min ( $m/z$  339). In drug metabolism not only is the sensitivity of the mass spectrometer important but the selectivity is also crucial, particularly when working with plasma samples.

Most methods of metabolite identification are done with online LC-MS. As mentioned earlier there is no ideal mass spectrometer for this type of work and the sample has to be reanalyzed several times on different types of mass spectrometer. The consequence is that metabolic investigation is often time-consuming. A concept has been described by Staack et al. [82] (Fig. 1.40) where, during the LC-MS run, fractions are collected onto a 96-well plate.

Either the information obtained during the data-dependent acquisition is sufficient or a fraction of interest can be re-analyzed by chip-based infusion at a flow rate ca.  $200 \text{ nl min}^{-1}$ . Due to the miniaturization sample consumption is very low (typically  $1\text{--}3 \text{ }\mu\text{L}$ ) and acquisition time is no longer critical. Therefore various MS experiments can be performed on various instruments, including  $\text{MS}^n$  and accurate mass measurements. An additional advantage is that the eluent can be removed and the infusion solvent can be optimized for positive or negative ion detection or for deuterium exchange measurements.

Advances in high resolution mass analyzers (TOF, FT-ICR, orbitrap) have greatly improved the detection and identification of metabolites based on accurate mass measurements. In single MS mode accurate mass determination is mainly used to differentiate between isobaric ions. Combined with LC-MS, it allows the detection of predicted metabolites by performing extracted ion current profiles



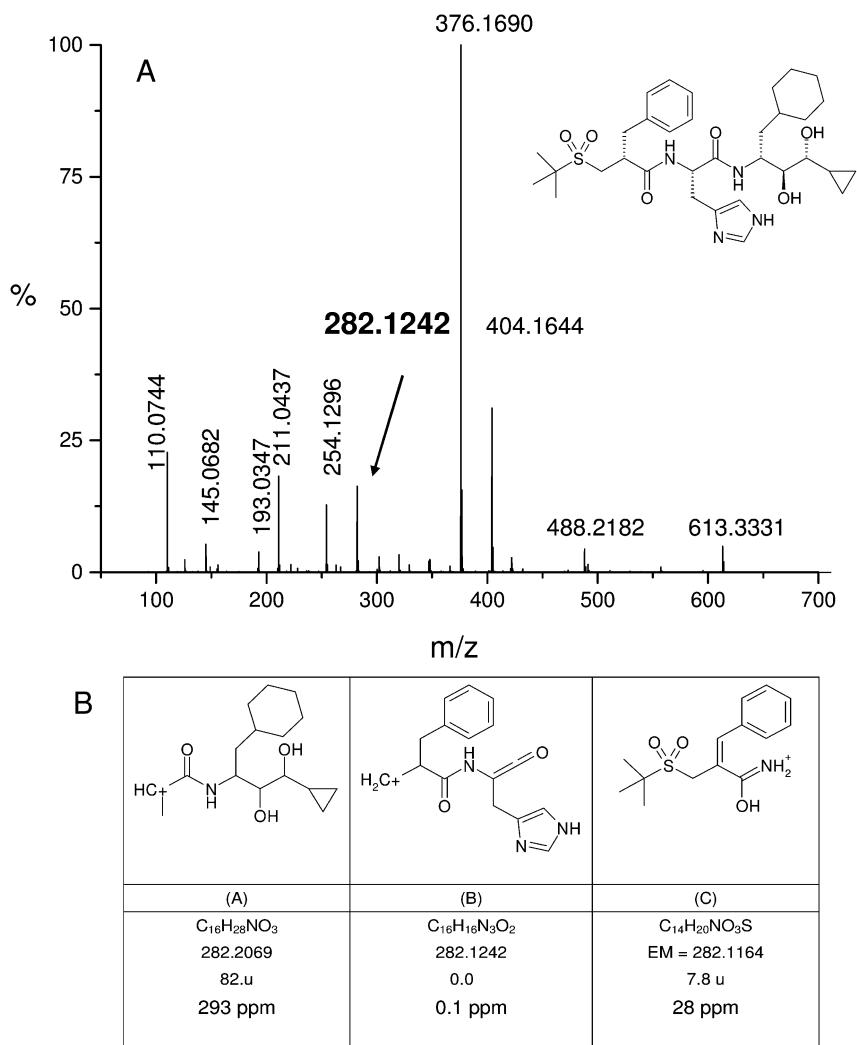


**Fig. 1.41** (A) Product ion spectrum of remikiren obtained on a QqTOF. (B) Software-predicted fragments (Mass Frontier, HighChem) for the ion at  $m/z$  282.

with much smaller mass windows than for unit mass resolution mass analyzers eliminating therefore background interferences. In MS/MS mode on hybrid systems (LIT-orbitrap, QqTOF, IT-TOF, FT-ICR) high resolution improves the interpretation of product ion spectra. As an example, in the product ion spectrum recorded at unit mass resolution spectra of bosentan and its phenol metabolites display an ion at  $m/z$  280. When performing the accurate mass measurements of this ion on a QqTOF it was found that bosentan generates an ion at  $m/z$

280.0835 and its phenol metabolite at  $m/z$  280.0628 [68]. It was shown that both ions were formed through a different cyclisation mechanism involving either the phenol or the amine substituent. The mass difference of 20.7 milliunits corresponds to the mass difference between  $\text{NH}_2$  and O.

The understanding of the fragmentation mechanism of the parent drug is very important for the metabolite assignment. The product ion spectrum of remikiren is illustrated in Fig. 1.41. Conventional spectra interpretation is time-consuming and the use of predictive fragmentation software such as Mass Frontier (High-Chem) can help to rationalize spectra interpretation [83]. In the case of the fragment at  $m/z$  282, three different fragments are proposed by the software. Only accurate mass measurement with an accuracy better than 10 ppm allowed selection of the right fragment (Fig. 1.41B, middle structure).

A similar approach using accurate mass measurements and predictive fragmentation software was also applied for the examination of the human microsomal metabolism of nefazodone using a linear ion trap–orbitrap hybrid mass spectrometer. Based on a single LC-MS run, using data-dependant acquisition, 15 metabolites of nefazodone could be identified in MS and MS/MS with a mass accuracy better than 3 ppm.

Zhang et al. [84] reported a strategy using a software mass defect filter to improve the detection of expected and unexpected metabolites in accurate mass LC-MS. Metabolic structural changes in the parent drug have an effect on the mass defect of the metabolites compared to the parent drug. As an example hydroxylation changes the mass defect by  $-5$  milliunits, demethylation by  $-23$  milliunits and glucuronation by  $+32$  milliunits. In fact most phase I and phase II metabolites have a mass defect window within 50 milliunits. It is therefore possible to apply a software filter which includes ions within a mass defect window relatively close to the parent drug and exclude ions, generally matrix interferences, which are outside the specified window. The application of the mass defect filter to a plasma sample spiked with omeprazole metabolites is illustrated in Fig. 1.42 [85].

For spectra interpretation and metabolite characterization accurate mass measurements become a must while it remains complementary to  $\text{MS}^n$ , precursor and neutral loss for identifying metabolites in complex biological matrices.

#### 1.6.4

#### Analysis of Proteins

The analysis for proteins present in plasma or a cell extract is a challenging task due to their complexity and the great difference between protein concentrations present in the sample. Simple mixtures of intact proteins can be analyzed by infusion with electrospray ionization and more complex ones by matrix assisted laser desorption ionization. MALDI is more suited for complex mixtures because for each protein an  $[\text{M}+\text{H}]^+$  signal is observed while for ESI multiply charged ions are observed. Surface enhanced laser desorption (SELDI) is a technique for the screening of protein biomarkers based on the mass spectrometric analysis of intact proteins [49]. However in most cases for sensitivity reasons mass spec-

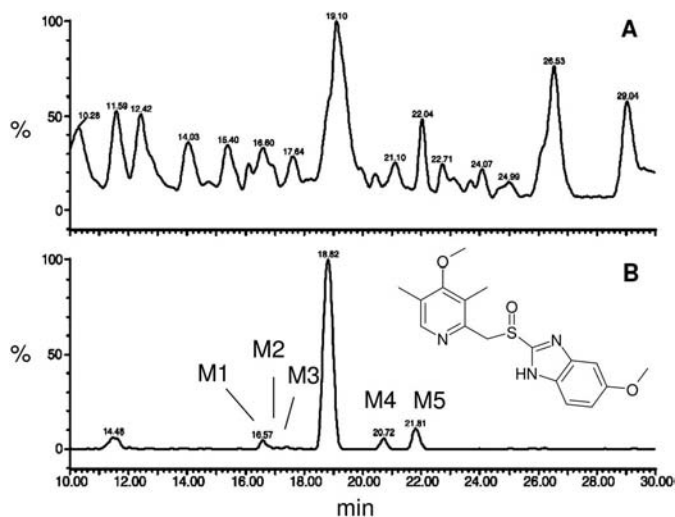


**Fig. 1.42** LC-MS profile of omeprazole metabolites spiked in plasma: (A) without mass defect filter, (B) with mass defect filter. Peaks: M1 mono-oxidation metabolite [+16 u, Mass defect (MD) +5 milliunits], M2 reduction and demethylation (−30 u, MD +10 milliunits), M3 mono-oxidation metabolite (+16 u, MD −5 milliunits), M4 reduction (−16 u, +5 milliunits), M5 mono-oxidation metabolite (+16 u, +5 milliunits). Adapted with permission from reference [85].

trometric analysis is performed at the peptide level after enzymatic digestion. Basically there are two approaches for the identification of complex mixtures of proteins (Fig. 1.43). The first is based on two-dimensional electrophoretic separation of intact proteins followed by trypsin digestion and matrix assisted laser desorption–time of flight (MALDI-TOF) detection. The second approach digests first the protein mixture and the resulting peptides are then separated by a two-dimensional chromatographic procedure using nanoliquid chromatography coupled to nanoelectrospray ionization.

Two-dimensional electrophoresis [86] is a well established technique for the separation of intact proteins. In the first dimension the proteins are separated based on their isoelectric point while the second dimension separates them based on their size. The presence on the gel of the proteins is revealed by Coomassie blue or silver staining. Under favorable conditions several thousand spots can be differentiated. The gel is digitized and computer-assisted analysis of the protein spot is performed. The spots of interest are excised either manually or automatically and then digested with trypsin. Trypsin cleaves proteins at the C-terminal side of lysine and arginine. In general one spot represents one protein and the peptides are analyzed by MALDI-TOF to obtain a peptide mass fingerprint. A peptide mass fingerprint involves the determination of the masses of all pep-

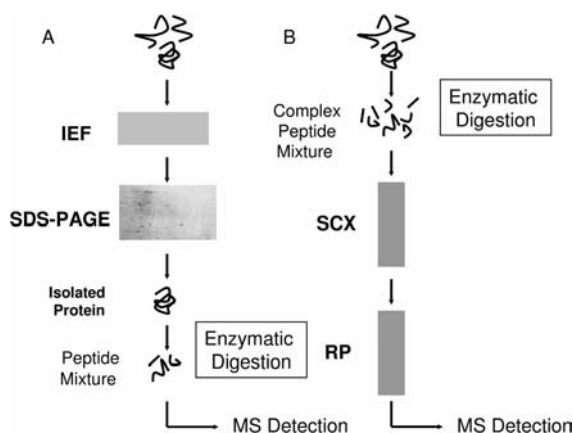


**Fig. 1.43** Strategies for protein identification. (A) 2D gel electrophoresis approach. (B) 2D liquid chromatography approach. *IEF* Isoelectric focusing, *SCX* strong cation exchange column, *RP* reverse phase column, *SDS-PAGE* sodium dodecyl sulfate polyacrylamide gel electrophoresis.

tides present in the digest. The list of peptides is then submitted to a database search to identify the protein. This approach does not work if several proteins are present in the same spot or if the sample is contaminated for example with keratin. The identification of the protein can be improved by sequencing selected peptides either by post source decay (PSD-MALDI) or tandem mass spectrometry (MALDI-TOF/TOF).

High-performance liquid chromatography (HPLC) represents an attractive alternative to two-dimensional electrophoresis for the separation of both proteins and peptides because of its chromatographic resolving power, reproducibility and its compatibility with MS detection. The use of multidimensional chromatography for the separation of complex protein and peptide mixtures has consequently seen increased use in proteomics studies [87, 88]. A typical approach involves the digestion with trypsin of an extract. Furthermore the preparation and handling of peptides is less tedious than with intact proteins and the whole process can be easily automated. A typical two-dimensional LC experiment (2D-LC) involves the initial separation (first dimension) of the resulting peptide mixture by their electrostatic charge using strong cation exchange (SCX) chromatography. In the second dimension peptides are then separated by their hydrophobicity using reversed phase (RP) chromatography coupled directly to ESI-MS. In a typical analysis of a complex protein mixture from a single sample the procedure is repeated about ten times with increasing salt concentration, resulting in a total analysis time of about 12 h.

As electrospray ionization is concentration-sensitive the last LC dimension uses a nano LC column with an internal diameter of 75  $\mu\text{m}$  to achieve maximum sen-

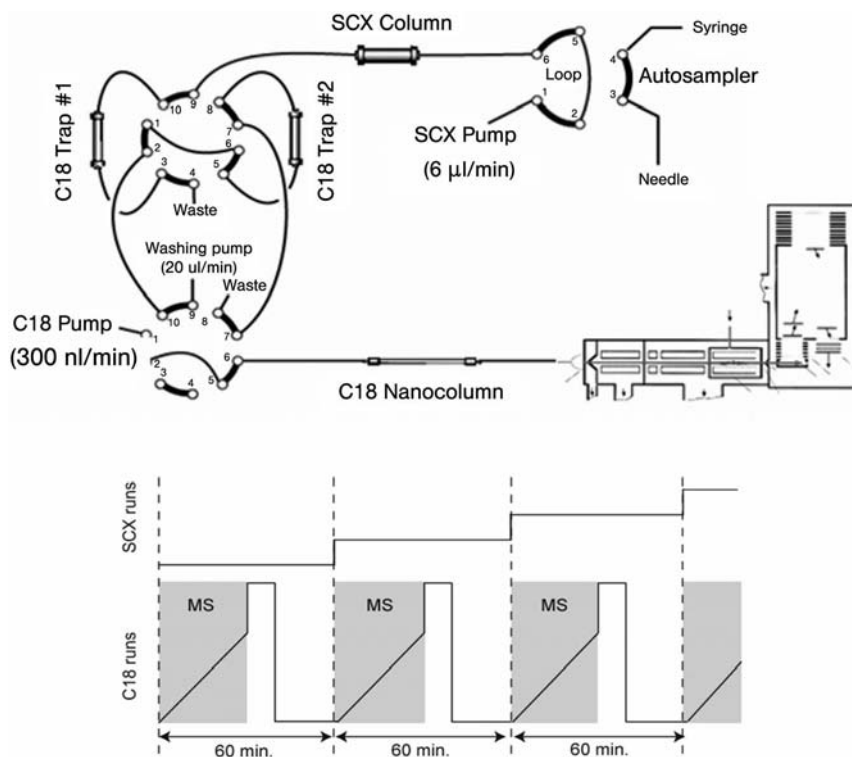


**Fig. 1.44** 2D-LC setup. The first ion exchange dimension is performed with a column with an i.d. of 1 mm, at a flow rate of  $50 \mu\text{L min}^{-1}$  while the second dimension uses a nanocolumn with an i.d. of 0.75 mm and a flow rate of  $300 \text{ nL min}^{-1}$ . First dimension ion exchange has ten salt steps: 0, 5, 10, 15, 20, 25, 50, 75, 100, 200 mM KCl. Second dimension is typically an organic gradient: 5% to 80% acetonitrile with 0.1% formic acid in 30 min.

sitivity while larger diameters are preferred for the first ion exchange dimension to be able to inject large sample amounts and volumes. A 2D-LC system is depicted in Fig. 1.44. Ion exchange elution can be performed with ammonium acetate buffers which are MS-compatible. More efficient is potassium chloride elution, but the drawback is that it affects the detection of peptides. Therefore it is necessary to implement trapping columns for desalting the fraction before transferring it in the second reversed phase LC dimension. At the end of the analysis all the data are processed together to generate a list of several hundred proteins. For this task efficient bioinformatics tools are essential.

Figure 1.45 illustrates a typical 2D nano LC-MS/MS analysis of a *Caenorhabditis elegans* extract. For each timepoint a single MS and a product ion spectrum are

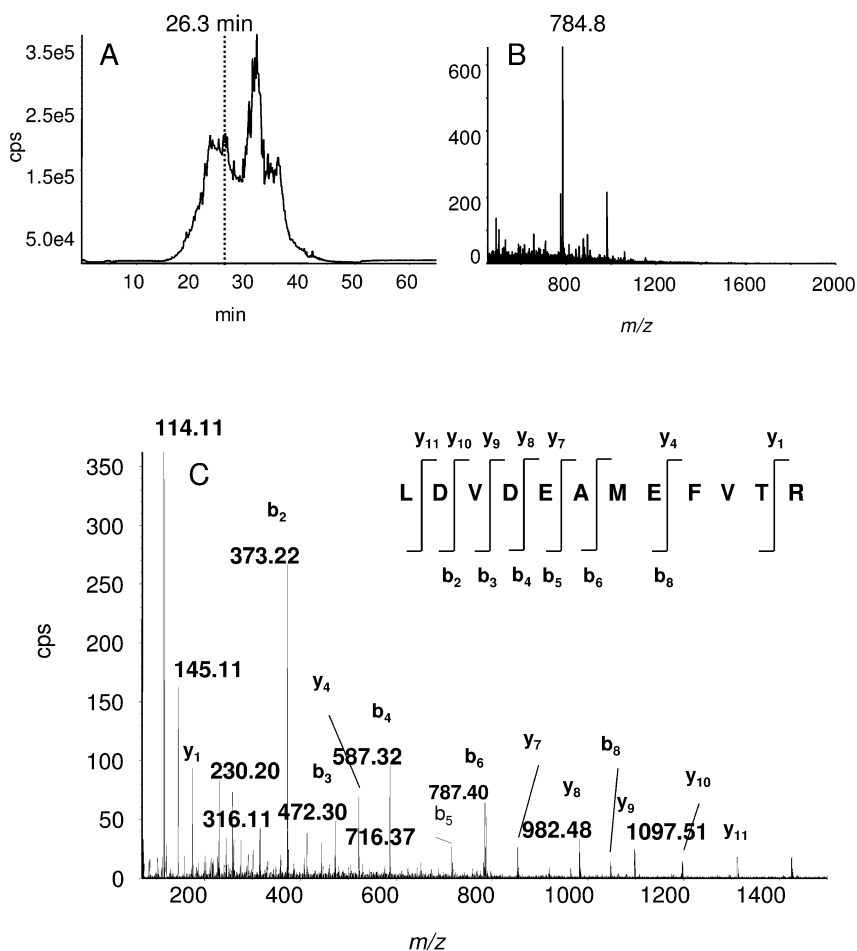


**Fig. 1.45** Example of a 2D nano LC-MS/MS analysis of a *C. elegans* extract. (A) Fraction 2, 4 mM KCl salt elution on the strong cation exchange column. (B) Full scan MS spectrum of the peak eluting at RT 26.3 min in (A). (C) product ion spectrum of the doubly charged precursor of (B) at  $m/z$  784.8. Y fragments are typical for C-terminal fragments while b ions are typical for N-terminal fragments.

recorded (Fig. 1.45B, C). With the help of bioinformatic tools the product ion spectrum can be automatically interpreted. The  $\gamma$  fragments are typical for C terminal fragments, while the  $b$  ions are typical for N-terminal fragments.

Two-dimensional-liquid chromatography (2D-LC) approaches are much easier to automate than 2D-electrophoresis. However 2D electrophoresis has the advantage that separation is performed at the protein and not at the peptide level and

that the proteins can be visualized by staining. With 2D-LC one has to wait for bioinformatics treatment to see if the experiment was successful.

## 1.7

### Perspectives

Mass spectrometry originated from quantitative measurements of the mass and charge of electrons [1]. Since that time the application of mass spectrometry has moved from the analysis of inorganic elements to organic molecules and finally to macromolecules. Over the past decade spectacular improvements were made in instrumental development regarding performance and new mode of operations in particular with hybrid instruments. Orbitrap, Fourier transform or triple quadrupole linear ion trap mass spectrometers could be used routinely only for the past few years and their potential is certainly not fully exploited yet. The strength of mass spectrometry lies in its sensitivity (femtomoles, attomoles); and in many applications the analyte of interest can be detected in its intact form. The challenge in life sciences bioanalysis is the diversity and the number of the molecules to analyze as well as the concentration range.

Analysis of pharmaceutical compounds in biological matrices with liquid chromatography coupled to mass spectrometry (LC-MS) has become a routine technique in many laboratories. However, certain issues such as non-standardized ionization response and matrix effects still need further investigation and improvement. The application of LC-MS for metabolomics studies [89] is gaining interest. Therefore, it is expected that accurate and high throughput quantitation of low molecular weight biomarkers will be one of the major challenges in the near future. Identification and quantification of proteins has progressed significantly; however in many cases the numbers of proteins which can be analyzed still remains limited. Electrospray ionization has been shown to be very powerful for single protein analysis but the technique is also well suited for the characterization of very large non-covalent complexes of proteins, which may lead to an increasing understanding of protein assemblies [90].

Single nucleotide polymorphism (SNP) genotyping has become a key technology in gaining a partial understanding of complex diseases or why patients react differently to drug treatment. Matrix assisted laser desorption especially with high speed laser allows real high throughput and is well suited for the analysis of oligonucleotides. MALDI is therefore an interesting approach for SNP discovery and genotyping, molecular haplotyping, methylation analysis, and RNA and allele-specific expression but needs further optimization before routine application [42, 91].

Significant progress has been realized in the miniaturization of separation sciences and mass spectrometric detection. Presently, the samples are transferred to highly specialized laboratories for analysis. But in the future it may become feasible to bring mass spectrometry as a portable technique to the bed for diagnostic or therapeutic monitoring.

**Table 1.6** Common definitions and abbreviations.

General	
$m/z$	Symbol used to denote the dimensionless quantity formed by dividing the mass of an ion in unified atomic mass units by its charge number (regardless of sign). $m/z$ should be written in italic and lower case. The Thomson (Th) is sometimes used as unit but it is not recommended.
$M^{+}$	Molecular ion, the ion results from the loss of one electron from the neutral molecule
$(M+H)^{+}$	Protonated molecule formed by the addition of a proton to a neutral molecule (the terms pseudo-molecular ion or quasi-molecular ion should not be used)
u	Symbol for atomic mass unit
Accurate mass	Experimentally determined mass of an ion that is used to determine an elemental formula. The precision of the measure is indicated in parts per millions (ppm).
Atomic mass	The average of the atomic masses of all the chemical element's isotopes (also known as atomic weight and average atomic mass)
Average mass	Mass of an ion or molecule calculated using the average mass of each element weighted for its natural isotopic abundance
Exact mass	Calculated mass of an ion or molecule containing a single isotope of each atom, most frequently the lightest isotope of each element, calculated from the masses of these isotopes using an appropriate degree of accuracy
Mass defect	The difference between the exact mass of an atom molecule, ion and its integer mass in MS. In physics, the mass defect represents the difference between the mass of an atom and the sum of the masses of its unbound constituents.
Mass defect filter (MDF)	A software filter which allows the removal of interference ions from drug metabolites in accurate mass liquid chromatography–mass spectrometry
Mass range	Operating $m/z$ range of a mass analyzer
Monoisotopic mass	Exact mass of an ion or molecule calculated using the mass of the most abundant isotope of each element
$M_r$	Relative molecular mass: mass of one molecule of a compound, with specified isotopic composition, relative to one-twelfth of the mass of one atom of $^{12}\text{C}$



Table 1.6 (continued)

Nominal mass	Mass of an ion or molecule calculated using the mass of the most abundant isotope of each element rounded to the nearest integer value and equivalent to the sum of the mass numbers of all constituent atoms
Ion	An atomic or molecular species having a net positive or negative electric charge
Metastable ion	An ion formed with an internal energy higher than the dissociation threshold but with a sufficient lifetime that it can exit the source and enter the mass spectrometer where it dissociates
Isotope	One of several forms of an element having the same atomic number but differing atomic masses
Base peak (BP)	The most intense peak in the spectrum
Total ion current (TIC)	The sum of all the separate ion currents contributing to the spectrum
Extracted ion current (XIC)	The current of a specified $m/z$ ion current
Mass resolving power	In a mass spectrum, the observed mass divided by the difference between two masses that can be separated: $m/\Delta m$ . The procedure by which $\Delta m$ was obtained and the mass at which the measurement was made should be reported.
Unit mass resolution	Means that a mass spectrometer is able to differentiate two peaks (generally the isotopes) distant of 1 $m/z$ unit
Mass resolution	Smallest mass difference ( $\Delta m$ ) between two equal magnitude peaks so that the valley between them is a specified fraction of the peak height
Ionization	
Even-electron ion	An ion containing no unpaired electrons in its ground electronic state
Odd-electron ion	An ion containing unpaired electrons in its ground state
EI	Electron impact ionization
PCI	Positive chemical ionization
NCI	Negative chemical ionization
API	Atmospheric pressure ionization: generic term for ionization techniques occurring at atmospheric pressure
ESI	Electrospray ionization: most commercial systems operate with pneumatically assisted electrospray (originally defined as ion spray)

Table 1.6 (continued)

Nano-ESI	Nanoelectrospray ionization: flow rates range from a few nanoliters per minutes to a few hundred nanoliters per minutes; nanoelectrospray is performed with pulled capillaries or on chips which serve as emitter
APCI	Atmospheric pressure chemical ionization
APPI	Atmospheric pressure photoionization
MALDI	Matrix assisted laser desorption ionization
Mass analyzer	
QqQ	Triple quadrupole: Q1 and Q3 are the mass resolving quadrupoles, q2 is the collision cell
QIT	Quadrupole ion trap: refers in general to a 3D ion trap instrument
LIT	Linear ion trap: refers in general to 2D ion trap; ion ejection is either axial or radial
QqQ <sub>LIT</sub>	Triple quadrupole linear ion trap instrument. In this instrument the quadrupole Q3 is operated either in RF/DC mode or in RF mode
QqTOF	Quadrupole–time of flight instrument
TOF-TOF	Tandem time of flight instrument
FT-ICR	Fourier transform ion cyclotron resonance instrument
MS <sup>n</sup>	Multistage mass spectrometry: applies generally for ion trap mass spectrometers
CID	Collision induced dissociation: the dissociation of ions after collisional excitation
PSD	A technique specific to reflectron time-of-flight mass spectrometers where product ions of metastable transitions or collision-induced dissociations generated in the drift tube prior to entering the reflectron are $m/z$ separated to yield product ion spectra
NL	Neutral loss spectrum
PIS	Product ion spectrum
PC	Precursor ion spectrum
SRM	Selected reaction monitoring mode

## 1.8

## Common Definitions and Abbreviations

The intention of this section is to provide to the reader a rapid and comprehensive reference for the most common definitions and acronyms used in mass spectrometry. Currently IUPAC has initiated a project to update and extend the definitions of terms related to the field of mass spectrometry. The definitions presented here (Table 1.6) are from the third draft document [16]. For more details and the latest updates, please consult [www.msterms.com](http://www.msterms.com).

## References

- Thomson, J. J.: Rays of positive electricity. *Proc. R. Soc.* **1913**, 89, 1–20.
- Budzikiewicz, H.; Grigsby, R. D.: Mass spectrometry and isotopes: a century of research and discussion. *Mass Spectrom. Rev.* **2006**, 25, 146–157.
- Dempster, A. J.: A new method of positive ray analysis. *Phys. Rev.* **1918**, 11, 316–324.
- Gohlke, R. S.: Time-of-flight mass spectrometry and gas–liquid partition chromatography. *Anal. Chem.* **1959**, 31, 535–541.
- Arpino, P.; Baldwin, M. A.; McLafferty, F. W.: Liquid chromatography–mass spectrometry. II. Continuous monitoring. *Biomed. Mass Spectrom.* **1974**, 1, 80–82.
- Ito, Y.; Takeuchi, T.; Ishii, D.; Goto, M.: Direct coupling of micro high-performance liquid chromatography with fast atom bombardment mass spectrometry. *J. Chromatogr.* **1985**, 346, 161–166.
- Caprioli, R. M.; Fan, T.; Cottrell, J. S.: A continuous-flow sample probe for fast atom bombardment mass spectrometry. *Anal. Chem.* **1986**, 58, 2949–2954.
- Blakley, C. R.; Vestal, M. L.: Thermospray interface for liquid chromatography/mass spectrometry. *Anal. Chem.* **1983**, 55, 750–754.
- Willoughby, R. C.; Browner, R. F.: Monodisperse aerosol generation interface for combining liquid chromatography with mass spectroscopy. *Anal. Chem.* **1984**, 56, 2626–2631.
- Finnigan, R. E.: Quadrupole mass spectrometers. *Anal. Chem.* **1994**, 66, 969A–975A.
- Paul, W.: *Electromagnetic Traps for Charged and Neutral Particles*, Nobel Lecture, 8 December, **1989**.
- Yost, R. A.; Enke, C. G.: Selected ion fragmentation with a tandem quadrupole mass spectrometer. *J. Am. Chem. Soc.* **1978**, 100, 2274–2275.
- Karas, M.; Hillenkamp, F.: Laser desorption ionization of proteins with molecular masses exceeding 10,000 daltons. *Anal. Chem.* **1988**, 60, 2299–2301.
- Fenn, J. B.; Mann, M.; Meng, C. K.; Wong, S. F.; Whitehouse, C. M.: Electrospray ionization for mass spectrometry of large biomolecules. *Science* **1989**, 246, 64–71.
- Sparkeman, D. O.: *MassSpec Desk Reference*, 1st edn, Global View Publishing, Pittsburgh, **2000**.
- Murray, K. K.; Boyd, R. K.; Eberlin, M. N.; Langley, G. J.; Li, L.; Naito, Y.: Standard definitions of terms relating to mass spectrometry, **2006**, available at: [www.msterms.com](http://www.msterms.com).
- Bristow, A. W. T.: Accurate mass measurement for the determination of elemental formula – a tutorial. *Mass Spectrom. Rev.* **2006**, 25, 99–111.
- Ausloos, P.; Clifton, C. L.; Lias, S. G.; Mikaya, A. I.; Stein, S. E.;

- Tchekhovskoi, D. V.; Sparkman, O. D.; Zaikin, V.; Zhu, D.: The critical evaluation of a comprehensive mass spectral library. *J. Am. Soc. Mass Spectrom.* **1999**, 10, 287–299.
- 19 Munson, B.: Development of chemical ionization mass spectrometry. *Int. J. Mass Spectrom.* **2000**, 200, 243–251.
- 20 Maurer, H. H.: Role of gas chromatography–mass spectrometry with negative ion chemical ionization in clinical and forensic toxicology, doping control, and biomonitoring. *Ther. Drug Monit.* **2002**, 24, 247–254.
- 21 Doroshenko, V. M.; Laiko, V. V.; Taranenko, N. I.; Berkout, V. D.; Lee, H. S.: Recent developments in atmospheric pressure MALDI mass spectrometry. *Int. J. Mass Spectrom.* **2002**, 221, 39–58.
- 22 Takats, Z.; Wiseman, J. M.; Gologan, B.; Cooks, R. G.: Mass spectrometry sampling under ambient conditions with desorption electrospray ionization. *Science* **2004**, 306, 471–473.
- 23 Cody, R. B.; Laramée, J. A.; Durst, H. D.: Versatile new ion source for the analysis of materials in open air under ambient conditions. *Anal. Chem.* **2005**, 77, 2297–2302.
- 24 Caldecourt, V. J.; Zakett, D.; Tou, J. C.: An atmospheric-pressure ionization mass spectrometer/mass spectrometer. *Int. J. Mass Spectrom. Ion Phys.* **1983**, 49, 233–251.
- 25 Bruins, A. P.; Covey, T. R.; Henion, J. D.: Ion spray interface for combined liquid chromatography/atmospheric pressure ionization mass spectrometry. *Anal. Chem.* **1987**, 59, 2642–2646.
- 26 Wilm, M.; Mann, M.: Analytical properties of the nano-electrospray ion source. *Anal. Chem.* **1996**, 68, 1–8.
- 27 Zhang, S.; Van Pelt, C. K.: Chip-based nano-electrospray mass spectrometry for protein characterization. *Exp. Rev. Proteom.* **2004**, 1, 449–468.
- 28 Kebarle, P.: A brief overview of the present status of the mechanisms involved in electrospray mass spectrometry. *J. Mass Spectrom.* **2000**, 35, 804–817.
- 29 Hopfgartner, G.; Bean, K.; Henion, J.; Henry, R.: Ion spray mass spectrometric detection for liquid chromatography: a concentration- or a mass-flow-sensitive device? *J. Chromatogr.* **1993**, 647, 51–61.
- 30 Zell, M.; Husser, C.; Hopfgartner, G.: Low picogram determination of Ro 48-6791 and its major metabolite, Ro 48-6792, in plasma with column-switching microbore high-performance liquid chromatography coupled to ion spray tandem mass spectrometry. *Rapid Commun. Mass Spectrom.* **1997**, 11, 1107–1114.
- 31 Carroll, D. I.; Dzidic, I.; Stillwell, R. N.; Haeghele, K. D.; Horning, E. C.: Atmospheric pressure ionization mass spectrometry. Corona discharge ion source for use in a liquid chromatograph-mass spectrometer-computer analytical system. *Anal. Chem.* **1975**, 47, 2369–2372.
- 32 Robb, D. B.; Covey, T. R.; Bruins, A. P.: Atmospheric pressure photoionization: an ionization method for liquid chromatography-mass spectrometry. *Anal. Chem.* **2000**, 72, 3653–3659.
- 33 Raffaelli, A.; Saba, A.: Atmospheric pressure photoionization mass spectrometry. *Mass Spectrom. Rev.* **2003**, 22, 318–331.
- 34 Bos, S. J.; Leeuwen, S. M.; Karst, U.: From fundamentals to applications: recent developments in atmospheric pressure photoionization mass spectrometry. *Anal. Bioanal. Chem.* **2006**, 384, 85–99.
- 35 Gallagher, R. T.; Balogh, M. P.; Davey, P.; Jackson, M. R.; Sinclair, I.; Southern, L. J.: Combined electrospray ionization–atmospheric pressure chemical ionization source for use in high-throughput LC-MS applications. *Anal. Chem.* **2003**, 75, 973–977.
- 36 Syage, J. A.; Hanold, K. A.; Lynn, T. C.; Horner, J. A.; Thakur, R. A.: Atmospheric pressure photoionization. II. Dual source ionization. *J. Chromatogr. A* **2004**, 1050, 137–149.

- 37 Takats, Z.; Wiseman, J. M.; Cooks, R. G.: Ambient mass spectrometry using desorption electrospray ionization (DESI): instrumentation, mechanisms and applications in forensics, chemistry, and biology. *J. Mass Spectrom.* **2005**, *40*, 1261–1275.
- 38 Cooks, R. G.; Ouyang, Z.; Takats, Z.; Wiseman, J. M.: Detection technologies: ambient mass spectrometry. *Science* **2006**, *311*, 1566–1570.
- 39 Tanaka, K.; Waki, H.; Ido, Y.; Akita, S.; Yoshida, Y.; To, Y.: Protein and polymer analysis up to  $m/z$  100,000 by laser ionization time-of-flight mass spectrometry. *Rapid Commun. Mass Spectrom.* **1988**, *2*, 151–153.
- 40 Rappsilber, J.; Moniatte, M.; Nielsen, M. L.; Podtelejnikov, A. V.; Mann, M.: Experiences and perspectives of MALDI MS and MS/MS in proteomic research. *Int. J. Mass Spectrom.* **2003**, *226*, 223–237.
- 41 Nielen, M.: MALDI Time-of-flight mass spectrometry of synthetic polymers. *Mass Spectrom. Rev.* **1999**, *18*, 309–344.
- 42 Gut, I. G.: DNA analysis by MALDI-TOF mass spectrometry. *Hum. Mutat.* **2004**, *23*, 437–441.
- 43 Schiller, J.; Suss, R.; Arnhold, J.; Fuchs, B.; Lessig, J.; Muller, M.; Petkovic, M.; Spalteholz, H.; Zschornig, O.; Arnold, K.: Matrix-assisted laser desorption and ionization time-of-flight (MALDI-TOF) mass spectrometry in lipid and phospholipid research. *Prog. Lipid Res.* **2004**, *43*, 449–488.
- 44 Cohen, L. H.; Gusev, A. I.: Small molecule analysis by MALDI mass spectrometry. *Anal. Bioanal. Chem.* **2002**, *373*, 571–586.
- 45 McCombie, G.; Knochenmuss, R.: Small-molecule MALDI using the matrix suppression effect to reduce or eliminate matrix background interferences. *Anal. Chem.* **2004**, *76*, 4990–4997.
- 46 Donegan, M.; Tomlinson, A. J.; Nair, H.; Juhasz, P.: Controlling matrix suppression for matrix-assisted laser desorption/ionization analysis of small molecules. *Rapid Commun. Mass Spectrom.* **2004**, *18*, 1885–1888.
- 47 Go, E. P.; Prenni, J. E.; Wei, J.; Jones, A.; Hall, S. C.; Witkowska, H. E.; Shen, Z.; Siuzdak, G.: Desorption/ionization on silicon time-of-flight/time-of-flight mass spectrometry. *Anal. Chem.* **2003**, *75*, 2504–2506.
- 48 Lewis, W. G.; Shen, Z.; Finn, M. G.; Siuzdak, G.: Desorption/ionization on silicon (DIOS) mass spectrometry: background and applications. *Int. J. Mass Spectrom.* **2003**, *226*, 107–116.
- 49 Tang, N.; Tornatore, P.; Weinberger, S. R.: Current developments in SELDI affinity technology. *Mass Spectrom. Rev.* **2003**, *23*, 34–44.
- 50 Caprioli, R. M.; Farmer, T. B.; Gile, J.: Molecular imaging of biological samples: localization of peptides and proteins using MALDI-TOF MS. *Anal. Chem.* **1997**, *69*, 4751–4760.
- 51 Rohner, T. C.; Staab, D.; Stoeckli, M.: MALDI mass spectrometric imaging of biological tissue sections. *Mech. Ageing Dev.* **2005**, *126*, 177–185.
- 52 Reyzer, M. L.; Hsieh, Y.; Ng, K.; Korfmacher, W. A.; Caprioli, R. M.: Direct analysis of drug candidates in tissue by matrix-assisted laser desorption/ionization mass spectrometry. *J. Mass Spectrom.* **2003**, *38*, 1081–1092.
- 53 March, R. E.; Todd, J. F. J.: *Quadrupole Ion Trap Mass Spectrometry*, 2nd edn (vol. 165), Wiley-Interscience, New York, **2005**, 346.
- 54 de Hoffmann, E.: Tandem mass spectrometry: a primer. *J. Mass Spectrom.* **1996**, *31*, 129–137.
- 55 Schwartz, J. C.; Wade, A. P.; Enke, C. G.; Cooks, R. G.: Systematic delineation of scan modes in multidimensional mass spectrometry. *Anal. Chem.* **1990**, *62*, 1809–1818.
- 56 Chin, K.; Channick, R.; Bosentan, B.: *Expert Rev. Cardiovasc. Ther.* **2004**, *2*, 175–182.
- 57 Paul, W.; Steinwedel, H.: A new mass spectrometer without magnetic field. *Zeitschrift für Naturforschung* **1953**, *8a*, 448–450.
- 58 Douglas, D. J.; Frank, A. J.; Mao, D.: Linear ion traps in mass spectrometry.

- try. *Mass Spectrom. Rev.* **2005**, 24, 1–29.
- 59 Schwartz, J. C.; Senko, M. W.; Syka, J. E. P.: A two-dimensional quadrupole ion trap mass spectrometer. *J. Am. Soc. Mass Spectrom.* **2002**, 13, 659–669.
  - 60 Hager, J. W.: A new linear ion trap mass spectrometer. *Rapid Commun. Mass Spectrom.* **2002**, 16, 512–526.
  - 61 Hopfgartner, G.; Varesio, E.; Tschäppät, V.; Grivet, C.; Emmanuel Bourgogne, E.; Leuthold, L. A.: Triple quadrupole linear ion trap mass spectrometer for the analysis of small molecules and macromolecules. *J. Mass Spectrom.* **2004**, 39, 845–855.
  - 62 Hopfgartner, G.; Zell, M.: Q trap MS: a new tool for metabolite identification, in *Using Mass Spectrometry for Drug Metabolism Studies*, ed. Korfmacher, W. A., CRC Press, **2004**.
  - 63 Mamyrin, B. A.: Time-of-flight mass spectrometry (concepts, achievements, and prospects). *Int. J. Mass Spectrom.* **2001**, 206, 251–266.
  - 64 Uphoff, A.; Grottemeyer, J.: The secrets of time-of-flight mass spectrometry revealed. *Eur. J. Mass Spectrom.* **2003**, 9, 151–164.
  - 65 Guilhaus, M.; Selby, D.; Mlynski, V.: Orthogonal acceleration time-of-flight mass spectrometry. *Mass Spectrom. Rev.* **2000**, 19, 65–107.
  - 66 Morris, H. R.; Paxton, T.; Dell, A.; Langhorne, J.; Berg, M.; Bordoli, R. S.; Hoyes, J.; Bateman, R. H.: High sensitivity collisionally-activated decomposition tandem mass spectrometry on a novel quadrupole/orthogonal-acceleration time-of-flight mass spectrometer. *Rapid Commun. Mass Spectrom.* **1996**, 10, 889–896.
  - 67 Chernushevich, I. V.; Loboda, A. V.; Thomson, B. A.: An introduction to quadrupole-time-of-flight mass spectrometry. *J. Mass Spectrom.* **2001**, 36, 849–865.
  - 68 Hopfgartner, G.; Chernushevich, I. V.; Covey, T.; Plomley, J. B.; Bonner, R.: Exact mass measurement of product ions for the structural elucidation of drug metabolites with a tandem quadrupole orthogonal-acceleration time-of-flight mass spectrometer. *J. Am. Soc. Mass Spectrom.* **1999**, 10, 1305–1314.
  - 69 Wolff, J. C.; Eckers, C.; Sage, A. B.; Giles, K.; Bateman, R.: Accurate mass liquid chromatography/mass spectrometry on quadrupole orthogonal acceleration time-of-flight mass analyzers using switching between separate sample and reference sprays. 2. Applications using the dual-electrospray ion source. *Anal. Chem.* **2001**, 73, 2605–2612.
  - 70 Martin, R. L.; Brancia, F. L.: Analysis of high mass peptides using a novel matrix-assisted laser desorption/ionisation quadrupole ion trap time-of-flight mass spectrometer. *Rapid Commun. Mass Spectrom.* **2003**, 17, 1358–1365.
  - 71 Vestal, M. L.; Campbell, J. M.: Tandem time-of-flight mass spectrometry. *Methods Enzymol.* **2005**, 402, 79–108.
  - 72 Suckau, D.; Resemann, A.; Schuerenberg, M.; Hufnagel, P.; Franzen, J.; Holle, A.: A novel MALDI LIFT-TOF/TOF mass spectrometer for proteomics. *Anal. Bioanal. Chem.* **2003**, 376, 952–965.
  - 73 Marshall, A. G.; Hendrickson, C. L.; Jackson, G. S.: Fourier transform ion cyclotron resonance mass spectrometry: a primer. *Mass Spectrom. Rev.* **1998**, 17, 1–35.
  - 74 Syka, J. E. P.; Marto, J. A.; Bai, D. L.; Horning, S.; Senko, M. W.; Schwartz, J. C.; Ueberheide, B.; Garcia, B.; Busby, S.; Muratore, T.; Shabanowitz, J.; Hunt, D. F.: Novel linear quadrupole ion trap/FT mass spectrometer: performance characterization and use in the comparative analysis of histone H3 post-translational modifications. *J. Proteome Res.* **2004**, 3, 621–626.
  - 75 Makarov, A.: Electrostatic axially harmonic orbital trapping: a high-performance technique of mass analysis. *Anal. Chem.* **2000**, 72, 1156–1162.

- 76 Makarov, A.; Denisov, E.; Kholomeev, A.; Balschun, W.; Lange, O.; Strupat, K.; Horning, S.: Performance evaluation of a hybrid linear ion trap/orbitrap mass spectrometer. *Anal. Chem.* **2006**, 78, 2113–2120.
- 77 Wiza, J. L.: Microchannel plate detectors. *Nucl. Instr. Methods* **1979**, 162, 587–601.
- 78 Birkinshaw, K.: Fundamentals of focal plane detectors. *J. Mass Spectrom.* **1997**, 32, 795–806.
- 79 Hopfgartner, G.; Bourgogne, E.: Quantitative high-throughput analysis of drugs in biological matrices by mass spectrometry. *Mass Spectrom. Rev.* **2003**, 22, 195–214.
- 80 Matuszewski, B. K.; Constanzer, M. L.; Chavez-Eng, C. M.: Strategies for the assessment of matrix effect in quantitative bioanalytical methods based on HPLC-MS/MS. *Anal. Chem.* **2003**, 75, 3019–3030.
- 81 Kostianen, R.; Kotiaho, T.; Kuuranen, T.; Auriola, S.: Liquid chromatography/atmospheric pressure ionization-mass spectrometry in drug metabolism studies. *J. Mass Spectrom.* **2003**, 38, 357–372.
- 82 Staack, R. F.; Varesio, E.; Hopfgartner, G.: The combination of liquid chromatography/tandem mass spectrometry and chip-based infusion for improved screening and characterization of drug metabolites. *Rapid Commun. Mass Spectrom.* **2005**, 19, 618–626.
- 83 Hopfgartner, G.; Vilbois, F.: The impact of accurate mass measurements using quadrupole/time-of-flight mass spectrometry on the characterisation and screening of drug metabolites. *Analisis* **2000**, 28, 906–914.
- 84 Zhang, H.; Zhang, D.; Ray, K.: A software filter to remove interference ions from drug metabolites in accurate mass liquid chromatography/mass spectrometric analyses. *J. Mass Spectrom.* **2003**, 38, 1110–1112.
- 85 Zhu, M.; Ma, L.; Zhang, D.; Ray, K.; Zhao, W.; Humphreys, W. G.; Skiles, G.; Sanders, M.; Zhang, H.: Detection and characterization of metabolites in biological matrices using mass defect filtering of liquid chromatography/high resolution mass spectrometry data. *Drug Metab. Dispos.* **2006**, 34, 1722.
- 86 Beranova-Giorgianni, S.: Proteome analysis by two-dimensional gel electrophoresis and mass spectrometry: strengths and limitations. *TrAC* **2003**, 22, 273–281.
- 87 Wolters, D. A.; Washburn, M. P.; Yates, J. R. III: An automated multidimensional protein identification technology for shotgun proteomics. *Anal. Chem.* **2001**, 73, 5683–5690.
- 88 Wang, H.; Hanash, S.: Multi-dimensional liquid phase based separations in proteomics. *J. Chromatogr. B* **2003**, 787, 11–18.
- 89 Dunn, W. B.; Bailey, N. J. C.; Johnson, H. E.: Measuring the metabolome: current analytical technologies. *Analyst* **2005**, 130, 606–625.
- 90 Benesch, J. L. P.; Robinson, C. V.: Mass spectrometry of macromolecular assemblies: preservation and dissociation. *Cur.Opin. Struc. Biol.* **2006**, 16, 245–251.
- 91 Sauer, S.: Typing of single nucleotide polymorphisms by MALDI mass spectrometry: Principles and diagnostic applications. *Clin. Chim. Acta* **2006**, 363, 95–105.

## **Part II**

**Studying target-ligand interactions analyzing  
the ligand by MS**





## 2

# Drug Screening Using Gel Permeation Chromatography Spin Columns Coupled with ESI-MS

*Marshall M. Siegel*

## 2.1

### Introduction

#### 2.1.1

##### Preface

The pharmaceutical industry has invested heavily in high throughput screening (HTS) technologies to find potential drug candidates present in large compound libraries that interact with a biological system of a potential therapeutic interest. Very often these screening techniques mimic the cellular function of the target protein. The HTS methods generally take considerable time to develop and are unique for each biological system of interest, but once developed they analyze single compounds in large arrays at high sensitivity, accounting for the high throughput capability of the methodology. The HTS methodology has been the technique of choice of pharmaceutical companies to initially screen corporate libraries for exploratory drug leads. Recently, however, a number of structurally based methods have been developed to screen corporate libraries based on the ability to observe non-covalent bonding between a protein of therapeutic interest and members of a compound library [1]. We will describe in this chapter the use of gel permeation chromatography (GPC) in the spin column mode with mass spectral detection as a reliable structural screening methodology that can be performed at high speed with large numbers of compounds, especially when analyzed as mixtures, requiring nearly no development time. This technology can be used as a primary screening technique as well as a secondary screening method to complement and verify results obtained with HTS methods.

#### 2.1.2

##### Direct and Indirect ESI-MS Analysis of Non-covalent Drug–Protein Complexes

Electrospray ionization mass spectrometry (ESI-MS) is a powerful technique for analyzing non-covalent complexes formed between small molecules and proteins.

Two ESI-MS approaches can be taken, namely, direct and indirect analysis of the complexes. Direct methods utilize exclusively ESI-MS to analyze the nature of the non-covalent complexes formed under native conditions in the condensed phase while analyzing the products in the gas phase. Indirect methods utilize biochemical and chromatographic methods for preparing and separating the complexes and ESI-MS as the ancillary detector for the individual products of the non-covalent complex, namely, the small molecules and the protein.

Direct analyses of non-covalent complexes between drug candidates and biopolymers have been studied extensively by ESI-MS. This subject has been reviewed comprehensively [2–10] and is also discussed in Chapter 10. The underlying principle of these ESI-MS studies is that the mass spectrometer directly analyzes, in the gas phase and in the absence of solvent, the complexes prepared in the condensed phase under native conditions, generally at a pH of  $\sim 7$  in water with a volatile buffer, most often ammonium acetate. Under these native conditions, the sensitivity of the ESI mass spectrometer is not optimum and there is no guarantee that the desolvated complex formed in the gas phase is not an artifact of the ion formation mechanism. In addition, the study of these complexes under native conditions is time-consuming because of the low sensitivity and difficulty in maintaining a stable instrument at the higher pressures needed to form and stabilize these protein complexes for mass spectral studies. Higher sensitivity is achieved under lower pH conditions and with more volatile solvents such as acetonitrile or methanol, however, these conditions denature the protein–drug complex.

A number of indirect methods have been developed with mass spectrometric detection to rapidly study non-covalent complexes for drug screening purposes [2]. Among the most promising and simple indirect methods that overcome the limitations described above for directly studying non-covalent complexes by mass spectrometry is the application of size exclusion techniques in the spin column format for the screening and analysis of drug–protein complexes under optimum mass spectral sensitivity conditions [11–13].

### 2.1.3

#### **Advantages of GPC Spin Columns**

A spin column is a short column packed with GPC media that is centrifuged (see Fig. 2.1A, B). The media used for GPC are also referred to as size exclusion chromatography and gel filtration chromatography media. The gel and sample are prepared with buffers compatible with processing the protein–drug complex in its native state. Upon loading the sample at the top of the column and centrifugation of the column, the lower molecular weight (MW) free ligands are separated rapidly from the higher MW protein and protein–ligand complexes. The free ligands are unfractionated and retained by the gel while the eluate, corresponding to the solvent front, passes unrestricted through the gel containing the protein and protein–ligand complexes. The GPC spin column eluate is then denatured

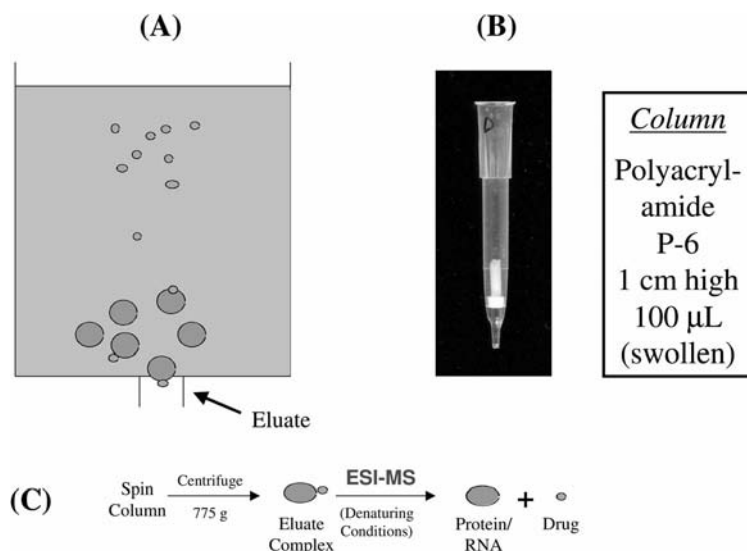


**Fig. 2.1** GPC spin column used for isolating protein/RNA–drug non-covalent complexes in the eluate upon centrifugation and the ESI-MS steps to detect the ligands upon denaturing of the protein/RNA–drug non-covalent complexes. (A) Spin column cartoon, (B) Photo of a miniature GPC spin column, (C) Schematic of GPC spin column/ESI-MS procedures.

and the free ligand is analyzed by flow-injection analysis or HPLC using ESI-MS under denaturing conditions (see Fig. 2.1C.) This procedure decouples the preparation (incubation), separation and analysis steps so that each step can be individually optimized in a flexible fashion. The methodology is simple to apply and rapid to implement and utilizes standard size exclusion and ESI mass spectrometry techniques under optimum conditions for sample preparation, isolation, detection, quantitation and automation.

An example of the GPC spin column/ESI-MS methodology for drug screening is illustrated in Fig. 2.2 for identifying a non-covalently bound inhibitor to a protein target. Figure 2.2A displays the ESI mass spectrum of an impure peptidic difluoromethyl ketone inhibitor (DFMK) before passing through the GPC spin column. Figure 2.2B displays the ESI mass spectrum after passage through the GPC spin column of the incubated mixture of impure DFMK with cytomegalovirus protease (CMVP). The impure inhibitor, upon passing through the GPC spin column, emerged as a purified major component together with the protease with which it formed a non-covalent complex. The gel retained all other impurity components. In this way, large numbers of drug candidates can be routinely screened with a protein target because the non-covalently bound drug candidates pass

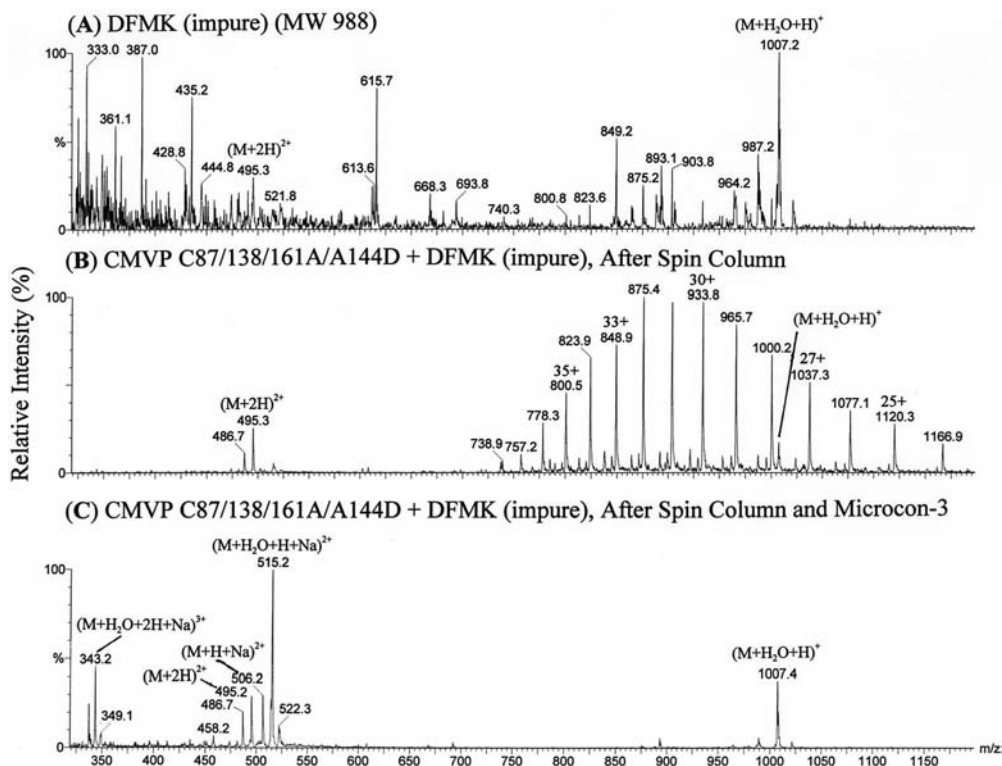


**Fig. 2.2** ESI mass spectra obtained from the GPC spin column/ESI-MS screening assay of non-covalently bound protease–inhibitor complexes. Enzymatically active CMVP A144D/C87A/C138A/C161A was used in this experiment. (A) Reference ESI mass spectrum of impure inhibitor DFMK (MW 988.5 Da). (B) ESI mass spectrum of the spin column eluate of CMVP A144D/C87A/C138A/C161A and DFMK, incubated at a

molar ratio of 1: ~10. (C) ESI mass spectrum of the microconcentrator filtrate (3 kDa cutoff centrifugal ultrafiltration membrane) obtained under denaturing conditions (3% acetic acid in 1:1 water:acetonitrile, v:v) from the non-covalently bound complex of CMVP A144D/C87A/C138A/C161A and DFMK generated from the GPC spin column eluate. Reprinted from reference [13] with permission from John Wiley & Son.

through the GPC spin column and are detected by ESI-MS while all the other drug candidates are retained by the GPC spin column and are not detected.

## 2.1.4

### Application of Equilibrium and Non-equilibrium Theory for the Analysis of GPC Spin Column Eluates

An excellent reference discussing the theory and applications of receptor binding is the text edited by E.C. Hulme entitled “*Receptor–ligand interactions: a practical approach*” [14].

### 2.1.4.1 Sample Prepared Under Equilibrium Conditions Prior to Spin Column Treatment

The binding of a small molecule ligand to a protein receptor follows a bimolecular association reaction with second-order kinetics. For the reversible reaction of a ligand L and a protein P to form a non-covalently bound complex C at equilibrium, Eq. (1) applies where  $k_{\text{on}}$  and  $k_{\text{off}}$  represent the forward and reverse mass transfer rate constants.



The equilibrium dissociation constant  $K_d$  is then given by:

$$K_d = [P][L]/[C] = k_{\text{off}}/k_{\text{on}} \quad (2)$$

If  $[P]_o$  and  $[L]_o$  are the initial total protein and ligand concentrations, respectively, where:

$$[P]_o = [P] + [C] \quad (3)$$

and:

$$[L]_o = [L] + [C] \quad (4)$$

the equilibrium in Eq. (2) can be transformed into a quadratic equation and solved, giving:

$$[C] = \frac{1}{2} (K_d + [P]_o + [L]_o) - \{1/4(K_d + [P]_o + [L]_o)^2 - [L]_o[P]_o\}^{1/2} \quad (5)$$

where  $[C]$  is the equilibrium concentration of the protein–ligand complex, referred to also as  $[C]_{\text{eq}}$ . Equation (5) can be used to calculate the concentration of complex present at equilibrium for initial protein and ligand concentrations and  $K_d$  during the incubation step in the GPC spin column screening experiment.

Typically, in most GPC spin column screening experiments, concentrations of the target protein and small molecule compounds are  $\geq 5 \mu\text{M}$ . Figure 2.3 illustrates the relationship between the concentration of the protein–ligand complex  $[C]$  present at equilibrium as a function of the binding constant for a variety of initial protein and ligand concentrations,  $[P]_o$  and  $[L]_o$ , respectively,  $\geq 5 \mu\text{M}$ . These initial concentrations are used so that sufficient complex is formed so that even weakly binding drugs with  $K_d$  values  $\leq 20 \mu\text{M}$  form complexes of sufficient concentration so that they are easily detectable using ESI-Time-of-Flight (ToF) mass spectrometry.

### 2.1.4.2 Calculation for Predicting the Concentration of Sample Complex Eluted From the Spin Column

The GPC spin column fractionation step is a non-equilibrium process. During the gel permeation chromatography step, the unbound small molecules in solu-

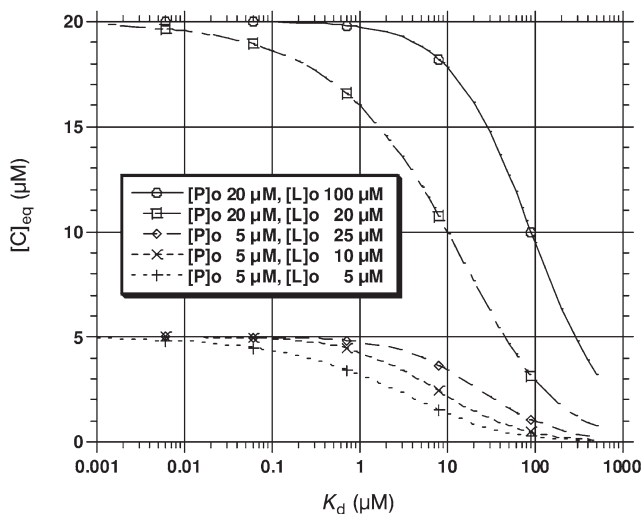


**Fig. 2.3** Plots of the concentration of the protein–ligand complex present at equilibrium  $[C]_{eq}$  ( $\mu\text{M}$ , shown as  $\mu\text{M}$ ) as a function of the binding constant  $K_d$  ( $\mu\text{M}$ ), with various initial concentrations of protein  $[P]_o$  and ligand  $[L]_o$ . Note that the  $[C]_{eq}$  values are the concentrations of the protein–ligand complex just prior to the GPC spin

column experiment. When initial concentrations of ligand and protein are  $\geq 5 \mu\text{M}$ , the concentration of complex produced for  $K_d$  values  $\leq 20 \mu\text{M}$  is  $\geq 1 \mu\text{M}$  of complex, a concentration considerably greater than the detection limit of modern ESI-ToF mass spectrometers.

tion are rapidly separated from the protein using centrifugation. At the start of GPC spin column centrifugation step (time = 0), the concentration of the protein–ligand complex is equal to the equilibrium concentration,  $[C]_{eq}$ . As the complex migrates through the column during centrifugation, it dissociates. If we assume that the protein–ligand complex dissociates in the column at a rate much faster than the association rate, then the concentration of the protein–ligand complex can be expressed by the first-order rate equation:

$$d[C]/dt = -k_{off}[C] \quad (6)$$

where  $k_{off}$  is the kinetic off-rate constant and  $t$  is the elution time. Note the use of underscores to designate concentrations not based on the law of mass action but rather based on non-equilibrium phenomena. Solving this equation, we obtain:

$$[C] = [C]_{eq} \exp(-k_{off}t) \quad (7)$$

Ultimately in the GPC spin column screening experiment, the complex present in the eluate is dissociated and the ligand molecules liberated from the protein are detected by mass spectrometry. The amount of ligand detected is essentially equivalent to the concentration of the protein–ligand complex that eluted from the GPC spin column. Equation (7) indicates that the amount of protein–ligand

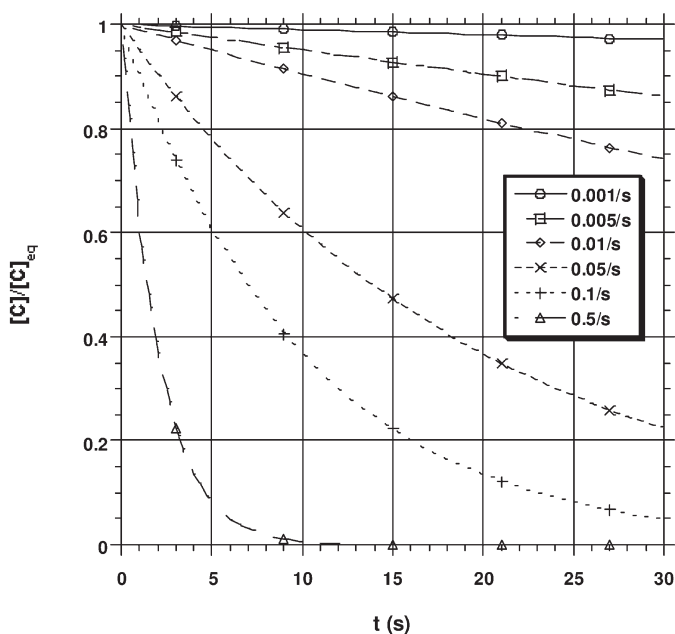


**Fig. 2.4** Plots of the fraction of complex ( $[C]/[C]_{eq}$ ) eluted from the spin column from the initial equilibrium state as a function of time for a variety of off-rate constants. Assuming a GPC spin column elution time of 15 s, greater than 20% of the initial equilibrium complex concentration is recovered in the GPC spin column eluate for off-rate constants less than  $0.1 \text{ s}^{-1}$ .

complex that survives the GPC spin column decreases exponentially as a function of the product of the off-rate constant and the elution time. Since the off-rate is controlled by the nature of the complex, the only GPC spin column parameter experimentally controllable is the spin time ( $t$ ). The shorter the spin time the greater the concentration of complex eluted from the spin column. Figure 2.4 plots the fraction of complex ( $[C]/[C]_{eq}$ ) eluted from the spin column from the initial equilibrium state as a function of time for a variety of off-rate constants. In most experiments, the spin column eluate is collected within about 15 s. Under these conditions, greater than 20% of the initial equilibrium complex concentration is recovered in the GPC spin column eluate for off rate constants less than  $0.1 \text{ s}^{-1}$ .

Since the limit of detection for small molecule ligands, with modern ESI-ToF mass spectrometers, is approximately  $\sim 0.05 \text{ } \mu\text{M}$ , the concentration of the protein–ligand complex prior to the GPC spin column treatment must be about  $0.25 \text{ } \mu\text{M}$ . For initial protein and ligand concentrations  $\geq 5 \text{ } \mu\text{M}$ , this corresponds to  $K_d$  values  $\leq 20 \text{ } \mu\text{M}$ , as indicated in Fig. 2.3. This is a desirable region for the GPC spin column studies, since one wants to be certain to detect ligands from the stronger as well as the weakest ligand binders.



Using sub-ambient temperatures for preparing the protein–ligand equilibrium mixtures and for centrifugation of the GPC spin column, the dissociation rate constant decreases and the off-rate diminishes, thereby expanding the kinetic window observable with GPC spin column screening to even weaker binders with  $K_d$  values  $>20 \mu\text{M}$ .

#### 2.1.4.3 Estimation of Relative Binding Affinities from GPC Spin-Column/ESI-MS Data

For a variety of ligands in a mixture with the same initial concentration  $[L]_0$ , such that  $[L]_0 > [C]$  and where the equilibrium concentration of the remaining protein is  $[P]$ , we can relate back to equilibrium conditions, and using Eq. 7 for computing the ratio of two components subscripted 1 and 2, we obtain:

$$\frac{K_{d1}}{K_{d2}} = \frac{[C_2]_{\text{eq}}}{[C_1]_{\text{eq}}} = \frac{[C_2] \exp(+k_{\text{off}2}t)}{[C_1] \exp(+k_{\text{off}1}t)} = \frac{[L_2] \exp(+k_{\text{off}2}t)}{[L_1] \exp(+k_{\text{off}1}t)} \quad (8)$$

Note that, in Eq. (8), the concentrations for the complex  $[C]$  and related ligand  $[L]$  are equal because the ligand is liberated from the complex by denaturing the complex. These non-equilibrium ligand concentration values are obtained by mass spectrometry from the denatured GPC spin column eluate. If the off-rates for the different compounds are the same,  $k_{\text{off}1} = k_{\text{off}2}$ , then:

$$\frac{K_{d1}}{K_{d2}} = \frac{[L_2]}{[L_1]} \quad (9)$$

i.e., the dissociation constants are inversely related to the ligand concentrations measured by mass spectrometry after elution from the GPC spin column. Equation (9) can be used to reliably estimate the unknown dissociation constants for related ligands in a mixture with a protein if the concentrations of the ligands in the GPC spin column eluate are quantitated and the dissociation constant for one of the ligands is known. Likewise for ligands, either in a mixture or as singletons, of initial equal concentrations when incubated with a protein, the relative binding affinities and relative dissociation constants for the ligands can be ranked based upon the ligand concentrations in the GPC spin column eluate as quantitated by mass spectrometry.

#### 2.1.4.4 Experimental Determination of the $K_d$ Value from GPC Spin-Column/ESI-MS Data

The expression for the equilibrium concentration of the protein–ligand complex  $[C]$ , described above using Eq. (5), can also be re-written in terms of the total initial protein concentration  $[P]_0$  such that:

$$[C] = \frac{([P]_0[L])}{(K_d + [L])} \quad (10)$$

and predicts a hyperbolic, saturable dependence of the concentration of the protein–ligand complex on the free ligand concentration. Equation (10) is a form of the simple Langmuir isotherm.

An experimentally most useful relationship occurs using Eq. (10), when the free ligand concentration  $[L]$  is equal to the dissociation constant  $K_d$ , namely,

$$[C] = [P]_o/2 \quad \text{when } [L] = K_d \quad (11)$$

i.e., the protein binding sites are half-saturated with ligand. Conversely, the free ligand concentration at 50% protein saturation is a measure of the  $K_d$ . The effective ligand concentration at 50% protein saturation is referred to as the  $EC_{50}$  and is equivalent to the  $K_d$ . Typically, the  $EC_{50}$  value is experimentally obtained by titrating various concentrations of ligand with a fixed initial protein concentration and measuring the concentration of complex formed, obtained in the GPC spin column/ESI-MS measurement. A plot of  $[C]/[P]_o$  vs  $\log_{10}[L]$  produces a sigmoidal shaped curve symmetrical about  $\log_{10} K_d$ . The  $K_d$  value can be read directly from the plot as the corresponding value of  $[L]$  where  $[C]/[P]_o$  is equal to 50%, the  $EC_{50}$  value. See the discussion in section 2.3.3.3 for an experimental application of this methodology.

## 2.2 Experimental

### 2.2.1 Spin Columns

Figure 2.1B illustrates a miniature GPC chromatographic column with a frit on the end used as a spin column. These miniature columns are commercially available in different sizes (Harvard Apparatus, Holliston, Mass.) and can be formatted as a microtiter plate consisting of an array of 96 miniature columns. Likewise, similarly sized miniature fritless spin columns are available with holes at the bottom of the column that are smaller than the diameter of the GPC media particles, thereby reducing possible sample and protein losses due to adherence to the frit (Glygen Corp., Columbia, Md.). Larger spin columns are also available (Pharmacia, BioRad). Miniature 96 GPC spin column arrays can be easily prepared with a Millipore (Danvers, Mass.) multiscreen filtration system containing a hydrophilic Durapore filter (with a pore diameter of 0.65  $\mu\text{m}$ ) at the bottom of each well [15, 16]. The system has a 96-well collection plate for the spin column eluate and samples can be either directly applied at the top of each column or preferably loaded simultaneously into all the columns using a 96-well top plate with pinholes (MDS Protana, Denmark) for transfer to the 96 columns upon centrifugation [16]. Commercially prepared 96-well size exclusion microplates are also available [AutoSeq96, GE Healthcare (Amersham Biosciences); SigmaSpin, Sigma–Aldrich].

**Table 2.1** GPC gel types and fractionation ranges.

Polyacrylamide (BioRad)		Sephadex (Pharmacia)	
Type	Fractionation Range	Type	Fractionation Range
P2	100–1,800 Da	G10	<700 Da
P4	800–4,000 Da	G15	<1,500 Da
P6	1,000–6,000 Da	G25	1,000–5,000 Da
P10	1,500–20,000 Da	G50	1,500–30,000 Da
P30	2,500–40,000 Da	G75	3,000–80,000 Da
P60	3,000–60,000 Da		
P100	5,000–100,000 Da		

### 2.2.2

#### Spin Column Media: Advantages and Disadvantages, Volatile vs Non-volatile Buffers

The most popular GPC gel media are polyacrylamides and sephadexes (see Table 2.1). When used in the spin column format, compounds with MWs within the fractionation range of the gels generally are retained in the pores of the gel beads and compounds with MWs greater than that of the fractionation range generally pass through the columns unrestricted. Since most protein and protein–drug complexes in pharmaceutical screening programs have MWs greater than 15 000 Da and the small molecules have MWs less than 1000 Da, the gel media used most often are the polyacrylamides P2, P4, P6 and the sephadexes G10, G15, G25. Highest sensitivity for identifying non-covalently bound small molecules to protein can occur using the GPC spin column/ESI-MS methodology when in control experiments the maximum amount of protein passes through the spin column. Likewise, in control experiments, all the small molecules should be retained on the column. In general, as the upper mass limit of the fractionation range for the gel media decreases, the amount of protein transmitted through the spin column increases with a greater risk for the transmission of the small molecule through the column. In screening studies with the insulin-like growth factor receptor (IGFr) protein (predicted MW 35 065 Da), the transmission of protein through identical spin column volumes for P6, G25 and P2 were 5%, 17% and 34%, respectively, relative to the response of the same amount of protein directly analyzed by ESI-MS. Clearly, P2 was the preferred gel since protein transmission was the highest and in control experiments none of the small molecules evaluated gave false positive results.

The gel media should be hydrated and washed with a buffer system compatible with maintaining the protein target in its native state. To thoroughly remove contaminants present in the gels, multiple washes are necessary. Sephadex beads

generally require more numerous washes than polyacrylamide beads. It is preferable to wash the columns with volatile buffers (ammonium acetate, ammonium bicarbonate systems) rather than non-volatile buffers (phosphate, sulfate systems) since they are more compatible with the ESI-MS assay and lead to minimal ion suppression. The gel columns are prepared by loading the washed gel into the column and centrifuging the column at 775 g for 3 min to gently remove excess buffer without dehydrating or drying the gel. This whole procedure of gel hydration, washing and column preparation can also be performed after loading dry gel into the miniature column and is the preferred method for preparing gel columns with 96-well microtiter plates. A useful spin column feature is the ability to exchange non-volatile buffers, often present in proteins, with the volatile buffers present in the spin column. If volatile buffers are present in the spin column eluate, flow injection ESI-MS is possible but if not HPLC ESI-MS is required.

All the GPC spin columns described above are inexpensive, disposable and designed for single use, avoiding all possibilities for cross contamination of samples. A very desirable feature of the GPC spin column technique is that the eluate contains principally only positive hits of non-covalently bound ligands and all other small molecules are absent, unlike other screening techniques, e.g., centrifugal ultrafiltration (see Chapter 4), where the tight binders are enriched while still retaining chemical noise from unenriched components of the mixture. On rare occasions, false positive results are obtained when a small molecule passes through the GPC spin column unfractionated, together with the protein and not as a non-covalently bound complex. This can be easily verified by assaying the small molecule alone in the absence of protein via the GPC spin column/ESI-MS methodology. From screening studies of large libraries, more false positive results were observed with sephadex beads than with polyacrylamide beads. The most common false positive results were obtained with organic molecules containing poly-carboxylic acid, poly-cyano, sulfate, poly-sulfate, phosphate and poly-phosphate moieties. Most of these compounds are not likely drug candidates.

### 2.2.3

#### **Preparing Non-covalent Complexes in Protein Buffer; Protein Concentration, Ligand Concentration, Incubation Time**

Non-covalent protein–drug complexes are prepared by incubating the drug with the native protein for 30–60 min in a compatible buffer. Volatile buffers are preferable over inorganic non-volatile buffers because mass spectral sensitivity is greater for samples prepared with volatile buffers. Often the libraries of drug candidates are prepared in DMSO solutions and are diluted with buffers similar to the ones used for the protein. The final DMSO concentration should be less than 5% so as not to denature the protein but to aid in solubilizing the drug candidates. Ideally, the drug candidates should be maintained in solution during the incubation process despite the fact that they often precipitate out of solution in the pH range normally utilized (pH 6–8) to maintain the protein in the native state.

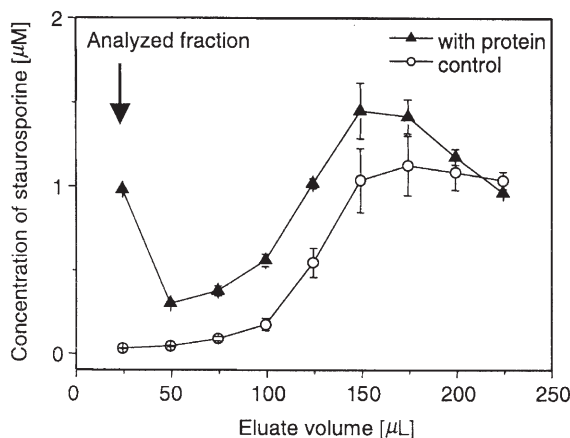
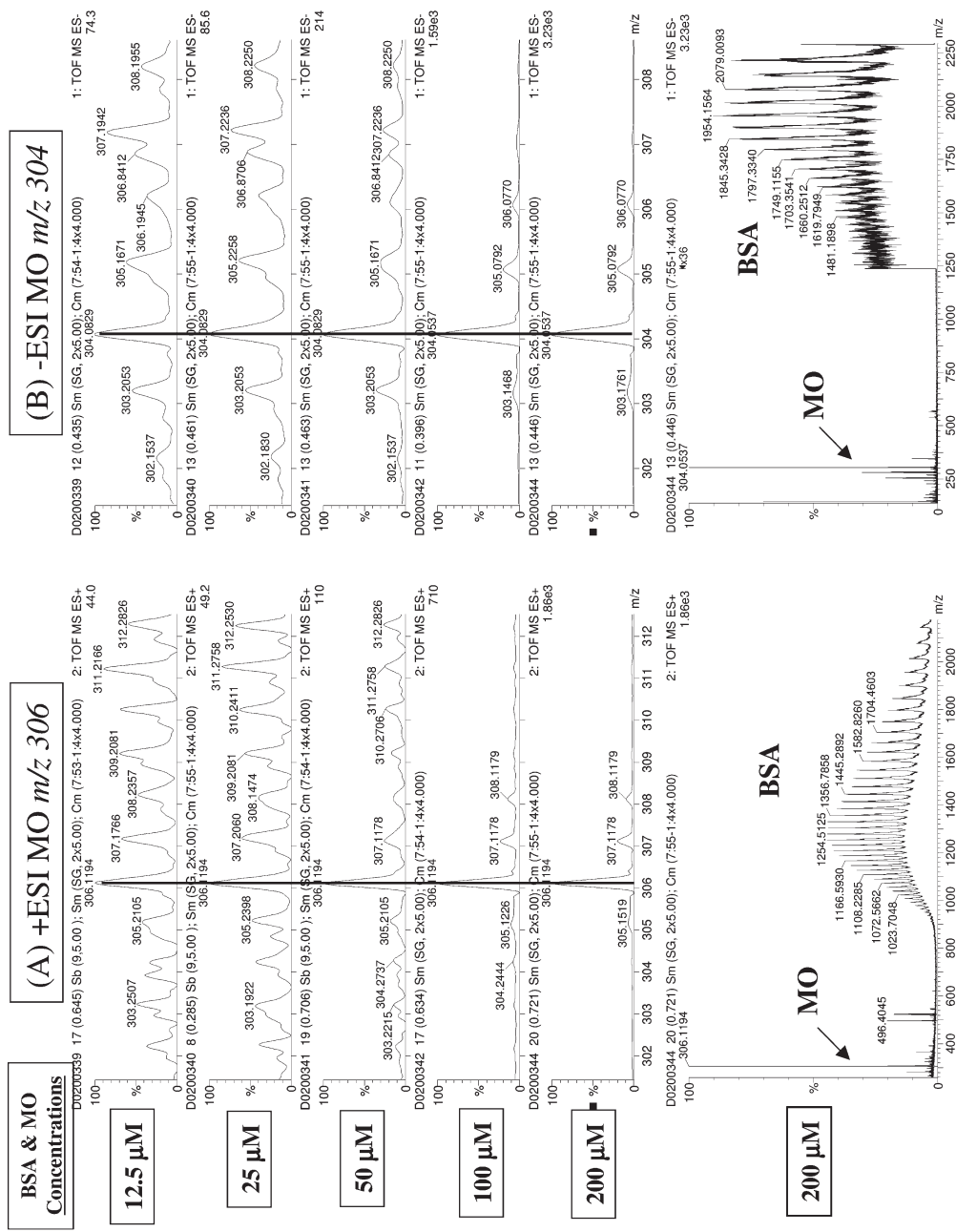


**Fig. 2.5** Concentrations of staurosporine in eluate fractions obtained in sequential GPC spin column/HPLC ESI-MS experiments. Mixtures of compounds were spiked with staurosporine and incubated with PKA (-▲-) and without PKA (-o-) as a control. The first eluate fraction shows the most significant ligand concentration difference between the protein-ligand and control samples. Reprinted from reference [16] with permission from Elsevier Science.

The concentrations of the incubated protein and drug candidates used are a function of the outcome desired. If very strongly bound ligands to protein are desired ( $K_d < 0.1 \mu\text{M}$ ) then lower concentrations of drug–protein mixtures are used; conversely, for weak binders ( $K_d > 10 \mu\text{M}$ ) higher concentrations are used. For screening campaigns for moderate binders ( $K_d$  0.1–10  $\mu\text{M}$ ) as well as strong binders using miniature spin columns of 100  $\mu\text{L}$  volume with ToF mass spectrometer detectors, generally, protein concentrations of 5–10  $\mu\text{M}$  with 5–10 times molar excess of drug candidates is sufficient. The volume of the protein–drug mixture utilized in the GPC spin column studies should be 10–15% of the miniature gel column volume. This small volume ratio is used so that the sample will not pass through open channels in the gel to the bottom of the column producing false positive results. Typically, 10  $\mu\text{L}$  volumes of protein–drug mixtures are used with miniature spin columns of 100  $\mu\text{L}$  volume. Screening studies for strong binders typically utilize protein concentrations of 0.25–5.0  $\mu\text{M}$  with 1–5 times

**Fig. 2.6** Titration assay of BSA and methyl orange (MO, MW 305 Da,  $K_d = 450 \mu\text{M}$ ) by GPC spin column/ESI-MS methodology as a function of [MO]/[BSA] molar ratios in the positive ionization mode (A) and the negative ionization mode (B). The mass spectra in the top five panels are exploded

views. The bottom panels of (A) and (B) illustrate the corresponding full spectra. The ion count for each spectrum is indicated in the upper right hand corner of each spectrum. A miniature 100  $\mu\text{L}$  P6 GPC spin column was used to assay 10  $\mu\text{L}$  samples.



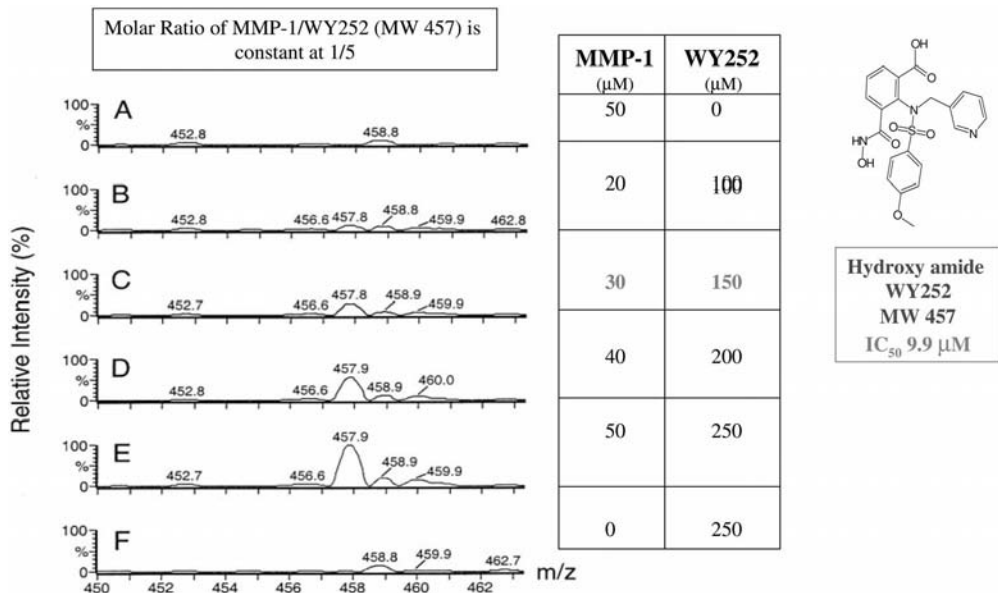


**Fig. 2.7** ESI mass spectra of ligands present in GPC spin column eluates have a linear response with increasing concentration: ESI (positive ionization mode) mass spectral analysis of the eluate from the GPC spin column titration of WY252 (MW 457 Da) with MMP-1 where the molar ratios of MMP-1/WY252 are constant at 1:5 while their individual concentrations linearly increase. The volume injected for each sample was

30  $\mu\text{L}$ . (A) MMP-1 alone at 50  $\mu\text{M}$  and (F) WY252 alone at 250  $\mu\text{M}$ , respectively. (B–E) increasing amount of MMP-1: (B) 20  $\mu\text{M}$ , (C) 30  $\mu\text{M}$ , (D) 40  $\mu\text{M}$  and (E) 50  $\mu\text{M}$ ; and increasing amount of WY252: (B) 100  $\mu\text{M}$ , (C) 150  $\mu\text{M}$ , (D) 200  $\mu\text{M}$  and (E) 250  $\mu\text{M}$ . Same absolute intensity scale for all panels. Reprinted from reference [15] with permission from the American Chemical Society.

molar excess of drug. Similarly for the study of weak binders, protein concentrations 15–200  $\mu\text{M}$  with 1–100 times molar excess drug can be used.

The unique property of the GPC spin column experiment is that the volume of sample loaded on to the spin column is the same volume of the eluate obtained after gentle centrifugation. Furthermore, when two GPC spin column experiments are performed, as described above, initially with an incubated protein–ligand sample in one column and with a ligand sample without protein as a control in another column, each followed by repeated elutions with buffer solutions, the most significant ligand concentration difference between the protein–ligand sample and the control sample is between the first collected fractions. This is illustrated in Fig. 2.5 for GPC spin column eluate fractions for a protein kinase A (PKA)–staurosporine sample and a control sample of staurosporine without PKA [16]. These fractionation experiments verify the fundamental principle of the GPC spin column methodology that only the first fractions of the protein–ligand

mixture and the control experiments are needed for non-covalent binding studies for drug screening.

Dose response titrations were used to demonstrate that the non-covalent binding in the GPC spin column/ESI-MS assay is a function of the protein and ligand concentrations. Methyl orange is a very weak binder to bovine serum albumin (BSA) with a  $K_d$  of 450  $\mu\text{M}$  and its passage through the GPC spin column can be visually monitored. A variety of equimolar concentrations of BSA and methyl orange were analyzed using the GPC spin column/ESI-MS methodology, as illustrated in Fig. 2.6 for both the positive and negative ESI ionization modes. The chemical noise level in these experiments is about 45 counts (note: the ion counts are indicated in the upper right hand corner of each spectrum.) Only background traces of the molecular ions for methyl orange ( $m/z$   $[\text{M}+\text{H}]^{1+}$ : 306;  $[\text{M}-\text{H}]^{1-}$ : 304) were observed in the mass spectra for equimolar concentrations 12.5  $\mu\text{M}$  and 25  $\mu\text{M}$ , i.e., the ion abundances were slightly greater than the chemical noise, while the methyl orange response grew with increasing equimolar concentrations from 50  $\mu\text{M}$  to 200  $\mu\text{M}$ . Visual observations of the column confirm these results. At the two lower concentrations, the orange color of methyl orange was confined to the top of the GPC spin column and with increasing concentrations the orange color moved down the column towards the top of the spin column frit, consistent with the ESI-MS intensity observations. Similar dose response titration studies have been reported with stronger binders, e.g., matrix metalloproteinase-1 (MMP-1) protein with a substituted hydroxyamide WY252 with an  $\text{IC}_{50}$  of 9.9  $\mu\text{M}$  (see Fig. 2.7) [15].

#### 2.2.4

##### **Sample Organization: Single Samples vs Mixtures, Mixture Set-up: Compatibility of Components, Plate Set-up**

Since the numbers of compounds to be assayed in a high throughput drug screening campaign are high (>25 000 samples) and the expected number of hits is relatively low (<0.5%), the GPC spin column assays are more efficiently done with mixtures of compounds. In the earliest reported work using the GPC spin column ESI-MS screening assay, mixtures of ten chemically compatible compounds were prepared [15]. An important additional criterion used for selecting the compounds for the mixtures was that the MW of each compound in the mixture differed by at least 3 Da to allow for clear identification of each component by the mass spectrometer, and thereby, the MW effectively becomes an identification tag for each compound screened in the assay. Additional considerations in the selection of compounds for the mixtures are solubility, structural diversity and drug-like characteristics [17]. Also, a reasonable balance of acidic and basic molecules was selected to avoid potentially drastic pH changes upon addition to the protein.

Schnier and coworkers [18] extended the GPC spin column ESI-MS assay for the analysis of a target protein with mixtures of 80 components (5  $\mu\text{M}$  protein, 1  $\mu\text{M}$  per compound). The compounds were pooled using two different procedures so that a specific compound is found in two wells with completely different



well-mates. Eighty microtiter plates were prepared where each plate contained 80 compounds and each compound occupied an individual well. One procedure combined the 80 samples from each of the microtiter plates into different wells of a new microtiter plate. The second procedure pooled each sample from similar wells of the 80 microtiter plates into individual wells of a second microtiter plate. Mixtures of 80 components each were found to be optimum for minimizing false positive GPC spin column eluates.

Most recently, Filpuzzi and coworkers incubated mixtures of 400 compounds with a protein and successfully analyzed for non-covalent binders using an array of GPC spin columns with ESI-MS detection in a very high throughput manner [16, 19, 20]. Compound mixtures of various sizes were evaluated when incubated with PKA spiked with staurosporine and in the absence of PKA. Mixtures of 400 compounds each at a concentration of 7  $\mu\text{M}$  and with a protein concentration of 10  $\mu\text{M}$  gave the best results, while mixtures with greater numbers of compounds gave increased numbers of false positive results.

#### 2.2.5

##### **Pooling Spin Column Eluates for Higher Throughput**

Perhaps the most efficient method to achieve higher sample throughput is to pool the GPC spin column eluates. Since the anticipated number of hits per eluate is very low, less than 0.05% or one hit per 2000 compounds, the average number of hits per eluate is less than one hit per large mixture. If the ESI-MS assay is performed using HPLC, sample volume due to pooling many eluates is not a problem since the sample is concentrated on the column. The main concern will be the amount of protein and its effect on the mass spectra. Often this is not a problem due to the low levels of protein used in the assays. However, the protein can be easily removed as discussed below in Section 2.2.10.

#### 2.2.6

##### **Manual vs Robotic Instrumentation for Sample Preparation and Acquiring Spin Column Eluates**

A considerable number of steps are required for preparing the samples, preparing the GPC spin columns, obtaining the eluates and operating the HPLC and mass spectrometer instruments. For secondary screening studies of small numbers of samples, these steps can be performed manually. However, for primary screening of large numbers of mixture samples, these operations are best performed robotically. The required robotic operations include: (i) preparation of compound mixtures, (ii) preparation of protein–compound mixtures, (iii) incubation of protein–compound mixtures, (iv) preparation of 96-well plate GPC spin columns, (v) loading of protein–compound mixtures onto the GPC spin columns, and (vi) centrifuging the 96-well plates and collecting the spin column eluates. A home-built robot for these sample preparation steps has been described [15] and is illustrated in Fig. 2.8. A number of these steps can be performed semi-

(A)



(B)

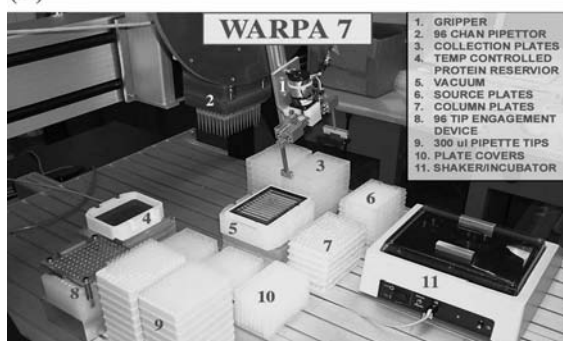


**Fig. 2.8** Broad (A) and detailed (B) views of a gel and sample preparation robot (WARPA7) for the GPC spin column/ESI-MS methodology. For panel (A) note the centrifuge (right end of table), shaker, sample reservoirs and robot arm with a 96-well pipettor. Reprinted from reference [15] with permission from the American Chemical Society.

automatically with commercially available solvent handling systems and human intervention. The final sample handling step is to load the 96-well collection plates, containing the GPC spin column eluates, into an HPLC autosampler for the injection of each sample into the mass spectrometer for analysis.

### 2.2.7

#### **ESI Mass Spectrometer: ESI, APCI, Photodissociation, Positive/Negative Ionization**

The mass spectrometer best suited for drug screening using the GPC spin column ESI-MS technique should be the most sensitive with reasonable resolution so that the low levels of compounds can be detected for the weakest binders. Modern ToF mass spectrometers are ideal for screening since they integrate the

ion intensities for maximum sensitivity with reasonable resolution. Scanning instruments such as ion traps and quadrupole mass spectrometers have been used as well but are less sensitive and have lower resolving powers. Despite the fact that most reported work has utilized electrospray ionization, since most drug like materials are quite polar, APCI and photodissociation sources can be used as well for less polar materials. Detection in both the positive and negative ionization modes is ideal and automatic switching between modes is possible. However, multiple ionization modes consume more protein and sample throughput is reduced versus a single ionization mode. Most reported work to date has been in the positive electrospray ionization mode.

### 2.2.8

#### **ESI Multi-sprayer (MUX) Technology; Sample Throughput; Protein Consumption**

For high throughput screening, Schnier reported assaying in parallel eight spin column eluates injected into eight ballistic gradient HPLC systems, which fed into an ESI mass spectrometer equipped with an eight-channel multisprayer system [18]. The cycle time for assaying eight wells in parallel, containing 640 compounds was 2 min, with injections in the overlay mode. Using this procedure, a GPC spin column kinase receptor ESI-MS assay was performed on 25 000 compounds, pooled twice, in 2.6 h. A total of 320 overlapping hits were observed between the two sample pools. It should be pointed out that, when using multisprayer sources, the achieved sensitivity for the mass spectrometer for each sample is approximately reduced by a factor equivalent to the number of sprayers. This can impact the number of hits observed because weak binders may not be detectable due to the sensitivity lost by the use of multiple sprayers.

Table 2.2 lists the number of samples that can be assayed per day using the multiple sprayer technology, assuming 2 min and 10 min per assay with four and eight sprayers. The numbers of samples assayed are quite impressive especially considering the amount of protein consumed per compound. Of course it should be pointed out that, by pooling four or eight GPC spin column eluates, the same efficiencies can be achieved as for the multisprayer systems; however, it is only necessary to use a single sprayer and not suffer the sensitivity losses as with the multisprayer system. It is also informative to compare sample throughput and protein consumption between the GPC spin column/ESI-MS technology with that of high throughput screening (HTS), the standard method used in exploratory pharmaceutical drug screening. As indicated in Table 2.2, the number of compounds assayed per day by GPC spin column/ESI-MS as mixtures of 80 or 400 compounds is equal to or exceeds the numbers assayed by HTS of single compounds, while the amount of protein consumed by GPC spin column methodology greatly exceeds (~15 times) the amount used by HTS. Note, however, that the tandem chromatographic method GPC reversed-phase (RP) HPLC with ESI-MS detection with mixtures of 3750 compounds greatly exceeds the numbers of compounds assayed per day by HTS and is comparable with the amount of protein consumed per compound by HTS.

**Table 2.2** GPC spin column/ESI-MS drug screening high throughput aspects: compounds assayed per day and protein consumed per compound.

# Compounds/Well	Analysis Time/Well	# Compounds Analyzed/Day			Protein Consumed/Compound	
		Single Sample	Mixture of 4 Wells/ 4-Way MUX	Mixture of 8 Wells/ 8-Way MUX	pmole/compound	µg/compound (MW Protein 25 kDa)
GPC-Spin Column/ESI-MS						
1 Compound/Well	2 min	720	2,880	5,760	100 <sup>a</sup>	2.5 <sup>a</sup>
10 Compounds/Well (Wyeth)	2 min	7,200	28,800	57,600	10 <sup>b</sup>	0.25 <sup>b</sup>
80 Compounds/Well (Amgen)	2 min	57,600	230,400	460,800	3.125 <sup>c</sup>	0.078 <sup>c</sup>
400 Compounds/Well (Novartis)	10 min	57,600	230,400	460,800	0.625 <sup>d</sup>	0.016 <sup>d</sup>
High Throughput Screening (HTS)						
HTS Binding Assay	1.8 sec [0.03 min]	50,000	~	~	0.040	0.0010
HTS Enzyme Assay	1.8 sec [0.03 min]	50,000	~	~	0.004	0.0001
GPC-RP HPLC/ESI-MS						
3,750 Compounds/Well (NeoGenesis/Schering-Plough)	6 min	900,000	~	~	0.027 <sup>e</sup>	0.0007 <sup>e</sup>

<sup>a</sup> 10 µL 10 µM Protein/Well.

<sup>b</sup> 10 µL 10 µM Protein/Well.

<sup>c</sup> 25 µL 5 µM Protein/Well.

<sup>d</sup> 25 µL 10 µM Protein/Well.

<sup>e</sup> 10 µL 10 µM Protein/Well.

### 2.2.9

#### Reversed Phase (RP) HPLC ESI-MS Considerations

Optimization of the RP HPLC system is critical for maximum sample throughput compatible with the mass spectrometer data acquisition capabilities. For highest throughput, the samples should be injected into the HPLC column or directly into the mass spectrometer using the overlay method, i.e., during the ESI-MS assay of a sample, the next sample is retrieved and prepared for injection immediately

upon completion of the previous assay. To further increase throughput, column switching should be coordinated with each injection, i.e., during the HPLC analysis of a sample an identical second HPLC column is conditioned for use immediately upon the completion of the prior HPLC ESI-MS assay. For high throughput primary drug screening, a 2-min ballistic gradient or a 10-min gradient with high solvent flow rates can be used. For secondary screens, 10- to 15-min gradients are used with lower solvent flow rates to optimize ESI-MS sensitivity.

### 2.2.10

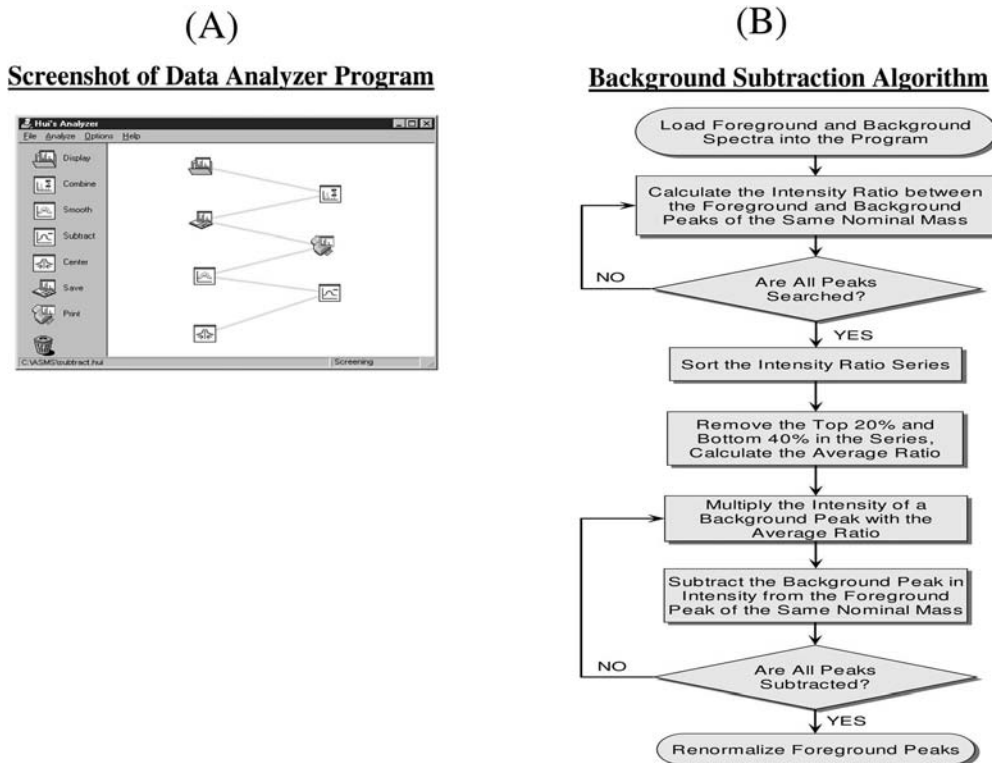
#### **Protein Removal for Optimum Sensitivity**

For small molecule screening, the presence of the multiply charged protein peaks is desirable since it confirms that the protein passed through the column with non-covalently bound drug. In most cases, the low mass origin for the distribution begins at about  $m/z$  700 and is often above the high mass cutoff for a desirable pharmaceutical. However, there are cases where a desired screening candidate may be above  $m/z$  700 and the protein peaks interfere with the drug candidate. In addition, the presence of the protein may cause ion suppression of the singly charged drug candidates and they may not be observed. Under such circumstances, it would be desirable to remove the protein before assaying the screened eluates. A number of methods have been proposed, including protein precipitation and protein adsorption (Porvair P3 protein precipitation filtration plate, Porvair Sciences, Shepperton, UK). Perhaps the most efficient method is to treat the spin column eluate with acid to liberate the drug from the protein and then apply centrifugal ultrafiltration (Millipore Microconcentrator) to the sample for separating the protein (retentate) from the drug (eluate). The ultrafiltration protein-free eluate is then analyzed by ESI-MS. This is illustrated in Fig. 2.2 for studies of the non-covalent interaction of a CMV protease mutant with DFMK. DFMK was available as an impure mixture producing a mass spectrum exhibiting low abundance molecular ions  $[M+2H]^{2+}$  and  $[M+H_2O+H]^{1+}$  (Fig. 2.2A). The mass spectrum for the GPC spin column eluate exhibited the protein peaks overlapping with the  $[M+H_2O+H]^{1+}$  ion and a clearly observed  $[M+2H]^{2+}$  ion (Fig. 2.2B). Upon removal of the CMV protein by centrifugal ultrafiltration, a highly sensitive ESI mass spectrum for the purified DFMK was obtained (Fig. 2.2C) [13].

### 2.2.11

#### **Data Reduction and Automated Interpretation of GPC Spin Column/ESI-MS Data**

The interpretation of the large amounts of data generated in a screening campaign cannot be performed manually. Customized software has been designed to automatically evaluate the data and search for the compounds that non-covalently bind to the protein [21, 22]. For flow injection ESI-MS data of GPC spin column eluates of ten component mixtures, the following steps were taken to automatically interpret the data. The raw data were combined, smoothed, background

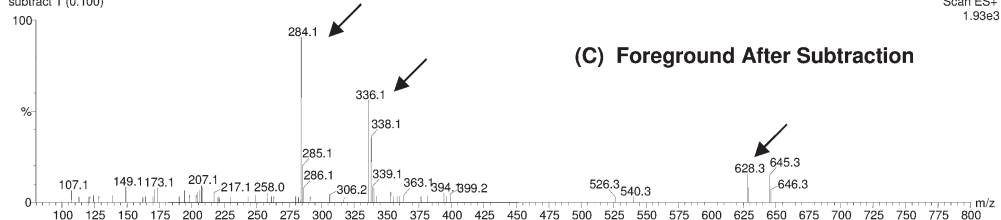
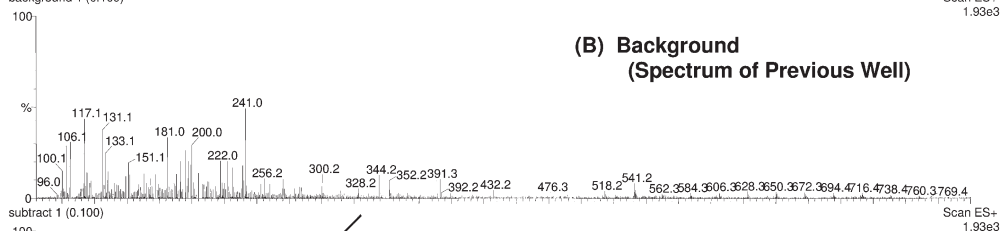
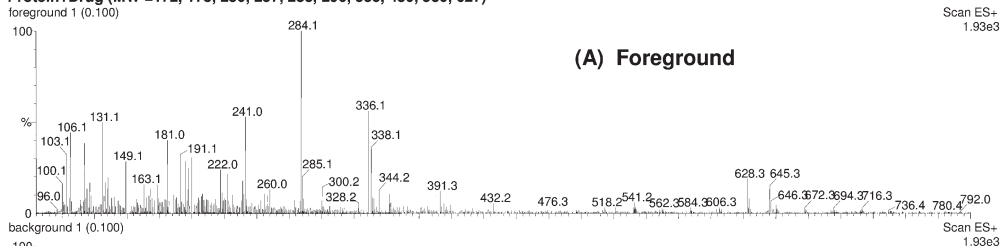


**Fig. 2.9** Automation software for data reduction and analysis of GPC spin column/ESI-MS drug screening data. (A) Screenshot of the data analyzer program for combining, smoothing, background subtracting and centering of raw mass spectral data. (B) Algorithm for background subtraction of the previous spectrum from the foreground spectrum including the normalization of the chemical noise between the two spectra.

subtracted and centroided as illustrated in the screenshot of the data analyzer program (Fig. 2.9A). To remove the chemical background from the spectrum of interest (foreground spectrum), the prior sample analyzed in the screening campaign was used as the background spectrum. The background spectrum was subtracted from the foreground spectrum after applying a multiplication factor to the background spectrum to normalize the chemical noise, as described in the background subtraction algorithm (Fig. 2.9B). Figure 2.10 illustrates the application of the chemical noise background subtraction algorithm to an eluate of a ten-component mixture. For the components in the mixture, the computed  $[M+H]^+$  values are matched with the observed values, the S/N ratios calculated for the observed ions and the theoretical isotopic distribution calculated and matched to the observed distribution. Each of these calculations are scored and weighted for

Protein+Drug (MW =172, 178, 230, 257, 283, 296, 335, 480, 580, 627)

05-Jun-2000 13:32:00

Scan ES+  
1.93e3

**Fig. 2.10** Application of the background subtraction algorithm between two consecutively acquired ESI mass spectra from GPC spin column eluates of ten-component mixtures incubated with RGS4 protein. (A) Foreground ESI mass spectrum for the GPC spin column eluate of a ten-component mixture incubated with RGS4 protein from well A1. (B) Background ESI mass spectrum corresponding to the GPC spin column

eluate of a ten-component mixture incubated with RGS4 from the well analyzed prior to well A1. (C) The foreground ESI mass spectrum for well A1 after subtraction of the background spectrum using the background subtraction algorithm described in Fig. 2.9B. Note the appearance in the subtracted mass spectrum of peaks corresponding to small molecules non-covalently bound to the RGS4 protein, indicated with bold arrows.

each compound in the mixture, and if the total score is greater than a predicted threshold value, the component is considered a “hit”. Generally, a scored S/N ratio greater than 25 is considered a “hit”. An example of an automatically generated drug screening report is illustrated in Fig. 2.11.

**Fig. 2.11** An automatically generated “drug screening ESI-MS report” for the ESI background subtracted mass spectrum, illustrated in Fig. 2.10C, obtained from the GPC spin column eluate of the ten-component mixture incubated with RGS4 protein from well A1. Note that the highlighted components are the three compound hits that non-covalently bind to the RGS4 protein.

# Automatically Generated Drug Screening Computer Report

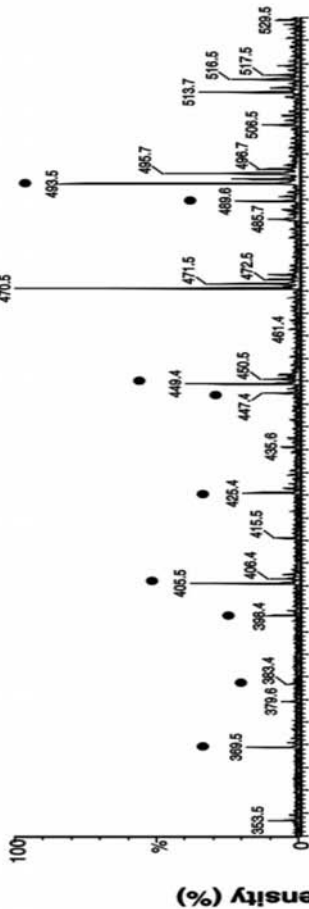
1: AL, C5 H12 N4 O2, 172.0960						
TIC = 3.38E+04 BG Ratio = 1.666404 Base Peak = 284.1 (1.75E+03)						
Mass	Matched Ion	Intensity	Abundance	Isotope	Fit	S/N
173.1	MH	8.8%	1.7%	87.0%		9
190.1	MNH4	3.4%	0.7%	86.6%		3
Score:	S/N	12/12	No Hit			
2: AL, C9 H6 N2 O3, 178.0378						
TIC = 3.38E+04 BG Ratio = 1.666404 Base Peak = 284.1 (1.75E+03)						
Mass	Matched Ion	Intensity	Abundance	Isotope	Fit	S/N
Score:	S/N	0/0	No Hit			
3: AL, C9 H18 N4 O3, 230.1379						
TIC = 3.38E+04 BG Ratio = 1.666404 Base Peak = 284.1 (1.75E+03)						
Mass	Matched Ion	Intensity	Abundance	Isotope	Fit	S/N
Score:	S/N	0/0	No Hit			
4: AL, C10 H9 Cl2 N3 O, 257.0123						
TIC = 3.38E+04 BG Ratio = 1.666404 Base Peak = 284.1 (1.75E+03)						
Mass	Matched Ion	Intensity	Abundance	Isotope	Fit	S/N
258.0	MH	5.8%	1.1%		0	5
Score:	S/N	5/5	No Hit			
5: AL, C14 H13 N5 S, 283.0892						
TIC = 3.38E+04 BG Ratio = 1.666404 Base Peak = 284.1 (1.75E+03)						
Mass	Matched Ion	Intensity	Abundance	Isotope	Fit	S/N
284.1	MH	100.0%	24.7%	96.3%		150
Score:	S/N	150/300	Hit			
6: AL, C14 H12 N6 O2, 296.1022						
TIC = 3.38E+04 BG Ratio = 1.666404 Base Peak = 284.1 (1.75E+03)						
Mass	Matched Ion	Intensity	Abundance	Isotope	Fit	S/N
149.1	M+2H	9.3%	1.8%		0	9
Score:	S/N	9/9	No Hit			
7: AL, C17 H19 Cl2 N3, 335.0956						
TIC = 3.38E+04 BG Ratio = 1.666404 Base Peak = 284.1 (1.75E+03)						
Mass	Matched Ion	Intensity	Abundance	Isotope	Fit	S/N
336.1	MH	6.1%	11.7%	82.9%		71
353.2	MNH4	6.1%	1.2%	76.3%		6
Score:	S/N	77/77	Hit			
8: AL, C23 H20 N4 O8, 480.1281						
TIC = 3.38E+04 BG Ratio = 1.666404 Base Peak = 284.1 (1.75E+03)						
Mass	Matched Ion	Intensity	Abundance	Isotope	Fit	S/N
Score:	S/N	0/0	No Hit			
9: AL, C37 H20 N6 O2, 580.1648						
TIC = 3.38E+04 BG Ratio = 1.666404 Base Peak = 284.1 (1.75E+03)						
Mass	Matched Ion	Intensity	Abundance	Isotope	Fit	S/N
291.1	M+2H	3.1%	0.6%		0	2
Score:	S/N	2/2	No Hit			
10: AL, C39 H41 N5 O3, 627.3209						
TIC = 3.38E+04 BG Ratio = 1.666404 Base Peak = 284.1 (1.75E+03)						
Mass	Matched Ion	Intensity	Abundance	Isotope	Fit	S/N
628.3	MH	17.2%	3.3%	89.5%		19
645.3	MNH4	16.3%	4.5%	90.4%		26
Score:	S/N	45/64	Hit			

Total Hits: 3 / 10 Noise Level = 15

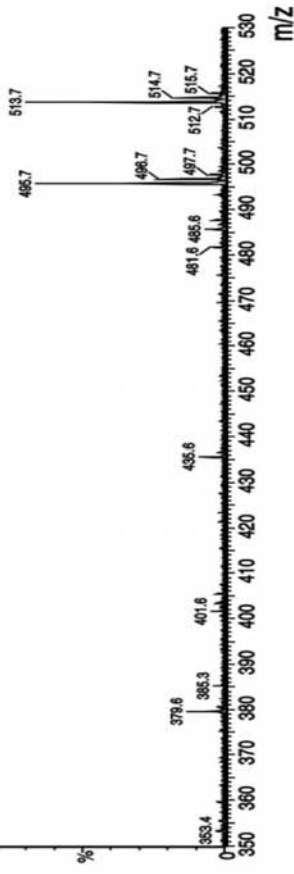


(A) MMP-1 with 10 Known Inhibitors

IC<sub>50</sub>'s 20 nM - 7 μM



(B) 10 Known Inhibitors without MMP-1



Structure	MW	IC <sub>50</sub> (nM)
	426	410
	494	46
	399	140
	406	760
	450	1000
	471	17
	370	3400
	448	1100
	384	7100
	491	540

## 2.3 Results

The GPC spin column/ESI-MS technology has been utilized for primary and secondary screening of drug candidates. For primary screens, large compound libraries are assayed in a high throughput mode to find new non-covalent binders to a target protein. For secondary screens, small subsets of libraries containing compounds believed to bind to a target protein, generally from data obtained using any drug screening technology, are evaluated by the GPC spin column/ESI-MS method to confirm or deny non-covalent binding.

### 2.3.1 Secondary Screens

#### 2.3.1.1 GPC Spin Column/ESI-MS Drug Screening Demonstration Papers

A number of authors demonstrated the early use of the GPC spin column/ESI-MS methodology as a valid way to screen for compounds non-covalently bound to a target protein [11–13, 15]. The behavior of a target protein MMP-1, with a known binding hydroxyamide compound WY252, was evaluated as a singleton and in the presence of a mixture of non-binding compounds. In both cases, no significant difference was observed in the ability to detect the known binder in the mixture. A dramatic illustration of the ability of the GPC spin column/ESI-MS assay to analyze a mixture (in the negative ionization mode) has been demonstrated with MMP-1 protein and ten known hydroxyamide inhibitors with an  $IC_{50}$  range of 9 nM to 7.1  $\mu$ M (Fig. 2.12A). Despite the wide range of  $IC_{50}$  values, all ten compounds were clearly observed in the ESI mass spectrum in the presence of MMP-1. None of the compounds were observed in the GPC spin column eluate when MMP-1 was not present (Fig. 2.12B).

#### 2.3.1.2 Estrogen Receptor Target

A secondary screen for compounds that bind non-covalently to estrogen receptor (ER, MW 67 kDa) was evaluated and illustrated for 17 $\beta$ -estradiol ( $K_d \sim 1$  nM, MW 272 Da), the control compound in the study (Fig. 2.13), and WY234 ( $K_d$  5  $\mu$ M, MW 253 Da; Fig. 2.14). 17 $\beta$ -Estradiol is a relatively less polar material and was studied in the negative atmospheric pressure chemical ionization (APCI) mode since it produced a weak APCI spectrum in the positive mode and no spec-

**Fig. 2.12** ESI (negative ionization mode) mass spectral analysis of the GPC spin column eluate of a mixture containing ten known MMP-1 inhibitors (A) with MMP-1 and (B) without MMP-1 (background). The  $[M-H]^{1-}$  ions for the ten compounds are indicated by solid circles (●) on the spectra.

The same absolute intensity scale is used for both panels. The mixture is composed of the compounds listed at the right of the figure with their corresponding  $IC_{50}$  values. Reprinted from reference [15] with permission from the American Chemical Society.

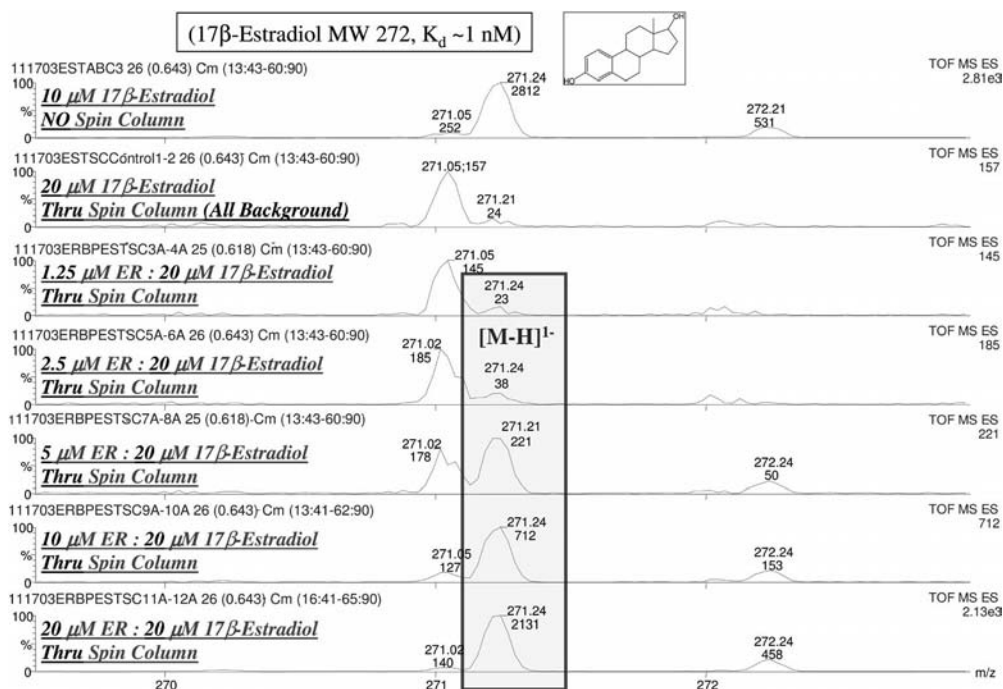


**Fig. 2.13** Negative ionization APCI mass spectra of the GPC spin column eluates of 20  $\mu$ M 17 $\beta$ -estradiol (MW 272 Da,  $K_d \sim 1$  nM) titrated with a variety of ER concentrations (1.25, 2.5, 5.0, 10.0, 20.0  $\mu$ M). A miniature P6 GPC spin column was used with 10- $\mu$ L samples, of which 2  $\mu$ L was injected into the APCI TOF mass spectrometer under low flow

conditions (15  $\mu$ L min $^{-1}$ ). Note that the high resolution capability of the TOF instrument resolves the 17 $\beta$ -estradiol peak from the lower nominal-mass chemical noise. The same absolute intensity scale is used for all panels. The masses and intensities of the peaks are labeled.

trum in either the positive or negative ESI modes. WY234 is a relatively polar material that produced spectra in both the positive and negative ESI modes. Both compounds were titrated with ER. The stronger binding 17 $\beta$ -estradiol exhibited a strong response at a molar ratio of 5  $\mu$ M ER/20  $\mu$ M 17 $\beta$ -estradiol (on the resolved shoulder of a chemical background peak at the same nominal  $m/z$  of 271 [M-H] $^{-1}$ ), while the weaker binding WY234 exhibited a strong response at the higher molar ratio of 60  $\mu$ M ER/300  $\mu$ M WY234 in both the positive and negative ESI modes.

### 2.3.1.3 Non-covalent Binding of Drugs to RNA/DNA Targets

The GPC spin column/ESI-MS method has been applied to a number of RNA problems of pharmaceutical interest as an expedient and sensitive method in drug development strategies involving RNA-metabolizing enzymes [23]. These include: (i) the profiling of drug candidates to identify ones that do not bind to

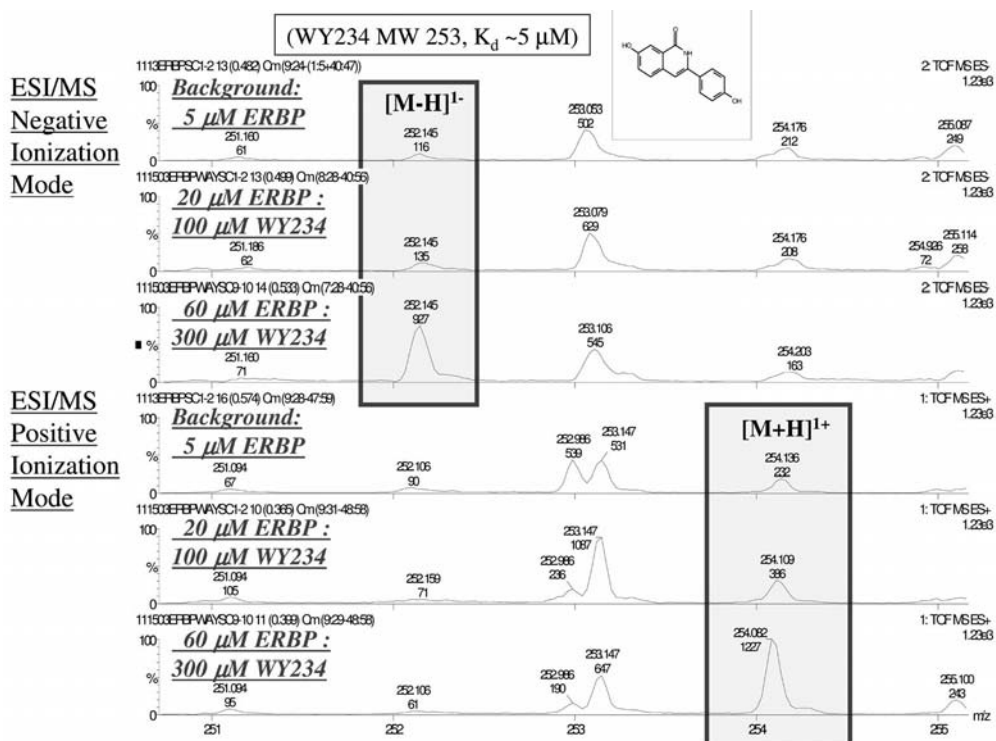


**Fig. 2.14** Positive and negative ionization ESI mass spectra of the GPC spin column eluates of WY234 (MW 253 Da,  $K_d \sim 1 \mu\text{M}$ ), a weak non-covalent binder, with ER, initially prepared at a variety of [WY234]/[ER] molar ratios. A miniature P6 GPC spin column was used with 10  $\mu\text{L}$  samples. The same absolute intensity scale is used for all panels. The masses and intensities of the peaks are labeled.

RNA, (ii) the screening for antiviral compounds that do not bind to RNA but bind specifically to target RNA polymerases, (iii) the evaluation of the binding of aminoglycosides to RNA, and (iv) the evaluation of the binding of DNA intercalators and minor groove binders to RNA.

Certain classes of drugs may be detrimental as therapeutic agents if binding to RNA/DNA is an undesirable secondary side-effect. Such molecules are very likely to be cytotoxic to cells by interfering with the cellular machinery for DNA replication, DNA transcription and RNA translation. Often the inhibition of an enzyme in an *in vivo* cell-based assay is due to the interaction of the drug candidate with the cell's RNA/DNA resulting in false positive results. To eliminate such results and identify only those drug candidates which react with RNA/DNA, a high throughput procedure was evaluated using the GPC spin column/ESI-MS method for screening pharmaceutical candidates by studying their interaction with model duplex and single stranded RNAs. Drug candidates that bind

non-covalently to RNA [23] or DNA can thereby be profiled either as single compounds or more efficiently as mixtures.

Three principal experiments were performed to identify potential drug candidates that bind non-covalently to RNA. The RNA/drug studies were performed under dilute and concentrated conditions using ethidium bromide, a known binder (intercalator) to RNA, as a reference RNA binding compound to validate the experimental strategy. In the first experiment, the formation of molecular ions of the compounds was ascertained under flow injection analysis in both the positive and/or negative ESI-MS ionization modes. In the second experiment, the GPC spin column eluates, recovered after incubation of the drug candidate in the buffer solution without RNA present, were analyzed by ESI-MS. Under these conditions the compounds should be fully retained in the GPC columns, which have a MW cutoff of about 6000 Da. However, any low-level detection of compounds provides a measure of “noise” for gauging false-positive controls. In the third experiment, the eluates recovered from reactions of the compounds with RNA were analyzed by ESI-MS. A biochemical control experiment showed that, under these conditions, the RNA is quantitatively recovered from the GPC spin column. However, the 125-mer RNA (MW 38 641 Da) does not produce an ESI mass spectrum in either the positive or negative ion modes. Compounds which passed through the GPC spin column due to non-covalent binding with the RNA, and which in the absence of RNA were retained by the column, would be flagged as unsuitable for further drug development. Using this technology, mixtures of drug candidates were analyzed, demonstrating a high throughput format for compound analysis. Figure 2.15 illustrates the positive ion ESI mass spectra obtained for a five-component mixture consisting of four drug candidates and ethidium bromide as a control under dilute conditions. Figure 2.15A illustrates the mass spectrum obtained under flow injection conditions, exhibiting molecular ions for ethidium bromide ( $[M]^{1+}$ :  $m/z$  314) and drug candidate WY311 ( $[M]^{1+}$ :  $m/z$  319). The other three components ionize in the negative ion mode but not in the positive ion mode. Figure 2.15B illustrates the mass spectrum obtained for the GPC spin column eluate of the mixture (in the absence of RNA). No ions were observed, indicating that the GPC spin column retained all the compounds. Figure 2.15C illustrates the mass spectrum obtained for the GPC spin column eluate of the mixture incubated in the presence of RNA. As expected ethidium bromide, which non-covalently binds to RNA, passed through the GPC spin column. However WY311, which was incubated with RNA, did not pass through the GPC spin column. The three negative ion compounds also do not pass through the GPC spin column in the absence and presence of RNA. Therefore, all four drug candidates have desirable pharmaceutical profiles in that they do not form non-covalent RNA:drug complexes.

RNA/drug studies with antiviral agents that target-specific RNA polymerases were conducted under dilute and concentrated conditions, viz. 0.25  $\mu$ M RNA/30  $\mu$ M drug and 10  $\mu$ M RNA/300  $\mu$ M drug, respectively, where the model RNA was a 125-mer with a MW of 38 641 Da. Ethidium bromide, a known binder (intercalator) to RNA, was used to validate the experiments under dilute and concentrated

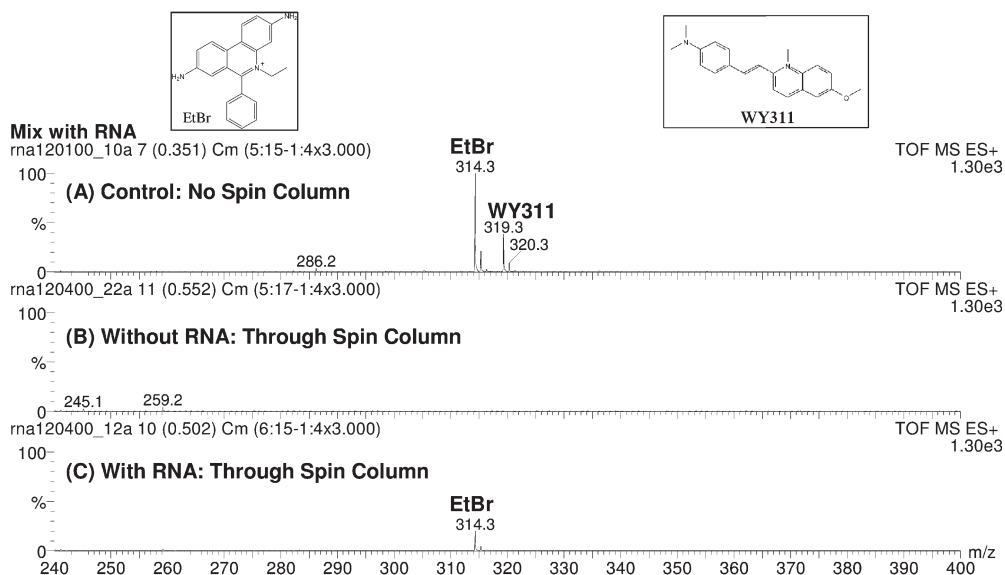


**Fig. 2.15** Positive ion ESI mass spectra under flow injection conditions for a five-component mixture. (A) Mass spectrum for the direct analysis of the mixture of which only two components ionize in the positive ion mode: ethidium bromide (MW 314 Da) and WY311 (MW 319 Da). (B) Mass spectrum of the GPC spin column eluate for the mixture without RNA present. Neither

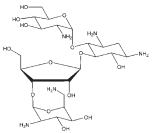
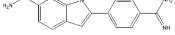
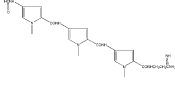
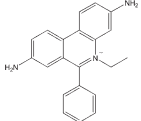
ethidium bromide or WY311 passed through the GPC spin column. (C) Mass spectrum of the GPC spin column eluate of the mixture incubated with RNA. In the presence of RNA, ethidium bromide passed through the GPC spin column as a non-covalent complex with RNA while WY311 did not pass through the GPC spin column and did not form a non-covalent complex with RNA.

conditions. In studies of seven antiviral drug candidates, three compounds at high concentrations exhibited binding to the 125-mer RNA while four compounds exhibited no binding under dilute and concentrated conditions. These results demonstrate that the latter four compounds, which under the different concentration conditions did not bind to the 125-mer RNA, are preferable anti-viral drug candidates.

Similar RNA-binding studies were performed with a variety of aminoglycosides and DNA-binding compounds, using ethidium bromide as a control. Table 2.3 summarizes the GPC spin column/ESI-MS results for paromomycin (an aminoglycoside) and DAPI (a DNA-binding compound), which both bind weakly to the 125-mer RNA. Distamycin (a DNA-binding compound) did not bind to the RNA, whereas ethidium bromide did. The results obtained in these studies further demonstrate that the detection of GPC spin column eluates with ESI-MS can be used successfully to screen, in a high throughput fashion, drug candidates that non-covalently bind to RNA. Likewise, these same procedures can be used to screen compounds that non-covalently bind to DNA.

**Table 2.3** GPC spin column/ESI-MS non-covalent binding studies of RNA with model RNA and DNA binding compounds (intercalators).

(I) No GPC spin column; (II), (III) Through GPC spin column

	Name	Paromomycin		DAPI		Distamycin		EtBr	
	Structure								
	MW	615		277		480		314	
(I) No GPC spin column	Ions (Control)	[M+H] <sup>1+</sup>	[M-H] <sup>1-</sup>	[M+H] <sup>1+</sup>	[M-H] <sup>1-</sup>	[M+H] <sup>1+</sup>	[M-H] <sup>1-</sup>	[M] <sup>1+</sup>	[M+Formic Acid-2H?] <sup>1-</sup>
	Intensity (Control)	82	24	2,320	1,640	2,600	569	20,800	303
(II) Through GPC spin column	Ions (without RNA)	[M+H] <sup>1+</sup>	[M-H] <sup>1-</sup>	[M+H] <sup>1+</sup>	[M-H] <sup>1-</sup>	[M+H] <sup>1+</sup>	[M-H] <sup>1-</sup>	[M] <sup>1+</sup>	[M+Formic Acid-2H?] <sup>1-</sup>
	Intensity (without RNA)	—	—	—	—	—	—	—	—
(III) Through GPC spin column	Ions (with RNA)	[M+H] <sup>1+</sup>	[M-H] <sup>1-</sup>	[M+H] <sup>1+</sup>	[M-H] <sup>1-</sup>	[M+H] <sup>1+</sup>	[M-H] <sup>1-</sup>	[M] <sup>1+</sup>	[M+Formic Acid-2H?] <sup>1-</sup>
	Intensity (with RNA)	32	15	132	76	—	—	13,900	134

RNA 125-mer MW 38,641 Da, Intensity = Ion Counts, Bio-Gel P6 Resin (1,000-6,000 Fractionation Range), RNA/Drug Ratios 10/300 mM/mM, Incubation Buffer 20 mM HEPES, 1 mM DTT, pH 7.5, Centrifuged 3 min at 775xg

2.3.1.4 Amgen Secondary Screens

Hits obtained in the primary screens of 80 compound mixtures (see Section 2.3.2.2) were rerun in the secondary screens as singletons.

2.3.1.5 Novartis Secondary Screens

Novartis GPC spin column/HPLC ESI-MS secondary screens were run in conjunction with their primary screens to confirm the hits found in the primary screen. The method used was identical to that of the GPC spin column/HPLC ESI-MS primary screen, as described in Section 2.3.2.3, except that the hits were run as singletons in triplicate.

2.3.2  
Primary Screens

2.3.2.1 RGS4 Protein Target

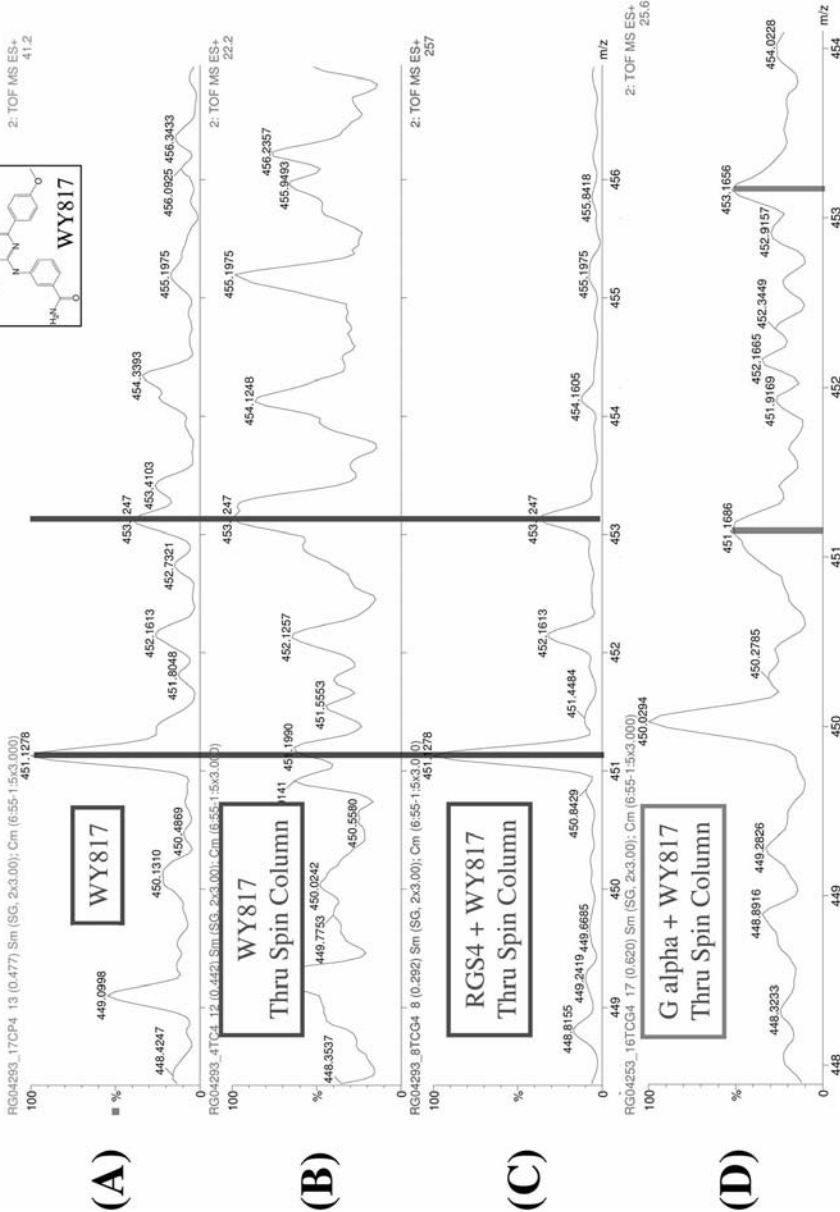
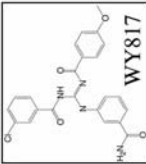
The GPC spin column/ESI-MS screening methodology was used to identify non-covalent inhibitors of regulator of G protein signaling (RGS4) protein. The RGS4 protein accelerates GTPase activity of the subunit of trimeric G protein and is indicated in central nervous system (CNS) disorders. Compounds were sought that

bind to RGS4, interfere with the binding of RGS4 to the G alpha protein, inhibit the endogenous GTPase activity of the G alpha protein ( $G_{i1}$ ) and are active in a luciferase yeast pheromone RGS4 response (functional) assay [24].

About 32 000 compounds were screened to identify compounds that bind non-covalently to RGS4 using the GPC spin column/ESI-MS methodology and 1720 compounds were identified to bind (including very weak binders) to RGS4 [15]. The 50 highest scoring compounds in the ESI-MS analyses were each evaluated by 2D  $^1\text{H}$ - $^{15}\text{N}$  HSQC NMR in the presence of RGS4 protein (see Section 2.3.3.2.2). Two compounds were found to be hits by generating RGS4 protein chemical shift perturbations; however, the region of the perturbations were not in the desired RGS4/G alpha interface region. These compounds still exhibited activity and suggested an allosteric binding site that prevented the necessary conformational change in RGS4 to bind G alpha. Nevertheless, using Lipinski's rules, the list of 1720 compounds was reduced to 743 compounds from which the top 150 candidates were screened in a RGS4/G alpha/GTPase assay. Two of these compounds were found to inhibit the RGS4 function in the GTPase assay. Furthermore, 58 compounds that tested positive in the luciferase pheromone RGS4 assay were also present in the hit list of 1720 compounds of the GPC spin column/ESI-MS assay. These results verify the validity of the GPC spin column/ESI-MS method for drug screening.

As a follow-up to the RGS4 primary screen, the GPC spin column/ESI-MS methodology was applied to a selected series of seven RGS4 drug candidates to identify those compounds that bind non-covalently to RGS4 and not to G alpha [24]. Three ESI-MS experiments were performed with each of the compounds. The first experiment ascertained the response factor for each of the molecular ions formed. The second experiment demonstrated that the drug candidates do not pass through the spin columns in the absence of the proteins. This experiment served as a control to validate the final experiments where the individual protein and drug candidates, after incubation, were passed through a spin column and the eluates analyzed by ESI-MS for residual non-covalently bound drug. Figure 2.16 illustrates the experimental results for compound WY817 (MW 450 Da). Figure 2.16A demonstrates the production of a molecular ion for 250 pg of WY817. Figure 2.16B demonstrates the absence of a molecular ion when  $\sim 100$   $\mu\text{g}$  of WY817 passed through the spin column. Figure 2.16C demonstrates the presence of WY817 when  $\sim 100$   $\mu\text{g}$  of WY817 were incubated in the presence of 25  $\mu\text{L}$  of 125  $\mu\text{M}$  RGS4. Finally, Fig. 2.16D demonstrates the absence of WY817 when  $\sim 100$   $\mu\text{g}$  of WY817 were incubated in 25  $\mu\text{L}$  of 37  $\mu\text{M}$  G alpha protein. These data demonstrate that WY817 satisfies a condition required for a potential small molecule drug candidate in that it non-covalently binds to RGS4 and does not bind to G alpha protein. Since high concentrations of compound and protein were used, WY817 is a weak non-covalent binder to RGS4. The results for all the seven drug candidates, all analyzed identically using the GPC spin column/ESI-MS screening methodology, are tabulated in Fig. 2.17. The relative affinities of the compounds to the proteins were determined from the observed ion abundances normalized to the response factors for each drug candidate. Four compounds

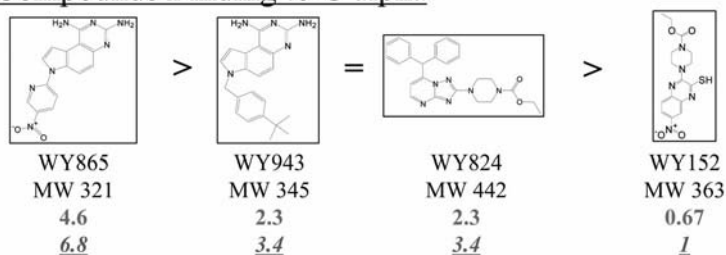




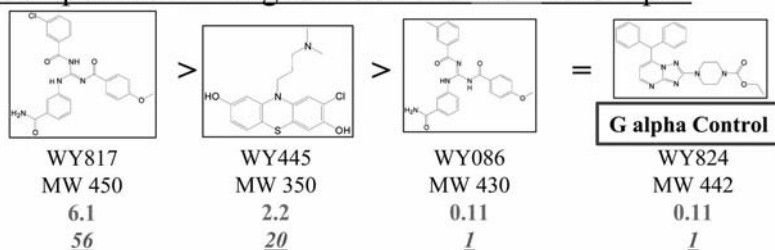
## RGS4/G alpha GPC/ESI Binding Orders

*Ratio of MS Response Thru Spin Column vs Response of ~250 pg of Compound and Normalized Values*

### Compounds Binding to G alpha



### Compounds Binding to RGS4 and NOT to G alpha



Key: Relative Mass Spec Response    *Normalized Mass Spec Response*

**Fig. 2.17** Relative non-covalent binding affinities of a variety of drug candidates to RGS4 and G alpha proteins based on the relative S/N ratios in the GPC spin column/ESI-MS assays to that of ~250 pg of the respective compound (normal font) and after normalizing all the values (underlined italics font).

were found to bind to G alpha and three compounds were found to bind to RGS4 but not to G alpha. The later three compounds have the required binding properties of desirable drug candidates for inhibiting RGS4 (note that compound WY824 bound to both G alpha and RGS4 proteins).

**Fig. 2.16** GPC spin column binding assay of RGS4 and G alpha proteins with WY817 (MW 450 Da). Positive ion ESI mass spectra for compound WY817, a weak binder to RGS4 protein and non-binder to G alpha protein. A miniature P6 GPC spin column was used. (A) ESI-MS response for ~250 pg of reference compound WY817 (no GPC spin column used), (B) ESI-MS response for GPC spin column (P6 gel, 1 cm long, 100 µL volume) eluate when ~100 µg of WY817 were passed

through the GPC spin column. Only chemical noise is observed. (C) ESI-MS response from GPC spin column eluate when ~100 µg of WY817 were incubated with 125 µM RGS4 protein in 25 µL (70 M WY817/1 M RGS4 protein). A moderate signal is observed. (D) ESI-MS response from GPC spin column eluate when ~100 µg of WY817 were incubated with 37 µM G alpha protein in 25 µL (240 M WY817/1 M G alpha protein). No signal is observed, only chemical noise.

### 2.3.2.2 Amgen Primary Screens

Primary screens were performed in duplicate on mixtures of 80 compounds (1  $\mu\text{M}$  per compound, 5  $\mu\text{M}$  protein), where samples in each mixture were orthogonally pooled so that no two compounds that are in one well are also together in another well. Primary hits were achieved when the same compound in two wells were observed. The GPC spin-column eluates were partially resolved using a reversed-phase C18 HPLC column (Waters Xterra 2.1  $\times$  20.0 mm) with a  $\sim$ 1-min ballistic gradient and total cycle time of 2 min. The HPLC eluates were analyzed with a Micromass eight-way MUX interfaced to an LCT ToF ESI-MS system. Achieved throughput was  $\sim$ 100 000 compounds per day.

### 2.3.2.3 Novartis Primary Screens

Typical Novartis screening campaigns utilized GPC spin columns constructed from 96-well plates where 400 compounds per well are assayed, utilizing 25  $\mu\text{L}$  of 10  $\mu\text{M}$  protein and 7  $\mu\text{M}$  of each compound, all in 2% DMSO. Primary hits are detected using microbore HPLC ESI-MS with a gradient run of 10 min with tandem column switching and ion trap MS detection. Figure 2.18 is an example of a primary screen model assay for a mixture of 400 compounds with PKA protein spiked with staurosporine ( $[\text{M}+\text{H}]^{1+}$ ;  $m/z$  467) and olomoucine ( $[\text{M}+\text{H}]^{1+}$ ;  $m/z$  299), strong binders to the PKA protein. The automatically acquired ESI

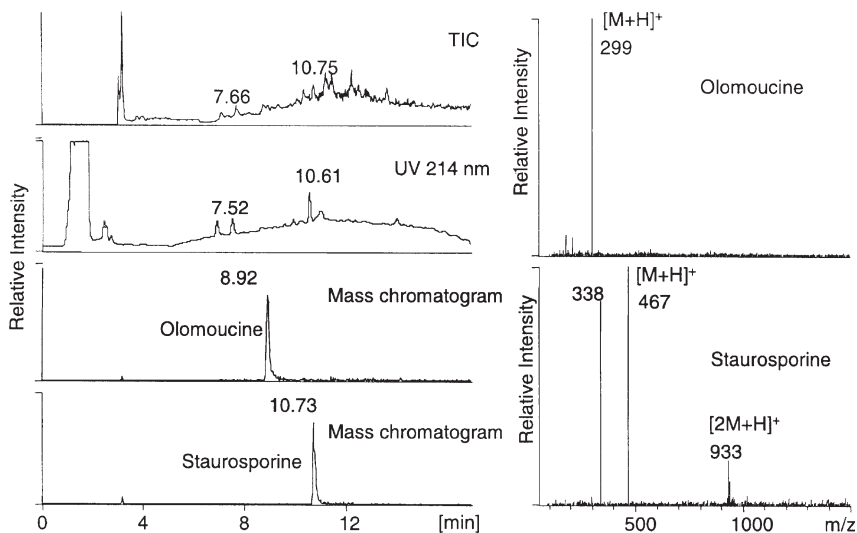


**Fig. 2.18** Raw data from a model GPC spin column/microbore HPLC ESI-MS primary screen of 400 compounds with PKA protein spiked with both staurosporine and olomoucine, known ligands of PKA. (Left) TIC, UV trace at 214 nm, and corresponding mass chromatograms for olomoucine and

staurosporine. (Right) ESI mass spectra for olomoucine and staurosporine obtained from the peaks of the mass chromatograms identifying both ligands. Reprinted from reference [16] with permission from Elsevier Science.

mass spectral and UV raw data illustrate the reliability of the GPC spin column methodology with HPLC ESI-MS and UV detection. The observed primary hits are confirmed by repeating the experiments with the single compounds in the presence and absence (control) of protein, in triplicate. In a screening campaign for ligands non-covalently bound to a ubiquitin-conjugating enzyme target (MW 25 kDa), the analysis of ~500 000 compounds took ~1 month, ~9 days for the primary screens (unattended operation) and the remainder of the time for data evaluation and the confirmation and control screens. Of the 151 compounds which were primary hits (0.03% hit rate), 23 compounds were confirmed hits (0.005% hit rate). The total amount of protein consumed was ~0.5  $\mu$ mol (~9 mg for the 25-kDa protein) and the cost of consumables was <\$10 000. This methodology has also been applied to orphan protein targets, molecular targets with unknown function, including transcription factors, adapter molecules, regulatory subunits, heat shock proteins, metal binding proteins, RNA binding proteins, phosphatases, oxidoreductases and other proteins [16, 19, 20]. IC<sub>50</sub> values up to the 10  $\mu$ M range were detectable using the GPC spin column/ESI-MS methodology. Detection of low-affinity ligands is most likely related to compounds with low off-rates in the GPC step.

### 2.3.3

#### Additional Spin Column Methods

##### 2.3.3.1 Competition Experiments of Inhibitor Mixture with Protein Target

Competition studies of ligand mixtures with a protein target can be efficiently evaluated using the GPC spin column/ESI-MS methodology [13]. The procedure involves quantitation using ESI-MS of the ligands initially present during incubation with a protein target under native conditions and after passing through a GPC spin column. This has been demonstrated for the binding competition between two ligands, a peptidic trifluormethylene ketone (TFMK) and a dibromoquinazalone (DBQ), with CMVP. An equimolar mixture of TFMK (MW 545 Da) and DBQ (MW 489 Da) was prepared with CMVP A144L. The molar ratios for CMVP A144L to each of the inhibitors in the mixture were 1:5:5. The CMVP-inhibitor mixture was incubated for 1 h at 25 °C and the spin column eluate was analyzed by ESI-MS. The ESI mass spectrum (Fig. 2.19C) exhibited peaks for both TFMK and DBQ. For quantitation purposes, individual ESI reference spectra were obtained from mixtures prepared (without GPC spin column analysis) as 1:1 molar ratios of CMVP A144L:TFMK (Fig. 2.19A) and CMVP A144L:DBQ (Fig. 2.19B). From the integrated areas of the reference compounds (Fig. 2.19A, B) and eluted compounds (Fig. 2.19C), the molar ratios of recovered CMVP A144L:TFMK:DBQ were calculated to be 1.0:0.2:2.2. These results suggest that DBQ prevents the binding of TFMK to CMVP. It is possible that DBQ and TFMK compete for the same site and that DBQ was more strongly bound to that site than TFMK. Alternatively, the binding of DBQ to more than one site of CMVP may induce a conformational change that prevents TFMK from binding.

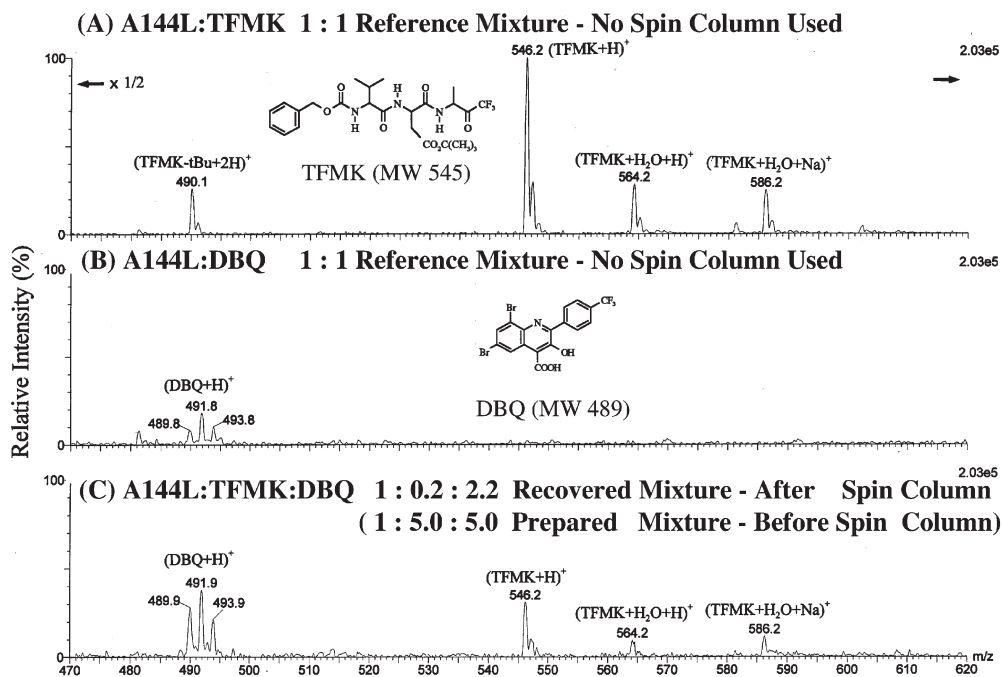


**Fig. 2.19** GPC spin column/ESI-MS non-covalent binding competition study to determine the relative binding affinities of CMVP A144L with TFMK (MW 545 Da) and DBQ (MW 489 Da). ESI mass spectra obtained from the GPC spin column screening assay for a mixture of the inhibitors TFMK and DBQ, which form non-covalent complexes with CMVP A144L. (A) ESI mass spectrum of a reference mixture (no GPC spin column used) consisting of a 1:1 molar ratio of CMVP A144L:TFMK. (B) ESI mass spectrum of a reference mixture (no spin column used) consisting of a 1:1 molar ratio of CMVP A144L:DBQ. (C) ESI mass spectrum of a spin column eluate of a

mixture of CMVP A144L:TFMK:DBQ with a recovered molar ratio of 1.0:0.2:2.2, initially prepared with molar ratios of 1:5:5, respectively. The molar ratio of CMVP A144L:TFMK:DBQ recovered after passing through the spin column was computed from the integrated areas of the peaks in Fig. 2.19A with respect to the corresponding reference peaks in Fig. 2.19B, C. Note that all spectra are normalized to the same intensity scale and were obtained using 10  $\mu$ L of the mixture where the protease concentration was 20  $\mu$ M in each sample. Reprinted from reference [13] with permission from John Wiley & Sons.

Competition binding experiments between mixtures of compounds and the insulin-like growth factor receptor (IGFr) protein were conducted to determine the relative binding affinities of the compounds to the IGFr protein. The IGFr protein is a potential target for inhibition by anti-cancer agents. The underlying theoretical assumptions for these competition studies are that, when the binding site and the off-rates for the drug candidates are identical, the relative ESI mass spectral responses for the drug candidates are inversely related to their  $K_d$ s ( $EC_{50}$ s) and  $IC_{50}$ s (see Section 2.1.4.3). Two mixtures of three compounds each

were prepared and incubated with IGFr protein. One compound, WY360, common to both mixtures, served as a reference/calibration point for comparing the affinities for all the compounds in both mixtures. Three experiments were performed for each mixture and the ESI mass spectral data for the molecular ion regions for each of the components are illustrated in Fig. 2.20. Figure 2.20A illustrates the molecular ions generated from the GPC spin column eluate of the drug mixtures incubated with IGFr. The S/N ratio for the molecular ion of each component was computed and these are listed in Table 2.4. Figure 2.20B illustrates the molecular ions generated for each component from the GPC spin column eluates of the mixtures without IGFr. This control experiment indicates that no compounds passed through the GPC spin columns, thereby validating the non-covalent binding results obtained when the IGFr protein was present with the compounds. Figure 2.20C illustrates the ESI mass spectral responses for each of the compounds present in the mixtures, each of equal concentration (without using GPC spin columns). The S/N ratios for each of the individual components in the mixture were determined and are listed in Table 2.4. The ratio of each ESI-MS response for the individual components for the spin column eluates when compared to that of the response factor for the pure drugs corresponds to the relative binding affinity for each of the compounds: the higher the ratio the stronger the non-covalent binding affinity and the lower the expected  $K_d$  and  $IC_{50}$ . The response of WY360 was used to normalize the responses from both mixtures. As indicated in Table 2.4, the order of the binding affinities measured by the GPC spin column/ESI-MS method correlates with the reported  $IC_{50}$  values. The dynamic range of measurable binding affinities using this technique is limited by the linear dynamic range of the signal detected by the ToF mass spectrometer used ( $\sim 10^3$  counts  $s^{-1}$ ) and the concentrations of the samples used in the experiments. In all these competition experiments, the concentrations of all the compounds are identical and greater than that of the protein.

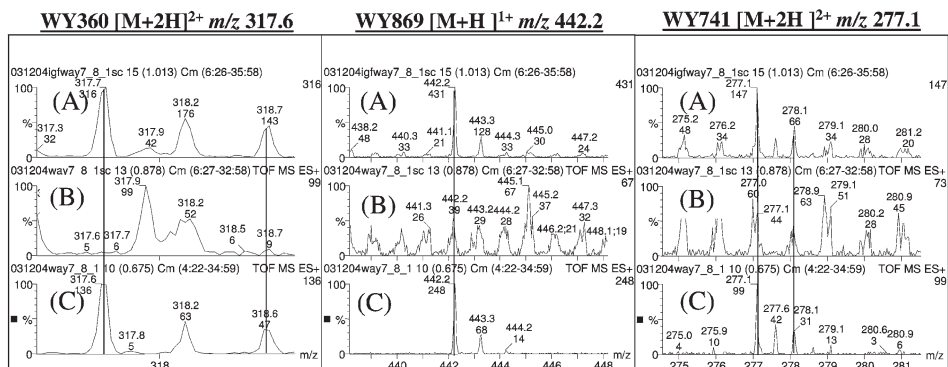
#### 2.3.3.2 GPC Spin Column/ESI-MS Determination of Binding Sites

An important question that needs to be addressed in any screening study is the determination of whether or not the ligand is non-covalently bound to the active site of the target protein. A number of simple GPC spin column ESI-MS screening methods have been developed to answer this question. These methods include the use of mutated proteins where the active site has been modified, GPC spin column/ESI-MS coupled with NMR (GPC spin column/MS/NMR) and displacement of known binders. Titration experiments with molar excesses of ligand to protein (described below in Section 2.3.3.2.4) can also be used to determine whether single or multiple binding sites are available in the protein.

##### 2.3.3.2.1 Comparing Non-covalent Binding of Ligand to Mutated Proteins

The GPC spin column/ESI-MS methodology with mutated CMV proteases was utilized to characterize the non-covalent binding site of ligand inhibitors [13]. The following illustration demonstrates the use of the GPC spin column screening technique to characterize non-covalent binding of TFMK to specific sites

## Mixture 1



## Mixture 2

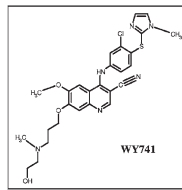
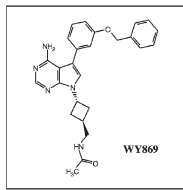
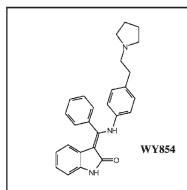
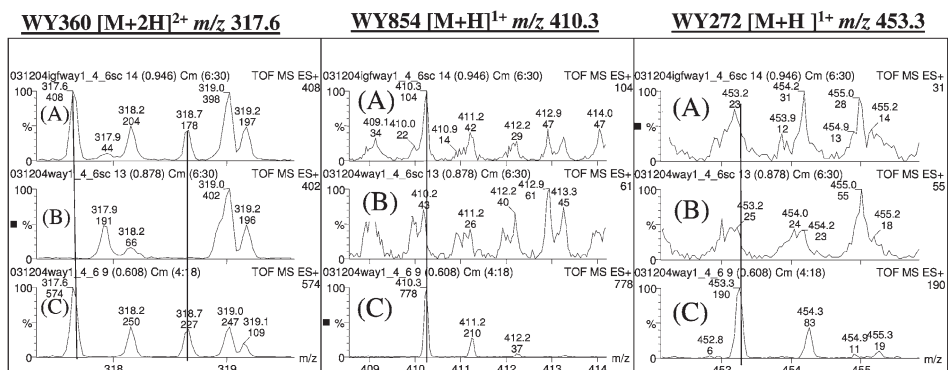


**Fig. 2.20** Non-covalent binding competition experiments between IGF $\alpha$  protein target and mixtures of compounds assayed using the GPC spin column/ESI-MS methodology. Mixture 1 compounds are WY360 (MW 633 Da), WY869 (MW 441 Da), and WY-741 (MW 552 Da). Mixture 2 compounds are WY360 (MW 633 Da), WY854 (MW 409 Da), and WY272 (MW 452 Da). Note that WY360 is present in both mixtures so that both mixtures can be correlated. The molecular ion region for the ESI mass spectra are illustrated for: (A) the GPC spin column

eluates of incubated components of mixtures 1 and 2 with IGF $\alpha$  protein in a molar ratio ( $\mu$ M) of 56:28, respectively, diluted 2 $\times$  with water and 10  $\mu$ L injection; (B) the GPC spin column eluates of incubated components of mixtures 1 and 2 originally each 56  $\mu$ M per compound, diluted 2 $\times$  with water and 10  $\mu$ L injection; and (C) direct infusion of mixtures 1 and 2 with each component 2.2  $\mu$ M, 1  $\mu$ L injection. The signal-to-noise ratios for the ESI-MS molecular ion peaks for each of the components of both mixtures are summarized in Table 2.4.

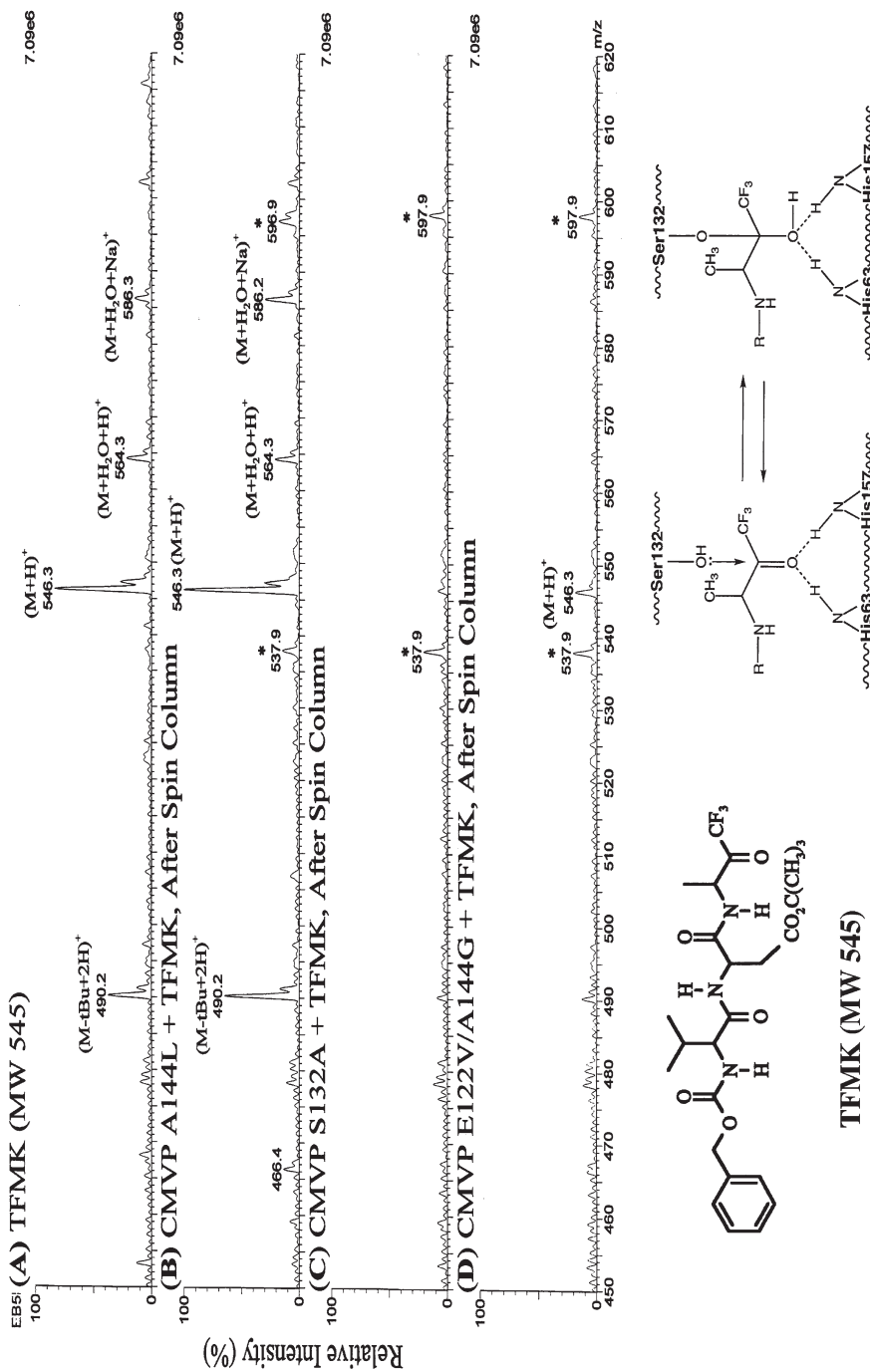
**Table 2.4** Relative competitive binding affinities computed from GPC spin column/ESI-MS data of IGF $\alpha$  protein for compounds in mixtures.

Mixture	Compound Number	<i>m/z</i>	MS Signal/ Noise Thru Spin Column (Fig. 2.20 A)	MS Signal/ Noise No Spin Column (Fig. 2.20 C)	MS Signal/ Noise Ratio of Ratios (Fig. 2.20 A/C)	Normalized Signal/Noise Ratio of Ratios	IC <sub>50</sub> (nM)
1	WY360	317.6	44.1	67.0	0.658	1	5
	WY869	442.2	13.4	61.0	0.219	0.332	40
	WY741	277.1	4.88	23.8	0.205	0.312	78
2	WY360	317.6	67.0	113.8	0.588	1	5
	WY854	410.3	2.06	74.3	0.028	0.047	121
	WY272	453.3	Not Detected	23.6	~	~	440

in CMVP by comparing the non-covalent binding affinities of the inhibitor to CMVP mutants A144L, S132A and E122V/A144G. CMVP A144L represents wild type CMVP (with respect to enzymatic activity) and is the reference protease for the binding studies. Serine residue 132 is the active site residue predicted to be responsible for nucleophilic attack of the DFMK class of inhibitors and is likely to be essential for the non-covalent binding of these inhibitors to CMVP. Mutation of S132 to an alanine residue in CMVP S132A inactivates the protease and is likely to prevent binding of the DFMK and TFMK class of inhibitors to the protease. Mutation of E122 to a valine residue in CMVP E122V/A144L has also been shown to destroy the enzymatic activity of CMVP [25] but the effect on inhibitor binding is not known.

The ESI mass spectrum for inhibitor TFMK (MW 545 Da), prior to passage through a GPC spin column (Fig. 2.21A), exhibits the characteristic molecular ions (M+H)<sup>1+</sup>, (M+H<sub>2</sub>O+H)<sup>1+</sup>, (M+H<sub>2</sub>O+Na)<sup>1+</sup> and (M+H<sub>2</sub>O+K)<sup>1+</sup> at *m/z* 546.3, 564.3, 586.3 and 602.1, respectively, as well as one fragment ion [M-C(CH<sub>3</sub>)<sub>3</sub>+2H]<sup>1+</sup> at *m/z* 490.2. In a control study, the ESI mass spectrum for the spin column eluate of pure TFMK (not illustrated) shows the absence of TFMK in the low mass region from *m/z* 415 to *m/z* 620. The ESI mass spectra of the spin column eluates of TFMK incubated with the CMVPs A144L, S132A and E122V/A144G (each originally prepared at a molar ratio of CMVP:TFMK of 1:40) are illustrated in Fig. 2.21B, C, D, respectively. All the spectra are normalized for the abundance of pure TFMK (in Fig. 2.21A) that corresponds to a ~1:1 molar ratio of CMVP:TFMK. (The ion distributions for the proteases occur over the *m/z* range of 750 to 1200 and are not depicted.) In a control study, the ESI mass spectrum of pure CMVP A144L (not illustrated) shows the presence of background peaks at *m/z* 538 and *m/z* 598, which correspond to solvent complexes of acetic acid (indicated with stars in Fig. 2.21B, C, D). From these data, it is evident that TFMK coelutes with CMVP A144L (in a CMVP:TFMK molar ratio





of  $\sim 1:1$ ), does not coelute with CMVP S132A and only very slightly coelutes with CMVP E122V/A144G (in a molar ratio of CMVP:TFMK of  $1:<0.05$ ).

The specificity of these coelution results are consistent with S132 as the active site nucleophile of CMVP and demonstrates that this screening methodology can detect specific binding of inhibitors to CMVP. From the crystal structure, the active site residues of CMVP are S132, H157 and H63 [26–29]. Mutation of S132 is therefore predicted to prevent binding to CMVP of active site directed inhibitors such as TFMK. A stabilized (reversible) hemiacetal protease–inhibitor complex is believed to have formed with CMVP A144L, as schematically illustrated in Fig. 2.21 (bottom). However, when S132 is replaced with a lipophylic amino acid residue such as alanine, the active site is destroyed and the mutated protease is incapable of tightly binding to the inhibitor. E122 is quite far from the active site and is involved in a salt bridge within the protease. Thus, the conformation of protease mutant E122V may be significantly different from the wild-type CMVP due to disruption of the salt bridge. CMVP E122V is enzymatically inactive and this study shows (Fig. 2.21D) that this mutant protease cannot bind significantly to the TFMK inhibitor.

### 2.3.3.2.2 GPC Spin Column/ESI-MS/NMR

The coupling of the GPC spin column/ESI-MS screening results with NMR (2D  $^1\text{H}$ - $^{15}\text{N}$  HSQC) is a powerful method for confirming that the non-covalent binders identified by the MS experiments truly bind at the predicted active site by observing NMR chemical shift perturbations in the vicinity of the protein active site [1, 15]. In contrast, the absence of chemical shift perturbations or a random distribution of chemical shift changes on the protein surface would imply a lack of an interaction of the compound with the protein or potentially the existence of non-specific binding. The development of the GPC spin column/MS/NMR assay

**Fig. 2.21** ESI mass spectra obtained from the GPC spin column/ESI-MS screening assay for a variety of CMVP mutants incubated with TFMK illustrating specificity of the protease–inhibitor complex. (A) ESI mass spectrum of inhibitor TFMK (MW 545 Da), no GPC spin column used. The TFMK response corresponds to that of the molar concentrations of protein used in panels B, C and D. (B) ESI mass spectrum of the GPC spin column eluate of CMVP A144L and TFMK, originally incubated at a molar ratio of 1:40. The measured  $[\text{CMVP A144L}]/[\text{TFMK}]$  molar ratio for the eluate is  $\sim 1:1$ . (C) ESI mass spectrum of the spin column eluate of CMVP S132A and TFMK, originally incubated at a molar ratio of 1:40. TFMK does not coelute. (D) ESI mass spectrum of CMVP E122V/A144G and

TFMK, originally incubated at molar ratio of 1:40. The measured  $[\text{CMVP E122V/A144G}]/[\text{TFMK}]$  molar ratio for the eluate is  $1:<0.05$ . The mass range illustrated only covers the inhibitor region and not the higher mass range for CMVP. The peaks labeled with stars (\*) at  $m/z$  538 and  $m/z$  598 are background peaks produced from the solvent (3% acetic acid in 1:1 water:acetonitrile, v:v). Note that all spectra are normalized to the same intensity scale. (Bottom) Scheme illustrating the stabilized (reversible) hemiacetal CMVP–inhibitor complex proposed between the triad of amino acid residues S132, H157 and H63 and TFMK. The wavy lines (~~~~) represent CMVP with the specific amino acid residues shown. Reprinted from reference [13] with permission from John Wiley & Sons.

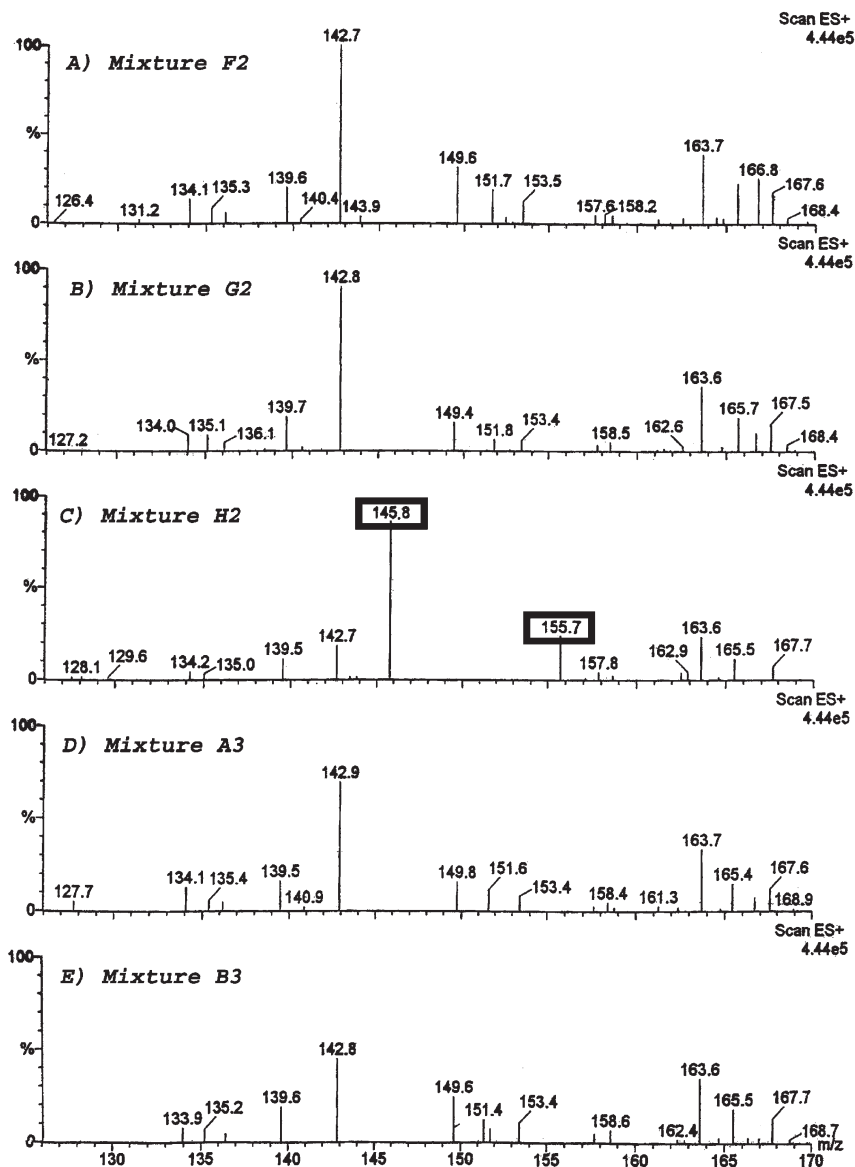


**Fig. 2.22** ESI mass spectra acquired from the GPC spin column eluates of five consecutive library mixtures, each of ten components, incubated with MMP-1 to screen for compounds non-covalently bound to the protein. (A), (B) and (D), (E) ESI mass spectra for mixtures F2, G2 and A3, B3, respectively, serve as background spectra for the ESI spectrum of the sample of interest

(C) mixture H2. Nearly all the ions are from the protein, buffer and solvent background except for the ions at  $m/z$  145.8 and  $m/z$  155.7. These two ions are protonated molecular ions for compounds with MWs of 145 Da and 155 Da that bind to MMP-1. Reprinted from reference [1] with permission from Elsevier Science.

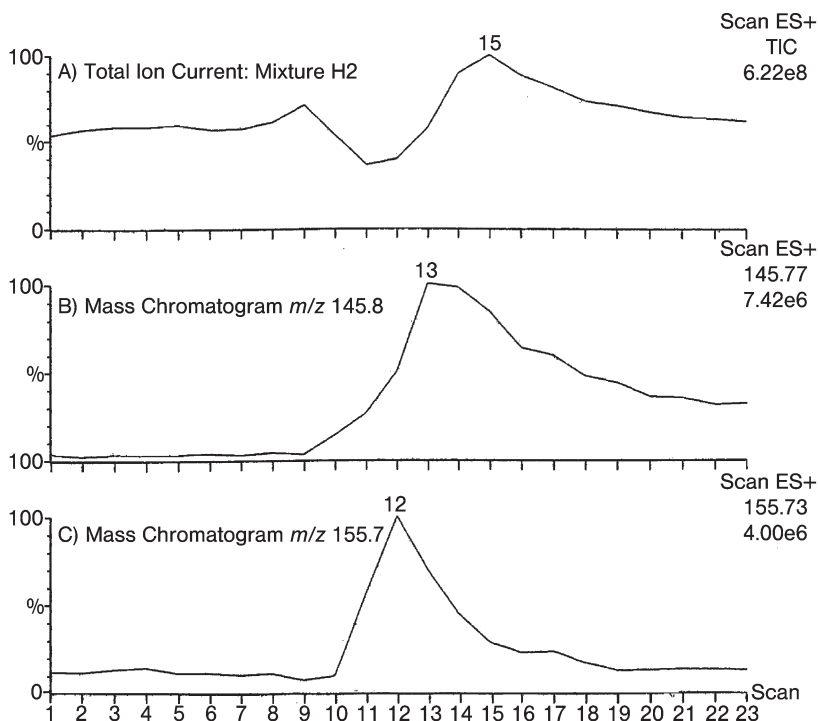


**Fig. 2.23** (A) ESI total ion chromatogram from mixture H2 (see Fig. 2.22C). Mass chromatograms for the components with (B)  $m/z$  145.8 and (C)  $m/z$  155.7 from the GPC spin column eluate originating from mixture H2 of ten components incubated with MMP-1 (the ESI mass spectrum for this mixture is illustrated as Fig. 2.22C). The evolution of

these peaks with time (scan numbers) demonstrates that these are unique components that eluted from the mixture while the other eight components were retained by the GPC spin column and not observed in the ESI mass spectrum. Reprinted from reference [1] with permission from Elsevier Science.

utilized MMP-1 (collagenase), a matrix metalloproteinase and a small compound library.

To demonstrate the screening of compounds for a potential anticancer program, a small chemical library was selected and mixtures of ten chemically compatible compounds were prepared where each compound had a different molecular weight. The mixtures were incubated with MMP-1 and analyzed using the GPC spin column/ESI-MS flow injection approach. The resulting mass spectral data were analyzed in two dimensions. The ESI mass spectra of the mixtures analyzed before and after the mixture of interest were compared to identify background peaks and new peaks associated with the mixture of interest. The second dimension analyzed was the evolution in time of the mass chromatograms for each of the components of the mixture to verify that they were components of the mixture and not from the instrumental chemical background that remained

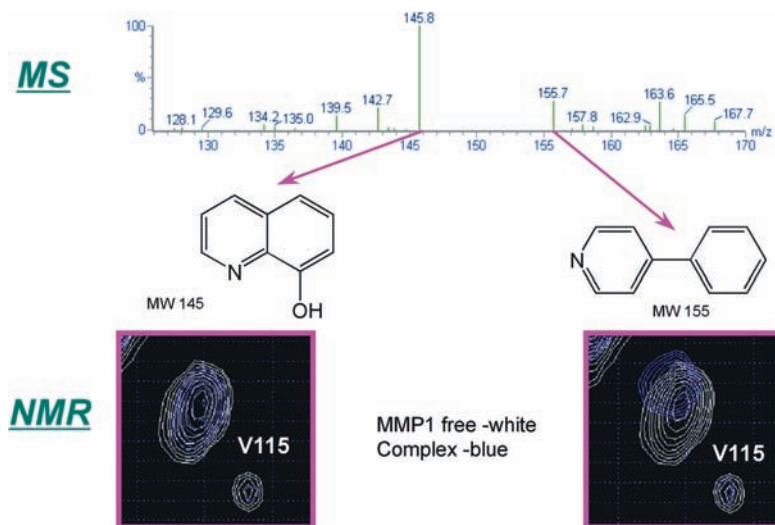


**Fig. 2.24** Screening results of GPC spin column/MS/NMR assay of MMP-1 protein with library mixture H2 (see Figs. 2.22C, 2.23), illustrating the complementary nature of the MS and NMR experiments in the MS/NMR MMP-1 assay. (Top) ESI mass spectrum of the GPC spin column eluate of the library mixture H2 shows the presence of molecular ions for two compounds (MWs 145 Da, 155 Da) indicating non-covalent binding to the MMP-1 protein. (Bottom) Expanded 2D  $^1\text{H}$ - $^{15}\text{N}$  HSQC NMR spectral regions of the MMP-1 protein in the presence

and absence of each of the two compounds (overlaid blue and white spectra, respectively) indicating that the *p*-phenyl pyridine (MW 155 Da) induces a chemical shift change for V115 in the MMP-1 active site while the 8-hydroxyquinoline (MW 145 Da) does not induce a chemical shift change at V115. Therefore, the *p*-phenyl pyridine binds non-covalently to the active site in MMP-1 while 8-hydroxyquinoline binds non-specifically to MMP-1. Reprinted from reference [1] with permission from Elsevier Science.

constant with time. Figure 2.22 illustrates a total of five mass spectra sequentially acquired, two from mixtures immediately prior to the mixture of interest (Fig. 2.22A, B), the mixture of interest (Fig. 2.22C) and two from mixtures immediately following the mixture of interest (Fig. 2.22D, E). Note that most of the mass spectral peaks in the mixture of interest (Fig. 2.22C) are present in most of the other spectra except for peaks at  $m/z$  145.8 and  $m/z$  155.7. Figure 2.23 illustrates the total ion chromatogram for the mixture of interest (Fig. 2.23A) and the mass chromatograms for the ions with  $m/z$  145.8 (Fig. 2.23B) and  $m/z$  155.7 (Fig. 2.23C). Note that, in both cases, mass chromatographic peaks evolve in time, confirming the fact that these two components with MWs 145 Da and 155 Da, respectively, passed through the GPC spin column non-covalently bound to MMP-1 and did not originate from the instrumental chemical background. These two compounds when analyzed in the same manner but in the absence of MMP-1 by GPC spin column/ESI-MS did not produce any detectable mass spectral peaks, further verifying that the compounds were non-covalently bound to MMP-1.

The two compounds with MWs 145 Da and 155 Da identified by GPC spin column/ESI-MS as non-covalent binders to MMP-1 were then each analyzed in the presence of MMP-1 by 2D  $^1\text{H}$ - $^{15}\text{N}$  HSQC NMR (Fig. 2.24). Chemical shift perturbations associated with the active site amide amino acid residue V115 was not observed for the MW 145 Da compound but was observed for the MW 155 Da compound. The NMR data verifies the fact that the MW 155 Da compound, corresponding to *p*-phenyl pyridine, was specifically bound to the MMP-1 active site while the MW 145 Da compound, corresponding to 8-hydroxyquinoline, was non-specifically bound to MMP-1. The *p*-phenyl pyridine compound was independently found by other NMR studies to bind to stromelysin (MMP-3) [30]. Limitations associated with the 2D  $^1\text{H}$ - $^{15}\text{N}$  HSQC NMR methodology are the need for  $^{15}\text{N}$ -enriched protein and the requirements of large quantities of protein due to the low sensitivity of the NMR experiments.

### 2.3.3.2.3 Displacement Experiments of Known Binders

At this point in time, no GPC spin column ESI-MS experiments have reported the displacement of a prepared non-covalently bound ligand with a protein with an even stronger binder. (Related competition experiments were described above in Section 2.3.3.1.) This type of experiment could be easily implemented using the GPC spin column/ESI-MS methodology and was recently demonstrated in the related screening methodology, utilizing in tandem the GPC and reversed phase HPLC methods with ESI-MS detection [31] (see Chapter 3). Typical experiments that can be routinely implemented using GPC spin column/ESI-MS techniques include the displacement of storosporine by stronger binders to kinases and the non-displacement/displacement of storosporine by allosteric binders.

### 2.3.3.2.4 Titration of Drug Using GPC Spin Column/ESI-MS: Coelution of Multiple Ligands Non-covalently Bound to Protein Target

A titration study was undertaken to determine the extent of non-covalent binding between the inhibitor DBQ (MW 489 Da) and the protein CMVP A144L. This experiment was conducted by incubating a fixed amount (50 pmol) of the protein CMVP A144L with from 0–40 mol excesses of DBQ. The incubated materials were then subjected to GPC spin column analysis, whereby the eluate containing the tightly bound inhibitor was analyzed by ESI-MS under denaturing conditions to quantitate the mole ratio of inhibitor to protease (D/P). Figure 2.25 illustrates the  $[\text{M}+\text{H}]^{1+}$  region of the ESI mass spectrum for these titration experiments. (Note the characteristic 1:2:1 dibromo isotopic intensity distribution.) Table 2.5 summarizes the quantitative results for these titration experiments by tabulating the  $[\text{drug}]/[\text{protein}]$  (D/P) molar ratios during the incubation reaction and after elution from the spin column. Figure 2.26 graphically illustrates a plot of the D/P mole ratios of the reaction vs the bound mixtures. Note that at low reaction D/P mole ratios, from 0 to 1, the slope of the curve rises rapidly and continuously levels off from reaction D/P mole ratios from 1 to 40. These results suggest that there may be specific non-covalent binding at low D/P mole ratios up to about 0.5 D/P mole ratios, but as the reaction D/P ratio increases less specific non-covalent

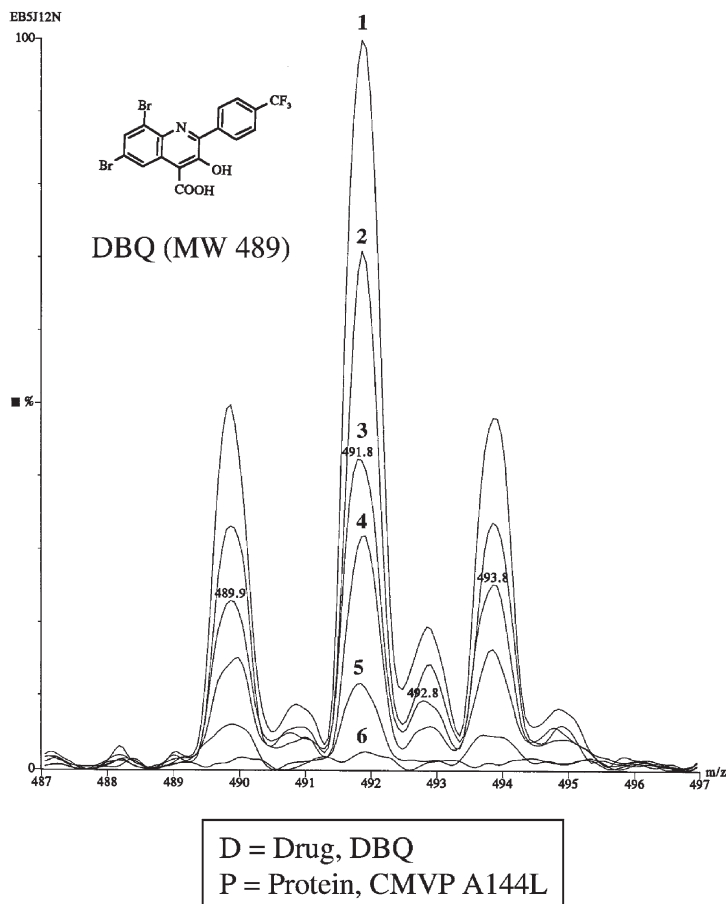


**Fig. 2.25** Positive ion ESI mass spectra of the molecular ion region of DBQ (MW 489 Da) in a titration study of the GPC spin column eluates of DBQ (Drug, D) incubated with CMVP A144L (Protein, P) with molar ratios of 1, 10, 20 and 40 of [D]/[P]. A reference ESI mass spectrum of DBQ and CMVP A144L of a molar ratio of 1:1 is also displayed. The amount of protein in all the experiments were kept constant at 50 pmol.

adducts are more abundant. Nevertheless, these simple GPC spin column/ESI-MS titration experiments demonstrate the usefulness of the technique to determine whether non-specific binding is likely with ligands to specific protein targets when excess ligand is present. Furthermore, as in this case, if excess drug non-covalently binds to the protein target, the ligand is probably unsuitable as a drug candidate. However, if as the reaction D/P ratio increases and the curve for the product D/P ratio asymptotically approaches 1, the ligand is reacting at a specific site in the protein target, most likely the active site. Recently, condensed

**Table 2.5** Mole ratios for titration of DBQ drug (D) and cytomegalovirus protease A144L (P) during incubation (Reaction) and after passing through a GPC spin column (Coeluted).

Spectrum <sup>+</sup>	D/P Mole Ratio <sup>#</sup>	
	Reaction	Coeluted
1	40	3.1
2	20	2.2
3	10	1.3
4	1*	1*
5	1	0.4
6	0	0

<sup>#</sup> P kept constant at 50 pmole.

\* Spiked standard (no spin column).

<sup>+</sup> See Figure 2.26.

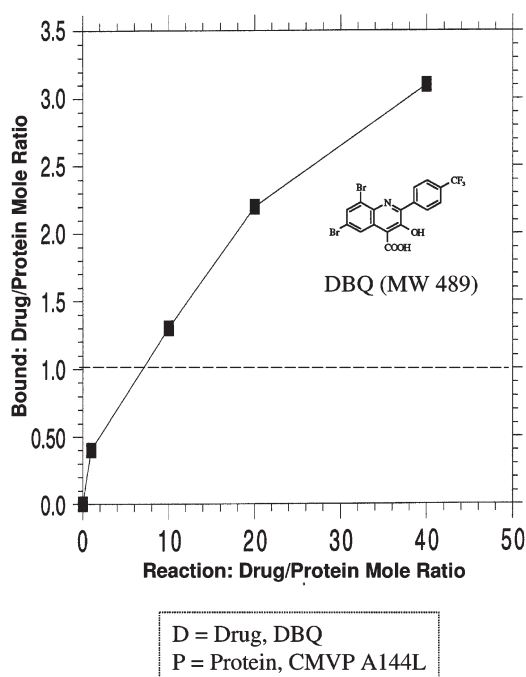


**Fig. 2.26** Plot of the DBQ (Drug, D)/CMVP A144L (Protein, P) molar ratios for the incubated concentrations as a function of the non-covalently bound concentrations as determined in the titration study of the GPC spin column eluates assayed by ESI-MS (see Table 2.5). The shape of the curve indicates that up to three drugs bind non-covalently and non-specifically to CMVP A144L.



phase H/D exchange methods have been developed to determine the stoichiometry of the ligand–protein interaction by monitoring by ESI-MS the mass shifts of the protein undergoing H/D exchange upon titration with a ligand [32–34] (see Chapter 11).

### 2.3.3.3 Obtaining MS $EC_{50}$ s and $K_d$ s for Ligands Non-covalently Bound to Protein Active Sites

In biological systems, the concentration needed to inhibit 50% of a cellular reaction is called the  $IC_{50}$  for that reaction and is often obtained by titrating a given reagent with a fixed biological system. Similarly, a spin-column mass spectral (MS)  $EC_{50}$  (or  $K_d$ ) can be obtained by analyzing the GPC spin-column ligand eluates from samples that were titrated with various concentrations with a fixed amount of protein. The mass spectral response for the ligand that non-covalently bound to the protein should produce a sigmoidal response curve and the concentration corresponding to 50% response from the extremes in the sigmoidal plot corresponds to the MS  $EC_{50}$ . The  $EC_{50}$  value corresponds to the  $K_d$  value for the protein–ligand complex. (See the theoretical discussion in Section 2.1.4.4.) Recently, Schnier and coworkers [18] demonstrated this application of the GPC spin-column ESI-MS technique for obtaining the MS  $EC_{50}$ s of a variety of compounds that non-covalently bind to a kinase protein. Figure 2.27 illustrates the

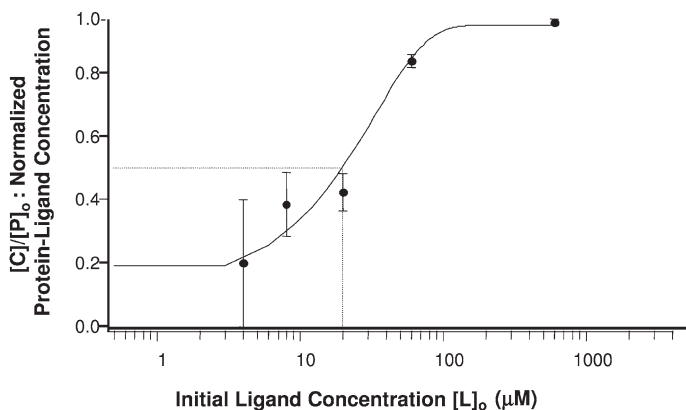


**Fig. 2.27** GPC spin column ESI-MS determination of MS  $EC_{50}$ s. Plot of fraction of known ligand inhibitor non-covalently bound to a fixed amount of kinase protein ( $[P]_0$ , 5  $\mu M$ ) as a function of initial ligand concentration  $[L]_0$ . The MS  $EC_{50}$  corresponds to the free ligand concentration  $[L]$  when 50% of the initial protein concentration is tied up as protein–ligand complex. At 50% of the

normalized protein–ligand concentration, the  $[L]_0$  value is read off the figure as 20  $\mu M$ . The corresponding free ligand concentration  $[L]$  is  $[L]_0 - [C]$ , see Eq. (4), where  $[C]$  is  $[P]_0/2.0$   $\mu M$  or 2.5  $\mu M$ . The MS  $EC_{50}$  value is therefore 17.5  $\mu M$ , reasonably consistent with the biological  $IC_{50}$  of 8  $\mu M$  (see reference [18]).

data obtained from a GPC spin-column ESI-MS titration of a known kinase inhibitor as a function of mass spectral ligand response and initial ligand concentration for a fixed protein concentration. From the sigmoidal fit of the mass spectral data, the MS EC<sub>50</sub> value was 17.5  $\mu$ M while the measured biological IC<sub>50</sub> kinase inhibitor value was 8  $\mu$ M. Good correlations were reported for the mass spectral EC<sub>50</sub> and biological IC<sub>50</sub> values for a variety of inhibitors.

#### 2.3.3.4 Multiple Passes Through Spin Columns – Finding Strongest Binders

An application of GPC spin column/ESI-MS methodology is to re-equilibrate the eluate of a spin column and pass it again through a second spin column to detect by ESI-MS the enriched tighter binding ligands at the expense of the weaker binding ligands [35]. This approach is applicable to mixtures of unknown structures and unknown concentrations for differentiating strong from weak binders. For these systems, the relative ESI-MS responses for different unknown compounds are not indicative of their relative binding affinities since their concentrations in the original mixture are unknown. Cycling the initial eluate through fresh GPC spin columns can deconvolute this. The strong binders will be selectively found in the eluates at the expense of the weak binders. After each pass of the eluate through the GPC spin column, the relative change in mass spectral response for the strong binder will be considerably less than that for the weak binder.

#### 2.3.3.5 Reverse Screening with GPC Spin Columns

A proposed method for screening mixtures of potential drug candidates, using GPC spin columns, is to analyze by ESI-MS the retained compounds after elution of the protein from the spin column [36]. In such studies, the absence of a ligand indicates strong affinity towards a target while the presence of a ligand indicates much weaker or no affinity. The disadvantage of this reverse GPC spin column screening methodology is that all the retained compounds in a mixture have to be eluted from the GPC spin column, identified and quantitated, while in the direct GPC spin column methodology only the desired non-covalent binders are detected in the eluate.

## 2.4 Conclusions

### 2.4.1

#### GPC Spin Column/ESI-MS: Ease of Use, Mixture Analysis, High Speed, Reliability, Uncoupling of GPC from ESI-MS and HPLC ESI-MS

The GPC spin column/ESI-MS screening protocol rapidly analyzes the ability of small organic molecules to bind non-covalently to target protein molecules.

The methodology takes advantage of and combines the inherent strengths of size exclusion gel chromatography in the spin column mode, reversed-phase HPLC and ESI-MS in a nearly universal high throughput screening approach. The methodology has been automated to screen large libraries of chemical compounds with known structures while optimizing each operational step and minimizing analysis time. The methodology has been successfully applied at a number of pharmaceutical institutions, resulting in the identification of a number of new and novel inhibitors/antagonists of proteins of therapeutic interest. The GPC spin column/ESI-MS screening methodology can complement and even supplement the cell-based assays presently in vogue for HTS and surely deserves exploration when HTS fails to identify compounds with desirable biological and chemical properties.

A unique feature of this technology is the uncoupling of the GPC spin column step from the (HPLC)/ESI-MS detection step, thereby permitting the optimization of each of the analytical steps to rapidly produce reliable drug discovery non-covalent binding data. The strength of this GPC spin column screening methodology is the direct identification in mixtures of the small minority of ligands that non-covalently bind to protein targets and the elimination of non-binding ligands from the eluate. A challenge for the GPC spin column/ESI-MS technique is the identification of ligands of low abundances and unknown structures, as found in very complex mixtures, such as natural products extracts, tissue extracts and combinatorial libraries, that bind non-covalently with protein targets. With advanced software and future instrumental developments, screening problems of this complexity will be solvable using the GPC spin column/ESI-MS technology.

The site of non-covalent binding of the ligand to the protein is not directly measurable by GPC spin column/ESI-MS. To directly obtain the binding site, X-ray and NMR techniques are used. Site directed mutagenesis and displacement of known binders coupled with GPC spin column/ESI-MS can be used to identify non-covalent binding sites.

#### 2.4.2

##### **Comparison of GPC Spin Column/HPLC ESI-MS with Tandem Chromatographic Method of GPC/HPLC ESI-MS**

In principle, the analytical results obtained by the GPC spin column/HPLC ESI-MS methodology described in this chapter should be similar to the results obtained using the tandem chromatographic method of GPC/reversed-phase HPLC ESI-MS described in Chapter 3. There are practical advantages for each method. Since each of the chromatographic and mass spectral steps are done serially for the GPC spin column/HPLC ESI-MS methodology, each of the steps can be performed and optimized individually. In the event of mass spectrometer failure, the production of spin column eluate samples can proceed and samples can be stored for future analysis. In contrast, the parallel methodology of tandem GPC/reversed-phase HPLC ESI-MS requires the simultaneous optimization of multi-

ple systems, with the concomitant risk of a downed system when there is a failure in any one of the units. However, the tandem GPC/reversed-phase HPLC ESI-MS requires less human intervention, provided all systems operate smoothly.

### 2.4.3

#### **Future Developments**

A number of future improvements in mass spectrometry, chromatography, microfluidics and automation will certainly improve the sensitivity, resolution and reliability in the GPC spin column/MS technology. Upon developing and implementing these newer technologies, the GPC spin column/MS screening technology will become another venue for reliable ultra-high throughput screening, complementing high throughput screening functional assays presently in use in numerous pharmaceutical and government laboratories.

##### **2.4.3.1 MS and HPLC Improvements**

Besides using the most recently developed ESI mass spectrometers with sensitivity and resolution improvements of  $10\times$  and  $3\times$ , respectively, principally with time-of-flight mass spectrometers, the most significant improvements in GPC spin column/HPLC ESI-MS screening will come from the application of ultra-performance liquid chromatography (UPLC) where the combination of a very high pressure liquid chromatograph together with LC columns containing particles of  $1.7\ \mu\text{m}$  has been demonstrated to produce chromatograms of remarkably improved resolution (peak widths of 5 s) with retention times also reduced by a factor of up to 10 times and with high sensitivity, generally  $3\text{--}10\times$  more than with conventional LC columns (Waters Acquity UPLC System) [37]. With these improvements in both LC and MS instrumentation, factors in sensitivity of  $30\text{--}100\times$  could be achieved vs presently used instrumentation, permitting more reliable detection of weaker signals in screening weak binders and enabling the use of smaller amounts of precious protein in a screening program, all achievable in considerably reduced cycle times.

##### **2.4.3.2 Use of Automated Nanospray for Greater Sensitivity and Smaller Sample Size (Less Protein/Drug)**

Maximum sensitivity and minimum use of sample resources are achieved in ESI-MS by spraying samples in the nanospray mode, which is inefficient in the manual mode but with recent technological advances can be fully automated [38–42]. Using the Advion automated nanospray system, the ultimate in sample sensitivity can be achieved for directly analyzing GPC spin column eluates with a reduced effect on signal suppression due to the presence of buffer ions. This technique should give strong response to molecules of low abundance, viz. weak non-covalent binders, and thereby conserve the amount of protein used in the GPC spin column assay. The down side of the nanospray technique is the longer data acquisition times needed to acquire spectra of high signal-to-noise ratio.

#### 2.4.3.3 Microfluidic Systems: Sensitivity, High Speed

Presently, chip-based microfluidic technologies are being developed which efficiently incorporate low-flow liquid chromatographic methods with low-flow chip-based nanoelectrospray devices in very low dead volume systems [43]. By analyzing the GPC spin column eluates in a microfluidic HPLC mode, these chip-based technologies offer potentially promising methodologies for achieving the idealized goals of high throughput drug screening by minimizing sample consumption while using ESI-MS as the optimum universal detector, operating with multiple sprayers [44, 45] in parallel with duty cycles approaching 100% for the analysis of produced ions [46].

#### 2.4.3.4 GPC Spin Column Eluates Analyzed by ESI/Ion Mobility/Mass Spectrometry

A future development for drug discovery using the GPC spin column/ESI-MS technique is to eliminate the HPLC/UPLC instrumentation in the analysis of the GPC spin column eluates and achieve the needed separation on a millisecond scale by use of an ion mobility (IM) interface to the ESI-ToF mass spectrometer. The ion mobility interface resolves compounds on the basis of their resistance to flow under an applied electric field and a buffer gas due to the differences in collision cross-sections (shapes, charges, masses) of the molecules. The IM/MS technique has the unique capability of resolving ligands that are structural isomers. This approach has been demonstrated for drug screening by Clemmer and co-workers for identifying members of a combinatorial peptide library that bind to ribonuclease S-protein using affinity selection chromatography for non-covalent binders and ESI/IM/MS for characterization of the ligands [47].

#### 2.4.3.5 GPC Spin Columns with Matrixless MALDI-MS and Gyros GPC Microfluidic ESI/MALDI-MS System

MALDI-MS techniques for high throughput drug screening are not as popular as the ESI-MS techniques. This is due in part to the facts that the  $m/z$  values of small drug molecules often overlap with the chemical noise of the MALDI matrix and that small drug molecules often fragment or rearrange, unlike peptides or oligonucleotides. In the near future, these disadvantages may be reduced dramatically with the use of porous silicon chips as MALDI targets [48–50] since no matrix is required, or with sol-gel derived polymeric matrixes which produce nearly no chemical background noise [51]. In addition, these laser desorption/ionization mass spectrometric methods, respectively referred to as DIOS and SGALDI, may produce molecular ions without any significant fragmentation and may even be more sensitive than traditional MALDI methods (see Chapter 8). The future prospects for these technologies become even more promising when GPC methods are coupled with the recently demonstrated microfluidic compact disc (CD) technology (Gyros System; Gyros AB, Uppsala, Sweden) for MALDI sample preparation [52, 53]. The design of the Gyros system is a natural for GPC spin column applications because when the CD is spun it behaves as a centrifuge to produce the spin column eluate. A significant breakthrough for drug screening will be

made when the microfluidic CD technology is developed in the GPC spin column mode coupled to ESI-MS as well as MALDI-MS in the IR and UV laser modes.

## Acknowledgements

The author greatly appreciates the technical comments and suggestions of Paul Schnier, Boris Cheskis, Anthony Amin and Scott Mayer and acknowledges his colleagues Ellen Baum, Robert Powers and Franklin Moy for inspiring and encouraging this work.

## References

- 1 R. Powers, M. M. Siegel: Applications of NMR and MS to anticancer drug discovery, in *Novel Anti-Cancer Agents: Strategies for Discovery and Clinical Testing*, ed. A. A. Adjei, J. K. Buolamwini, Elsevier Science, New York, **2006**, pp 107–190.
- 2 M. M. Siegel: Mass spectrometry-based drug screening assays for early phases in drug discovery, in *Integrated Strategies for Drug Discovery Using Mass Spectrometry*, ed. Mike S. Lee, John Wiley & Sons, **2005**, pp 27–70.
- 3 M. M. Siegel: Early discovery drug screening using mass spectrometry, *Curr. Top. Med. Chem.* **2002**, 2, 13–33.
- 4 J. A. Loo: Electrospray ionization mass spectrometry: a technology for studying noncovalent macromolecular complexes, *Int. J. Mass Spectrom.* **2000**, 200, 175–186.
- 5 J. A. Loo, V. Thanabal, H.-Y. Mei: Studying noncovalent small molecule interactions with protein and RNA targets by mass spectrometry, *Mass Spectrom. Biol. Med.* **2000**, 2000, 73–90.
- 6 J. A. Loo, K. A. Sannes-Lowery: Studying noncovalent interactions by electrospray ionization mass spectrometry, *Mass Spectrom. Biol. Mater.* **1990**, 1998, 345–367.
- 7 J. A. Loo: Studying noncovalent protein complexes by electrospray ionization mass spectrometry, *Mass Spectrom. Rev.* **1997**, 16, 1–23.
- 8 S. A. Hofstadler, R. H. Griffey: Analysis of noncovalent complexes of DNA and RNA by mass spectrometry, *Chem. Rev.* **2001**, 101, 377–390.
- 9 R. D. Smith, J. E. Bruce, Q. Wu, Q. P. Lei: New Mass spectrometric methods for the study of noncovalent associations of biopolymers, *Chem. Soc. Rev.* **1997**, 26, 191–202.
- 10 A. J. R. Heck: Ligand fishing by mass spectrometry, *Spectrosc. Eur.* **1999**, 11, 12, 14, 16, 17.
- 11 M. M. Siegel, K. Tabei, G. A. Bebernitz, E. Z. Baum: A rapid method for screening low molecular weight compounds non-covalently bound to proteins using size exclusion and mass spectrometry applied to inhibitors of human cytomegalovirus protease, in *Proceedings of the American Society for Mass Spectrometry and Allied Topics* (45th ASMS Conference), Palm Springs, CA, **1997**, WPD 124.
- 12 Y. M. Dunayevskiy, J.-J. Lai, C. Quinn, F. Talley, P. Vouros: Mass spectrometric identification of ligands selected from combinatorial libraries using gel filtration, *Rapid Commun. Mass Spectrom.* **1997**, 11, 1178–1184.
- 13 M. M. Siegel, K. Tabei, G. A. Bebernitz, E. Z. Baum: Rapid methods for screening low molecular mass compounds non-covalently bound to proteins using size exclusion and mass spectrometry applied to inhibitors of human

- cytomegalovirus protease, *J. Mass Spectrom.* **1998**, 33, 264–273.
- 14 E. C. Hulme (ed.): *Receptor–Ligand Interactions: A Practical Approach*, Oxford University Press, Oxford, **1992**.
  - 15 F. J. Moy, K. Haraki, D. Mobilio, G. Walker, R. Powers, K. Tabei, H. Tong, M. M. Siegel: MS/NMR: a structure-based approach for discovering protein ligands and for drug design by coupling size exclusion chromatography, mass spectrometry, and nuclear magnetic resonance spectroscopy, *Anal. Chem.* **2001**, 73, 571–581.
  - 16 I. Muckenschnabel, R. Falchetto, L. M. Mayr, I. Filipuzzi: SpeedScreen: label-free liquid chromatography-mass spectrometry-based high-throughput screening for the discovery of orphan protein ligands, *Anal. Biochem.* **2004**, 324, 241–249.
  - 17 E. J. Martin, R. E. Critchlow, D. C. Spellmeyer, S. Rosenberg, K. L. Spear, J. M. Blaney: Diverse approaches to combinatorial library design, *Pharmacochem. Libr.* **1998**, 29, 133–146.
  - 18 P. D. Schnier, R. Deblanc, G. Woo, W. Gigante, J. Cheetham: Ultra-high throughput affinity mass spectrometry for screening protein receptors, in *Proceedings of the 51st ASMS Conference on Mass Spectrometry and Allied Topics*, Montreal, **2003**, WPC 049.
  - 19 I. Filipuzzi: SpeedScreen, a label-free, affinity-based high-throughput screening technology for the discovery of orphan protein ligands, *Chimia* **2004**, 58, 585–587.
  - 20 H. Zehender, F. le Goff, N. Lehmann, I. Filipuzzi, L. M. Mayr: SpeedScreen: the “missing link” between genomics and lead discovery, *J. Biomol. Screen.* **2004**, 9, 498–505.
  - 21 H. Tong, D. Bell, K. Tabei, M. M. Siegel: Automated data massaging, interpretation, and e-mailing modules for high throughput open access mass spectrometry, *J. Am. Soc. Mass Spectrom.* **1999**, 10, 1174–1187.
  - 22 H. Tong, K. Tabei, F. Moy, R. Powers, M. M. Siegel: Software package for the analysis of high-throughput drug screening data obtained by ESI/MS, in *Proceedings of the American Society for Mass Spectrometry and Allied Topics* (48th ASMS Conference), Long Beach, **2000**, pp 935–936 (WPH320).
  - 23 H. Tong, K. Tabei, A. Amin, M. Olson, G. Bebernitz, M. M. Siegel: Identification of compounds non-covalently bound to RNA using GPC spin columns with ESI MS detection, in *Proceedings of the 49th American Society of Mass Spectrometry Conference on Mass Spectrometry & Allied Topics*, Chicago, **2001**, Poster Th 274.
  - 24 M. M. Siegel, Y. Wang, C. Bender, A. Gilbert, K. Young: Applications of GPC spin column/ESI-MS for identifying non-covalent inhibitors of RGS4 protein, a potential CNS target, in *Proceedings of the 52nd ASMS Conference on Mass Spectrometry and Allied Topics*, Nashville, **2003**.
  - 25 S. Thaisrivongs, D. T. Pals, W. M. Kati, S. R. Turner, L. M. Thomasco, W. Watt: Design and synthesis of potent and specific renin inhibitors containing difluorostatine, difluorostatone, and related analogs, *J. Med. Chem.* **1986**, 29, 2080–2087.
  - 26 H. S. Shieh, R. G. Kurumbail, A. M. Stevens, R. A. Stegeman, E. J. Sturman, J. A. Pak, A. J. Wittwer, M. O. Palmier, R. C. Wiegand, B. C. Holwerda, W. C. Stallings: Three-dimensional structure of human cytomegalovirus protease, *Nature* **1996**, 383, 279–282.
  - 27 X. Qiu, J. S. Culp, A. G. DiLella, B. Hellmig, S. S. Hoog, C. A. Janson, W. W. Smith, S. S. Abdel-Meguid: Unique fold and active site in cytomegalovirus protease, *Nature* **1996**, 383, 275–279.
  - 28 L. Tong, C. Qian, M. J. Massariol, P. R. Bonneau, M. G. Cordingley, L. Lagace: A new serine-protease fold revealed by the crystal structure of human cytomegalovirus protease, *Nature* **1996**, 383, 272–275.
  - 29 P. Chen, H. Tsuge, R. J. Almassay, C. L. Gribbskov, S. Katoh, D. L. Vanderpool, S. A., Margosiak, C. Pinko, D. A. Mathews, C.-C. Kan:

- Structure of the human cytomegalovirus protease catalytic domain reveals a novel serine protease fold and catalytic triad, *Cell* **1996**, *86*, 835–843.
- 30 P. J. Hajduk, G. Sheppard, D. G. Nettlesheim, E. T. Olejniczak, S. B. Shuker, R. P. Meadows, D. H. Steinman, G. M. Carrera, Jr., P. A. Marcotte, J. Severin, K. Walter, H. Smith, E. Gubbins, R. Simmer, T. F. Holzman, D. W. Morgan, S. K. Davidsen, J. B. Summers, S. W. Fesik: Discovery of potent nonpeptide inhibitors of stromelysin using SAR by NMR. *J. Am. Chem. Soc.* **1997**, *119*, 5818–5827.
  - 31 D. A. Annis, N. Zazef, C.-C. Chuang, M. P. Scott, H. M. Nash: A general technique to rank protein–ligand binding affinities and determine allosteric versus direct binding site competition in compound mixtures. *J. Am. Chem. Soc.* **2004**, *126*, 15495–15503.
  - 32 M. M. Zhu, R. Chitta, M. L. Gross: PLIMSTEX: a novel mass spectrometric method for the quantification of protein–ligand interactions in solution. *Int. J. Mass Spectrom.* **2005**, *240*, 213–220.
  - 33 M. M. Zhu, D. L. Rempel, M. L. Gross: Modeling data from titration, amide H/D exchange, and mass spectrometry to obtain protein–ligand binding constants. *J. Am. Soc. Mass Spectrom.* **2004**, *15*, 388–397.
  - 34 M. M. Zhu, D. L. Rempel, Z. Du, M. L. Gross: Quantification of protein–ligand interactions by mass spectrometry, titration, and H/D exchange: PLIMSTEX. *J. Am. Chem. Soc.* **2003**, *125*, 5252–5253.
  - 35 R. G. Davis, R. J. Anderegg, S. G. Blanchard: Iterative size-exclusion chromatography coupled with liquid chromatographic mass spectrometry to enrich and identify tight-binding ligands from complex mixtures, *Tetrahedron* **1999**, *55*, 11653–11667.
  - 36 P. A. Wabnitz, J. A. Loo: Drug screening of pharmaceutical discovery compounds by micro-size exclusion chromatography/mass spectrometry, *Rapid Commun. Mass Spectrom.* **2002**, *16*, 85–91.
  - 37 J. R. Mazzeo, U. D. Neue, M. Kele, R. S. Plumb: Advancing LC performance with smaller particles and higher pressure, *Anal. Chem.* **2005**, *77*, 460A–467A.
  - 38 T. N. Corso, G. A. Schultz, J. Li, C. G. Alpha, B. I. Smith, N. A. Shinde, J. C. Ackerman, G. S. Sheldon: A microchip-based multi-nozzle nanoelectrospray device, in *Proceedings of the 50th ASMS Conference on Mass Spectrometry and Allied Topics*, Orlando, **2002**, MPM 390, 1350.pdf, available at: [www.advion.com](http://www.advion.com).
  - 39 S. Zhang, C. K. Van Pelt, G. A. Schultz: Rapid, fully automated nano-ESI/MS/MS analysis of excised 2D gel spots by the nanomate robot and ESI chip, in *Proceedings of the 50th ASMS Conference on Mass Spectrometry and Allied Topics*, Orlando, **2002**, ThPB 025, 1549.pdf, available at: [www.advion.com](http://www.advion.com).
  - 40 C. K. Van Pelt, S. Zhang, J. D. Henion: Characterization of a fully automated nanospray system with mass spectrometric detection for proteomic analyses, *J. Biomol. Tech.* **2002**, *13*, 72–84.
  - 41 K. Benkestock, C. K. Van Pelt, T. Åkerud, A. Sterling, P.-O. Edlund, J. Roeraade: Automated nanoelectrospray mass spectrometry for protein–ligand screening by noncovalent interaction applied to human H-FABP and A-FABP, *J. Biomol. Screen.* **2003**, *8*, 247–256.
  - 42 S. Zhang, C. K. Van Pelt, D. B. Wilson: Quantitative determination of noncovalent binding interactions using automated nanoelectrospray mass spectrometry, *Anal. Chem.* **2003**, *75*, 3010–3018.
  - 43 R. E. Moore, L. Licklider, D. Schumann, T. D. Lee: A microscale electrospray interface incorporating a monolithic, poly(styrene-divinylbenzene) support for online liquid chromatography/tandem mass spectrometry analysis of peptides and proteins, *Anal. Chem.* **1998**, *70*, 4879–4884.



- 44 H. Liu, C. Felten, Q. Xue, B. Zhang, P. Jedrzejewski, B. L. Karger, F. Foret: Development of multichannel devices with an array of electrospray tips for high-throughput mass spectrometry, *Anal. Chem.* **2000**, 72, 3303–3310.
- 45 K. Tang, Y. Lin, D. W. Matson, T. Kim, R. D. Smith: Generation of multiple electrosprays using microfabricated emitter arrays for improved mass spectrometric sensitivity, *Anal. Chem.* **2001**, 73, 1658–1663.
- 46 S. Zhang, X. Huang: A microchip electrospray device and column with affinity adsorbents and use of the same, *PCT Int. Appl.* **2002**, 59 pp, WO 0266135 A1 20020829.
- 47 C. A. S. Barnes, D. E. Clemmer: Assessment of purity and screening of peptide libraries by nested ion mobility-TOFMS: identification of RNase S-protein binders. *Anal. Chem.* **2001**, 73, 424–433.
- 48 Z. Shen, J. J. Thomas, C. Averbuj, K. M. Broo, M. Engelhard, J. E. Crowell, M. G. Finn, G. Siuzdak: Porous silicon as a versatile platform for laser desorption/ionization mass spectrometry, *Anal. Chem.* **2001**, 73, 612–619.
- 49 G. E. Siuzdak, J. Buriak, J. Wei: Improved desorption/ionization of analytes from porous light-absorbing semiconductor, *PCT Int. Appl.* **2000**, 76 pp, WO0054309 A1 20000914.
- 50 J. Wei, J. M. Buriak, G. Siuzdak: Desorption-ionization mass spectrometry on porous silicon, *Nature* **1999**, 399, 243–246.
- 51 Y.-S. Lin, Y.-C. Chen: Laser desorption/ionization time-of-flight mass spectrometry on sol-gel-derived 2,5-dihydroxybenzoic acid film, *Anal. Chem.* **2002**, 74, 5793–5798.
- 52 M. Holmquist, A. Palm, J. Engström, U. Selditz, P. Andersson: High-speed protein digestion, sample preparation and MALDI-TOF MS peptide mapping on a microfluidic compact disc (CD), in *Proceedings of the 50th ASMS Conference on Mass Spectrometry and Allied Topics*, Orlando, **2002**, WPP 238, 2066.pdf, available at: [www.gyros.com](http://www.gyros.com).
- 53 M. Gustafsson, E. Togan-Tekin, G. Ekstrand, R. Känge, P. Andersson, S. Wallenborg: A CD microlaboratory for improved protein identification by MALDI MS, in *Proceedings of the 50th ASMS Conference on Mass Spectrometry and Allied Topics*, Orlando, **2002**, ThPA 004, 1558.pdf, available at: [www.gyros.com](http://www.gyros.com).

### 3

## **ALIS: An Affinity Selection–Mass Spectrometry System for the Discovery and Characterization of Protein–Ligand Interactions**

*Allen Annis, Cheng-Chi Chuang, and Naim Nazef*

### **3.1**

#### **Introduction**

The biological efficacy of a small molecule drug candidate is coupled to its binding characteristics for its therapeutically relevant biomolecular target. The compound's most important binding characteristics include its affinity, binding site, and dissociation rate. Therefore, in any drug discovery program, considerable medicinal chemistry effort is expended to optimize these binding features of a drug candidate. In the early stages of the drug development process, progress towards improving a compound's binding features is typically followed using *in vitro* biochemical assays that measure a compound's effect on the conversion of one biological molecule into another, and other, orthogonal techniques that directly measure the binding characteristics of a lead compound for its receptor. These two methods are complementary, since direct protein–ligand binding assays provide the medicinal chemist with independent confirmation that activity observed in a biochemical assay correlates with specific binding to the target of interest, and that biochemical activity is not due to off-target binding, unwanted interaction with substrates or cofactors, or due to undesirable physical properties such as insolubility and target co-precipitation.

Techniques to directly characterize protein–ligand interactions play an increasingly vital role in the pharmaceutical discovery and development process. Direct binding assays are valuable not only to complement known techniques for determining the activity of ligands for well established classes of protein targets, but they are also critical for the pursuit of emerging drug targets that have no functional assay with which to evaluate potential ligands. In some cases, these techniques may be the only recourse for quantifying binding potency in a drug discovery program. For instance, advances in genome and proteome analysis are rapidly increasing the number of human and pathogen proteins identified as targets for small molecule therapy of human disease [1]. While these proteins may be synthesized and purified as targets for small-molecule therapy, many lack biochemical assays to discover and evaluate the binding properties of potential drug

candidates, are only available in minute quantities, or lack endogenous ligands for affinity determination using competitive binding assays. Even classic targets with well established biochemical assays are yielding new avenues for therapy through non-traditional points of intersection along their reaction pathway, requiring sophisticated *in vitro* assays for the discovery and evaluation of new drug candidates. As an example, potential small-molecule therapeutics that bind to and prevent phosphorylation of their basal kinase targets require complex, “coupled” assays to characterize their activities using purely biochemical means [2]. In instances where no such coupled assay exists, direct methods to measure protein–ligand binding characteristics are essential.

### 3.1.1

#### State of the Art

An ideal technology to directly characterize protein–ligand binding would have the following properties: (1) it would require no labeling of the target or small molecules with radioisotopes, fluorophores, or other moieties, and no covalent modification to immobilize the protein target or small molecules on a surface would be necessary; (2) the ideal technique could selectively identify the compound that is responsible for the observed output; (3) it would be solution-based, and amenable to all cofactors, salts, metal ions, and detergents necessary for proper protein folding and stability; and (4) it would require only modest amounts of a purified protein target for its implementation.

#### 3.1.1.1 Spectroscopic and Biophysical Methods

Unfortunately, few analytical tools for evaluating protein–ligand interactions comprise all, or even most, of these properties. The most commonly used solution-phase methods for binding affinity determination are spectroscopic in nature, and typically measure nuclear magnetic resonance (NMR), ultraviolet light absorbance, circular dichroism, or fluorescence changes caused by protein–ligand interactions [3]. These methods, especially ones based on NMR chemical shift changes, have the benefit in certain circumstances of indicating where the ligand is binding to its target [4]. However, spectroscopic methods often require isotopic or fluorescence labeling of the ligand or receptor [5]. Thermophysical techniques, such as isothermal or differential scanning calorimetry, require no chemical modification for their use, and in addition to measuring binding affinities these methods can also yield thermodynamic parameters of binding.

Though both spectroscopic techniques and calorimetric methods enable cofactors, buffers and metal ions to be included in the binding reaction, these methods are unfortunately very consumptive of purified protein. Partly to mitigate the difficulty of high protein consumption, binding affinity measurement techniques based on surface-immobilized receptors have been developed. These techniques include affinity chromatography and surface plasmon resonance (SPR) spectroscopy, with instruments using SPR and other biosensor techniques available commercially [6, 7]. While surface methods are operationally simple to execute and can yield useful kinetic parameters that describe binding interactions, such

methods require chemical modification of the receptor for attachment, possibly occluding ligand binding sites or otherwise affecting binding interactions.

### 3.1.1.2 Mass Spectrometry-based Methods

Affinity measurement techniques based on mass spectrometry (MS) are of increasing interest due to the exquisite sensitivity and unique selectivity possible with MS [8]. In addition to low protein consumption, these techniques enjoy the benefit of having all reaction components in solution. Affinity selection–MS (AS-MS) screening methods have been implemented using a number of hardware configurations [9–21] and all include the following steps: (1) an affinity selection step, where the protein is equilibrated with one or more potential ligands, leading to the formation of a complex of the protein with any compound capable of binding; (2) the resulting receptor–ligand complexes are separated from non-binding mixture components; and (3) ligands are identified by MS or MS/MS [9–21]. Since its first description in 1991 [22], a number of researchers have reported methods that use the direct analysis of non-covalent protein–ligand complexes by electrospray ionization–MS (ESI-MS), especially ultra-sensitive nanospray techniques, to study binding interactions [23, 24]. However, these methods require the non-covalent complexes to survive the transition to the gas phase, and there is conflicting data on the correlation of gas-phase affinity measurements with solution-phase interactions [25]. Also, these and other related MS affinity measurement techniques do not tolerate non-volatile salts or buffers, or high co-factor, metal ion, or detergent concentrations that may be necessary for proper protein folding and stability. Though not rigorously affinity selection methods, techniques that are based on hydrogen–deuterium exchange–MS [26], including the PLIMSTEX [28] method described in Chapter 11, and the SUPREX [29, 30] method, enable thermodynamic and equilibrium binding affinity estimates using high-sensitivity MALDI-MS analysis. Diffusion-based MS methods using laminar flow features in capillaries also enable the measurement of protein–ligand binding constants [32].

To take advantage of the high sensitivity and selectivity inherent to MS, while permitting greater flexibility in binding reaction conditions, hyphenated methods based on multidimensional chromatography–MS have been developed to study small molecule–protein interactions [33]. Several variants, both step-wise and integrated, have been reported and are described in detail in this book, including size-exclusion chromatography (SEC) coupled with reverse-phase chromatography–MS (RPC-MS; this Chapter), gel filtration “spin-column”–MS (Chapter 2 [13, 34, 35]) ultrafiltration–MS (Chapter 4), frontal affinity chromatography–MS (Chapter 6 [36]), and affinity capillary electrophoresis–MS. While most reports demonstrate these methods for screening small molecule combinatorial libraries for affinity selection-based drug discovery [37, 38], Blom and co-workers described a way to quantify the binding affinities of individual compounds for their protein target by SEC-RPC-MS, and researchers at NeoGenesis demonstrated a mixture-based, competitive binding method using SEC-RPC-MS to rank binding affinities and classify ligand–ligand competition as direct or allosteric (see below) [12, 39].

An important advantage of MS-based techniques lies in their ability to simultaneously distinguish multiple components from complex reactions, enabling mixture-based analysis. As mentioned above, this feature has been exploited primarily for the discovery of ligands from pools of compounds synthesized by combinatorial chemistry techniques. However, this advantage is also useful for evaluating the binding properties of multiple protein–ligand interactions in compound mixtures, including simultaneous affinity measurements, binding site classification by ligand–ligand competition analysis, and mixture-based dissociation rate determination. A multiplexed approach to evaluating these binding characteristics enables combinatorial synthesis methods to be applied to the affinity optimization process. Medicinal chemists can thereby optimize the structure and affinity of lead compounds while minimizing the need for synthesis and purification of individual ligands, which is the most time-consuming aspect of the affinity optimization process. This approach can dramatically decrease the time, expense, and effort required to optimize a lead molecule, as the synthesis and purification of discrete compounds is reserved for only the most interesting ligands that require more detailed functional studies. Also, the ability to multiplex compounds for follow-up evaluation enables the rapid triage of multiple hits from a high-throughput screening (HTS) campaign. HTS often generates multiple compound series for which no objective assessment can be made a priori as to the likelihood of any one series progressing through medicinal chemistry optimization. A well designed, mixture-based optimization can enable the collection of critical data that can be used to identify the most promising series from an HTS screen for further follow-up.

This chapter describes a hardware platform for affinity selection–MS using continuous SEC, and the application of this platform to characterizing the binding interactions that most directly impact the medicinal chemistry component of the drug development process. The first application is a technique for quantitatively measuring absolute protein–ligand binding affinities, commonly expressed as the equilibrium binding constant  $K_d$ . The second method relies on ligand–ligand competition to yield two valuable results from mixtures of compounds: (1) to distinguish same-site versus different, or allosteric, binding by multiple ligands to the same target, thus providing insight into the location of ligand binding; and (2) to simultaneously measure the affinities of multiple ligands to the target. Last, a method is presented for measuring the dissociation rates of small molecule ligands from their protein targets, either as individual compounds or as pools. Examples are shown for several drug targets of contemporary interest in the pharmaceutical industry.

## 3.2

### ALIS: An Affinity Selection–Mass Spectrometry System based on Continuous SEC

The schematic shown in Fig. 3.1 describes an optimized, integrated SEC-RPC-MS-based affinity selection platform developed at NeoGenesis, dubbed the

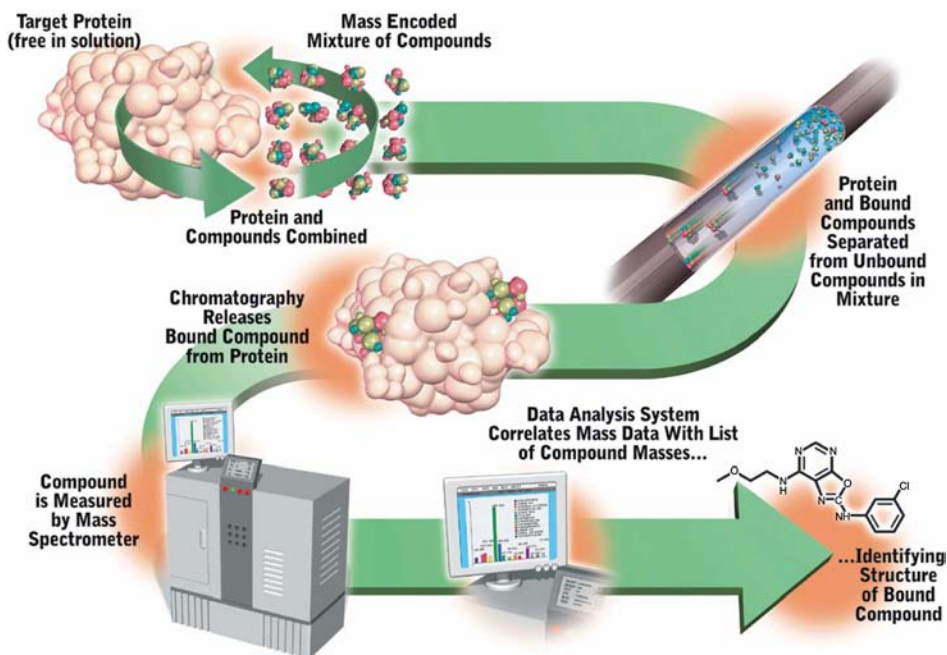


**Fig. 3.1** Schematic of ALIS, an automated ligand identification system that uses continuous size-exclusion chromatography for the study of protein–ligand interactions.

Automated Ligand Identification System, or ALIS [40]. The ALIS system incorporates the following components: (1) an affinity selection stage, where a protein target binds to ligands of moderate to high affinity ( $K_d$  values of 10  $\mu\text{M}$  to sub-nanomolar); (2) an SEC step that separates the protein–ligand complexes from unbound compounds; (3) an RPC step that dissociates the ligands from the complex; and (4) identification and quantitation of the dissociated ligands by MS.

In the affinity selection step, a protein target is incubated with one or more compounds in a physiologically relevant buffer containing any necessary cofactors, salts, metal ions, and detergents. The ALIS system is generic with respect to target class, and the binding reaction can be performed using proteins of virtually any variety, including both soluble targets and membrane-associated proteins; enzymes such as proteases, kinases, and phosphatases; nuclear hormone receptors; and G protein-coupled receptors (GPCRs). Genomic targets from bacterial or viral pathogens, especially novel target proteins that are derived from lethal gene product deletions but are of otherwise unknown function, can be readily studied to yield potential anti-infective compounds. Since the binding reaction is solution based, potential ligands can query all protein surfaces and not just the “active site,” enabling the discovery of ligands that act through allosteric binding and other mechanisms. The use of high-sensitivity MS enables ALIS to be

used to characterize protein–ligand interactions while consuming only microgram amounts of a purified, soluble protein target.

### 3.2.1

#### ALIS System Design

All the chromatography steps of the ALIS process are accomplished using a single suite of hardware. As described in reference [38], in the ALIS system the SEC and RPC-MS systems are directly coupled through a single valve. This strategy reduces sample loss due to non-specific interaction with multiple surfaces or through additional sample transfer steps, allowing maximum sample recovery, improved system reliability, and good sample-to-sample reproducibility. Also, since sample handling and tracking are minimized, improved workflow efficiency enables a highly automated, “screening sample-to-results” process.

ALIS uses continuous SEC to isolate protein–ligand complexes from unbound library members. Samples containing a target protein, protein–ligand complexes, and unbound compounds are injected onto an SEC column, where the complexes are separated from non-binding components by a rapid SEC step. As shown in Fig. 3.2, the SEC column eluate is monitored using UV detectors to confirm that the early-eluting protein fraction, which elutes in the void volume of the SEC column, is well resolved from unbound components that are retained on the column. After the peak containing the protein and protein–ligand complexes elutes from the primary UV detector, it enters a sample loop where it is excised from the flow stream of the SEC stage and transferred directly to the LC-MS via a valving mechanism. A second UV detector positioned after the valve records the SEC components not delivered to the LC-MS. The primary detector shows the separation of the protein peak from unbound library members, and by comparing the

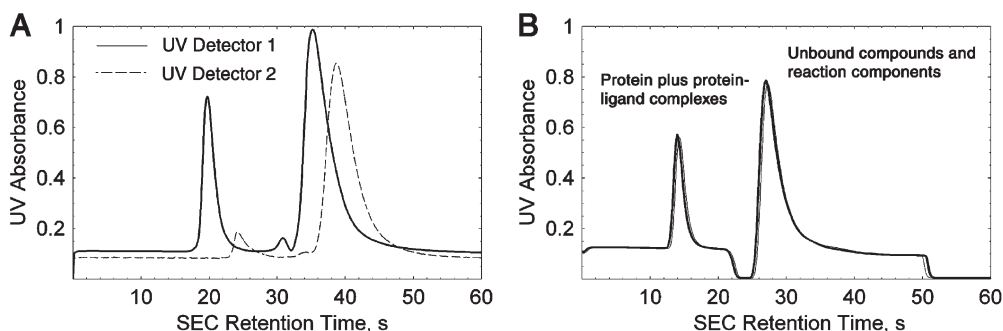


**Fig. 3.2** SEC chromatograms from typical ALIS experiments. (A) UV responses from detectors positioned before and after a sampling valve show that the protein–ligand complex, eluting at 20 s, is excised from the SEC stream for transfer to RPC-MS. (B) An overlay of ten SEC chromatograms demonstrates ALIS sample-to-sample reproducibility. Reprinted from [40] with permission from Elsevier.

two UV detector outputs, an operator can determine whether any unbound library members might have been introduced to the MS. Another important operational advantage of this configuration is demonstrated in Fig. 3.2B. In this screenshot, an overlay of SEC chromatograms from a series of ALIS experiments shows good symmetry and reproducibility for the protein peak, indicating no deleterious interactions with the library or sample preparation that may cause misshapen or absent protein peaks.

Following the SEC stage, the band containing protein–ligand complexes is immediately transferred to an RPC column where ligands are dissociated from the protein and trapped on the RPC stationary phase. The dissociated ligands are eluted into a mass spectrometer for analysis, and automated software algorithms search the mass spectral data to identify the ligands by their molecular weight. ALIS reports only compounds that bind directly to the target of interest, preventing false positives that arise from off-target activity or interactions with substrates or other reagents. Since ALIS directly identifies bound components by MS, the incidence of false positives based on “bulk effects” and non-specific binding is lower than that of biochemical assays that yield a secondary readout of activity.

### 3.3

#### Discovery of Ligands from Combinatorial Libraries

The ALIS platform has been used to successfully screen a variety of therapeutically valuable proteins against combinatorial libraries of small, drug-like compounds, yielding novel ligands to a number of targets, including targets of unknown function identified by genomic and proteomic profiling, well established targets in the pharmaceutical industry, and popular but notoriously intractable (or “hard”) targets for which the discovery of small molecule drugs has proven difficult [41]. Mixture-based combinatorial libraries are designed using software algorithms [42] to minimize the amount of mass redundancy present at both the library synthesis and library pooling stages, while insuring that each member is constructed from building blocks chosen to maximize the diversity of shape and functionality [43]. As such, each library member is self-encoded by its molecular weight [44, 45].

As an example, the bifunctional epoxy ester core ( $\pm$ )-2 was reacted with building blocks 3–18 to yield solution-phase library NGL127A443 containing nominally 512 substitutionally and stereochemically unique compounds (Figs. 3.3, 3.4). Of these, 82% have a molecular weight unique to 0.050 amu. This library was combined with four other 500-member libraries to form a 2500-member primary library that was screened against the important antibacterial target dihydrofolate reductase (DHFR, also known as Fol-A).

This screening experiment yielded the monochlorinated DHFR ligand **1** at  $m/z$  515.24, corresponding to an  $[M+H]^+$  ion with a monoisotopic molecular weight of 514.23 amu. No signal for this ion was evident in an ALIS control experiment with DHFR in the absence of the screening library (Fig. 3.5). Table 3.1 shows a



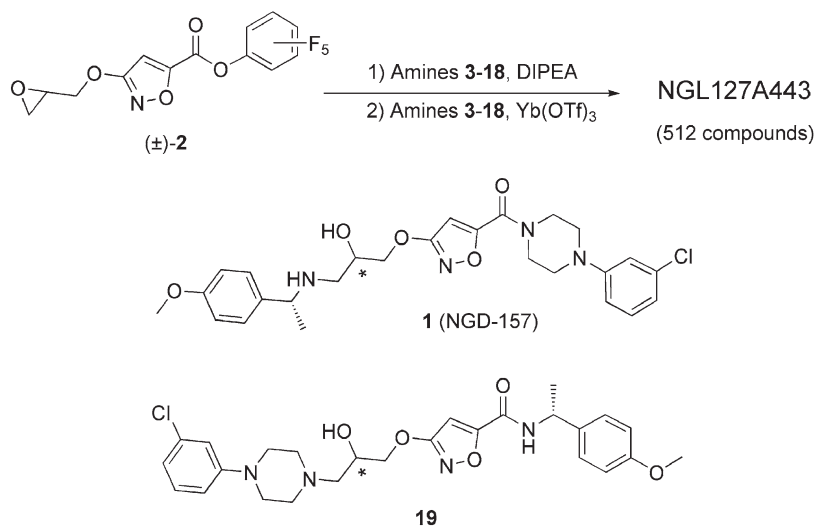


**Fig. 3.3** Synthetic scheme for mass-encoded library NGL127A443 containing isobaric positional isomers **1** and **19**. Reprinted from [40] with permission from Elsevier.

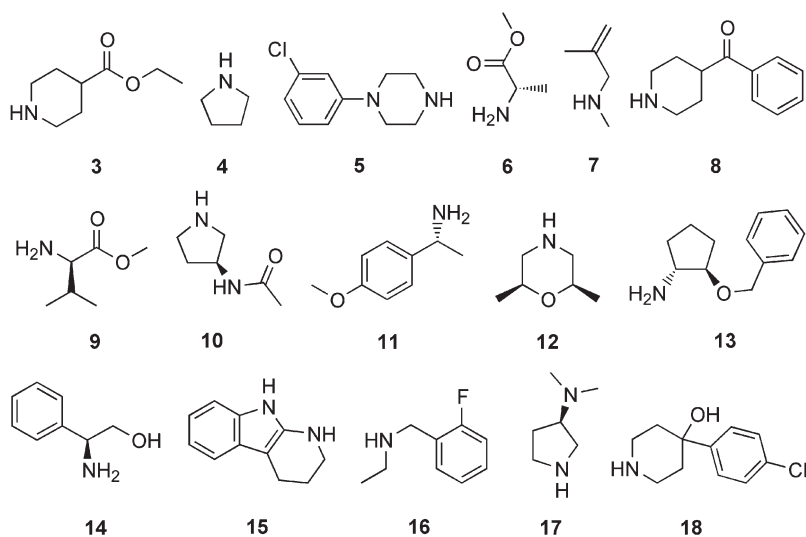


**Fig. 3.4** Amine building blocks used in the synthesis of library NGL127A443. Reprinted from [40] with permission from Elsevier.

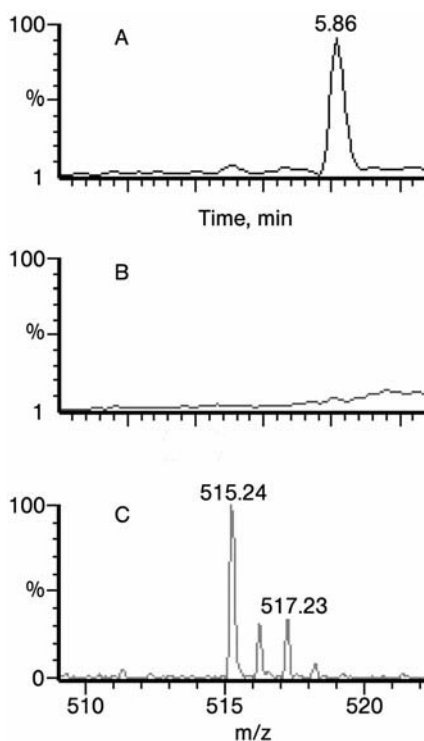


**Fig. 3.5** (A) Extracted ion chromatogram (XIC) of  $m/z$  515.2 ( $M+H$ )<sup>+</sup> from an ALIS experiment with DHFR and NGL127A443. (B) XIC of  $m/z$  515.2 from control experiment (no library). (C) Mass spectrum of the region near  $m/z$  515.2 underlying the XIC peak in A. Reprinted from [40] with permission from Elsevier.

portion of the membership of the 2500-member screening library; only one of the five combined libraries contains a monochlorinated member within 0.05 amu of the measured molecular weight.

An independent affinity selection experiment confirmed that the ligand originated from library NGL127A443. Compound **1**, also known as NGD-157, and its positional isomer **19** were then synthesized as purified, discrete compounds for ALIS binding confirmation and measurement of their binding affinity, competition profiles versus other, known DHFR ligands, and their biological activity. As demonstrated in detail below, NGD-157 was found to bind specifically to the active site of DHFR with a  $K_d$  of  $3.5 \pm 1.7$   $\mu$ M. Isomer **19** was found to be inactive in ALIS binding experiments and in bacterial growth inhibition assays.

The discovery of DHFR inhibitor NGD-157 demonstrates that ALIS is an efficient system for identifying novel, bioactive lead compounds from large combinatorial libraries. A single ALIS experiment containing over 2500 compounds is complete in under 10 min, allowing more than 250 000 compounds to

**Table 3.1** A portion of the membership of the ALIS screening library, composed of NGL127A443 (library 3 in this table) and four other libraries, which yields DHFR ligand **1** (NGD-157, entry 11). Compounds of similar exact molecular weight (EMW) are distributed among the five pooled libraries to minimize mass overlap and simplify hit deconvolution. Reprinted from [40] with permission from Elsevier.

Entry	EMW	Formula	Library				
			1	2	3	4	5
1	511.2220	C <sub>29</sub> H <sub>29</sub> N <sub>5</sub> O <sub>4</sub>			♦		
2	511.2318	C <sub>27</sub> H <sub>33</sub> N <sub>3</sub> O <sub>7</sub>	♦				
3	511.2318	C <sub>27</sub> H <sub>33</sub> N <sub>3</sub> O <sub>7</sub>		♦			
4	511.2431	C <sub>26</sub> H <sub>33</sub> N <sub>5</sub> O <sub>6</sub>				♦	
5	511.2482	C <sub>28</sub> H <sub>34</sub> N <sub>3</sub> O <sub>5</sub> F			♦		
6	511.2642	C <sub>23</sub> H <sub>37</sub> N <sub>5</sub> O <sub>8</sub>	♦				
7	511.2795	C <sub>27</sub> H <sub>37</sub> N <sub>5</sub> O <sub>5</sub>					♦
8	512.2383	C <sub>25</sub> H <sub>32</sub> N <sub>6</sub> O <sub>6</sub>		♦			
9	512.2999	C <sub>28</sub> H <sub>40</sub> N <sub>4</sub> O <sub>5</sub>		♦			
10	513.2475	C <sub>27</sub> H <sub>35</sub> N <sub>3</sub> O <sub>7</sub>			♦		
11	514.1983	C <sub>26</sub> H <sub>31</sub> ClN <sub>4</sub> O <sub>5</sub>			♦		
12	514.2791	C <sub>27</sub> H <sub>38</sub> N <sub>4</sub> O <sub>6</sub>					♦
13	514.2791	C <sub>27</sub> H <sub>38</sub> N <sub>4</sub> O <sub>6</sub>		♦			
14	515.1823	C <sub>26</sub> H <sub>30</sub> N <sub>3</sub> O <sub>6</sub> Cl			♦		
15	515.2631	C <sub>27</sub> H <sub>37</sub> N <sub>3</sub> O <sub>7</sub>			♦		
16	515.2631	C <sub>27</sub> H <sub>37</sub> N <sub>3</sub> O <sub>7</sub>					♦
17	515.2631	C <sub>27</sub> H <sub>37</sub> N <sub>3</sub> O <sub>7</sub>				♦	
18	515.2631	C <sub>27</sub> H <sub>37</sub> N <sub>3</sub> O <sub>7</sub>		♦			
19	516.1940	C <sub>26</sub> H <sub>30</sub> ClN <sub>4</sub> FO <sub>4</sub>			♦		

be screened from a single 96-well plate of libraries per day. Only 10 pmol (0.5 µg) of protein is consumed per sample, and the ALIS screening campaign for *Escherichia coli* DHFR against 1500, 2500-member libraries, representing >3 500 000 compounds, consumed a total of 1.0 mg protein.

It is important to note that the same ALIS hardware and software used for combinatorial library screening is applicable to characterizing protein–ligand interactions using the methods described below.

### 3.4

#### Quantitative Binding Affinity Measurement

The first measure of a candidate compound's efficacy in a drug discovery program is its specific binding affinity to a desired biomolecular target. Therefore,

the development of improved methods to accurately determine the absolute binding affinities of drug-like small molecules to their receptors is an active and fruitful area of research. Most methods for absolute affinity quantitation (as compared to relative affinity measurements based on displacement of a known inhibitor) rely on titration of a receptor by a ligand and readout of a signal corresponding to formation of the receptor–ligand complex. In the case of spectroscopic methods, the readout is based on emission or absorption of electromagnetic radiation; for thermophysical methods such as isothermal calorimetry, the readout is based on emission of heat. In ALIS, the protein–ligand complex concentration is determined from the MS signal measured for the ligand after its dissociation from the complex. This section describes a straightforward ALIS-based titration method to quantify the binding affinities between unlabelled small molecules and their native protein targets.

### 3.4.1

#### Theory

Single-site binding of a ligand to a receptor is described by the following equilibrium expression, here using nomenclature familiar from Michaelis–Menten kinetic analyses, with  $E$  representing the receptor (for example, an enzyme) and  $S$  representing the ligand (for example, an enzyme's substrate):



The protein–ligand binding affinity is usually expressed as the equilibrium dissociation constant,  $K_d$ , which is described by the following relationship between the concentrations of free receptor  $[E]$ , free ligand  $[S]$ , and the receptor–ligand complex  $[ES]$ :

$$K_d = \frac{[E][S]}{[ES]} \quad (2)$$

Some titration methods utilize high ligand-to-receptor ratios to simplify data analysis, and in these cases depletion of the ligand concentration by binding to the target can be ignored, which simplifies the analysis. In the ALIS method, the receptor and ligand concentrations are comparable in magnitude and ligand depletion must be explicitly considered as the titration results are analyzed. Expressions for free receptor and ligand may be written in terms of total receptor and total ligand concentrations  $[E]_0$  and  $[S]_0$ , respectively:

$$\begin{aligned} [E] &= [E]_0 - [ES], \\ [S] &= [S]_0 - [ES] \end{aligned} \quad (3)$$

These values can be substituted into the original expression defining  $K_d$ . Here, no assumptions or simplifications regarding ligand depletion are made:

$$K_d = \frac{([E]_0 - [ES])([S]_0 - [ES])}{[ES]} \quad (4)$$

Solving this quadratic equation for protein–ligand receptor concentration  $[ES]$  yields the following expression. Here, the protein–ligand complex concentration  $[ES]$  is defined in terms of the  $K_d$  and the total receptor and ligand concentrations  $[E]_0$  and  $[S]_0$ :

$$[ES] = \frac{1}{2} (K_d + [S]_0 + [E]_0 - \sqrt{(K_d + [S]_0 + [E]_0)^2 - 4[E]_0[S]_0}) \quad (5)$$

ALIS measures the MS response of the ligand following its dissociation from the protein–ligand complex. Therefore, the magnitude of the MS response corresponds to the equilibrium concentration of the receptor–ligand complex concentration  $[ES]$  times the compound’s MS calibration factor  $C_{MS}$ , which depends on the ionization efficiency and other molecular properties of the ligand:

$$\text{MS Response} = C_{MS}[ES] \quad (6)$$

Substituting this expression into the equation above yields a new expression relating the MS response to four variables: the total ligand concentration  $[S]_0$ , which is the known, independent variable in a titration experiment; the  $K_d$ , which is the dependent variable of interest; the total receptor concentration  $[E]_0$ ; and the MS response calibration factor  $C_{MS}$ :

$$\begin{aligned} \text{MS Response} \\ = \frac{C_{MS}}{2} (K_d + [S]_0 + [E]_0 - \sqrt{(K_d + [S]_0 + [E]_0)^2 - 4[E]_0[S]_0}) \end{aligned} \quad (7)$$

Therefore, plotting the ALIS MS response from a titration series versus the total ligand concentration yields a saturation binding curve that can be fit to this equation by nonlinear regression analysis to yield the  $K_d$  of the ligand of interest.

The MS response calibration factor  $C_{MS}$  can be determined independently by injecting samples of known ligand concentration into the MS and correlating the response with the amount injected. This allows quantitative determination of the receptor–ligand complex concentration at each data point of the titration, and enables accurate measurement of the total receptor concentration  $[E]_0$  as the asymptote of the saturation binding curve. However, in practice it is simpler to fit the titration curve data to yield the MS calibration factor by non-linear regression, since this obviates the need to create calibration curves for each ligand under study. Another advantage of fitting the MS response factor is that any minor losses of ligand in the ALIS system (for example, due to protein–ligand complex dissociation during the SEC stage) are corrected for and do not influence the  $K_d$  estimate. In the absence of a calibration curve, solving for the MS response factor

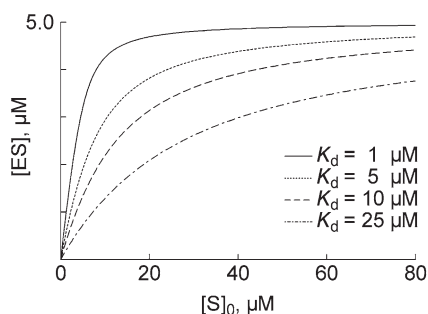


**Fig. 3.6** Simulated ALIS saturation binding experiments for ligands of varying affinity to a single-site receptor present at 5.0  $\mu\text{M}$  concentration.

$C_{\text{MS}}$  by regression analysis may not yield an accurate value for either this variable or for  $[E]_0$ , as the two variables are highly coupled in the regression results. Fortunately, the fit value of the  $K_d$  variable is not so highly coupled, and can be determined with good confidence [46].

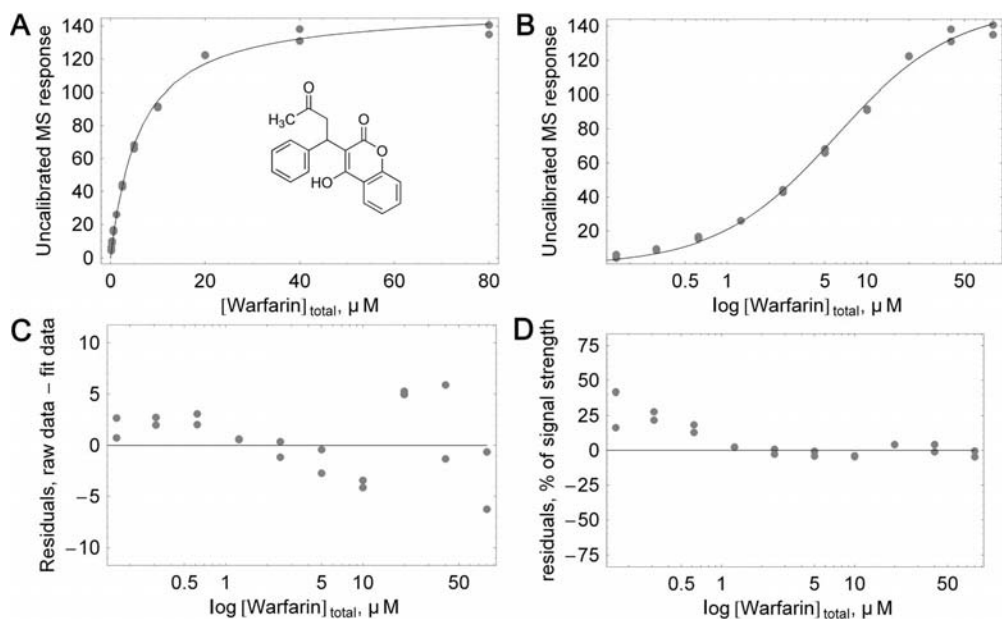


**Fig. 3.7** ALIS titration experiment for warfarin vs 5.0  $\mu\text{M}$  HSA. Duplicate injections shown. (A) Fitting the data by nonlinear regression analysis yields a  $K_d$  of  $5.6 \pm 1.0 \mu\text{M}$ . (B) Data from A, plotted as a sigmoidal curve to better show the fit at low titrant concentrations. (C) Residuals plotted as absolute and (D) as percent of signal.

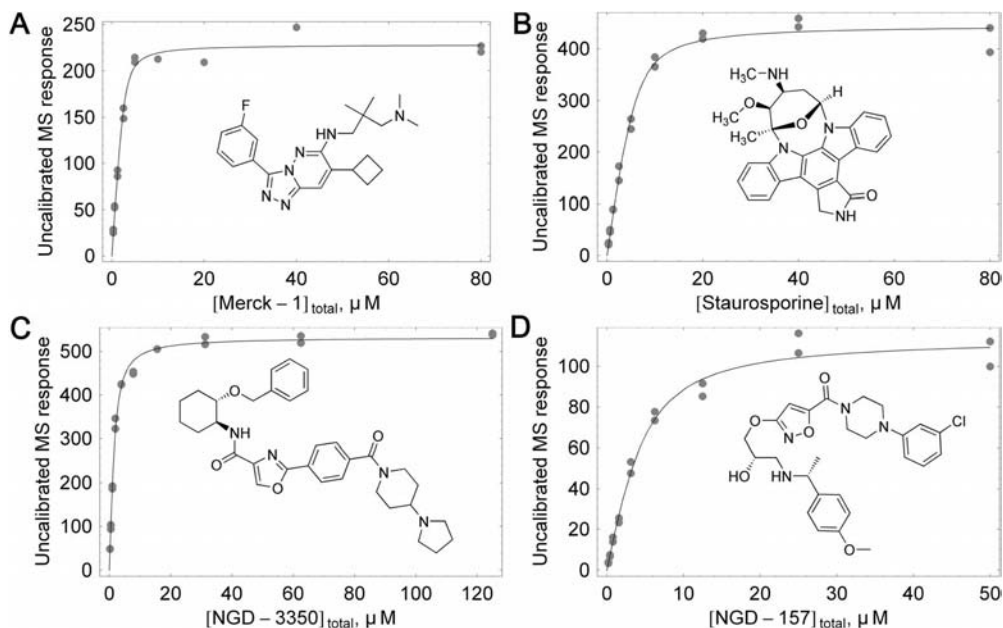


**Fig. 3.8** Examples of the ALIS-based  $K_d$  titration experiment for a variety of compounds and protein targets. (A) Compound "Merck-1" vs 5.0  $\mu\text{M}$  Akt-1,  $K_d = 0.3 \pm 0.1 \mu\text{M}$ . (B) Staurosporine vs 4.5  $\mu\text{M}$  JNK1,  $K_d = 1.0 \pm 0.4 \mu\text{M}$ . (C) NGD-3350 vs 2.5  $\mu\text{M}$  M<sub>2</sub> receptor,  $K_d = 0.7 \pm 0.1 \mu\text{M}$ . (D) NGD-157 vs 5.0  $\mu\text{M}$  DHFR,  $K_d = 3.5 \pm 1.7 \mu\text{M}$ .

### 3.4.2

#### Simulations and Experimental Results

Figure 3.6 shows the simulated titration of a receptor at a fixed concentration by increasing concentrations of a ligand that binds a single site. Because the receptor concentration is fixed, the ligands saturate the receptor at high concentrations, and the amount of receptor–ligand complex present asymptotically approaches the total receptor concentration. Importantly, the rate at which saturation occurs – the steepness of the hyperbolic portion of the binding curve – depends on the binding affinity.

Such a titration using ALIS is operationally simple to execute. First, samples of varying ligand concentration are generated by serial dilution (for example, 80, 40, 20, 10...  $\mu\text{M}$ ), and then each sample is incubated with a fixed concentration of the receptor, and subsequently injected on the SEC-RPC-MS system for analysis. Figure 3.7 shows the results of such a titration experiment for the small molecule ligand warfarin binding to human serum albumin (HSA, 5  $\mu\text{M}$ ) as its protein target. The x-axis of this plot is the total warfarin concentration, which includes both bound and unbound ligand. Fitting the raw data to the equation above yields a  $K_d$  value of  $5.6 \pm 1.0 \mu\text{M}$ , which is consistent with literature values determined by

frontal affinity chromatography and other methods [47]. The sigmoidal representation of this data and plots of the residuals of the curve fit demonstrate how well the model fits the raw data.

Further examples of the ALIS-based  $K_d$  measurement are shown in Fig. 3.8. Here, in Fig. 3.8A, titration of Akt-1 kinase (PKB- $\alpha$ ) by the known ligand Merck-1 yields a  $K_d$  value of  $0.3 \pm 0.1 \mu\text{M}$ , which correlates with its reported  $\text{IC}_{50}$  value of  $0.4 \mu\text{M}$  [48]. Figure 3.8B shows binding of Staurosporine to Jun N-terminal kinase 1 (JNK1), yielding a  $K_d$  value of  $1.0 \pm 0.4 \mu\text{M}$ , which corresponds well to its  $\text{IC}_{50}$  value of  $0.5 \mu\text{M}$ . As a further example, Figure 3.8C shows that NGD-3350 binds its GPCR target, the  $\text{M}_2$  muscarinic acetylcholine receptor, with a  $K_d$  of  $0.7 \pm 0.1 \mu\text{M}$ , which compares to its  $K_i$  value of  $0.2 \mu\text{M}$  [49]. Finally, the DHFR ligand NGD-157, described in the preceding section, yields a  $K_d$  value of  $3.5 \pm 1.7 \mu\text{M}$  by ALIS titration shown in Fig. 3.8D. Independent isothermal calorimetry experiments indicate that NGD-157 binds DHFR with a  $K_d$  of  $5.9 \mu\text{M}$  [50].

Titration experiments in the presence of allosteric-binding proteins, peptides, and cofactors can indicate whether a ligand's binding affinity is positively or negatively affected by binding of the allosteric ligand. The next section of this chapter describes a method of determining ligand–ligand binding cooperativity where two ligands are detectable by ALIS.

### 3.5

#### Competition-based Binding Site Determination and Affinity Ranking in Mixtures

The location on a target protein at which a potential drug lead binds is a key determinant of its biological efficacy. For example, the mechanistic basis of many therapeutic compounds, especially those that target enzymes, involves *in vivo* competition by the drug with another ligand or cofactor for a particular binding site on the protein target [53]. Therefore, the ability to characterize the binding site of a small molecule ligand with respect to known cofactors, substrates, or other small molecule drugs having known binding sites is of paramount importance in the drug discovery process. Techniques to classify ligands according to binding site are especially important for protein targets where no atomic-resolution structural data is available (for example, from NMR or x-ray crystallographic analysis), including GPCRs and other membrane-associated proteins.

The ability of a known competitor ligand to displace a target-bound library member – as measured by ALIS – reveals the binding site classification and affinity ranking of mixture components [36]. In practice, affinity selection experiments are performed with samples containing a constant concentration of the ligand(s) of interest and serially increasing concentrations of a competitor ligand. In these experiments, the ALIS responses of the ligands and the competitor reflect the equilibrium concentrations of each protein–ligand complex.

The competitor used in these experiments may be either a known ligand or MS-sensitive substrate or cofactor for the target of interest, a representative chosen from multiple ligand classes discovered in a high-throughput screening cam-



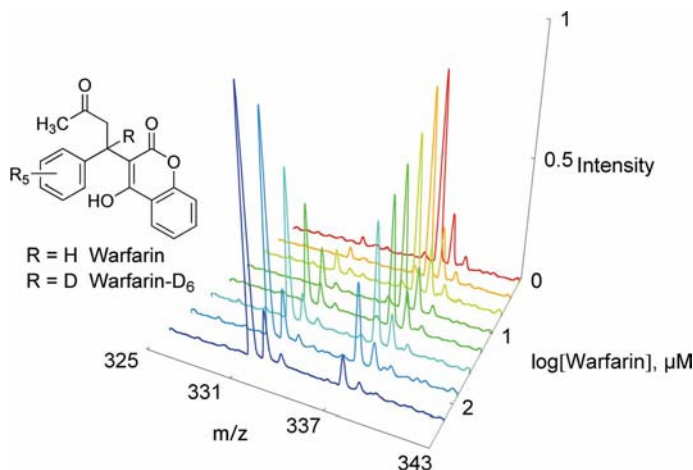


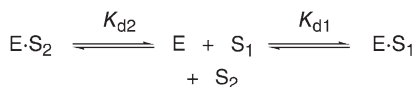
**Fig. 3.9** ALIS-MS results for the titration of 5  $\mu\text{M}$  HSA with warfarin in the presence of a 5  $\mu\text{M}$  concentration of its stable isotope-labeled congener warfarin-D<sub>6</sub>. Increasing concentrations of warfarin reduce the response of warfarin-D<sub>6</sub> due to isosteric binding competition. Reprinted from [39] with permission from the American Chemical Society.

paign, or the progenitor of a series of structural analogs synthesized for affinity ranking. If two ligands bind at different sites, the method can yield their absolute binding affinity and a quantitative assessment of the degree of allosteric cooperativity between them.

### 3.5.1

#### Binding Site Classification

The example shown in Fig. 3.9 demonstrates this technique for the HSA ligand warfarin in competition with its stable isotope-labeled congener warfarin-D<sub>6</sub>. Here, the concentration of the receptor and deuterated ligand are held constant while warfarin is added at increasing concentrations. The ALIS MS response of warfarin increases while the response of warfarin-D<sub>6</sub> diminishes as it is competed from its binding site on HSA. This is an absolute example of direct binding competition (Scheme 3.1), since the labeled and unlabeled compounds bind the same site with identical affinities, yet are distinguishable by their different molecular weights. Importantly, if two compounds bind the same site, the *ratio* of the ALIS



**Scheme 3.1** Isosteric competition diagram.

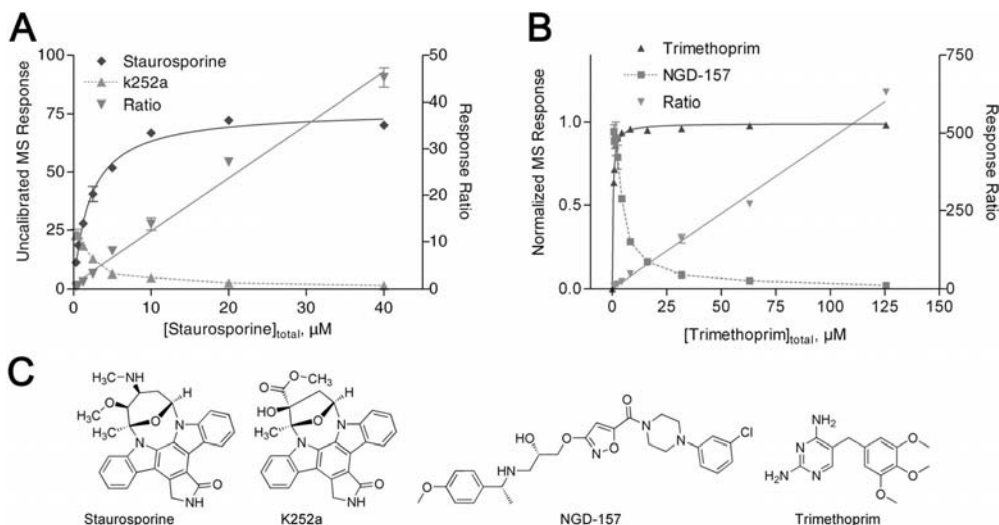
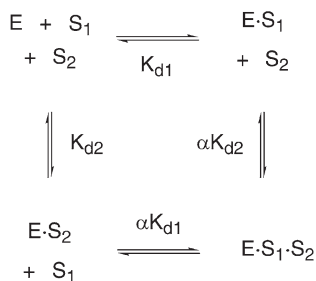


**Fig. 3.10** Examples of isosteric binding competition. (A) ALIS-MS results for the titration of 5  $\mu\text{M}$  Zap-70 by staurosporine in the presence of a 5  $\mu\text{M}$  concentration of its structural congener K252a; and (B) titration of 5  $\mu\text{M}$  DHFR with the known DHFR inhibitor trimethoprim in the presence of ligand NGD-157 at 5  $\mu\text{M}$  concentration. Linear MS response ratios in these experiments are consistent with direct binding competition. (C) Compound structures.

responses for two competing ligands will be linear as a function of increasing titrant.

As another example of direct binding competition, Fig. 3.10 shows competition profiles for the emerging immunosuppression target Zap-70 kinase [54] using staurosporine and its structural congener K252a, both well known ligands for active sites of nearly all protein kinases. As expected, these two structurally similar ligands yield a linear ratio of MS responses, consistent with direct binding competition. Though ATP has poor sensitivity in electrospray ionization MS, the Zap-70 example demonstrates that a known ATP-binding site inhibitor such as staurosporine can be used in ALIS as an ESI-MS-sensitive surrogate of ATP or other nucleotide ligand. As another example, and one that demonstrates the method for two compounds of very different structure, the DHFR ligand NGD-157 (whose  $K_d$  determination was shown previously in Fig. 3.8) is directly competitive with the known DHFR ligand trimethoprim [55] as shown by the linear response ratio plotted in Fig. 3.10B.

ALIS competition experiments can also demonstrate whether two ligands bind allosterically with respect to one another. Such allosteric binding can be positively cooperative, where binding by one ligand enhances binding by a second; or negatively cooperative, such that binding by the first diminishes binding by a second; or non-cooperative, so binding by one has no effect on the binding of another li-



**Scheme 3.2** Allosteric competition diagram.

gand. Scheme 3.2 shows the ternary complex model of allosteric binding [56]. In this model, ligands  $\text{S}_1$  and  $\text{S}_2$  bind distinct sites on receptor  $\text{E}$  with dissociation constants  $K_{d1}$  and  $K_{d2}$ , respectively. However, if both ligands bind simultaneously to the receptor, they may affect each other's binding constant by an amount described as the binding cooperativity factor, denoted here as  $\alpha$ . For example,  $\text{S}_1$  binds to  $\text{E}$  with dissociation constant  $K_{d1}$ , but it also binds to the binary complex  $\text{E} \cdot \text{S}_2$  to form ternary complex  $\text{E} \cdot \text{S}_1 \cdot \text{S}_2$  with dissociation constant  $\alpha K_{d1}$ . Where  $\alpha > 1$ , allosteric interaction by one of the ligands increases the dissociation constant of the other, resulting in negative binding cooperativity. Where  $\alpha < 1$ , positive cooperativity results, and if  $\alpha = 1$ , binding by one ligand has no effect on the binding of the other [57].

ALIS cannot separate binary protein–ligand complexes from allosterically bound ternary complexes; all protein–ligand species co-elute from the SEC stage. The measured recovery of a particular ligand therefore represents the sum of the protein–ligand complexes containing that ligand. As a consequence, the ratio of the ALIS MS responses of a titrated competitor versus an allosteric ligand will not be a straight line, as was the case with direct competition; rather the ratio plot will be an asymptotically bound hyperbolic curve if the two ligands can form a ternary complex with the protein target.

The Akt-1 kinase ligand NGD-28835, discovered by ALIS screening of mass-encoded libraries against the basal form of its target [58], provides an example of allosteric binding interaction. As shown in the ALIS titration experiment for Akt-1 and NGD-28835 versus staurosporine in Fig. 3.11, the ALIS response for staurosporine is diminished to a constant value while the titrant response plateaus as the receptor reaches saturation. This yields an asymptotically bound response ratio, indicating allosteric binding with respect to staurosporine and detection of a ternary complex of Akt-1, staurosporine, and NGD-28835 by ALIS. This result is consistent with NGD-28835 binding outside the ATP-binding pocket of Akt-1, and indicates negative binding cooperativity by NGD-28835.

Compounds that inhibit Akt-1 are of increasing interest as possible oncology therapeutics [59]. Akt-1 is a multi-domain protein that is known to be activated after binding of its pleckstrin homology (PH) domain to its endogenous target. A report from researchers at Merck indicates that their Akt-1 inhibitor does

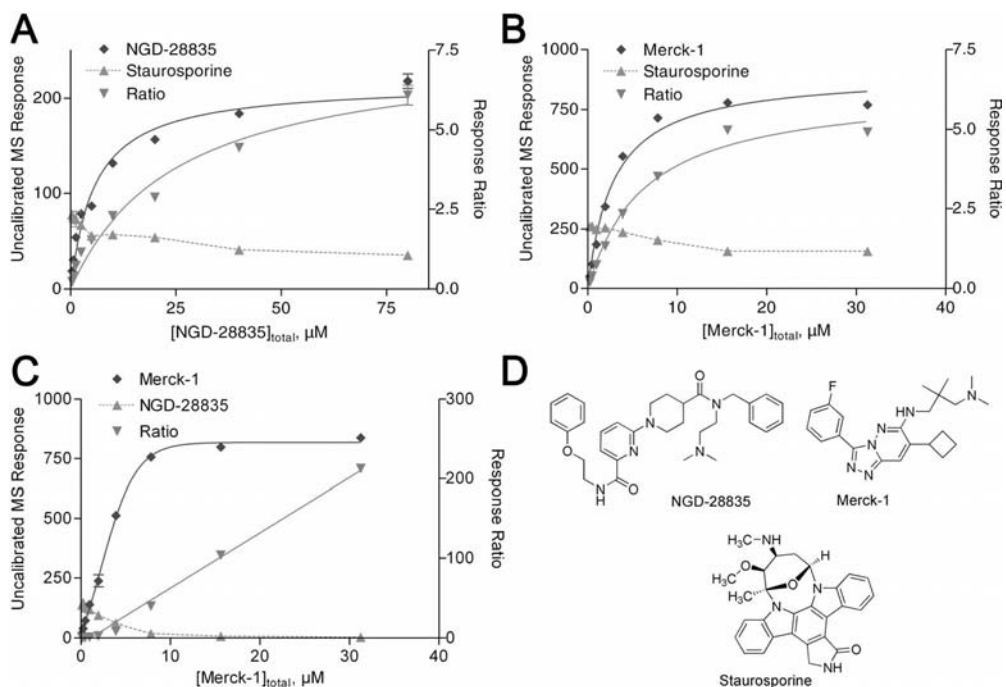


**Fig. 3.11** Examples of allosteric binding competition. Titration of 5  $\mu\text{M}$  Akt-1 plus 5  $\mu\text{M}$  staurosporine by: (A) NGD-28835 and (B) Merck-1 does not yield linear response ratios for the two competing ligands. Asymptotically bound response ratios indicate allosteric binding between these two

ligands and staurosporine. (C) Titration of 5  $\mu\text{M}$  Akt-1 plus 5  $\mu\text{M}$  NGD-28835 by Merck-1 does yield a linear ratio of MS responses, indicating these two compounds bind the same site on Akt-1. (D) Compound structures.

not bind to the kinase domain; rather, it binds Akt-1 at its PH domain [60]. ALIS competition experiments between staurosporine and the Merck compound (Merck-1) indicate allosteric binding between these two ligands, as evidenced by the hyperbolic ratio plot of the ALIS responses in the titration experiment shown in Fig. 3.11B.

NGD-28835 and Merck-1 both bind allosterically with respect to staurosporine. To test whether NGD-28835 and Merck-1 bind the *same* site, ALIS competition experiments were conducted with these two compounds. Though they are structurally dissimilar, a linear ratio plot in Fig. 3.11C confirms isosteric binding for these two compounds, indicating that they both bind the PH domain and effect a biological response through this mechanism, rather than through traditional binding to the kinase active site. It is noteworthy that the ALIS competition method can discern the binding sites of ligands to the inactive form of a receptor (here, the basal form of a kinase), which is a challenging task using traditional biochemical assays.

## 3.5.2

## Affinity Ranking in Compound Mixtures

Advances in chemical synthesis have enabled considerable sophistication in the construction of diverse compound libraries to probe protein function [61, 62]. However, few general techniques exist that can directly assess binding mechanisms and evaluate ligand affinities in a multiplexed format. To realize the full potential of combinatorial chemistry in the drug discovery process, generic and efficient tools must be applied that combine mixture-based techniques to characterize protein–ligand interactions with the strengths of diversity-oriented chemical synthesis.

ALIS-based techniques enable researchers to rank the affinity of multiple ligands for a protein receptor while simultaneously showing whether the ligands bind the same site as a competitor ligand or bind an allosteric site. As a simple example to describe the basis of the method, the warfarin versus warfarin- $D_6$  competition data shown previously in Fig. 3.9 yields sigmoidal curves when normalized and plotted on a logarithmic axis (Fig. 3.12). The total competitor concentration at which each protein–ligand complex concentration (here, warfarin- $D_6$ ) is reduced to half its value in the absence of the competitive ligand is defined as the affinity competition experiment 50% inhibitory concentration ( $ACE_{50}$  value) and is dependent upon the  $K_d$  of the ligand and other experimental parameters (Fig. 3.12A). The  $ACE_{50}$  value, which describes the concentration of the competitor required to compete out 50% of the ligand of interest, is the converse of the ordinary definition of a biochemical or biophysical  $IC_{50}$ , which describes the concentration of the ligand of interest required to compete out 50% of a

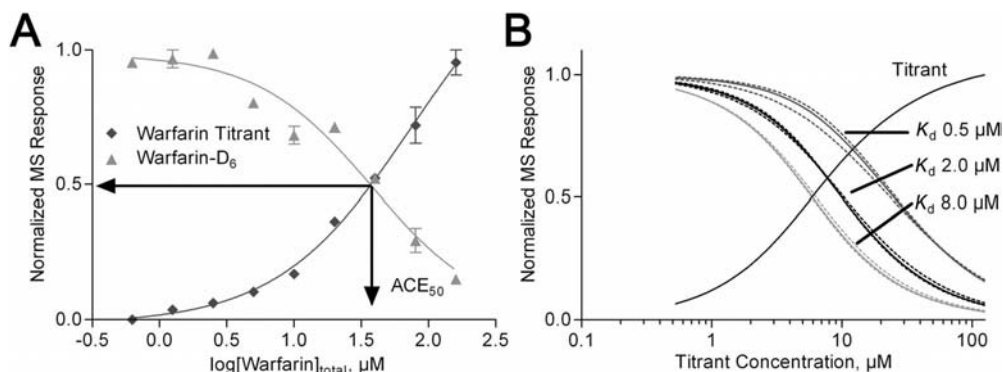


**Fig. 3.12** The ALIS affinity competition experiment 50% inhibitory concentration ( $ACE_{50}$ ) method. (A) The warfarin versus warfarin- $D_6$  ALIS competition data from Fig. 3.9, normalized and plotted on a logarithmic axis, yields the  $ACE_{50}$  value, which is the titrant concentration at which the ligand binding is reduced by 50%. (B) Simulated

$ACE_{50}$  experiment for a three-component mixture. Dashed lines indicate variation of that component's concentration by  $\pm 3$ -fold (an overall 9-fold difference) highlighting that the method is insensitive to ligand concentration. See text for details. Reprinted from [39] with permission from the American Chemical Society.

known compound, for example, a radioligand. In contrast to a conventional  $IC_{50}$  value, a higher  $ACE_{50}$  value indicates a higher-affinity ligand: greater competitor concentration is required to displace the compound of interest from the binding site.

Though the ALIS  $ACE_{50}$  method resembles a radioligand displacement assay, the MS-based readout enables multiple components to be measured simultaneously, an advantage which is not possible using radiochemical or fluorescence methods. Fig. 3.12B demonstrates a simulated titration of a three component mixture where the total concentration of all pool components (1  $\mu M$  each, 3  $\mu M$  total) is less than the total receptor concentration (simulated at 5  $\mu M$ ). Under these conditions, individual library components bind independently to the excess receptor and compete only with the titrant, and not with one another, and the  $ACE_{50}$  value of each component depends upon its  $K_d$ . The dashed lines simulate variation in the concentration of each component by a factor of  $\pm 3$  (an overall nine-fold difference in concentration). As the simulation shows, the  $ACE_{50}$  values are insensitive to ligand concentration: Over a nine-fold variation in the concentration of any ligand, the  $ACE_{50}$  values are virtually unchanged. This feature is valuable because it allows the  $ACE_{50}$  method to be applied where the concentrations of the mixture components are not accurately known; for example, to the direct products of a mixture-based combinatorial chemical synthesis. As such, the method enables unpurified combinatorial mixtures to be used for the affinity optimization of a lead compound's chemical structure, a problem of great importance in the pharmaceutical industry.

The  $ACE_{50}$  method for ranking compounds by their protein–ligand binding affinity is demonstrated in Fig. 3.13 for a mixture of ligands to the  $M_2$  receptor. This mixture contains representatives of compounds of different structural classes, including analogs of NGD-3346, discovered by ALIS screening of combinatorial libraries. The known  $M_2$  active site inhibitor atropine was used as the titrant against 2.0  $\mu M$   $M_2$  in the presence of 0.5  $\mu M$  per component compound pool. The  $ACE_{50}$  curves indicate clear differences in affinity, with NGD-3350 exhibiting a higher affinity than its structural congeners NGD-3348 and NGD-3346. This result correlates well with those from independent biochemical activity measurements and ALIS-based  $K_d$  titration experiments. ALIS saturation binding experiments with the individual  $M_2$  ligands yield the same rank-order of affinities as revealed by the  $ACE_{50}$  experiment:  $K_d$ s of 0.7, 2.1, 2.9, and 6.2  $\mu M$  were measured for NGD-3350, NGD-3348, NGD-3346, and NGD-3344, respectively. The compound with the highest  $ACE_{50}$  value, NGD-3350, has the best  $K_d$  at 0.7  $\mu M$ , and this compound also shows the best biochemical activity in a cell-based cAMP assay [63]. In a tissue-based assay for  $M_2$  antagonism, NGD-3350 yields an  $IC_{50}$  of 9.6  $\mu M$  [64, 65]. Only this compound shows significant activity in tissue, consistent with the remaining compounds all having lower affinity as determined by  $ACE_{50}$  ranking, ALIS  $K_d$  titration, and  $M_2$  antagonist activity in the cAMP assay.

It is also noteworthy that the  $ACE_{50}$  technique for affinity ranking also allows mixture components to be classified as either allosteric or directly competitive with another ligand of interest. In the  $M_2$  example, reanalyzing the sigmoidal  $ACE_{50}$  curves in Fig. 3.13 as the ratio plots instead shows that the response ratios

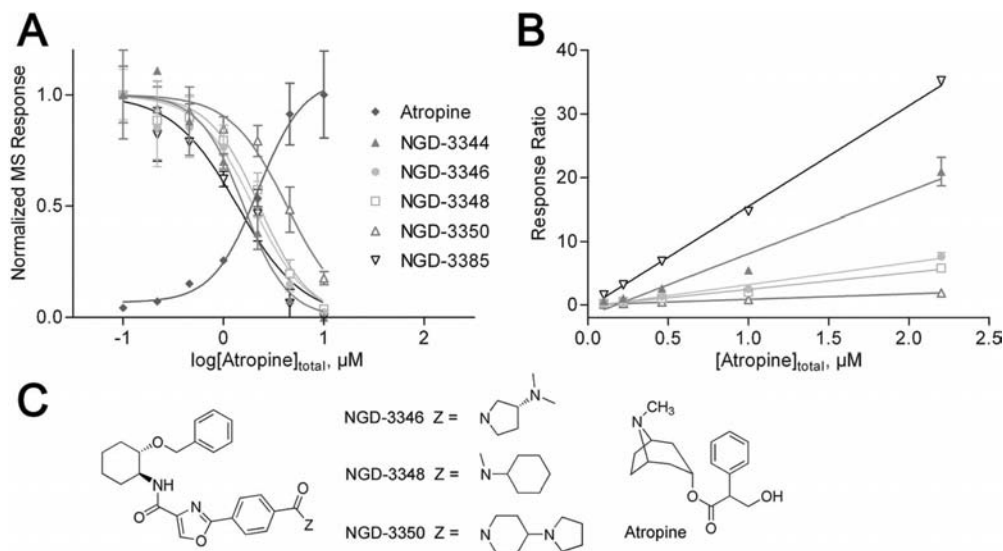


**Fig. 3.13** The ACE<sub>50</sub> method demonstrated for a mixture of ligands at 1  $\mu\text{M}$  per component to the M<sub>2</sub> receptor at 5  $\mu\text{M}$  concentration. (A) NGD-3350 requires the greatest competitor concentration to be competed from the receptor, indicating that it is the highest affinity ligand. (B) Ratio plots indicate direct binding competition with atropine. (C) Select compound structures. Reprinted from [39] with permission from the American Chemical Society.

are linear, indicating that all the ligands examined are directly competitive with atropine. Consistent with this result, the biochemical assays mentioned above all show that the ligands tested, like atropine, are antagonists of M<sub>2</sub>.

These results highlight the ability of the ACE<sub>50</sub> method to simultaneously rank-order compounds by affinity, especially mixtures of structural analogs synthesized by combinatorial chemistry techniques. The method is particularly valuable for identifying those compounds with improved affinity relative to a progenitor, for example, the improved affinity of NGD-3350 relative to its parent NGD-3346. Through multiple iterations of combinatorial analog synthesis and ACE<sub>50</sub> analysis, structure–activity relationships can be developed for the compound series and the potency of the initial hit can be optimized, even in the absence of a biochemical assay.

### 3.6

#### Protein–Ligand Dissociation Rate Measurement

The biological efficacy of a drug candidate depends critically on the rate at which it dissociates from its therapeutically relevant target biomolecule. As described in

greater detail below, the binding affinity of a small molecule for its receptor also depends upon its dissociation rate (or “off-rate”). Therefore, within a series of compounds having comparable association rates (“on-rates”), compounds with slower off-rates have, by definition, greater affinity for their protein target. Also, the more slowly a compound dissociates from its receptor, the more time it spends on the receptor effecting its desired biological outcome, and the less time it is subject to metabolism, excretion, or off-target binding and undesired side-effects. Therefore, for highly potent compounds in the advanced stages of a medicinal chemistry optimization program, compounds of similar potency can be ranked according to off-rate as a secondary measure of their potential efficacy. Also, very slow dissociation kinetics can contribute to slow clearing of a drug, which can be problematic in the event of adverse reactions such as an undesired allergic response. Therefore, methods to accurately determine the dissociation kinetics for protein–ligand interactions are of great value to the drug discovery process.

This section describes the theoretical principles underlying an ALIS-based method for determining protein–ligand dissociation rates for single ligands and for ligands which are components of mixtures. The basis of the method resembles a “cold quench” radioligand technique common to receptor biology, where a large excess of an inhibitor (or quench) ligand of equal or better affinity than the compound under study is added to an equilibrated protein–ligand binding reaction. As soon as any protein–ligand complex spontaneously dissociates, the freed protein is quenched by the excess of inhibitor so no protein–ligand complex can re-form. Therefore, the concentration of the protein–ligand complex will diminish with time after addition of an excess of inhibitor, and the rate of its diminution, which depends on the protein–ligand dissociation kinetics, can be measured by ALIS. The method is demonstrated by simultaneously measuring the protein–ligand dissociation rates of a number of ligands to the Zap-70 kinase.

### 3.6.1

#### Theory

The single-site equilibrium binding of a small molecule ligand  $S$  with its receptor  $E$  can be expressed as the chemical reaction shown here:



The dissociation rate (or “off-rate”) of the protein–ligand complex  $ES$  is characterized by the first-order rate constant  $k_{\text{off}}$  and depends on the concentration of protein–ligand complex  $[ES]$ :

$$\text{dissociation rate} = -k_{\text{off}}[ES] \quad (9)$$

The association rate (or “on-rate”) can be likewise defined as the product of the association rate constant  $k_{\text{on}}$ , in units of  $\mu\text{M}^{-1} \text{ s}^{-1}$ , the concentration of free pro-



tein  $[E]$ , and the concentration of free ligand  $[S]$ :

$$\text{association rate} = k_{on}[E][S] \quad (10)$$

The overall rate of change in the concentration of protein–ligand complex with time is the sum of its rate of formation and its rate of depletion:

$$\frac{d[ES]}{dt} = k_{on}[E][S] - k_{off}[ES] \quad (11)$$

It should also be noted that when the rate of change in the protein–ligand complex concentration is zero (by definition, when the system is at equilibrium), this equation reduces to the equilibrium expression below, with the binding affinity constant  $K_d$  defined as the ratio of the dissociation rate  $k_{off}$  to the association rate  $k_{on}$ :

$$K_d = \frac{[E][S]}{[ES]} = \frac{k_{off}}{k_{on}} \quad (12)$$

As mentioned above in a qualitative sense, it can be seen from this equation that, for a given association rate constant  $k_{on}$ , a lower value of dissociation rate constant  $k_{off}$  yields a smaller value of  $K_d$  and hence a higher equilibrium concentration of the desired protein–ligand complex.

The half-life ( $t_{1/2}$ ) of binding is another convenient metric for comparing dissociation rates. For a first-order process such as protein–ligand complex dissociation, the half-life is defined from the dissociation rate constant  $k_{off}$  as follows:

$$t_{1/2} = \frac{\ln(2)}{k_{off}} = \frac{0.693}{k_{off}} \quad (13)$$

In the absence of any protein–ligand re-association (for example, under hypothetical conditions of infinite dilution of the complex), the half-life is the time required for half of the complex to decay to unbound protein and ligand.

As mentioned previously, the concentrations of free protein  $[E]$  and free ligand  $[S]$  are related to the total protein and ligand concentrations  $[E]_0$  and  $[S]_0$  by the following relationships:

$$\begin{aligned} [E] &= [E]_0 - [ES], \\ [S] &= [S]_0 - [ES] \end{aligned} \quad (14)$$

Substituting these expressions into the equations above yields a new expression that enables the interaction kinetics to be readily modeled for single-site, reversible binding between a protein and a single ligand:

$$\frac{d[ES]}{dt} = k_{on}([E]_0 - [ES])([S]_0 - [ES]) - k_{off}[ES] \quad (15)$$

In analogy to the single-ligand, single-site equilibrium described above, competitive binding between a ligand  $S$  and an inhibitor ligand  $I$  is described by the following equation:



Here, free protein  $E$  can react either with ligand  $S$  to form the complex  $ES$ , or react with free inhibitor  $I$  to form complex  $EI$ . It follows that the overall rate of change in the concentrations of protein–ligand complexes  $[ES]$  and  $[EI]$  is described by the following simultaneous differential equations:

$$\frac{d[ES]}{dt} = k_{S-on}([E]_0 - [ES] - [EI])([S]_0 - [ES]) - k_{S-off}[ES] \quad (17)$$

$$\frac{d[EI]}{dt} = k_{I-on}([E]_0 - [ES] - [EI])([I]_0 - [EI]) - k_{I-off}[EI] \quad (18)$$

The kinetics of a system of competing ligands can be modeled by simultaneous numerical solution of these two equations given initial values for the system parameters, including the total protein concentration  $[E]_0$ , the total ligand and total inhibitor concentrations  $[S]_0$  and  $[I]_0$ , the rates of association and dissociation for the interacting components of the mixture  $k_{S-on}$ ,  $k_{S-off}$ ,  $k_{I-on}$ , and  $k_{I-off}$ , and initial values for  $[ES]$  and  $[EI]$ . Note that simultaneous solution of these equations where the initial value of  $[ES]$  is not zero allows the behavior of the system to be modeled versus time upon addition of an excess of inhibitor.

### 3.6.2

#### Simulations

Figure 3.14 shows the results of mathematical modeling experiments that simulate the ALIS response for a protein–ligand complex versus time when subjected to changes in inhibitor concentration and variation in other parameters. Figure 3.14A models a system consisting of 5  $\mu\text{M}$  protein and 1  $\mu\text{M}$  ligand with typical association and dissociation rates ( $k_{S-on} = 0.1 \mu\text{M}^{-1} \text{ s}^{-1}$ ,  $k_{S-off} = 0.01 \text{ s}^{-1}$ ,  $k_{I-off} = 0.01 \text{ s}^{-1}$ ) to which has been added a large excess of inhibitor by 1:1 dilution of the original, equilibrated protein–ligand mixture with 100  $\mu\text{M}$  inhibitor while keeping the total ligand concentration constant. This would be a typical experimental implementation of the “cold quench” method for determining protein–ligand dissociation rates using ALIS. As mentioned above, the rate at which the inhibitor competes with the ligand for the protein depends upon both the dissociation rate of the protein–ligand complex and the rate of association of the inhibitor and protein; this figure shows the expected ALIS protein–ligand recovery for inhibitors of varying association rate. Dilution of the protein with a non-associating inhibitor ( $k_{I-on} = 0$ ) containing an equal total concentration of

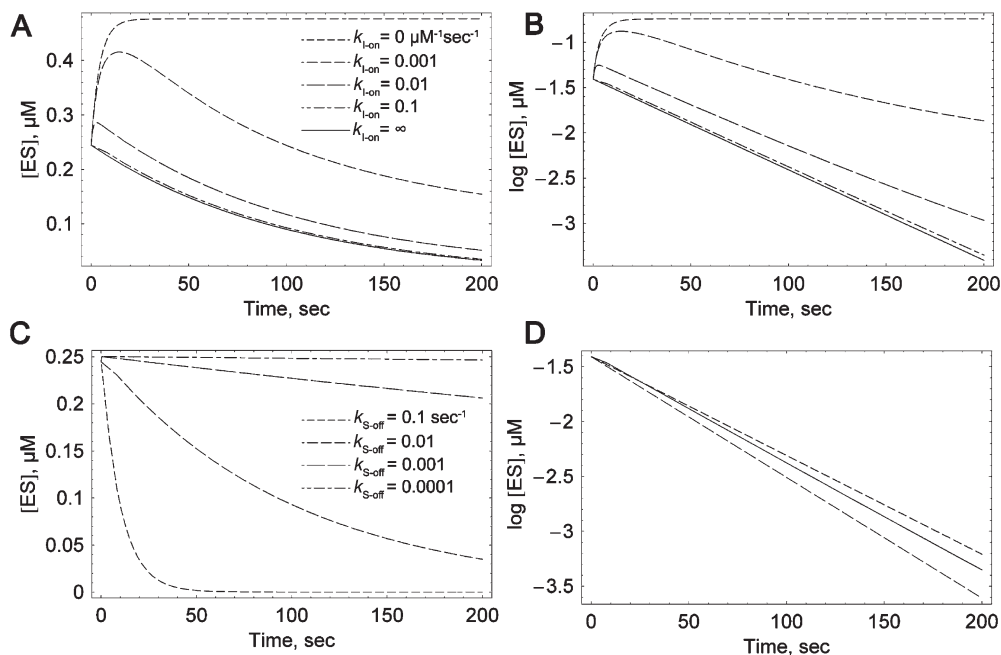


**Fig. 3.14** Simulated ALIS-based dissociation rate measurements. See text for details. (A) Quench experiments modeled at varying inhibitor association rates. Even with a very slow-binding inhibitor, the decay curve resembles pure first-order dissociation kinetics. (B) Data in (A), shown on a log axis. (C) Simulated ALIS quench experiment with varying protein–ligand dissociation rates,

showing how the method can be used to rank compounds by off-rate. (D) Correlation between the modeled ALIS quench experiment and the theoretical decay curve expected from infinite dilution. The modeled decay curve (solid line) is shown for  $k_{off} = 0.01 \text{ s}^{-1}$  and theoretical curves (dashed lines) are shown for rates  $\pm 10\%$  of this value.

ligand as the equilibrated protein–ligand mixture causes the total protein and protein–ligand complex concentrations to initially drop to 50% of their original value, then (in the absence of active inhibitor) the system restores itself to a new equilibrium. However, in the presence of an excess of an associating inhibitor ( $k_{l-on} \neq 0$ ) any free protein is rapidly quenched by the inhibitor, so no protein–ligand complex *ES* can re-form. Therefore, as soon as any protein–ligand complex *ES* spontaneously dissociates, the rate of which depends upon  $k_{s-off}$ , the freed protein is quenched by the excess of inhibitor. As such, the measurable concentration of the protein–ligand complex will diminish with time after addition of an excess of inhibitor. It can be seen that even with a very slow-binding inhibitor ( $k_{l-on} = 0.001 \text{ } \mu\text{M}^{-1} \text{ s}^{-1}$ ) the slope of the decay curve approaches that of the integrated rate expression resulting from pure first-order dissociation kinetics (for example, under conditions of infinite dilution):

$$[ES] = [ES]_0 e^{k_{S-off} \cdot t} \quad (19)$$

Since the decay follows an exponential function, the similarity between the simulated decay curve slopes and the theoretical, infinite dilution ideal is even more apparent when the plots are compared in log space, as shown in Fig. 3.14B.

The utility of this method for measuring and comparing multiple ligands' dissociation rates is demonstrated by the simulations in Fig. 3.14C. This figure demonstrates a system consisting of 5  $\mu\text{M}$  protein and 1  $\mu\text{M}$  ligand, with a typical protein–ligand association rate and varying protein–ligand dissociation rates, to which has been added a large excess of inhibitor by 1:1 dilution of the original, equilibrated protein–ligand mixture. The model shows that the ALIS quench method can distinguish compounds of varying off-rate.

Figure 3.14D shows the degree of correlation for the rate of decay of the protein–ligand complex in a modeled ALIS quench experiment and the theoretical decay curve expected from infinite dilution. The modeled decay curve is shown for  $k_{S-off} = 0.01 \text{ s}^{-1}$  and theoretical curves are shown for dissociation rates  $\pm 10\%$  of this value. The results indicate that the measured dissociation rate is well within  $\sim 10\%$  of the actual value, a very good approximation of the actual dissociation rate given the simplicity of this experimental method.

Since the simulated decay curve closely matches the theoretical exponential decay curve expected from pure first-order dissociation kinetics, the experimental data can be fit to this simple function using available curve-fitting algorithms to extract dissociation rate information about each ligand. Following the quench of an equilibrated mixture of a protein and a ligand or ligands of interest, protein–ligand complex concentration values measured by consecutive ALIS experiments yield quantitative estimates of the dissociation rate of each ligand, and the rates of multiple ligands in a mixture can be compared.

### 3.6.3

#### Experimental Results

The ALIS-based off-rate measurement method was applied to a proprietary series of Zap-70 Kinase inhibitors. First, an  $\text{ACE}_{50}$  experiment was conducted to demonstrate that the compounds bind the same site as the quench reagent staurosporine. As shown in Fig. 3.15, sigmoidal plots indicate that, with the exception of one compound, the  $\text{ACE}_{50}$  values were all very similar to one-another. Linear ratio plots of the same  $\text{ACE}_{50}$  data confirm that the compounds all bind isosterically with respect to the quench reagent, a necessary prerequisite for effective competition.

The mixture of these compounds at 0.5  $\mu\text{M}$  per component was equilibrated with a 5  $\mu\text{M}$  concentration of the protein target, then the reaction was quenched with excess staurosporine (100  $\mu\text{M}$ ) and analyzed using ALIS every 7 min. The measured protein–ligand complex MS responses were normalized and fit to the exponential decay function above, as shown in Fig. 3.16. The raw data fit the ex-

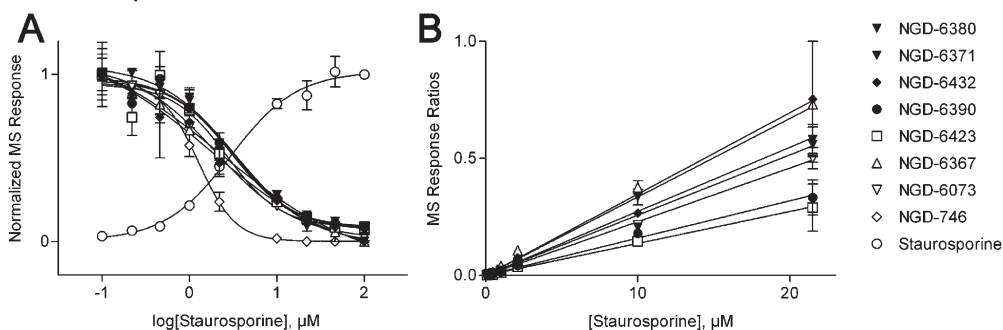


**Fig. 3.15** (A) An ALIS competition experiment with a proprietary series of Zap-70 kinase inhibitors at  $0.5 \mu\text{M}$  per component plus receptor at  $5 \mu\text{M}$  concentration yields similar  $\text{ACE}_{50}$  values, indicating that all but one of the compounds have similar  $K_d$ s. (B) Linear ratio plots of the  $\text{ACE}_{50}$  data in (A) confirm that the compounds all bind isosterically with respect to staurosporine.

ponential function well; the fit for one of the compounds shown as an example. Varying rates of dissociation were observed for the mixture components, which was surprising given the very similar  $\text{ACE}_{50}$  values mentioned above, and similar  $\text{IC}_{50}$  values determined from independent biochemical measurements (Table 3.2) [66]. This result emphasizes the importance of having orthogonal methods to assess protein–ligand interactions when evaluating and prioritizing compounds for lead discovery: Despite comparable protein–ligand binding affinities, the off-rates for these compounds vary over an order of magnitude. This aspect these compounds’ binding properties could have considerable effects on other aspects of

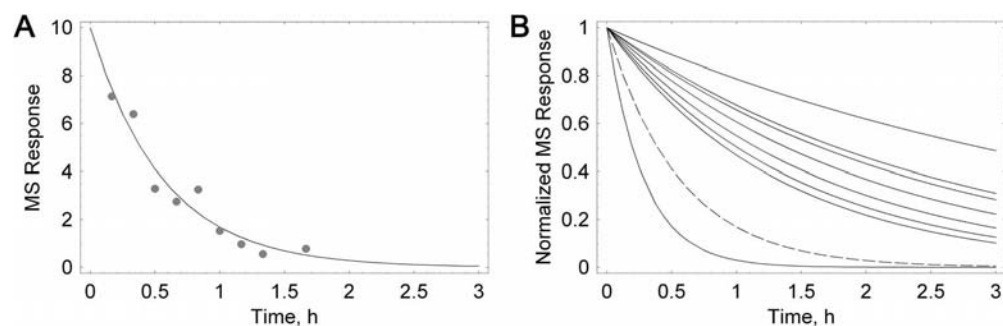


**Fig. 3.16** The ALIS-MS responses from a dissociation rate experiment for a mixture of Zap-70 ligands using staurosporine as the quench reagent. See text for details. (A) The raw data and its fit curve for NGD-6367, one of the compounds in the mixture. (B) The exponential decay curves fit to normalized

ALIS-MS response data. Each curve (left to right) corresponds to the compounds listed in Table 3.1 (top to bottom). NGD-6367, from (A), is shown as a dashed line. For clarity, the raw data points are not shown in (B).

**Table 3.2** IC<sub>50</sub> values and protein–ligand dissociation half-lives for a proprietary series of Zap-70 Kinase inhibitors.

Entry	Compound ID	IC <sub>50</sub> , nM	t <sub>1/2</sub> , min
1	NGD-746	3000	11.8 ± 2.6
2	NGD-6367	160	23.4 ± 3.0
3	NGD-6380	80	54.2 ± 6.6
4	NGD-6390	130	55.0 ± 12.4
5	NGD-6371	100	60.5 ± 8.6
6	NGD-6073	170	99.6 ± 13.5
7	NGD-6432	110	99.6 ± 23.5
8	NGD-6862	90	107.9 ± 23.0
9	NGD-6423	150	175.5 ± 48

their optimization as drug leads, including pharmacokinetic, metabolism, and excretion profiles.

The dissociation rates of certain protein–ligand complexes can be affected by binding of allosteric ligands. This effect is especially well known for GPCRs, where the dissociation of active site antagonists can be retarded by binding of an allosteric ligand. In GPCRs, this effect is attributed to blocking the channel in which the antagonists bind, thus inhibiting their escape from their binding site. The ALIS quench method can be used to evaluate the effect of an allosteric ligand on the dissociation rate of another ligand [49]. The M<sub>2</sub> receptor ligands N-methyl scopolamine (NMS) and W-84 bind allosterically with respect to one another, with binding by one reducing the affinity of binding by the other. Figure 3.17 shows the result of quenching an equilibrated mixture of the M<sub>2</sub> receptor plus NMS by

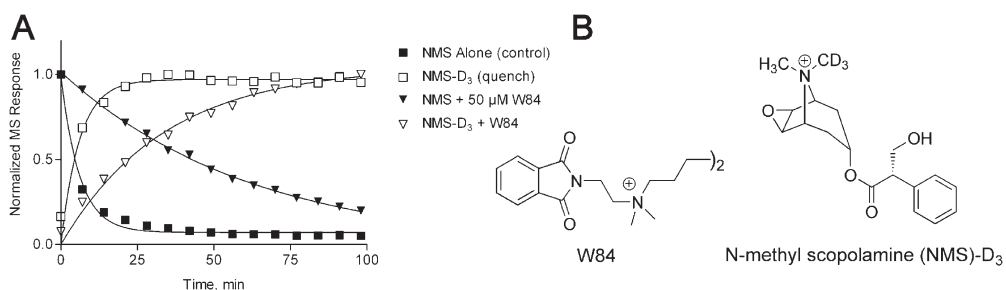


**Fig. 3.17** (A) ALIS-MS results from quenching an equilibrated mixture of 2.0 μM M<sub>2</sub> receptor plus 1.5 μM NMS by 200 μM of the isosteric ligand NMS-D<sub>3</sub>, in the presence and absence of the known allosteric ligand W-84 at 50 μM concentration. Binding by the allosteric ligand W-84 decreases the off-rate of NMS. (B) Compound structures.

the isosteric ligand NMS-D<sub>3</sub>, both in the presence and absence of the known allosteric ligand W-84. These ALIS experiments show that the presence of the allosteric ligand decreases the off-rate of NMS, which is consistent with similar experiments performed by radioligand binding analysis [52].

The ALIS “quench” method for dissociation rate measurement uses little protein and requires no biochemical assay for its implementation, yet the method readily yields quantitative values for the dissociation rates of the protein–ligand complexes. The technique can be used with pools of ligands to provide a quantitative rank ordering of the dissociation rates of all the components of the mixture. Since it is not necessary to know the exact concentrations of the ligands under study, the dissociation rate assessment can be performed using impure compounds, such as unpurified compound mixtures derived from combinatorial chemistry synthesis. The method does not require a foreknowledge of active protein concentration to measure and rank ligands based on their rates of dissociation. As such, the technique is self-contained and does not rely upon an external measure of protein activity as one of its input parameters.

### 3.7

#### Conclusions

The ALIS system enables several useful techniques for studying protein–ligand interactions, and is generally applicable to a broad range of protein classes, including serum proteins, kinases, and GPCRs. The methods described here require neither tagging of the ligands nor the existence of a biochemical assay, as they rely purely on the MS readout of an affinity selection experiment for their implementation.

ALIS-based titration experiments yield an absolute measure of protein–ligand binding affinities without assumptions regarding ligand depletion or other simplifications. No competitor ligand is necessary for the method’s implementation, and it can readily measure the affinity of active-site or allosteric ligands to a receptor. Also, the titration method can be used to validate that a protein synthesized and purified by biochemical techniques retains specific ligand binding ability, and that the binding affinity correlates with that expected from orthogonal methods to confirm proper protein folding.

The ALIS ACE<sub>50</sub> method enables the simultaneous classification of ligands of dissimilar structure according to their binding site. This capability can assist the development of structure–activity relationships and understanding protein–ligand interactions in multi-domain or multi-subunit targets, even in the absence of atomic resolution structure data. As shown in the examples above, the ACE<sub>50</sub> method enables the triage of multiple hits arising from high-throughput screening according to binding site and target-specific binding affinity, and facilitates combinatorial library-based structural optimization of these hits to high-affinity lead compounds. This method is especially useful as a tool for the study of allosteric ligands, facilitating the advancement of compounds with improved target

specificity engendered by binding at sites distinct from those conserved within protein families [67].

Dissociation rate measurement using ALIS mimics the radioligand quench method; however, because the ALIS readout is MS-based, it is readily adapted to mixture-based analysis. This feature facilitates medicinal chemistry optimization of protein–ligand off-rates using combinatorial synthesis techniques. The ability to measure the effect of allosteric ligands on the dissociation rate of an active site ligand is also demonstrated, and this ability highlights the advantages of using ALIS for the in-depth study of protein–ligand interactions.

While the methods described in this chapter have been optimized for affinity selection–MS using continuous SEC, they are readily adaptable to spin-column, gel permeation, or other well validated and highly accessible two-stage AS-MS designs. The use of AS-MS for studying protein–ligand interactions, especially for the discovery of ligands from pools of compounds, has been reported by a number of experts in the pharmaceutical industry and academia over the past decade. Due to the advantages offered by AS-MS, it can be anticipated that these techniques will be increasingly applied by medicinal and synthetic organic chemists, biochemists, analytical chemistry experts and other researchers throughout the pharmaceutical discovery community.

### 3.8 Future Directions

Advances in mass spectrometry, especially innovations leading to more efficient ionization techniques and higher sensitivity detector systems, will enable the characterization of protein–ligand binding interactions using ever smaller quantities of purified protein target. Improvements in separation technologies may even allow these techniques to be explored using partially purified protein preparations, or in an especially optimistic view, using unpurified cellular or tissue extracts.

New MS hardware and software designs allow more researchers to utilize MS-based techniques without specialized training. Engineering advances that yield complete “lab-on-a-chip” systems are enabling miniaturized chromatography systems that integrate all stages of sample preparation, separation, and introduction to high-sensitivity detector systems. These innovations may lead to the commercial availability of easily accessible instrumentation, so that the techniques presented here will become widely available to researchers in all areas of drug discovery and less limited to specialized laboratories.

Future improvements of the methods presented here will include modifications that enable determination of the thermodynamic parameters of protein–ligand binding interactions. For example, ALIS-based  $K_d$  or off-rate measurements at varying temperatures could yield useful relationships between chemical structures and binding thermodynamics. Ready access to such information, especially for targets that otherwise require complex bioassays for their study, could posi-



tively impact the medicinal chemistry optimization component of the drug discovery process in unanticipated ways.

## Acknowledgements

The authors gratefully acknowledge Satish Jindal, Jerry Shipps, Arshad Siddiqui, and Charles Whitehurst for valuable discussions and critical reading of the manuscript, Ciamac Moallemi, Kieth Mason, and Vladimir Bozin for lending their mathematical expertise, and Yongmin Hou for experimental assistance.

## References

- 1 Falb, D., Jindal, S.: Chemical genomics: bridging the gap between the proteome and therapeutics. *Curr. Opin. Drug Discovery Dev.* **2002**, 5, 532–539.
- 2 Reviewed in: Knight, Z.A., Shokat, K.M.: Features of selective kinase inhibitors. *Chem. Biol.* **2005**, 12, 621–637.
- 3 Windzor, D.J., Sawyer, W.H.: *Quantitative Characterization of Ligand Binding*. Wiley-Liss, New York, **1995**.
- 4 Hajduk, P., Meadows, R.P., Fesik, S.W.: NMR-based screening in drug discovery. *Q. Rev. Biophys.* **1999**, 32, 211–240.
- 5 Gradl, G., Gunther, R., Sterrer, S.: Fluorescence correlation spectroscopy (FCS): measuring biological interactions in microstructures. *BioMethods* **1999**, 10, 331–351.
- 6 Day, Y.S., Baird, C.L., Rich, R.L., Myszkowski, D.G.: Direct comparison of binding equilibrium, thermodynamic, and rate constants determined by surface- and solution-based biophysical methods. *Protein Sci.* **2002**, 11, 1017–1025.
- 7 Cunningham, B.T., Li, P., Schulz, S., Lin, B., Baird, C., Gerstenmaier, J., Genick, C., Frankwang, E.F., Laing, L.: Label-free assays on the bind system. *J. Biomol. Screen.* **2004**, 9, 481–490.
- 8 Reviewed in: Kelly, M.A., McLellan, T.J., Rosner, P.J.: Strategic use of affinity-based mass spectrometry techniques in the drug discovery process. *Anal. Chem.* **2002**, 74, 1–9.
- 9 Kaur, S., McGuire, L., Tang, D., Dollinger, G., Heubner, V.: Affinity selection and mass spectrometry-based strategies to identify lead compounds in combinatorial libraries. *J. Prot. Chem.* **1997**, 16, 505–511.
- 10 Dunayevskiy, Y.M., Lai, J.-J., Quinn, C., Talley, F., Vouros, P.: Mass spectrometric identification of ligands selected from combinatorial libraries using gel filtration. *Rapid Comm. Mass Spectrom.* **1997**, 11, 1178–1184.
- 11 Wieboldt, R., Zweigenbaum, J., Henion, J.: Immunoaffinity ultra-filtration with ion spray hplc/ms for screening small-molecule libraries. *Anal. Chem.* **1997**, 69, 1683–1691.
- 12 Blom, K.F., Larsen, B.S., McEwen, C.N.: Determining affinity-selected ligands and estimating binding affinities by online size exclusion chromatography/liquid chromatography-mass spectrometry. *J. Comb. Chem.* **1999**, 1, 82–90.
- 13 Siegel, M.M., Tabei, K., Bebernitz, G.A., Baum, E.Z.: Rapid methods for screening low molecular mass compounds non-covalently bound to proteins using size exclusion and mass spectrometry applied to inhibitors of human cytomegalovirus proteases. *J. Mass Spectrom.* **1998**, 33, 264–273.

- 14 Davis, R.G., Anderegg, R.J., Blanchard, S.G.: Iterative size-exclusion chromatography coupled with liquid chromatographic mass spectrometry to enrich and identify tight-binding ligands from complex mixtures. *Tetrahedron* **1999**, 55, 11653–11667.
- 15 Moy, F.J., Haraki, K., Mobilio, D., Walker, G., Powers, R., Tabei, K., Tong, H., Siegel, M.M.: MS/NMR: A structure-based approach for discovering protein ligands and for drug design by coupling size exclusion chromatography, mass spectrometry, and nuclear magnetic resonance spectroscopy. *Anal. Chem.* **2001**, 73, 571–581.
- 16 Zhao, Y.-Z., van Breemen, R.B., Nikolic, D., Huang, C.-R., Woodbury, C.P., Schilling, A., Venton, D.L.: Screening solution-phase combinatorial libraries using pulsed ultrafiltration/electrospray mass spectrometry. *J. Med. Chem.* **1997**, 40, 4006–4012.
- 17 Colton, I.J., Carbeck, J.D., Rao, J., Whitesides, G.M.: Affinity capillary electrophoresis: a physical-organic tool for studying interactions in biomolecular recognition. *Electrophoresis* **1998**, 19, 369–382.
- 18 Dunayevskiy, Y.M., Lyubarskaya, Y.V., Chu, Y.-H., Vouros, P., Karger, B.L.: Simultaneous measurement of nineteen binding constants of peptides to vancomycin using affinity capillary electrophoresis-mass spectrometry. *J. Med. Chem.* **1998**, 41, 1201–1204.
- 19 Chu, Y.-H., Dunayevskiy, Y.M., Kirby, D.P., Vouros, P., Karger, B.L.: Affinity capillary electrophoresis-mass spectrometry for screening combinatorial libraries. *J. Am. Chem. Soc.* **1996**, 118, 7827–7835.
- 20 Davidson, W., Hopkins, J.L., Jeanfavre, D.D., Barney, K.L., Kelly, T.A., Grygon, C.A.: Characterization of the allosteric inhibition of a protein–protein interaction by mass spectrometry. *J. Am. Soc. Mass Spectrom.* **2003**, 14, 8–13.
- 21 Muckenschnabel, I., Falchetto, R., Mayr, L.M., Filipuzzi, I.: SpeedScreen: label-free liquid chromatography-mass spectrometry-based high-throughput screening for the discovery of orphan protein ligands. *Anal. Biochem.* **2004**, 324, 241–249.
- 22 Ganem, B., Li, Y.-T., Henion, J.D.: Detection of noncovalent receptor–ligand complexes by mass spectrometry. *J. Am. Chem. Soc.* **1991**, 113, 6294.
- 23 Loo, J.A.: Electrospray ionization mass spectrometry: a technology for studying noncovalent macromolecular complexes. *Int. J. Mass Spectrom.* **2000**, 200, 175–186.
- 24 Heck, A.J.R., Van den Heuvel, R.H.H.: Investigation of intact protein complexes by mass spectrometry. *Mass Spectrom. Rev.* **2004**, 23, 368–389.
- 25 Clark, S.M., Konermann, L.: Diffusion measurements by electrospray mass spectrometry for studying solution-phase noncovalent interactions. *J. Am. Soc. Mass Spectrom.* **2003**, 14, 430–441.
- 26 Breuker, K.: New mass spectrometric methods for the quantification of protein–ligand binding in solution. *Angew. Chem. Int. Ed.* **2004**, 43, 22–25.
- 27 No reference.
- 28 Zhu, M.M., Rempel, D.L., Gross, M.L.: Modeling data from titration, amide H/D exchange, and mass spectrometry to obtain protein–ligand binding constants. *J. Am. Soc. Mass Spectrom.* **2004**, 15, 388–397.
- 29 Powell, K.D., Fitzgerald, M.C.: Accuracy and precision of a new H/D exchange- and mass spectrometry-based technique for measuring the thermodynamic properties of protein–peptide complexes. *Biochemistry* **2003**, 42, 4962–4970.
- 30 Powell, K.D., Fitzgerald, M.C.: High-throughput screening assay for the tunable selection of protein ligands. *J. Comb. Chem.* **2004**, 6, 262–269.
- 31 Zhu, M.M., Rempel, D.L., Gross, M.L.: Modeling data from titration,

- amide H/D exchange, and mass spectrometry to obtain protein–ligand binding constants. *J. Am. Soc. Mass Spectrom.* **2004**, 15, 388–397.
- 32 Clark, S.M., Leait, D.G., Konermann, L.: Taylor dispersion monitored by electrospray mass spectrometry: a novel approach for studying diffusion in solution. *Rapid Commun. Mass Spectrom.* **2002**, 16, 1454–1462.
  - 33 Reviewed in: Schermann, S.M., Simmons, D.A., Konermann, L.: Mass spectrometry-based approaches to protein–ligand interactions. *Expert Rev. Proteomics* **2005**, 4, 475–485.
  - 34 Zehender, H., Le Goff, F., Lehmann, N., Filipuzzi, I., Mayr, L.M.: SpeedScreen: the “missing link” between genomics and lead discovery. *J. Biomol. Screen.* **2004**, 9, 498–505.
  - 35 Huyer, G., Kelly, J., Moffat, J., Zamboni, R., Zongchao, J., Gresser, M.J., Ramachandran: affinity selection from peptide libraries to determine substrate specificity of protein tyrosine phosphatases. *Anal. Biochem.* **1998**, 258, 19–30.
  - 36 Ng, E.S.M., Yang, F., Kameyama, A., Palcic, M.M., Hinds Gaul, O., Schriemer, D.C.: High-throughput screening for enzyme inhibitors using frontal affinity chromatography with liquid chromatography and mass spectrometry. *Anal. Chem.* **2005**, 77, 6125–6133.
  - 37 Reviewed in: Triolo, A., Altamura, M., Cardinali, F., Sisto, A., Maggi, C.A.: Mass spectrometry and combinatorial chemistry: a short outline. *J. Mass Spectrom.* **2001**, 36, 1249–1259.
  - 38 Flarakos, J., Morand, K.L., Vouros, P.: High-throughput solution-based medicinal library screening against human serum albumin. *Anal. Chem.* **2005**, 77, 1345–1353.
  - 39 Annis, D.A., Nazef, N., Chuang, C.-C., Scott, M.P., Nash, H.M.: A general technique to rank protein–ligand binding affinities and determine allosteric versus direct binding site competition in compound mixtures. *J. Am. Chem. Soc.* **2004**, 126, 15495–15503.
  - 40 Annis, D.A., Athanasopoulos, J., Curran, P.J., Felsch, J.S., Kalghatgi, K., Lee, W.H., Nash, H.M., Orminati, J.P.A., Rosner, K.E., Shipps Jr., G.W., Thaddupathy, G.R.A., Tyler, A.N., Vilenchik, L., Wagner, C.R., Wintner, E.A.: An affinity selection-mass spectrometry method for the identification of small molecule ligands from self-encoded combinatorial libraries. discovery of a novel antagonist of *E. coli* dihydrofolate reductase. *Int. J. Mass. Spectrom.* **2004**, 238, 77–83.
  - 41 Coburn, C.A., Stachel, S.J., Li, Y.-M., Rush, D.M., Steele, T.G., Chen-Dodson, E., Holloway, M.K., Xu, M., Huang, Q., Lai, M.-T., DiMuzio, J., Crouthamel, M.-C., Shi, X.-P., Sardana, V., Chen, Z., Munshi, S., Kuo, L., Makara, G.M., Annis, D.A., Tadikonda, P.K., Nash, H.M., Vacca, J.P., Wang, T.: Identification of a small molecule nonpeptide active site beta-secretase inhibitor that displays a nontraditional binding mode for aspartyl proteases. *J. Med. Chem.* **2004**, 47, 6117–6119.
  - 42 Nash, H.N., Birnbaum, S., Wintner, E.A., Kalghatgi, K., Shipps, G., Jindal, S.: U.S. Patent 6 207 861.
  - 43 Wintner, E.A., Moallemi, C.C.: Quantized surface complementarity diversity (QSCD): a model based on small molecule-target complementarity. *J. Med. Chem.* **2000**, 43, 1993–2006.
  - 44 Carell, T., Wintner, E.A., Sutherland, A.J., Rebek, J. Jr: New promise in combinatorial chemistry: synthesis, characterization, and screening of small-molecule libraries in solution. *Chem. Biol.* **1995**, 2, 171–183.
  - 45 Hughes, I.: Design of self-coded combinatorial libraries to facilitate direct analysis of ligands by mass spectrometry. *J. Med. Chem.* **1998**, 41, 3804–3811.
  - 46 As a simplistic explanation, consider solving two coupled equations where  $A \cdot B = 24$  and  $A \cdot B \cdot C = 48$ . It is clear that  $C = 2$ , since  $2 \cdot 24 = 48$  is the only solution for  $C$  that gives the correct result. However, the pair  $(A,$

- B) could be (4, 6) or (3, 8) or (2, 12), etc., since the product of either of these pairs is 24.
- 47 The  $K_d$  for HSA binding to racemic warfarin has been reported for 3–6  $\mu\text{M}$  by various techniques, including frontal analysis and equilibrium dialysis, and is temperature- and pH-dependent. See: Loun, B., Hage, D.S.: Chiral separation mechanisms in protein-based HPLC columns. 1. Thermodynamic studies of (R)- and (S)-warfarin binding to immobilized human serum albumin. *Anal. Chem.* **1994**, 66, 3814–3822.
  - 48 International Patent WO 02/083139, **2002**.
  - 49 Whitehurst, C.E., Nazef, N., Annis, D.A., Hou, Y., Murphy, D.M., Spacciopoli, P., Yao, Z., Ziebell, M. R., Cheng, C.-C., Shipps, G.W. Jr, Felsch, J.S., Lau, D., Nash, H.M.: Discovery and characterization of orthosteric and allosteric muscarinic  $M_2$  acetylcholine receptor ligands by affinity selection–mass spectrometry. *J. Biomol. Screen.* **2006**, 11, 194–207.
  - 50 Smith, K., Windsor, W.: personal communication.
  - 51 Caufield, M.P., Birdsall, N.J.M.: *Pharmacol. Rev.* **1998**, 50, 279–290.
  - 52 Trankle, C., Andresen, I., Lambrecht, G., Mohr, K.: *Mol. Pharmacol.* **1998**, 53, 304–312.
  - 53 Robertson, J.G.: Mechanistic basis of enzyme-targeted drugs. *Biochemistry* **2005**, 44, 5561–5571.
  - 54 Shimizu, Y.: Tuning the function of ZAP-70 in vivo. *Trends Immunol.* **2001**, 22, 541–542.
  - 55 McCormack, J.J.: The rational design, mechanistic study and therapeutic application of chemical compounds, in *Comprehensive Medicinal Chemistry*, ed. Hansch, C., Sammes, P.G., Taylor, J.B., Pergamon Press, Elmsford, **1990**, p. 271.
  - 56 Reviewed in: Christopoulos, A.: Allosteric binding sites on cell-surface receptors: novel targets for drug discovery. *Nat. Rev. Drug Discov.* **2002**, 1, 198–210.
  - 57 Ehlert, F.L.: Estimation of the affinities of allosteric ligands using radioligand binding and pharmacological null methods. *Mol. Pharmacol.* **1998**, 33, 187–194.
  - 58 Scott, M.P., Makara, G., Nan, Y., Mansoor, F., Takonda, P., Liu, B., Hou, Y., Whitehurst, C., Falb, D., Siddiqui, A., Alaoui-Ismaili, M.H.: Identification of novel and selective Akt-1 inhibitors using affinity-based screening of both basal and activated forms of Akt-1. *Am. Assoc. Cancer Res. Meet.* **2003**, Poster.
  - 59 Bellacosa, A., Testa, J.R., Staal, S.P., Tsichilis, P.N.: A role for akt in mediating the estrogenic functions of epidermal growth factor and insulin-like growth factor. *Science* **1991**, 254, 274–277.
  - 60 Barnett, S.F., Defeo-Jones, D., Fu, S., Hancock, P.J., Haskell, K.M., Jones, R.E., Kahana, J.A., Kral, A.M., Leander, K., Lee, L.L., Malinowski, J., Mcavoy, E.M., Nahas, D.D., Robinson, R.G., Huber, H.E.: Identification and characterization of pleckstrin-homology-domain-dependent and isoenzyme-specific Akt inhibitors. *Biochem J.* **2005**, 385, 399–408.
  - 61 Burke, M.D., Berger, E.M., Schreiber, S.L.: Generating diverse skeletons of small molecules combinatorially. *Science* **2003**, 302, 613–618.
  - 62 Schreiber, S.L.: The small-molecule approach to biology. Chemical genetics and diversity-oriented organic synthesis make possible the systematic exploration of biology. *Chem. Eng. News* **2003**, 81, 51–61.
  - 63 cAMP-Screen<sup>TM</sup> chemoluminescent immunoassay system, Applied Biosystems, 850 Lincoln Centre Dr., Foster City, CA 94404, USA.
  - 64 Lambrecht, G., Feifel, R., Wagner-Roder, M., Strohmman, C., Zilch, H., Tacke, R., Wailbroeck, M., Christophe, J., Boddeke, H., Mutschler, E.: Affinity profiles of hexahydro-sila-difenidol analogues at muscarinic receptor subtypes. *Eur. J. Pharmacol.* **1989**, 168, 71–78.
  - 65 Lundblad, L.K.A., Persson, C.G.A.: The epithelium and the pharma-

- cology of guinea pig tracheal tone in vitro. *Br. J. Pharmacol.* **1988**, 93, 909–917.
- 66** Braunwalder, A.F., Yarwood, D.R., Sills, M.A., Lipson, K.E.: Measurement of the protein tyrosine kinase activity of c-src using time-resolved fluorometry of europium chelates. *Anal Biochem.* **1996**, 238, 159–164.
- 67** Trankle, C., Andresen, I., Lambrecht, G., Mohr, K.: M<sub>2</sub> receptor binding of the selective antagonist AF-DX 384: possible involvement of the common allosteric site. *Mol. Pharmacol.* **1998**, 53, 304–312.
- 68** May, L.T., Christopoulos, A.: Allosteric modulators of G protein-coupled receptors. *Curr. Opin. Pharmacol.* **2003**, 3, 1–6.

## 4

# Library Screening Using Ultrafiltration and Mass Spectrometry

*Timothy E. Cloutier and Kenneth M. Comess*

### 4.1

#### Introduction

The early stages of new drug discovery in the pharmaceutical industry rely on many steps in the identification and optimization of small drug molecules. These include target identification, assay development, high throughput screening (HTS), hit characterization, and medicinal chemistry optimization. A current problem with this approach is that more funds are spent on drug discovery than those returned from the steadily decreasing number of drugs reaching the market. In order to continue down this avenue of discovery, it is essential that new strategies and technologies be developed and adopted to reverse this trend. One way to do so is to identify and work with more novel and highly validated molecular targets, using genomic, proteomic, and reverse chemical genetic efforts (the elucidation of target function through identification of target-specific small molecule ligands, and subsequent study of their phenotypic effects; see [1] and references therein), coupled with developing cheaper and faster HTS technologies. HTS includes both activity- and affinity-based methodologies, and plays a variety of roles in drug discovery. Most commonly, HTS is used in a methodical search for potential drug leads of molecular targets through cell-based or purified protein-based assays [2, 3]. While activity-based screening can be very robust and efficient, allowing interrogation of many thousands of compounds per day against a single target, affinity-based screening can allow for even greater overall efficiency by screening multiple targets against hundreds of thousands of compounds per day. Furthermore, affinity screening techniques in conjunction with mass spectroscopy (MS) can very efficiently characterize and rank order the primary and deconvoluted hits, greatly facilitating hit-to-lead identification.

In the past decade, MS has become an indispensable tool for the pharmaceutical industry at each stage in drug discovery (see Table 4.1 [4]). Primarily, MS has been employed at the drug development stage. However, due to major advances in affinity-based MS technologies, it is readily becoming a common tool for hit identification in the drug discovery process (see Table 4.2 [4]). A common theme

**Table 4.1** Major components of drug discovery phase and their challenges. Included from [4] with permission from Wiley Periodicals.

Phase	Numbers of compounds	Role or opportunity for MS-based methods
Initial lead discovery	Start with $\sim 10^6$ ; prefer 10–100 hits	Limited by massive installed base of other methods. Current paradigm requires only single-point estimate of activity, because low-potency hits are expected (therefore, power of MS-based systems may overmatch the task). Mass-based recognition of compounds may be thwarted by isobaric compounds or impurities.
Lead optimization	Start with 1–4 hits; expand to 100–1000 by library technology	May be optimum location for use of MS; at this stage, there is interest in accurately determining the respective affinities of compounds derived from the initial leads. Requires screening shift to a secondary assay that could introduce a lag time following early screening phase.
Candidate selection	From a small set of advanced leads, serial synthesis is used to identify final candidate	Limited, as complex mixtures or large numbers of compounds are no longer being assayed; more traditional pharmaceutical methods can be applied. Use of MS methods introduced in earlier phases may continue.

for most of these strategies involves massive screening of large chemical libraries or natural products against molecular target proteins to identify potential lead compounds for therapeutics based on compound–target interactions. However, few methods actually allow for both target and ligand(s) to be screened in solution so as to preserve the natural state of both target and small ligand(s). This chapter will provide an overview of how affinity-based MS in combination with ultrafiltration is used in hit identification in the new drug discovery process. We will give examples from our own work and others to emphasize the impact that affinity-based MS has had in new drug discovery. We will cover the importance of developing rapid, highly efficient ultrafiltration affinity-based hit identification strategies, briefly review the principles of specific MS technologies used in these endeavors, and describe the many ways ultrafiltration-based MS is utilized in affinity high throughput screening in today's pharmaceutical industries.

The recent advent of efficient high throughput affinity-based techniques has greatly impacted the new drug discovery process. Such affinity-based technologies have helped begin to answer crucial questions at the earliest possible stage of drug discovery: (i) is the biological target druggable?, (ii) how structurally diverse is the selection of novel small molecules?, and (iii) do selected compounds allow for rapid structure–activity relationship (SAR) development to get lead com-

**Table 4.2** MS-based methods proposed for use in lead discovery.  
Included from [4] with permission from Wiley Periodicals.

Method	Target	Potential leads	Principle	Reference
Frontal-affinity chromatography-MS	Immobilized in a column	Pumped through column	Compounds in dynamic equilibrium with immobilized target. Unbound and weakly bound compounds eluted earlier than bound. Mass-specificity in detection identifies compounds	(Schriemer et al., 1998)
Pulsed ultrafiltration-MS	Mixed with multiple compounds in solution	Mixed with target in solution	Target mixed with potential ligands is placed over ultrafiltration membrane; when pressure is applied, ligands showing affinity for the protein are selectively concentrated; later, they are identified by MS	(Zhao et al., 1997)
Affinity size exclusion-MS	Mixed with multiple compounds in solution	Mixed with target in solution	Rapid molecular exclusion fractionation in a spin column separates target-ligand complexes from unbound compounds; MS identifies binders	(Kaur et al., 1997)
Ultrafiltration-MS	Mixed with multiple compounds in solution	Mixed with target in solution	Target mixed with ligands and subjected to centrifugal ultrafiltration; binding compounds separated from non-binders that are washed to waste; ligands bound to target are eluted by acidification and detected by MS	(Wieboldt, Zweigenbaum, & Henion, 1997)



Table 4.2 (continued)

Method	Target	Potential leads	Principle	Reference
Affinity capillary electrophoresis-MS	In electrophoretic buffer	In running buffer for CE	Bound ligands measured by mobility change of ligand upon interaction with target in electrophoretic buffer and identified by MS	(Chu et al., 1996)
Surface plasmon resonance-MS	Coupled to optical sensor surface	Flow across sensor surface	Change in surface refractive index to detect presence of a binding partner for an immobilized target; MS identifies the binding partner	(Sonksen et al., 1998; Nelson & Krone, 1999)
Affinity capture-MS	Immobilized on beads	Incubated with immobilized target	Bead-bound target mixed with potential ligands; unbound ligands removed by washing; bound ligands eluted and identified by ES-MS/MS	(Kelly et al., 1996)
Noncovalent affinity-MS	In gas phase	Mixed with one or multiple targets	Direct mass analysis of target-ligand mixture; complex of a ligand with a given target (or multiple targets) is identified directly from its mass using very soft ionization from volatile buffer	(Hofstadler et al., 1999)

pounds to the clinic faster? In order to facilitate the development of new screening methodologies many companies utilize existing technologies as platforms for developing new screening campaigns.

For example, Graffinity Pharmaceutical Design GmbH (Heidelberg) [5] uses Rapid Array Informed Structure Evolution (RAISE™), a surface plasmon resonance detection methodology, to identify novel target-specific compounds by flowing soluble proteins over gold surface immobilized fragments isolated from a combinatorial chemistry-derived library. 3-Dimensional Pharmaceuticals (now part of Johnson & Johnson) uses fluorescence-based thermal shift assays in a microplate, high throughput format to monitor ligand-induced stabilization of

proteins. The technique has several advantages, namely that the general applicability of the thermal shift assay circumvents timely and costly development steps, and the assay is indiscriminant to any prior knowledge of protein function [6].

Finally, measuring amide hydrogen/deuterium (H/D) exchange in proteins, monitored by protein mass spectrometry, has been used to monitor ligand binding-induced shifts in protein stability [7–9]. The first technology SUPREX (stability of *un*purified proteins from rates of H/D exchange) uses a fluorescence-based thermal shift assay, developed in a microplate, high throughput format, to monitor ligand-induced stabilization of proteins [7]. Protein stability is assessed by following the extent of H/D exchange during a multi-point urea titration and establishing the midpoint for protein unfolding. When ligand binders are added protein stability is enhanced and a higher urea concentration is required to reach this midpoint. By choosing an appropriate single urea concentration ( $\sim 3$  M) the ability of individual ligands to influence protein stability can be measured, and this has been exploited as a high throughput screening technology. Briefly, test compounds (at  $6\text{ }\mu\text{M}$ ) are placed in microtiter plate wells, followed by deuterated exchange buffer that contains a constant urea concentration, and this mixture is allowed to equilibrate [7]. Target protein is then added in small volumes ( $10\text{ }\mu\text{L}$ ) to a final concentration of  $1\text{ }\mu\text{M}$  and equilibrated for 30 min. Next, H/D exchange is quenched with trifluoroacetic acid, the sample is concentrated and desalted using chromatography columns, and placed at  $-20\text{ }^{\circ}\text{C}$  to prevent H/D back-exchange. Finally, the samples are analyzed using MALDI-MS. A caveat is that the ligands must be in significant excess of both the protein concentration and the  $K_D$  of protein–ligand complex, which offers the possibility of compound solubility issues. For example, Powell and Fitzgerald alluded that ligand concentrations in excess of  $100\text{ }\mu\text{M}$  may be required to measure  $10\text{ }\mu\text{M}$   $K_D$  binding if a modest shift in stability toward unfolding is observed. Such high compound concentrations suggest solubility may be a limiting issue. The second technology PLIMSTEX (quantification of protein ligand interactions by mass spectrometry, titration and H/D exchange) monitors differences in H/D exchange of amide hydrogens of a target protein resulting from the interaction with a ligand by ESI-MS (see Chapter 11).

Notably, all of the above technologies function by observing quantitative functional changes or chemical modifications in the target protein, rather than the ligand. A disadvantage to this paradigm is that the ligands must be present in significant excess of both the protein concentration and the  $K_D$  of the biological reaction. Considering the  $K_D$  range of  $500\text{ nM}$  to  $5\text{ }\mu\text{M}$  as typical in early stage drug discovery, there is significant concern about compound solubility. Conversely, techniques that monitor ligands directly, rather than protein behavior, have the advantage of being performed at protein excess. Under these conditions, compound solubility typically is less of an issue because their concentrations can be held much lower, at least several-fold less than the  $K_D$  and near the limits of MS detection. However, a major caveat to protein-excess screening paradigms is that protein consumption becomes a limiting factor. Hence, for these campaigns to be successful in early-stage drug discovery, constantly evolving strategies for re-

ducing target protein consumption must be implemented. Many companies have circumvented this obstacle by moving to much larger compound screening mixtures. With the advent of MS-based readout in affinity screening methodologies, the monoisotopic masses unique to each individual compound can be directly measured with MS, even in large mixes containing closely related monoisotopic redundant neighbors, allowing for target-specific ligands to be readily identified.

Several affinity screening methodologies that include MS-based readout and work under protein-excess conditions have been developed in the past decade [1]. Some examples include affinity selection/mass spectrometry (ASMS; Abbott Labs [10]), size exclusion chromatography with LC-ESI-MS (see Chapter 2 and 3 [11–19]), the use of coupled or non-coupled pulsed ultra-filtration/mass spectrometry (summarized in this chapter [11, 20–23]), restricted access phase chromatography (see Chapter 5 [24, 25]), capillary electrophoresis [26, 27], target shift mass spectrometry [28], and multitarget affinity/specificity screening (MASS, see Chapter 10 [29, 30]).

Importantly, the central difficulty for high throughput affinity-based screening techniques is how to screen large compound collections in a realistic timeframe. Each of the above techniques has strengths and limitations with respect to assay development time, screening throughput, specialized protein requirements, and specialized library design requirements [11, 22, 31]. For example, for those techniques requiring the immobilization of reaction components (such as protein or compound tagging), there is the possibility for artifacts in protein character (alteration in conformation, inactivation of key residues) or limitations in library chemistry. Additionally, most affinity screening techniques coupled with MS become overwhelmed when hundreds of thousands of library compounds are screened per target, yet a consensus of operational and theoretical studies from HTS over the past ten years has indicated that screening is most effective by maximizing library size [32–34]. Hence, until we develop a more concrete understanding of small molecule structural diversity, and subsequently apply that knowledge to synthesizing small libraries that encompass the entire chemical effector space, our best chance of identifying a good starting point for medicinal chemistry optimization will increase only as the total number of compounds screened increases. Furthermore, as the library size and number of targets increases, a general concern about affinity-based screening is that the identification of a large number of non-selective, promiscuous, compounds can be overwhelming so that the best, selective compounds may be overlooked. Evidence for the above concerns is that most of these referenced techniques have been successful in screening only relatively small libraries, relatively small mixtures of compounds, and even fewer have reported the discovery of bona fide new lead(s).

To address these concerns, we at Abbott Laboratories developed a high throughput screening method that is efficient and robust enough to allow study of many targets against very large libraries on the basis of affinity. The method contains an adjustable selection stringency and a computational filter for removing promiscuous compounds that bind non-selectively to proteins in general. As discussed below, the method enabled the discovery of a novel compound series that

binds specifically and inhibits the UDP-MurNac-pentapeptide synthetase enzyme MurF, which catalyzes the final step in synthesis of the bacterial peptidoglycan cell wall precursor, addition of D-Alanine-D-Alanine to UDP-MurNac-tripeptide. Targeting the UDP-MurNac-pentapeptide synthetic pathway has been a goal of antibacterial research for years [35]. Two chemically related compounds were rapidly determined to be the most potent and selective ligands in a library of 123 405 compounds, screened in large pools of ~2700 compounds per mixture with a stringency set by the protein concentration of 10  $\mu$ M. The identification of this novel MurF inhibitor series led to a medicinal chemistry optimization effort described in detail elsewhere [36].

## 4.2

### Ultra-high Throughput Filtration-based Affinity Screening as a Discovery Tool

#### 4.2.1

##### Affinity Selection/Mass Spectrometry

We have developed a high throughput ultrafiltration affinity screening method coupled to MS (affinity selection/mass spectrometry; ASMS), which works with any soluble target and small molecule library (including natural products)<sup>1</sup>. ASMS is amenable to parallelization, efficient and robust enough to allow study of many targets against very large libraries on the basis of affinity, yet designed to identify target-specific binders over a broad range of affinities, and it provides both rank ordering and affinity measurements of bound ligand(s). Because we work at excess protein, relative to individual compounds, the protein concentration drives the binding reaction. Also, assay stringency is both adjustable and dependent on that protein concentration. Furthermore, we have developed a computational method to remove promiscuous compounds that bind non-selectively to proteins in general, greatly reducing our “false positive” hit rates. We have demonstrated the validity of ASMS with numerous targets and screening paradigms [10, 37], establishing it as a very powerful drug discovery tool.

We recently reported the discovery of a new class of inhibitors to an essential *Streptococcus pneumoniae* cell wall biosynthesis enzyme, MurF, by our novel affinity screening method [10]<sup>1</sup>. The strategy involved screening very large mixtures of diverse small organic molecules against the protein target on the basis of equilibrium binding, followed by iterative ultrafiltration steps and ligand identification by mass spectrometry. Hits from any affinity-based screening method often can be relatively non-selective ligands, sometimes referred to as “nuisance” or “promiscuous” compounds. Ligands selective in their binding affinity for the MurF

1) Sections of text and figures are included with permission from Sage Publications and Corwin Press.

target were readily identified through electronic subtraction of an empirically determined subset of promiscuous compounds in the library without subsequent selectivity panels. The complete strategy for discovery and identification of novel specific ligands can be applied to all soluble protein targets and a wide variety of ligand libraries.

#### 4.2.2

##### Primary Screening Strategy

The general method for ASMS is shown in Fig. 4.1. In ASMS, the target concentration is generally set at 5–10  $\mu\text{M}$ , so that at equilibrium, ligands with affinities of no weaker than  $K_D \sim 10 \mu\text{M}$  will be significantly bound and, therefore, retained in the ultrafiltration steps. The minimal concentration of each small molecule is dictated by the eventual need to detect ligands by mass spectrometry after several cycles of ultrafiltration and subsequent extraction. In order to ensure detection just above baseline for the vast majority of compounds, which vary in inherent ionization properties and efficiency of mass spectrometric visibility, the starting compound concentration is set at 1.5  $\mu\text{M}$  per compound. The mixture

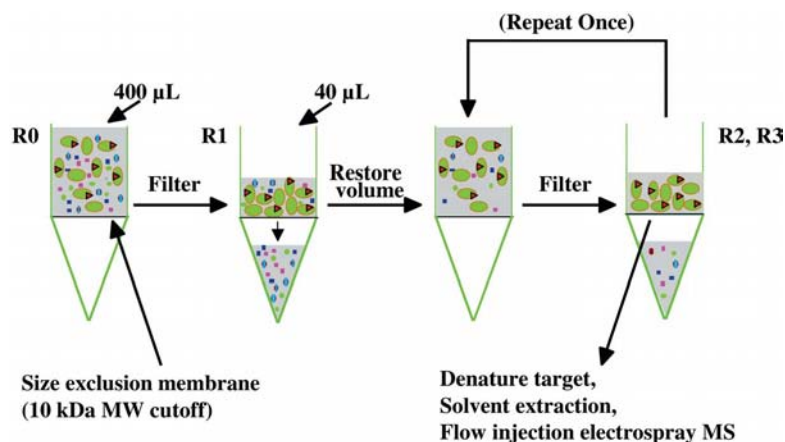


**Fig. 4.1** Schematic of the ASMS experiment format. In primary screening, several thousand compounds are included in a single tube and allowed to equilibrate with the target protein under excess target concentration relative to individual compound ligands. The concentration of each compound is 1.5  $\mu\text{M}$  relative to 5–10  $\mu\text{M}$  target protein. Hence at equilibrium the amount of ligand bound is directly related to both the target concentration and the intrinsic  $K_D$  of the ligand. Multiple rounds of

ultrafiltration are used to separate protein-bound ligands from non-ligands free in solution in order to increase the signal for ligands over background of non-ligands. Sampling and analysis takes place only at the end of the final round of selection. In the deconvolution/retesting phase, 10–30 compounds are included per tube, and 10% of the initial ("R0") volume is sampled as well as the entire volume at the end of R3. Included from [10] with permission from SAGE Publications.

size is set to be as large as possible to minimize the quantity of protein required and increase the throughput for screening the maximum number of compounds, while still trying to maintain a condition of excess free target. By screening  $\sim 2700$  compounds per mixture, the combined small molecule concentration is  $\sim 4$  mM, or  $\sim 400$  times in excess of the target protein. However, in a diverse small molecule mixture of 2700 compounds, very few compounds are anticipated to have  $K_D < 10$   $\mu$ M, or even  $K_D < 100$   $\mu$ M, so that the probability of competitive binding leading to the loss of a high affinity ligand is very low. For example, in small molecule screening using an NMR affinity screening method [38], the frequency of compounds with  $K_D < 1$  mM is  $\sim 0.25\%$  [9]. Therefore, if there are on average  $\sim 7$  very weak ligands (0.25% of 2700) per mixture, in aggregate these are in equimolar concentration with the target protein, and the protein will still be mostly unbound.

Multiple rounds of selection are carried out in order to increase the signal over background. When 90% of the volume is filtered, the initial equilibrium bound fraction of each compound is retained, in addition to a constant residual 10% (unbound) from the remaining volume. Though unbound ligands are being depleted during filtration, the initial equilibrium quantity of bound ligand is maintained because the protein concentration is also increasing at the same rate. For example, a ligand with  $K_D = [\text{protein}]$  will be approximately 50% bound initially. As half the volume has passed through the filter, half of the free ligand has passed through (or 25% of the total), but now  $[\text{protein}] = 2K_D$ , so 66% of the remaining 75% of the ligand will be bound, which is equal to 50% of the original ligand still bound. In other words, the use of ultrafiltration results in a continuous equilibrium such that the relative enrichment can be achieved on the basis of equilibrium rather than dissociation rate, particularly for weak binding compounds with  $K_D$  values in the low micromolar range (which typically equilibrate on a timescale that is faster than the volume reduction). After each round of selection, the volume is restored to the initial volume, but so is the initial protein concentration. Successive rounds of selection result in exponential enrichment of ligands such that the final concentrations will be inversely correlated to the  $K_D$  of each ligand (i.e., compounds with the highest affinity, or lowest  $K_D$ , will be the most abundant).

By adjusting the target concentration, the screening stringency can be altered. Given the starting concentration of each compound in the mixture and the post-selection processing for mass spectrometric detection, the ASMS method is designed so that compounds that cannot bind (i.e., those that have  $K_D > 10 \times [\text{protein}]$ ) are just below the limit for detection in the mass spectrometer, whereas those with the desired affinity ( $K_D \sim [\text{protein}]$ ) will be  $>10\times$  above the background as the only remaining peaks. In practice, for the majority of the library a compound with affinity equal to the protein concentration will be robustly identified, while a weaker binder will show less consistent results. However, compounds with weaker  $K_D$  values, on the order of three-fold above the protein concentration, can also be readily observed when the compounds are especially well extracted and/or ionized in the mass spectrometer.

Parallelization of the processing of individual filter units can lead to extremely high throughput. Our compound library is split into two sets, which we screen in duplicate against every target. In the past a single replicate for either set was screened at the bench in one day. It then took two days or more for mass spectra to be acquired and analyzed due to experimental, equipment, computational, software, and database limitations. Our first step to improve ASMS throughput was to design a methodology that allows for both replicates to be performed simultaneously, greatly reducing the total bench time per target; the entire library can now be screened in duplicate in two days. Time-consuming steps were eliminated by the addition of more automation and by setting absolute time limits for each stage. We have greatly accelerated the data handling by processing and analyzing data in parallel on three or four computers simultaneously. We have improved our custom ASAE.NET automated picking software, resulting in faster analysis and better communication with our databases (data not shown) [39]. Furthermore, we now stagger target screening such that two bench scientists and one mass spectrometrists can screen four or five targets at one time. Such process enhancements allow entire screens of a library of approximately 500 000 compounds to be completed in 2.5 weeks. Finally, switching from electrospray mass spectrometric analyses to LC-ESI-MS has afforded a nearly ten-fold increase in compound sensitivity and resolution. Such an enhancement in sample analysis suggests that we may be able to lower our protein and compound concentrations even further to help reduce our total protein consumption.

After affinity selection, an organic solvent extraction step separates ligands from the protein and prepares them for electrospray mass spectrometric analyses in both positive and negative ionization modes. The protocol was experimentally selected for efficient extraction of the widest range of drug-like [40] and lead-like [41, 42] compounds in the compound collection. The mass spectra of samples are processed and either inspected visually or by the aid of ASAE.NET analysis software (data not shown) [39]. Peaks that stand out by comparison with the local background are identified as primary hits. In addition, spectra obtained with other compound mixtures are examined to determine whether the  $m/z$  ratio of identified peaks are unique to a particular mixture. Peaks with the same  $m/z$  ratio in spectra from multiple compound mixtures are generally artifacts, such as contaminants in the protein preparation. To ensure that hits are not missed, peaks are picked even if they are barely enriched over background. The false positives inherent in the noise near background are easily eliminated in the subsequent deconvolution step. The peaks of interest are converted into a list of potential ligands (hits). Each peak, however, corresponds on average to six mass-redundant compounds, with only one typically being responsible for the apparent binding. Therefore, only ~17% of the primary hits are expected to demonstrate binding in subsequent retesting and deconvolution experiments. The primary screen for MurF ligands utilized 45 mixtures of approximately 2700 compounds each and was run in a single day. A duplicate screen was run on a second day. In the MurF screen, 434 peaks were identified as potential hits from the first experiment, ranging in monoisotopic mass from 249.09 Da to 773.50 Da. The number

of peaks in each of the 45 mixtures ranged from one to 35. In the duplicate screen, 390 peaks were identified as potential hits, with 157 peaks overlapping between the duplicate screens. Compounds from the overlapping peaks were assembled into a primary hit list of 1147 compounds for subsequent retesting and confirmation.

#### 4.2.3

##### Retesting and Deconvolution Strategy

In the retesting and deconvolution phase of the procedure new compound mixtures were made based on the results of primary screening. These contained from nine to 14 compounds and no monoisotopic mass redundancy. Since most mass spectrometric peaks picked as hits in the primary screen contain more than one compound, and only one compound per peak is likely to be a binder, the non-mass redundant retest mixtures are unlikely to contain more than a few bona fide ligands, so once again target excess is maintained. Both the initial (round zero, R0, prior to first round of filtration) and final (round three, R3, after three rounds of selection) mixtures are sampled. The free target concentration is in excess over individual ligands, so the amount of compound bound at equilibrium can be estimated according to Eq. (1).

$$\text{Bound Fraction} = \frac{[\text{Target}]}{[\text{Target}] + K_D} \quad (1)$$

The amount of free ligand is disregarded in this estimation.  $K_D$  can be estimated according to the following, where R0 and R3 represent either a raw signal intensity or signal to local background ratio according to Eqs. (2–4).

$$\text{FR} \equiv \text{Fraction Retained} = \left( \frac{\text{R3}}{\text{R0}} \right)^{1/3} \quad (2)$$

(average per round)

$$\text{FB} \equiv \text{Fraction Bound} = \frac{\text{FR}(+) - \text{FR}(-)}{1 - \text{FR}(-)} \quad (3)$$

+/- = presence/absence  
of protein

$$K_D = [\text{Protein}] \left( \frac{1 - \text{FB}}{\text{FB}} \right) \quad (4)$$

During the deconvolution phase of screening, careful control of the pre- and post-filtration volumes are required to ensure both a rank ordering of binding strengths and estimation of the  $K_D$  value. The post-filtration volumes are controlled by use of a novel pressure limited equilibrium filtration device for selection steps. Operationally, all of R3 is sampled for analysis and 10% of R0 is sampled. Therefore, when the compound  $K_D$  is equal to the protein concentration, the R3 signal will be approximately equal to the R0 signal, and an R3 signal generated through selection in the absence of protein will be 100-fold (rather than



1000-fold) less than the R0 signal. Compounds whose  $K_D$  values are ten-fold or more below the protein concentration appear as peaks with approximately ten times the intensity of the R0 peak, assuming a linear dose response in the mass spectrometer. Using the example of a compound with  $K_D = [\text{protein}]$  and a starting compound concentration of 1.5  $\mu\text{M}$  in a volume of 400  $\mu\text{L}$ , 75 pmol of compound remains after three rounds (600 pmol divided by two, three times). Since the final samples are split into three aliquots, for positive ion analysis, negative ion analysis, and a backup sample as needed, approximately 25 pmol of material is available for analysis. By measuring the signal intensity or signal/background ratio for a compound before and after selection, the  $K_D$  value can be estimated.

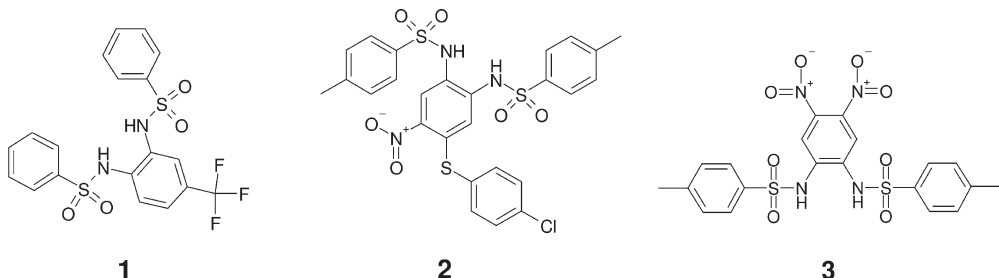
#### 4.2.4

##### Promiscuous Compound Filter

In activity-based HTS campaigns, secondary counterscreens frequently are applied in order to exclude artifacts, such as compounds that inactivate the substrate or detection method rather than the target of interest. One advantage of an affinity-based HTS strategy is that there are no additional reagents, substrates, or cofactors in the assay to increase the potential for false positives due to such artifacts. Additionally, any false positive ligands that do occur should be similar for all targets because the assay format and detection method is identical for every target screened. Aggregated compounds that cannot pass through the 10 000 Da molecular weight cutoff filters are an example. Interestingly, because of the requirement in ASMS for ligands to be dissociated before MS detection, ASMS will not detect reactive compounds bound covalently to a target protein (a common source of false-positive hits in activity-based screens). Compounds that have promiscuous or non-specific affinity for a variety of proteins are another potential problem for HTS, including ASMS. Furthermore, while certain chemotypes seem to recur as non-specific hits in HTS (activity or affinity), some individual members within a class can have just enough selectivity to hit in very few screens due to the relatively high stringency. This can lead to a significant waste of time trying to optimize these into quality lead compounds, as the series can rarely attain drug-like selectivity.

After screening and deconvolution of primary hits from dozens of targets by our ASMS technique it became apparent that the frequency of compound overlap between targets was high but aggregated compound occurrences were very low. Aggregated compounds could be detected in two ways: (i) by showing apparent binding to every target in the primary screen, and (ii) by showing a very high retention in the absence of protein. Non-selective but non-aggregated ligands were discovered as expected, and exhibited a range of  $K_D$  values as measured in deconvolution experiments. Therefore, simply adjusting the stringency or rejecting hits above a certain  $K_D$  threshold cannot easily eliminate these non-selective ligands. Many distinct structural classes or chemotypes were observed, but a phenylsulfoamide series represented by compounds 1–3 appeared most often.

Compound 1 has been resolved as a ligand for ten distinct protein targets out of 16 target screens run, compound 2 as a ligand for 13 out of 40 screens, and compound 3 as a ligand for 12 out of 45 screens. The apparent  $K_D$  value depends on the particular target, with compound 2, for example, having affinities ranging from 1  $\mu\text{M}$  to 30  $\mu\text{M}$  for different targets.

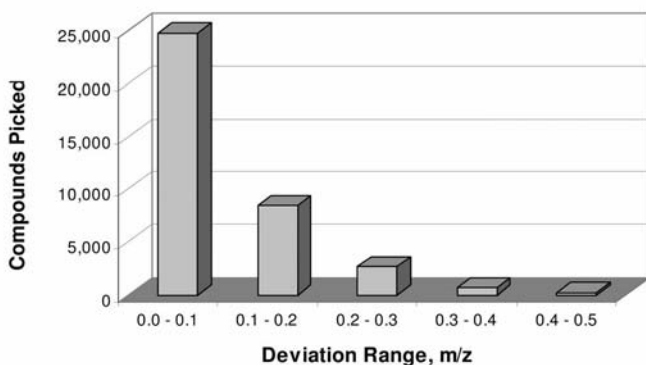


We reasoned that a low stringency ASMS screening campaign might allow identification of non-selective ligands, thereby enabling prioritization of hits that are most likely to be useful leads by virtue of their relatively selective affinity. We also observed that different protein targets varied widely in their propensity to bind promiscuous ligands. This suggests that targets could be profiled for selective chemical tractability. Once a compound library is profiled for the non-specific ligands, the information can be used for all other screens to prioritize compounds for follow-up against specific targets and to prioritize targets based on the likelihood that they can be bound selectively by small molecules. Blood serum, whose principal component is albumin, is known for its ability to bind reversibly to a very large variety of ligands. For this reason, serum was employed as a model target for general non-specific binding. While serum protein binding can be engineered out in a medicinal chemistry campaign on a given series, and serum protein binding is not intrinsically a criterion for deprioritizing a particular lead compound, in the case of affinity-based screening, the leads most likely to be optimized into drugs should be those with selective affinity for a target. Subsequent medicinal chemistry for potency, pharmacokinetic, and other properties, will likely result in some degree of binding to serum proteins which needs to be considered in the context of the rest of the properties, but candidates with target-selective binding interactions make easier starting points for a medicinal chemistry campaign than do non-selective ligands, since non-selective hydrophobicity tends to increase during optimization [41–43].

Our goal was to divide the screening library into two populations, a set of compounds with extremely low probability of promiscuous binding and as small a set as possible that would contain all serum protein ligands under our ASMS conditions; the latter is called the promiscuous compound filter (PCF) list. To do this, screening was carried out at several serum concentrations and in several replicates in order to gather sufficient data for analysis. Figure 4.2 shows statistics from running 45 mixtures containing a total of 123 405 compounds in duplicate

**A**

Experiment	Serum Dilution	Compounds Picked			MurF Hits / Serum Hits	Serum Hits / Total Library
		Positive Ion	Negative Ion	Unique Cpds		
1	2%	4,071	13,082	16,281	44%	13%
2	2%	4,184	12,301	15,741	44%	13%
3	10%	7,530	10,861	17,734	46%	14%
4	10%	5,530	13,338	17,990	47%	15%
5	20%	8,928	11,123	19,054	45%	15%
6	20%	5,447	12,703	17,439	50%	14%
<i>Total Unique:</i>		<i>16,097</i>	<i>24,082</i>	<i>36,748</i>	<i>65%</i>	<i>30%</i>

**B**

**Fig. 4.2** Serum ASMS screen results. Statistics are shown for six primary ASMS screens run against various dilutions of fetal calf serum. Compounds picked, number of compounds corresponding to ligand peaks within a defined  $m/z$  range of the center of the ligand peak. (A) Complete statistics for both positive and negative ion mass spectra; all compounds within a 0.5  $m/z$  unit range of ligand peaks are included. Unique compounds are obtained by combining experimental data and removing duplicates. MurF Hits/Serum Hits: percentage of the 1147 matched unique compounds described in the text that intersect with the unique compounds identified from specific experiments 1–6 or that intersect with the

combined list of unique compounds. Serum Hits/Total Library: number of unique compounds identified in specific experiments 1–6 (or the combined list of unique compounds) divided into the total library of 123 405 compounds. In the last line of the table “Total Unique”, the results from experiments 1–6 are summarized. The first three entries represent the total number of different entries from experiments 1–6 in each column. The ratios given in last two entries are calculated from the total number of unique serum hits (i.e., 36 748). (B) The expected  $m/z$  positions of compounds mostly occur close to the center of ligand binding peaks. Included from [10] with permission from SAGE Publications.

against prepared serum diluted to 2%, 10%, and 20% of its neat concentration (the latter corresponding to approximately 0.1 mM albumin, thus providing the desired low stringency). All compounds whose exact monoisotopic mass falls within 0.5 Da of a peak were annotated.

Fig. 4.2A shows the percentage of compounds on the MurF primary hit list that overlap with the primary hit list for each serum screen and the percentage of the entire library within the serum hit list. Note that these range from 44% to 50%, so that in each case the serum screen is hitting MurF ligands with higher than random (13–15%) frequency. If MurF bound only selective ligands then the serum list would be irrelevant, and one would expect the percentage of MurF hits on the serum list to be no higher than that determined by random chance based on the percentage of the entire library contained on the serum hit list. The decision to use the combined list of 36 748 compounds that occur at least once in any of the serum screens as the PCF list was made on the basis of efficiency. The highest percentage overlap with serum compounds occurs when the MurF hit list is compared to the combined PCF list. In this case, 65% of the MurF hits are from the PCF list, even though it only contains 30% of the total library. Since the majority of the unique compounds within 0.5  $m/z$  units of a peak are very close to the center of the peak, as indicated by a graph of the distribution of deviations (Fig. 4.2B), we included all compounds within 0.5  $m/z$  units to further ensure that the PCF list contained all possible serum protein ligands.

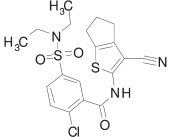
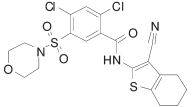
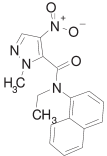
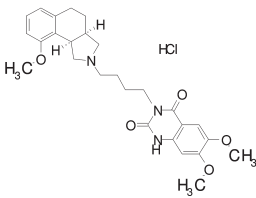
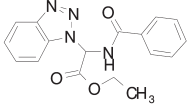
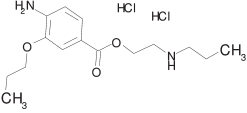
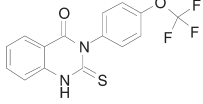
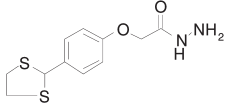
#### 4.2.5

#### MurF Lead Discovery

To efficiently identify compounds of interest for further study in biochemical or cell-based assays, the candidate ligands remaining after promiscuous compound filtering were deconvoluted in small non-mass-redundant mixtures. The eight deconvoluted hits are shown in Table 4.3, along with their enzyme inhibition values. The two best ligands (compounds 4 and 5) also are structurally related and were discovered in different initial screening mixtures. ASMS binding data is shown in Fig. 4.3. Both compounds were ionized in the negative ion mass spectrometry mode, and the characteristic halogen isotope patterns at  $M + 2$  for the monochloro (4) and dichloro (5) functional groups are evident both in primary screening (Fig. 4.3A) and deconvolution testing (Fig. 4.3B, C). Signal intensities are much weaker in primary screening than in deconvolution, most likely because of ionization of the very low levels ( $>1$  pmol) of several thousand nonligands remaining in a mixture after affinity selection. Nevertheless, the signal is still adequate so that these and other hits were selected in the primary screen. Subsequent structure–activity relationship (SAR) studies were conducted to increase the potency of this series, and several analogs with  $IC_{50}$  values in the 20–70 nM range have been synthesized [36]. Additional biophysical studies using X-ray crystallography and NMR have confirmed the active site binding and specificity of the compound series (data not shown).

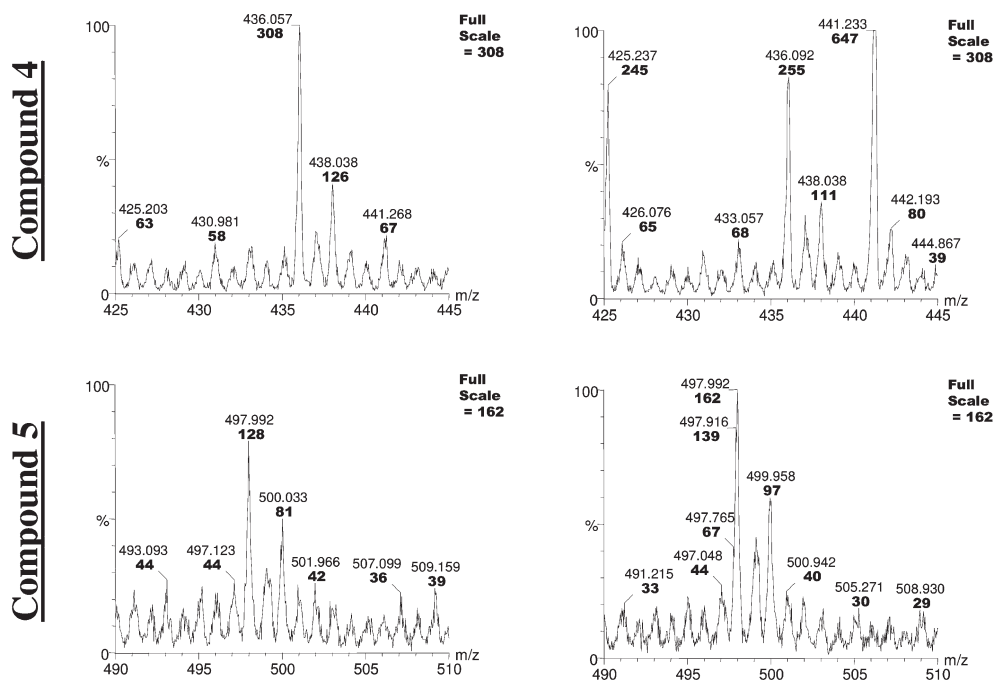
ASMS combined with a novel promiscuous ligand filtering procedure led to the discovery of a potent series of MurF inhibitors. The lead discovery methods were highly parallel, robust, and efficient. One key to success of this very straightforward screening process is the large number of compounds in each primary screening mixture. Without this feature, protein consumption would be prohib-

**Table 4.3** Comparison of MurF ASMS screening-based binding constants and MurF activities from the radiolabeled phosphate release assay. Included from [10] with permission from SAGE Publications.

Compound	Structure	$K_D$ Estimate ( $\mu\text{M}$ )	MurF $\text{IC}_{50}$ ( $\mu\text{M}$ ) <sup>b</sup>
4		3	8
5		$2 \pm 3^a$	1
6		6	> 50
7		11	> 50
8		12	> 50
9		15	30
10		17	19
11		22	> 50

<sup>a</sup> Value obtained from average of triplicate analyses in both positive and negative ion modes.

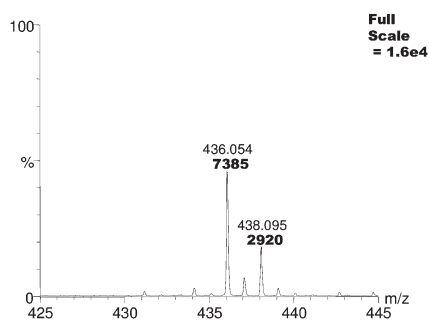
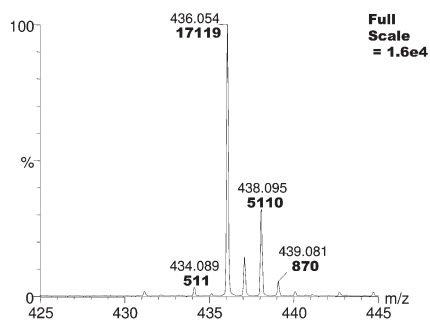
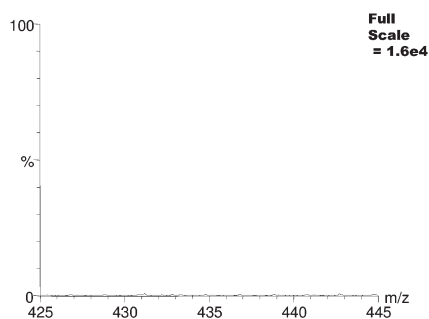
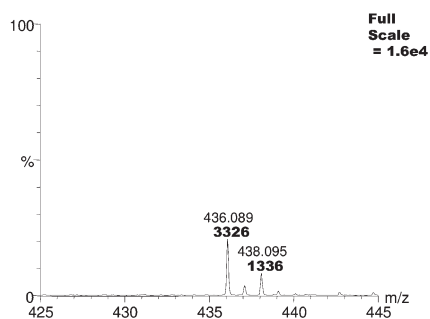
<sup>b</sup> Values obtained from dose response curves, with the exception of Compounds 9 and 10, which were extrapolated from a single 10  $\mu\text{M}$  dose in duplicate (Included with permission from SAGE publications. [10])

**A****Experiment 1****Experiment 2**

**Fig. 4.3** Primary screening and deconvolution stage mass spectra. (A) The region of the negative ion mass spectra containing the ions of interest is shown for two compounds, in two replicate primary screening experiments. Full-scale y-axis intensity values are normalized to 308 counts per second for compound 4 ( $m/z \sim 436$ ) and 162 counts per second for compound 5 ( $m/z \sim 498$ ).

itive, and the logistics of manipulating a larger number of smaller mixtures would be difficult. While larger mixtures of compounds result in an increase in mass redundancy and therefore a concomitant increase in the number of compounds that need to be deconvoluted and retested, the overall efficiency is greatly increased.

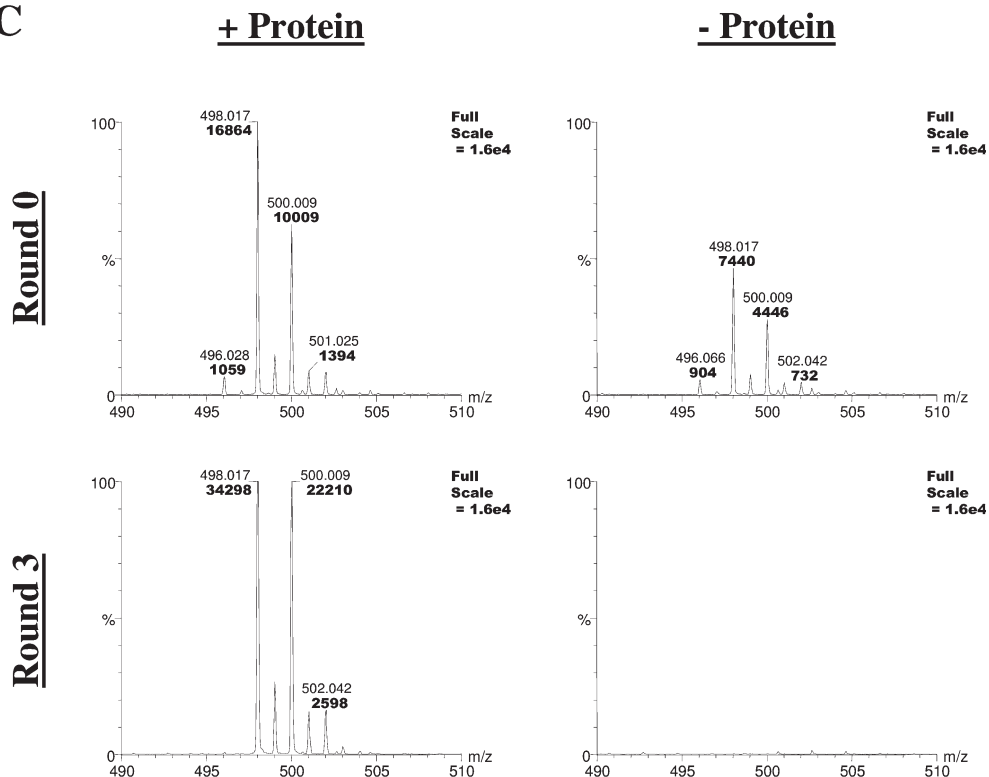
There are approximately 2700 compounds per primary screening mixture, and the readout is in essence multiplexed; the ligands are individually ionized and identified in the mass spectrometer according to their exact mass positions. The readout, however, does not unambiguously identify compounds, as multiple compounds in a single mixture may have the same mass, i.e., a particular peak may correspond to as many as 31 compounds with closely related masses. The protein excess over individual compounds coupled with the rarity of potent ligands within a randomly assembled library minimizes competition between ligands for

**B****+ Protein****- Protein****Round 0****Round 3**

**Fig. 4.3 (B)** Deconvolution experiments for compound **4**. The compound is screened in a much smaller mixture than in primary screening and with no mass redundancy. Both round 0 data (before affinity selection) and round 3 data (after three rounds of affinity selection) are shown, where round 0 represents a sampling prior to any ultrafiltration. Round 0 and round 3 samples undergo identical denaturation/solvent extraction procedures. Data were generated

both with (+protein) and without any protein present (−protein), in order to observe whether compound retention by ultrafiltration is protein-dependent. Compounds shown here are observed in mass spectra in round 0 regardless of the presence or absence of protein in the starting sample and are observed in round 3 only in the presence of protein. Spectra are normalized to an intensity of 16 000 counts per second.

available sites. In the theoretical case where the number of ligands overwhelms the number of target sites the apparent affinity of ligands will be reduced. Caution must be used in assembling libraries of either biomolecular or combinatorial origin because these could have problems with weak binding as a class [32, 33]. This could result in significant competition, making individual higher affinity ligands undetectable. With a sufficiently diverse collection of compounds this is not a concern.

**C**

**Fig. 4.3** (C) Deconvolution experiments for compound 5, performed as in (B). Round 0 spectra in (B) and (C) likely are more intense in the presence of protein than in its absence due to protein preventing compound binding to the ultrafiltration membrane. Included from [10] with permission from SAGE Publications.

The retesting/deconvolution phase of screening utilizes small mixtures of non-mass-redundant compounds. A balance of stringent rejection criteria and emphasis on reduction of false negatives is maintained during this phase. While in theory 90% of the compound is lost in each round of selection in the absence of protein, an actual protein-free selection is carried out for each mixture in order to increase accuracy and decrease false positives. At one extreme, compounds that form large aggregates [44, 45] could appear to be ligands in the protein-containing selection even if they cannot, in fact, bind to the target, but such compounds will also demonstrate an equivalent fraction retained per round of selection in the absence of protein. When this occurs, the fraction bound [Eq. (3)] calculates approximately to zero, and no  $K_D$  estimate is made. Additionally, the set of four spectra [R0(+protein), R0(−protein), R3(+protein), and R3(−protein)]



for each putative deconvoluted ligand is scored visually for verification of appropriate ligand behavior. Based on a survey of several thousand randomly chosen compounds, approximately 80% of the library compounds are visible under the experimental conditions (data not shown). The remainder may be poorly extracted, show poor sensitivity to electrospray ionization, or have an incorrectly assigned structure and formula due to degradation or rearrangement during storage. Although a limitation of the method is its bias toward generally more MS visible compounds, compound structural series that are identified through traditional high-throughput screening techniques, such as fluorescence polarization assay, are also discovered in ASMS screens [37]. The total time required for the screen from primary screening through retesting and deconvolution is under three weeks, and it can be further reduced by automation.

The concept of promiscuous compound filtering was implemented for ASMS screening as a means to prioritize hits based on their potential value as drug leads, but it also may be used to prioritize targets. Note that 65% of the MurF hits resulted in overlap with the total combined PCF list. In 34 ASMS screens run against targets across several areas of pharmaceutical research, we have observed that 36–92% of primary hits for individual protein targets overlap with compounds on the PCF list. Since targets vary widely in their tendency to bind compounds on the PCF list, it is tempting to believe that targets with higher frequency of overlap with the PCF list will pose a more difficult challenge in drug discovery either because of a similarity to serum proteins or a binding site that is ideal for promiscuous compounds in general. Medicinal chemistry directed at these kinds of targets, even with initial leads that show some binding selectivity, may result in optimized compounds that have undesired binding affinity for other proteins if the nature of the active site on the target is inherently similar to other proteins in the ability to bind promiscuous classes of small molecules. Targets that result in hit lists with very high overlap with the PCF list may be considered less desirable even if a few selective hits are discovered, though this is only speculation at this point. The difference in the propensity of various proteins to bind to the major classes of promiscuous compounds is one of the more interesting results of these experiments and would require more study in order to fully understand all of the ramifications on the drugability of different kinds of targets.

Although there must be “innocent bystanders” present in the PCF list, the mass redundancy of the primary screening mixtures makes this unavoidable. The time cost of deconvoluting all serum binders would be prohibitive. Our strategy still costs the time spent in screening the 45 compound mixtures, six times (Fig. 4.2). However, in addition to allowing prioritization of hits and targets, the PCF list filtering also reduces the cost of retesting and deconvolution if the hits overlapping the PCF list are not pursued. For MurF, the initial list of 1147 matched compounds was reduced to 402 compounds by application of the promiscuous compound filter. This meant that only 30 mixtures of 13 compounds needed to be tested in the deconvolution step instead of 86 mixtures. At this rate, the investment in upfront promiscuous compound filtering is realized after screening just five targets. The research cost of attempting to optimize the chem-

ically intractable compounds and targets that application of promiscuous compound filtering may eliminate, however, is likely to be much higher. Importantly, the PCF list is used to electronically filter hits as a means of prioritizing hits, but no information is lost. One can also choose to deconvolute those hits that overlap with the PCF list, with the expectation that many, but not all, of the hits identified will subsequently be shown to exhibit non-specific protein binding, e.g., compounds 1–3.

ASMS is applicable to combinatorial and traditional libraries of small molecules, peptides, and carbohydrates, although with libraries that may share some non-specific affinity for particular targets, large mixtures should be tested to ensure that there is not significant aggregate binding of the mixture (discussed above). No protein tag or protein molecular weight constraints are required. Like other affinity techniques for HTS, ASMS identifies compounds that bind to a target without regard to function, and its speed, efficiency, and applicability to all soluble targets makes it appropriate for genomics and proteomics targets. For example, we screened the inactive form of a given kinase with the intent of identifying a non-active site binder that would prevent target activation required for downstream activity. In doing so, we isolated a small molecule that bound to an extraneous site that exhibits kinase specific and selective inhibition (data not shown). Of note is the ligand confirmation efficiency built into the system. In most HTS screen formats, chemical matter showing activity or binding must be independently confirmed for structural integrity [46]. In ASMS, ligands are identified from their mass spectrometric peak position, so the only opportunity for misidentification is via a structural isomer. ASMS can be complementary to activity screening, but also can be useful in identifying ligands for targets with particularly difficult or expensive activity assays. While one novel class of MurF ligands discovered here clearly was optimizable for *in vitro* potency, no whole-cell antibacterial activity has been demonstrated for this series, even after steps were taken to address potential issues of cellular permeability and active transport of compounds out of the cell [36]. The discovery of the MurF ligands demonstrates the utility and advantages of the lead discovery methods described here.

## 4.3

### **Additional Affinity Screening Methodology That Includes Mass Spectrometry-based Readout**

#### 4.3.1

##### **Pulsed Ultrafiltration MS**

Pulsed ultrafiltration MS (PUF-MS) represents an inline high throughput affinity screening method with a variety of potential uses in the discovery and development of pharmaceuticals [22]. The in-line combination of solution-phase equilibration, ultrafiltration, and electrospray liquid chromatography mass spectrometry (LC-ESI-MS) facilitates the identification of high affinity target-specific

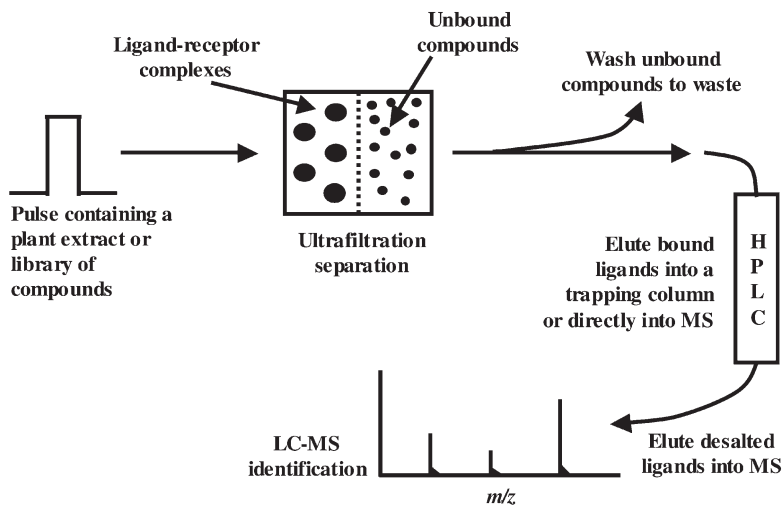


**Fig. 4.4** Scheme of pulsed ultrafiltration–mass spectrometry (PUF-MS) to screen chemical mixtures for compounds that bind to a macromolecular receptor. The ultrafiltration membrane traps a receptor in solution, but allows low molecular weight

compounds to pass through. Bound ligands are eluted from the chamber by destabilizing the ligand–receptor complex with an organic solvent or pH change. The ligands are characterized with MS. Included from [22] with permission from Wiley Periodicals.

ligand(s), and also allows for potential reuse and/or recovery of the target proteins. PUF-MS has been used for rapid screening of several drugs to determine their effect on metabolism, and to characterize various primary metabolites (i.e., microsomal cytochromes P450 [21]). During PUF-MS, soluble target is equilibrated with modest compound mixtures of ~20 molecules for approximately 20 min and injected into the ultrafiltration chamber (the “pulse”). As shown in Fig. 4.4 [21], the target protein is trapped in solution on one side of the chamber by an ultrafiltration porous membrane of defined mass selectivity (i.e., a 10 kDa molecular weight cutoff). The sample is then flushed for a predetermined amount of time (8–10 min) with water to remove unbound ligands. Van Breemen and colleagues demonstrated that during the washing step more than 98% of the unbound compounds diffused out from the ultrafiltration chamber, reducing their concentration to background levels in the electrospray mass spectra. The wash may be discarded to waste or monitored continuously by the mass spectrometer (Fig. 4.4). Next, the ligand-target complex in the mobile phase is disrupted by addition of organic solvent (i.e., 50:50 v/v methanol:water) or pH changes, thereby releasing bound ligand(s) into the mass spectrometer for identification. In this manner, the ultrafiltration chamber functions as a solution-phase extraction device.

In a continuous infusion mode, the mass spectrometer acts as the detector for target-specific small molecules exiting the sample chamber. Each compound's intrinsic unique mass results in specific elution profile that is recorded for quanti-

tation. Specifically, by integrating the area under each spectra curve for a given compound's mass signal the total amount of target-specific ligand can be calculated. If the starting concentrations of a ligand and target protein are known, then one can calculate the compound's relative  $K_D$  for that target. Hence, both kinetic and thermodynamic parameters can be simultaneously deduced from these ligand-binding studies for multiple ligands against a single protein target.

Similar to ASMS, in pulsed ultrafiltration screening assays it is important to keep the target concentration in excess of the compound concentration. In general, a protein concentration is chosen to be approximately equal to the  $K_D$  of the weakest ligands. For example, the use of 1  $\mu\text{M}$  protein permits the detection of target-specific binders that exhibit  $K_D$  values of 0.1–1.0  $\mu\text{M}$ . The ratio of receptor and ligand concentrations, or selection stringency, determines the number of “hits” that might be obtained when screening large compound mixtures. High receptor concentrations typically result in larger numbers of hits because weaker ligands will be identified together with the high-affinity compounds. With screening libraries that contain large mixtures, even with diverse structures, excess protein is required to minimize competition between ligands so that all of the potential hits may be detected. When this experiment is conducted in the presence of a high molecular weight protein, elution of a compound with no target-specific affinity (non-binder) follows the same profile as without target. However, if affinity exists between a compound and the target, its elution profile is perturbed. A caveat, though, is that if the binding reaction exhibits a very rapid off rate the total area under the curve for that compound is unaltered. Binding-induced shifts in a compound's elution profile over time are interpreted in terms of the binding affinity [47].

There are several advantages and disadvantages with PUF-MS with respect to other affinity selection techniques. In contrast to ASMS, the equilibration and filtration steps are coupled to the mass spectrometer, and the rate limiting steps therefore are the lengthy equilibration time required for ligand binding and wash time to remove unbound ligands. For precious protein samples, however, an advantage is that protein usage can be minimized in this inline technique. If the protein can be treated in a manner that releases bound ligands but does not irreversibly denature the protein (for example, by careful choice of organic solvent or pH shift), then the protein may be used repeatedly. Additionally, compound handling steps are minimized in an inline procedure and the potential for compound loss to surfaces and introduction of adventitious contaminants is minimized. In addition, like ASMS, affinity selection reactions occur in solution; screening covalently immobilized proteins or ligands can compromise protein and/or ligand native conformations or binding characteristics. A disadvantage that PUF-MS shares with ASMS is the proclivity for non-specific binding of small molecules to the ultrafiltration membrane. This necessitates certain controls. Specifically, because the elution of a given binder from the chamber is slowed by reversible protein association and dissociation, relative to controls performed in the absence of protein, the elution profiles of such a binder differ between these two cases. Using differential equations that describe solution fluidity and ligand–

target association, quantitative thermodynamic and kinetic information can be derived from the degree of difference between their elution profiles [47, 48].

Finally, several features inherent to PUF-MS suggest this methodology is a potentially powerful tool in new drug discovery. Predominantly, it has been demonstrated to be applicable to “reverse pharmacology” studies in which a given receptor of interest has been identified and isolated, but novel small molecules that bind to the receptor are needed [22]. Also, the binding behavior of these ligands can be quantitatively measured (association constants or binding rates). There is also evidence that PUF-MS is very effective for metabolic screening [49]. van Breemen and colleagues accurately identified novel phase I metabolites of xenobiotic compounds generated in the presence of cytochromes P450. Also, pulsed ultrafiltration was used to screen four natural products extracts for the metabolic formation of electrophilic quinoid metabolites [22]. Using tandem MS approaches, the chemical diversity of the mixtures did not compromise the ability of PUF-MS to detect such reactive metabolites because tandem MS can selectively detect fragment ions from glutathione adducts, using neutral-loss scanning or precursor-ion scanning [22]. These applications demonstrate the versatility of PUF-MS and are likely to be valuable in new drug discovery endeavors.

#### 4.4

#### Conclusions and Future Directions

Many of the key steps in early drug discovery have benefited from the application of affinity-based mass spectroscopy screening technologies, including lead identification in HTS, target identification and purification, the characterization of modification sites on proteins, and the detection and optimization of preclinical candidates. Although many affinity methods have been around for decades, only recently have their utility been truly recognized and shown great promise in supporting the pharmaceutical industry’s future lead discovery needs. When combined with mass spectrometry, affinity techniques offer high-resolution structural and biophysical insights into lead identification. They have been used to address some difficult and limiting factors in the early stages of drug discovery, including exploring the drugability of a biological target, providing both rank ordering and affinity measurements of bound ligand(s), and facilitating rapid SAR development to get lead compounds to the clinic faster. The development of several high throughput ultrafiltration affinity screening methods coupled to MS have greatly aided these endeavors. Such technologies work with any soluble target and small molecule library, they are amenable to parallelization, allowing for efficient and robust study of many targets against very large libraries on the basis of affinity, and they are designed to identify target-specific binders over a broad range of structural classes and affinities. The growing efficacy of these methodologies have surfaced at a time where the need for more efficient HTS assays and tools used for early lead identification in the pharmaceutical industry is at its highest point in history. Presently, more funds are spent on drug discovery than

those returned from the steadily decreasing number of drugs reaching the market, and the result is increasing economic pressure on many big pharmaceutical companies. However, based on the promising reports of late, we anticipate a significant increase in the number of leads identified using affinity-based mass spectrometry technologies in the near future.

## References

- 1 Comess KM, Schurdak ME: Affinity-based screening techniques to enhance lead discovery. *Curr Opin Drug Discov Devel* **2004**, 7, 411–416.
- 2 Bleicher KH, Böhm H-J, Müller K, Alanine AI: Hit and lead generation: beyond high-throughput screening. *Nat Rev Drug Discov* **2003**, 2, 369–378.
- 3 Walters WP, Namchuk M: Designing screens: how to make your hits a hit. *Nat Rev Drug Discov* **2003**, 2, 259–266.
- 4 Geoghegan KF, Kelly MA: Biochemical applications of mass spectrometry in pharmaceutical drug discovery. *Mass Spectrom Rev* **2005**, 24, 347–366.
- 5 Freundlieb S, Garner J: *New Drugs* **2002**, 3, 54–60.
- 6 Pantoliano MW, Petrella EC, Kwasnoski JD, Lobanov VS, Myslik J, Graf E, Carver T, Asel E, Springer BA, Lane P, Salemme FR: High-Density miniaturized thermal shift assays as a general strategy for drug discovery. *J Biomol Screen* **2001**, 6, 429–440.
- 7 Powell KD, Fitzgerald MC: High-throughput screening assay for the tunable selection of protein ligands. *J Comb Chem* **2004**, 6, 262–269.
- 8 Zhu MM, Rempel DL, Du Z, Gross ML: Quantification of protein-ligand interactions by mass spectrometry, titration, and H/D exchange: PLIMSTEX. *J Am Chem Soc* **2003**, 125, 5252–5253.
- 9 Zhu MM, Hambley D, Gross ML: Quantitation of protein–ligand interactions in solution by H/D exchange (PLIMSTEX), chapter 11.
- 10 Comess KM, Schurdak ME, Voorbach MJ, Coen M, Trumbull JD, Yang H, Gao L, Tang H, Cheng X, Lerner CG, McCall JO, Burns DJ, Beutel BA: An ultra-efficient affinity-based high throughput screening process: application to bacterial cell wall biosynthesis enzyme MurF. *J Biomol Screen* **2006**, 11, 736–742.
- 11 Siegel MM, Tabei K, Bebernitz GA, Baum EZ: Rapid methods for screening low molecular mass compounds non-covalently bound to proteins using size exclusion and mass spectrometry applied to inhibitors of human cytomegalovirus protease. *J Mass Spectrom* **1998**, 33, 264–273.
- 12 Lenz GR, Nash HM, Jindal S: Chemical ligands, genomics, and drug discovery. *Drug Discov Today* **2000**, 5, 145–156.
- 13 Muckenschnabel I, Falchetto R, Mayr LM, Filipuzzi I: SpeedScreen: label-free liquid chromatography–mass spectrometry-based high-throughput screening for the discovery of orphan protein ligands. *Anal Biochem* **2004**, 324, 241–249.
- 14 Zehender H, Le Goff F, Lehmann N, Filipuzzi I, Mayr LM: SpeedScreen: The “missing link” between genomics and lead discovery. *J Biomol Screen* **2004**, 9, 498–505.
- 15 Siegel MM: Drug screening using gel permeation chromatography spin columns coupled with ESI-MS, chapter 2.
- 16 Annis DA, Nazef N, Chuang CC, Scott MP, Nash HM: A general technique to rank protein-ligand binding affinities and determine allosteric versus direct binding site

- competition in compound mixtures. *J Am Chem Soc* **2004**, 126, 15495–15503.
- 17 Coburn CA, Stachel SJ, Li YM, Rush DM, Steele TG, Chen-Dodson E, Holloway MK, Xu M, Huang Q, Lai MT, DiMuzio J, Crouthamel MC, Shi XP, Sardana V, Chen Z, Munshi S, Kuo L, Makara GM, Annis DA, Tadikonda PK, Nash HM, Vacca JP, Wang T: Identification of a small molecule nonpeptide active site beta-secretase inhibitor that displays a nontraditional binding mode for aspartyl proteases. *J Med Chem* **2004**, 47, 6117–6119.
  - 18 Annis DA: *Int J Med Sci* **2004**, 238, 77–83.
  - 19 Annis A, Chuang C-C, Nazef N: An affinity selection-mass spectrometry system for the discovery and characterization of protein–ligand interactions, chapter 3.
  - 20 Shin YG, van Breemen RB: Analysis and screening of combinatorial libraries using mass spectrometry. *Biopharm Drug Dispos* **2001**, 22, 353–372.
  - 21 van Breemen RB, Huang CR, Nikolic D, Woodbury CP, Zhao YZ, Venton DL: Pulsed ultrafiltration mass spectrometry: a new method for screening combinatorial libraries. *Anal Chem* **1997**, 69, 2159–2164.
  - 22 Johnson BM, Nikolic D, van Breemen RB: Applications of pulsed ultrafiltration–mass spectrometry. *Mass Spectrom Rev* **2002**, 21, 76–86.
  - 23 Wieboldt R, Zweigenbaum J, Henion J: immunoaffinity ultrafiltration with ion spray HPLC/MS for screening small-molecule libraries. *Anal Chem* **1997**, 69, 1683–1691.
  - 24 van Elswijk DA, Tjaden UR, van der Greef J, Irth H: Mass spectrometry-based bioassay for the screening of soluble orphan receptors. *Int J Mass Spectrom* **2001**, 210/211, 625–636.
  - 25 Irth H: Continuous-flow systems for ligand binding and enzyme inhibition assays based on mass spectrometry, chapter 5.
  - 26 Hughes DE, Waters JL, Dunayevskiy YM: Capillary electrophoretic method to detect target-binding ligands and to determine their relative affinities. US Patent 6 524 866, **2003**.
  - 27 Hughes DE, Karger BL, Waters JL, Dunayevskiy YM: Method to detect and analyze tight-binding ligands in complex biological samples using capillary electrophoresis and mass spectrometry. US Patent 6 432 651, **2002**.
  - 28 Griffey RH, Hofstadler SA, Sannes-Lowery KA, Ecker DJ, Crooke ST: Determinants of aminoglycoside-binding specificity for rRNA by using mass spectrometry. *Proc Natl Acad Sci USA* **1999**, 96, 10129–101233.
  - 29 Cummins LL, Chen S, Blyn LB, Sannes-Lowery KA, Drader JJ, Griffey RH, Hofstadler SA: Multitarget affinity/specificity screening of natural products: finding and characterizing high-affinity ligands from complex mixtures by using high-performance mass spectrometry. *J Nat Prod* **2003**, 66, 1186–1190.
  - 30 Hofstadler SA, Sannes-Lowery KA: Interrogation of covalent complexes by ESI-MS: A powerful platform for high throughput drug discovery, chapter 10.
  - 31 Siegel MM: Early discovery drug screening using mass spectrometry. *Curr Top Med Chem* **2002**, 2, 13–33.
  - 32 Goodnow RA Jr.: Current practices in generation of small molecule new leads. *J Cell Biochem* **2001**, 37, 13–21.
  - 33 Goodnow R Jr: Small molecule lead generation processes for drug discovery. *Drugs Future* **2002**, 27, 1165–1180.
  - 34 Martin YC, Kofron JL, Traphagen LM: Do structurally similar molecules have similar biological activity? *J Med Chem* **2002**, 45, 4350–4358.
  - 35 El Zoeiby A, Sanschagrin F, Levesque RC: Structure and function of the Mur enzymes: development of novel inhibitors. *Mol Microbiol* **2003**, 47, 1–12.
  - 36 Gu YG, Florjancic AS, Clark RF, Zhang T, Cooper CS, Anderson DD, Lerner CG, McCall JO, Cai Y, Black-Schaefer CL, Stamper GF, Hajduk PJ,

- Beutel BA: Structure–activity relationships of novel potent MurF inhibitors. *Bioorg Med Chem Lett* **2004**, 14, 267–270.
- 37 Qian J, Voorbach MJ, Huth JR, Coen ML, Zhang H, Ng S-C, Comess KM, Petros AM, Rosenberg SH, Warrior U, Burns DJ: Discovery of novel inhibitors of Bcl-xL using multiple high-throughput screening platforms. *Anal Biochem* **2004**, 328, 131–138.
  - 38 Hajduk PJ, Meadows RP, Fesik SW: NMR-based screening in drug discovery. *Q Rev Biophys* **1999**, 32, 211–240.
  - 39 Comess KM, Trumbull JD, Park C, Chen Z, Judge RA, Voorbach MJ, Coen M, Gao L, Tang H, Kovar P, Cheng X, Schurdak ME, Zhang H, Sowin T, Burns DJ: Kinase drug discovery by affinity selection/mass spectrometry (ASMS): application to DNA damage checkpoint kinase Chk1. *J Biomol Screen* **2006**, 11, 743–754.
  - 40 Lipinski CA, Lombardo F, Dominy BW, Feeney PJ: Experimental and computational approaches to estimate solubility and permeability in drug discovery and development settings. *Adv Drug Deliv Rev* **1997**, 23, 3–25.
  - 41 Oprea TI, Davis AM, Teague SJ, Leeson PD: Is there a difference between leads and drugs? A historical perspective. *J Chem Inf Comput Sci* **2001**, 41, 1308–1315.
  - 42 Teague SJ, Davis AM, Leeson PD, Oprea T: The design of leadlike combinatorial libraries. *Angew Chem Int Ed Engl* **1999**, 38, 3743–3748.
  - 43 Rishton GM: Nonleadlikeness and leadlikeness in biochemical screening. *Drug Discov Today* **2003**, 8, 86–96.
  - 44 McGovern SL, Caselli E, Grigorieff N, Shoichet BK: A common mechanism underlying promiscuous inhibitors from virtual and high-throughput screening. *J Med Chem* **2002**, 45, 1712–17122.
  - 45 McGovern SL, Shoichet BK: Kinase inhibitors: not just for kinases anymore. *J Med Chem* **2003**, 46, 1478–1483.
  - 46 Golebiowski A, Klopfenstein SR, Portlock DE: Lead compounds discovered from libraries: part 2. *Curr Opin Chem Biol* **2003**, 7, 1–18.
  - 47 van Breemen RB, Nikolic D, Xu X, Xiong Y, van Lieshout M, West CE, Schilling AB: Development of a method for quantitation of retinol and retinyl palmitate in human serum using high-performance liquid chromatography–atmospheric pressure chemical ionization–mass spectrometry. *J Chromatogr A* **1998**, 794, 245–251.
  - 48 Zhao YZ, van Breemen RB, Nikolic D, Huang CR, Woodbury CP, Schilling A, Venton DL: Screening solution-phase combinatorial libraries using pulsed ultrafiltration/electrospray mass spectrometry. *J Med Chem* **1997**, 40, 4006–4012.
  - 49 Nikolic D, van Breemen RB: Screening for inhibitors of dihydrofolate reductase using pulsed ultrafiltration mass spectrometry. *Comb Chem High Throughput Screen* **1998**, 1, 47–55.





## 5

# Continuous-flow Systems for Ligand Binding and Enzyme Inhibition Assays Based on Mass Spectrometry

Hubertus Irth

### 5.1

#### Introduction

High-throughput screening (HTS) technologies have become one of the most important tools in modern drug discovery to accelerate the development of novel lead compounds [1]. HTS technologies have been developed and implemented that are able to test tens of thousands of compounds or more per day for their activity in various assay types, ranging from receptor binding and enzyme inhibition to whole-cell assays. While HTS techniques are highly efficient in the screening of pure compound samples, the screening of complex mixtures is more demanding, involving a close coordination between chemical analysis, sample fractionation and biological screening.

Complex mixtures in drug discovery are samples originating from natural products, reaction mixtures from solution-phase combinatorial chemistry and *in vitro* or *in vivo* metabolic profiling. In all cases, non-active sample constituents at widely different concentration ranges are present next to an unknown number of pharmacologically active compounds. Identification requires fractionation, mostly performed by off-line liquid chromatography (LC), in combination with fraction collection. Fractionation can be performed prior to or after primary screening of, for example, natural product extracts [2, 3] and or combinatorial chemistry libraries [4, 5], but always requires a follow-up screening step. The whole process of screening and fractionation must be repeated until the bioactive compound against the molecular target is isolated. It is obvious that this process can be very laborious and time-consuming.

In recent years, analytical screening technologies were described that facilitate the determination and identification of bioactive compounds in complex mixtures. Both high-performance liquid chromatography (HPLC) [6–8] and capillary electrophoresis (CE) [9–11] were employed to separate the compound mixture during or prior to the biological screening. In contrast to the microtiter plate format dominating HTS assays, analytical screening assays are carried out in continuous-flow systems to be compatible with the separation technique em-

ployed. Both receptor ligand binding and enzyme inhibition assays were compatible with the continuous-flow assay formats.

Both modern microtiter plate and continuous-flow biochemical assays are based on fluorescence detection principles as the most common readout principle. These assay types require fluorescent labels to generate a readout signal reflecting the affinity of the compound(s) tested for the biomolecular target. In more advanced systems, mass spectrometry (MS) was used in parallel to simultaneously measure MS and MS-MS spectra of biologically active compounds. Methods using LC-UV/MS [12–14] and LC-fluorescence/MS [15, 16] allowed the simultaneous detection of bioactivity and characterization of the bioactive molecules in a single analysis. While fluorescence based biochemical assays typically are characterized by a high detection sensitivity and robustness, the need to prepare a fluorescent label or substrate that retains a significant receptor or enzyme affinity often hampers the speed of assay development. Also, in complex samples, the presence of natively fluorescent compounds with excitation/emission spectra, that overlap the spectra of the fluorescent label, may complicate data interpretation.

In the present review, we focus on the use of MS for the detection of both chemical and biochemical characteristics of bioactive compounds present in complex mixtures. The biochemical assays on which these methodologies are based rely on the direct or indirect detection of binding interactions by MS.

## 5.2

### Continuous-flow Enzyme Assays Based on Mass Spectrometry

#### 5.2.1

##### Assay Principle

The assay principle for MS-based enzyme inhibition assay is shown in Fig. 5.1. The assay is based on the mass spectrometric detection of reaction products of

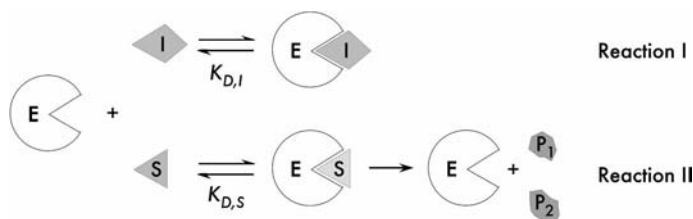


**Fig. 5.1** Principle of MS-based enzyme assays. Enzyme (E) molecules react with the substrate (S) to form an enzyme-substrate complex (ES), leading, for example, to a subsequent cleavage into two products  $P_1$  and  $P_2$ .  $P_1$  and  $P_2$  are monitored continuously by ESI-MS. The injection of an inhibitor, I, results in the temporary formation of an inactive enzyme-inhibitor (EI) complex, resulting in a reduction of  $P_1$  and  $P_2$  and negative peaks in the corresponding mass traces.

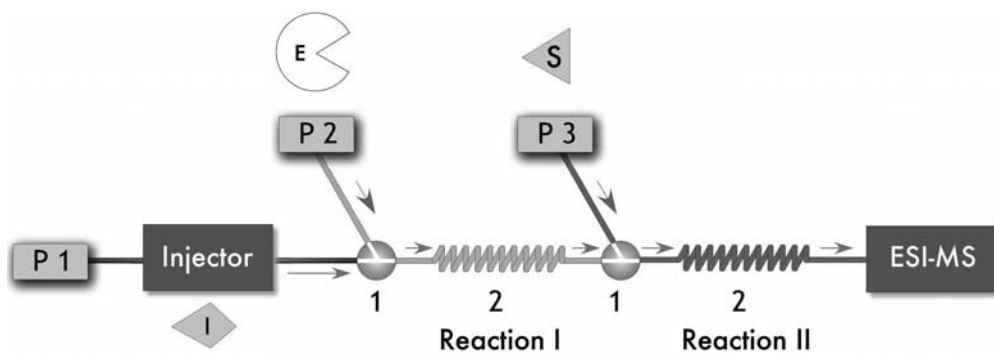


**Fig. 5.2** Analytical set-up for on-line enzyme assays based on ESI-MS. P1: Carrier/HPLC pump. P2: HPLC pump delivering enzyme solution. P3: HPLC pump delivering substrate solution. 1: Mixing union. 2: Microcoil reactor. In case of on-line coupling to HPLC, the HPLC column is inserted

between the autoinjector and the first mixing union. In the first microcoil reactor, the enzyme inhibition takes place (reaction I, Fig. 5.1) whereas in the second microcoil reactor, the enzyme substrate reaction proceeds (reaction II, Fig. 5.1).

the enzyme–substrate reaction at their specific  $m/z$  values. The presence of inhibitors in the sample results in a concentration change of both substrate and product due to the temporary inhibition of the enzyme. The hardware implementation is shown in Fig. 5.2. Compounds eluting from the HPLC column or injected into a flow injection (FI) system are mixed with the enzyme solution that is continuously infused via a mixing union. In the first microcoil reactor the reaction between the sample components and the enzyme takes place (reaction I, Fig. 5.1). In the absence of active compounds, the enzyme molecules pass the reactor unaltered and reach the second mixing union where a solution of substrate is infused. In the second microcoil reactor (reaction II, Fig. 5.1), the enzyme substrate reaction is allowed to proceed, the reaction time being determined by the volume of the reactor and the total flow rate which is the sum of the flow rates of the HPLC pump, and the pumps delivering the enzyme and substrate solutions, respectively. Typically the total reaction time is between 30 s and 5 min, depending on the type of enzyme assay. The enzyme substrate reaction results in products that are detected by electrospray ionization MS (ESI-MS) at their respective  $m/z$  values. In the absence of inhibitors, a constant concentration of products is formed, leading to a constant baseline of extracted ion current chromatograms (EIC) of the products. An inhibitor that is injected into a FI system or that elutes from the HPLC column temporarily inhibits the enzyme, leading to a decrease of the product concentration that results in a negative peak in the corresponding EICs. In order to correct for ion suppression effects, system monitoring compounds (SMC) are added to both the enzyme and substrate solutions. Only those compounds are considered to be inhibitors that produce a negative peak in the products EICs but no peaks in either of the SMC traces.

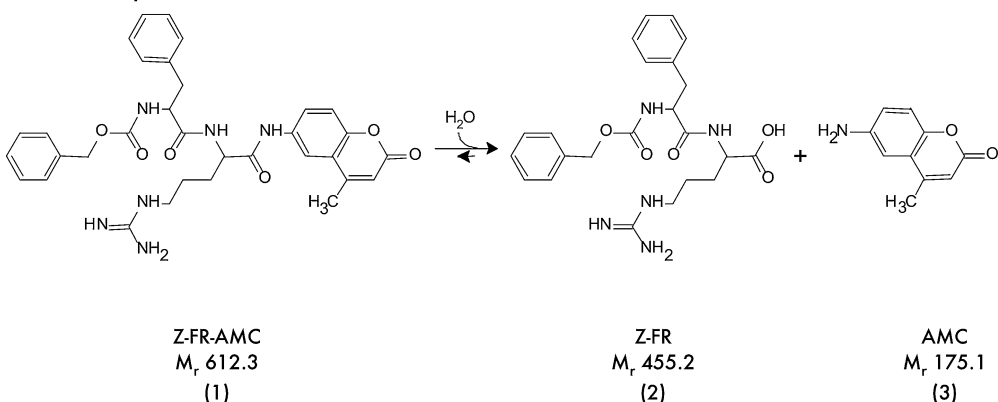


**Fig. 5.3** Substrate conversion reaction for cathepsin B. Substrate Z-FR-AMC is converted by cathepsin B into two products, Z-FR and AMC, that are employed as reporter molecules at their corresponding  $m/z$  traces.

## 5.2.2

### ESI-MS Assay of Cathepsin B

#### 5.2.2.1 MS Assay Development for Cathepsin B

In a first example, we demonstrate the implementation of a homogeneous substrate conversion-based protease assay using the enzyme cathepsin B [17]. Cathepsin B belongs to the group of lysosomal cysteine proteinases, which comprises an important group of enzymes involved in many physiological and pathological processes, such as intracellular protein turnover [18], cancer invasion and metastasis [19, 20]. Cathepsin B catalyzes the hydrolysis of Z-FR-AMC (substrate, N-CBZ-Phe-Arg 7-amino-4-methylcoumarin hydrochloride,  $M_r$  612.3), resulting in two products, Z-FR and AMC (see Fig. 5.3). Figure 5.4a depicts the ESI-MS spectrum obtained after analysis of the enzymatic reaction. It shows the enzymatic cleavage products of Z-FR-AMC, AMC ( $m/z$  175.9) and Z-FR ( $m/z$  456.1). In addition, the spectrum shows the uncleaved substrate ( $m/z$  613.1) and the two SMCs (biotin,  $m/z$  244.9, and cAMP,  $m/z$  329.9). Figure 5.4b shows the ESI-MS spectrum of the reaction mixture after addition of a cathepsin B inhibitor, E-64. The inhibition of cathepsin B results in a strong decrease of the Z-FR and AMC signals. Furthermore, the presence of the E-64 ( $m/z$  358.1) signal demonstrates the potential of the current methodology to simultaneously obtain chemical and biological information of potential enzyme inhibitors.

#### 5.2.2.2 Compatibility of Cathepsin B Assay with MS Detection

A key requirement for the successful on-line coupling of enzyme assays to ESI-MS is the solvent and buffer compatibility. Enzyme assays are mostly performed in nonvolatile buffers, such as HEPES, TRIS, and PBS. Moreover, additives are

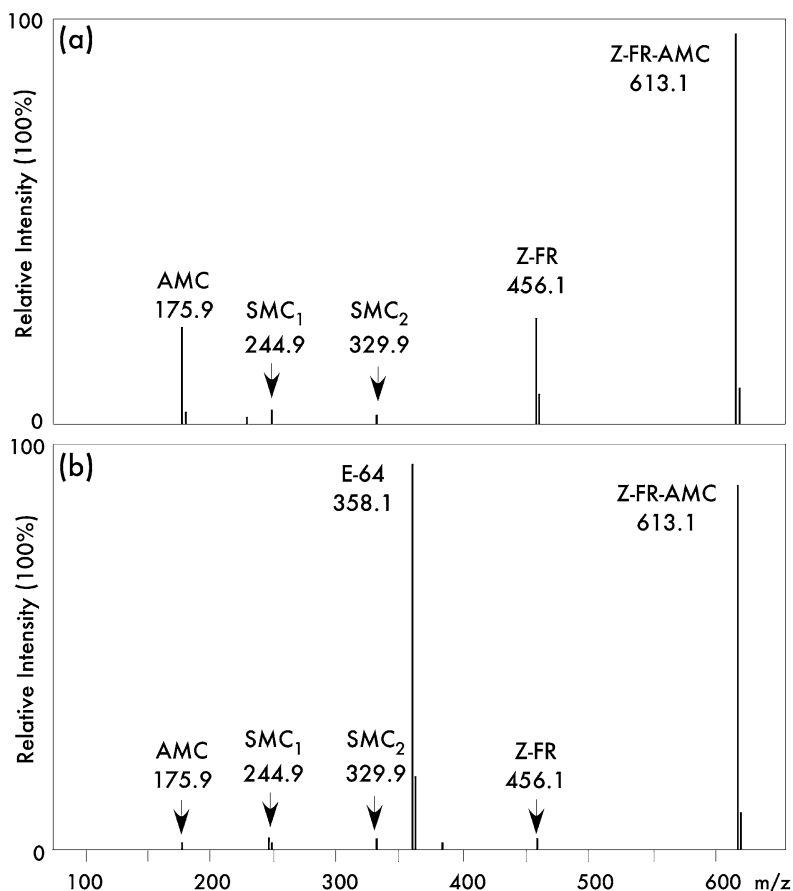


**Fig. 5.4** Monitoring of the enzymatic reaction and cathepsin B inhibition by ESI-MS. MS instrument: Shimadzu LCMS-2010 single-stage quadrupole mass spectrometer. (a) The ESI-MS spectrum obtained after analysis of the enzyme reaction, containing the cleavage products AMC ( $m/z$  175.9) and Z-FR ( $m/z$  456.1);  $m/z$  244.9 and  $m/z$  329.9 belong to

the system monitoring compounds,  $m/z$  613.1 belongs to the substrate Z-FR-AMC. (b) The ESI-MS spectrum obtained after addition of the inhibitor E-64 to the enzymatic assay. The signal intensities of AMC ( $m/z$  175.9) and Z-FR ( $m/z$  456.1) are very low as a result of the cathepsin B inhibition;  $m/z$  358.1 corresponds to E-64.

added to maintain enzyme activity and stability and to prevent nonspecific surface binding of the proteins. Nonvolatile salts and additives, however, may contaminate the ion source of the mass spectrometer and cause ion suppression in ESI-MS, which results in a decreased MS performance [21]. Consequently, we choose to perform the enzyme–substrate reaction under buffer/salt conditions that are routinely used in ESI-MS, omitting commonly used additives and non-volatile buffers and salts. Experiments demonstrated that cathepsin B was active in a carrier solution containing solely ammonium formate and 1,4-dithioerythri-

tol (pH 7.0). Organic modifiers, such as methanol or acetonitrile used for elution in (gradient) reversed-phase chromatogram represent another point of concern. In the past, we have shown that biochemical assays can be performed in the presence of organic modifier concentrations up to 15% as long as the reaction time does not exceed 3–5 min. Similar results were obtained for cathepsin B, in which the presence of 10% methanol in the enzyme–substrate reaction (20% in the column) leads to an 11% decrease of product formation. Despite this decrease in enzyme activity, limits of detection (LODs) obtained with the current system compare well with LODs reported, for example, for fluorescence-based readouts for the same enzyme, illustrating the benefits of using ESI-MS as readout technique.

#### 5.2.2.3 On-line Coupling of MS-based Cathepsin B Assay to HPLC

The continuous-flow MS enzyme assay format allows the continuous screening of sample components present in a carrier flow for enzyme inhibition activity. This allows the integration of this assay format in a reversed-phase HPLC system, allowing the screening of complex mixtures after chromatographic separation. For this purpose, a reversed-phase C18 column was inserted between the autoinjector and the mixing union for the addition of the enzyme solution (see Fig. 5.2). Furthermore, a 1:3 flow splitter was placed between the HPLC column and the enzyme assay, resulting in a total flow of  $50 \mu\text{L min}^{-1}$  directed toward the enzyme assay. The remaining  $150 \mu\text{L min}^{-1}$  was directed toward waste; in other applications, this flow may be used for UV, fluorescence, or ELSD measurements to obtain additional chemical data on bioactive analytes.

To optimize the on-line HPLC enzyme assay setup, a mixture of five flavonoids spiked with two cathepsin B inhibitors, E-64 and leupeptin, was used as a test sample. Figure 5.5 shows the mass chromatograms obtained when analyzing this mixture by ESI-MS. Figure 5.5a shows the total ion current (TIC) chromatogram of the test mixture, indicating that the TIC does not provide any information about the (bioactive) compounds injected. Figure 5.5b, c depicts the mass chromatograms of the products AMC ( $m/z$  176) and Z-FR ( $m/z$  456), respectively, reflecting the enzyme inhibition activity of compounds eluting from the HPLC column. The bioactive compounds E-64 and leupeptin cause a temporary decrease of the concentration AMC and Z-FR, detected as negative peaks. The peak heights depend on the concentration of the inhibitor and its binding affinity.

The process of compound characterization and identification is illustrated for the bioactive peaks with retention time ( $t_R$ ) 7.5 min. Figure 5.5g shows the mass spectrum recorded at 7.5 min, obtained after applying background subtraction. Figure 5.5i depicts the EIC chromatograms of the three most abundant masses, together with the EICs of AMC ( $m/z$  176) and Z-FR ( $m/z$  456), reflecting the bioactivity signal. The  $m/z$  613 is not plotted as EIC, because this represents the protonated substrate. Since the active compounds enter the mass spectrometer synchronously with AMC and Z-FR, their identification can be performed on the basis of a retention time and peak shape match. On the basis of this matching, the mass chromatograms for  $m/z$  427 and  $m/z$  459 are identified to correspond

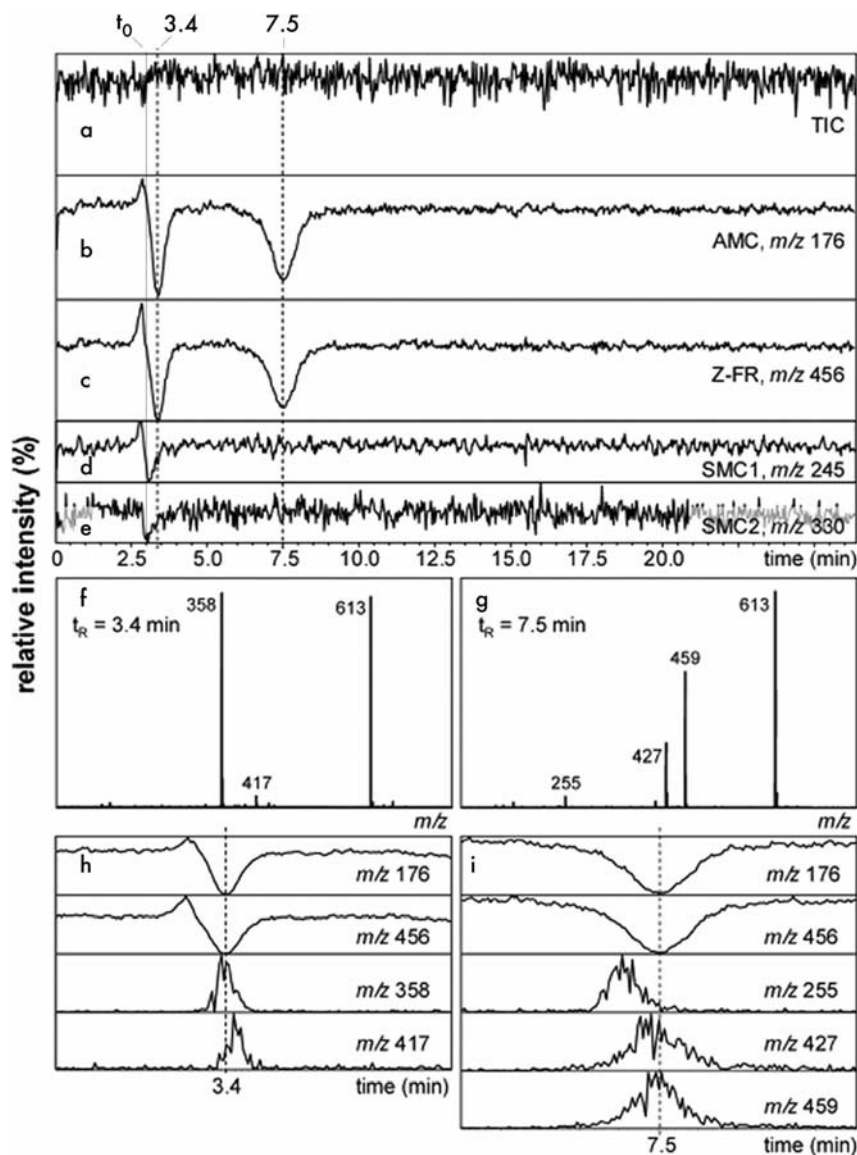


**Fig. 5.5** On-line HPLC bioactivity screening of a mixture of five flavonoids spiked with two cathepsin B inhibitors, E-64 and leupeptin using acetylcholinesterase as biological target. MS instrument: Shimadzu LCMS-2010 single-stage quadrupole mass spectrometer. (a) TIC chromatogram of the mixture, scan range  $m/z$  75–750; (b) mass chromatogram of AMC ( $m/z$  176); (c) mass

chromatogram of Z-FR ( $m/z$  456); (d) mass chromatogram of SMC1 ( $m/z$  245); (e) mass chromatogram of SMC2 ( $m/z$  330); (f) mass spectrum recorded at  $t_R = 3.4$  min; (g) mass spectrum recorded at  $t_R = 7.5$  min; (h) EICs of the most abundant peaks shown in the mass spectrum recorded at  $t_R = 3.4$  min; (i) EIC of the most abundant peaks shown in the mass spectrum recorded at  $t_R = 7.5$  min.



with the bioactive compound. The mass chromatogram of  $m/z$  255 shows a mismatch in both retention time and peak profile and can be excluded from further data interpretation. The mass chromatograms of  $m/z$  427 and  $m/z$  459 correspond with  $[\text{leupeptin} + \text{H}]^+$  and  $[\text{leupeptin} + \text{H} + \text{methanol}]^+$ . A similar scheme allowed the identification of negative peak at  $t_R = 3.4$  min, resulting in E-64 ( $m/z$  358).

When using MS-based biochemical assays for the screening of complex mixtures, it is essential to perform control experiments to prove that the apparent reduction in product concentrations is, indeed, caused by inhibition of cathepsin B and not by ionization suppression. First of all, the mass chromatograms of the two SMCs (see Fig. 5.5d, e) show no negative peaks at the retention times of the two bioactive peaks, only at the dead time. In addition, we tested the behavior of the overall system in the absence of active enzyme. For this purpose, a solution identical in composition to the enzyme assay solution was used in the continuous-flow reaction detection system. This solution contained deactivated cathepsin B and the products AMC and ZFR. Injections of E-64 did not result in any decrease of the AMC and Z-FR signals, proving that the negative peaks measured under assay conditions, indeed, were the result of cathepsin B deactivation and not of ionization suppression of the AMC and Z-FR signals. Finally, it is important to mention that the peak shapes of the peaks in the AMC and Z-FR chromatograms are virtually identical. It is highly unlikely that ionization suppression due to the injection of E-64 would be identical for substrate conversion products. In conclusion, these control measurements unambiguously confirm that the decrease of product formation monitored by ESI-MS is, indeed, exclusively caused by the presence of cathepsin-B inhibitors in the HPLC effluent.

#### 5.2.2.4 Screening of Natural Products for Cathepsin B Activity

We analyzed various natural extracts that were previously tested in a fluorescence-based cathepsin B assay in order to demonstrate the applicability of the current method for screening real-life samples. The screening result of a nonspiked fungi extract is represented in Fig. 5.6. A methanol gradient was used for elution of the sample components. The increasing amount of methanol resulted in an improved ESI-MS sensitivity for AMC and Z-FR, but simultaneously decreased enzymatic activity. The corresponding baseline instability can clearly be seen in the mass chromatograms of AMC and Z-FR. Nevertheless, data interpretation was still possible, even at the highest methanol concentration level applied. The AMC and Z-FR mass chromatograms (see Fig. 5.6b, c) show several synchronous negative peaks, of which the first peak at 3.0 min is the injection peak. In a procedure similar to the one described above, mass spectra were constructed from the negative peaks at  $t_R$  43.3, 51.8, and 55.6 min. As an example, the EICs of the possible bioactive compounds for peak 43.3 min are shown in Fig. 5.6f–j. The retention times of the peaks in Fig. 5.6g, i, j match with the negative peak at 43.3 min. Considering the peak shape of  $m/z$  230, it is unlikely that this compound has caused the negative peak at  $t_R$  43.3 min, because the peak shape is rather different than the peak shape of the bioactive peak. It is more reliable that either

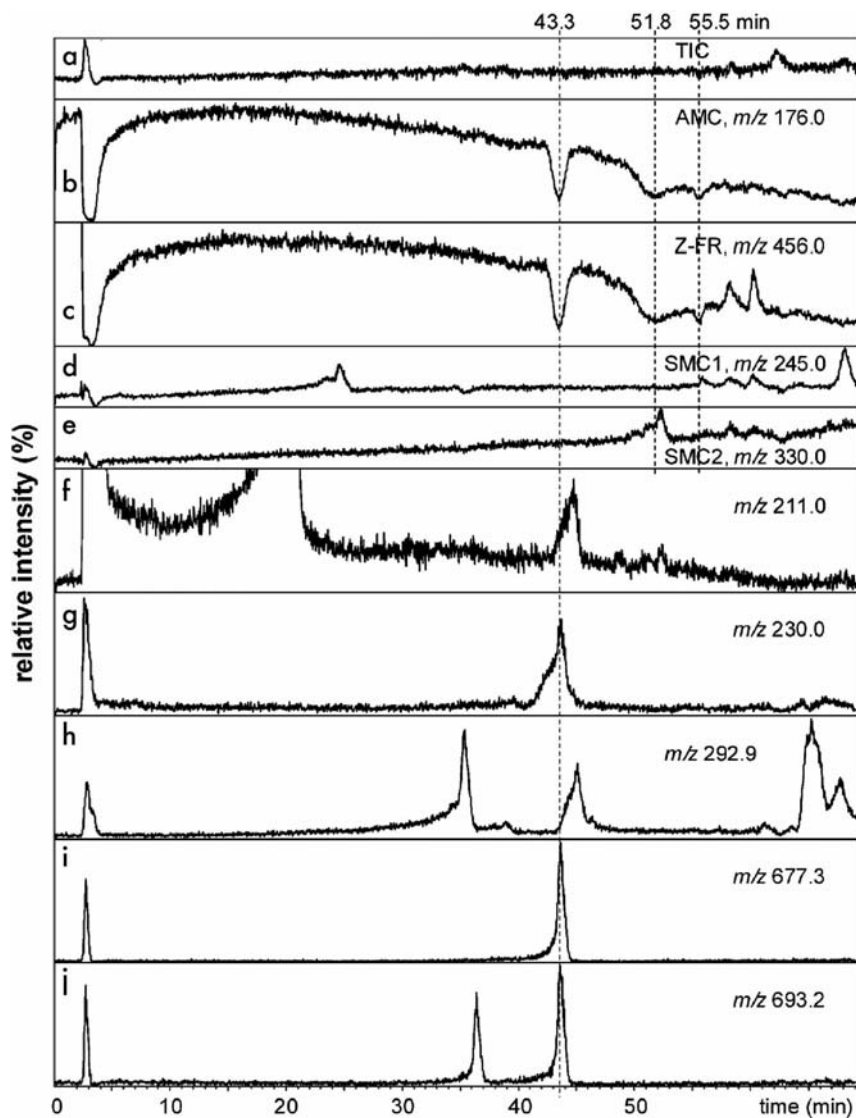


**Fig. 5.6** On-line HPLC bioactivity screening of a fungi extract using acetylcholinesterase as biological target. MS instrument: Shimadzu LCMS-2010 single-stage quadrupole mass spectrometer. (a) TIC chromatogram of the mixture, scan range  $m/z$  50–1000; (b) mass chromatogram of AMC ( $m/z$  176.0); (c) mass chromatogram of Z-FR ( $m/z$  456.0); (d) mass chromatogram of SMC1 ( $m/z$  245.0); (e)

mass chromatogram of SMC2 ( $m/z$  330.0); (f–j) mass chromatogram of various  $m/z$  values, which were present as an abundant peak in the mass spectrum recorded at  $t_R = 43.3$  min: (f) mass chromatogram of  $m/z$  211.0; (g) mass chromatogram of  $m/z$  230.0; (h) mass chromatogram of  $m/z$  292.9; (i) mass chromatogram of  $m/z$  677.3; (j) mass chromatogram of  $m/z$  693.2.

$m/z$  677.3 or  $m/z$  693.2 or both compounds were bioactive, because the peak shapes are identical. Most likely is that  $m/z$  677.3 and  $m/z$  693.2 are  $[M+Na]^+$  and  $[M+K]^+$  of a molecule with a molecular mass of 654 Da. Regarding the other negative peaks, possible bioactive compounds showed an  $m/z$  199.1 for the peak at 51.8 min, and an  $m/z$  279.1 for the peak at 55.6 min (EICs not shown). The results of this screening measurement, that is, the number of active compounds in the extract, their retention times, and molecular masses serve as starting points for further structure elucidation experiments (data not shown).

### 5.2.3

#### ESI-MS Assay of Acetylcholinesterase

##### 5.2.3.1 MS Assay Development for Acetylcholinesterase

In the following example we describe the implementation of a mass spectrometric assay for acetylcholinesterase (AChE) [22]. AChE plays an important role in the nervous system. This enzyme rapidly hydrolyzes the active neurotransmitter acetylcholine into the inactive compounds choline and acetic acid. Amongst others, low levels of acetylcholine in the synaptic cleft are associated with Alzheimer's disease [23, 24]. Patients afflicted by this disease may benefit from inhibition of AChE activity thereby increasing ACh level.

Traditionally, plants are a rich source of AChE inhibitors. People from the Caucasus used bulbs of snowdrops (*Galanthus* sp.) to treat forgetfulness [25]. The active compound in this plant has been isolated and called galanthamine. Other plant-derived AChE inhibitors used for treatment of Alzheimer's disease include Huperzine A from *Huperzia serrata* and Rivastigmine (Exelon). The latter is a derivative from physostigmine isolated from the calabar bean, *Physostigma venenosum*.

In order to develop an MS-based screening method for AChE, we used a continuous-flow fluorescence assay [26] as the starting point and adapted the assay conditions to MS-compatible conditions using the assay format described in Fig. 5.1. In this assay, the synthetic non-fluorescent AChE substrate 7-acetoxy-1-methyl quinolinium iodide (AMQI) is hydrolyzed into the highly fluorescent 7-hydroxy-1-methyl quinolinium iodide (HMQI). First, it was assessed whether AChE was still active in volatile buffer and whether ionic strength influenced AChE activity. Batch measurements indicated that the reaction proceeded most efficiently in 50 mM potassium phosphate whereas AChE activity proceeded at a somewhat slower rate in 10 mM ammonium hydrogencarbonate; the addition of 180  $\mu$ M sodium chloride to the 10 mM ammonium hydrogencarbonate did not influence enzyme activity as compared with the 10 mM ammonium hydrogencarbonate buffer. Although somewhat slower in volatile buffers, enzyme activity is sufficiently high for assay purposes.

Figure 5.7 demonstrates the implementation of the assay and shows the read-out in the MS that was obtained for injections of the AChE inhibitor galanthamine at 0, 1, and 10  $\mu$ M. Figure 5.7a shows the extracted ion chromatogram of galanthamine, Fig. 5.7b shows the extracted ion chromatogram of HMQI (prod-

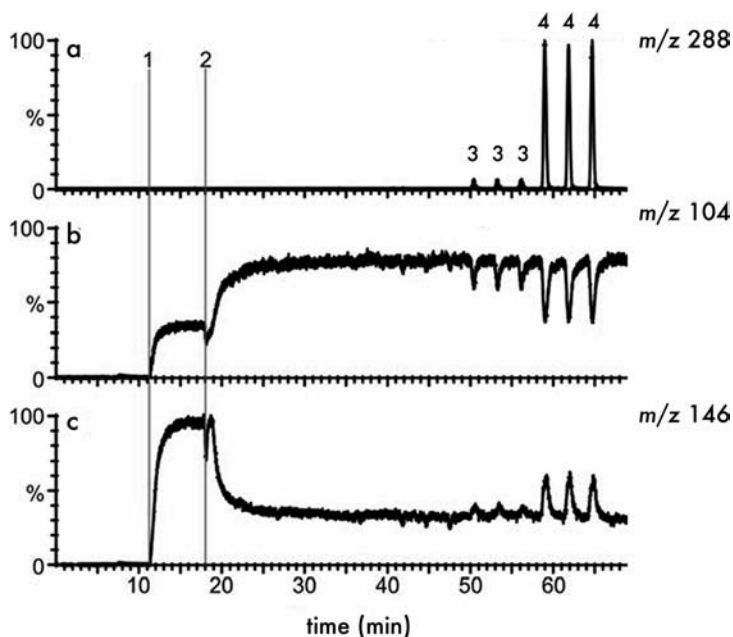


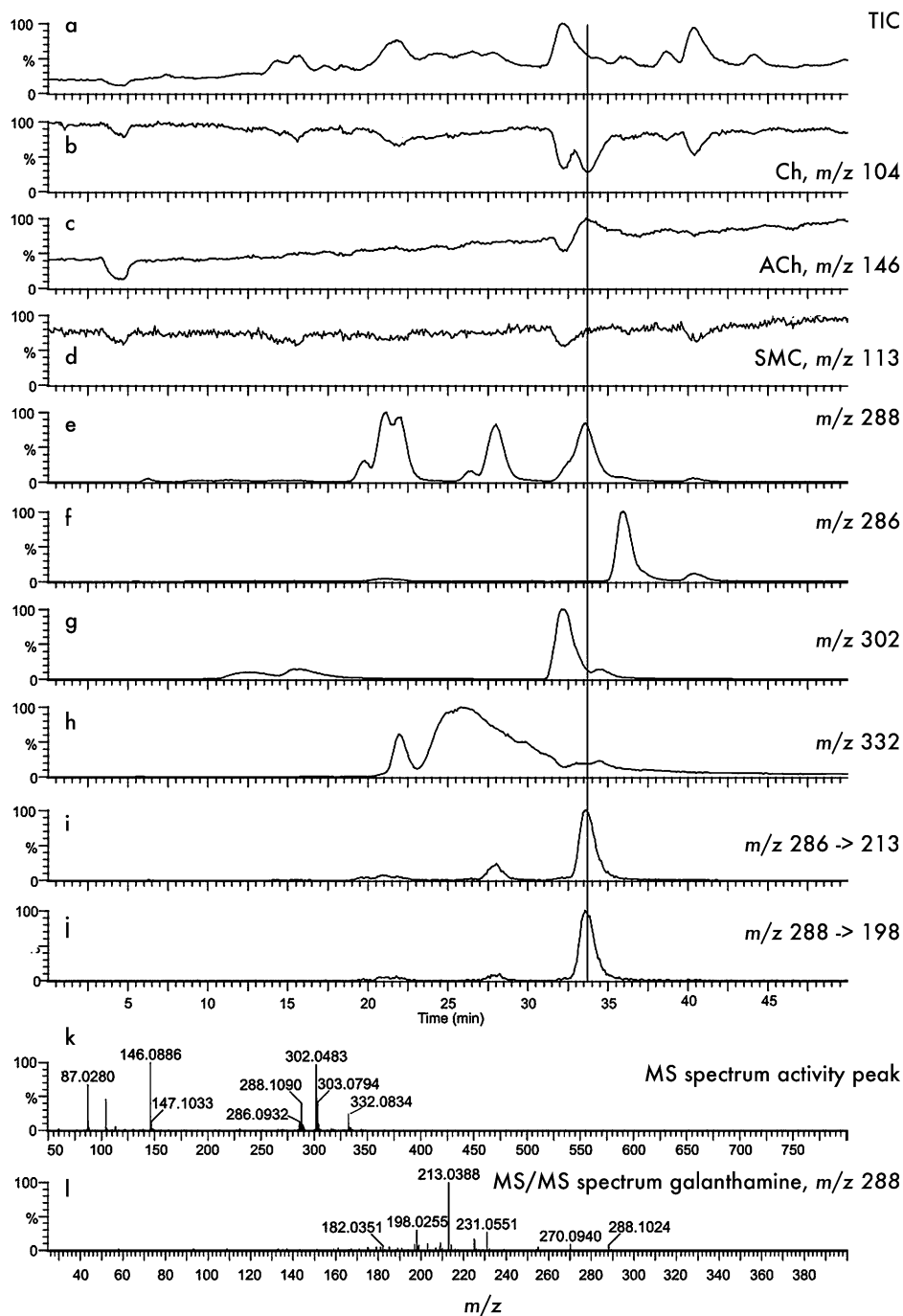
**Fig. 5.7** AChE-catalyzed hydrolysis of the fluorescent substrate AMQI in volatile buffer monitored by mass spectrometry. Line 1: Start of the substrate pump delivering AMQI. Line 2: Start of the enzyme pump delivering AChE. Peak 3: Injection of 0.1  $\mu$ M galanthamine. Peak 4: Injection of 1.0  $\mu$ M galanthamine. MS instrument: Q-ToF2 (Waters) equipped with a Waters Z-spray electrospray (ESI) source. (a) Mass chromatogram of  $m/z$  288 (galanthamine); (b) mass chromatogram of  $m/z$  104

(choline); (c) mass chromatogram of  $m/z$  146 (acetylcholine). Assay conditions: the carrier solution consisted of 95% 10 mM ammonium bicarbonate, pH 7.8, 5% methanol; the AChE solution (0.25 units AChE  $\text{mL}^{-1}$ ) was prepared in 10 mM ammonium bicarbonate, pH 7.8. The substrate solution consisted of 30  $\mu$ M acetylcholine dissolved in 97.5% 10 mM ammonium bicarbonate, pH 7.8, and 2.5% methanol; all reagents were pumped at a flow of 20  $\mu\text{L min}^{-1}$ .

uct trace), whereas Fig. 5.7c shows the extracted ion chromatogram of AMQI (substrate trace). The line marked with the number 1 indicates the position at which the substrate pump was switched on, whereas the line marked with the number 2 indicates the position at which the AChE pump was started. When the substrate pump was switched on, a clear increase in the substrate trace was observed. However, also a sharp increase in the product trace was evident, indicative of autolysis of the substrate.

Upon starting the AChE pump, a ready decrease in the substrate and a matching increase in the product trace was observed. Injections of galanthamine resulted in a negative peak in the product trace and a positive peak in the substrate trace, accurately matching the peaks observed in the galanthamine trace.

As AMQI was both an expensive and unstable artificial substrate, it was replaced by the native substrate of AChE, acetylcholine that is both cheap and



readily detected by MS. As acetylcholine and its product choline were both readily detected by MS, cheap, and acetylcholine being the native substrate of AChE, this substrate was chosen for further studies.

### 5.2.3.2 Assay Validation and Stability

To test for assay stability, the assay was run overnight and every 80 min an injection of 5  $\mu$ M galanthamine was performed. The assay proved to be stable for over 13 h, but was terminated when maximum data file size was reached. Subsequently, IC<sub>50</sub> curves of galanthamine were recorded by injection of 10  $\mu$ L galanthamine at a concentration of 0, 0.01, 0.025, 0.05, 0.1, 0.25, 0.5, 1, 2.5, 5, 10, and 25  $\mu$ M. IC<sub>50</sub> values were calculated using product peak height as a measure of inhibitory activity. Six galanthamine IC<sub>50</sub> curves were recorded over a period of 14 days and the interday variation as calculated from the determined IC<sub>50</sub> values was 16.2%.

IC<sub>50</sub> curves were also recorded for various other inhibitors and the corresponding IC<sub>50</sub> values were calculated. The determined IC<sub>50</sub> values of 9-aminoacridine, galanthamine, gallamine, (–)-Huperzine A and thioflavin T were 0.12  $\mu$ M, 0.38  $\mu$ M, 6.4  $\mu$ M, 0.46  $\mu$ M, and 3.2  $\mu$ M, respectively. It was difficult to compare these values with comparable values in literature since often different types of AChE, or AChE isolated from different organisms were used and different assay conditions were applied. However, the relative activities of the used inhibitors compared well with those reported in literature, except for (–)-huperzine A, which was found to be relatively less active than was expected.

### 5.2.3.3 Screening of Natural Products for Acetylcholinesterase Activity

To test whether the system was effective in a real screening experiment, an extract was made of *Narcissus* cv “Bridal Crown” bulbs. Although species of the genus *Narcissus* are known to contain galanthamine, no information was available about the galanthamine content in this variety.

Figure 5.8a presents the TIC of the MS experiment whereas Fig. 5.8b shows the corresponding choline trace. In the choline trace three major negative peaks were detected. However, two of those peaks also showed negative peaks in the SMC trace (Fig. 5.8d), corresponding with major peaks in the TIC. Also, one of these peaks matched with a negative peak in the acetylcholine trace. However, at the retention time indicated by the solid line a negative peak was observed in the choline trace and a matching positive peak in the acetylcholine trace, and no

**Fig. 5.8** Analysis of a *Narcissus* extract by HPLC coupled to the MS-based AChE assay. MS instrument: Q-ToF2 (Waters) equipped with a Waters Z-spray electrospray (ESI) source. (a) Total ion current (TIC); (b) product trace (choline)  $m/z$  104; (c) substrate trace (acetylcholine)  $m/z$  146; (d)

system monitoring compound (SMC) detected at  $m/z$  113; (e–j) MS traces, MS and MS/MS spectra for bioactive compound detected at an elution time of 33.5 min; (k) MS spectrum of active peak at  $t = 33$  min; (l) MS/MS spectrum of galanthamine.

peak in the SMC trace, excluding ion suppression and thus indicating that these peak was caused by AChE inhibitory activity. A mass spectrum of the peak area was recorded (Fig. 5.8k), and the extracted ion chromatograms of the most prominent  $m/z$  values were constructed (Fig. 5.8e–h). Of these extracted ion chromatograms only the extracted ion chromatogram of  $m/z$  of 288 showed a peak matching with the activity peak. Although other compounds having an  $m/z$  of 288 eluted from the column, they did not show any sign of activity in the acetylcholine and choline traces. The  $m/z$  of 288 corresponded with the calculated  $M+H^+$  of galanthamine. The MS/MS spectrum of galanthamine is presented in Fig. 5.8l. From the TOF-MS/MS data from the extract, extracted ion chromatograms of the major  $m/z$  values, 198 and 213, present in the MS/MS spectrum of galanthamine were constructed (Fig. 5.8i, j). Both extracted chromatograms of these  $m/z$  values showed a peak matching the activity peak indicating that indeed galanthamine is responsible for the AChE inhibitory activity present in the *Narcissus* extract. Albeit to a lesser extent, these daughter ions also showed peaks at the same retention time as the peaks present in the extracted ion chromatogram of  $m/z$  288. This indicates that the other masses may be derivatives of galanthamine that fragment during ionization. The amount of galanthamine was determined by connecting the HPLC system to the MS. Performing an MS/MS experiment using the height of the daughter peak  $m/z$  288  $\rightarrow$  198 to quantify galanthamine, it was established that 1  $\mu$ M galanthamine was present in the 50 $\times$  diluted crude extract that was injected in the screening assay.

## 5.2.4

### Miniaturization of Electrospray MS Assays

#### 5.2.4.1 Chip-based Electrospray MS Assays

Unlike fluorescence detection, MS-based detection methods maintain their sensitivity when moving from normal-bore chromatography columns to capillary and nano LC systems. MS-based bioassays are therefore particularly suited for miniaturization. Conventional assays are operated at reagent flow rates of 20–50  $\mu$ L  $\text{min}^{-1}$ . By using electrospray MS as readout, flow rates of 1  $\mu$ L  $\text{min}^{-1}$  and lower could be envisaged, which is particularly useful for assays comprising expensive reagents.

We have demonstrated the feasibility of miniaturized MS assays by converting the cathepsin B assay described in Section 5.2.2 to a chip format, using the same substrate and products for the MS-based readout [27]. The assay set-up is identical to the format described in Fig. 5.1. The advantages of chips as microreactors over fused silica capillaries are in their compactness, strength, greater degrees of freedom in design and material, and the presence of hair-pin curves to increase the diffusion rate.

Miniaturizing a conventional-flow screening system (macro-scale system) to a chip-based system comprises a number of changes, such as flow rates, reagent supply, and the material. While the conventional system with the open tubular reactors is restricted to polymer reactors, the choice of materials for the chip is

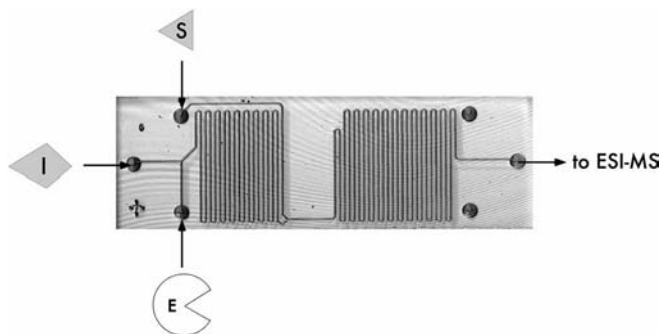


**Fig. 5.9** Design of the chip-based enzyme ESI-MS assay. MS instrument: Ion-trap mass spectrometer (LCQ Deca, Thermo Electron). I: Sample components/inhibitors injected by flow injection or eluting from capillary HPLC column. E: Infusion pump delivering the enzyme cathepsin B. S: infusion pump delivering the substrate Z-FR-AMC. Micro-chip design: Vrije Universiteit Amsterdam. Micro-chip production: Micronit Microfluidics BV (Enschede, The Netherlands).

much larger, like glass, silicon, plastic, quartz, and fused silica. The design of the chip (see Fig. 5.9) is mainly dictated by the flow rates compatible with electrospray MS. In order to achieve proper mixing on the microchip, flow rates of  $2 \mu\text{L min}^{-1}$  for capillary LC and  $1 \mu\text{L min}^{-1}$  for both enzyme and substrate solutions were chosen. The choice of a total flow rate in the chip of  $4 \mu\text{L min}^{-1}$  resulted in reaction times of 32 s and 36 s in the two reactors, respectively. In comparison with the macro-scale system, the flow rates of both enzyme and substrate were reduced by a factor of 25. Employing the optimum concentrations of the macro-scale system did not result in sufficient product formation for screening. For that reason, the enzyme concentration was increased 5-fold, having an overall decrease in enzyme and substrate consumption of  $5\times$  and  $25\times$ , respectively.

#### 5.2.4.2 Chip Performance

Extra column band broadening is a key concern when implementing chip-based microfluidics in a capillary LC system. Band broadening negatively influences the sensitivity for bioactivity detection, as the sensitivity is dependent on the height of the inhibitor peaks in the product trace(s). Both the design of the microreactors and the connections to the LC column and mass spectrometer are crucial. The band broadening was investigated by flow-injection of the inhibitor E-64 at various flow rates and injection volumes by calculating the peak width at half height (FWHM). Data were obtained by experiments using an autosampler connected to a UV detector in the absence and presence of the chip.

As expected, the lower flow rates and injection volumes resulted in broader peaks when using the microfluidic system. At an injection volume of  $0.1 \mu\text{L}$ , 85% of the band broadening can be contributed to the microfluidic chip, independent of the flow rate. The reason is that the connections and channels of the chip



increased the extra column volume and thus the sample dilution. At larger injection volumes (1  $\mu\text{L}$ ), the percentage of band broadening that can be contributed to the chip was less (60%). A reason for this difference could be that diffusion at the borders of the sample plug is relatively more problematic for smaller volumes.

The band broadening and the analyte dilution resulting from extracolumn band broadening were compared between the microfluidic chip system and the conventional macro-scale system. For a proper comparison, we calculated the analyte concentration at the peak maximum of the bioactive peaks ( $C_{\text{max}}$ ) from E-64 injections in both systems. It turned out that the dilution factor when comparing the concentration at peak maximum with the injected concentration was only 10% higher for the microfluidic chip system in comparison to the conventional macro-scale system.

#### 5.2.4.3 Sensitivity of the Chip-based MS Screening System

The sensitivity of the microfluidic system was determined by measuring calibration curves of four cathepsin B inhibitors. The inhibitors caused negative peaks in the product mass chromatograms by inhibiting cathepsin B and thus the substrate turnover. The measured order of affinities of the four inhibitors is in agreement with the affinities determined in microtiter plate assays and the macro-scale system.

LODs and  $\text{IC}_{50}$  values were derived from the calibration measurements and compared with the conventional system. The concentration LODs of the microfluidic system were six times higher under similar experimental conditions, while the  $\text{IC}_{50}$  values were four times higher. These differences could be caused by less efficient mixing of sample and reagents in the chip compared with the macro-scale system. Despite the more unfavorable detection limit compared to the macro-scale system, the LODs are still in the concentration range for bioactivity screening, while the complete system is miniaturized to a micro-scale level. In addition, the absolute LODs and  $\text{IC}_{50}$  values with the chip were four times and six times lower, respectively, which means that less sample is required for screening.

### 5.3

#### Continuous-flow Ligand Binding Assays Based on Mass Spectrometry

##### 5.3.1

##### Assay Principle

Next to the detection of enzyme inhibition, ESI-MS can also be used to monitor protein–ligand interaction, employing an assay format similar to fluorescence-based receptor assays. Using a similar continuous-flow analytical screening system as shown in Fig. 5.2, a competitive assay can be set up using ESI-MS to measure the interaction of the analyte(s) with an affinity protein such as an antibody, receptor or enzyme [28]. Figure 5.10 shows the equilibrium reactions that form the basis of the assay concept. In a first step, the sample was injected into a con-

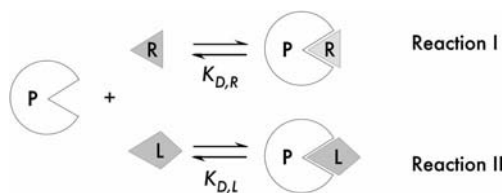


**Fig. 5.10** Principle of competitive ligand binding MS assays. Protein (P) molecules react with the test ligand (L) to form a protein–ligand complex (PL). The extent of complex forming is monitored by the addition of a bioactive reporter ligand (R) resulting in the formation of protein–reporter complex (PR). The concentration free R is directly dependent on the concentration and affinity of L; R is monitored by ESI-MS at its corresponding  $m/z$  trace.

tinuous-flow reaction system and allowed to react with the affinity protein for 10–20 s. In the second step, a reporter ligand was added to saturate the remaining free binding sites of the affinity protein. The reaction time was 10–20 s and depended mainly on the binding constant of reporter ligand–affinity protein complex. The reaction time was chosen in a way that the association of free affinity protein molecules with the reporter ligand is favored whereas the dissociation of the analyte–affinity protein complex is negligible. Finally, the concentration of free reporter ligand was detected using ESI-MS in the SIM mode.

Generally, in biochemical analysis a phosphate buffer is used to mimic physiological conditions (about pH 7.5). The percentage of organic modifier is usually kept as low as possible to prevent denaturation of the proteins. In addition, a blocking reagent such as Tween-20 is added to prevent non-specific binding of the protein (and protein–ligand complex) to the surface of reaction capillaries. However, nonvolatile additives in the eluent, such as phosphate buffer and blocking reagent, are not compatible with MS detection. Various reaction conditions were monitored using a series of MS-compatible solvents and compared with the responses observed in the fluorescence detection.

### 5.3.2

#### Optimization of MS Conditions

Different organic and inorganic buffers, such as ammonium acetate, ammonium formate, HEPES, Gly-Gly, and triethanolamine, were selected to study the response of biotin and fluorescein–biotin in MS and compared to phosphate buffer. Biotin and fluorescein–biotin were dissolved in the carrier solution compositions of buffer (10 mM; pH 7.5)/methanol (50:50, v/v) at concentrations of  $10 \text{ ng } \mu\text{l}^{-1}$ . Both infusion and  $20 \text{ } \mu\text{l}$ -loop injection experiments were performed with detection by MS in full-scan and SIM mode. Main optimization criteria are the maximum response of biotin and fluorescein–biotin with lowest interference of the carrier solution. HEPES, Gly-Gly, and triethanolamine give very high background response, which significantly hampers the detection of biotin and fluorescein–

biotin. Phosphate buffer and ammonium acetate/ammonium formate give a factor  $10\times$  and  $100\times$  less background response, respectively. As regards to sensitivity, ammonium acetate and ammonium formate gave the highest response for biotin and fluorescein–biotin. Consequently, all stock solutions were prepared in methanol (biotin/fluorescein–biotin) or ammonium formate ( $10\text{ mmol L}^{-1}$ ; pH 7.5, protein).

In order to select a carrier solution composition which would provide an overall maximum response for MS detection, two modifiers were selected, acetonitrile and methanol, and two buffers, i.e. ammonium acetate ( $10\text{ mmol L}^{-1}$ ; pH 7.5) and ammonium formate ( $10\text{ mmol L}^{-1}$ ; pH 7.5). Biotin and fluorescein–biotin were dissolved in various binding buffer–organic solvent mixtures ranging from 90:10 (v/v) to 50:50 (v/v) at two concentration levels ( $0.01\text{ ng }\mu\text{L}^{-1}$ ,  $1\text{ ng }\mu\text{L}^{-1}$ ) and  $20\text{ }\mu\text{L}$  were injected and analyzed by MS in full-scan and SIM mode. The maximum response was found with 50% methanol, which was about a factor  $2\times$  higher than for 10% methanol. Since the proteins can denature or protein–ligand complexes can dissociate at relatively low percentages of organic modifier in further experiments only 10% methanol is used in the carrier solution.

### 5.3.3

#### On-line Continuous-flow Biochemical Interaction

Figure 5.11 illustrates the basic performance of the on-line MS assay. For comparison, a homogenous fluorescence assay has been set up in parallel. For this purpose, the carrier flow was split after the second microcoil reactor, with 90% of the total flow being directed to a fluorescence detector (Fig. 5.11a) and 10% to the MS (Fig. 5.11b). The affinity interaction between streptavidin and biotin was chosen to study the characteristics of an on-line MS biochemical assay. Fluorescein–biotin was used as reporter ligand for both fluorescence and MS in the SIM mode ( $m/z\ 390$ ) detection. In the fluorescence mode, the homogeneous biochemical assay is based on the quenching of the fluorescein–biotin fluorescence upon binding to streptavidin.

At point (1) in Fig. 5.11a, solely carrier buffer is pumped by all pumps (carrier pump, affinity protein pump, reporter ligand pump) resulting in stable baseline in both detectors. At point (2), fluorescein–biotin is added to the reporter ligand pump leading to an increase of the background signal in both detectors. After stabilization of the system, streptavidin is added to the affinity protein pump at point (3). The reaction of streptavidin and fluorescein–biotin leads to an almost complete disappearance of free fluorescein–biotin and, consequently, to a reduction of the baseline to the original level. When injecting active analytes such as biotin (points labeled 4), the concentration of free, unbound streptavidin is reduced in reaction 1, leading to an increase of the free fluorescein–biotin concentration after reaction 2 and a positive signal in both the MS and fluorescence detector. MS is shown to mimic the similar response patterns in the continuous-flow experiment as those observed with fluorescence detection. The decrease of

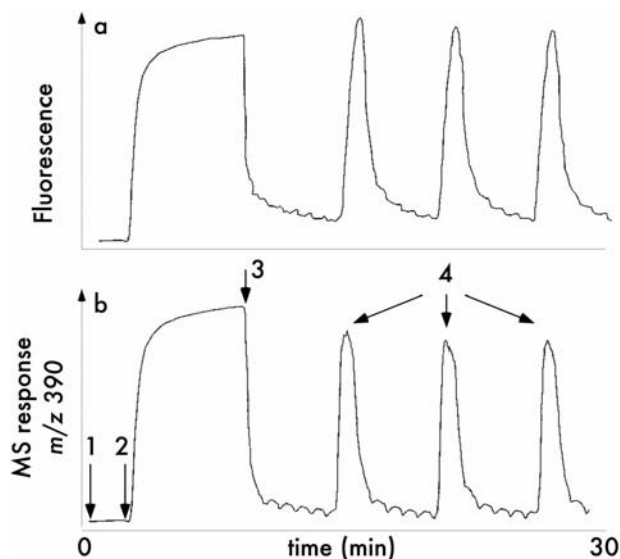


**Fig. 5.11** On-line continuous-flow monitoring of biochemical interaction with (a) fluorescence and (b) MS SIM ( $m/z$  390) detection. Fluorescein–biotin (96 nM), streptavidin (32 nM), 20- $\mu$ L loop injections of 1000 nM biotin ( $n = 3$ ). MS instrument: Q-ToF2 (Waters) equipped with a Waters Z-spray electrospray (ESI) source. Point 1: Carrier pump, protein and reporter ligand pumps

are delivering background buffer. Point 2: Fluorescein–biotin (reporter molecule) is added, resulting in an increase of both the fluorescence and MS-SIM signal. Point 3: streptavidin is added, resulting in a decrease of the free fluorescein–biotin concentration. Point 4: injection of the active ligand biotin leads to positive peak due to the displacement of bound reporter ligand.

the unbound fluorescein–biotin concentration upon addition of streptavidin at point (3) indicates that complex formation occurs and that the fluorescein biotin–streptavidin complex does not dissociate during the ionization phase. Complete protein–ligand complexes have been reported to stay intact in the ESI-MS process; however, gentle experimental conditions should be applied.

Furthermore, when using 96 nM fluorescein–biotin and 32 nM streptavidin, an injection of 1  $\mu\text{mol L}^{-1}$  of biotin results in an almost complete blocking of streptavidin and, consequently, the maximum peak height possible under the current conditions is about 95% of the highest point (3), indicating that apparent binding of biotin to streptavidin is in the order of  $>95\%$ .

Because the interaction between biotin and streptavidin is strong ( $K_a = 0.6 \times 10^{15} \text{ L mol}^{-1}$ ) with a relatively fast association rate ( $k_{+1} = 2.4 \times 10^7 \text{ L mol}^{-1} \text{ s}^{-1}$ ) and slow dissociation rate ( $k_{-1} = 0.4 \times 10^{-7} \text{ s}^{-1}$ ), the reaction times are fast, i.e. 10–20 s. Furthermore, the addition of reporter ligand is performed only after the analyte protein reaction has taken place in coil I, avoiding a displacement reaction that would substantially increase the overall reaction time.

Hence the reaction coil volumes were kept as small as possible to reduce band-broadening, i.e. 17  $\mu\text{L}$  and 33  $\mu\text{L}$ , for coil I and coil II, respectively.

### 5.3.4

#### Monitoring Bioactive Compounds

The biochemical MS assay performance was studied for various biotin derivatives, such as biotin ( $m/z$  245), N-biotinyl-6-aminocaproic acid hydrazide ( $m/z$  372), biotin-hydrazide ( $m/z$  259), N-biotinyl-L-lysine ( $m/z$  373) and biotin-N-succinimidelester ( $m/z$  342). These five different bioactive compounds were consecutively injected into the biochemical MS assay. Figure 5.12 shows triplicate injections in the biochemical MS-based system of the different active compounds. Each compound binds to streptavidin, hence the MS responses of peaks of the reporter ligand (fluorescein–biotin,  $m/z$  390) are similar. The use of SIM allows specific components to be selected and monitored, e.g. protonated molecule of the biotin derivatives. In this case, no peaks were observed for biotin-N-succinimidelester ( $m/z$  342), because under the applied conditions fragmentation occurred to  $m/z$  245. In combination with full-scan MS measurements, the molecular mass of active compounds can be determined simultaneously to the biochemical measurement.

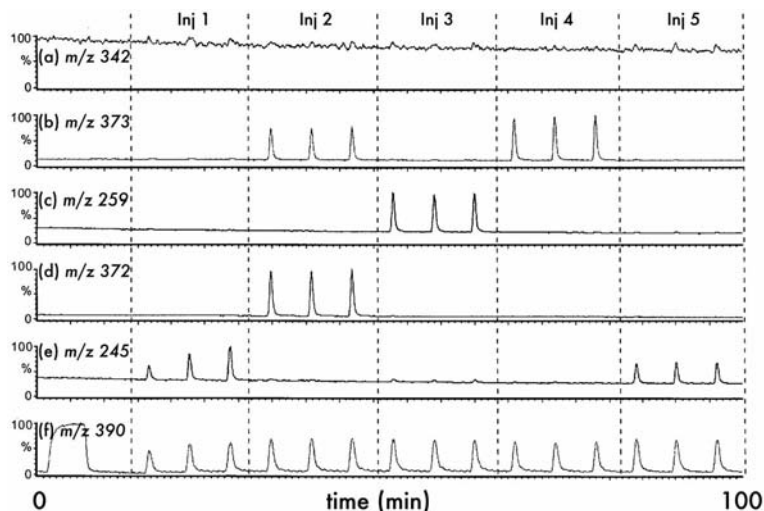


**Fig. 5.12** On-line continuous-flow monitoring of bioactive compounds using fluorescein–biotin/streptavidin assay. MS instrument: Q-ToF2 (Waters) equipped with a Waters Z-spray electrospray (ESI) source. Triplicate injections of (a) biotin-N-succinimidelester ( $m/z$  342), (b) N-biotinyl-L-lysine ( $m/z$  373),

(c) biotin hydrazide ( $m/z$  259), (d) N-biotinyl-6-aminocaproic hydrazide ( $m/z$  372), (e) biotin ( $m/z$  245), (f) monitoring of fluorescein–biotin ( $m/z$  390) as reporter molecule for ligand binding to streptavidin. Fluorescein–biotin 96  $\text{nmol L}^{-1}$ , streptavidin 32 nM, and all ligand injections are 1  $\mu\text{M}$ .

## 5.3.5

**Antibody–Antigen Interactions**

In order to assess the applicability of MS to study antibody–antigen interactions we used a model system comprising FAB fragments of anti-digoxigenin antibodies. Digoxin and digoxigenin are ligands having approximately the same affinity for the anti-digoxigenin antibodies. Both compounds can therefore be used as either analyte or reporter ligand. The same MS-based biochemical assay set-up was used as for the streptavidin/biotin system. Because the interaction between anti-digoxigenin antibodies and digoxin is weaker ( $K_a = \text{approx. } 10^9 \text{ L mol}^{-1}$ ) with a relatively slower association rate and dissociation rate than streptavidin/biotin, a longer reaction time is preferred. Therefore a reaction coil volume of 65  $\mu\text{L}$  was chosen for reaction I resulting in a reaction time of 39 s.

The interaction of digoxigenin with the anti-digoxigenin antibodies was measured by incubating various concentrations of digoxigenin with 200 nM anti-digoxigenin antibodies and subsequent injection into the FI–MS system. The interaction was monitored by observing the response of digoxigenin in MS at  $m/z$  408.4. In comparison with the calibration line obtained by injection of digoxigenin in the absence of antibodies, a significant decrease of the digoxigenin response was observed for all digoxigenin concentrations injected. In order to demonstrate that the decrease of the free digoxigenin concentration upon incubation with anti-digoxigenin antibodies is based on specific interactions, the same experiment was repeated, but the anti-digoxigenin antibodies were first incubated with a large excess (2  $\mu\text{M}$ ) of digoxin, i.e. a competing ligand. The resulting calibration curve is almost identical with the calibration for digoxigenin measured in the absence of antibodies indicating that digoxigenin is prevented from binding to the antibody due to an excess of competing ligand. A similar behavior was observed when digoxin instead of digoxigenin was used as reporter ligand.

These experiments clearly demonstrate that ESI-MS is suitable for monitoring antibody–antigen interactions by selectively detecting free ligand molecules in the presence of antibody–ligand complexes. Moreover, the development of MS-based biochemical assays is rather straightforward since any detectable analyte can principally be used as reporter ligand. The sensitivity of the biochemical assay depends mainly on the detection sensitivity of the reporter ligand and its binding affinity for the affinity protein. Since digoxin and digoxigenin have similar binding affinities for the anti-digoxigenin antibodies, similar assay sensitivities are obtained when using both compounds as reporter ligands.

## 5.3.6

**Continuous-flow Multi-protein Binding Assays Using Electrospray MS**

The assay principle shown in Fig. 5.10 has the potential of multiplexing, i.e. performing several assays in parallel, by pumping mixtures of receptors, i.e. streptavidin and anti-digoxigenin and reporter ligands, i.e. fluorescein–biotin and digoxin [29]. Clearly this approach will only be feasible for those assays

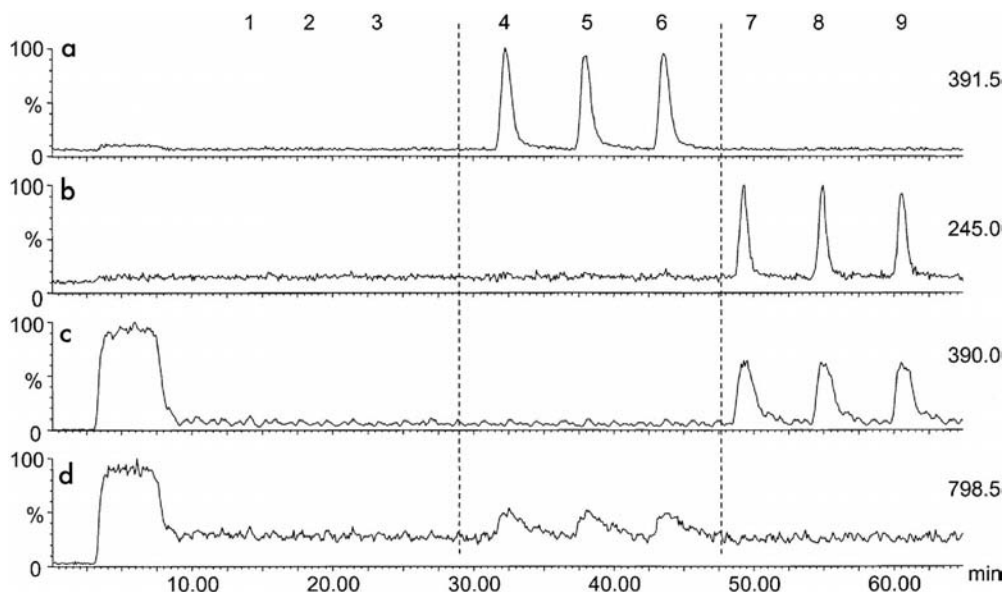


**Fig. 5.13** On-line continuous-flow, multi-protein biochemical assay. MS instrument: Q-ToF2 (Waters) equipped with a Waters Z-spray electrospray (ESI) source. Extracted-ion chromatograms of (a) digoxigenin ( $m/z$  391.5), (b) biotin ( $m/z$  245.0), (c) fluorescein-biotin/streptavidin ( $m/z$  390.0) assay and (d) digoxin/anti-digoxigenin ( $m/z$  798.5) assay. Triplicate injections were performed WITH blank (peaks 1–3), 1  $\mu$ M digoxigenin (peaks 4–6) and 1  $\mu$ mol L<sup>-1</sup> biotin (peaks 7–9).

where no cross-reactivity exists between receptors and reporter ligands. Batch experiments (data not shown) revealed that there is no cross-reactivity for ligands binding either to streptavidin or anti-digoxigenin.

The parallel biochemical assay was performed by dissolving both receptor proteins in one solution and the two reporter ligands in one other solution. Both reporter ligands (fluorescein-biotin and digoxin) were pumped together with one pump. The receptors (streptavidin and anti-digoxigenin) were pumped with another pump. Figure 5.13 shows the extracted-ion chromatograms for both reporter molecules. The two lower traces represent the reporter molecule digoxin ( $m/z$  798.5) and the reporter molecule fluorescein-biotin ( $m/z$  390.0), respectively. Triplicate injections of blank, 1  $\mu$ M digoxigenin, and 1  $\mu$ M biotin were performed. As expected, the injection of an active compound resulted in an increase in the concentration of the respective unbound reporter molecule. In addition, peaks were observed in the extracted-ion chromatograms of biotin and digoxigenin. This is a result of the fact that the concentration injected into the carrier solution is a large excess compared to the concentration of receptor present in the carrier solution.

## 5.4

### MS Assay Based on Dissociation of Isolated Protein–Ligand Complexes

#### 5.4.1

##### Assay Set-up

The MS assay principles discussed in Sections 5.2 and 5.3 have in common that they rely on the availability of appropriate reporter molecules, i.e. chemical compounds that indicate the presence of bioactive ligands through a change of concentration. In many instances, it is not straightforward to get access to these compounds, e.g. in the case of orphan receptors where no active ligands are yet found. In this section we describe an assay format that relies on the detection of bioactive ligands after dissociation from their target protein [30]. The general principle of this reporter-free biochemical MS assay format is outlined in Fig. 5.14. The assay is based on three sequential steps, i.e. the incubation of the sample with the affinity protein, the quantitative separation of free and protein-bound compounds, and the dissociation of the protein–ligand complexes. Ligands released from the protein are subsequently detected by LC-MS.

The hardware implementation is shown in Fig. 5.15. After injecting the sample into the carrier phase, a plug of affinity protein is added during a period of 60 s, i.e. a time interval which ensures that, under the conditions described, the entire sample is able to react with the target proteins. By introducing a protein plug instead of constantly adding the target proteins to the carrier phase, a considerable reduction in affinity protein consumption is achieved. Subsequently, by implementing a short column packed with a C18 restricted-access (RA) column material (e.g. Lichrosorb ADS C18; Merck, Darmstadt, Germany), low molecular mass molecules, which did not form an affinity complex during the reaction period, are trapped inside the small hydrophobic pores of the RA beads. In contrast, the high

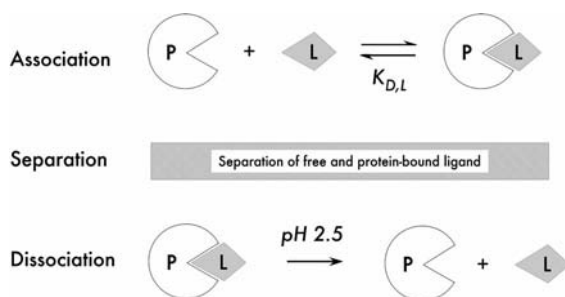


**Fig. 5.14** Principle of label-free ligand binding MS assays. Protein (P) molecules react with the test ligand (L) to form a protein–ligand complex (PL). Unbound compounds are separated from PL by passage through a restricted-access column. Subsequently, PL is dissociated at low pH, and active ligands L are detected by LC-ESI-MS.



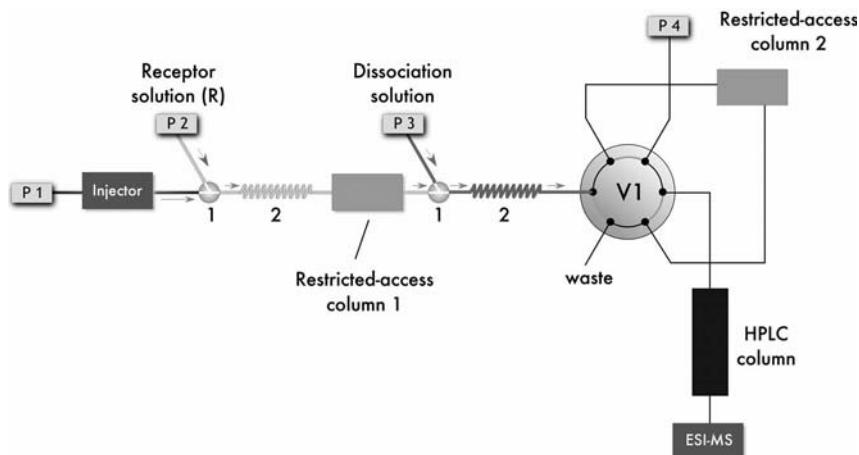


**Fig. 5.15** Analytical set-up for on-line label-free assay based on ESI-MS. MS instrument: Ion-trap mass spectrometer (LCQ Deca, Thermo Electron). P1: Carrier/HPLC pump. P2: HPLC pump delivering receptor solution. P3: HPLC pump delivering dissociation solution. P4: HPLC pump for final LC-MS analysis of released ligands. 1: Mixing union. 2: Microcoil reactor. V1: injection valve.

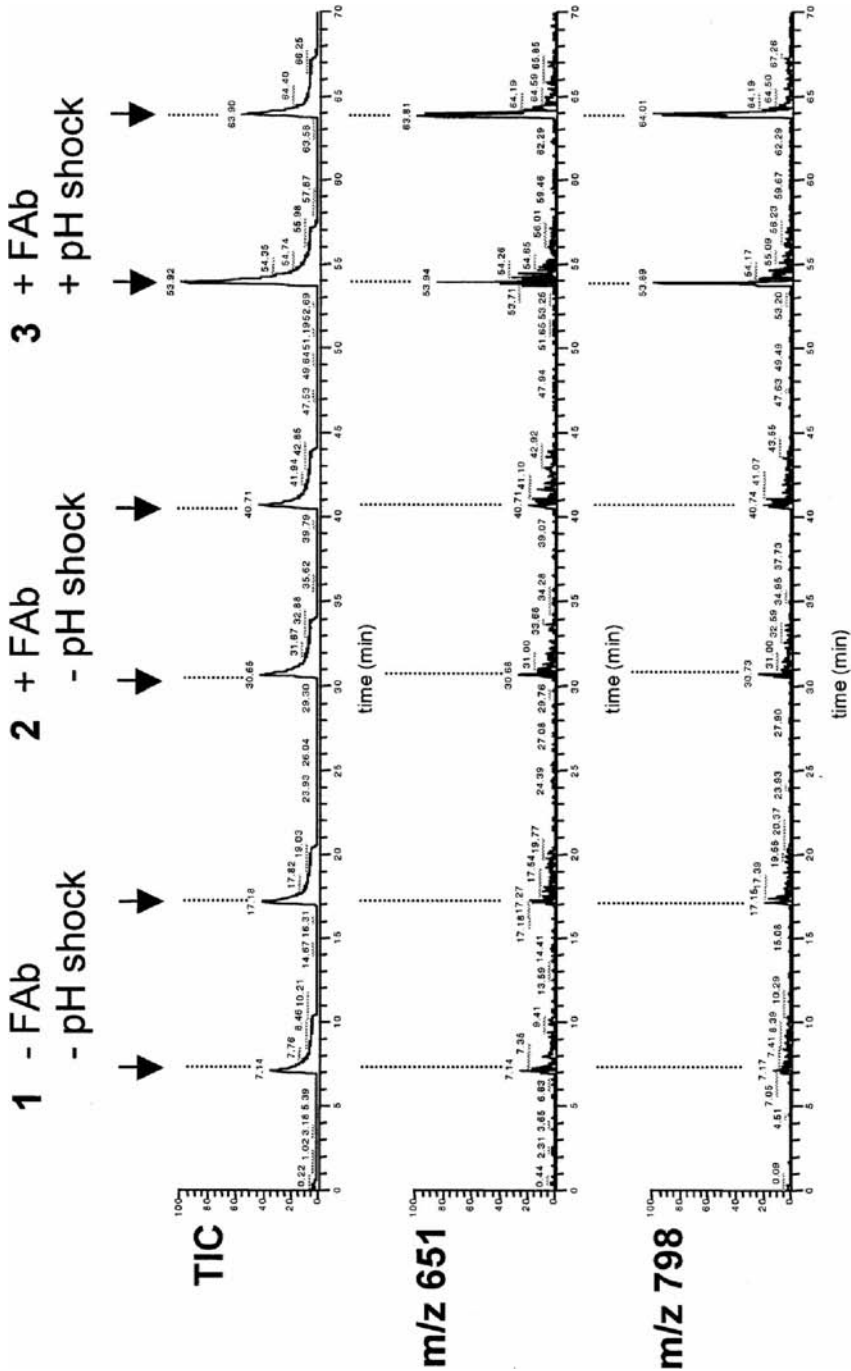
molecular mass affinity proteins and complexes are allowed to pass the RA column unretained, as their size prevents diffusion into the small hydrophobic pores. Nonspecific binding of these proteins is largely avoided because of the hydrophilic nature of the surface of the RA beads. As a result, a fast and efficient separation is achieved between those compounds that either do not or only weakly form an affinity complex with the target protein and those that do. Besides efficiently separating the bound molecules from the unbound molecules, implementation of RA columns expands the range of affinity interactions, which can be monitored using the current setup, to higher  $K_D$  values as a result of the short residence times onto the RA column. As the affinity complexes typically pass the RA columns within seconds, affinity-complex dissociation becomes less pronounced when compared with other separation methods, such as size exclusion chromatography. Subsequently, after passing the first RA column, the affinity complex is subjected to a dissociation step based on a pH change, which disrupts the affinity interaction between target protein and bioactive compound. After dissociation of the affinity complex, separation of the free bioactive compound and the target protein is easily accomplished by introducing a second RA column. Ligands, originating from the dissociated affinity complex, are trapped within the hydrophobic pores, whereas the target protein passes the RA column unretained and is directed towards waste. In this way, bioactive compounds are isolated from nonactive molecules as well as from the affinity proteins. After this loading

phase, which typically takes 2 min, the second RA column is washed extensively with 1% acetic acid to remove the majority of the impurities, such as salts, originating from sources such as reagent solutions and samples. Subsequently the second RA column is switched into a 75% MeOH/2 mM ammonium acetate solution, which is constantly introduced into the ESI probe. Trapped bioactive compounds are eluted from the RA column in a well defined matrix at a flow rate of  $50 \mu\text{L min}^{-1}$  and are subsequently analyzed by MS, using data-dependent scanning. This way, characteristic MS and  $\text{MS}^n$  ( $n = 2$  or  $3$ ) data of bioactive compounds are recorded during a single run. Molecular mass information is obtained from the MS data, whereas a mass fingerprint of the bioactive molecule is provided by  $\text{MS}^n$  spectra.

#### 5.4.2

##### Flow Injection Label-free MS Assay

To demonstrate proper functioning of the MS-based bioassay and illustrate the potential for orphan target screening, a model system using anti-digoxigenin antibodies was chosen, and digoxin samples were injected under several bioassay conditions. The presence of digoxin onto the second RA column was evaluated by monitoring the reconstructed ion currents of two  $m/z$  values, 651.1 and 798.2, that were characteristic for digoxin under the conditions applied. Figure 5.16 shows the results of digoxin injections ( $1 \mu\text{M}$ ) using three different bioassay conditions. First, digoxin was injected into a bioassay system in which the anti-digoxigenin FAb as well as the dissociation solution were replaced by buffer (10 mM ammonium acetate, pH 6.7). The ion current traces for  $m/z$  651 and 798 are comparable to those obtained for blank injections, thus indicating that digoxin is efficiently trapped onto the first RA column. The ion current peaks, which can be observed in the total, as well as extracted ion current profiles are caused by the introduction of residual ions and solvent (DMSO), which were not completely removed from the RA column during flushing. During a second step, anti-digoxigenin FAb was added to the biochemical assay, while the dissociation solution was still replaced by buffer. Again, the digoxin injections showed hardly any increase in ion current, indicating that the affinity complexes formed passed both the first and second RA columns. Finally, digoxin was injected into a complete bioassay system containing both the affinity protein as well as the dissociation solution. The ion current traces of  $m/z$  651 and 798 both clearly show a significant increase in intensity compared with the previous digoxin injections. From these experiments it can be concluded that the affinity complexes between digoxin and anti-digoxigenin FAb were indeed formed, passed the first RA column, and finally were dissociated by the pH shock applied. As a result, digoxin molecules were trapped onto the second RA column and were detected by full-scan MS analysis after column desorption. Under these semi-optimized conditions, digoxin could be detected down to 250 nM, whereas the relative standard deviation of  $1 \mu\text{M}$  digoxin injections equaled 13.0% ( $n = 5$ ).



## 5.4.3

**Flow Injection Label-free MS Assay Screening of Natural Extracts**

To demonstrate proper functioning of the MS-based bioassay for anti-digoxigenin antibodies using complex sample matrices, higher plant extracts were diluted ten times with 10 mM TRIS buffer (pH 7.0), spiked with digoxin (250 nM), and subsequently analyzed. Figure 5.17 shows an example of such a spiked extract. First, an unspiked aliquot of the extract was injected into the MS-based bioassay of which the first RA column was removed (no target present). Consequently, moderately polar to hydrophobic compounds present in the sample were trapped onto the second RA column and were eluted towards the MS detector. The principle of the MS-based bioassay was then demonstrated by reinserting the RA column again, followed by the injection of a spiked aliquot of the same plant extract in the presence of protein target. As can be seen in Fig. 5.17, the first RA column efficiently traps the non-bioactive molecules, which were present in the plant extract. The bioactive compound digoxin, however, is successfully isolated from the plant extract and can clearly be observed in the MS spectrum ( $m/z$  859.2 and 902.0). By injecting spiked and unspiked aliquots of natural extracts, the ability of the bioassay format to rapidly detect ligands for protein targets, such as soluble orphan receptors, is demonstrated.

## 5.5

**Future Prospects**

We have shown that electrospray MS is a valuable tool in the screening of bioactive compounds, the main advantages being in the area of complex mixture screening. The potential of MS to provide a chemical fingerprint of the bioactive compounds next to binding/inhibition properties is unique and in fact only matched by similar approaches using NMR. Next to the assay formats described in this article, many more formats have been successfully demonstrated in literature. It is worthwhile to mention the detection of intact protein-ligand complexes by ESI-MS or MALDI-TOF MS as alternative to the assay concepts described in this article that mainly rely on reporter molecules or the detection of dissociated ligands.

**Fig. 5.16** Demonstration of MS-based bioassay functionality. Injections represent standard solutions of 1  $\mu$ M digoxin samples. MS instrument: Ion-trap mass spectrometer (LCQ Deca, Thermo Electron).  $m/z$  651 represents the  $[(M-S)+H]^+$  ion of digoxin with S indicating one sugar moiety;  $m/z$  798

represents the ammonium ion of digoxin. 1: Affinity protein and pH dissociation solution replaced by buffer solutions. 2: pH dissociation solution replaced by buffer solution. 3: All MS-based bioassay solutions installed.

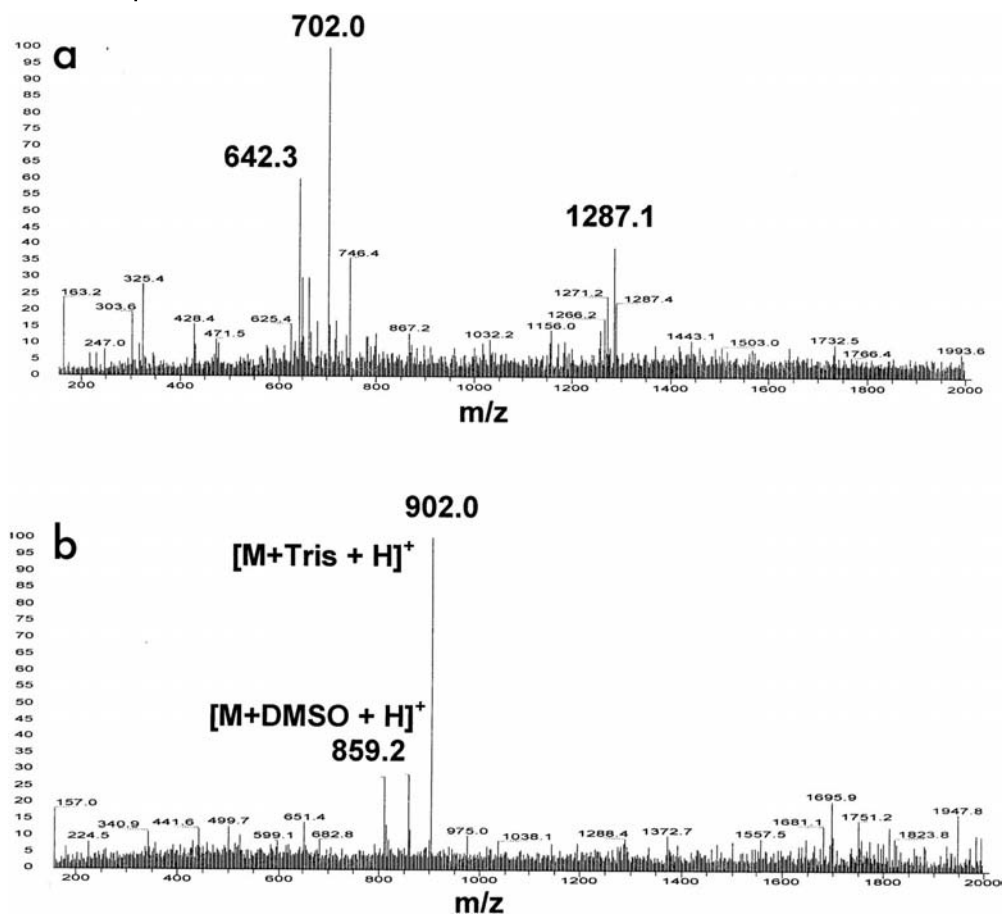


**Fig. 5.17** Demonstration of MS-based bioassay functionality using a plant extract. MS instrument: Ion-trap mass spectrometer (LCQ Deca, Thermo Electron). (a) MS analysis of pure extract by direct injection onto restricted-access column 2 in the absence of affinity protein. (b) Analysis of the same natural extract spiked with digoxin using the label-free MS assay method as shown in Fig. 5.15.

One has to emphasize that MS also is associated with several drawbacks when it comes to bioactivity screening. First of all, the optimum, native conditions for bioactivity screening (pH 7.2, addition of 150 mM sodium chloride) are entirely incompatible with optimum conditions for MS detection which, for ESI-MS, typically require acidic pH values and the presence of organic modifiers to enhance ionization properties of the analytes. Assay development for MS-based assays therefore mainly requires the testing of different assay conditions, particularly the replacement of nonvolatile buffers with MS-compatible volatile buffers. Furthermore, it is essential to monitor ion suppression effects, for example, by the

addition of system-monitoring compounds, as shown in this article. Ion suppression may very well lead to wrongful assignments of bioactivities which is particularly harmful if it leads to false negative results. Assay development should therefore also comprise the design of control experiments, e.g. omitting proteins in binding studies, addition of competitors, in order to allow an accurate assessment of the biochemical properties of bioactive substances.

Miniaturization is a key aspect when implementing MS-based assays. The high sensitivity of ESI-MS in capillary or nano-LC mode favors the use of miniaturized assay formats. Both open-tubular capillaries and chip-based designs enable the establishment of low deadvolume microfluidic assays; however, one should keep in mind that injection volumes for miniaturized analytical systems are substantially lower than in macrofluidic systems. In our experience, it is essential to integrate on-line preconcentration methods, for example, solid-phase extraction or on-column focusing of analytes, to enable larger injection volumes, to achieve the detection limits relevant for screening in a drug discovery environment.

With the development of high-resolution MS instruments such as FT-ICR MS, mass spectrometry will certainly gain in importance for studying key properties of hit and lead compounds in the early stages of drug discovery. In view of the diversity of many protein targets to be screened, it is in our opinion advisable to rely on a broad portfolio of assay formats rather than focusing on a single approach. Next to the methodologies described in this contribution, assay formats detecting protein–ligand complexes by, for example, MALDI-TOF MS should also be considered.

## Acknowledgements

We wish to thank Shimadzu BioSciences and Agilent Technologies for their support in MS instrumentation. Furthermore we thank Kiadis BV (Groningen, The Netherlands) for financial support and fruitful discussions.

## References

- 1 A. Smith: Screening for drug discovery: the leading question. *Nature* **2002**, 418, 453–459.
- 2 K. Robards: Strategies for the determination of bioactive phenols in plants, fruit and vegetables. *J Chromatogr A* **2003**, 1000, 657–691.
- 3 M. A. Strege: High-performance liquid chromatographic-electrospray ionization mass spectrometric analyses for the integration of natural products with modern high-throughput screening. *J Chromatogr B Biomed Sci Appl* **1999**, 725, 67–78.
- 4 C. Enjalbal, J. Martinez, J. L. Aubagnac: Mass spectrometry in combinatorial chemistry. *Mass Spectrom Rev* **2000**, 19, 139–161.
- 5 V. Swali, G. J. Langley, M. Bradley: Mass spectrometric analysis in combinatorial chemistry. *Curr Opin Chem Biol* **1999**, 3, 337–341.
- 6 K. J. Miller, A. C. Herman: Affinity chromatography with immunochemical detection applied to the

- analysis of human methionyl granulocyte colony stimulating factor in serum. *Anal Chem* **1996**, 68, 3077–3082.
- 7 A. J. Oosterkamp, M. T. Villaverde Herraiz, H. Irth, U. R. Tjaden, J. van der Greef: Reversed-phase liquid chromatography coupled on-line to receptor affinity detection based on the human estrogen receptor. *Anal Chem* **1996**, 68, 1201–1206.
  - 8 T. Schenk, G. J. Breel, P. Koevoets, S. van den Berg, A. C. Hogenboom, H. Irth, U. R. Tjaden, J. van der Greef: Screening of natural products extracts for the presence of phosphodiesterase inhibitors using liquid chromatography coupled online to parallel biochemical detection and chemical characterization. *J Biomol Screen* **2003**, 8, 421–429.
  - 9 A. Belenky, D. Hughes, A. Korneev, Y. Dunayevskiy: Capillary electrophoretic approach to screen for enzyme inhibitors in natural extracts. *J Chromatogr A* **2004**, 1053, 247–251.
  - 10 H. Y. Cheung, W. P. Lai, M. S. Cheung, F. M. Leung, D. J. Hood, W. F. Fong: Rapid and simultaneous analysis of some bioactive components in *Eucommia ulmoides* by capillary electrophoresis. *J Chromatogr A* **2003**, 989, 303–310.
  - 11 L. Ma, X. Gong, E. S. Yeung: Combinatorial screening of enzyme activity by using multiplexed capillary electrophoresis. *Anal Chem* **2000**, 72, 3383–3387.
  - 12 Y. F. Hsieh, N. Gordon, F. Regnier, N. Afeyan, S. A. Martin, G. J. Vella: Multidimensional chromatography coupled with mass spectrometry for target-based screening. *Mol Diversity* **1997**, 2, 189–196.
  - 13 K. Ingkaninan, C. M. de Best, R. van der Heijden, A. J. Hofte, B. Karabatak, H. Irth, U. R. Tjaden, J. van der Greef, R. Verpoorte: High-performance liquid chromatography with on-line coupled UV, mass spectrometric and biochemical detection for identification of acetylcholinesterase inhibitors from natural products. *J Chromatogr A* **2000**, 872, 61–73.
  - 14 G. R. Lenz, H. M. Nash, S. Jindal: Chemical ligands, genomics and drug discovery. *Drug Discov Today* **2000**, 5, 145–156.
  - 15 U. Schobel, M. Frenay, D. A. van Elswijk, J. M. McAndrews, K. R. Long, L. M. Olson, S. C. Bobzin, H. Irth: High resolution screening of plant natural product extracts for estrogen receptor alpha and beta binding activity using an online HPLC-MS biochemical detection system. *J Biomol Screen* **2001**, 6, 291–303.
  - 16 D. A. van Elswijk, O. Diefenbach, S. van der Berg, H. Irth, U. R. Tjaden, J. van der Greef: Rapid detection and identification of angiotensin-converting enzyme inhibitors by on-line liquid chromatography-biochemical detection, coupled to electrospray mass spectrometry. *J Chromatogr A* **2003**, 1020, 45–58.
  - 17 A. R. de Boer, T. Letzel, D. A. van Elswijk, H. Lingeman, W. M. Niessen, H. Irth: On-line coupling of high-performance liquid chromatography to a continuous-flow enzyme assay based on electrospray ionization mass spectrometry. *Anal Chem* **2004**, 76, 3155–3161.
  - 18 E. Shaw, R. T. Dean: The inhibition of macrophage protein turnover by a selective inhibitor of thiol proteinases. *Biochem J* **1980**, 186, 385–390.
  - 19 L. Herszenyi, M. Plebani, P. Carraro, M. De Paoli, G. Roveroni, R. Cardin, F. Foschia, Z. Tulassay, R. Naccarato, F. Farinati: Proteases in gastrointestinal neoplastic diseases. *Clin Chim Acta* **2000**, 291, 171–187.
  - 20 J. E. Koblinski, M. Ahram, B. F. Sloane: Unraveling the role of proteases in cancer. *Clin Chim Acta* **2000**, 291, 113–135.
  - 21 R. Bonfiglio, R. C. King, T. V. Olah, K. Merkle: The effects of sample preparation methods on the variability of the electrospray ionization response for model drug compounds. *Rapid Commun Mass Spectrom* **1999**, 13, 1175–1185.
  - 22 C. F. de Jong, R. J. Derks, B. Bruyneel, W. Niessen, H. Irth: High-

- performance liquid chromatography–mass spectrometry-based acetylcholinesterase assay for the screening of inhibitors in natural extracts. *J Chromatogr A* **2006**, 1112, 303–310.
- 23 R. T. Bartus, R. L. Dean 3rd, B. Beer, A. S. Lipka: The cholinergic hypothesis of geriatric memory dysfunction. *Science* **1982**, 217, 408–414.
  - 24 H. M. Greenblatt, H. Dvir, I. Silman, J. L. Sussman: Acetylcholinesterase: a multifaceted target for structure-based drug design of anticholinesterase agents for the treatment of Alzheimer's disease. *J Mol Neurosci* **2003**, 20, 369–383.
  - 25 M. Heinrich, H. L. Teoh: Galanthamine from snowdrop – the development of a modern drug against Alzheimer's disease from local Caucasian knowledge. *J Ethnopharmacol* **2004**, 92, 147–162.
  - 26 I. K. Rhee, N. Appels, T. Luijendijk, H. Irth, R. Verpoorte: Determining acetylcholinesterase inhibitory activity in plant extracts using a fluorimetric flow assay. *Phytochem Anal* **2003**, 14, 145–149.
  - 27 A. R. de Boer, B. Bruyneel, J. G. Krabbe, H. Lingeman, W. M. Niessen, H. Irth: A microfluidic-based enzymatic assay for bioactivity screening combined with capillary liquid chromatography and mass spectrometry. *Lab Chip* **2005**, 5, 1286–1292.
  - 28 A. C. Hogenboom, A. R. de Boer, R. J. Derks, H. Irth: Continuous-flow, on-line monitoring of biospecific interactions using electrospray mass spectrometry. *Anal Chem* **2001**, 73, 3816–3823.
  - 29 R. J. Derks, A. C. Hogenboom, G. van der Zwan, H. Irth: On-line continuous-flow, multi-protein biochemical assays for the characterization of bioaffinity compounds using electrospray quadrupole time-of-flight mass spectrometry. *Anal Chem* **2003**, 75, 3376–3384.
  - 30 D. A. van Elswijk, U. R. Tjaden, J. van der Greef, H. Irth: Mass spectrometry-based bioassay for the screening of soluble orphan receptors. *Int J Mass Spectrom* **2001**, 210/211, 625–636.





## 6

# Frontal Affinity Chromatography – Mass Spectrometry for Ligand Discovery and Characterization

*Nora Chan, Darren Lewis, Michele Kelly, Ella S.M. Ng,  
and David C. Schriemer*

## 6.1

### Introduction

In the reductionist approach to drug discovery, where a disease state is approached through target-driven ligand development, mass spectrometry (MS) does not yet play a prominent role. It has a comfortable home in target characterization and preclinical studies of lead compounds – upstream and downstream of the initial discovery phase – but is rarely considered a tool for the initial discovery phase. Impressive engines of lead discovery have been developed based on optical technologies, with large appetites for compound archives and combinatorial library products. Drug discovery assays involving mass spectrometry face stiff competition with these high-volume, wellplate assays. But MS-based systems need not be wielded in a competitive manner. The advantage to mass spectrometry lies in its ability to characterize compounds in mixtures with high sensitivity and only moderate requirements for sample purification. Thus, when MS is considered as a detector for drug discovery applications, it is appropriate to leave the high-volume, single-compound analyses to the array technologies currently implemented in screening laboratories. If MS is to play a significant role in lead discovery, it will be to extend access to chemical diversity, for example in screening less well defined mixtures of potential ligands such as natural product extracts. Frontal affinity chromatography–mass spectrometry (FAC-MS) is an analytical concept that offers a generalized approach to compound screening via MS, and while it can be utilized as an assay for single compounds, it is well adapted to deriving compound-specific binding data from complicated mixtures that would confound plate-based bioassays. In this chapter we will present the fundamentals of the FAC-MS technique and describe system advancements and recent applications, which together suggest a strong role for the technique in lead discovery.

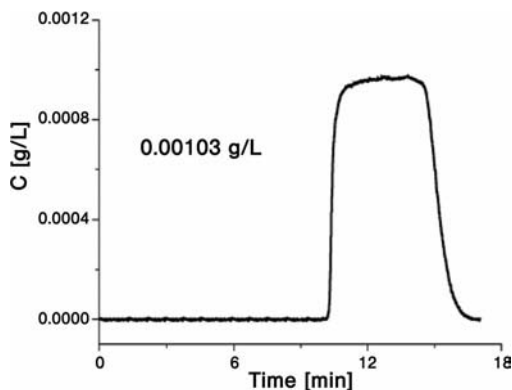


**Fig. 6.1** A breakthrough curve generated by the frontal analysis method [31]. The analysis represents a high-volume injection of caffeine through a reversed-phase column, at a concentration representative of the linear region of the binding isotherm. Adapted with permission from Elsevier.

#### 6.1.1

##### The Basic Frontal Method

Frontal analysis (FA) is perhaps the most straightforward of all chromatographic methods. To operate the method, one continuously infuses sample through a stationary phase and monitors breakthrough times. The goal of such analyses is not to separate components of the mixture, but simply to explore the nature of the interaction between column and compound. An example can be found in Fig. 6.1. Here, a large volume sample of caffeine is injected onto a  $C_{18}$  column, sufficient to achieve breakthrough conditions. In this experiment, a single point determination of the breakthrough volume immediately provides a measurement of the amount of compound bound, while a concentration series accurately describes the isotherm governing the compound/stationary phase interaction – different models of interaction behavior can then be applied to rationalize the interaction.

The method has a rich history in the characterization of compound–stationary phase interactions as it supports the determination of *thermodynamics* and *kinetics* of interaction between a solute and a stationary phase. What has emerged from these studies is the recognition of FA as the premier chromatographic method for generating interaction data; high precision and accuracy are a direct result of making measurements under undistorted dynamic equilibrium conditions. These advantages offer the opportunity to “dissect” the molecular basis for molecular interactions. For example, FA supports the determination of complexity in solute–sorbert interactions as shown in Fig. 6.2, by revealing distinct binding modes. This figure demonstrates that a “simple” interaction between a small molecule nortryptiline and a  $C_{18}$  column is better described as a convolution of

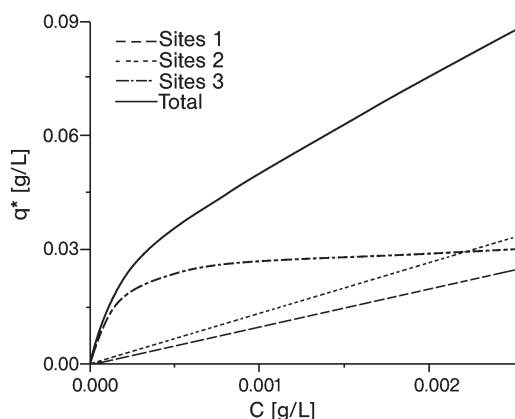


**Fig. 6.2** An example of a binding isotherm generated from frontal affinity data. This example shows that nortryptiline on a  $C_{18}$  reversed-phase column exhibits complex binding behavior. At least three distinct binding modes exist between the compound and the stationary phase [31].  $q^*$  represents the concentration of bound nortryptiline and  $C$  the total concentration of applied nortryptiline. Adapted with permission from Elsevier.

at least three distinct types of interaction. This sort of information is useful in the development of advanced materials for high performance chromatography.

Its application to the measurement of biochemical interactions is intuitive – simply replace the conventional analytical stationary phase with ligand, protein, DNA or any relevant biomolecule. A large-scale version of the method was first described in 1975 by Ken-Ichi Kasai [1] and referred to as frontal affinity chromatography (FAC). The method finds application in the process engineering field, where adsorbents are used to study the interaction of proteins on immobilized ligands, for the purpose of optimizing purification schemes [2–4]. The realization of the analytical benefits of FAC was later in coming [5–7]. Through extensive miniaturization of the affinity columns, sensitive FAC assays have been implemented that are comparable to the amounts used in sensitive biosensor applications [8].

Developing a FAC assay for discovering or characterizing molecular interactions involves effort comparable with most bioassay development exercises. Optimal buffer conditions need to be determined, including the use of necessary co-factors (e.g. divalent cations, secondary ligands). Column design requires a valid immobilized form of the protein, ligand or other biomolecule. This is no more problematic than similar requirements found in surface plasmon resonance (SPR) assays and many plate-based assays. It is worth emphasizing that, with the production of recombinant proteins and the ability to selectively insert affinity tags, much of the complexity involved in this stage of assay development has been removed. In addition, new developments in protein entrapment suggest

that covalent immobilization can be circumvented in certain situations, as will be discussed in Section 6.3.

### 6.1.2

#### FAC – Basic Theory

The simplest binding event involves the interaction of a ligand with a single class of binding sites. There may be multiple, equivalent sites in a given target molecule but the model assumes their independence. This basic binding function stems from the familiar law of mass action and when expressed as a function of the measurable quantity in a FAC experiment it takes the following form, Eq. (1):

$$(V - V_0) = \frac{B_t}{[A]_0 + K_d} \quad (1)$$

The breakthrough volume  $V$  for a ligand is corrected by the breakthrough volume of the ligand in the absence of the binding event,  $V_0$ . This is a difficult number to obtain in practice so a structurally related nonligand is often used to assess  $V_0$ .  $B_t$  refers to the dynamic capacity of the affinity column for the ligand,  $[A]_0$  the infusion concentration of the ligand and  $K_d$  the dissociation constant for the interaction. We may recognize this formalism as one example of a nonlinear convex binding isotherm. Figure 6.3 shows the basic elements that comprise a break-

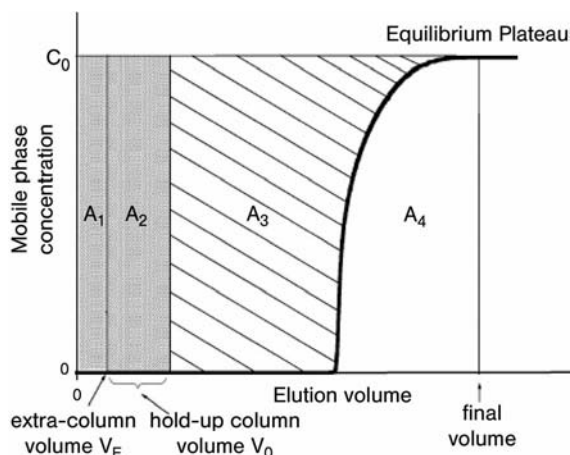


**Fig. 6.3** A dissection of the frontal chromatogram [31]. The breakthrough curve is represented by the thick line. The two gray/hatched surfaces on the left side ( $A_1$ ,  $A_2$ ) represent the mass of compound in the extra- and dead-column volumes. Area  $A_3$  represents the mass of the compound adsorbed to the stationary phase. Adapted with permission from Elsevier.

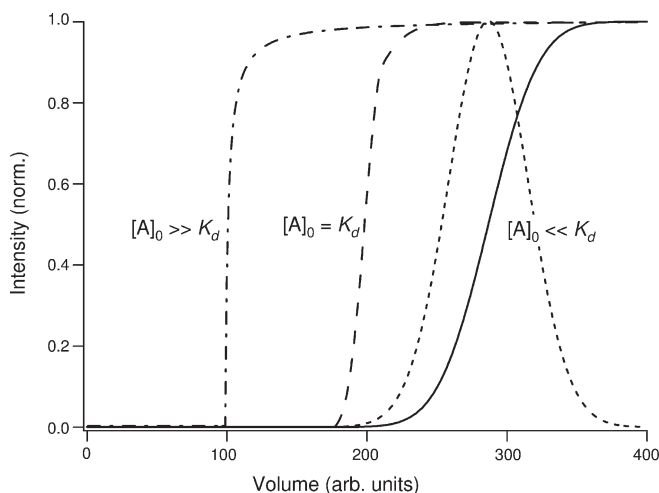


**Fig. 6.4** The effects of ligand concentration on the FAC chromatogram [8]. A given ligand experiences an accelerated breakthrough as its concentration increases. Under linear chromatographic conditions ( $[A]_0 \ll K_d$ ), there is a direct relationship with zonal chromatography, where the breakthrough curve is coincident in retention time with the

zonal peak (short dashed trace). At higher ligand concentration, the breakthrough shifts to earlier elution times (i.e. lower elution volumes) and exhibit a noticeable “sharpening” of the curve (long-dash trace, dot-dash trace). Adapted with permission from the American Chemical Society.

through curve, and Fig. 6.4 the effect of ligand concentration on both the appearance of the curve and the breakthrough volume. At high dilution relative to the  $K_d$  of the particular interaction, the breakthrough volume is insensitive to slight changes in ligand concentration and has actually achieved its maximum value. Under these dilute conditions, FAC operates in the linear region of the binding function.

### 6.1.3

#### FAC Advantages

There are numerous advantages to the FAC approach that differentiate it from many forms of bioassay – MS-dependent or otherwise. The FAC method offers thermodynamic and kinetic binding data from the breakthrough curves. As with the classical application of the FA method, the quality of the data is superb relative to other chromatographic or electrophoretic methods [9, 10]. It is an equilibrium method, as opposed to systems that rely upon the separation of bound from unbound, and this forms the basis of its accuracy.

The most significant figure of merit is the breakthrough volume and assuming a simple equilibrium model, this volume is used to determine the dissociation

constant for the interaction being studied. These values may be measured by any appropriate detector and it is interesting to note that no detector calibration is required, nor does the accuracy of the volume depend on the efficiency of the column. A membrane, cartridge or high-efficiency microbore column can all basically provide the same  $V$  (and thus  $K_d$ ) [11].

In other words, many different styles of affinity construct can be built, all of which can support breakthrough volume measurements. This is a liberating concept, as one can imagine making cheaper/simpler cartridges for high volume applications and more specialized columns for higher precision in follow-on measurements. It is also significant that the detector does not play a significant role in the assay, aside from monitoring breakthrough volumes. The detector is simply required to determine when breakthrough occurs and, as we will see, MS does provide some unique advantages in this regard.

A subtle but unique advantage to the method stems from the distinction between detecting the *compound* rather than the *binding event*. Essentially, FAC achieves molecular interaction analysis in a *concentration-independent* manner. Many assay types generate a signal that is in some way proportional to the amount of bound ligand. According to the law of mass action, this implies that the  $K_d$  of an interaction strongly determines successful detection, and means that a weak interaction cannot be detected as sensitively as a strong interaction. Low concentrations relative to the  $K_d$  of the interaction always generate the maximum breakthrough volume, as will be shown below, and so as long as the detector is sufficiently sensitive, the FAC method can detect interaction  $K_d$  values ranging from millimolar to picomolar without modifying the assay. This is an important advantage. Developments in MS detection ensure that we can “find” low abundance hits/ligands that may be present in the sample well below their  $K_d$  values. For example, a 10 mM  $K_d$  ligand present at a concentration of 1 nM would be difficult to detect with capture/wash methods as washing conditions would likely remove the bound ligand. This sets the method apart from biosensors in which the signal strength is directly related to the amount bound. While the high sensitivity of SPR-based biosensors can ameliorate this to a degree, there are clear advantages to removing the dependency on  $K_d$  value for detecting a binding event.

There are no inherent limitations to the nature of the interaction that can be probed with the FAC method. This too stems from an uncoupling of the binding event and the detector. The method can be applied to simple binary interactions between protein and small molecule, but also to protein–protein interactions, protein–cell interactions and virtually any interaction that can be modeled in a flow system. Some of the more elegant examples include drug interaction with whole cells [12] and membrane-bound receptors from brain homogenates [13]. Ultimately, the limitations are dictated by what can be detected from a stream of column effluent.

While it is possible for a FAC experiment to require excessive sample in order to equilibrate the column and generate a breakthrough curve, this can be easily

prevented during column design. Lowering the binding capacity of the affinity column brings with it reduced sample requirements [10]. In practice, miniaturization to easily-constructed micro-cartridges supports sub-picomol amounts of immobilized protein and similar amounts of sample. This is comparable to modern biosensor technology in both operation and consumption of sample.

#### 6.1.4

#### FAC Disadvantages

No method for quantifying molecular interactions is foolproof, and FAC is no exception. The primary concern with FAC relates to assay development – it can take considerable time and effort to design the assay, in which a protein or some other appropriate biomolecule requires immobilization. The classical concern with immobilization-dependent assays involves preservation of relevant activity; it is not uncommon for initial attempts to be completely unsuccessful especially when chemical labelling strategies are used (e.g. Schiff base reactions between a protein and an amino-resin). More common is the generation of a partially deactivated protein stationary phase, which begs the question whether the loss of activity is simply a “percentage problem” or reflective of an alteration of protein structure/dynamics. Most often this can be resolved by comparing the results generated by FAC analysis of a known ligand, to that generated by an independent assay. Obviously this requires some idea of what structural features constitutes a ligand. This represents the key restriction to extending this assay type to true “orphan receptors” or newly discovered target molecules: this knowledge may not be readily available. It is almost always true that a successful immobilization/retention strategy can be developed and in some cases the immobilized form is much closer to *in vivo* conditions than true homogeneous assays (consider membrane-bound receptors for example).

The FAC method offers the opportunity to measure binding events in an environment of undistorted equilibrium, which is a strength but also an analytical challenge. There is no inherent purification or enrichment, and as a result the chosen detector must meet some stringent performance requirements. Systems have used simple UV-based flow cell detectors, which is entirely appropriate for very simple single-compound analyses. The FAC-FD system of Hirabayashi incorporates fluorescence detection of labelled marker ligands, as a sensitive and selective means of quantifying an interaction and is particularly useful in higher screening-rate single-compound analyses, where the fluorescently labelled ligand is used competitively [14]. Both approaches preserve the essence of the FAC advantage (accurate/precise measurements, access to a wide range of binding strengths), but both need a high degree of purity in the samples to be analyzed. This is required for most plate-based or biosensor-based assay systems, and does not provide significant justification for developing a FAC assay, aside from validating the results of other methods or exploring very weak interactions.



## 6.2

### Enabling FAC with MS Detection

This detection limitation prompted the development of a FAC-MS method, which significantly expands the scope of the method to complex mixtures of compounds. An MS approach removes the requirement for labelling compounds to enhance a fluorescent signal and minimizes the need to pre-purify the samples to be analyzed. Monitoring numerous compounds via their respective  $m/z$  values enables the determination of individual breakthrough curves from mixtures and offers powerful insights into multi-ligand behavior. At the simplest level, this combination of technologies (FAC, MS) provides the opportunity to rank-order binding strength in a single experiment, immediately placing the discovery of new ligands in a relational context. However, the opportunity to monitor multiple breakthrough curves without ligand labelling presents additional advantages. To illustrate, we will consider two different classes of methods: direct and indirect.

#### 6.2.1

##### Direct FAC-MS Methods for Compound Binding Data

The direct FAC-MS method is characterized by an online coupling of mass spectrometry with the FAC cartridge [7]. This is usually enabled with electrospray as an ionization method especially when monitoring drug-like molecules, although MALDI has also proven useful [15, 16]. MS detection might seem less significant when making binding measurements on single ligands; however it is very important when making these measurements that the void volume be accurately determined. This can be approximated by co-infusing one or more compounds that are not expected to bind to the stationary phase. For example, our laboratory uses a collection of peptides, oligosaccharides or low concentration buffer components (e.g. nonbuffering Tris concentration) to make  $V_0$  measurements, and therefore MS detection is essential. Guiochon has demonstrated that weaker ligands are particularly prone to inaccuracies in the estimation of  $V_0$ . MS detection enables a more accurate assessment of  $V_0$  through multiple sampling.

One of the most useful adaptations of the direct FAC-MS method for quantitating a binding event is referred to as the *staircase method* (Fig. 6.5). In this method, successively higher concentrations of test ligand are infused and the breakthrough volumes induced by the concentration increments are determined [9, 10]. As with all thorough studies of a binding event, these measurements are best conducted over a wide concentration range so that the binding isotherm is adequately sampled. This staircase method avoids long washing steps between injections; such long washes can be problematic for affinity columns that have a short lifetime. The concentration-series data can be linearized very simply according to Eq. (2) [10]:

$$[A]_{0,j} + y_j = B_t \left( \frac{1}{V_j - V_0} \right) - K_d \quad (2)$$

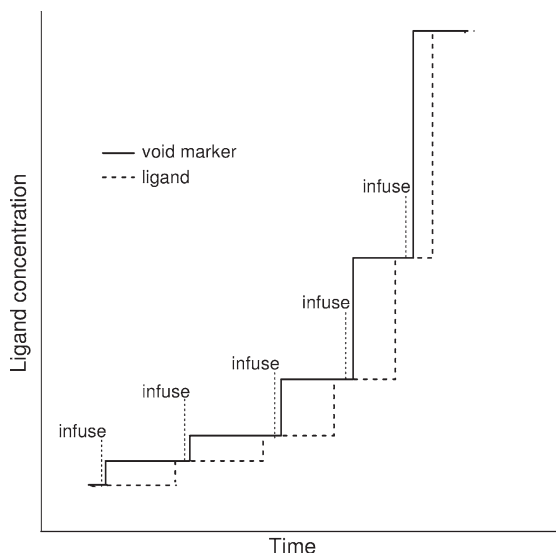


**Fig. 6.5** A diagram of the modified staircase approach. In this procedure, ligand and void marker are infused at increasingly higher concentrations. It differs from the normal procedure in that column washing between infusions is not performed. This is the simplest of FAC techniques for measuring ligand  $K_d$ .

where:

$$y_j = \frac{\sum_{i=1}^{j-1} ([A]_{0,i} - [A]_{0,i-1})(V_i - V_0)}{V_j - V_0}$$

A plot of  $[A]_0 + y$  versus reciprocal breakthrough volume supports the determination of  $B_t$  and  $K_d$  by linear regression analysis. As with all FAC methods for ligand characterization, the cartridge does not require precalibration before a measurement is made, because  $B_t$  is a product of the measurement. One disadvantage of this method is that any error in the earlier measurements is carried forward in subsequent ones; however the speed of these measurements and the ability to accurately measure  $V_0$  usually makes this the method of choice.

These sorts of analyses are limited only by the ability of the chosen mass spectrometer to detect the test-compound under infusion–buffer conditions. In many cases, there will not be a problem even at low nanomolar compound concentrations, but in others MS will be hard-pressed to detect compounds even at micromolar concentrations. The online FAC-MS system will always be challenged by the inherent incompatibility of routine assay buffers with MS, but there are opportunities to reconfigure either the ion source or the buffer composition for

the demands of the analysis. For example, detection of steroids may benefit from an APCI source over electrospray, whereas a MALDI source may have greater tolerance for higher ionic strength buffers. A powerful alternative involves the insertion of a FAIMS (high field *asymmetric waveform ion mobility* spectrometry) device [17] after electrospray ionization. We have shown that compounds buffered in full-strength PBS (~150 mM NaCl) can be successfully detected in an online FAC-MS experiment, whereas a simple selected ion reaction monitoring of the compound was unsuccessful (data not shown). In our experience, sub-micromolar to low millimolar  $K_d$  values can be successfully characterized with the on-line method under a wide range of buffer conditions. Every increment in MS sensitivity further extends the  $K_d$  range over which the direct method can function.

### 6.2.2

#### Direct Method for Discovering and Ranking Multiple Ligands

The above discussion presents the utility of the FAC-MS method as a supportive tool for higher-throughput discovery initiatives, in which hits might well be carried forward after their binding parameters are carefully re-measured and validated, and related to the data from the other hits. When incorporating MS detection, this evaluation may be done all at once. It is easy to see how a single ligand can be detected in a large pool of nonligands, but what if there exists a competitive multi-ligand environment?

Let us first consider the nature of the breakthrough curves when multiple ligands are present, and do so through the presentation of an example. Figure 6.6 shows the breakthrough curves for three isobaric compounds ( $m/z$  359) and a void marker, generated in a sorbitol dehydrogenase FAC assay. Two different MS/MS transitions were monitored, to resolve the individual breakthrough curves for the three ligands. What is immediately obvious from this example is that the breakthrough curves deviate from simple sigmoidal shapes. Most biomolecular interactions are modeled with a nonlinear binding isotherm reflective of saturable binding events, thus one ligand can actively compete with another [18]. When this is established in flowing system as encountered in a FAC assay, ligand displacement occurs in a predictable fashion, assuming equilibrium conditions. This produces a displacement of the weaker ligand(s) and represents the only condition under which *ligand enrichment* can occur in a constant-infusion system.

The shape of this displacement feature is dictated by the kinetics of binding and the overall efficiency of the cartridge. Notice that the first breakthrough (359  $\rightarrow$  162 transition) is peak-like in nature, while the second breakthrough (359  $\rightarrow$  188 transition) appears as a regular sigmoidal curve. The third breakthrough (359  $\rightarrow$  162 transition) is also a sigmoid curve. So in this example, while it is not clear which stereoisomer is the strongest or weakest, it is clear that the *positional* isomer is intermediate in binding strength between two stereoisomers. This indicates that stereochemistry is significant for this interaction, and most likely that a common binding site is accessed. Under ideal, infinitely fast condi-

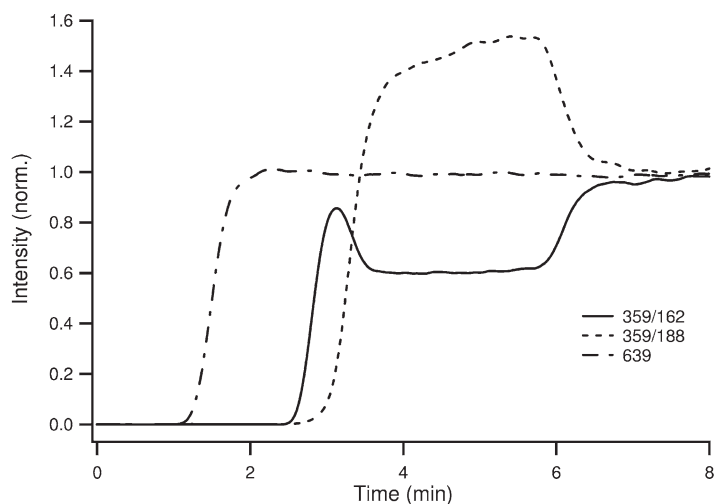


**Fig. 6.6** Demonstration of the displacement phenomenon that occurs when FAC experiments are conducted in the nonlinear region of the binding isotherm. Three isobaric ligands ( $m/z$  359) are infused at micromolar concentration through a sorbitol dehydro-

genase FAC assay, as monitored by a triple quadrupole mass spectrometer in MRM mode. The solid trace represents two stereoisomers and the dashed trace a positional isomer. The dot-dash trace represents a nonbinding void marker ( $m/z$  639).

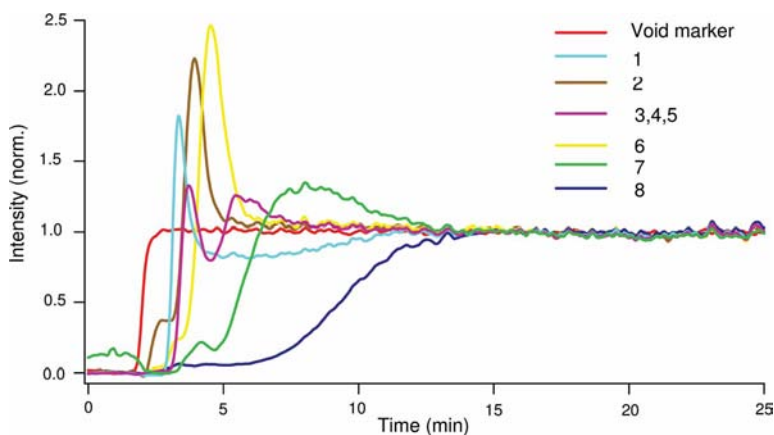


**Fig. 6.7** A FAC-MS experiment for ligand ranking. Eight ligands for sorbitol dehydrogenase were infused, spanning a  $K_d$  range of 2  $\mu$ M to 8 nM [10]. All ligands were applied at 1  $\mu$ M concentration, ensuring operation in the nonlinear region of the binding isotherm. Adapted with permission from Elsevier.

**Table 6.1** The order of breakthrough for the example of Fig. 6.7 closely parallels the IC<sub>50</sub> values from independent determinations using plate-based activity assays [10]. K<sub>d</sub> values were measured for the strongest and weakest ligands in separate FAC-MS experiments.

Compound	FAC-MS RANK ORDER	IC <sub>50</sub> (nM)	K <sub>d</sub> (nM)
1	Weakest	3300	2200.0
2		340	nd
3		660	nd
4		270	nd
5		39	nd
6		<10 (K <sub>i</sub> )>	nd
7		86	nd
8	Strongest	41	8

tions of mass transfer, all displacements or breakthroughs would be rectangular in shape. Under real-world conditions where ligand-binding kinetics dominate, the resulting finite mass transfer rates serve to “smooth” these features into peaks and sigmoids [8].<sup>1</sup>

FAC has a remarkable capacity to resolve/rank-order ligands even under fully saturating levels of compound. The example in Fig. 6.7 shows the evolution of multiple-ligand breakthroughs under conditions where the cartridge saturation is over 99.9%. A mixture of eight ligands generates a rank order as determined by measurement of breakthrough volumes, which follows the general trend of IC<sub>50</sub> values (3.3 μM to 39 nM; Table 6.1).

Note that the mixture contains the three isobaric ligands discussed above, and even under these saturating conditions, the method can resolve three orders of magnitude K<sub>d</sub> values. A multi-ligand, equilibrated environment supports the K<sub>d</sub> measurement of both the strongest and the weakest ligand, which provides the opportunity to “bracket” the rank order with accurate dissociation constants [19]. In theory, the ligands with intermediate binding strength could also be quantitated, requiring knowledge of ligand concentration and a measurement of rollup amplitude [11]. This may be possible in certain applications (e.g. screening of mixtures constructed from single compound stock solutions) but, in more challenging screenings as encountered using natural product extracts or crude mixture syntheses, a bracketed rank order is the best that can be achieved.

Deng and Sanyal have suggested that FAC is not applicable to ligands with low on- and off-rates [20]. As will be shown below, this is not true particularly when indirect FAC methods are applied, but it is also misleading in direct assays as described in this section. With flow-rate programming, for example, slow kinetics

1) These displacements (or “roll-ups”) can only occur if there is competition for a common binding site, or a strongly-negative

allosteric linkage between two distal sites, with the further requirement that the allosteric effector have a lower K<sub>d</sub>.

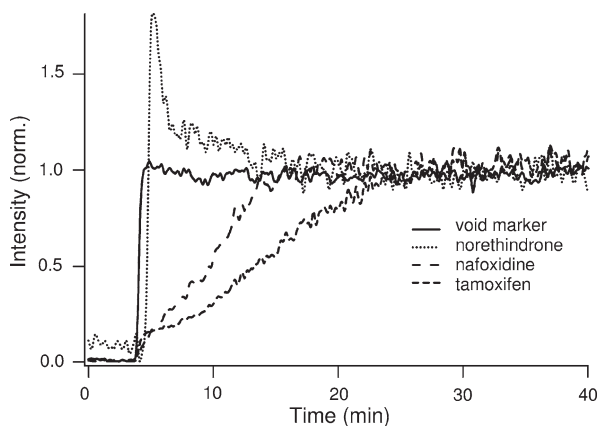


**Fig. 6.8** Breakthrough curves for ligands infused through an estrogen receptor  $\beta$  FAC assay. Slow tight-binding ligands (nafoxidine and tamoxifen) exhibit diffuse breakthrough curves, while ligands with rapid kinetics exhibit sharper curves (norethindrone). Dehydroisoandrosterone, a ligand intermediate between norethindrone and nafoxidine, was undetected in this experiment.

need not be limiting. Nevertheless it is true that any flowing system must consider the impact of mass transfer rates on the quality of the data. As an example, consider Fig. 6.8. Here, we screened a mixture of  $\sim 100$  compounds in an estrogen receptor  $\beta$  FAC assay. The two stronger ligands (nafoxidine and tamoxifen) are known to possess extremely slow off-rates yet the FAC method not only detects these as ligands, it also correctly estimates their ranking. Under the temporal conditions of this experiment, neither nafoxidine nor tamoxifen rapidly establish equilibrium on the FAC cartridge. In this situation, ligands with slower on-rates will elute ahead of those with faster on-rates. Notice also the severely extended breakthrough curves for both ligands, indicative of slow on-rates [9]. So rather than an inherent limitation, the FAC-MS method is useful for detecting slow kinetics in much the same way as optical biosensors. Admittedly, theoretical treatments of breakthrough curves for on- and off-rate measurements have not yet received wide application to biomolecular interaction data from FAC. It is also true that, if on-rates are very low ( $<100 \text{ M}^{-1} \text{ s}^{-1}$ ), the direct FAC method may miss them. But for the simple purpose of ligand discovery, we suggest that FAC cartridges be operated at low linear flow rates without concern that slow/tight-binding ligands may be missed (this will be revisited in the next section). Notice that the FAC data in this example only shows breakthrough curves for three of the four expected ligands. Dehydroisoandrosterone is undetectable at the concentrations chosen, but the weakest of the four ligands (norethindrone) has been displaced – clearly indicating the presence of another ligand and indicating the utility of the displacement as a useful check for completeness of the analysis.

Mass spectrometry enables the type of direct analyses described, but it does have its limitations. Online operation forces detection at infusion concentrations, in salty buffer and under complex mixture conditions. General ion suppression results from the buffer and mixture components, and mixture complexity can tax the resolution of even the best mass spectrometers. Increasing compound concentration is not the answer, as this leads to problems of solubility and increased compound consumption. We have found that the online method can work successfully for up to 100 compounds per analysis, but the false negative rate becomes appreciable [21]. As an alternative for ligand discovery purposes, we have developed a FAC-LC/MS system in which FAC effluent is sampled and analyzed by LC/MS [19]. This system offers the ability to concentrate mixture components and introduces another dimension to the data in order to tolerate more complex mixtures (Fig. 6.9). Using this system, we have screened approximately 1000 modified trisaccharide acceptor analogs targeting immobilized N-

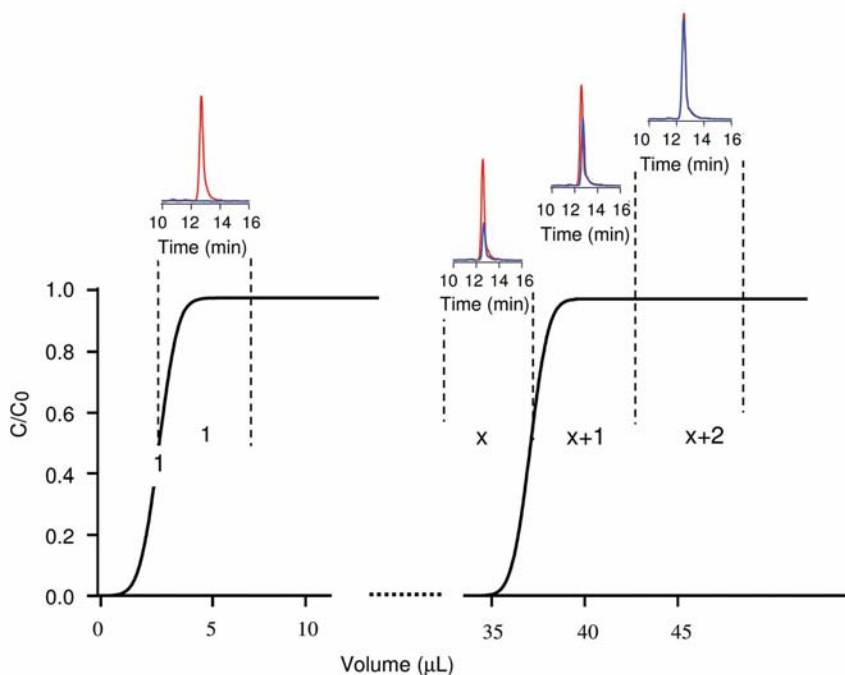


**Fig. 6.9** Schematic of FAC effluent sampling strategy for insertion of an LC/MS step to increase ruggedness of the discovery mode of analysis, as applied to high throughput screening for ligands to GnT-V [19]. The insets represent LC/MS data for a strong ligand for four fractions of FAC effluent (1, x, x + 1, x + 2). Blue traces represent the

extracted ion chromatogram of the compound eluted from the GnT-V column, and red indicates the extracted ion chromatogram (XIC) from a blank column. The insets are referenced to idealized online FAC-MS chromatograms for the strong ligand. Adapted with permission from the American Chemical Society.

**Table 6.2** Summary of the hit data obtained from the GnT-V screening using the FAC-LC/MS method [19]. Hits are categorized based on an arbitrary binning strategy, where breakthrough times are converted into approximate  $K_d$  values. Adapted with permission from the American Chemical Society.

Rank order (1 – weak, to 4 – strong)	Number of Hits in Library (~1000 compounds)	Approximate $K_d$ Values ( $\mu\text{M}$ )
1	42	$\geq 3$
2	6	1.5–3
3	3	1.0–1.5
4	1	0.6

acetylglucosaminyltransferase V (GnT-V), an enzyme regulating the branching pattern of N-linked oligosaccharides on glycoproteins [22]. Increased expression of active GnT-V has been reported in mammary, hepatocellular, and pancreatic cancer [23, 24] and it has been suggested that inhibition of GnT-V could represent a useful treatment for cancer [25]. With an LC/MS system incorporating hydrophilic interaction chromatography (HILIC) for oligosaccharide separation, we have discovered four quality ligands (with  $K_d$ s in the 0.6–1.5  $\mu\text{M}$  range, measured in separate FAC-MS experiments), from a large mixture possessing an overall hit rate of approximately 5% (Table 6.2).

Fractionating the FAC effluent for LC/MS processing reduces resolution in hit determination, as the breakthrough volumes for each hit can only be estimated, however coarse fractionation will suffice for screening purposes. The insertion of an LC step avoids a dependency on MS-compatible assay buffers and provides an increase in sensitivity along with the ability to detect lower concentrations of ligand; this is important when screening large mixtures as high total library concentrations can induce compound precipitation. Based on this work, screening rates exceeding 5000 compounds  $\text{day}^{-1}$  are easily achieved with a simple LC/MS system, at compound concentrations 10- to 100-fold less than the online method. With automation and more highly resolving LC/MS systems, these screening rates could easily exceed 50 000 compounds  $\text{day}^{-1}$ , assuming mixtures of approximately 5000 compounds each.

There are really only two situations in modern drug discovery where this sort of capacity for high-volume mixture screening may be needed. First, natural product extracts can be screened to detect low-abundance compounds present in the complex matrix of nonligand species. Some interesting work has been published in this area [26], and will be described below. Second, split-pool synthetic combinatorial libraries can be quickly surveyed, possibly as a method for surveying chemical space prior to launching an expanded parallel-chemistry effort for library creation. Blending pre-existing collections of individual compounds is possible in



order to take advantage of the efficiency of the screening method, however these benefits may be eroded due to the effort in reformatting compound collections at time of use. Given the pre-existing investment in large-scale screening systems, the niche for FAC-MS in a screening laboratory is likely *before* and *after* the main screening exercise – during library development, and hit evaluation or secondary screening.

### 6.2.3

#### Indirect Methods

There are alternative modes of FAC-MS operation that are useful in HTS, secondary screening, and lead development. These modes are designed around monitoring the impact of a ligand (or mixture of ligands) on the breakthrough volume of a *pre-selected* ligand, which we refer to as an *indicator*. In a typical experiment, the protein stationary phase is equilibrated with the test ligand by adding it to the running buffer. After an infusion period suitable to ensure equilibrium, the *indicator* ligand is injected. An accelerated breakthrough for the indicator ligand is observed, to a degree determined by the concentration of the test ligand [10]. The data resulting from these experiments can be linearized according to Eq. (3), where the ligands  $A_1$  (with  $K_{d,1}$ ) and  $A_2$  (with  $K_{d,2}$ ) represent the indicator and test ligand, respectively.

$$\frac{1}{1 - \frac{(V - V_0)_i}{(V - V_0)_0}} = 1 + \frac{K_{d,2}}{[A_2]_i} \left( 1 + \frac{[A_1]_0}{K_{d,1}} \right) \quad (3)$$

The indexing of 0 to  $i$  refers to infusions of ligand  $A_2$  at progressively higher concentrations, with the corresponding indicator measurements of  $V - V_0$ . Appropriate indicator ligands are relatively weak ( $K_d$ s  $> 10 \mu\text{M}$ ), allowing for infusion under linear isotherm conditions and rapid indicator kinetics. In this way Eq. (4) applies, and the indicator ligand simply functions as tool to measure the reduction in column capacity due to the test ligand (hence the term “indicator” and not “competitive” ligand). Under these conditions, the term within large brackets in Eq. (3) disappears and the most accurate data is generated.

$$(V - V_0) = \frac{B_i}{K_d} \quad (4)$$

We have used this approach in the FAC-MS analysis of a number of challenging receptor–ligand systems [10]; overcoming nonspecific binding effects and slow on-rates is a particular strength of this method. As discussed in the previous section, nafoxidine (an estrogen antagonist used in the treatment of breast cancer) is a slow-tight binder targeting the ligand binding domain of estrogen receptor- $\beta$  [27]. By using a weak-binding steroid as an indicator ligand, the equilibrium  $K_d$  value was measured to be 23 nM, comparable with other methods. We find this

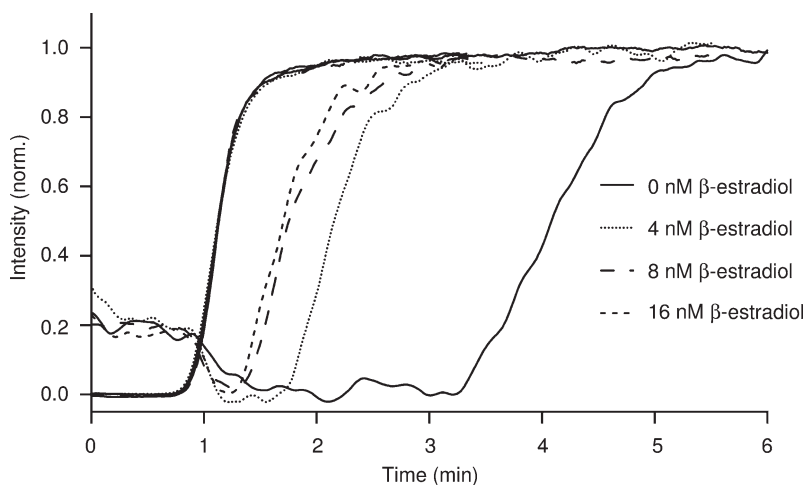


**Fig. 6.10** Breakthrough behavior for a weak indicator ligand (norethindrone) in the presence of an increasing concentration of the strong ligand  $\beta$ -estradiol [10]. These ligands access the ligand-binding domain of estrogen receptor  $\beta$ . Displayed is an overlay of four chromatograms showing breakthrough curves of norethindrone after

successive equilibrations with  $\beta$ -estradiol. Corresponding void marker traces at each concentration of  $\beta$ -estradiol are also shown (overlaid at a breakthrough time of  $\sim 1$  min). A  $K_d$  of 1.3 nM was determined by this method. Adapted with permission from Elsevier.

method to be extremely useful for  $K_d$  measurements of single ligands in general: weak ligands are easy to obtain for most biomolecular interactions and they usually present rapid kinetics. For our FAC-MS work, we typically select indicators in the range of  $10\ \mu\text{M}$  to  $1\ \text{mM}$   $K_d$ , and apply them at low micromolar concentrations. However, the  $K_d$  of the indicator ligand can be much lower than  $10\ \mu\text{M}$ , as long as equilibrium conditions can be met.

These analyses are rapid, usually limited by the incubation time for the test compound on the cartridge. Figure 6.10 shows the breakthrough curves for an indicator analysis of  $\beta$ -estradiol, demonstrating that each “probe” of binding capacity with the indicator can be achieved in approximately five minutes. Full equilibration with low concentration, high-affinity test ligands can require large volumes, however. For example, the  $4\ \text{nM}$  estradiol infusion concentration was applied at  $50\ \mu\text{L min}^{-1}$  for 100 min (5 mL). This is unavoidable, as full cartridge equilibration is required. A lower-capacity cartridge can always be implemented if this is an issue, as the equilibration volume is directly proportional to column capacity.

The displacement-based rollup feature described above can also be used to detect test–ligand binding. Under equilibrium conditions, integrating the rollup provides a means of measuring the  $K_d$  of the stronger ligand, but this is a less reliable method than that described above; resistance to mass transfer makes the rollup hard to quantitate with accuracy, especially under low occupancy condi-

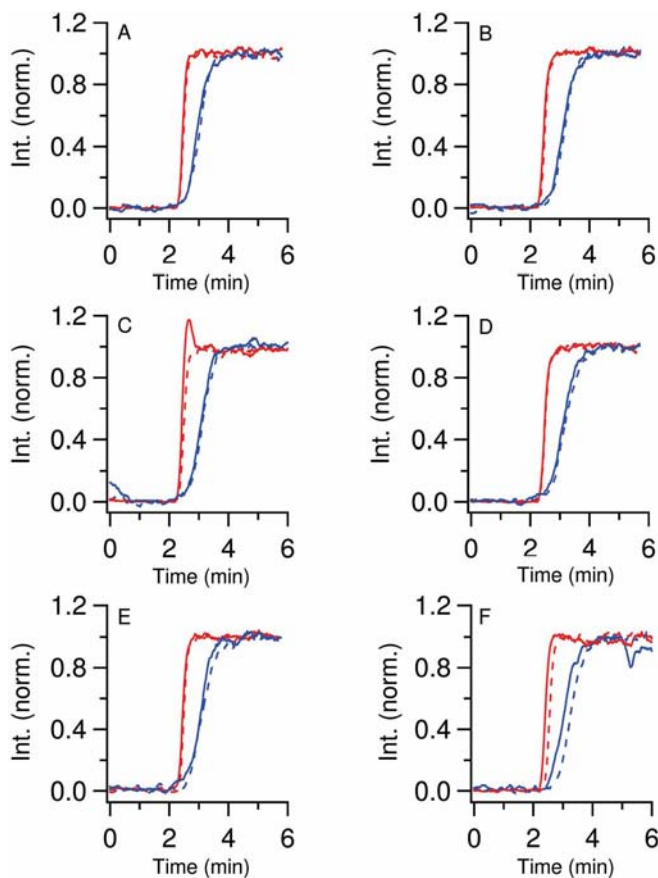


**Fig. 6.11** Using rollups to efficiently pre-screen mixtures for the presence of “hits”. In this example, six mixtures of approximately 90 compounds each (A–E) were screened in a dual protein FAC assay ( $\beta$ -galactosidase, GS1B4). The dashed red and blue curves in each chromatogram represent the breakthroughs of the  $\beta$ -galactosidase and GS1B4 indicators, respectively, in the absence of the

mixtures. The solid red and blue curves in each chromatogram represent the breakthroughs of the  $\beta$ -galactosidase and GS1B4 indicators, respectively, in the presence of the mixtures. In this example, mixture C was quickly determined to be the only mixture with a hit against one of the proteins ( $\beta$ -galactosidase). Adapted with permission from Elsevier.

tions ( $[\text{ligand}] < K_d$ ). It is far more useful as a quick test for the presence of stronger ligands in a mixture. Figure 6.11 illustrates that this mode of indicator analysis can readily pinpoint mixtures containing hits of greater affinity than the indicator, and opens the door to multiplexed “pre-screening”, where mixtures can be interrogated against multiple proteins in one experiment [10]. This mode of analysis works best when the indicator is present at a concentration equivalent to its  $K_d$  value. The example in Fig. 6.11 involves screening mixtures of approxi-

mately 90 compounds from the Optiverse (Tripos) library against a dual-target column containing immobilized  $\beta$ -galactosidase and GSIB4<sup>2</sup>. Monitoring only the indicators allows a quick survey to determine which mixture should proceed to deconvolution, offering a rapid means to reduce the screening burden. In this example, a rollup in mixture three indicates the presence of a ligand for  $\beta$ -galactosidase stronger than the indicator.

This mode successfully avoids false positives arising from mixtures containing many weak ligands – a classic problem when conducting mixture screening. Again, a method such as this would find its ideal application in the screening of single-pot syntheses and/or natural product extracts where deconvolution is particularly time-consuming. Note that in these pre-screening applications, a fluorescently labelled indicator ligand may offer a simpler instrumental solution, although multiplexing the analysis would require differential, multi-color labelling.

### 6.3

#### System Advancements – Fluidics, Immobilization, Detection

The methods described above establishes FAC as an alternative means of generating reliable binding data, and it is most comparable to optical biosensor technology in its performance, requirements and benefits. The marriage with mass spectrometry enables the characterization of complex mixtures (an advantage over biosensors), but most descriptions of FAC with or without MS detection have simply used fluidic systems and columns not ideally suited to the FAC experiment. This section considers some of the issues confronting FAC, recent progress in system design and data analysis, and some selected new applications that further widen the opportunities of FAC.

#### 6.3.1

##### Column

A quality FAC assay presents certain column design constraints. Most researchers' experience with affinity chromatography involves the use of gravity-fed sample flows through large-bore column beds constructed of loosely packed agarose-based particulate supports. Large excess column capacities are usually designed into such systems, specifically to maximize the capture of a ligand, and little attention is paid to the surface area occupied by the capture molecule. The first objective in designing a new FAC assay, in contrast, is to optimize the amount of

2)  $\beta$ -Galactosidase recognizes  $\beta$ -Gal compounds, whereas the lectin GSIB4 selectively recognizes  $\alpha$ -Gal compounds. All six mixtures were doped with low-micromolar concentrations of the respective indicators (1S,4S isomer of 4-hydroxy-2,2-

dimethyl-cyclopent-1-yl 1-thio- $\beta$ -D-galactopyranoside as a known binder for  $\beta$ -galactosidase [15] and 4-phenyl-2-butanone-4-thio- $\alpha$ -D-galactopyranoside [racemate] as a binder for GSIB4).

immobilized capture molecule per unit column volume. In most situations, this should be as high as possible without introducing unwanted interactions between adsorbed molecules due to molecular crowding. This serves to minimize nonspecific binding. Current commercially available microparticulate solid phase supports have not been developed with this in mind, as opposed to chip surfaces in SPR. In a FAC experiment, any retention mechanism in the system will directly contribute to the measured breakthrough volume. In the worst case, nonspecific binding can completely override specific associations and, while we have shown that indirect methods can overcome this limitation, this does erode the utility of mixture screening. These are not new problems, as assay developers have long struggled with nonspecific associations. In our laboratory, we prefer to use passivated silica where possible. Passivation usually involves bonded hydroxyl coatings (glycerol or polyvinyl alcohol) as well as physisorbed protein, the goal being the masking of inevitable “hot-spots” in most particulate materials. Nonspecific binding is impossible to “solve” but stationary phases can be adapted to the analysis based on the class of molecules targeted. For example, we have found that oligosaccharide-based compounds can be successfully analyzed through cartridges constructed from beaded, polyol-coated polystyrene–divinylbenzene, whereas neutral heterocyclic organic compounds respond better to silica-based supports. Ultimately, the requirements for preserving protein activity usually dictates the freedom of design; for example immobilization of the enzyme GnT-V on silica led to its rapid inactivation, whereas immobilization on a polymeric support actually increased the stability of the enzyme compared to the enzyme in solution [19].

Some degree of nonspecific binding can be tolerated in FAC. In most situations nonspecific binding is characterized by weak retention mechanisms, which means that the contribution of such binding to the measured breakthrough volume is independent of ligand concentration and easily corrected in a concentration-series experiment. For discovery-based applications where large mixtures are processed, operating at maximal mixture dilution ensures that breakthrough volumes are dominated by the specific interaction [19].

In any case, high densities of capture molecule ensure that unwanted nonspecific binding sites are minimized and that the breakthrough curves can be interpreted from the standpoint of the specific interaction. If high densities are achieved, this presents an interesting design problem: the amount of stationary phase required for a FAC column is exceedingly small, on the order of 100 nL or less for a cartridge presenting 1–5 pmol of protein (assuming a 100-nm pore diameter material as a model). Most commercially available porous affinity supports are based on large beads ( $>30\text{ }\mu\text{m}$ ) that cannot be packed into small capillary cartridges of 100  $\mu\text{m}$  inner diameter or less. A larger system can be designed and used successfully in FAC experiments, but this is wasteful of sample. Most recently, we have implemented nonporous 5  $\mu\text{m}$  spheres for FAC, which are easier to pack into small cartridges. These nonporous supports present a reduced surface area over the porous ones ( $>$  a factor of ten) and their only drawback is that they present a larger pressure drop over the cartridge length, but this is man-

ageable with newer fluidic systems we have designed. The excellent diffusion characteristics of these nonporous particles are an added advantage. While it is true that accurate breakthrough curve measurements can be made with low efficiency columns [11], sharper breakthrough curves support greater precision in multi-ligand mixture analysis and will be essential for measuring a wide range of rate constants.

Recent developments in the Brennan laboratory offer exciting possibilities for streamlining the generation of FAC columns. This laboratory has adapted *in situ* sol–gel technology for the capture of proteins directly from solution. Briefly, silica sols are prepared from diglycerylsilane and (3-aminopropyl)triethoxysilane with various additives to preserve protein function, in the presence of protein. In one example, dihydrofolate reductase (DHFR) was added in a “single-pot” sol–gel preparation and cast within fused silica capillaries [28]. The resulting monolithic column was successful in trapping DHFR within mesopores and preserving the activity of approximately 25% of this protein. The monolith could sustain pressure-driven flow and appears to support sufficiently rapid mass transfer (Figs. 6.12, 6.13). The issues with column reusability were attributed to a nonoptimum buffer rather than an inherent limitation of the entrapment procedure. This sol–gel procedure is an elaboration on well established entrapment methods [29], but with the added advantage of stability and better flow properties. Interestingly, none of the examples presented thus far demonstrate competitive behavior between multiple ligands (i.e. displacement); in the FAC analysis of trimethoprim and pyrimethamine a reversed order of elution based on  $K_d$  is described, but this could simply be due to the shift towards an on-rate limited situation for higher affinity compounds, as described earlier. Erosion of dynamic competition between ligands could occur if the sol–gel allows convective mixing of the entrapped protein; however the bimodal pore structure of these materials would

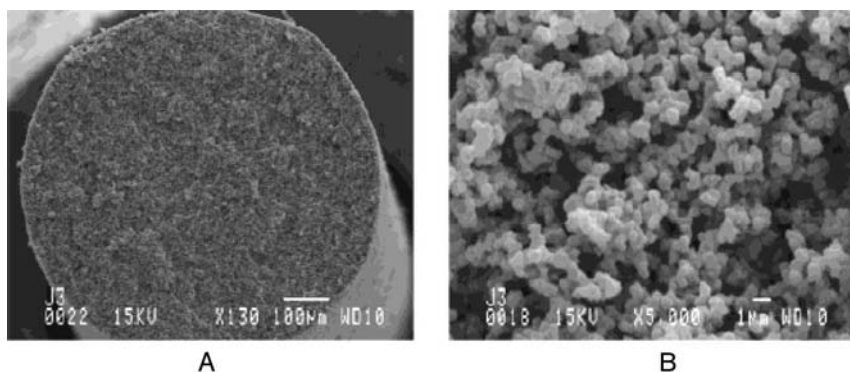


**Fig. 6.12** Scanning electron microscopy images of a sol-gel derived column material (A) a rigid rod and (B) a magnification of the bimodal pore structure in the resulting monolithic material [28]. Adapted with permission from the American Chemical Society.

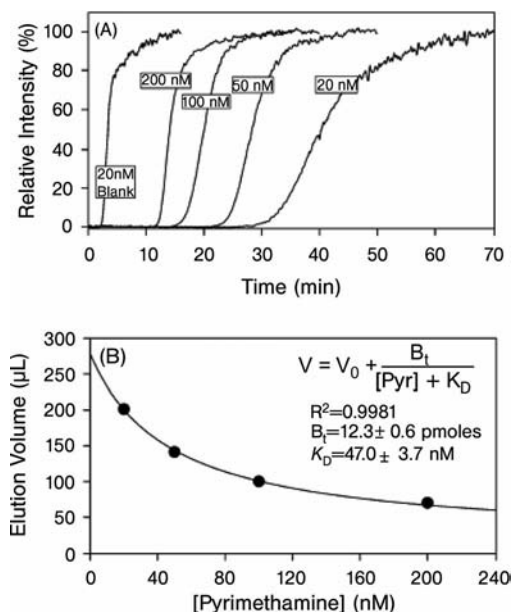


**Fig. 6.13** Measurement of FAC data for a range of pyrimethamine concentrations applied to sol-gel-entrapped dehydrofolate reductase: (A) overlay of breakthrough curves and (B) nonlinear regression analysis of the fit to the measured breakthrough volumes from A [28]. Adapted with permission from the American Chemical Society.

suggest the constructs closely approximate immobilized systems. In any case, the sol-gel preparation is a powerful addition to conventional immobilization strategies and will serve to further shorten assay development times as well as broaden the class of proteins that can be screened by the technique. An obvious disadvantage to the entrapment method is that interaction analysis is only possible between molecular species that are widely different in hydrodynamic radius, a similar restriction experienced by screening systems based on size exclusion chromatography.

As the only requirement for conducting basic FAC experiments is the immobilization or entrapment of the target molecule in a construct that supports forced flow, many strategies for immobilization can be considered. The Wainer lab has successfully used immobilized artificial membranes as a method to retain membrane associated species and demonstrated that multiple receptors from rat brain homogenates could be successfully probed. Earlier work by Lundahl described the entrapment of liposomes and even whole cells [29]; all of these entrapment constructs can be tolerated in FAC experiments provided that forced flow does not generate excessive pressure drops across the column, potentially leading to phase collapse. In this regard, the sol-gel method shows the greatest promise

of all the entrapment methods for sustaining high efficiency FAC driven by high pressure flows, but full immobilization would be required for the highest efficiency.

From this discussion, there is an obvious advantage to FAC in that the assay development approach is extremely flexible and adaptable to the requirements of the interaction to be studied. It is worth mentioning that the effort placed on creating a FAC cartridge is never wasted – it can be used as a simple capture/elute tool for alternative screening approaches, and even in preclinical studies that require methods for monitoring drug candidates and their active metabolites [30].

### 6.3.2

#### System

One of the benefits of FAC is the simplicity of the fluidic system; all that is required is to continuously infuse the solution of ligand(s) through a packed bed. Inspection of most breakthrough curves might suggest that the analyses reflect “poor” chromatography, because breakthrough curves can appear extremely diffuse. As was discussed, this is usually due to the actual binding event, but such curves can mask poor column performance as well. To capitalize on the strength of FAC for generating accurate binding data, proper attention should be paid to the fluidic system. Early systems used simple syringe pumps or conventional HPLC systems for higher flow rates. As the columns continue to diminish in capacity, neither system is appropriate as stable low flow is difficult to achieve. Syringe pumps in particular should not be used for obtaining binding data, as flow rate variations can be as high as  $\pm 20\%$  at low  $\mu\text{L min}^{-1}$  flow rates.

We have designed new pumps based on a 250  $\mu\text{L}$  positive displacement pump, an integrated electronic inlet/outlet valve, and an inline flow sensor. The pump operates at nano- to micro-flow rates using feedback from the inline flow sensor. During operation, the feedback signal is used to dynamically clamp the output flow to a desired value, in this way achieving flow-rate stability of better than 1% even below 100  $\text{nl min}^{-1}$  [19]. These nanofluidic modules are capable of operating at 5000 psi, suitable to drive our FAC cartridges incorporating 5  $\mu\text{m}$  nonporous particles. Because they dynamically respond to preserve constant flow rates, they are particularly well suited to conventional injection systems, where sample is loaded through a “superloop”; upon injection, the loop pressure is rapidly equilibrated to the system pressure and stable flow rates are generated. This allows us to make measurements of binding data with CVs of 2% or better [19].

Inclusion of a second pump for effluent dilution and transfer supports both online and offline MS analysis. As shown above, fraction collection followed by LC/MS analysis significantly expands the performance characteristics of the FAC method, but the effluent can also be sampled for MALDI-based analysis. Advantages to this method include greater salt tolerance over the electrospray approach, extension to complex mixtures of protein and archiving of the run. MALDI is generally considered to possess higher peak capacity than electrospray (at least



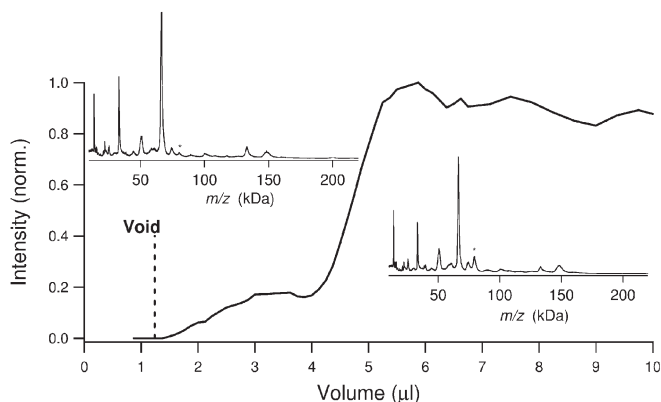


**Fig. 6.14** Infusion of dilute human serum through a transferrin-binding protein B (TbpB) FAC assay. Insets demonstrate MALDI-TOF spectra acquired before (2 min) and after (7 min) the principal breakthrough curve for transferrin, shown as a solid black trace representing  $m/z \sim 80\,000$ . The asterisk denotes the  $m/z$  of human transferrin [15].

for peptides and proteins). Neither ionization method when applied to the unfractionated effluent is expected to have the peak capacity of the LC/MS approach, but with the MALDI method the effluent can be sampled more extensively, making it an excellent choice of less complex mixtures. We demonstrated the utility of FAC-MALDI/MS in the detection of transferrin binding to transferrin-binding protein B (TbpB) subunit, a peripheral outer membrane lipoprotein from bacteria essential for iron uptake direct from human serum [15] (e.g. *Neisseriaceae* spp). In this experiment, a soluble form of TbpB was expressed with a recombinantly introduced biotin tag, in place of the lipid anchor. This construct was immobilized on 5  $\mu\text{m}$  nonporous streptavidin beads; approximately 1.7 pmol of active TbpB was bound. Dilute human serum was infused through the column and the effluent spotted on a MALDI plate in 15 s intervals. The breakthrough curve for transferrin could be readily detected by MALDI (Fig. 6.14). The double-plateau nature of the breakthrough likely reflects weakly bound apotransferrin, followed by the more strongly retained iron-loaded form. We have also shown that this effluent can be sampled for proteomics analysis and protein discovery, where fractions are digested with trypsin and the resulting peptides compared against each other using LC-MS/MS datasets. This should be an attractive alternative to conventional pathway discovery which uses bead-based pulldowns and washes. FAC supports the discovery of weaker or transient interactions, which most often go undetected in conventional pulldowns. A drawback to the approach is that each fraction may require laborious 2D-LC-MS/MS analysis to array the contents of the fractions.

More recently, Brennan has shown that FAC-MALDI-MS can be used to screen small molecules, relying upon MRM transitions to overcome the chemical noise generated by the matrix [16]. This is an acceptable approach for known compounds, but for ligand discovery from uncharacterized mixtures, ion selection

will be difficult. More appropriate may be the DIOS (desorption/ionization on silica) surfaces that support matrix-free desorption of small molecules.

### 6.3.3

#### Breakthrough Curve Detection and Data Analysis

Whatever the application, MS-based analyses of FAC effluent will always be faced with the need to support a wide range of buffer components, ranging from variable ionic strength, surfactant levels to required cofactors. In select situations such as indicator analyses, online methods may be appropriate but it is clear that the insertion of an intermediate LC step offers significantly improved performance. This changes the nature of the data analysis, from the detection of sigmoidal breakthrough curves to peak detection and differential analysis across multiple fractions.

For online applications, breakthrough volume measurements are a simple matter of determining the inflection point when such curves are symmetrical, and a first derivative analysis can be useful in determining inflection points. Frequently the breakthrough curves are asymmetric at higher ligand concentration, where the binding isotherm can be nonlinear (see Fig. 6.4, for example). In this situation, the breakthrough volume is defined as the intensity-weighted midpoint. For offline applications involving LC/MS analysis of effluent fractions breakthrough curves are detected as peaks (Fig. 6.9) from extracted ion chromatograms. Chromatographic peaks *apparent* in the control representing the unprocessed mixture but *absent* in an assay fraction indicates the presence of a hit; the quality of the hit is in turn determined by the fraction where compound breakthrough occurs. Automation of this process for large mixtures is necessary, as large volumes of data are generated. One approach involves the application of a component detection algorithm, to identify all features within an extracted ion chromatogram of significance, and then identifying differences between each feature and the control based on a user-defined tolerance (e.g. area differences > 10%). A requirement for successful ligand detection using this method is reproducibility in LC/MS, which we have shown is possible even with less-stable forms of chromatography such as HILIC [19]. We note that software developed for quantitative proteomics applications perform similar functions, and can be co-opted for use in high-throughput FAC systems.

Typically, discovery-style high-throughput experiments are single-point determinations designed solely to identify hits rather than characterize the interactions. Infusions of isolated, newly discovered ligands over a concentration series provides the opportunity to map out the binding isotherm. Most frequently a single or multi-term Langmuir equation is sufficient to describe the data for straightforward binary interactions [31]. Careful measurement of these isotherms, however, can reveal much about the nature of the binding event, and a simple Langmuir relationship need not be assumed. Affinity chromatography has been used to determine coupling constants between ligands exhibiting allosteric behavior, and FAC-MS represents an excellent method for making such measurements.

## 6.4

### Select Applications

Some newer applications of FAC-MS have been described, which suggest that the technology has a strong role to play in the drug discovery process for an extremely broad range of molecular interactions.

The method has been applied as a “global kinase binding assay”, in which both ATP and substrate binding sites could be monitored in the same experiment using indicator methods described above (Fig. 6.15) [32]. A similar FAC-MS assay was developed around the anticancer target kinase, EphB2 and the data compared to an ELISA for the same protein [33]. In this work, a series of known kinase inhibitors were interrogated by both methods using the indicator approach focusing on the ATP binding site, and the correlation between FAC and ELISA data was strong.

The method has been used as an adjunct to virtual library screening, in which a set of compounds was screened against a pharmacophoric model of the ATP

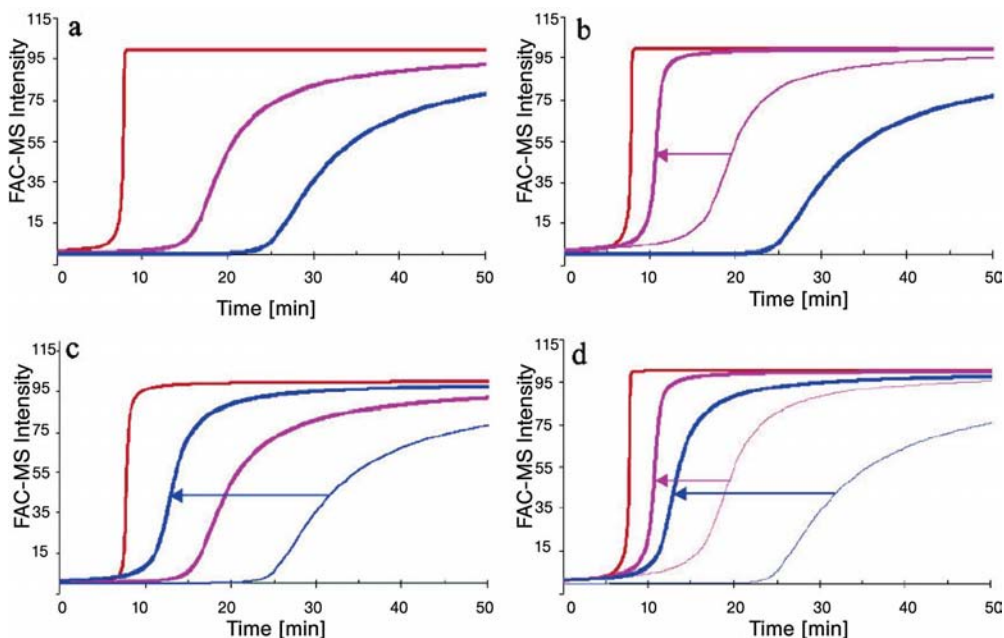


**Fig. 6.15** FAC-MS chromatograms of dual indicators for protein kinase C $\alpha$  [32]. (a) In the chromatograms, the red lines correspond to a void marker, the blue lines correspond to the substrate-site indicator chelerythrine chloride and the magenta lines correspond to the ATP-site indicator PD153035. Arrows

indicate respective shifts when screening. (b) WHI-P180, an ATP-site binder, (c) inhibitor peptide 19–36, a substrate-site binder and (d) both WHI-P180 and inhibitor peptide 19–36. Adapted with permission from the American Chemical Society.

binding site in EphB2 [34]. This serves to “weed out” compounds that do not conform to the model and thus would likely show a reduced probability of generating hits in a real screen. In this example, the authors reduced their library from an initial 50 542 unique compounds to 468, which were then acquired and screened via FAC-MS. These were then binned into mixtures of nine compounds each and screened using a simple indicator analysis. While this method only provides a bulk measurement of inhibition (i.e. does not discriminate between many weak binders and single stronger binders), the use of very small mixture sizes makes this approach feasible. Even so, it was shown that over half of the mixtures generated measurable indicator shifts, and that larger mixtures may have rendered this particular indicator method ineffective. Nevertheless, mixtures with low to moderate hit rates would benefit from this sort of prescreen [10]. Four mixtures generating the largest shifts were further investigated – individual components were screened using a single-point indicator experiment, and the results correlated well with ELISA data for the individual hits.

Nonprotein screening exercises have also been developed around the FAC method. We have demonstrated that affinity constructs can be formulated around immobilized 16S A-site rRNA, and used to screen aminoglycoside-binding to the A-site domain. An online experiment was performed, where it could be shown that neamine, lividomycin and paromomycin eluted in the expected order based on previous studies [35]. Interestingly, FAC columns constructed around immobilized RNA could not be regenerated after ligand binding, requiring that a new column be used for each experiment. With column volumes of 800 nL, this is not a difficulty as many columns can be prepared from a single batch of stationary phase.

FAC-MS has been used recently in antiviral development projects to discover two small molecule natural products inhibiting the entry of SARS-Coronavirus into Vero-E6 cells [26]. A range of Chinese herbs (121 different species) were extracted in 85% ethanol and screened via online FAC-MS (using an electrospray TOF instrument), through a column containing the SARS S2 protein. The authors estimate that ~130 compounds with  $K_{ds}$  under 10  $\mu\text{M}$  were discovered by FAC-MS, and of these hits, two molecules (luteolin and tetra-O-galloyl- $\beta$ -D-glucose) exhibited low micromolar EC50s in an infection assay using a pseudotyped virus, correlating well with their highest binding strength in the FAC assay. These two molecules exhibit an activity far superior to glycyrrhizin, another small molecule recently reported to exhibit antiSARS-CoV activity [36].

## 6.5

### Summary and Evaluation

Several years after its demonstration as a viable approach to interrogating ligand binding events in mixtures, FAC-MS systems, immobilization strategies and methods have advanced to the degree where FAC assays can be constructed around most molecular interactions relevant to the drug discovery industry. Aside

from the utility of the frontal analysis method to support sensitive, accurate  $K_d$  measurements on single ligands, perhaps the most significant opportunity for FAC in ligand discovery is through the screening of “imperfect” mixtures. Under equilibrium conditions, ligands elute in order of their binding strength regardless of their concentrations, thus determination of hit “quality” is simply by inspection. This makes the method useful for screening single-pot combinatorial synthetic mixtures, or natural product extracts where compound concentrations are nonequivalent. Most initial screening exercises do not begin with the detection of  $K_d$ s  $< 1 \mu\text{M}$  so the ability for FAC to detect ligands in a concentration-independent manner promotes efficient use of finite compound collections. Improved LC/MS technology can array entire mixture compositions in reproducible fashion, as evidenced by applications in combinatorial library analysis and proteomics. This suggests that FAC-MS has a growing opportunity to assume an expanded role in high-throughput screening exercises. Although it should not be viewed as a replacement to established HTS operations, the inherent simplicity of the method suggests that FAC-MS can broaden access to chemical diversity at early stages in drug discovery.

## References

- 1 Kasai, K., Ishii, S.: Quantitative analysis of affinity chromatography of trypsin. A new technique for investigation of protein–ligand interaction. *J Biochem* **1975**, 77, 261–264.
- 2 Bellofiore, P., Petronzelli, F., De Martino, T., Minenkova, O., Bombardi, V., Anastasi, A. M., Lindstedt, R., Felici, F., De Santis, R., Verdoliva, A.: Identification and refinement of a peptide affinity ligand with unique specificity for a monoclonal anti-tenascin-C antibody by screening of a phage display library. *J Chromatogr A* **2006**, 1107, 182–191.
- 3 Guiochon, G.: Csaba Horvath and preparative liquid chromatography. *J Chromatogr A* **2005**, 1079, 7–23.
- 4 Subramanian, A., Hommerding, J.: Interaction of immunoglobulin G with modified chitosan. *J Liquid Chromatogr Related Technol* **2004**, 27, 2671–2688.
- 5 Hirabayashi, J., Hashidate, T., Arata, Y., Nishi, N., Nakamura, T., Hirashima, M., Urashima, T., Oka, T., Futai, M., Muller, W. E. G., Yagi, F., Kasai, K.: Oligosaccharide specificity of galectins: a search by frontal affinity chromatography. *Biochim Biophys Acta* **2002**, 1572, 232–254.
- 6 Hirabayashi, J., Arata, Y., Kasai, K.: Glycome project: concept, strategy and preliminary application to *Caenorhabditis elegans*. *Proteomics* **2001**, 1, 295–303.
- 7 Schriemer, D. C., Bundle, D. R., Li, L., Hindsgaul, O.: Micro-scale frontal affinity chromatography with mass spectrometric detection: A new method for the screening of compound libraries. *Angew Chem Int Ed* **1998**, 37, 3383–3387.
- 8 Schriemer, D. C.: Biosensor alternative: frontal affinity chromatography. *Anal Chem* **2004**, 76, 440A–448A.
- 9 Guiochon, G., Shirazi, S. G., Katti, A. M.: *Fundamentals of Preparative and Nonlinear Chromatography*, Academic Press, Toronto, **1994**.
- 10 Chan, N. W., Lewis, D. F., Rosner, P. J., Kelly, M. A., Schriemer, D. C.: Frontal affinity chromatography-mass spectrometry assay technology for multiple stages of drug discovery: applications of a chromatographic

- biosensor. *Anal Biochem* **2003**, 319, 1–12.
- 11 Kasai, K., Oda, Y. J.: Frontal affinity chromatography: theory for its application to studies on specific interaction of biomolecules. *J Chromatogr* **1986**, 376, 33–47.
  - 12 Lundqvist, A., Lundahl, P.: Chromatography on cells and biomolecular assemblies. *J Chromatogr B Biomed Sci Appl* **1997**, 699, 209–220.
  - 13 Moaddel, R., Cloix, J.-F., Ertem, G., Wainer, I. W.: Multiple receptor liquid chromatographic stationary phases: the co-immobilization of nicotinic receptors,  $\gamma$ -amino-butyric acid receptors, and N-methyl-D-aspartate receptors. *Pharm Res* **2002**, 19, 104–107.
  - 14 Nakamura, S., Uchiyama, N., Kuno, A., Kominami, J., Tatsumi, N., Osaka, Y., Maruyama, S., Ueda, T., Hirabayashi, J.: Comprehensive interaction analysis between lectins and PA-oligosaccharides by an automated frontal affinity chromatography (FAC) system. *Glycobiology* **2004**, 14, 1189–1189.
  - 15 Slys, G., Middleditch, M., Schriemer, D. C.: in *50th ASMS Conference on Mass Spectrometry and Allied Topics*, Orlando, **2002**.
  - 16 Kovarik, P., Hodgson, R. J., Covey, T., Brook, M. A., Brennan, J. D.: Capillary-scale frontal affinity chromatography/MALDI tandem mass spectrometry using protein-doped monolithic silica columns. *Anal Chem* **2005**, 77, 3340–3350.
  - 17 Guevremont, R.: High-field asymmetric waveform ion mobility spectrometry: a new tool for mass spectrometry. *J Chromatogr A* **2004**, 1058, 3–19.
  - 18 Winzor, D. J., Sawyer, W. H.: *Quantitative Characterization of Ligand Binding*, John Wiley & Sons, New York, **1995**.
  - 19 Ng, E. S., Yang, F., Kameyama, A., Palcic, M. M., Hindsgaul, O., Schriemer, D. C.: High-throughput screening for enzyme inhibitors using frontal affinity chromatography with liquid chromatography and mass spectrometry. *Anal Chem* **2005**, 77, 6125–6133.
  - 20 Deng, G., Sanyal, G.: Applications of mass spectrometry in early stages of target based drug discovery. *J Pharm Biomed Anal* **2006**, 40, 528–538.
  - 21 Chan, N. W., Lewis, D. F., Hewko, S., Hindsgaul, O., Schriemer, D. C.: Frontal affinity chromatography for the screening of mixtures. *Comb Chem High Throughput Screen* **2002**, 5, 395–406.
  - 22 Dennis, J. W., Granovsky, M., Warren, C. E.: Glycoprotein glycosylation and cancer progression. *Biochim Biophys Acta* **1999**, 1473, 21–34.
  - 23 Fernandes, B., Sagman, U., Auger, M., Demetrio, M., Dennis, J. W.: Beta-1-6 branched oligosaccharides as a marker of tumor progression in human breast and colon neoplasia. *Cancer Res* **1991**, 51, 718–723.
  - 24 Yao, M., Zhou, D. P., Jiang, S. M., Wang, Q. H., Zhou, X. D., Tang, Z. Y., Gu, J. X.: Elevated activity of N-acetylglucosaminyltransferase V in human hepatocellular carcinoma. *J Cancer Res Clin Oncol* **1998**, 124, 27–30.
  - 25 Ko, J. H., Miyoshi, E., Noda, K., Ekuni, A., Kang, R. J., Ikeda, Y., Taniguchi, N.: Regulation of the GnT-V promoter by transcription factor Ets-1 in various cancer cell lines. *J Biol Chem* **1999**, 274, 22941–22948.
  - 26 Yi, L., Li, Z., Yuan, K., Qu, X., Chen, J., Wang, G., Zhang, H., Luo, H., Zhu, L., Jiang, P., Chen, L., Shen, Y., Luo, M., Zuo, G., Hu, J., Duan, D., Nie, Y., Shi, X., Wang, W., Han, Y., Li, T., Liu, Y., Ding, M., Deng, H., Xu, X.: Small molecules blocking the entry of severe acute respiratory syndrome coronavirus into host cells. *J Virol* **2004**, 78, 11334–11339.
  - 27 Griffin, R. J., Fontana, G., Golding, B. T., Guiard, S., Hardcastle, I. R., Leahy, J. J., Martin, N., Richardson, C., Rigoreau, L., Stockley, M., Smith, G. C.: Selective benzopyranone and pyrimido[2,1-a]isoquinolin-4-one inhibitors of DNA-dependent protein kinase: synthesis, structure-activity studies, and radiosensitization of a

- human tumor cell line in vitro. *J Med Chem* **2005**, 48, 569–585.
- 28 Hodgson, R. J., Chen, Y., Zhang, Z., Tleugabulova, D., Long, H., Zhao, X., Organ, M., Brook, M. A., Brennan, J. D.: Protein-doped monolithic silica columns for capillary liquid chromatography prepared by the sol-gel method: applications to frontal affinity chromatography. *Anal Chem* **2004**, 76, 2780–2790.
- 29 Gottschalk, I., Li, Y. M., Lundahl, P.: Chromatography on cells: analyses of solute interactions with the glucose transporter Glut1 in human red cells adsorbed on lectin-gel beads. *J Chromatogr B Biomed Sci Appl* **2000**, 739, 55–62.
- 30 Comess, K. M., Schurdak, M. E.: Affinity-based screening techniques for enhancing lead discovery. *Curr Opin Drug Discov Dev* **2004**, 7, 411–416.
- 31 Gritti, F., Guiochon, G.: Critical contribution of nonlinear chromatography to the understanding of retention mechanism in reversed-phase liquid chromatography. *J Chromatogr A* **2005**, 1099, 1–42.
- 32 Slon-Usakiewicz, J. J., Dai, J. R., Ng, W., Foster, J. E., Deretey, E., Toledo-Sherman, L., Redden, P. R., Pasternak, A., Reid, N.: Global kinase screening. Applications of frontal affinity chromatography coupled to mass spectrometry in drug discovery. *Anal Chem* **2005**, 77, 1268–1274.
- 33 Slon-Usakiewicz, J. J., Ng, W., Foster, J. E., Dai, J. R., Deretey, E., Toledo-Sherman, L., Redden, P. R., Pasternak, A., Reid, N.: Frontal affinity chromatography with MS detection of EphB2 tyrosine kinase receptor. 1. Comparison with conventional ELISA. *J Med Chem* **2004**, 47, 5094–5100.
- 34 Toledo-Sherman, L., Deretey, E., Slon-Usakiewicz, J. J., Ng, W., Dai, J. R., Foster, J. E., Redden, P. R., Uger, M. D., Liao, L. C., Pasternak, A., Reid, N.: Frontal affinity chromatography with MS detection of EphB2 tyrosine kinase receptor. 2. Identification of small-molecule inhibitors via coupling with virtual screening. *J Med Chem* **2005**, 48, 3221–3230.
- 35 Sannes-Lowery, K. A., Griffey, R. H., Hofstadler, S. A.: Measuring dissociation constants of RNA and aminoglycoside antibiotics by electrospray ionization mass spectrometry. *Anal Biochem* **2000**, 280, 264–271.
- 36 Cinatl, J., Morgenstern, B., Bauer, G., Chandra, P., Rabenau, H., Doerr, H. W.: Glycyrrhizin, an active component of liquorice roots, and replication of SARS-associated coronavirus. *Lancet* **2003**, 361, 2045–2046.

## 7

### MS Binding Assays – An Alternative to Radioligand Binding

*Georg Höfner, Christine Zepperitz, and Klaus T. Wanner*

#### 7.1

##### Introduction

The development of the receptor concept by Langley, Ehrlich, Clark and others at the end of the nineteenth and the beginning of the twentieth century provided the basis for understanding pharmacological effects on a molecular basis [1, 2]. Today pharmacological receptors are understood to be signal transducing proteins that selectively and reversibly bind an endogenous signal molecule (or a synthetic analog), and then undergo a conformational change and mediate a cellular answer as a consequence. Among them are intracellular receptors of the nuclear receptor superfamily and membrane-bound receptors such as ion channel-coupled receptors, kinase-coupled receptors or G protein-coupled receptors [3].

For a long time no highly sensitive detection methods existed for the analysis of pharmacological effects, in the sense of receptor–ligand interactions, at a molecular level, even though receptors were already accepted as primary targets for biologically active compounds. Direct characterization of receptors, which are usually present in tissue preparations only in subnanomolar concentrations, was only possible after pure radioisotopes such as  $^3\text{H}$  or  $^{125}\text{I}$  were available that allowed the production of radioligands [4]. The beginnings of radioligand binding assays are dated differently in the literature [1, 5–7]. They have definitely found widespread use since the mid 1970s [8]. Since the early 1990s radioligand binding assays have been increasingly automated, miniaturized and adapted to the requirements of high-throughput screening [9]. Recently, with the advent of modern fluorescence techniques, binding assays based on fluorophore-labeled ligands were established and gained importance for a variety of targets [10–15].

As binding assays provide a means to characterize the affinity of test compounds to defined targets, they play a very important, not to say an essential role in the drug discovery process. Next to the advantage of effective quantitation, the use of a marker, i.e. a labeled ligand – either with a radioisotope or a fluorophore – has, however, also serious immanent disadvantages. As the performance of mass spectrometry continues to improve, it appears therefore obvious to conduct



binding assays in analogy to radioligand binding assays employing a native, i.e. unlabeled, ligand as a marker and to quantify this marker by mass spectrometry. In this chapter the feasibility of this approach, named MS binding assays in analogy to radioligand binding assays, will be outlined.

Since MS binding assays closely resemble conventional radioligand binding assays, the most important fundamentals and the relevance of radioligand binding assays but also their limitations are discussed first. Next, the basic considerations for the establishment of the MS binding assays are described and finally some applications addressing typical, pharmacologically relevant membrane-bound targets are presented.

## 7.2

### Radioligand Binding Assays

Radioligand binding assays are a relatively simple but at the same time a very important and efficient tool to study target–ligand interactions. Since they are very widely used in drug discovery and have been described extensively, this section only discusses their fundamental aspects and those aspects that are important for the description of the MS binding assays below. More detailed information can be found in the relevant literature [6, 7, 16–21].

Radioligand binding assays depend on the use of a radioligand addressing the target of interest. Depending on the assay type performed (e.g. saturation, competition or kinetic experiments) different information is obtained. All types have in common that a radioligand as a marker is first incubated with a target. After a period of time, that is dependent on the aim of the experiment, the target and the radioligand bound to it are separated from the rest of the incubation mixture and, as a last step, the amount of bound radioligand is quantified by measuring the radioactivity. As a result the total binding, that is the specific binding (i.e. binding of the marker to the target) and the nonspecific binding (i.e. binding of the marker to different binding sites independent from the target) is obtained. To ascertain the specific binding, being relevant for the binding assay, the nonspecific binding has to be determined in a separate experiment [7, 16, 17, 21].

#### 7.2.1

##### General Principle

##### 7.2.1.1 Saturation Assays

Saturation assays are used to characterize the affinity of the radioligand to the target as well as to determine the target density. In saturation assays, in a series of experiments a constant target concentration ( $T_{\text{tot}}$ ) is incubated with an increasing concentration of marker ( $M_{\text{tot}}$ ). The amount of bound radioligand determined after the equilibrium is reached represents total binding. Nonspecific binding is defined in a control experiment where the target is incubated with the marker in the presence of a great excess of a competitor, i.e. another ligand with high

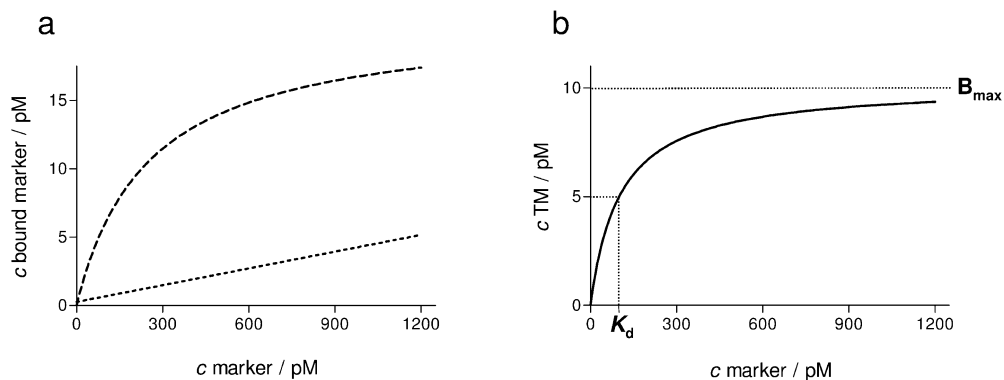


**Fig. 7.1** Typical saturation binding experiment: (a) Hypothetical binding isotherm for total binding (---) and straight line for nonspecific binding (---). (b) Saturation binding isotherm for specific binding after subtraction of nonspecific binding from total binding ( $B_{\max} = 10$  pM,  $K_d = 100$  pM).

affinity to the target. Plotting the specific binding of the marker (target–marker complex, TM, calculated from total and nonspecific binding) against the concentration of the free marker (M) gives a saturation isotherm (Fig. 7.1). This provides the equilibrium dissociation constant ( $K_d$ ) of the marker represented by the concentration of the free marker yielding a target occupancy of 50% [see Eqs (1), (2)].



$$K_d = \frac{[T] \cdot [M]}{[TM]} \quad \text{for } [TM] = [T] = \frac{1}{2} [T_{\text{tot}}] \Rightarrow K_d = [M] \quad (2)$$

From the plateau of the saturation isotherm, the maximal occupancy of the target  $B_{\max}$  can be determined that corresponds to the target concentration in the binding assay. Preferably, the target is used in concentrations of  $T_{\text{tot}} \ll K_d$ , as under these conditions the concentration of TM remains low compared to the concentration of the free marker M and therefore M can be replaced by  $M_{\text{tot}}$  for the analysis of the binding experiment [7, 16, 17, 21].

### 7.2.1.2 Competition Assays

Competition assays are used to determine indirectly, that is by quantifying the binding of a radioligand, the affinity of a test compound to a target. In such an experiment the target is incubated in the presence of a constant concentration of  $M_{\text{tot}}$  ( $M_{\text{tot}} \sim K_d$ ) and of varying concentrations of the test compound under conditions that allow an equilibrium to be attained. As a result of the competition between marker and test compound the binding of the marker to the target is reduced with increasing concentrations of the test compound. Plotting the specific binding of the marker against the free concentration of the test compound gives a

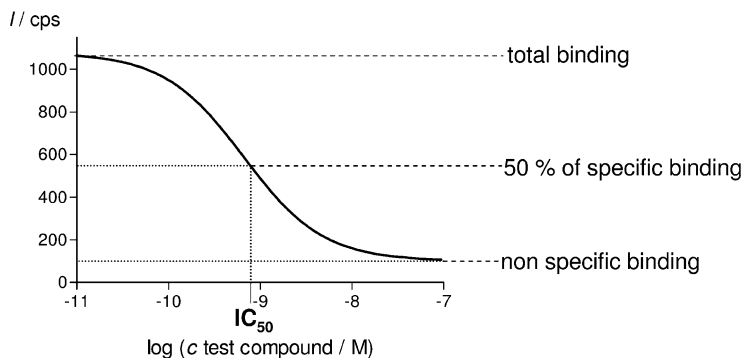


**Fig. 7.2** Typical competitive binding experiment. The hypothetical test compound is an inhibitor of marker binding with an  $IC_{50}$  of 0.66 nM ( $\log c = -9.2$ ). Specific binding covers approx. 980 units of signal intensity ( $I$ ).

competition curve (Fig. 7.2) yielding the  $IC_{50}$  value, i.e. the concentration of test compound required to reduce the specific binding of the radioligand by 50%.

The affinity constant of the test compound  $K_i$  can in turn be calculated from the  $IC_{50}$  value, the  $K_d$  of the marker and the concentration of M according to Cheng-Prusoff [see Eq. (3)] [22]. Since the concentration of free marker (M) is usually not determined in radioligand binding assays, it should be noted that the calculation of  $K_i$  according to Eq. (3) based on  $M_{tot}$  yields only reliable results if the depletion of the marker is negligible (i.e. <5% to 10% [7, 17, 21]). In competition experiments performed under typical conditions ( $T_{tot} \ll K_d$ ,  $M_{tot} \sim K_d$ ) this criterion is fulfilled.

$$K_i = \frac{IC_{50}}{1 + \frac{[M]}{K_d}} \quad (3)$$

### 7.2.1.3 Kinetic Assays

Kinetic assays give access to the binding reaction's forward and reverse rate constants, i.e. the association rate constant  $k_{+1}$  and the dissociation rate constant  $k_{-1}$  that characterize the association and the dissociation of the target–marker complex and the  $K_d$  [see Eq. (4)].

$$K_d = \frac{k_{-1}}{k_{+1}} \quad (4)$$

To determine the association rate constant  $k_{+1}$  a constant target concentration is incubated with a constant marker concentration. The experiment is stopped after different periods of time and the amount of marker bound to the target quanti-

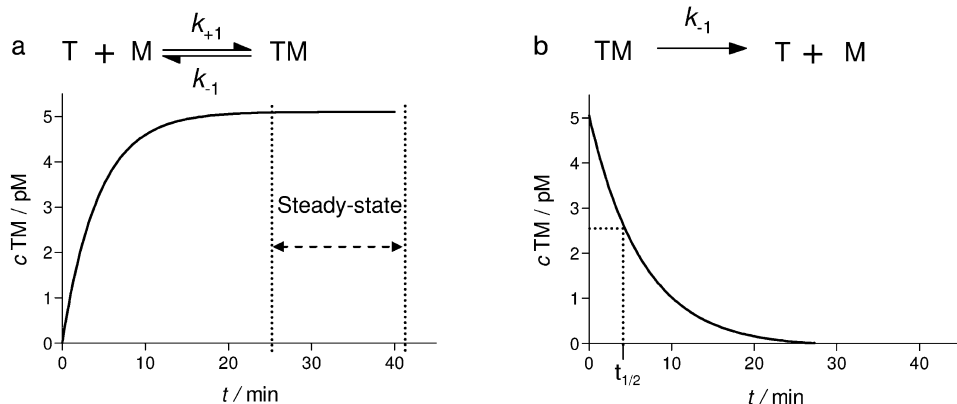


**Fig. 7.3** Kinetic binding experiments: (a) Typical association experiment where binding between target (T) and marker (M) reaches steady state after approx. 25 min. (b) Typical dissociation experiment with a half-life of target–marker complex (TM) of approx. 4.5 min.

fied. In dissociation assays, constant concentrations of target and marker are first incubated until equilibrium is reached. Next, dissociation is started under conditions suppressing the association reaction almost completely, e.g. by “infinite” dilution or addition of a large excess of a competitor. The course of the dissociation is registered by measuring the amount of the bound marker after different periods of time. The association rate constant  $k_{+1}$  and dissociation rate constant  $k_{-1}$  can be determined from the association and dissociation diagrams (Fig. 7.3) compiled from the experimental data [7, 16, 17, 21].

### 7.2.2

#### Application

Though there are hardly any restrictions to choosing a target, pharmacological receptors are investigated most frequently. The nature of the receptor, whether it is membrane-bound or soluble, determines which separation technique is used to terminate the binding assay. For the former, filtration or centrifugation are favored as separation steps, while for the latter suitable methods are gel filtration, equilibrium dialysis, precipitation or adsorption of the nonbound marker by charcoal [23, 24].

The marker should display both an affinity to and a selectivity for the target that is as high as possible while generating as little nonspecific binding as possible. The  $K_d$ -values of the suitable markers are typically in the range between 100 pM and 10 nM, enabling the separation of the target–marker complex from the non-bound marker and the subsequent washing steps without noticeable dissociation [7, 16, 17, 21].

From the three basic radioligand binding assay types, competition experiments are no doubt most frequently applied in the drug discovery process, since they allow the characterization of the affinity of any kind of test compound to a defined target [7, 16, 17, 21]. To meet the increasing challenge of throughput in this area, filtration assays and later on assays based on gel filtration as the separation step were established already in the 1990s, using a 96-well plate format [6, 9, 25]. By now filtration assays can be accomplished in a completely automated form [26]. Next to these technical improvements, new “homogeneous” techniques have been developed since the 1980s that omit the separation step obligatory in conventional radioligand binding assays [27–30]. These methods, based on the scintillation proximity principle, differ from conventional radioligand binding assays in that the target is first bound on beads or on the surface of microtiter plates which are impregnated with scintillator molecules. After being incubated with the radioligand, the sample can be measured without separating bound from nonbound marker, since only those radioligands in the immediate vicinity of the scintillator molecules, i.e. those bound to the immobilized target, cause emissions of light. This technique, despite the advantage of a high throughput, also has some drawbacks in comparison to conventional radioligand binding assays, e.g. a higher degree of nonspecific binding, the necessity of higher radioligand concentrations and occasionally a reduced affinity of the marker for the target due to the immobilization of the latter [26, 31].

Modern high-throughput screening knows a number of very different rivalling strategies and test systems for the detection and optimization of new lead structures [32–34]. Homogeneous “mix and measure assays” avoiding a separation step are generally preferred. Conventional radioligand binding assays, however, are an indispensable tool that represent the “gold standard” for the characterization of new test compounds and for the investigation of structure activity relationships [1, 25]. As a simple, robust, flexible, fast, and comparatively inexpensive technology, they are still of great importance for the pharmaceutical industry as well as for companies like Novoscreen and CEREP that specialize in receptor screening [35, 36].

### 7.2.3

#### **Disadvantages and Alternatives**

Next to the advantages, like outstanding sensitivity of quantitation, the use of radioligands also has some inherent disadvantages. Since handling radioisotopes in organic syntheses requires relatively high safety standards and is subject to broad legal restrictions, the production of radioligands is expensive and also restricted to a few specialized institutions. For the user this means a sizeable expense and a limited number of commercially available radioligands. Performing radioligand binding assays according to legal requirements adds further costs. Among them are those for specially equipped rooms or the disposal of radioactive waste. The nature of the radionuclide causes its own problems. Radionuclides with a short

half life have to be used within a correspondingly short time, while radionuclides with a long half life generate additional problems with regard to their storage and disposal. Very often the radioactive decay leads also to destruction, raising the question of the chemical purity of the radioligand after longer storage.

Next to radioisotopes, any other label allowing the detection of a ligand with sufficient sensitivity can be employed in binding assays. The preferred markers, apart from radioligands, are ligands conjugated to a fluorophore [37–40]. Since background fluorescence causes problems when measuring the fluorescence in the presence of the receptor material [41], either the nonbound fluorescent marker has to be quantified in conventional binding assays after separation or, alternatively, the bound fluorescent marker after being liberated from the target. Binding assays based on time-resolved fluorescence (TRF) or fluorescence polarization (FP) [10–12] have gained particular attraction. TRF assays usually employ ligands labeled with lanthanide chelates (e.g.  $\text{Eu}^{3+}$  chelate) and are used for a great variety of targets [12, 13, 42–44]. Measuring the amount of bound or the nonbound marker generally requires a separation step and the addition of an enhancer solution since the matrix of the binding sample hinders optimal quantitation. FP allows the distinction between nonbound and bound fluorescent markers in homogenous phase based on the restricted rotation of fluorescent markers bound to a target. Commonly, fluorescent markers originating from peptides are employed for FP applications; however, recently some examples using fluorescent markers originating from small molecules have been described as well [14, 15, 45]. Other fluorescence-based methods to investigate target–ligand interactions use fluorescence correlation spectroscopy (FCS) or fluorescence resonance energy transfer (FRET) [8, 12, 46].

Despite successful examples of fluorescence-based binding assays and the relevance of radioligand binding assays in the drug discovery process, two major inherent disadvantages regarding any labeling strategy remain. First of all, labeling always means an additional synthetic effort. In addition to the labeling process, very often a new synthetic route has to be established to obtain a suitable precursor for the labeling reaction. Secondly, labeling of a ligand can decrease its affinity. Replacing a stable isotope with a radioisotope (e.g.  $^3\text{H}$  with  $^1\text{H}$ ) does usually not change the ligand in this respect, whereas the substitution by a radioisotope with different electronic properties (e.g. replacing  $^1\text{H}$  with  $^{125}\text{I}$ ) may cause a significant decrease in affinity. In the case of labeling a native ligand with a large fluorophore – compared to a radioisotope – a severe decrease in affinity can frequently be observed. This is especially true for small molecules and seriously limits the use of fluorophore-labeled ligands in binding assays [12, 41, 47].

However, the determination of affinity does not necessarily have to rely on labeled ligands. It is also possible with native ligands when using suitable detection methods, as for example nuclear magnetic resonance (NMR), surface plasmon resonance (SPR), acoustic biosensors or calorimetry [48, 49]. A particularly versatile and sensitive detection principle for the investigation of interactions between targets and native ligands is mass spectrometry [50].

### 7.3

#### MS Binding Assays

The increasing performance of mass spectrometry as well as the development of particularly gentle but also effective ionization techniques like matrix-assisted laser desorption ionization (MALDI) and electrospray ionization (ESI) provided the opportunity to directly study binding of native ligands at defined targets [51, 52] (see also Chapter 1). The first MS based methods to measure target–ligand interactions were described in the beginning of the 1990s [53]. Later on, in 1995, Henion and coworkers reported the determination of the affinity constants of glycopeptide antibiotics like vancomycin at peptides representing target partial structures. They attained this goal by analyzing the target–ligand complexes and the free ligands in parallel directly in the gas phase by ESI-MS [54]. By now, a great variety of different methods to study target–ligand interactions qualitatively or quantitatively based on mass spectrometry have been published [50, 52, 55, 56].

In contrast to most of the other detection methods that can be employed for the characterization of target–ligand interactions, mass spectrometry also allows the identification of structurally unknown ligands. Due to this almost exclusive potential, mass spectrometry has an outstanding position in the screening of combinatorial libraries. The principle to filter hits based on their affinity to the target from a set of different test compounds is called affinity selection. The majority of screening techniques based on mass spectrometry follow the affinity selection principle, and several of these have achieved an impressive efficiency, for example the automated ligand identification system (ALIS, see Chapter 3) established by NeoGenesis (now part of Schering Plough) and affinity selection mass spectrometry (ASMS, see Chapter 4) established by Abbott or SpeedScreen from Novartis [57].

Although these and many other successful approaches for the MS determination of a compound's affinity are regarded as being well established, their application is still reserved to specialists as they require the application of comparatively complex and high sophisticated techniques. The method presented below is therefore deliberately employing a comparatively simple principle: the MS quantitation of native markers in binding assays that are conducted in analogy to radioligand binding assays. This method has been termed "MS binding assays".

MS binding assays share all the advantages of conventional radioligand binding assays, the principle is very simple, they are robust, comparatively cheap, flexible and universally applicable, without the disadvantages caused by a label. Basically, the binding assay itself can be performed exactly as a radioligand binding assay. However, after separation of the bound from the nonbound native marker, the marker quantitation is done by mass spectrometry. As the quantitation method for the marker can be used for all binding samples in the same way, MS analysis creates a modicum of effort. The prerequisites for the native marker are first of all – just as in radioligand binding assays – that it shows a high affinity and selectivity for the target and, at the same time, as little nonspecific binding as possible. Secondly, the marker should be quantifiable by mass spectrometry with a sensitivity as high as possible.

In one point, however, MS binding assays differ fundamentally from radioligand binding assays. In radioligand binding assays it is of little importance whether the marker (i.e. the radioligand) is free or bound to the target during quantitation, since measuring the radioactivity detects both the bound and the already dissociated marker in the same way. This is not the case in MS binding assays, where the free marker and the bound marker (i.e. the target–marker complex) give rise to different signals. Additionally, the exact mass spectrometric quantitation of the marker poses a formidable challenge, particularly if the concentrations to be determined lie in the picomolar range or below (as typical in radioligand binding experiments).

As it is often difficult to prevent dissociation of the target–marker complex during quantitation, this problem can be solved by first separating the target–marker complex from the nonbound marker and, in a second step, liberating the bound marker from the complex for the mass spectrometric quantitation. MS binding studies of this type will be discussed in Section 7.3.2. Alternatively, MS binding studies can be also conducted by quantifying the amount of nonbound marker in the binding sample instead of bound marker (as the amount of bound marker can be calculated from the amounts of total marker and nonbound marker). While the latter method allows to complete the experiment without the additional step of liberating the marker from the target–marker complex it is subject to some restrictions concerning the experimental procedure. Examples for this procedure are given below in Section 7.3.1.

### 7.3.1

#### MS Binding Assays Quantifying the Nonbound Marker

In radioligand binding assays, binding of the marker is always quantified by the amount of marker bound to the target. The practicality of a procedure that in contrast quantifies the nonbound marker to indirectly determine the amount of bound marker has been shown by applications which examined the binding of fluorescent markers to nicotinic acetylcholine and benzodiazepine receptors [37, 38]. Although very different from conventional binding assays with regard to the design of the binding experiment, the principle to quantify the nonbound marker by LC-MS has also been realized in a sophisticated “continuous flow” approach (as described in Chapter 5).

Competition experiments performed as conventional radioligand binding assays are characterized by a nominal marker concentration in the range of its  $K_d$  value, while the concentration of the target is set at, by comparison, a significantly lower level (i.e.  $[M_{\text{tot}}] \approx K_d \gg [T_{\text{tot}}]$ ). In radioligand binding assays this set up is possible since the resulting amount of bound marker (TM) is quantified by scintillation counting, that is sensitive enough to reliably measure TM in concentrations  $\ll K_d$ . In MS binding assays where the amount of nonbound marker is to be quantified the situation is completely different. If an MS binding assay of this kind were to be conducted under the same conditions as a radioligand binding assay, the differences between the concentrations of the free marker ( $\Delta M$ ) that



result from changes in the concentrations of the bound marker (TM) would be imperceptible or, at least, extremely hard to detect, because these differences would be so small in relation to the concentration of M that they would hardly exceed the uncertainty regarding the quantitation of M by MS. This problem can be avoided if the concentration of the bound marker (TM) is increased considerably in comparison to the nominal marker concentration ( $M_{\text{tot}}$ ). This can be achieved by increasing the concentration of the target ( $T_{\text{tot}}$ ) in comparison to the concentration used in radioligand binding assays. The result of an increasing concentration of the target is exemplified in the following for  $[T_{\text{tot}}] \approx K_d$  while the other conditions remain the same  $\{[M_{\text{tot}}] \approx K_d, \text{ see Eq. (5)}\}$ .

$$[M_{\text{tot}}] = [\text{TM}] + [M] = [T_{\text{tot}}] = [\text{TM}] + [T] = K_d \quad (5)$$

Solving Eq. (2) (Section 7.2.1) for the conditions given in Eq. (5) leads to Eq. (6).

$$[\text{TM}] = \frac{3 - \sqrt{5}}{2} \cdot K_d \approx 0.38 K_d \quad (6)$$

Neglecting nonspecific binding, Eq. (6) reveals that a considerable fraction (c. 38%) of the total amount of the marker is bound to the target ( $[\text{TM}] = 0.38 K_d = 0.38 [T_{\text{tot}}] = 0.38 [M_{\text{tot}}]$ ). This means that the changes in the fraction of the bound marker caused in competition experiments, result in a significant change in the concentration of the nonbound marker (M). For saturation and kinetic experiments, however, this concept is more difficult to apply.

In competition experiments that quantify the nonbound marker, as discussed here, the concentration relations are intentionally fixed in a manner that ensures that a significant fraction of the marker is bound ( $[\text{TM}] > 0.1 [M_{\text{tot}}]$ ). Therefore, marker depletion has to be considered when analyzing the data. This can be done by means of Eq. (7), for example [16].

$$K_i = \frac{IC_{50}}{2 \frac{([M_{50}] - [M_0])}{[M_0]} + 1 + \frac{[M_{50}]}{K_d}} \quad (7)$$

$K_i$ : equilibrium dissociation constant of the test compound,  
 $IC_{50}$ : concentration of test compound reducing specific binding of the marker to 50%,  $[M_{50}]$ : concentration of the free marker at the  $IC_{50}$ -value,  
 $[M_0]$ : concentration of the non bound marker in the absence of a competitor,  $K_d$ : equilibrium dissociation constant of the marker.

Furthermore it has to be taken into account that the nonbound marker has to be quantified out of a matrix containing all the dissolved compounds of the binding sample. To avoid ion suppression of the marker, it is therefore necessary to either use a buffer compatible with MS (i.e. a volatile buffer), or alternatively to remove the matrix of the binding sample prior to quantitation of the nonbound marker.

### 7.3.1.1 Competition Assays for D<sub>1</sub> and D<sub>2</sub> Dopamine Receptors

#### 7.3.1.1.1 Dopamine Receptors

Dopamine receptors belong to the group of G protein-coupled receptors (GPCRs) [58]. GPCRs are integral membrane proteins that, after binding the respective endogenous messengers, transduce signals into the interior of a cell through interaction with heterotrimeric G proteins. More than 600 different genes coding for GPCRs were discovered on the human genome. Currently, they are the most frequently addressed targets in drug development [59]. Disturbed dopaminergic neurotransmission is linked to a number of diseases of the central nervous system, including Morbus Parkinson and schizophrenia [58]. Therefore, binding assays for dopamine receptors play a crucial role in the development of new drugs for the relevant indications. So far five different subtypes of dopamine receptors (D<sub>1-5</sub>) have been found. They can be classified into two groups according to their signal transduction and pharmacology, D<sub>1</sub> and D<sub>5</sub> on one side and D<sub>2-4</sub> on the other. D<sub>1</sub> and D<sub>2</sub> are the subtypes that occur most frequently in the brain [58]. Taking the determination of the affinity of test compounds for dopamine D<sub>1</sub> and D<sub>2</sub> receptors as a typical issue of the modern drug discovery process, it will be exemplified here how competitive MS binding assays based on the quantitation of the nonbound marker can be accomplished easily.

#### 7.3.1.1.2 Competition Assays for Dopamine D<sub>1</sub> Receptors

As described above conducting competitive MS binding assays is dependent on certain prerequisites. Crude membrane preparations from pig striatum could be shown to be a suitable source for D<sub>1</sub> receptors in preliminary radioligand binding assays. Furthermore it turned out that the binding assays can be conducted in 50 mM ammonium formate instead of the Tris buffer generally used. A further decisive fact was that the D<sub>1</sub> receptor density in the membrane preparation was high enough to reach a target concentration in the range of the  $K_d$  of SCH 23390 (Fig. 7.4) that was chosen as a marker.

Employing the D<sub>1</sub> receptor selective compound SCH 23390 as marker, well known from radioligand binding assays ( $K_d$  for [<sup>3</sup>H]SCH 23390 = 0.53 nM) [60], had a two-fold advantage: first, the experimental conditions for the binding experiment could be adopted from respective radioligand binding assays, and secondly, it enabled a very simple validation of the results obtained from MS binding assays by means of radioligand binding assays. Finally, with the development of a LC-ESI-MS/MS method that allowed a reliable quantitation of SCH 23390 in concentrations below 100 pM, the requirements for using SCH 23390 as a marker in competitive MS binding assays were fulfilled.

The binding experiments were conducted with 1.25 nM SCH 23390 and D<sub>1</sub> receptors in concentrations of roughly 0.5–0.8 nM in a total volume of 250  $\mu$ L, applying different concentrations of the test compound. Separating the nonbound marker from the target preparation (containing the bound marker) was accomplished by centrifugation. The resulting supernatant was subsequently analyzed by LC-ESI-MS/MS without further purification (Fig. 7.5).

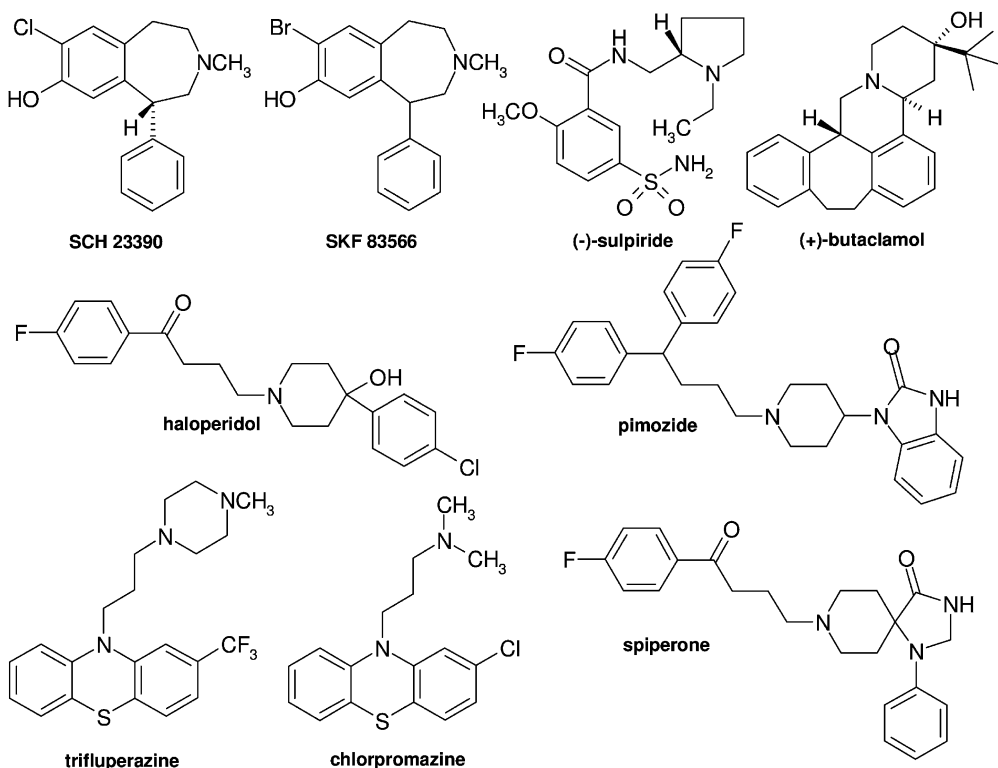


**Fig. 7.4** Structures of compounds used in competitive MS binding assays for dopamine D<sub>1</sub> and D<sub>2</sub> receptors.

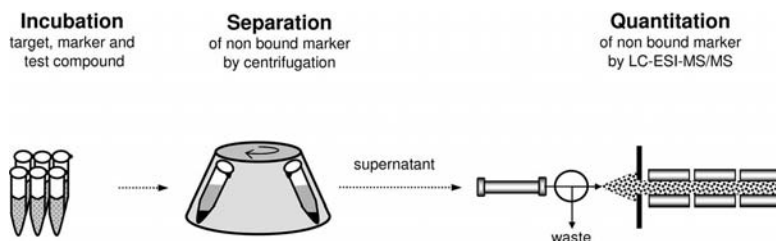


**Fig. 7.5** Schematic flowchart of the competitive MS-binding assay quantifying the nonbound marker employed for dopamine D<sub>1</sub> receptors. After incubation of the target (D<sub>1</sub> receptor) in presence of the marker (SCH 23390) and a test compound, the binding samples are centrifuged to separate bound from nonbound marker. The nonbound marker in the resulting supernatant is quantified by LC-ESI-MS/MS without further sample preparation.

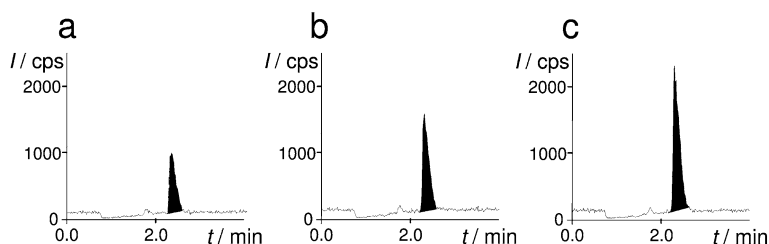


**Fig. 7.6** Nonbound SCH 23390 in a competitive MS binding assay for dopamine D<sub>1</sub> receptors monitored at a transition from 288.1 → 91.2 *m/z* from binding samples without or with (+)-butaclamol. Intensity (*I*) is shown: (a) without (+)-butaclamol, (b) with 30 nM (+)-butaclamol, (c) with 10 μM (+)-butaclamol. (a–c) Representative chromatograms after HPLC separation (RP8 column; solvent: CH<sub>3</sub>CN/0.1% HCOOH in H<sub>2</sub>O 1:1; 300 μL min<sup>-1</sup>).

Figure 7.6 exemplifies the results for the dopamine antagonist (+)-butaclamol (Fig. 7.4).

In the absence of the test compound (total binding) the signal of the nonbound marker was low (Fig. 7.6a) and intensified with increasing concentrations of (+)-butaclamol (Fig. 7.6b). The signal obtained in the presence of 10 μM (+)-butaclamol (Fig. 7.6c) corresponds to the difference between the total marker concentration [*M*<sub>tot</sub>] and nonspecific binding. Hence, the difference between the maximum signal ( $\cong$  [*M*<sub>tot</sub>] – nonspecific binding) and the minimum signal ( $\cong$  [*M*<sub>tot</sub>] – specific binding – nonspecific binding) represents specific SCH 23390 binding.

With the data obtained in this way competition curves could be generated for (+)-butaclamol (Fig. 7.7). A number of other dopamine antagonists were studied

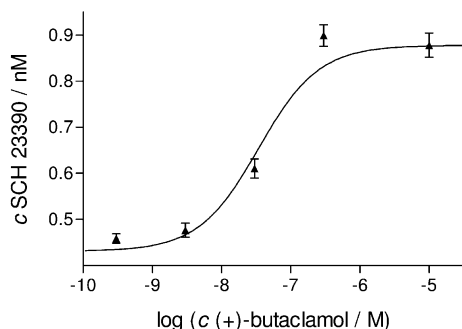


**Fig. 7.7** Representative binding curve obtained by nonlinear regression from a competitive MS binding assay for dopamine D<sub>1</sub> receptors, in which (+)-butaclamol competes with SCH 23390 as marker. The points describe nonbound SCH 23390 quantified by LC-ESI-MS/MS. Data reflect means ( $\pm$ s) from binding samples, each performed in quadruplicate.

**Table 7.1** Affinities (mean  $\pm$  SEM,  $n = 3$ ) for dopamine antagonists at  $D_1$  receptors obtained by MS-binding assays and radioligand binding assays, respectively [61].

	SCH 23390		[ $^3$ H]SCH 23390
	IC <sub>50</sub> (nM)	K <sub>i</sub> (nM)	K <sub>i</sub> (nM)
(+)-Butaclamol	36 $\pm$ 3	11 $\pm$ 1	5.4 $\pm$ 1.9
Chlorpromazine	1700 $\pm$ 40	620 $\pm$ 10	300 $\pm$ 40
Haloperidol	1620 $\pm$ 170	220 $\pm$ 60	110 $\pm$ 2
Pimozide	13 000 $\pm$ 700	4700 $\pm$ 200	2500 $\pm$ 500
SKF 83566	5.9 $\pm$ 1.0	1.9 $\pm$ 0.3	2.7 $\pm$ 0.6
(S)-Sulpiride	>10 000	>10 000	>10 000
Trifluoperazine	1300 $\pm$ 100	460 $\pm$ 40	215 $\pm$ 20

in the same way and their affinity constants calculated from the resulting competition curves (Table 7.1, Fig. 7.4).

To validate the results, the test compounds were examined in radioligand binding assays under comparable conditions. In this case, however, according to the common procedure in conventional radioligand binding assays, a target concentration  $[T_{\text{tot}}] \ll K_d$  was employed, and [ $^3$ H]SCH 23390 bound to the target was quantified after filtration (Table 7.1). The  $K_i$  values determined [according to Eq. (7), Section 7.3.1) in the MS binding assays tend to be slightly higher than those determined in radioligand binding assays. However, most importantly the ranking of the  $K_i$  values is in good accordance for both test systems [61].

### 7.3.1.1.3 Competition Assays for Dopamine $D_2$ Receptors

The method was also applied to the  $D_2$  receptor. In this case however, an incubation medium with nonvolatile components frequently used in radioligand binding assays consisting of 50 mM Tris-HCl, 120 mM NaCl, 5 mM  $MgCl_2$ , 5 mM KCl and 1 mM EDTA was deliberately employed to demonstrate that the incubation medium in MS binding assays quantifying the nonbound marker is not restricted to volatile buffers. As in the  $D_1$  receptor binding assay, a crude membrane fraction of pig striatum was used as the source for the  $D_2$  receptors and with spiperone (Fig. 7.4) again the native form of a well established radioligand was chosen as a marker. Preliminary experiments showed, as expected, that the signal of the marker was substantially suppressed, when the nonbound marker was analyzed by LC-ESI-MS/MS directly out of the matrix of the binding sample. Therefore a solid phase extraction (SPE) method was employed to remove most of the interfering sample matrix and to enhance the spiperone signal, allowing the binding experiments to be successfully performed. After incubating spiperone in

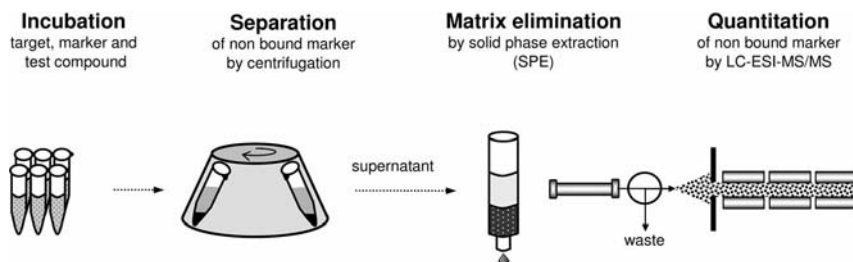


**Fig. 7.8** Schematic flowchart of the competitive MS-binding assay quantifying the nonbound marker employed for dopamine D<sub>2</sub> receptors including matrix elimination. After incubation of the target (D<sub>2</sub> receptor) in presence of the marker (spiperone) and a test compound, the binding samples are centrifuged to separate bound from nonbound marker. The nonbound marker in the resulting supernatant is quantified after SPE by LC-ESI-MS/MS.

a concentration of 1.25 nM with D<sub>2</sub> receptors in a concentration of ~400 pM in a total volume of 500  $\mu$ L nonbound spiperone could be quantified reliably by LC-ESI-MS/MS after SPE of the supernatant obtained after centrifugation (Figs. 7.8, 7.9).

In this way, the affinities of (+)-butaclamol, chlorpromazine and (*S*)-sulpiride (Fig. 7.4) for the D<sub>2</sub> receptor were characterized. The competition curves obtained [e.g. for (+)-butaclamol, Fig. 7.10] were as expected, but showed an unusually

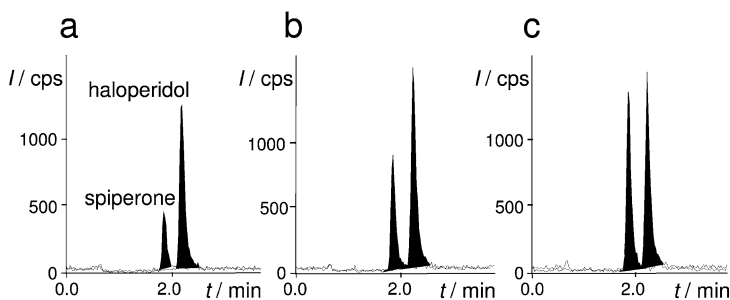


**Fig. 7.9** Nonbound spiperone in a competitive MS binding assay for dopamine D<sub>2</sub> receptors monitored at a transition from 396.0  $\rightarrow$  123.0  $m/z$  from binding samples without or with (+)-butaclamol. Intensity (*I*) is shown: (a) without (+)-butaclamol, (b) with 100 nM (+)-butaclamol, (c) with 10  $\mu$ M (+)-butaclamol. (a–c) Representative

chromatograms after SPE on Oasis HLB cartridges followed by HPLC separation (RP8 column; solvent: CH<sub>3</sub>CN/0.1% HCOOH in H<sub>2</sub>O 30:70, 150  $\mu$ L min<sup>-1</sup>). All samples (supernatants) were spiked with haloperidol (0.875 nM, 396.0  $\rightarrow$  123.0  $m/z$ ) as internal standard.

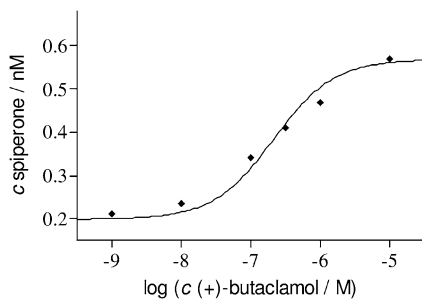


**Fig. 7.10** Representative binding curve obtained by nonlinear regression from a competitive MS-binding assay for dopamine D<sub>2</sub> receptors, in which (+)-butaclamol competes with spiperone as marker. The points describe nonbound spiperone quantified by LC-ESI-MS/MS. Data reflect means (±s) from binding samples each performed in triplicate.

high amount of nonspecific binding [defined as the remaining binding in the presence of 10  $\mu$ M (+)-butaclamol].

Nevertheless, they easily allowed the determination of IC<sub>50</sub> values of the test compounds and the calculation of the respective K<sub>i</sub> values [according to Eq. (7), Section 7.3.1, Table 7.2].

The reliability of the SPE-LC-ESI-MS/MS quantitation method of the non-bound marker spiperone was verified in identical binding assays employing [<sup>3</sup>H]spiperone as marker and (S)-sulpiride as test compound, again quantifying the nonbound marker but this time by scintillation counting. Both the run of the competition curve and the K<sub>i</sub> value determined for (S)-sulpiride were in good accordance with the results from the MS binding assays (Table 7.2).

The entire binding experiment was further validated by characterizing the test compounds in a conventional [<sup>3</sup>H]spiperone radioligand binding assay. This control experiment was conducted in analogy to the MS binding experiment except

**Table 7.2** Affinities (mean ± SEM, n = 3) for dopamine antagonists at D<sub>2</sub> receptors obtained by MS-binding assays and by radioligand binding assays, respectively [62]. n.d. Not determined.

	Spiperone (nonbound)		<sup>3</sup> H]Spiperone (nonbound)		<sup>3</sup> H]Spiperone (bound)	
	IC <sub>50</sub> (nM)	K <sub>i</sub> (nM)	IC <sub>50</sub> (nM)	K <sub>i</sub> (nM)	IC <sub>50</sub> (nM)	K <sub>i</sub> (nM)
(+)-Butaclamol	140 ± 50	43 ± 10	n.d.	n.d.	44 ± 8	8.7 ± 1.8
Chlorpromazine	560 ± 90	220 ± 20	n.d.	n.d.	120 ± 10	23 ± 3
(S)-Sulpiride	210 ± 30	65 ± 8	110 ± 25	45 ± 9	120 ± 20	25 ± 4

that the concentration of the receptor ( $T_{\text{tot}}$ ) was  $\ll K_d$  and the bound radioligand was quantified after filtration as a separation step. For the test compounds (+)-butaclamol, chlorpromazine and (S)-sulpiride, the resulting  $K_i$  values determined by conventional [ $^3\text{H}$ ]spiperone binding assays were 2.5- to 10-fold lower than those established by MS binding studies (Table 7.2) [62]. The reasons for the, partly considerable, deviations are still unknown. However, they are obviously not the result of the mass spectrometric quantitation as the identically conducted control experiment quantifying nonbound [ $^3\text{H}$ ]spiperone using (S)-sulpiride as competitor had yielded results similar to the MS binding assay. The main cause is presumably the large amount of membrane fraction required to obtain a sufficient concentration of binding sites for the marker. Particularly, the lipophilic test compounds (+)-butaclamol and chlorpromazine might show a high amount of nonspecific binding to the membrane fraction resulting in ligand depletion which would easily explain the rise of  $\text{IC}_{50}$  and  $K_i$  values, respectively. Of course this problem could be effortlessly solved by employing a more appropriate receptor source with a higher receptor density, e.g. a membrane fraction of a heterologous expression system, or by using a more powerful mass spectrometer.

### 7.3.1.2 Library Screening and Competition Assays for $\mu$ -Opioid Receptors

#### 7.3.1.2.1 Opioid Receptors

Opioid receptors also belong to the group of G protein-coupled receptors. Besides controlling pain perception, they control functions as widely different as breathing, gastrointestinal motility, diuresis, temperature regulation, or cognitive processes. Binding assays for opioid receptors are therefore indispensable for the search for potential drugs in many indication areas. Opioid receptors can be divided into three subtypes,  $\mu$ -,  $\kappa$ - and  $\delta$ -receptors. The pharmacologic effects mediated by these receptor subtypes are considerably different. Therefore, radioligand binding assays characterizing the affinity of test compounds at opioid receptor subtypes represent an essential primary screening tool in the search for, e.g. new analgesics [63, 64].

The competitive MS binding assays for  $\mu$ -opioid receptors were established using a membrane fraction of CHO-K1 cells that express human  $\mu$ -receptors in contrast to the native brain membrane preparations used in the dopamine receptor MS binding assays. The use of a heterologously expressed target offers the advantage that a relatively high concentration of a comparatively pure target can be employed, which in turn means that the requirement on the marker's affinity and selectivity as well as the sensitivity required for the quantitation of the marker is less demanding.

#### 7.3.1.2.2 Library Screening with Identification of Hits

MS binding assays are also useful for library screening with subsequent hit identification. The concept is simple. First, a library is searched for active compounds in a competitive binding assay. If the result is positive (which is indicated by an increase of the marker signal), the target bound hit is liberated and identified.



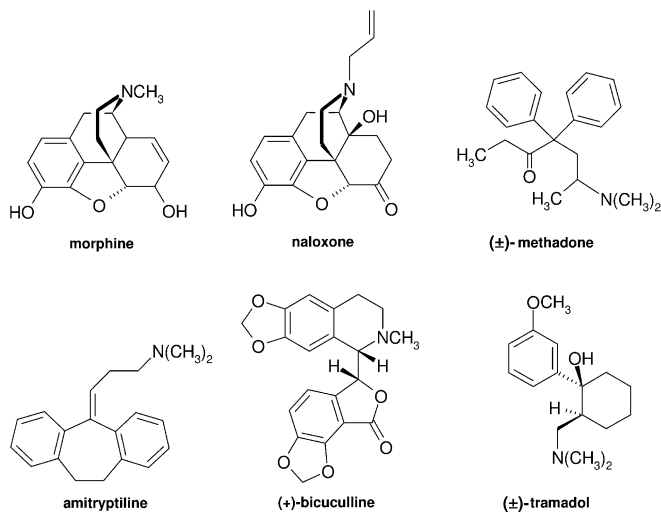


**Fig. 7.11** Structures of compounds used in competitive MS binding assays for  $\mu$ -opioid receptors.

Two artificial compound libraries were chosen as compound mixtures, of which library 1 was composed only of “dummy” ligands (acetanilide, amitryptiline, benzoic acid, (+)-bucuculline, 4-chloraniline, 2,3-dichloraniline, methylbenzoate, phenol, tramadol; see Fig. 7.11), whereas library 2 contained, in addition to these compounds, naloxone, a known  $\mu$ -opioid receptor ligand.

The assay was conducted at 10 nM morphine (Fig. 7.11) which had been chosen as native marker and a  $\mu$ -opioid receptor concentration of 5.5 nM (in 50 mM Tris-HCl, 5 mM  $\text{MgCl}_2$ ). After incubation and centrifugation to separate the non-bound marker, the resulting supernatants were directly analyzed by LC-ESI-MS/MS. Control experiments without competitor (representing total binding) revealed 2.32 nM nonbound morphine whereas 7.73 nM nonbound morphine were found in the presence of 50  $\mu\text{M}$  ( $\pm$ )-methadone (representing  $[\text{M}_{\text{tot}}] - \text{nonspecific binding}$ , Fig. 7.11, Table 7.3). Experiments employing the libraries at final concentrations of 1  $\mu\text{M}$  and 10 nM per compound led in the case of library 1 to a concentration of nonbound morphine in the range of the control experiment without competitor. In the binding samples containing library 2, however, the concentration of nonbound morphine was significantly higher than in the control experiment without competitor (Table 7.3).

Accordingly, library 2 in contrast to library 1 must contain (at least) one ligand that, in concentrations of 1  $\mu\text{M}$  and 10 nM, is capable of reducing the specific binding of morphine to the  $\mu$ -opioid receptor. Considering the composition of the two libraries, the conclusion that the component with an affinity for the  $\mu$ -opioid receptor must be naloxone is naturally trivial, but this issue could also be addressed by further examining the relevant binding samples (Fig. 7.12).

**Table 7.3** Nonbound morphine in MS binding assays at  $\mu$ -opioid receptors [65].

Conditions		Morphine
Compound	Concentration	Nonbound
Control	—	2.32 nM
( $\pm$ )-Methadone	50 $\mu$ M	7.73 nM
Library 1	10 nM	2.76 nM
Library 1	1 $\mu$ M	2.03 nM
Library 2	10 nM	5.02 nM
Library 2	1 $\mu$ M	7.92 nM

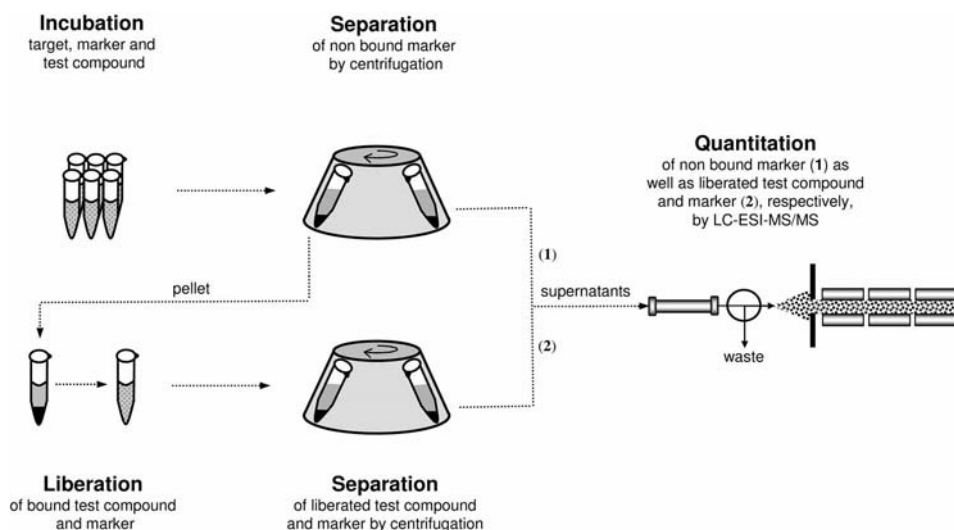


**Fig. 7.12** Schematic flowchart of the competitive MS binding assay for  $\mu$ -opioid receptors including liberation of bound marker and test compounds, respectively. After incubation of the target ( $\mu$ -opioid receptor) in the presence of the marker (morphine) and a compound library, the binding samples are centrifuged to separate bound from nonbound marker. Subsequently, the nonbound marker in the resulting supernatant is quantified by LC-ESI-MS/MS without further sample preparation (route 1).

In the case that a signal reduction for the nonbound marker is caused by a compound library, the respective pellet remaining after centrifugation is resuspended in buffer containing a large excess of competitor [( $\pm$ )-methadone] to liberate the bound marker and bound library components. After centrifugation, the marker and the hits liberated from the target are analyzed in the resulting supernatant by LC-ESI-MS/MS (route 2).

To this end, the pellets remaining from the competitive MS binding assay were, after several washing steps, resuspended in binding buffer and incubated with a great excess of competitor (50  $\mu\text{M}$  ( $\pm$ )-methadone) to liberate the unknown bound ligand (as well as the bound marker). Then the supernatants obtained by centrifugation were analyzed by LC-ESI-MS/MS. In addition to morphine as the marker, naloxone was identified as the hit that had been searched for. Thereby, the relative concentrations of marker (2.93 nM) and hit (2.30 nM) pointed to the fact that the hit had a similar affinity to the  $\mu$ -opioid receptor as the marker [65].

#### 7.3.1.2.3 Competition Assays Taking the Depletion of Marker and Ligand into Account

Unlike radioligand binding assays that only allow quantitation of the radioligand itself, binding assays based on MS detection offer the opportunity to quantify any additional ligand. This allows another interesting application: competitive MS binding assays observing both the concentration of the marker and the test compound at the same time (via their nonbound portion). In competition curves, the concentration of the bound (and accordingly in this case the nonbound) marker is plotted against the concentration of the test compound. Of course, in the strict sense of the law of mass action, the free and not the nominal concentration of the test compound is relevant for the competition curve. Competition curves generated by radioligand binding assays however, are usually based on the nominal concentration of the test compound which can deviate substantially from its free concentration (due to specific as well as nonspecific binding). Therefore, quantitation of the nonbound test compound would enhance the accuracy of the affinity determined for the test compound by eliminating this source of error.

This strategy was realized in a competitive MS binding assay examining the affinity of naloxone for  $\mu$ -opioid receptors (with morphine as marker under the conditions described above for library screening). The respective experiments led

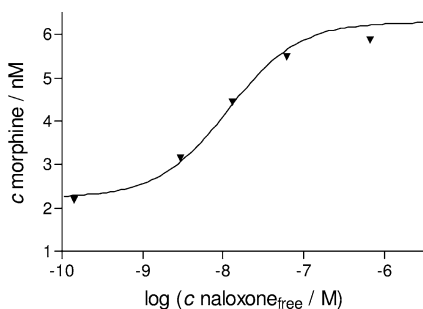


**Fig. 7.13** Representative binding curve obtained by nonlinear regression from a competitive MS binding assay for  $\mu$ -opioid receptors, in which naloxone competes with morphine as marker. The points describe nonbound morphine quantified by LC-ESI-MS/MS at concentrations of nonbound naloxone determined simultaneously by LC-ESI-MS/MS.

to the binding curve shown in Fig. 7.13 in which the concentration of the non-bound marker is plotted against the concentration of free naloxone.

Taking depletion of the marker [according to Eq. (7), Section 7.3.1] and the ligand (by analyzing the binding curve based on the concentration of free naloxone) into account, a  $K_i$ -value of naloxone for  $\mu$ -receptors of 1.6 nM was calculated (using a  $K_d$  value of 2.0 nM for morphine, according to Raynor et al. [66]). Without correction for free naloxone, a  $K_i$  value of 7.9 nM was obtained. Interestingly, the first but not the second value is in surprisingly good accord with the result of Raynor et al., who in a conventional radioligand binding assay with [ $^3\text{H}$ ]DAMGO as marker determined a  $K_i$  value of 1.4 nM for naloxone at human  $\mu$ -receptors [66].

### 7.3.2

#### MS Binding Assays Quantifying the Bound Marker

Another promising setup for MS binding assays is the quantitation of the bound native marker. Such MS binding experiments would allow “transferring” already established radioligand binding studies with relatively small effort to the format of MS binding assays and produce comparable results. Additionally, this approach has several other advantages.

Considering the higher target concentrations generally necessary for MS binding assays with quantitation of the nonbound marker, it is obvious that a depletion of the test compound can very easily occur (particularly if  $K_i < K_d$ ). In case of MS binding assays with quantitation of the bound marker this should be less of a concern, as the target concentrations are, in general, distinctly lower (see Section 7.3.1 and [67]).

It is also interesting to note that MS binding assays performed in analogy to a radioligand binding assay determining the amount of bound native marker allows binding assays that would only be possible with radioligands in some kind of a “mixed mode”: it is not always possible to examine the entire concentration range with pure radioligands (“hot only”) due to the restricted availability, high costs or low affinity of the radioligand. Therefore, conducting saturation assays requires that mixtures of labeled and unlabeled, i.e. “hot” and “cold”, markers are used [36, 68].

To conduct MS binding assays with ligand liberation, similar prerequisites have to be met as generally described for MS binding assays (see Section 7.3). Besides high affinity and selectivity of the marker for the target, these include in this setup a quantitation method with a sufficient sensitivity, or in other words with a lower limit of quantitation (LLOQ) low enough to reliably quantify the low quantities of marker commonly present in such studies. For this last point, one important aspect is also the target density of the target material used in the assay: A sufficient amount of marker should be bound to ensure that a satisfactory signal intensity is reached. Yet binding of the marker and ligand should still be kept low enough to ensure that depletion is less than 10%. Also in this context, cell lines heterologously expressing the desired target seem advantageous [69–71].

The separation of the target–marker complex from the free marker can be achieved with different techniques (e.g. centrifugation or filtration). When conducting binding experiments with membrane-bound targets, filtration is generally preferred due to its speed and effectiveness.

One of the essential steps when developing MS binding assays quantifying the bound marker is the liberation of the marker from the target–marker complex retained, e.g. in the filter, and its quantitation in the relevant eluate [39, 72–75]. A very practical way to implement this is using filter plates in the 96-well format with suitable vacuum manifolds where elution can be directed to another 96-well plate. Generally, glass fiber filters are often used in radioligand binding assays which are also available in different versions in the 96-well format [72].

The liberation of the marker from the target–marker complex after separation should be complete and reproducible and include both the specifically and non-specifically bound marker. To achieve this, common methods for protein denaturation should be suitable (e.g. change in pH value, addition of organic solvents, chaotropic salts, detergents or increase in temperature) [76, 77]. However, it has to be kept in mind that the denaturation method should not interfere with the subsequent quantitation. When using ESI-MS for quantitation for example, high salt concentrations can lead to signal suppression and impair the LLOQ of the method [78, 79]. Therefore, denaturation with organic solvents seems to be more advantageous when using ESI-MS for quantitation.

A practical advantage of MS binding assays quantifying the bound marker after liberation is the “decoupling” of biological binding assay and analytical MS quantitation. In this case the choice of buffer is less restricted as the incubation buffer is mostly removed in the separation step and therefore can contain, for example, high salt concentrations or other additives that would negatively influence MS quantitation. For the denaturation the only aspect that has to be kept in mind is that a method is chosen with which the marker is transferred into a solution that does not interfere with the quantitation.

However, the solution obtained after denaturation might include, depending on the application, other components besides the liberated marker (“matrix”). If a small amount of target material is used in the binding assay, the quantity of remaining matrix will be so low that it hardly disturbs the quantitation and the sample can be measured directly by LC-MS without further sample preparation (e.g. membrane filtration or solid phase extraction [78]).

In the following, an example of this new kind of MS binding experiment is presented as a straightforward alternative to conventional radioligand binding assays and suitable for the performance of saturation, competition and kinetic binding assays [80].

### 7.3.2.1 Saturation Assays for mGAT1

#### 7.3.2.1.1 GABA Transporters

$\gamma$ -Amino butyric acid (GABA) is the most important inhibitory neurotransmitter in the central nervous system. In the last three decades, GABAergic neuro-

transmission was linked, directly or indirectly, to a variety of neuro-pathological and psychiatric medical conditions, e.g. epilepsy, Huntington's chorea, Parkinson, Tardive dyskinesia, schizophrenia, anxiety, depression and other behavioral disorders. The GABA transporters (GATs) that remove the neurotransmitter from the synaptic cleft after its release are very interesting targets for the development of new agents for the indications listed above [81]. Inhibitors of these transporters can extend the presence of GABA in the synaptic cleft and therefore increase the inhibitory effect of the neurotransmitter. For the GABA transporters that are a part of the superfamily of  $\text{Na}^+/\text{Cl}^-$ -dependent transporters four subtypes are known. Among them the transporter subtype most frequently found in the brain is GAT1, an already validated target in the search for anticonvulsants [82–85]. A successful example is the agent tiagabine, an effective and selective inhibitor of GAT1 which has already been introduced in the therapy of epilepsy in the form of the drug Gabitril [81–83, 85–88].

For *in vitro* screening of new ligands at GABA transporters uptake assays are generally used which measure the uptake of [ $^3\text{H}$ ]GABA into whole cells or synaptosomes [89–92]. However, this type of assay has significant practical drawbacks. It is necessary to employ whole cells or synaptosomes that have to stay intact during the entire course of the experiment, i.e. also during the separation step, since the breakdown of the cell membrane or the synaptosome would cause a loss of substrate ([ $^3\text{H}$ ]GABA). In contrast, conventional binding assays which determine not the functionality but the affinity for the GABA transporter have the advantage that membrane fractions are sufficient for these experiments [93, 94].

In 1990, Braestrup and coworkers reported the first radioligand binding assay for GABA transporters [95–97]. The radioligand they employed in their experiments was [ $^3\text{H}$ ]tiagabine. Unfortunately, neither [ $^3\text{H}$ ]tiagabine nor other radioligands for binding assays to GAT1 are readily commercially available. There is, however, no shortage of affine and selective ligands for GAT1 [98]. This is another intriguing fact highlighting the advantages of MS binding assays which can be conducted without a labeled marker.

#### 7.3.2.1.2 Basic Principles

The MS binding assay quantifying the amount of bound marker for the murine GAT1 transporter (mGAT1) was conducted as follows: The source of mGAT1 was a recombinant cell line that expressed the transporter in sufficient density [99]. Of the several possible ligands selective for GAT1, NO 711 (1f in Fig. 7.17) [96, 100] was chosen as a marker because the compound not only shows a high affinity and selectivity for GAT1 but can also be quantified in very low concentrations by LC-ESI-MS/MS (LLOQ = 18 pM; see Fig. 7.14).

It had been shown that 50 mM Tris-citrate buffer with 1 M NaCl was a suitable incubation buffer for the binding to GAT1 [95]. The high salt concentration in this incubation buffer caused no problems in the new MS binding assays, since most of the incubation buffer was removed before the liberation step. The separation of the bound from the nonbound marker was conducted by filtration over glass fiber filters as common in radioligand binding assays.

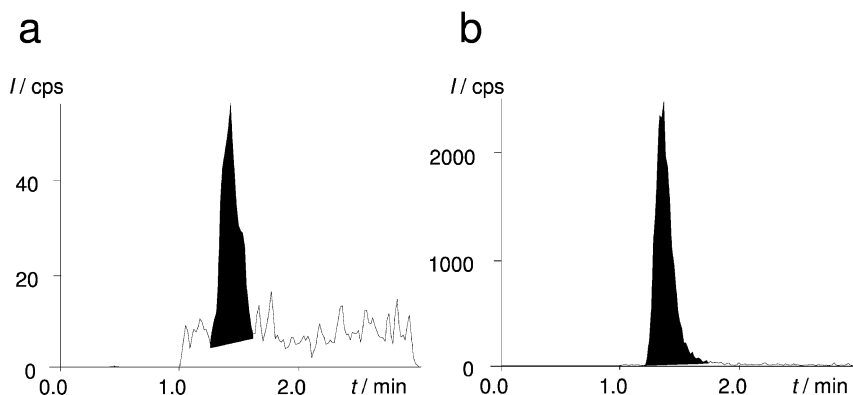


**Fig. 7.14** Example for standard matrix sample. Matrix was obtained by incubation of mGAT1-membrane preparation in Tris-NaCl buffer ( $\sim 10$   $\mu\text{g}$  protein content), subsequent filtration and elution with methanol. This empty matrix was then spiked with NO 711 and  $[\text{}^2\text{H}_{10}]\text{NO}$  711 to obtain standard matrix samples for LC-MS method validation purposes. (a) Trace for 0.015 nM NO 711 (mass transition  $381 \rightarrow 180$ ,  $m/z$ ). (b) Trace for 1 nM  $[\text{}^2\text{H}_{10}]\text{NO}$  711 ( $391 \rightarrow 190$ ,  $m/z$ ) in the same sample.

For the liberation of the bound marker from the marker–target complex, a simple denaturation with methanol proved to be extremely effective. A drying step before the methanol denaturation and an internal standard (deuterated analog of NO 711,  $[\text{}^2\text{H}]\text{NO}$  711; **1g** in Fig. 7.17) added to the denaturation reagent further improved the precision of the method. The initially bound marker liberated this way was collected in a 96-well plate and quantified by an isocratic RP-HPLC method followed by ESI-MS/MS detection via the internal standard (see Fig. 7.14). Figure 7.15 gives an overview over the procedure of an MS binding assay with liberation of the bound marker.

### 7.3.2.1.3 MS Saturation Assays

According to the procedure for the MS binding assays described above, saturation assays with the native marker NO 711 were conducted at mGAT1, after the incubation period was determined (see Section 7.3.2.3). A constant target concentration (10–20  $\mu\text{g}$  protein per well, according to Bradford;  $\sim 1$  nM mGAT1) was incubated with increasing NO 711 concentrations (2–200 nM) and allowed to reach equilibrium. After separation over the 96-well glass fiber filter plates, bound marker was liberated and quantified by LC-ESI-MS/MS. A representative saturation isotherm resulting from these experiments is given in Fig. 7.16.

The results of this saturation assay were validated by direct comparison to conventionally conducted radioligand binding assays using  $[\text{}^3\text{H}]\text{NO}$  711 as marker [80, 100]. Not only due to financial considerations, hot/cold dilutions had to be used in the radioligand binding assays, in contrast to the MS binding assays

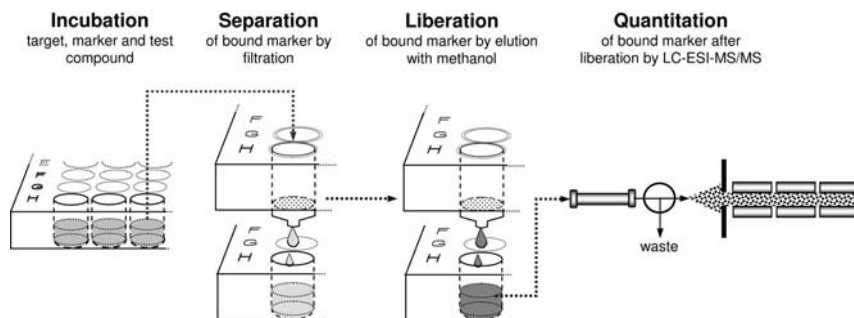


**Fig. 7.15** Schematic flowchart of MS binding assays quantifying bound marker. Incubation of the target (mGAT1) in presence of the marker (NO 711) and a test compound is conducted in a 96-well plate. The bound marker is separated from the nonbound marker by vacuum filtration. In the next step the target bound marker remaining on the filter is liberated with methanol. Finally, the liberated marker is quantified by LC-ESI-MS/MS.

where the entire marker concentration range could be covered with native (“cold”) marker only. As can be seen from Table 7.4, the values of  $K_d$  and  $B_{max}$  determined in both binding studies are in good accord with each other.

Clearly, as indicated by these results, MS binding assays quantifying the originally bound marker can be performed in the same manner as radioligand binding assays to determine the affinity constant of a marker and they are just as efficient.

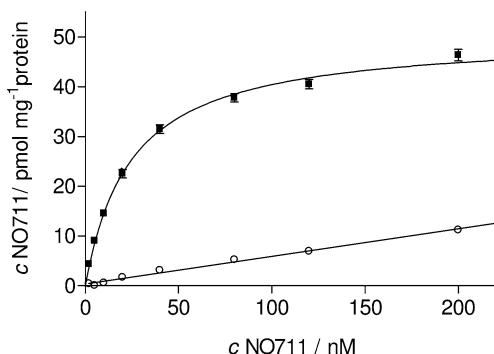


**Fig. 7.16** Saturation isotherm of NO 711 binding to mGAT1-membrane fraction as measured in MS binding experiments. One representative example from a series of identical experiments is shown. Total binding of NO 711 (■; 10  $\mu$ g protein according to Bradford). Nonspecific binding (○) measured as binding of NO 711 in the presence of 10 mM GABA. Each data point depicts the mean  $\pm$  SEM from triplicate values.



**Table 7.4** Comparison of results from saturation binding experiments using native NO 711 in MS binding experiments and [ $^3\text{H}$ ]<sub>2</sub>NO 711 in radioligand binding experiments. All values represent mean  $\pm$  SEM from independent experiments [80].

	MS binding	Radioligand binding
$K_d$	$23.4 \pm 2.19$ nM ( $n = 15$ )	$35.9 \pm 1.81$ nM ( $n = 19$ )
$B_{\text{max}}$	$34.6 \pm 4.02$ pmol/mg protein ( $n = 14$ )	$26.0 \pm 2.64$ pmol/mg protein ( $n = 22$ )

### 7.3.2.2 Competition Assays for mGAT1

Additionally, MS binding assays comparable to competitive radioligand binding assays were conducted for the target–marker system mGAT1/NO 711. A wide variety of ligands with different lipophilicity and affinity to the target were tested (see Fig. 7.17). The experiments were conducted in a way that a constant concentration of both the target (10–20  $\mu\text{g}$  protein per well, according to Bradford) and the marker (10 nM NO 711) were incubated with increasing concentrations of each test compound under conditions, as described for the saturation experiments. The bound native marker was then quantified by LC-MS/MS after the separation and liberation steps. From the binding curves obtained, the affinity constants of the test compounds ( $K_i$ ) were calculated using the Cheng–Prusoff equation [see Eq. (3), Section 7.2.1], since marker-depletion was negligible (see Fig. 7.18 for a representative example for compound (**S**)-**3b**).

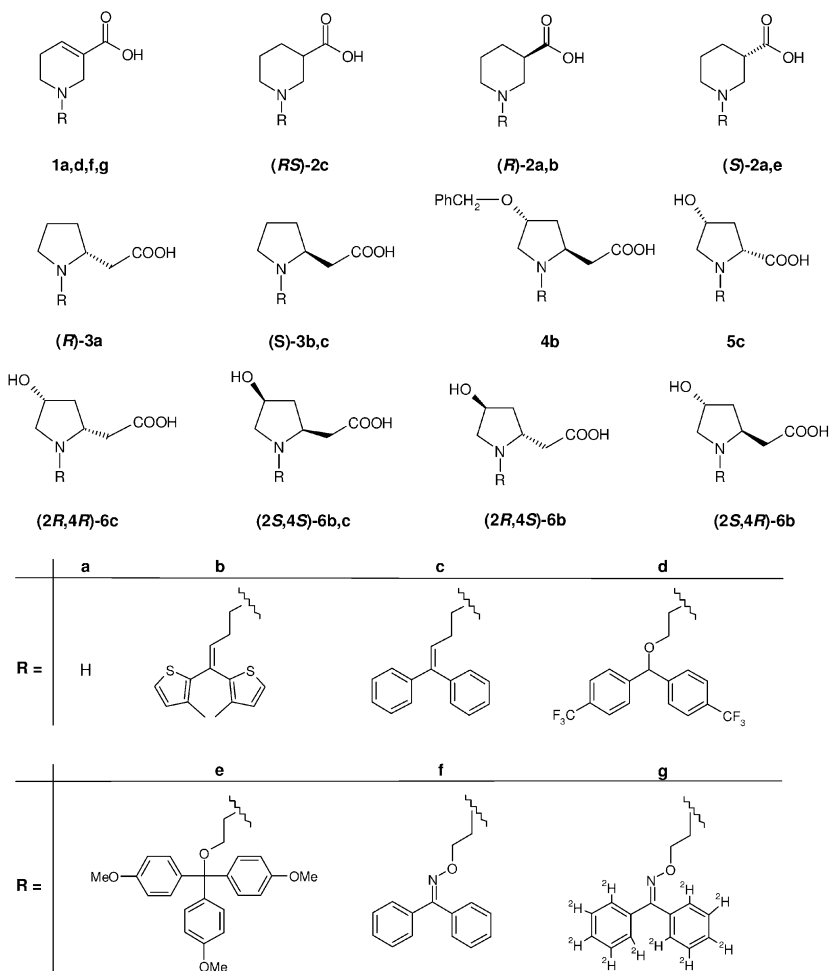
The results of the competitive MS binding assays quantifying the bound marker were again compared to conventional radioligand binding assays (based on [ $^3\text{H}$ ]NO 711) for the same test compounds. Table 7.5 shows the results of both the competitive MS binding studies and the competitive radioligand binding assays in comparison.

Figure 7.19 shows a direct correlation between  $\text{p}K_i$  values derived from the MS binding assays described above and those from radioligand binding assays. The rise of the graph of  $1.010 \pm 0.01604$  shows ( $r^2 > 0.99$ ) that  $\text{p}K_i$  values resulting from both binding assays are nearly identical.

### 7.3.2.3 Kinetic Assays for mGAT1

For the establishment of saturation and competitive MS binding assays described above, association and dissociation assays with mass spectrometric quantitation of the native marker had also been conducted.

In association assays, a constant NO 711 concentration (in the region of  $K_d$ ) was incubated with the target. Using the previously described method, the binding experiments are terminated after different periods of time and quantified by LC-ESI-MS/MS. The binding curve derived from the data is shown in Fig. 7.20. It



**Fig. 7.17** Structures of compounds tested in competitive MS binding assays quantifying bound marker.

is clearly visible that the binding of the marker to the target reaches steady state after approximately 30 min. The observed association rate constant  $k_{\text{obs}}$  calculated from these experiments amounted to  $0.19 \pm 0.01 \text{ min}^{-1}$ .

A further characteristic of ligand–target interaction is the dissociation rate constant. Dissociation experiments are not only an important criterion for the establishment of binding assays, they also can show the reversibility of the specific marker binding at the target [16], which is usually verified by dissociation experiments (see also Section 7.2.1). In the MS binding assays presented here, GABA was used as a competitor to initiate dissociation. The experiment was then termi-

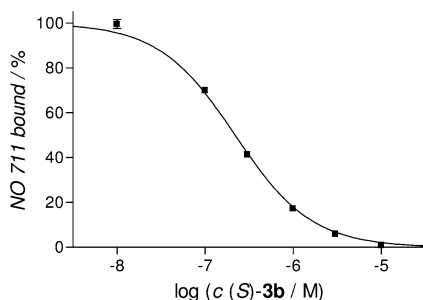


**Fig. 7.18** Representative binding curve for competitive MS-binding experiments quantifying bound marker. Compound (S)-3b was tested (see Fig. 7.17 for structure). Data points represent specific binding of the marker NO 711 (mean  $\pm$  SEM from triplicate values).

**Table 7.5** Affinities (mean  $\pm$  SEM,  $n = 3$ ) for GAT1 inhibitors at mGAT1–membrane preparation obtained in competitive binding experiments using NO 711 for competitive MS binding quantifying bound marker and [ $^3\text{H}_2$ ]NO 711 in competitive radioligand binding [80].

Test compound	MS binding $K_i$ ( $\mu\text{M}$ )	Radioligand binding $K_i$ ( $\mu\text{M}$ )
GABA	$83.2 \pm 8.9$	$115 \pm 4.9$
<i>Trans</i> -4-aminocrotonic acid (TACA)	$221 \pm 7.5$	$233 \pm 25$
D,L-4-Amino-3-hydroxybutyric acid	$3719 \pm 279$	$5280 \pm 294$
D,L-3-Amino- <i>n</i> -butyric acid	$1043 \pm 266$	$1341 \pm 48.8$
(S)-4-Amino-2-hydroxy butyric acid	$251 \pm 28$	$236 \pm 34$
Guvacine ( <b>1a</b> )	$146 \pm 16$	$157 \pm 21$
CI 966 ( <b>1d</b> )	$0.245 \pm 0.024$	$0.180 \pm 0.018$
SKF89976 A [( <i>RS</i> )- <b>2c</b> ]	$0.192 \pm 0.007$	$0.186 \pm 0.008$
( <i>R</i> )-Nipectic acid [( <i>R</i> )- <b>2a</b> ]	$32.3 \pm 3.3$	$24.5 \pm 4.2$
Tiagabine[( <i>R</i> )- <b>2b</b> ]	$0.041 \pm 0.009$	$0.059 \pm 0.009$
( <i>S</i> )-Nipectic acid [( <i>S</i> )- <b>2a</b> ]	$1049 \pm 116$	$1324 \pm 280$
( <i>S</i> )-SNAP 5114 [( <i>S</i> )- <b>2e</b> ]	$27.4 \pm 1.1$	$34.3 \pm 2.0$
( <i>R</i> )-Homoproline [( <i>R</i> )- <b>3a</b> ]	$444 \pm 85$	$528.0 \pm 3.5$
( <i>S</i> )- <b>3b</b> <sup>a</sup>	$0.179 \pm 0.012$	$0.212 \pm 0.003$
( <i>S</i> )- <b>3c</b> <sup>a</sup>	$0.075 \pm 0.006$	$0.082 \pm 0.001$
<b>4b</b> <sup>b</sup>	$55.1 \pm 3.93$	$32.7 \pm 1.02$
<b>5c</b> <sup>b</sup>	$6.96 \pm 0.321$	$6.70 \pm 0.85$
(2 <i>R</i> ,4 <i>R</i> )- <b>6c</b> <sup>b</sup>	$3.53 \pm 0.39$	$3.45 \pm 0.22$
(2 <i>S</i> ,4 <i>S</i> )- <b>6b</b> <sup>b</sup>	$0.517 \pm 0.065$	$0.421 \pm 0.05$
(2 <i>S</i> ,4 <i>S</i> )- <b>6c</b> <sup>b</sup>	$1.13 \pm 0.28$	$1.07 \pm 0.18$
(2 <i>R</i> ,4 <i>S</i> )- <b>6b</b> <sup>b</sup>	$0.954 \pm 0.07$	$1.44 \pm 0.08$
(2 <i>S</i> ,4 <i>R</i> )- <b>6b</b> <sup>b</sup>	$1.20 \pm 0.26$	$0.921 \pm 0.11$

<sup>a</sup> Reference [105].

<sup>b</sup> Reference [106].

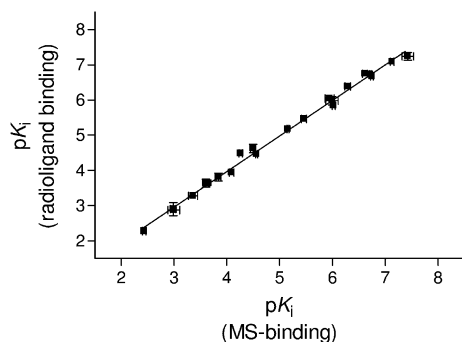


**Fig. 7.19** Correlation between  $pK_i$  values from competitive MS binding assays and radioligand binding assays.

nated after a range of different time periods and the marker subsequently quantified by LC-ESI-MS/MS. The resulting dissociation curve is depicted in Fig. 7.21. It shows the typical curve progression for a reversible binding of a ligand to its target [96, 101]. The dissociation rate constant calculated from these experiments was  $k_{-1} = 0.094 \pm 0.003 \text{ min}^{-1}$ .

Knowing the rate constants of the target–marker binding experiment gives a different way to determine the dissociation constant  $K_d$  independently from saturation experiments [see Eq. (4) in Section 7.2.1]. For this purpose, the association rate constant  $k_{+1}$  has to be calculated from  $k_{\text{obs}}$  according to Eq. (8):

$$k_{+1} = \frac{(k_{\text{obs}} - k_{-1})}{[M_{\text{tot}}]} \quad (8)$$

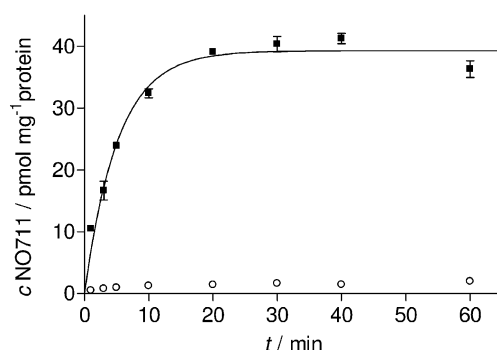


**Fig. 7.20** Kinetic MS binding study quantifying bound marker – association experiment. Total binding (■) of NO 711 (20 nM; incubation temperature 37 °C) to mGAT1. Nonspecific binding (○) was determined as binding of NO 711 in the presence of 10 mM GABA. One representative example is shown. Data points represent each mean  $\pm$  SEM from triplicate values.

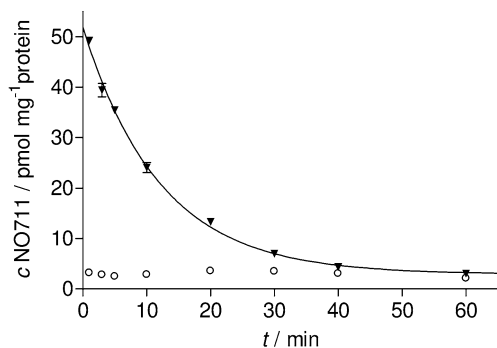


**Fig. 7.21** Kinetic MS binding study quantifying bound marker – dissociation experiment. Total binding (▼) of NO 711 (20 nM; incubation temperature 37 °C) to mGAT1. GABA (10 mM) was added after 60 min preincubation to initiate dissociation ( $t = 0$  min). Nonspecific binding (○) was determined as binding of NO 711 in the presence of 10 mM GABA. One representative example is shown. Data points represent each mean  $\pm$  SEM from triplicate values.

This yielded a  $k_{+1}$  of  $0.0091 \pm 0.002 \text{ nM}^{-1} \text{ min}^{-1}$  for NO 711 binding to mGAT1. Hence, the equilibrium dissociation constant calculated from kinetic MS binding experiments resulted in  $K_d = 11.7 \pm 2.5 \text{ nM}$ . This is in good accord with  $K_d$  determined in MS saturation binding experiments and confirms the validity of the new setup.

## 7.4

### Summary and Perspectives

As the examples described here show, the goals that so far have been pursued with radioligand binding assays can, in principle, also be achieved with MS binding assays based on the mass spectrometric quantitation of native, i.e. nonlabeled markers. MS binding assays can be conducted in an experimental setup in analogy to radioligand binding assays, i.e. quantifying the amount of marker bound to the target. In contrast to radioligand binding assays, however, the quantitation in MS binding assays does not proceed at the level of the target–marker complex directly after its separation from the binding sample. In MS binding assays, the marker is liberated from the target–marker complex, before it is quantified by LC-ESI-MS/MS. In this way, the basic types of binding assays, saturation, competition and kinetic assays can be realized. Under certain conditions (with a significant amount of  $M_{\text{tot}}$  being bound to the target T), MS binding assays can also be arranged in a way that the nonbound marker can be quantified by LC-ESI-MS/MS directly from the supernatant obtained by centrifugation of the binding sample.

Irrespective of certain limitations, this method offers the opportunity to efficiently conduct competitive binding assays.

Although the applications presented here are exclusively based on membrane-bound targets, MS binding assays are not restricted to them. Generally, every kind of target can be examined in MS binding assays as long as suitable markers are available. The search for suitable markers, however, is in contrast to radioligand binding assays (or assays based on fluorescent markers), greatly facilitated by a much wider repertoire of potential markers, since they are used in their native, i.e. unlabeled form. The most demanding task in MS binding assays, the reliable mass spectrometric quantitation of the marker, is increasingly facilitated by the continuously improving sensitivity of modern mass spectrometers. If the sensitivity of the mass spectrometer tends to limit the quantitation of the marker in the binding assay, it is still possible to partly compensate this problem by choosing a higher target concentration than commonly used in radioligand binding assays.

The throughput that can be achieved in MS binding assays depends on both the workflow chosen for the binding experiments as well as the mass spectrometric quantitation of the marker. In the binding experiments itself, the throughput is – just as in radioligand binding assays – primarily dependent on the separation step. MS binding assays based on filtration as separation step can be performed in a 96-well plate format just as easily as radioligand binding assays. But in the analytical setup described here, HPLC dictates the speed of quantitation. Although quantitation in MS-binding assays generally requires more time than measuring radioactivity, the applications above show that it is possible to process several hundred samples a day, even with a very simple instrumentation. Since high-sensitivity quantitation of an analyte in a biological matrix by LC-MS is a quite frequent topic in the life sciences (e.g. in pharmacokinetics, see Chapter 13) there are a number of possibilities to significantly accelerate this process [78, 102–104].

Even though MS binding assays follow the principle of radioligand binding assays, their potential significantly exceeds that of the radioligand binding assays as shown by the applications described above. It is, for example, possible to use the marker in the binding assays, even in very high concentrations, or to identify structurally unknown hits in a library. To mention only one further example for other feasible options, it should be possible to track several targets simultaneously in one MS binding assay.

In summary, MS binding assays can be applied comparatively easily and universally without the inherent disadvantages of labeling. Thereby their reliability is approximately equal to that of radioligand binding assays. Therefore, it can be expected that MS binding assays will find increasing use in drug discovery.

## Acknowledgement

We thank Monika Simon for her assistance with editing and proofreading.

## References

- 1 Williams, M., Mehlin, C., Triggle, D. J.: Receptor targets in drug discovery and development, in *Burger's Medicinal Chemistry and Drug Discovery*, Vol. ii: *Drug Development*, ed. Abraham, D. J., John Wiley & Sons, New York, **2003**, pp 319–355.
- 2 Jenkinson, D. H.: Classical approaches to the study of drug–receptors interactions, in *Textbook of Receptor Pharmacology*, ed. Foreman, J.C., Johansen, T., CRC Press, Boca Raton, **2003**, pp 3–78.
- 3 Höfliger, M. M., Beck-Sickinger, A. G.: Receptor–ligand interaction, in *Protein–Ligand Interactions. From Molecular Recognition to Drug Design*, ed. Böhm, H.-J., Schneider, G., Wiley–VCH, Weinheim, **2003**, pp 107–135.
- 4 Hulme, E. C.: Preface, in *Receptor–Ligand Interactions. A Practical Approach*, ed. Hulme, E. C., IRL Press, Oxford, **1992**.
- 5 Wang, J.-X., Yamamura, H. I., Wang, W., Roeske, W. R.: The use of the filtration technique in *in vitro* radioligand binding assays for membrane-bound and solubilized receptors, in *Receptor–Ligand Interactions. A Practical Approach*, ed. Hulme, E. C., IRL Press, Oxford, **1992**, pp 213–234.
- 6 Sweetnam, P. M., Price, C. H., Ferkany, J. W.: Mass ligand screening as a tool for drug discovery and development, in *Burger's Medicinal Chemistry and Drug Discovery*, vol. i: *Principles and Practice*, ed. Wolff, M. E., John Wiley & Sons, New York, **1995**, pp 697–731.
- 7 Haylett, D. G.: Direct measurement of drug binding to receptors, in *Textbook of Receptor Pharmacology*, ed. Foreman, J.C., Johansen, T., CRC Press, Boca Raton, **2003**, pp 153–180.
- 8 Vogel, H. G.: Introduction. Strategies in drug discovery and evaluation, in *Drug Discovery and Evaluation. Pharmacological Assays*, ed. Vogel, H. G., Springer, Berlin, **2002**, pp 1–22.
- 9 Major, J. S.: Challenges of high throughput screening against cell surface receptors. *J. Recept. Signal Transduction Res.* **1994**, 15, 595–607.
- 10 Pope, A.J., Haupts, U.M., Moore, K.J.: Homogenous fluorescence readouts for miniaturized high-throughput screening: theory and practice. *Drug Discov. Today* **1999**, 4, 350–362.
- 11 Hovius, R., Vallotton, P., Wohland, T., Vogel, H.: Fluorescence techniques: shedding light on ligand–receptor interactions. *Trends Pharmacol. Sci.* **2000**, 21, 266–273.
- 12 Hemmlia, I., Mikkala, V.-M.: Time-resolution in fluorometry technologies, labels, and applications in bioanalytical assays. *Crit. Rev. Clin. Lab. Sci.* **2001**, 38, 441–519.
- 13 Handl, H. L., Gillies, R. J.: Lanthanide-based luminescent assays for ligand–receptor interactions. *Life Sci.* **2005**, 77, 361–671.
- 14 Tota, M.R., Daniel, S., Serotina, A., Mazina, K.E., Fong, M.F., Longmore, J., Strader, C.D.: Characterization of a fluorescent substance P analog. *Biochemistry* **1994**, 33, 13079–13086.
- 15 Turcatti, G., Vogel, H., Chollet, A.: Probing the binding domain of the NK2 receptor with fluorescent ligands: evidence that heptapeptide agonists and antagonists bind differently. *Biochemistry* **1995**, 34, 3972–3980.
- 16 Hulme, E. C., Birdsall, N. J. M.: Strategy and tactics in receptor-binding studies, in *Receptor–Ligand Interactions. A Practical Approach*, ed. Hulme, E. C., IRL Press, Oxford, **1992**, pp 63–176.
- 17 Bennett, J. P. Jr, Yamamura, H. I.: Neurotransmitter, hormone, or drug receptor binding methods, in *Neurotransmitter Receptor Binding*, ed. Yamamura, H. I., Enna, S. J., Kuhar, M. J., Raven Press, New York, **1985**, pp 61–89.
- 18 Williams, M., Sills, M. A.: Quantitative analysis of ligand–receptor interaction, in *Comprehensive Medicinal Chemistry*, vol. iii:

- Membranes & Receptors*, ed. Emmett, J. C., Pergamon Press, Oxford, **1990**, pp 45–80.
- 19 Titeler, M.: Binding theory and methodology, in *Receptor Pharmacology and Function*, ed. Williams, M., Glennon, R. A., Timmermans, P. B. M. W. M., Marcel Dekker, New York, **1989**, pp 17–45.
  - 20 Rahman, A., Choudhary, M. I., Thomsen, W. J.: Radioligand binding assays, in *Bioassay Techniques for Drug Development*, ed. Rahman, A., Choudhary, M. I., Thomsen, W. J., Harwood Academic Publishers, Amsterdam, **2001**, pp 179–218.
  - 21 Bylund, D.B., Deupree, J. D., Toews, M.L.: Radioligand-binding methods for membrane preparations and intact cells, in *Methods in Molecular Biology*, vol. 259: *Receptor Signal Transduction Protocols*, ed. Willars, G. B., Challiss, R.A.J., Humana Press, Totowa, **2004**, pp 1–28.
  - 22 Cheng, Y.-C., Prusoff, W.H.: Relationships between the inhibition constant ( $K_i$ ) and the concentration of inhibitor which causes 50 per cent inhibition ( $IC_{50}$ ) of an enzymatic reaction. *Biochem. Pharmacol.* **1973**, 22, 3099–3108.
  - 23 Hulme, E. C., Buckley, N. J.: Receptor preparations for binding studies, in *Receptor–Ligand Interactions. A Practical Approach*, ed. Hulme, E. C., IRL Press, Oxford, **1992**, pp 177–212.
  - 24 Jones, S. A., Parks, D. J., Klierer, S. A.: Cell-free ligand binding assays for nuclear receptors. *Methods Enzymol.* **2003**, 364, 53–71.
  - 25 Liu, J., Zacco, A., Piser, T. M., Scott, C. W.: Microplate gel-filtration method for radioligand-binding assays. *Anal. Biochem.* **2002**, 308, 127–133.
  - 26 Shrikhande, A., Courtney, C., Smith, D., Melch, M., McConkey, M., Bergeron, J., Wong, S. K.-F.: Fully automated radioligand binding filtration assay for membrane-bound receptors. *BioTechniques* **2002**, 33, 932–937.
  - 27 Bosworth, N., Towers, P.: Scintillation proximity assay. *Nature* **1989**, 341, 167–168.
  - 28 Minor, L.K.: Assays for membrane tyrosine kinase receptors: methods for high-throughput screening and utility for diagnostics. *Expert Rev. Mol. Diagn.* **2005**, 5, 561–571.
  - 29 Brown, B.A., Cain, M., Broadbent, J., Tompkins, S., Henrich, G., Joseph, R., Casto, S., Harney, H., Greene, R., Delmondo, R., Ng, S.: in *High Throughput Screening*, ed. Devlin, J.P., Dekker, New York, **1997**, pp 317–328.
  - 30 Wu, S., Liu, B.: Application of scintillation proximity assay in drug discovery. *Biodrugs* **2005**, 19, 383–392.
  - 31 Van der Hee, R. M., Deurholt, T., Gerhardt, C. C., de Groene, E.: Comparison of 3 AT<sub>1</sub> receptor binding assays: filtration assay, Screenready™ target and WGA Flashplate®. *J. Biomol. Screening* **2005**, 10, 118–126.
  - 32 Walters, W. A., Namchuk, M.: Designing screens: how to make your hits a hit. *Nat. Rev. Drug Discov.* **2003**, 2, 259–266.
  - 33 Houston, J. G., Banks, M. N.: High-throughput screening for lead discovery, in *Burger's Medicinal Chemistry and Drug Discovery*, vol. ii: *Drug Development*, ed. Abraham, D. J., John Wiley & Sons, New York, **2003**, pp 37–69.
  - 34 Griersiefen, H., Hilgenfeld, R., Hillisch, A.: modern methods of drug discovery: an introduction, in *Modern Methods of Drug Discovery*, ed. Hillisch, A., Hilgenfeld, R., Birkhäuser, Basel, **2003**, pp 1–18.
  - 35 Noël, F., Mendonça-Silva, D. L., Quintas, L. E. M.: Radioligand binding assays in the drug discovery process: potential pitfalls of high throughput screenings. *Arzneim. Forsch./Drug Res.* **2001**, 51, 169–173.
  - 36 Rovati, G. E.: Ligand-binding studies: old beliefs and new strategies. *Trends Pharmacol. Sci.* **1998**, 19, 365–369.
  - 37 Takeuchi, T., Rechnitz, G.A.: Nonisotopic receptor assay for benzodiazepine receptors for utilizing



- a fluorophore labelled ligand. *Anal. Biochem.* **1991**, 194, 250–255.
- 38 Chen, L., Takeuchi, T., Rechnitz, G. A.: Development of a nonisotopic acetylcholine receptor assay for the investigation of cholinergic ligands. *Anal. Chim. Acta* **1992**, 267, 55–62.
  - 39 Janssen, M.J., Ensing, K., de Zeeuw, R.A.: A fluorescent receptor assay for benzodiazepines using coumarin-labeled desethylflumazenil as ligand. *Anal. Chem.* **2001**, 73, 3168–3173.
  - 40 Pedersen, S. E., Lurtz, M. M., Papineni, R. V. L.: Ligand-binding methods for analysis of ion channel structure and function. *Methods Enzymol.* **1999**, 294, 117–135.
  - 41 McGrath, J. C., Arrias, S., Daly, C. J.: Fluorescent ligands for the study of receptors. *Trends Pharmacol. Sci.* **1996**, 17, 393–399.
  - 42 Takeuchi, T., Nishikawa, T., Matsukawa, R., Matsui, J.: Nonisotopic receptor assay for benzodiazepine drugs using time-resolved fluorometry. *Anal. Chem.* **1995**, 67, 2655–2658.
  - 43 Inglese, J., Samama, P., Patel, S., Burbaum, J., Stroke, I. L., Appell, K. C.: Chemokine receptor–ligand interactions measured using time-resolved fluorescence. *Biochemistry* **1998**, 37, 2372–2377.
  - 44 Gao, X., Hsu, C.-K., Heinz, L. J., Morin, J., Shi, Y., Shukla, N. K., Smiley, D. L., Xu, J., Zhong, B., Sliker, L. J.: Europium-labeled melanin-concentrating hormone analogues: ligands for measuring binding to melanin-concentrating hormone receptors 1 and 2. *Anal. Biochem.* **2004**, 328, 187–195.
  - 45 Parker, G. J., Law, T. L., Lenoch, F. J., Bolger, R. E.: Development of high throughput screening assays using fluorescence polarization: nuclear receptor–ligand-binding and kinase/phosphatase assays. *J. Biomol. Screen.* **2000**, 5, 77–88.
  - 46 Pramanik, A.: Ligand-receptor interactions in live cells by fluorescence correlation spectroscopy. *Curr. Pharm. Biotechnol.* **2004**, 5, 205–212.
  - 47 Price, G.W., Riley, G.J., Middlemiss, D.N.: Biological evaluation of novel compounds, in *Medicinal Chemistry Principles and Practice*, ed. King, F. D., Royal Society of Chemistry, Cambridge, **2002**, pp 91–117.
  - 48 Lundqvist, T.: The devil is still in the details – driving early drug discovery forward with biophysical experimental methods. *Curr. Opin. Drug Discov. Dev.* **2005**, 8, 513–519.
  - 49 Cooper, M.A.: Advances in membrane receptor screening and analysis. *J. Mol. Recogn.* **2004**, 17, 286–315.
  - 50 Siegel, M. M.: Mass-spectrometry-based drug screening assays for early phases in drug discovery, in *Integrated Strategies for Drug Discovery Using Mass Spectrometry*, ed. Lee, M. S., John Wiley & Sons, New York, **2005**, pp 27–70.
  - 51 Daniel, J.M., Friess, S.D., Rajagopalan, S., Wendt, S., Zenobi, R.: Quantitative determination of noncovalent binding interactions using soft ionisation mass spectrometry. *Int. J. Mass Spectrom.* **2002**, 216, 1–27.
  - 52 Van Breemen, R. B.: Mass spectrometry and drug discovery, in *Burger's Medicinal Chemistry and Drug Discovery*, vol. i: *Drug Discovery*, ed. Abraham, D. J., John Wiley & Sons, New York, **2003**, pp 583–610.
  - 53 Ganem, B., Li, Y.-T., Henion, J.: Detection of noncovalent receptor–ligand complexes by mass spectrometry. *J. Am. Chem. Soc.* **1991**, 113, 6294–6296.
  - 54 Lim, H.-K., Hsieh, Y.L., Ganem, B., Henion, J.: Recognition of cell-wall peptide ligands by vancomycin group antibiotics: studies using ion spray mass spectrometry. *J. Mass Spectrom.* **1995**, 30, 708–714.
  - 55 Schermann, S., Simmons, D.A., Konermann, L.: Mass spectrometry-based approaches to protein–ligand Interactions. *Expert Rev. Proteomics* **2005**, 2, 475–485.
  - 56 Geoghegan, K.F., Kelly, M.A.: Biochemical applications of mass spectrometry in pharmaceutical drug

- discovery. *Mass Spectrom. Rev.* **2005**, 24, 347–366.
- 57 Muckenschnabel, I., Falchetto, R., Mayr, L.M., Filipuzzi, I.: SpeedScreen: label-free liquid chromatography-mass spectrometry-based high-throughput screening for the discovery of orphan protein ligands. *Anal. Biochem.* **2004**, 324, 241–249.
  - 58 Missale, C., Nash, R., Robinson, S.W., Jaber, M., Caron, M.D.: Dopamine receptors: from structure to function. *Physiol. Rev.* **1998**, 78, 189–225.
  - 59 Bleicher, K. H., Böhm, H.-J., Müller, K., Alanine, A. I.: Hit and lead generation: beyond high throughput screening. *Nat. Rev.* **2003**, 2, 369–378.
  - 60 Billard, W., Ruperto, V., Crosby, G., Iorio, L.C., Barnett, A.: Characterization of the binding of <sup>3</sup>H-SCH 23390. A selective D-1 receptor antagonist ligand, in rat striatum. *Life Sci.* **1984**, 35, 1885–1893.
  - 61 Höfner, G., Wanner, K.T.: Competitive binding assays simply done with a native marker and mass spectrometric quantification. *Angew. Chem. Int. Ed.* **2003**, 42, 5235–5237; *Angew. Chem.* **2003**, 115, 5393–5395.
  - 62 Niessen, K.V., Höfner, G., Wanner, K.T.: Competitive MS binding assays for dopamine D<sub>2</sub> receptors employing spiperone as anative marker, *ChemBioChem* **2005**, 6, 1769–1775.
  - 63 Rees, C., Hunter, J. C.: Opioid receptors, in *Comprehensive Medicinal Chemistry*, vol. iii: *Membranes & Receptors*, ed. Emmett, J. C., Pergamon Press, Oxford, **1990**, pp 45–80.
  - 64 Aldrich, J.V., Virgil-Cruz, S.C.: Narcotic analgetics, in *Burger's Medicinal Chemistry and Drug Discovery*, vol. vi: *Nervous System Agents*, ed. Abraham, D. J., John Wiley & Sons, New York, **2003**, pp 329–481.
  - 65 Wanner, K., Höfner, G., Bertling, W.: Method for determining the binding behaviour of ligands which specifically bind to target molecules. US patent US 20040232077 A1.
  - 66 Raynor, K., Kong, H., Mestek, A., Bye, L.S., Tian, M., Liu, J., Yu, L., Reisine, T.: Characterization of the cloned human mu opioid receptor. *J. Pharmacol. Exp. Ther.* **1995**, 272, 423–428.
  - 67 Goldstein, A., Barrett, R. W.: Ligand dissociation constants from competition binding assays: errors associated with ligand depletion. *Mol. Pharmacol.* **1987**, 13, 603–609.
  - 68 Bylund, D. B., Murrin, L. C.: Radioligand saturation binding experiments over large concentration ranges. *Life Sci.* **2000**, 67, 287–2911.
  - 69 Tate, C. G., Grisshammer, R.: Heterologous expression of G protein-coupled receptors. *Trends Biotechnol.* **1996**, 14, 426–430.
  - 70 Turner, G. J., Reusch, R., Winter-Vann, A. M., Martinez, L., Betlach, M. C.: Heterologous gene expression in a membrane-protein-specific system. *Protein Express. Purif.* **1999**, 17, 312–323.
  - 71 Kalipatnapu, S., Pucadyil, T. J., Harikumar, K. G., Chattopadhyay, A.: Ligand binding characteristics of the human serotonin<sub>1A</sub> receptor heterologously expressed in CHO cells. *Biosci. Receptors* **2004**, 24, 101–115.
  - 72 Janssen, M.J., Ensing, K., de Zeeuw, R.A.: Improved benzodiazepine radioreceptor assay using the MultiScreen® assay system. *J. Pharm. Biomed. Anal.* **1999**, 20, 753–761.
  - 73 Zhang, H., Pan, Y.: Affinity ultrafiltration of DNA topoisomerases-targeted compounds determined with HPLC/ESI-MS for drug candidate screening. *J. Zhejiang Univ. Sci.* **2004**, 5, 900–905.
  - 74 Sun, Y., Gu, C., Liu, X., Liang, W., Yao, P., Bolton, J. L., van Breemen, R. B.: Ultrafiltration tandem mass spectrometry of estrogens for characterization of structure and affinity for human estrogen receptors. *J. Am. Soc. Mass Spectrom.* **2005**, 16, 271–279.
  - 75 Liu, J., Carr, S., Rinaldi, K., Chandler, W.: Screening estrogenic oxidized by-products by combining ER binding

- and ultrafiltration. *Environ. Toxicol. Pharmacol.* **2005**, 20, 269–278.
- 76 Biddlecombe, R. A., Pleasance, S.: Automated protein precipitation by filtration in the 96-well format. *J. Chromatogr. B* **1999**, 734, 257–265.
  - 77 Janssen, M. J., Ensing, K., de Zeeuw, R. A.: Improved benzodiazepine radioreceptor assay using the MultiScreen® assay system. *J. Pharm. Biomed. Anal.* **1999**, 20, 753–761.
  - 78 Hopfgartner, G., Bourgogne, E.: Quantitative high-throughput analysis of drugs in biological matrices by mass spectrometry. *Mass Spectrom. Rev.* **2003**, 22, 195–214.
  - 79 Mei, H., Hsieh, Y., Nardo, C., Xu, X., Wang, S., Ng, K., Korfmacher, W. A.: Investigation of matrix effects in bioanalytical high-performance liquid chromatography/tandem mass spectrometric assays: application to drug discovery. *Rapid Commun. Mass Spectrom.* **2003**, 17, 97–103.
  - 80 Zepperitz, C., Höfner, G., Wanner, K. T.: MS-binding assays: kinetic, saturation, and competitive experiments based on quantitation of bound marker as exemplified by the GABA transporter mGAT1. *ChemMedChem* **2006**, 1, 208–217.
  - 81 Belebony, R. O., Gomes Carolino, R. O., Baldocchi Pizzo, A., Castellan-Baldan, L., Coutinho-Netto, J., Ferreira dos Santos, W., Cysne Coimbra, N.: Pharmacological and biochemical aspects of GABAergic neurotransmission: pathological and neuropsychobiological relationships. *Cell. Mol. Neurobiol.* **2004**, 24, 707–728.
  - 82 Iversen, L.: Neurotransmitter transporters: fruitful targets for CNS drug discovery. *Mol. Psychiatry* **2000**, 5, 357–362.
  - 83 Dalby, N. O.: Inhibition of gamma-aminobutyric acid uptake: anatomy, physiology and effects against epileptic seizures. *Eur. J. Pharmacol.* **2003**, 479, 127–137.
  - 84 Chen, N.-H., Reith, M. E. A., Quick, M. W.: Synaptic uptake and beyond: the sodium- and chloride-dependent neurotransmitter transporter family SLC6. *Pflugers Arch. Eur. J. Physiol.* **2004**, 447, 519–531.
  - 85 Conti, F., Minelli, A., Melone, M.: GABA transporters in the mammalian cerebral cortex: localization, development and pathological implications. *Brain Res. Rev.* **2004**, 45, 196–212.
  - 86 Czuczwar, S. J., Patsalos, P. N.: The new generation of GABA enhancers potential in the treatment of epilepsy. *CNS Drugs* **2001**, 15, 339–350.
  - 87 Laughlin, T. M., Tram, K. V., Wilcox, G. L., Birnbaum, A. K.: Comparison of antiepileptic drugs tiagabine, lamotrigine, and gabapentin in mouse models of acute, prolonged, and chronic nociception. *J. Pharmacol. Exp. Ther.* **2002**, 302, 1168–1175.
  - 88 Genton, P., Guerrini, R., Perucca, E.: Tiagabine in clinical practice. *Epilepsia* **2001**, 42, 42–45.
  - 89 Iversen, L. L., Neal, M. J.: The uptake of [<sup>3</sup>H]GABA by slices of rat cerebral cortex. *J. Neurochem.* **1968**, 15, 1141–1149.
  - 90 Iversen, L. L., Kelly, J. S.: Uptake and metabolism of  $\gamma$  aminobutyric acid by neurones and glial cells. *Biochem. Pharmacol.* **1975**, 24, 933–938.
  - 91 Sutcliffe, R. J., Davies, C. C., Bowery, N. G.: GABA release and uptake measured in crude synaptosomes from genetic absence epilepsy rats from Strasbourg (GAERS). *Neurochem. Int.* **1999**, 34, 415–425.
  - 92 Clausen, R. P., Moltzen, E. K., Perregaard, J., Lenz, S. M., Sanchez, C., Falch, E., Frølund, B., Bolvig, T., Sarup, A., Larsson, O. M., Schousboe, A., Krogsgaard-Larsen, P.: Selective inhibitors of GABA uptake: synthesis and molecular pharmacology of 4-N-methylamino-4,5,6,7-tetrahydrobenzo[d]isoxazol-3-ol analogues. *Bioorg. Med. Chem.* **2005**, 13, 895–908.
  - 93 Bylund, D. B., Toews, M. L.: Radioligand binding methods: practical guide and tips. *Am. J. Physiol. Lung Cell. Mol. Physiol.* **1993**, 265, L421–L429.
  - 94 Bylund, D. B., Deupree, J. D., Toews, M. L.: Radioligand-binding methods

- for membrane preparations and intact cells. *Methods Mol. Biol.* **259**, 1–28.
- 95 Braestrup, C., Nielsen, E. B., Sonnewald, U., Knutsen, J. S., Andersen, K. E., Jansen, J. A., Frederiksen, K., Andersen, P. H., Mortnesen, A., Suzdak, P.D.: (*R*)-*N*-[4,4-bis(3-methyl-2-thienyl)but-3-en-1-yl]nipecotic acid binds with high affinity to the brain  $\gamma$ -aminobutyric acid uptake carrier. *J. Neurochem.* **1990**, *54*, 639–647.
  - 96 Suzdak, P. D., Frederiksen, K., Andersen, K. E., Sørensen, P. O., Knutsen, L. J. S., Nielsen, E. B.: NNC-711, a novel potent and selective  $\gamma$ -aminobutyric acid uptake inhibitor: pharmacological characterization. *Eur. J. Pharmacol.* **1992**, *223*, 189–198.
  - 97 Suzdak, P. D., Foged, C., Andersen, K. E.: Quantitative autoradiographic characterization of the binding of [<sup>3</sup>H]tiagabine (NNC 05-328) to the GABA uptake carrier. *Brain Res.* **1994**, *647*, 231–241.
  - 98 Soudijn, W., van Wijngaarden, I.: The GABA transporter and its inhibitors. *Curr. Med. Chem.* **2000**, *7*, 1063–1079.
  - 99 Kragler, A., Höfner, G., Wanner, K. T.: Novel parent structures for inhibitors of the murine GABA transporters mGAT3 and mGAT4. *Eur. J. Pharmacol.* **2005**, *519*, 43–47.
  - 100 Knutsen, L. J. S., Andersen, K. E., Lau, J., Lundt, B. F., Henry, R. F., Morton, H. E., Nærum, L., Petersen, H., Stephensen, H., Suzdak, P. D., Swedberg, M. D. B., Thomsen, C., Sørensen, P. O.: Synthesis of novel GABA uptake inhibitors. 3. diaryloxime and diarylviny ether derivatives of nipecotic acid and guvacine as anticonvulsant agents. *J. Med. Chem.* **1999**, *42*, 3447–3462.
  - 101 Barakat, L., Bordey, A.: GAT-1 and reversible GABA transport in bergmann glia in slices. *J. Neurophysiol.* **2002**, *88*, 1407–1419.
  - 102 Ackerman, B.L., Berna, M.J., Murphy, A.T.: Recent advances in use of LC/MS/MS for quantitative high-throughput bioanalytical support of drug discovery. *Curr. Top. Med. Chem.* **2002**, *2*, 53–66.
  - 103 Niessen, W.M.A.: Progress in liquid chromatography–mass spectrometry instrumentation and its impact on high-throughput screening. *J. Chromatogr. A* **2003**, *1000*, 413–426.
  - 104 Hopfgartner, G., Varesio, E.: New approaches for quantitative analysis in biological fluids using mass spectrometric detection. *Trends Anal. Chem.* **2005**, *24*, 583–589.
  - 105 Wanner, K., Füle, G., Höfner, G.: WO 0014064, **2000** (Chem. Abstr. **2000**, *132*, 194656).
  - 106 Zhao, X., Hoegl, C. E., Hoefner, G. C., Wanner, K. T.: Synthesis and biological evaluation of new GABA-uptake inhibitors derived from proline and from pyrrolidine-2-acetic acid. *Eur. J. Med. Chem.* **2005**, *40*, 231–247.



## 8

### Laser Desorption Assays – MALDI-MS, DLOS-MS, and SAMDI-MS

*Martin Vogel, Andy Scheffer, André Liesener, and Uwe Karst*

#### 8.1

##### MALDI-MS Assays

##### 8.1.1

##### Principles of MALDI

Although lasers had been applied in the early 1980s for desorbing analytes from e.g. metal surfaces, ionization efficiency of this direct desorption approach was only poor and strong fragmentation was observed. Even worse, laser desorption was mainly restricted to molecules up to a mass of  $\sim 1000$  Da, thus being incompatible with most applications in bioanalysis. In 1988, Karas and Hillenkamp [1] introduced matrix-assisted laser desorption/ionization (MALDI) as a new ionization technique which turned out to be ideally suited for bioanalytical mass spectrometry. In MALDI, the analytes are co-crystallized in an organic matrix, which mostly consists of small organic molecules that are able to absorb light at a characteristic wavelength (Fig. 8.1). Ideally, this absorption maximum is compatible with the laser wavelength used for desorption. The matrix-to-analyte ratio is predominantly in the range of 1000 to 10 000.

After matrix and sample have been deposited onto the MALDI target, the solvent is evaporated, and the crystalline surface is desorbed by nanosecond laser pulses with energies of  $10^6$ – $10^7$  W cm $^{-2}$  (Fig. 8.2). Thus, matrix molecules absorb the laser energy, and in a complex series of electronic excitation, relaxation and rapid thermal extension, parts of the crystalline surface evaporate. During this process, both matrix and analyte molecules are transferred into the gas phase. Provided that the laser energy was not too high, analyte molecules, e.g. proteins, peptides etc., are ionized without showing significant fragmentation.

As the laser pulse is in the nanosecond range, a fast mass spectrometer has to be coupled in series. In most cases, MALDI is connected to a time-of-flight (TOF) mass spectrometer with which  $m/z$  ratios are determined by precisely measuring the time an ion needs to pass from the ion source to the detector. Besides its abil-

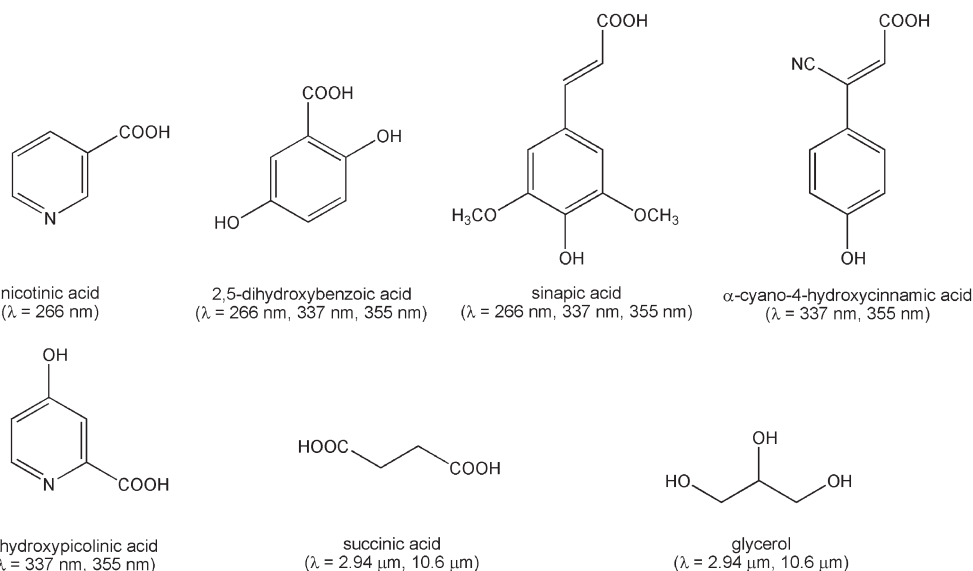


**Fig. 8.1** An overview on commonly used MALDI matrices. Depending on the analytes that have to be investigated and depending on the provided laser wavelength, the appropriate matrix has to be selected. The absorption maxima of the respective compounds are given in brackets.

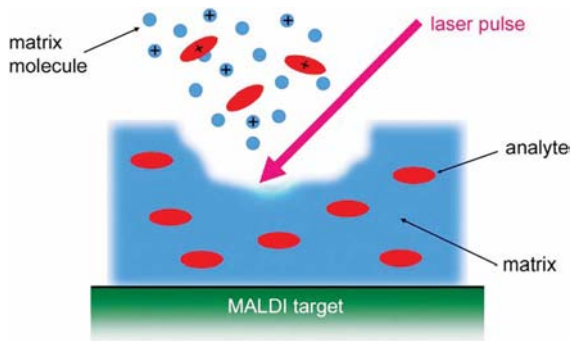


**Fig. 8.2** Principle of the MALDI process. Initially, analyte and matrix are co-crystallized. After evaporation of the solvent, a nanosecond laser pulse is directed onto the crystalline surface, and both matrix and analyte molecules are desorbed. A complex reaction cascade leads to the formation of charged analyte molecules that reach the mass spectrometer without significant fragmentation.

ity for fast measurements, TOF-MS offers advantageous ion transmission, which allows to also detect low ion fluxes originating from the MALDI source.

### 8.1.2

#### Application of MALDI-MS in Bioanalysis

Since the end of the 1980s, MALDI has been employed for the analysis of proteins, peptides, oligonucleotides, and polymers in a wide range of applications. Owing to its high tolerance regarding the presence of biological matrices and biological sample constituents, and owing to its advantageous ionization efficiencies for high molecular weight compounds, MALDI-MS has been established as a versatile tool especially in the field of proteomics [2]. Several approaches using MALDI-MS for the monitoring of enzymatic conversions have been introduced over recent years [3–6]. In 2001, Kang et al. developed a high-throughput protocol for the automated determination of enzymatic activities by MALDI-MS [7]. As an enzymatic model system, they used the lipase-catalyzed conversion of *rac*-1-phenylethylamine (Fig. 8.3).

For reliable quantification, the deuterium-labelled substrate ( $d_5$ -phenylethylamine) was added to the matrix as internal standard. To circumvent the problem of crystal inhomogeneities, 100 acceptable spectra were measured from seven to ten different positions of one sample spot and averaged. The MALDI-MS assay was validated with a gas chromatography-based quantification scheme and was found to be in good compliance. This methodology obviously allows a reliable quantification of the low molecular weight analytes of interest. Nevertheless, the need for isotopically labelled compounds as internal standards is still a bottleneck, as these are usually rather expensive or have to be laboriously synthesized.

The potential of the MALDI-MS-based assay scheme for the quantification of low molecular weight products and substrates directly from reaction mixtures has been described by Bungert et al. [8]. The glucose oxidase-based conversion of glucose to gluconolactone and the carboxypeptidase A-mediated cleavage of hippuryl-L-phenylalanine were chosen as model systems (Fig. 8.4).

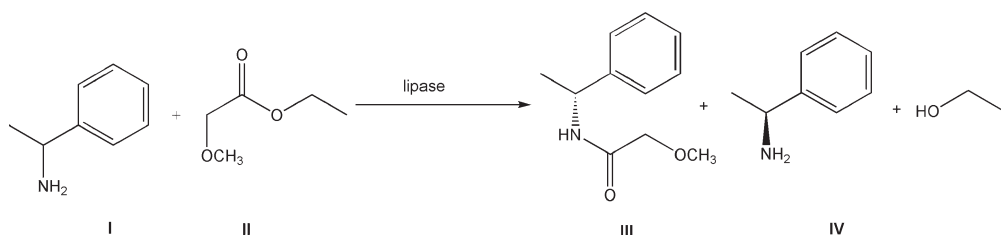


**Fig. 8.3** Lipase-catalyzed formation of 2-methoxy-N-[(1R)-1-phenylethyl]-acetamide (III) and (S)-phenylethylamine (IV). The reaction uses racemic 1-phenylethylamine (I) and ethylmethoxyacetate (II) as educts and is carried out in methyl-*tert*-butylether. As a byproduct, ethanol is formed.



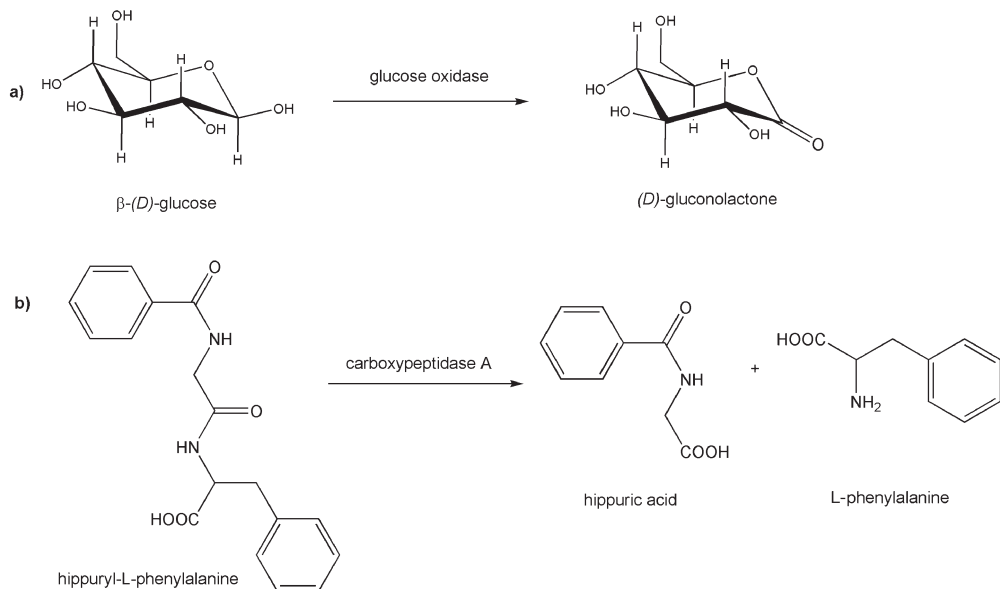


**Fig. 8.4** (a) In the presence of oxygen, the glucose oxidase-catalyzed oxidation of  $\beta$ -D-glucose leads to the formation of gluconolactone. (b) Carboxypeptidase A selectively cleaves the substrate, hippuryl-L-phenylalanine, thus leading to the formation of hippuric acid and phenylalanine.

Time-resolved reaction profiles for both enzymatic reactions were obtained by simultaneous determination of the respective substrate and product concentrations without the need for time-consuming sample preparation steps. The results were in good agreement with those from a standard UV absorbance-based assay. In another study by the same group, a liquid ionic matrix was employed instead of using a crystalline solid matrix, thus minimizing the negative effects on the quantification by sample spot inhomogeneities [9]. The method was applied to screen the enzymatic activity of ten pyranose oxidase variants towards glucose (Fig. 8.5).

Each sample was mixed with the ionic liquid matrix (2,5-dihydroxybenzoic acid/pyridine) containing  $^{13}\text{C}$ -labelled glucose as internal standard and spotted on the target. MALDI-MS analysis generated reaction profiles by the simultaneous determination of product and substrate concentrations for each enzyme variant. The reaction profiles could be used to sort the enzyme variants into five different classes.

In 2006, Greis and co-workers reported on the application of MALDI-TOF MS as a tool for rapid inhibitor screening [10]. Different kinases (protein kinase C- $\alpha$ , cAMP-dependent protein kinase) in combination with their substrates were assayed, and the inhibitory potencies of staurosporine and three novel compounds were determined. For all four compounds,  $\text{IC}_{50}$  values could be determined, and

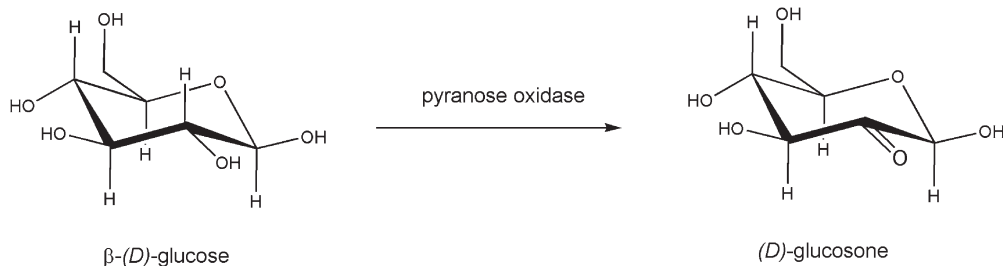


**Fig. 8.5** The pyranose oxidase-catalyzed oxidation of  $\beta$ -D-glucose leads to the formation of glucosone. Educt and product differ by 2 Da.

staurosporine was found to possess the highest inhibitory potency. In the field of drug discovery, selectivity of an inhibitor, i.e. of a potential drug substance, plays a significant role. As many enzymes exist as members of enzyme families, an inhibitor would only be useful as a drug candidate in those cases, where it selectively inhibits the target enzyme. Therefore, the inhibitory potency of staurosporine towards both protein kinases was assayed by means of MALDI-TOF MS. In accordance with literature data, it was found that staurosporine shows ten times higher inhibitory activity for protein kinase C- $\alpha$  than for cAMP-dependent protein kinase. Although LC/MS-based approaches are still the method of choice in the field of quantitative enzyme activity screening, MALDI-TOF MS has thus shown to be a versatile alternative in all those cases where minimal sample preparation is required and high-throughput analysis is desirable.

## 8.2

### DIOS: Desorption/Ionization on Silicon

#### 8.2.1

##### Principles of DIOS

A severe problem when quantifying low molecular weight compounds by means of MALDI-MS is the potential interference of matrix signals with the analyte signals in the low-mass region. Furthermore, target preparation, i.e. co-crystallization of matrix and sample, is often time-consuming: Due to inhomogeneous distribution of analyte molecules within the matrix crystal, shot-to-shot reproducibility (generation of so-called "hot spots") and sample-to-sample reproducibility remain mostly poor. Several factors like matrix compound selection, pH value of sample solution, ratio of matrix to analyte molecules, target surface, and sample drying method are critical for the crystallization process and have to be carefully optimized [11]. To overcome the limitations related to the use of a matrix, direct laser desorption/ionization without the use of a matrix is no alternative for bioanalytical mass spectrometry, as significant analyte degradation is fre-

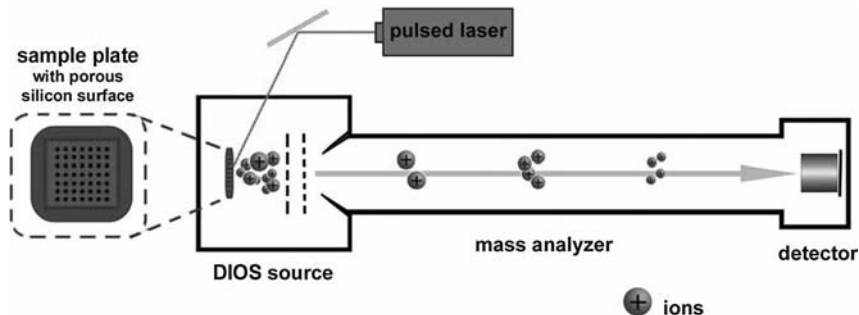


**Fig. 8.6** Schematic set-up of a DIOS-TOF-MS system. Initially, the sample is deposited on the porous silicon surface. Subsequently, a laser pulse is directed to the silicon surface, and the analytes are desorbed. Ions that are generated are transferred into a time-of-flight mass spectrometer.

quently observed upon direct exposure to the laser beam. Therefore, Wei et al. developed a matrix-free strategy based on the pulsed laser desorption/ionization of molecules from a porous silicon surface (DIOS) [12]. In a DIOS experiment, the analytes in solution are spotted onto a porous silicon target, evaporated to dryness, and ionized by a laser pulse. The generated ions are then detected by a mass spectrometer. The set-up of a DIOS-MS system is schematically shown in Fig. 8.6.

Porous silicon is generated from flat crystalline silicon by using a galvanostatic or chemical etching procedure [12–14]. Thus, a thin layer in the submicrometer range is formed, which comprises a nanocrystalline structure and shows bright photoluminescence upon irradiation with UV light [12]. By modulating etching conditions and by selecting the appropriate silicon wafer precursors, characteristics of the formed silicon surface, e.g. morphology and porosity, can be controlled. Porous silicon has narrow pores (typically 50–100 nm) and a large surface area reaching up to several hundred  $\text{m}^2 \text{cm}^{-3}$ . The porous silicon surface may either be used in its metastable silicon hydride form, comprising Si–H endgroups, or in its functionalized form by covalently attaching organic groups, e.g. dodecyl, ethyl, phenyl, or ethylphenyl substituents. Actually, the more hydrophobic surfaces yield higher signals [12].

Due to the hydrophobicity of the silicon surface, samples are typically dissolved in water or mixtures of water and methanol. While samples dissolved in pure non-polar solvents tend to spread over the whole surface, aqueous/organic mixtures form droplets that stay localized to a small surface area. Additionally, mixtures also guarantee that the sample penetrates sufficiently deep into the silicon. Spotted volumes are typically in the low microliter to submicroliter range. Traditionally, sample spotting in DIOS-MS is carried out using pipettes, which mostly suffers from an inhomogeneous analyte distribution. This can be overcome by

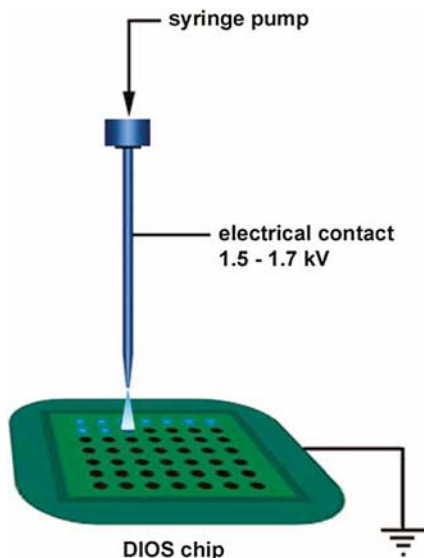


**Fig. 8.7** Electrospray deposition (ESD). During the ESD process, an electrospray capillary is used to generate small positively charged droplets containing the analytes. The droplets are sprayed onto the silicon surface, where a uniform and thin layer is formed.

the application of electrospray deposition (ESD) [15]. During the ESD process, small positively charged droplets are sprayed onto the porous silicon chip and form a uniform thin layer of the analyte (Fig. 8.7). Subsequent to spotting, the chip is evaporated to dryness. Analysis can then be performed by using standard MALDI-MS equipment, i.e. pulsed laser set-up and TOF mass spectrometer.

Regarding the ionization process, it is believed that – similar to MALDI – the porous structure of silicon serves as a scaffold for both solvent and analyte molecules while, simultaneously, the high UV absorptivity of the material enables an efficient transfer of the laser pulse energy towards the analyte molecules [14]. A major advantage of DIOS is the fact that little to no fragmentation is induced by the desorption/ionization process. However, the mass range of the methodology is limited to analytes of a molecular weight below 18 000 Da, with the highest efficiency for analytes below 3000 Da [16].

Although DIOS-MS is mainly a tool for qualitative analysis, many examples have shown that quantitative analysis is possible when internal standards are used. These may either be isotope-labelled – mostly deuterated – compounds or structurally related analogues. For example, subsequent to electrospray deposition, amino acids such as phenylalanine and tyrosine have been successfully quantified by means of DIOS-MS using their deuterated analogues as internal standards.

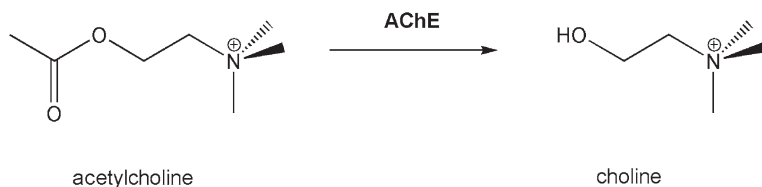


**Fig. 8.8** The acetylcholinesterase-catalyzed cleavage of acetylcholine. The product, choline, is characterized by a mass loss of 42 Da.

### 8.2.2

#### Application of DIOS in Bioanalysis

Desorption/ionization on porous silicon has been successfully applied to the direct mass analysis of a variety of analytes and analyte mixtures, e.g. from exocrine tissues as well as from single neurons. In forensic analysis, DIOS-MS was applied for the analysis of small molecular weight polymers from biological samples, e.g. spermicides or polyethylene glycol polymers. But it has also been applied in the fields of drug discovery [17] or fatty acid analysis [18]. DIOS-MS has early been used for the monitoring of enzymatic reactions, too. In 2001, Thomas et al. investigated a multi-enzyme system comprising of a glucosidase (mannosidase II), a lipase (phospholipase A<sub>2</sub>) and an esterase (acetylcholinesterase, AChE) and their respective substrates [19]. All reactions were carried out directly on the silicon surface. Subsequent to quenching, which was accomplished by the evaporation of the solvent, direct DIOS-MS analysis of the dried reaction mixture was performed. AChE was reacted with its substrate acetylcholine, and deuterated choline was used as an internal standard for quantification (Fig. 8.8).

A time-resolved reaction profile was generated by plotting the choline formation vs time, and inhibition of acetylcholinesterase by three different inhibitors was studied in three independent reactions on a single target plate, thus allowing screening the inhibitory activities within 15 min, including sample preparation time. In order to assay mannosidase II, an oxidized silicon surface was used on which best signal responses of the carbohydrate analytes were obtained. The possibility to tailor the silicon's surface properties is thus one of the major advantages of DIOS-MS analysis when different reaction mixtures are concerned. The activity of phospholipase A<sub>2</sub> was determined by reacting the enzyme with a triacylglycerol phospholipid, which yielded a lysophospholipid species upon enzymatic conversion (Fig. 8.9). After 30 min of incubation directly on the DIOS chip, the product species could be monitored in the MS as their sodium and potassium adducts.

A further advantage, as described by Thomas et al. [19], is the possibility of protein identification that follows the functional characterization of the enzyme. The activity of an enzyme is initially determined by following the substrate consumption and product formation in the first assay (Fig. 8.10). Since no matrix components are present in the sample spot, the immobilized enzyme is then directly

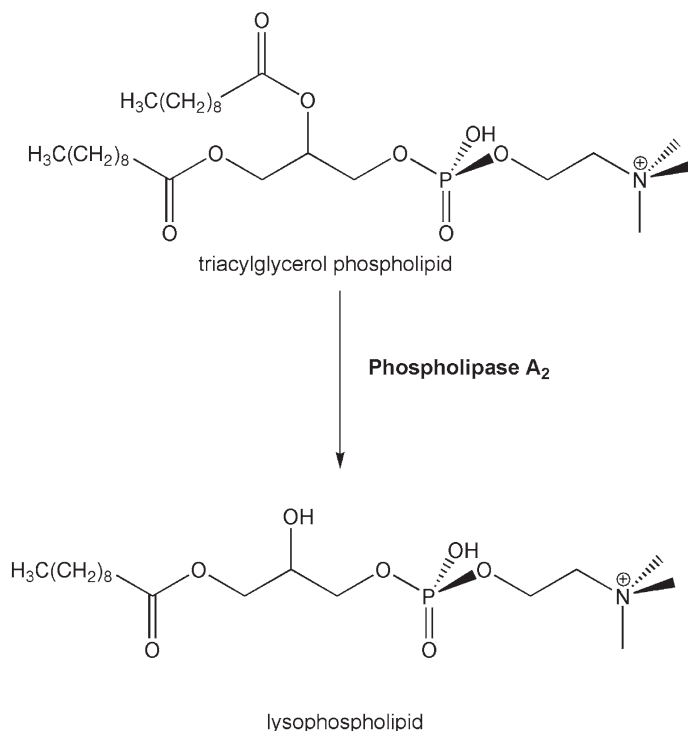


**Fig. 8.9** The activity of phospholipase A<sub>2</sub> can be determined by following the consumption of the triacylglycerol phospholipid and the formation of the lysophospholipid.

digested with site-specific proteases. Afterwards, the digest is analyzed again by means of DIOS-MS and the protein fragments generated can be used for the correct identification of the protein.

An automated DIOS-MS-based approach as screening assay for enzymatic activities and enzyme inhibitors was published in 2004 [20]. A DIOS-MS plate-reader assay was employed in an enzyme activity screening, searching for new enzymes with activity similar to phenylalanine hydroxylase (PAH). Determination of kinetic parameters as a measure of catalytic activities was carried out by varying the substrate concentration and monitoring product formation as well as substrate consumption. For quantification, deuterium-labelled phenylalanine and tyrosine as internal standards were used. In a second set of experiments, the DIOS-MS plate reader assay was employed in a screening for potential inhibitors of acetylcholinesterase. The library of potential inhibitors comprised more than 900 compounds, including some known reference inhibitors. All enzymatic reactions in the study were carried out offline and aliquots of the reaction mixtures were spotted onto the DIOS target. Thus, speed and precision of sample deposition become the most crucial point for the application of this system. Employing

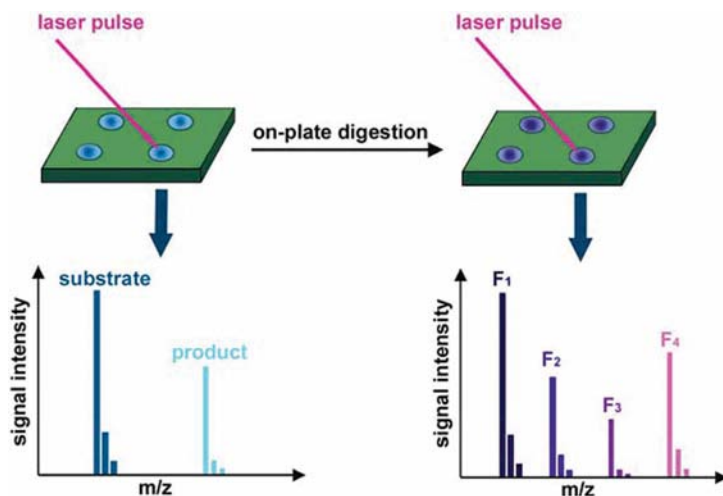


**Fig. 8.10** Sequential functional characterization and structural identification of an enzyme. Initially, information about the activity is obtained by assessing substrate consumption and product formation. Afterwards, the enzyme is digested on the plate, and the formed peptide fragments ( $F_1$ – $F_4$ ) are determined by means of mass spectrometry.

an electrospray deposition device (Fig. 8.7), sample homogeneity could be significantly improved. With this approach, the high potential of DIOS-MS-based assays as a tool in high-throughput screening for either determining enzymatic activities or detecting potential inhibitors has been clearly demonstrated. Nevertheless, it should be noted that the number of different enzymatic systems studied by this interesting technique is still rather small and the exact mechanism of the ionization by DIOS is not yet fully understood.

The surface of the porous silicon chip offers multiple possibilities for the covalent coupling of functional groups. Thus, functionalization of a DIOS target by immobilization of trypsin was described by Xu et al. [21]. The enzyme was immobilized using cyanuric chloride as coupling agent following an amino-functionalization (Fig. 8.11).

It could be shown that the immobilized enzyme retained its bioactivity and the kinetic parameters for the trypsin-catalyzed proteolysis of an appropriate substrate were determined. However, the value for  $v_{\max}$  was found to be lower than for free trypsin, thus indicating a slight loss of activity likely to be related to the immobilization of the enzyme. The trypsin-functionalized DIOS target was used for peptide-mapping analysis of two model proteins: cytochrome *c* and bovine serum albumin (BSA) were incubated on the target and after evaporation to dryness directly analyzed by means of DIOS-MS. The signal intensity of the peptide fragments generated was found to be low, which might be due to the surface modification. Therefore, a small amount of a typical MALDI matrix ( $\alpha$ -cyano-4-

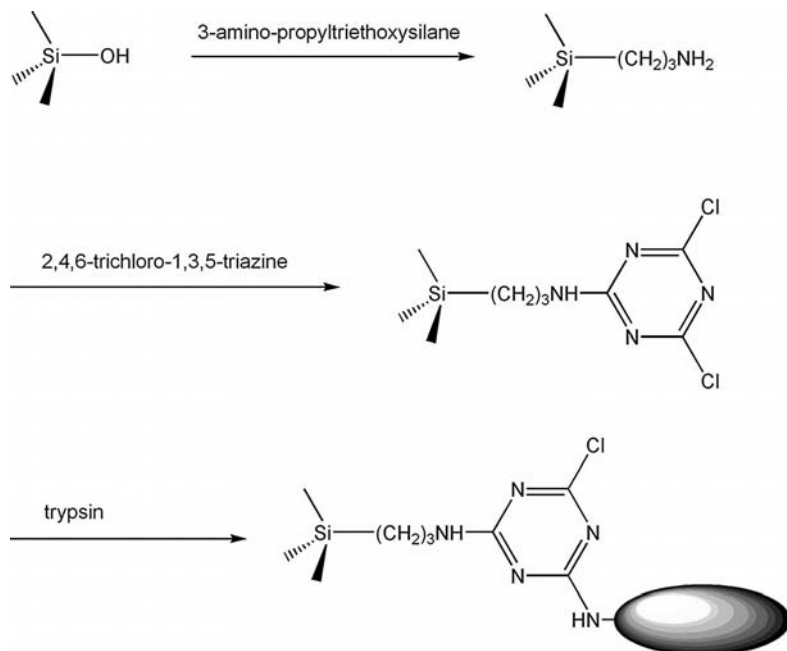


**Fig. 8.11** Covalent coupling of trypsin to a silicon surface. In a first step, free silanol groups are reacted with 3-amino-propyltriethoxysilane. The amino-functionalized surface is then treated with 2,4,6-trichloro-1,3,5-triazine (cyanuric chlorid). Finally, trypsin is covalently bound via a free amino group of the protein.

hydroxycinnamic acid) was added to increase the signal response significantly. In the presence of matrix, 19 peptide fragments could be assigned for cytochrome *c* and 54 peptide fragments for BSA. This means that the DIOS-MS approach can be “converted” into a MALDI-MS scheme for enhancing signal intensities, when needed.

## 8.3

### SAMDI: Self-assembled Monolayers for MALDI-MS

#### 8.3.1

##### Principles of SAMDI-MS

Mrksich and co-workers developed a MALDI-based assay scheme making use of a target surface modification by self-assembled monolayers (SAMs) [22]. This combination of SAMs and MALDI is predominantly called SAMDI (self-assembled monolayers for MALDI). For SAMDI, a self-assembled monolayer with reactive end groups is used in order to covalently bind enzyme substrates to a surface. To



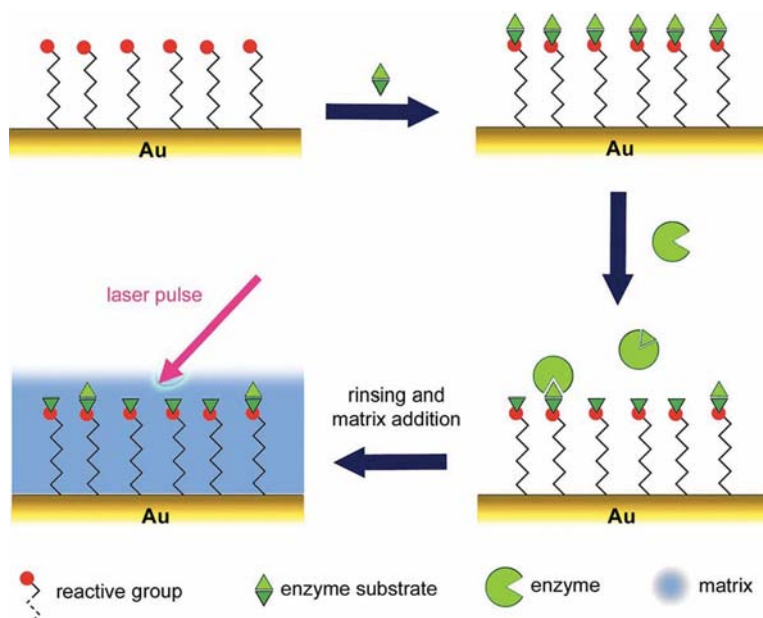


**Fig. 8.12** Scheme of the SAMDI principle. To a self-assembled monolayer (SAM) with reactive end groups, enzyme substrates are immobilized. During incubation with an enzyme solution, the bound substrates are converted into the product compounds. The reaction is quenched by rinsing the surface. Finally, matrix is added, the solvent is evaporated, and the surface is analyzed by means of MALDI-MS.

monitor enzymatic activity, the functionalized surface is incubated with the solution containing the enzyme of interest. After quenching the enzymatic reaction by rinsing the surface, matrix is added, and by means of MALDI, substrate consumption and product formation can be monitored (Fig. 8.12).

This hybrid set-up combines the high selectivity of a functionalized surface with the versatile ionization efficiency of MALDI. The SAMs applied in the approach presented by Mrksich et al. were designed in order to present a mixture of oligo(ethylene glycol) groups and substrates, e.g. peptides or carbohydrate ligands, as terminal groups. It is crucial to use oligo(ethylene glycol), because it prevents non-specific interactions of proteins with the surface, thus ensuring that all interactions of proteins in solution occur with the immobilized substrates. To ensure a maximum of accessibility to the immobilized substrates, SAMs presenting the substrate and oligo(ethylene glycol) terminal groups in a ratio of 1:4 are created. In contrast to DIOS-MS, where the porous silicon replaces the MALDI matrix, SAMs in SAMDI only serve as surfaces for the selective immobilization of analytes. Ionization is later on supported by the addition of classical MALDI matrices. This method was used in several studies published by the same group.

## 8.3.2

**Application of SAMDI in Bioanalysis**

The use of functionalized monolayers in monitoring enzymatic activities was tested using  $\beta$ -1,4-galactosyltransferase as model enzyme and immobilized *N*-acetylglucosamine as substrate. The enzyme solution was incubated on SAM-modified target surfaces. Subsequent to incubation, the target was rinsed, an appropriate matrix was applied, and the surface was analyzed by means of MALDI-MS. By varying the incubation times, time-resolved reaction profiles were obtained. The yield of the enzymatic conversion could be calculated from the ratio of the product signal to the sum of product and substrate signal intensities [22].

An approach to multiplexing analysis was presented by Min et al. [23], who developed a SAMDI-based assay scheme to screen for the activity of different kinases. In this assay scheme, peptide substrates were used that are specific for one type of kinase. A mixture of four substrates was immobilized on the SAM. After incubation with an appropriate kinase, the target surface was rinsed, thus stopping the reaction. Matrix was deposited on the surface and MALDI-MS analysis was carried out (Fig. 8.13). By monitoring the signal intensities for the substrates

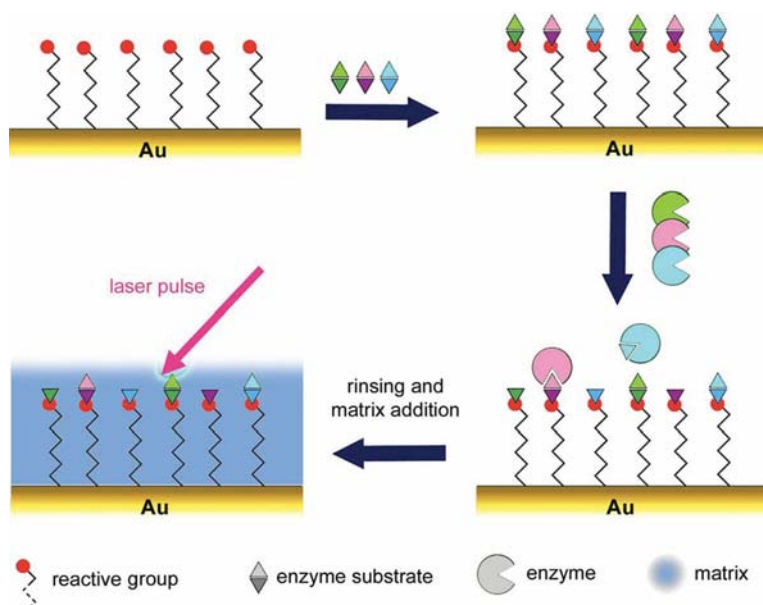


**Fig. 8.13** A multiplexing SAMDI-MS assay. In this case, a mixture of three substrates is immobilized on the SAM. After incubation with appropriate enzyme solutions, the enzymatic reaction is quenched by rinsing the surface. Subsequently, matrix is deposited on the surface and MALDI-MS is carried out. Consumption of all three substrates can thus be determined in parallel.

and the products, enzymatic activity was determined, thus demonstrating the feasibility of the SAMDI approach for multiplexing analysis of enzymatic activities.

In a second series of experiments, the quantification of enzyme inhibition by means of SAMDI-MS was studied. For quantitative studies, two different kinases were incubated separately with varying amounts of known inhibitors on the modified target surface. The inhibition of the respective reactions in the presence of the inhibitors was determined by MALDI-MS, and  $IC_{50}$  values for both kinases could be generated. However, the reported  $IC_{50}$  value for the inhibition of casein kinase I was significantly higher than the value that had been determined from a different assay scheme. A possible explanation for this may be the differences between a liquid-phase reaction and a surface/liquid-phase reaction. Furthermore, the general problem of accurate quantification of the analytes in MALDI may have been contributed to this deviation.

Furthermore, SAMDI-MS methods have been developed that may be used as screening procedure for the identification of anthrax lethal factor inhibitors [24]. Anthrax lethal factor is a zinc-dependent protease. An oligopeptide, which is cleaved by the enzyme at a proline position, served as a model substrate and was immobilized on the SAM-modified surface of a MALDI target. The target plate comprised an array of 100 gold-coated and SAM-modified sample spots. For initial screening, different mixtures – each consisting of eight potential inhibitors – were added to an aliquot of the enzyme solution. These mixtures were then incubated on the target sample spots. After the enzyme reactions had been stopped, matrix was added and MALDI-MS analysis was performed. Inhibition activity was assessed, when no or only small product signal intensity was observed. Then, the compounds present in those wells, where complete or partial inhibition was observed, were screened individually. Thus, one compound could be identified which completely inhibited the enzymatic activity of anthrax lethal factor. Incubation of the enzyme in the presence of varying amounts of inhibitor and determination of the relative amount of product formed during the reactions enabled quantification of the inhibition activity. Based on these assays, an  $IC_{50}$  value for the inhibitor could be calculated that fitted well to the value obtained by a photometric reference assay. With this example, the high potential of SAMDI-MS for chemical screening of inhibitory activity in a high-throughput environment such as drug discovery has been impressively demonstrated. A variation of the SAMDI-MS approach for monitoring enzymatic conversions has been presented by Min et al. within a so-called pull-down assay scheme (Fig. 8.14) [25].

In this pull-down assay, the enzymatic reaction is carried out completely in solution. Samples taken from the reaction mixture are then transferred to a SAM-modified MALDI target, on which the remaining substrate and the reaction product are selectively immobilized. Subsequent to the extraction of the analytes, the target is rinsed, treated with matrix, and MALDI-MS analysis is carried out. A major advantage of this assay scheme is that the inherent danger of negative influences on the reaction kinetics, which may be caused by immobilization of the substrate as in standard SAMDI-MS-based assay formats, is circumvented. Additionally, by selective extraction of the analytes of interest and removal of the other

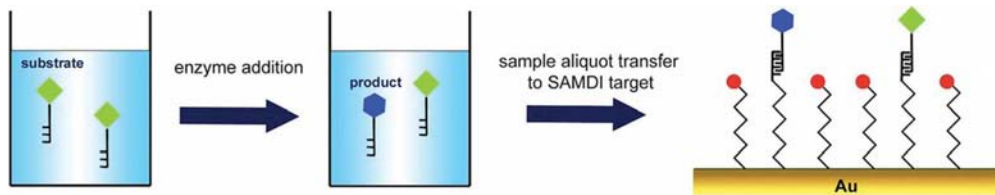


**Fig. 8.14** Scheme of a pull-down assay. The enzymatic reaction is completely carried out in solution. Upon enzyme addition, substrate is consumed, and product is formed. Sample aliquots are taken at several time points from the reaction mixture and are taken to a SAM, which has been modified with selective end groups. The latter are able to bind both substrate and product. Finally, matrix is added, and the SAM is analyzed by means of MALDI-MS.

reaction mixture constituents, the chemical background during the MS analysis can be significantly reduced.

Recently, a SAMDI-MS assay was described by means of which endogenous caspase protease activities in cell lysates can be determined [26]. Similar to the assay used to determine anthrax lethal factor inhibitors, peptide substrate SAMs for either caspase-3 or -8 were treated with cell lysates. In contrast to fluorescence assays, also longer peptide substrates could be used, thus enabling a better resolution of the two caspase activities.

## 8.4

### Conclusion

Since its introduction some 20 years ago, MALDI-MS has been established as a standard technique for a large variety of applications within the field of bioanalytical mass spectrometry, ranging from protein identification to enzyme activity screening. Quantitative analysis has long been a challenge, but, with the use of isotopically labelled standards, it is steadily obtaining more attention.

In contrast to established MALDI-MS techniques, DIOS-MS is a comparatively new technique. However, over the last five years, it has been gaining steadily more attention and promising results have already been obtained in all those cases, where interference from classic MALDI matrices needed to be avoided. Owing to the fact that DIOS-MS is still a juvenile technique, it is hard to predict future developments, but especially in the field of silicon modifications further promising developments can be foreseen, accompanied by new applications.

SAMDI as a merger of the rapidly growing field of SAMs and the established MALDI-MS is an even more recent technique. Interesting assay formats and applications have already been described combining the selectivity of SAMs with the efficiency of MALDI. Nevertheless, there are, up to now, too few applications in order to predict in which way SAMDI is going to develop. For future applications,

especially in the field of medicinal chemistry with its evident need for high-throughput systems, the parallel immobilization of various biomolecules to one SAM may turn out to be a versatile tool whenever rapid screening of drug candidates, enzymes or inhibitors is concerned.

## References

- 1 Karas, M., Hillenkamp, F.: Laser desorption/ionization of proteins with molecular masses exceeding 10 000 Daltons. *Anal. Chem.* **1988**, 60, 2299–2301.
- 2 Fenselau, C.: MALDI MS and strategies for protein analysis. *Anal. Chem.* **1997**, 69, 661A–665A.
- 3 Kokko, K.P., Dix, T.A.: Monitoring neurotensin [8–13] degradation in human rat serum utilizing matrix-assisted laser desorption/ionization time-of-flight mass spectrometry. *Anal. Biochem.* **2002**, 308, 34–41.
- 4 Petkovic, M., Müller, J., Müller, M., Schiller, J., Arnold, K., Arnold, J.: Application of matrix-assisted laser desorption/ionization time-of-flight mass spectrometry for monitoring the digestion of phosphatidylcholine by pancreatic phospholipase A<sub>2</sub>. *Anal. Biochem.* **2002**, 308, 61–70.
- 5 Shimazaki, Y., Sugarawa, Y., Manabe, T.: Nondenaturing two-dimensional electrophoresis enzyme profile involving activity and sequence structure of cytosol proteins from mouse liver. *Proteomics* **2004**, 4, 1406–1411.
- 6 Shimazaki, Y., Sugarawa, Y.: Activity and sequence structure analysis of cytosolic dehydrogenase by mass spectrometry after separation by nondenaturing two-dimensional electrophoresis. *Anal. Biochem.* **2004**, 328, 87–89.
- 7 Kang, M.-J., Tholey, A., Heinze, E.: Application of automated matrix-assisted laser desorption/ionization time-of-flight mass spectrometry for the measurement of enzyme activities. *Rapid Commun. Mass Spectrom.* **2001**, 15, 1327–1333.
- 8 Bungert, D., Heinze, E., Tholey, A.: Quantitative matrix-assisted laser desorption/ionization mass spectrometry for the determination of enzyme activities. *Anal. Biochem.* **2004**, 326, 167–175.
- 9 Bungert, D., Bastian, S., Heckmann-Pohl, D.M., Giffhorn, F., Heinze, E., Tholey, A.: Screening of sugar converting enzymes using quantitative MALDI-ToF mass spectrometry. *Biotechnol. Lett.* **2004**, 26, 1025–1030.
- 10 Greis, K.D., Zhou, S., Burt, T.M., Carr, A.N., Dolan, E., Easwaran, V., Evdokimov, A., Kawamoto, R., Roesgen, J., Davis, G.F.: MALDI-TOF MS as a label free approach to rapid inhibitor screening. *J. Am. Soc. Mass Spectrom.* **2006**, 17, 815–822.
- 11 Kang, M.J., Tholey, A., Heinze, E.: Quantification of low molecular mass substrates and products of enzyme catalyzed reactions using matrix-assisted laser desorption/ionization time-of-flight mass spectrometry. *Rapid Commun. Mass Spectrom.* **2000**, 14, 1972–1978.
- 12 Wei, J., Buriak, J., Siuzdak, G.: Desorption–ionization mass spectrometry on porous silicon. *Nature* **1999**, 401, 243–246.
- 13 Cullis, A.G., Canham, L.T., Calcott, P.D.J.: The structural and luminescence properties of porous silicon. *J. Appl. Phys.* **1997**, 82, 909–965.
- 14 Shen, Z., Thomas, J.J., Averbuj, C., Broo, K.M., Engelhard, M., Crowell, J.E., Finn, M.G., Siuzdak, G.: Porous silicon as a versatile platform for laser desorption/ionization mass spectrometry. *Anal. Chem.* **2001**, 73, 612–619.
- 15 Go, E.P., Shen, Z., Harris, K., Siuzdak, G.: Quantitative analysis with desorption/ionization on silicon

- mass spectrometry using electrospray deposition. *Anal. Chem.* **2003**, 75, 5475–5479.
- 16 Lewis, W.G., Shen, Z., Finn, M.G., Siudzak, G.: Desorption/ionization on silicon (DIOS) mass spectrometry: background and applications. *Int. J. Mass Spectrom.* **2003**, 226, 107–116.
  - 17 Deng, G.J., Sanyal, G.: Applications of mass spectrometry in early stages of target based drug discovery. *J. Pharmaceut. Biomed. Anal.* **2006**, 40, 528–538.
  - 18 Budimir, N., Blais, J.C., Fournier, F., Tabet, J.C.: The use of desorption/ionization on porous silicon mass spectrometry for the detection of negative ions for fatty acids. *Rapid Commun. Mass Spectrom.* **2006**, 20, 680–684.
  - 19 Thomas, J.J., Shen, Z., Crowell, J.E., Finn, M.G., Siudzak, G.: Desorption/ionization on silicon (DIOS): a diverse mass spectrometry platform for protein characterization. *Proc. Natl. Acad. Sci. USA* **2001**, 98, 4932–4937.
  - 20 Shen, Z., Go, E.P., Gamez, A., Apon, J.V., Fokin, V., Greig, M., Ventura, M., Crowell, J.E., Blixt, O., Paulson, J.C., Stevens, R.C., Finn, M.G., Siudzak, G.: A mass spectrometry plate reader: monitoring enzyme activity and inhibition with a desorption/ionization on silicon (DIOS) platform. *ChemBioChem* **2004**, 5, 921–927.
  - 21 Xu, S., Pan, C., Hu, L., Zhang, Y., Guo, Z., Li, X., Zou, H.: Enzymatic reaction of the immobilized enzyme on porous silicon studied by matrix assisted laser desorption/ionization-time of flight-mass spectrometry. *Electrophoresis* **2004**, 25, 3669–3676.
  - 22 Su, J., Mrksich, M.: Using mass spectrometry to characterize self-assembled monolayers presenting peptides, proteins, and carbohydrates. *Angew. Chem. Int. Ed.* **2002**, 41, 4715–4718.
  - 23 Min, D.H., Su, J., Mrksich, M.: Profiling kinase activities by using a peptide chip and mass spectrometry. *Angew. Chem. Int. Ed.* **2004**, 43, 5973–5977.
  - 24 Min, D.H., Tang, W.J., Mrksich, M.: Chemical screening by mass spectrometry to identify inhibitors of anthrax lethal factor. *Nat. Biotechnol.* **2004**, 22, 717–723.
  - 25 Min, D.H., Yeo, W.S., Mrksich, M.: A method for connecting solution-phase enzyme activity assays with immobilized format analysis by mass spectrometry. *Anal. Chem.* **2004**, 76, 3923–3929.
  - 26 Su, J., Rajapasksha, T.W., Peter, M.E., Mrksich, M.: Assays of endogenous caspase activities: a comparison of mass spectrometry and fluorescence formats. *Anal. Chem.* **2006**, 78, 4945–4951.



## **Part III**

**Studying target-ligand interactions analyzing  
intact target-ligand complexes by MS**





## 9

## Tethering: Fragment-based Drug Discovery by Mass Spectrometry

Mark T. Cancilla and Daniel A. Erlanson

## 9.1

### Introduction

Pressure to keep early phase pipelines filled with drug leads has heightened interest in developing innovative technology to discover drug-like molecules. One alternative and effective approach for generating small-molecule inhibitors is “fragment-based drug discovery”, a process which identifies one or more low-affinity, low molecular weight, drug-like “fragments” and subsequently elaborates or combines them to make compounds that are analogous to a high throughput screening (HTS) hit [1–3]. Fragment-based discovery has an advantage over traditional HTS because it samples more chemical “diversity space” with significantly fewer molecules (thousands for fragment-based approaches compared to millions in traditional HTS formats) [4].

One pervasive challenge in fragment-based discovery is how to identify small chemical fragments that bind only weakly to target biological molecules. Currently, several different screening techniques are used for discovering such fragments: functional binding assays [5], NMR-based screening [6–8], crystallography-based screening [9–10] and mass spectrometry-based methods [11–15]. All have unique advantages and limitations.

For mass spectrometry, modern ionization methodologies such as electrospray ionization (ESI) [16] and matrix-assisted laser desorption ionization (MALDI) [17], along with advances in current mass spectrometry platforms, would seem ideal for the rapid discovery of fragments, but detecting molecules possessing millimolar binding affinities is not trivial. Mass spectrometry-based ligand binding assays such as non-covalent mass spectrometry and the myriad of front-end, affinity-based mass spectrometry techniques (such as AS-MS [18]) are not ideal for detecting such low affinity ligands. To overcome these barriers, we developed a discovery technology, *Tethering* [19], centered on detecting fragment–protein conjugates by LC/MS. Among fragment-based approaches, *Tethering* is unique in using a covalent, reversible bond to stabilize the interaction between a fragment and a target protein. The bond forms is stable only when there is inherent

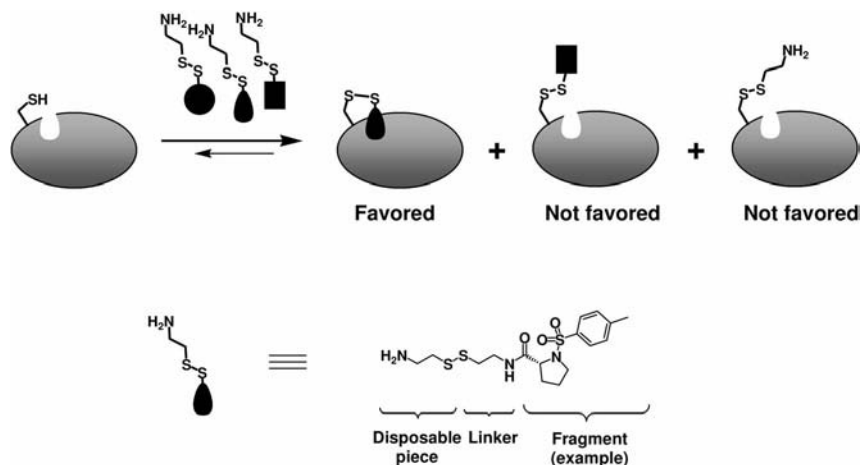


**Fig. 9.1** Tethering schematic. A fragment will be selected if it has inherent affinity for the protein and binds in the vicinity of the cysteine residue. An example disulfide-containing fragment is shown below, illustrating the variable portion, the linker, and the cysteamine piece that is lost when the fragment forms a disulfide bond with the protein.

affinity between the ligand and the protein target. The fragment is then rapidly identified using electrospray mass spectrometry to detect the modified, intact protein.

The general process of Tethering is outlined in Fig. 9.1. First, a cysteine residue is either co-opted or introduced into a target protein. Metaphorically, the cysteine residue serves as a fishing line to capture fragments (fish) that bind near the cysteine. The protein is incubated with pools of thiol-containing small molecule fragments which are conjugated to a common, hydrophilic thiol (such as cysteamine) for improved water solubility. By controlling the redox conditions in the experiment with exogenous reducing agents, equilibria can be established so that the cysteine residue in the protein *reversibly* forms disulfide bonds with individual fragments. If no fragments have affinity for the interrogated area of the protein, no fragment should bind more favorably than any other, and a pool of fragments will produce a statistical mixture of different protein–fragment complexes, plus unmodified and cysteamine-modified protein. However, if a fragment has inherent affinity for the protein and binds near the cysteine residue, the fragment–protein conjugate will be stabilized, and this complex will predominate. A fragment thus selected can be easily identified through mass spectrometry of the equilibrium mixture: if each fragment in a pool has a unique molecular weight, so will the resulting protein–fragment conjugates. These captured fragments then serve as starting points for conversion to non-covalent ligands by removal of the thiol functionality and chemical optimization.

In the following pages, we present an overview of the theory, practice, and uses of Tethering. First we examine the experimental nuances of the screening meth-

odology. Next we demonstrate how the technology can be used in the active sites of enzymes to identify fragments, which can then be elaborated to more potent inhibitors. The final section considers how Tethering can be used not only to identify fragments but also to link these fragments to more rapidly identify starting points for drug discovery.

## 9.2

### Reduction to Practice

#### 9.2.1

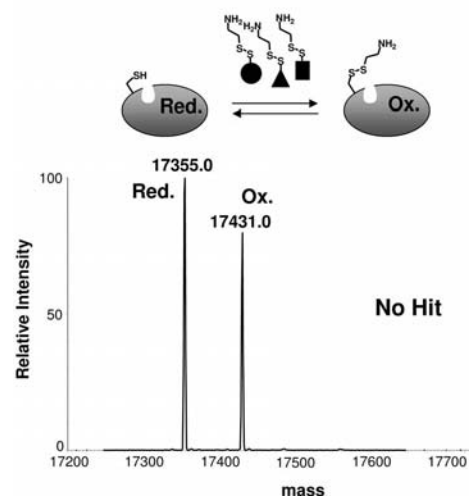
##### Technique

To prepare a biological target for Tethering, the target protein must contain a cysteine residue near an area of interest (e.g. an enzyme active site or a “hot-spot” of a protein–protein interface). If no native cysteines are in a suitable location, a cysteine can be introduced at an appropriate spot via site-directed mutagenesis. One potential limitation of Tethering is this need to generate cysteine-containing mutant proteins, but with site-directed mutagenesis and protein expression, this is rarely a significant hurdle. Tethering does require sufficient knowledge about a protein’s structure to inform where to place the cysteine; while a crystal structure is not required, a good model of the protein is essential. The most labor-intensive requirement for Tethering is the synthesis of a library of disulfide-containing fragments: very few disulfide-containing fragments are commercially available, and introducing a disulfide onto a fragment requires at least one additional chemical step. Sunesis Pharmaceuticals has synthesized a library of roughly 18 000 disulfide-containing fragments. They are pooled into groups of roughly ten fragments, each with a unique molecular weight in a given pool. The development and production of our Cys-mutants and disulfide-containing library are reviewed elsewhere [12].

In Tethering, the protein target is screened by mixing the target with each pool under reducing conditions that enhance disulfide exchange. 2-Mercaptoethanol (in the low millimolar concentration range) is used as the reductant due to its redox potential ( $-0.196$  V at pH 7) [21]. Disulfide exchange allows a reduced cysteine on the protein to react with each disulfide-containing fragment. After equilibrium is established, the reaction mixture is injected into an LC/ESI-MS instrument, a system which is ideally suited for measuring protein modification by allowing both rapid on-line sample clean-up and the ability to accurately measure intact protein mass.

As we optimized Tethering we used a variety of mass spectrometers. In our experience, the sensitivity and high resolution of TOF analyzers has provided the most rapid and accurate analyses of intact proteins. An example of an ESI-TOF data set from a standard experiment is illustrated in Fig. 9.2. Figure 9.2A is the deconvoluted mass spectrum of a Cys-mutant target protein after equilibration

a



b

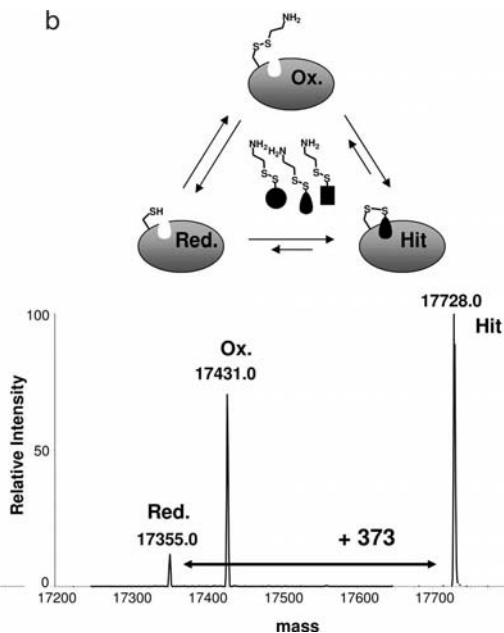


**Fig. 9.2** (a) Deconvoluted ESI-TOF mass spectrum of a Cys-containing target protein equilibrated with a pool of ten disulfide-containing fragments with no hit discovered. Red. Reduced or unmodified protein; Ox. protein oxidized by cysteamine. (b) Deconvoluted ESI-TOF mass spectrum of the same protein representing a strong hit from a different pool of ten disulfide-containing fragments. The mass of the protein has shifted according to the mass of the fragment captured by the protein.

with a pool of ten disulfide-containing compounds from a single well in a 96-well plate. The two peaks represent the unmodified protein (17 355 Da) and the protein oxidized with either 2-mercaptoethanol or cysteamine, the solubilizing functionality that is common to all library members (17 431 Da). The detection of cysteamine modification indicates proper disulfide scrambling has occurred, and time-course experiments demonstrate when the reaction mixture is at equilibrium. In this pool, none of the ten disulfide-containing fragments had any detectable affinity for the target. In contrast, Fig. 9.2B is the deconvoluted mass spectrum representing a hit from a different pool of ten disulfide-containing compounds. The mass of the protein has shifted 373 Da, due to a shift in the complex equilibria towards a protein–fragment conjugate. The disulfide bond is stabilized due to contributions from the affinity between the protein and the fragment, and the covalently modified protein conjugate is easily identified by LC/ESI-MS.

Tethering is also amenable to high throughput sample analysis, and analytical methods have been streamlined to routinely investigate thousands of protein–

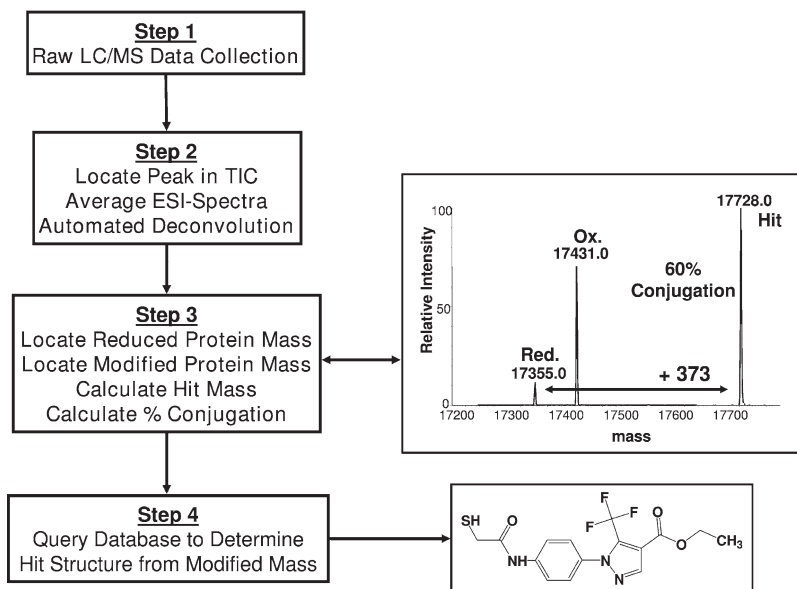


**Fig. 9.3** Flowchart illustrating how data is automatically handled and processed to yield the chemical structure of a hit. The LC/MS systems have been integrated with software to automatically deconvolute each protein charge state distribution and determine potential protein conjugation and obtain the structure of a hit by database searching.

fragment interactions on a daily basis. The reaction mixtures are set up in 96 well plates and standard autosamplers inject the equilibrated reaction mixtures into the LC/MS system. Ballistic HPLC gradients are used to rapidly load, desalt and elute the proteins using C4 guard columns with a total run time of 2–3 min per analysis. To expedite data handling, each LC/MS system has been integrated with customized software to automatically deconvolute each spectrum, determine potential protein conjugation, and obtain the structure of a hit by database searching (Fig. 9.3). After the raw data set is collected, it is transferred to a processing computer where the charge state distribution of the protein is located in the total ion count (TIC), the spectra are averaged and each averaged charge state distribution spectrum is deconvoluted to a zero charge state spectrum, revealing the accurate mass of the protein and any potential modifications.

Next, custom software is used to interrogate the deconvoluted data set to identify the protein's mass and the intensity of the peak, determine any potential modification above a user-defined intensity threshold and, if there is a hit, calculate the mass and the relative conjugation of the fragment. In fact, the percent conjugation is used as a measure of relative affinities of the fragment hits. Since the library is mass encoded (all compounds in a well have a unique mass), the calculated mass of any hits are queried into a database to identify their structures.

## 9.2.2

**Advantages**

The reversible covalent bond formation in Tethering has both advantages and disadvantages. On the positive side, ESI/mass spectrometry detects hits rapidly. As a “positive” detection method, it is less prone to false positives than are typical inhibition assays [22]. Since the bond must be within several Ångströms of the cysteine residue, it roughly indicates where fragments bind. Moreover, the bond facilitates modeling and crystallography: if the fragment is not highly soluble, the non-covalent complex may be difficult to crystallize and the disulfide-bonded complex is more likely to yield a structure. A related advantage is that the stoichiometry of the fragment in the complex is exactly one-to-one.

Of course, the very ability to detect real but weak binders is a double-edged sword. Typical affinities for fragments are initially weak (in the millimolar range). They can be improved through chemical optimization, but optimizing a very weakly binding fragment can be challenging. However, a second-generation version of the technology, *Tethering with extenders*, largely solves this problem (see below).

## 9.3

**Finding Fragments: Thymidylate Synthase Proof of Principle**

We first applied Tethering to thymidylate synthase (TS). This enzyme converts deoxyuridine monophosphate (dUMP) to thymidine monophosphate (dTMP), an activity essential for DNA synthesis. The cancer drug 5-fluorouracil irreversibly inhibits TS, and a selective inhibitor of a non-human form of the enzyme could yield a new antibiotic or antifungal drug [23].

In addition to its biological interest, TS was ideally suited for developing Tethering [11]. It is well characterized both structurally and mechanistically, and the many inhibitors developed for the enzyme demonstrate that it is a “druggable” target. Moreover, the active site contains a nucleophilic cysteine residue. Although the *Escherichia coli* version of the enzyme we used contains four other cysteine residues, crystallography revealed these to be largely non-surface exposed, and they did not interfere with our experiments.

Initial experiments screened pools of ten compounds, each present in roughly ten-fold excess over TS, with a total disulfide concentration of about 2 mM and a reducing agent (2-mercaptoethanol) concentration of 1 mM. After screening about 1200 compounds, we saw a strong selection for N-phenyl-sulfonamide-substituted proline fragments, as represented by N-tosyl-D-proline (Fig. 9.4). In a separate experiment, this fragment could even be selected from a pool of 100 compounds, each present at roughly the same concentration as TS. However, larger pools have more compounds with similar molecular weights, making data more challenging to interpret. In practice, pools of five to ten compounds strike a balance between throughput and unambiguous interpretation.

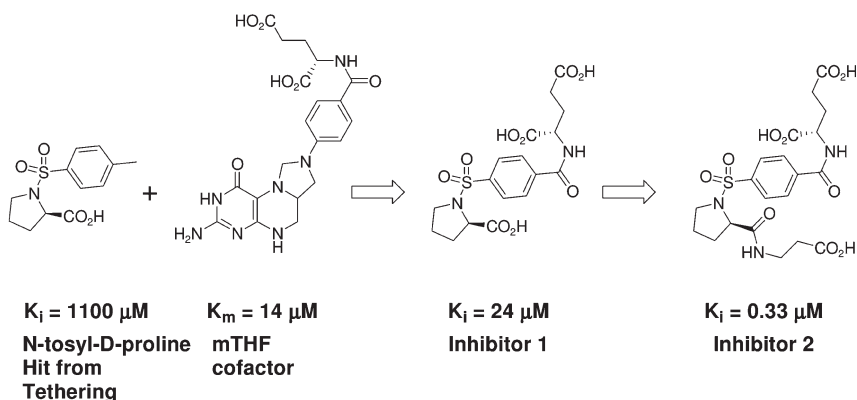


**Fig. 9.4** Improvements in potency of N-tosyl-D-proline. Structural analyses revealed that the glutamate moiety from the mTHF cofactor could be appended to the hit from Tethering, and further elaboration led to a submicromolar inhibitor.

A critical feature of Tethering is that thermodynamics govern disulfide bond formation. To ensure that fragment selection was thermodynamic rather than kinetic, we added a reducing agent (2-mercaptoethanol). Without reducing agent, the active-site cysteine reacts with whichever disulfide it encounters first, usually the solubilizing element common to all library members. Although even a small amount of reducing agent allows disulfide exchange, the N-tosyl-D-proline fragment could tolerate strongly reducing conditions. In fact, even in the presence of

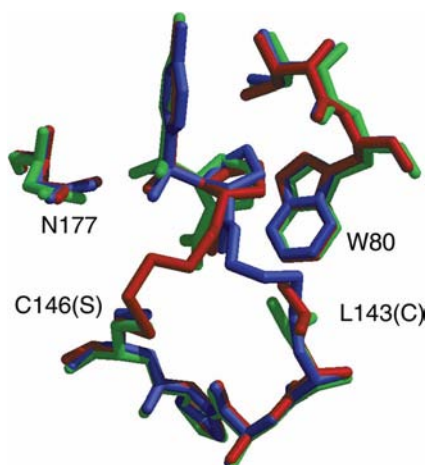


**Fig. 9.5** Structures of TS with the N-tosyl-D-proline fragment bound through two different cysteine residues (red, blue) or non-covalently bound (green). Reprinted from [12] with permission.



20 mM of 2-mercaptoethanol, where the ratio of reductant to disulfide was 10:1, a mass corresponding to N-tosyl-D-proline conjugation was still prominent.

Screens with chemically similar fragments showed that although substitutions around the aromatic moiety and in the stereochemistry of the proline residue did not disrupt the fragment's affinity, the proline residue itself was essential. Crystallography of N-tosyl-D-proline covalently linked to TS explained these structure–activity relationships (SAR): the proline residue sits snugly within a hydrophobic pocket, and one of the sulfonamide oxygen atoms makes a hydrogen bond to Asn 177 on the enzyme, but the phenyl ring is in a relatively open area (Fig. 9.5).

To learn whether the disulfide bond itself changed how the fragment binds, we determined the crystal structure of N-tosyl-D-proline bound non-covalently to TS. As shown in Fig. 9.5, the “free” fragment binds in a nearly identical manner to the disulfide-linked fragment, demonstrating that the covalent linkage does not affect how the fragment binds.

To test whether nearby cysteines would be suitable for Tethering, we mutated the active-site cysteine to a serine and introduced a new cysteine nearby (C146S, L143C). When we performed Tethering on this mutant enzyme, we also strongly selected N-tosyl-D-proline, and when we solved the X-ray crystal structure we found that this fragment binds in a manner very similar to the other structures, despite the very different trajectories that the disulfide linkage takes (Fig. 9.5). The lack of influence of the disulfide attachment on the fragment's binding mode, along with the fact that the fragment could be strongly selected from more than one cysteine residue, suggested the inherent fragment affinity was more important energetically than the specifics of how it was linked to the protein.

Enzymatic assays determined the inhibitory potential of N-tosyl-D-proline: the fragment has a  $K_i$  of 1.1 mM, so weak that it likely would be missed in any conventional screen. However, the crystal structure shows that the phenyl group binds in a similar position to the para-amino-benzoic acid moiety of the natural co-factor, methylenetetrahydrofolate (mTHF); by simply grafting the glutamate moiety from this co-factor onto N-tosyl-D-proline, we boosted the affinity 40-fold to 24  $\mu$ M. A small library of compounds with substitutions off the proline yielded a compound with a  $K_i$  of 330 nM, three orders of magnitude more potent than the original fragment (Fig. 9.4). Overall, applying Tethering to TS demonstrated the capability of mass spectrometry to selectively discover weak, disulfide-containing fragments that were optimized into lead-like compounds.

## 9.4

### Finding and Linking Fragments in One Step: Tethering with Extenders

#### 9.4.1

#### Caspase-3

One of the biggest challenges in fragment-based drug discovery is not finding fragments but linking them. In the case of TS (above), we used structure-based

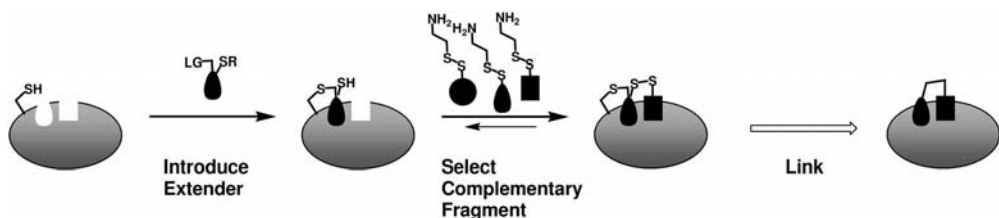


**Fig. 9.6** Tethering with extenders. An extender is used to modify a residue in the protein; the extender has some inherent affinity for the protein and also contains a thiol that can be used for Tethering. When a complementary fragment is identified, this can be linked with binding elements from the extender to generate a potent inhibitor. (LG = leaving group).

drug design to improve the potency of a fragment identified from Tethering. However, the true combinatorial power of fragment-based approaches only becomes apparent when two fragments are linked together to generate a potent inhibitor. For a general method to link fragments, we invented *Tethering with extenders* [24].

Tethering with extenders (Fig. 9.6) takes a fragment that binds a protein at a desired site, and modifies the fragment so that it becomes a platform for Tethering. This fragment needs only to have modest affinity and could come from a previous experiment using Tethering or other sources. The fragment is modified to contain an electrophile that reacts with a cysteine on the target protein, plus a potentially masked thiol residue. The resulting modified fragment is called an “extender.” After the extender forms a covalent complex with the protein target, the thioester (if present) can be deprotected to reveal the thiol for Tethering. Fragments identified through these screens can be identified through the mass spectrometry and deconvolution process used for Tethering without extenders.

The two-dimensional connectivity between the extender and any fragments identified from subsequent screens will be known, even if the exact placement of both fragments is not. With this knowledge, binding elements from the extender can be easily connected to newly discovered fragments. In theory, the resulting molecule should have two separate binding elements and bind the target molecule more tightly than either fragment alone.

We tested this strategy on the enzyme caspase-3, a cysteine-aspartyl protease that is one of the central “executioners” of apoptosis. Excess apoptosis is attributed to a variety of diseases, from stroke to Alzheimer’s Disease to sepsis, making caspase-3 a popular drug target [25]. The enzyme also made an ideal starting point for constructing extenders. It is well characterized both structurally and mechanistically and contains an active site cysteine residue that is irreversibly alkylated by small molecule inhibitors.

The first extender we constructed is shown in Fig. 9.7. Mass spectrometry showed we could modify caspase-3 cleanly and quantitatively with this molecule, even though the large subunit of the enzyme contains four other cysteine residues. We could also fully deprotect the thioester to reveal a free thiol. Screens

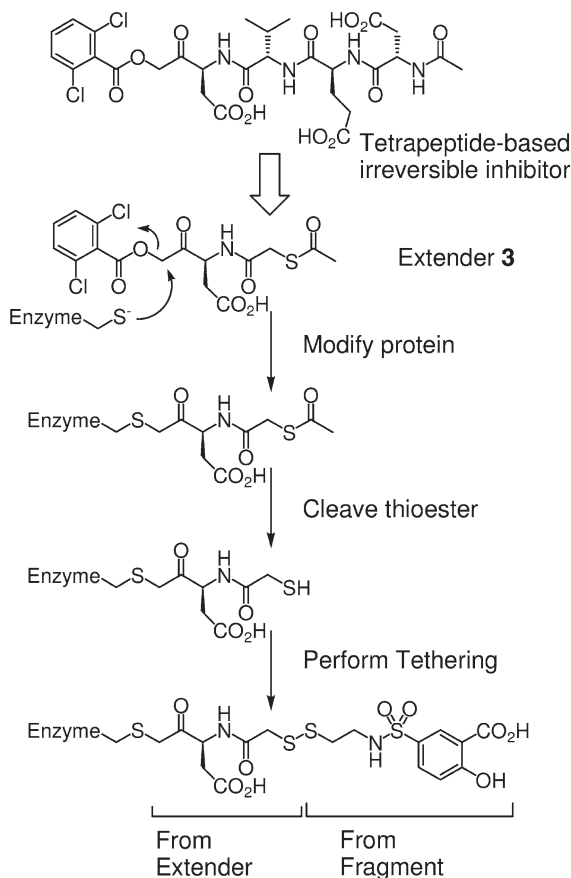


**Fig. 9.7** Tethering with extenders on caspase-3. The extender (3) covalently modifies the protein and can then be deprotected to reveal a thiol for Tethering. One of the strongest hits is the salicylic acid derivative shown.

against a library of about 7000 disulfide-containing fragments yielded one strong hit, a sulfamoyl salicylic acid (Fig. 9.7). By simply replacing the disulfide bond with two methylenes and replacing the irreversible warhead with a reversible aldehyde, we created an inhibitor with  $K_i = 2.8 \mu\text{M}$ . By rigidifying the linker, we boosted the affinity to 200 nM. Further medicinal chemistry allowed us to obtain 20 nM inhibitors (Fig. 9.8) [24–26].

To ensure the technique could be generalized, we constructed a second extender to explore a slightly different area of the protein. We modified caspase-3 with this extender, deprotected the thioester, and screened the conjugate against our fragment library. We did not rediscover the salicylic acid hit from our first extender screen, but we did identify several other hits, including a thiophene sulfone. When this fragment was linked to the extender, the resulting inhibitor

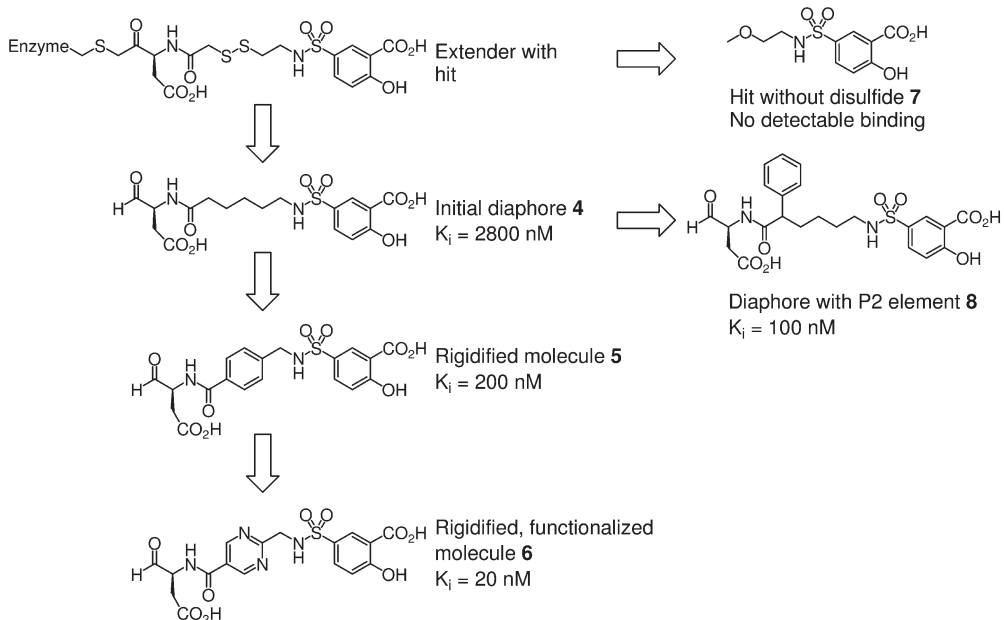


**Fig. 9.8** Evolution of a fragment from Tethering with extenders to a potent caspase-3 inhibitor. Simple replacement of the disulfide linker with an alkyl linker resulted in a low micromolar inhibitor (**4**), and rigidification (**5**) and functionalization (**6**) of this linker led to increasingly potent inhibitors. The salicylic acid hit itself (**7**) had no detectable binding.

had  $K_i = 330 \text{ nM}$  [24]. These examples illustrate the speed with which Tethering with extenders can lead to potent inhibitors. Moreover, these inhibitors are non-peptidic, and so more useful as drug leads.

We used crystallography to understand the binding mode of these fragments. The structure of the salicylic acid fragment bound through the disulfide is shown in Fig. 9.9a, superimposed upon the structure of a tetrapeptide-based inhibitor. Significantly, the two inhibitors occupy roughly the same volume, and make many of the same contacts, but do so using very different chemical moieties. Moreover, the S2 pocket in the salicylic acid structure is collapsed, while the S4 pocket expands to make room for the larger salicylic acid moiety. By introducing a substituent that bound in the S2 pocket, we boosted affinity by nearly two orders of magnitude (Fig. 9.8) [27].

All of these features contrast with the structure of the second extender-fragment complex, shown in Fig. 9.9b. Here, the extender forces itself into the S2 pocket, but the disulfide linker then curves back to place the thiophene sulfone into the S4 pocket. The sulfone makes some of the same hydrogen bonds as the salicylic acid and the aspartyl residue in the tetrapeptide but with completely different chemistry. The flexibility of caspase-3 to accommodate different

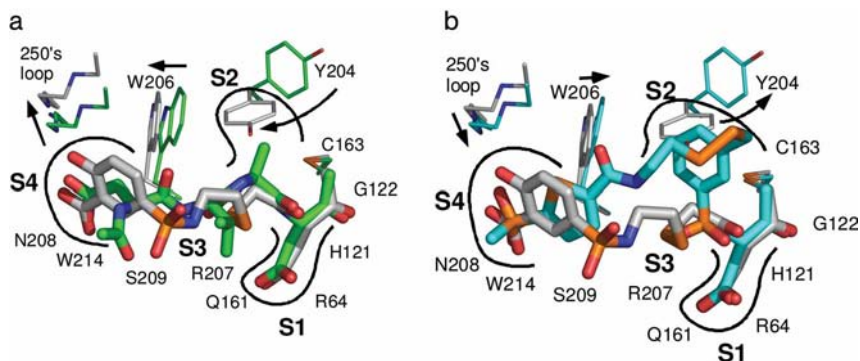


**Fig. 9.9** (a) Structure of the salicylic acid fragment covalently bound to caspase-3 (gray), superimposed on a tetrapeptide-based inhibitor (green). Note the collapse of the S2 pocket and the widening of the S4 pocket to accommodate the salicylic acid moiety. (b) Structure of a second fragment covalently bound to caspase-3 (blue) superimposed on

the salicylic acid fragment. Here the S2 pocket is intact, and the linker takes an alternative path to arrive in the S4 pocket. Reprinted from [25] with permission. The molecular graphics in this and all other figures were done using the program PyMol (see DeLano, W. L. (2004) PyMOL, available at: <http://pymol.sourceforge.net/>).

inhibitors emphasizes the ability of Tethering to identify fragments that would not have been easy to predict using structure-based design.

#### 9.4.2

##### Caspase-1

Tethering with extenders was also used to identify inhibitors to the anti-inflammatory target caspase-1 [28, 29]. In this case, one of the same extenders previously designed for caspase-3 selected an entirely different set of fragments. This is consistent with different substrate peptide sequence preferences: WEHD for caspase-1 vs DEVD for caspase-3 [30].

As with caspase-3, these hits were converted into potent, soluble inhibitors by replacing the disulfide linkage with a simple alkyl linkage (Fig. 9.10). As in the case of caspase-3, rigidifying the linker could improve affinity, as could introducing a hydrophobic moiety at the S2 position. Several of these molecules demonstrated activity in cellular assays and selectivity for caspase-1 over the closely related caspase-5. Crystallography of several of these molecules in complex with caspase-1 revealed that they bind in an extended conformation as expected, but that the S2 pocket that collapses in caspase-3 remains open in caspase-1.

## 9.5

### Conclusions

This chapter has presented an introduction to Tethering with a focus on how mass spectrometry enables the technology to rapidly find inhibitors to drug

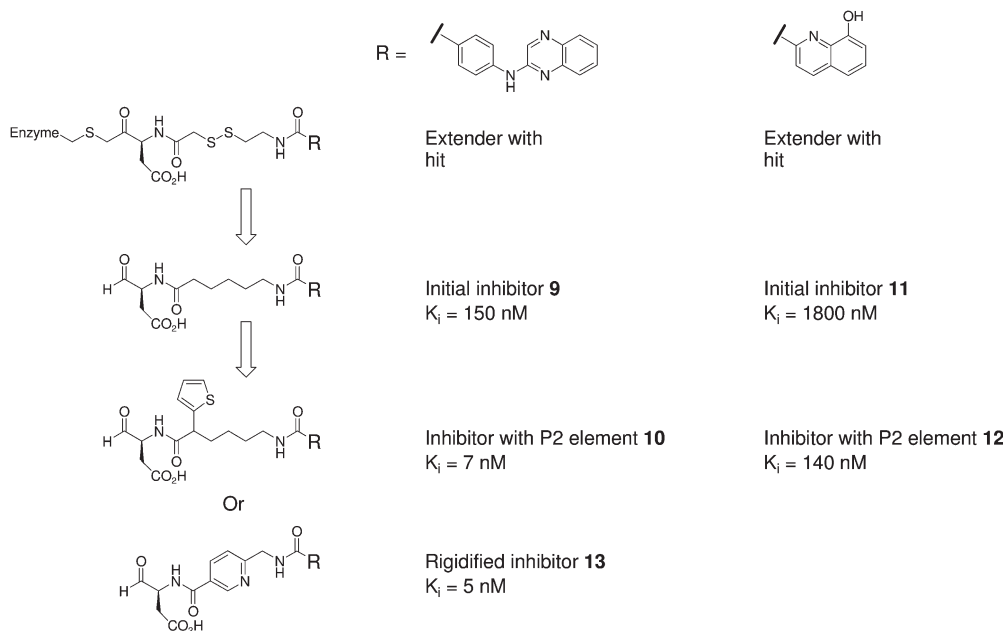


**Fig. 9.10** Tethering with extenders to identify caspase-1 inhibitors. Two of the hits from tethering are shown, as are inhibitors derived from them.

targets. The technology has also been employed to identify inhibitors to protein-protein interactions and to identify fragments that bind to allosteric sites [31–34]. Although mass spectrometry has been critical in most applications of Tethering, in some cases functional screens are sufficient, particularly where MS is challenging, such as membrane-bound proteins [35–36].

As a fragment-identification method, Tethering is one of many possible approaches. The technique is unique because it uses a covalent bond, which ensures that fragments bind in a stoichiometric fashion, and also allows rapid identification of low-affinity fragments through mass spectrometry. Tethering can target specific sites and wide-ranging conformations of a protein. Moreover, there is some evidence that by employing mass spectrometry, Tethering can identify fragments that bind more weakly than those identified by other methods. For example, the sulfamoyl salicylic acid fragment identified in caspase-3 showed no detectable inhibition by itself. Although this increases the range of fragments accessible to the medicinal chemist, it does raise the question of whether some fragments may be so weak as to be essentially useless for further development. Nonetheless, given the success observed thus far, we believe there are many untapped opportunities for Tethering.

## Acknowledgements

We thank all of our colleagues at Sunesis Pharmaceuticals for their contributions, without which Tethering would not have been possible, and Monya L. Baker for editorial assistance. Portions of this chapter appeared in a similar form in a previous book in this series [20], and Marcus D. Ballinger and James A. Wells both contributed to the editing of these sections.

## References

- 1 Erlanson, D.A., McDowell, R.S., O'Brien, T.: Fragment-based drug discovery. *J. Med. Chem.* **2004**, 47, 3463–3482.
- 2 Rees, D.C., Congreve, M., Murray, C.W., Carr, R.: Fragment-based lead discovery. *Nat. Rev. Drug Discov.* **2004**, 3, 660–672.
- 3 Jahnke, W., Erlanson, D.A. (Eds): *Fragment-Based Approaches in Drug Discovery. Vol 34 in series Methods and Principles in Medicinal Chemistry (Series Eds: R. Mannhold, H. Kubinyi, G. Folkers).* Weinheim, Germany: Wiley-VCH; 2006.
- 4 Lipinski, C.A.H., All, L.: Navigating chemical space for biology and medicine. *Nature* **2004**, 432, 855–861.
- 5 Maly, D.J., Choong, I.C., Ellman, J.A.: Combinatorial target-guided ligand assembly: identification of potent subtype-selective c-Src inhibitors. *Proc. Natl Acad. Sci. USA* **2000**, 97, 2419–2424.
- 6 Shuker, S.B., Hajduk, P.J., Meadows, R.P., Fesik, S.W.: Discovering high-affinity ligands for proteins: SAR by NMR. *Science* **1996**, 274, 1531–1534.
- 7 Hajduk, P.J., Gerfin, T., Boehlen, J.M., Haberli, M., Marek, D., Fesik, S.W.: High-throughput nuclear magnetic resonance-based screening. *J. Med. Chem.* **1999**, 42, 2315–2317.
- 8 Huth, J.R., Sun, C.: Utility of NMR in lead optimization: fragment-based approaches. *Comb. Chem. High. Throughput Screen.* **2002**, 5, 631–643.
- 9 Nienaber, V.L., Richardson, P.L., Klighofer, V., Bouska, J.J., Giranda, V.L., Greer, J.: Discovering novel ligands for macromolecules using X-ray crystallographic screening. *Nat. Biotechnol.* **2000**, 18, 1105–1108.
- 10 Congreve, M.S., Davis, D.J., Devine, L., Granata, C., O'Reilly, M., Wyatt, P.G., Jhoti, H.: Detection of ligands from a dynamic combinatorial library by X-ray crystallography. *Angew. Chem. Int. Ed. Engl.* **2003**, 42, 4479–4482.
- 11 Erlanson, D.A., Braisted, A.C., Raphael, D.R., Randal, M., Stroud, R.M., Gordon, E.M., Wells, J.A.: Site-directed ligand discovery. *Proc. Natl Acad. Sci. USA* **2000**, 97, 9367–9372.
- 12 Erlanson, D.A., Wells, J.A., Braisted, A.C.: Tethering: fragment-based drug discovery. *Annu. Rev. Biophys. Biomol. Struct.* **2004**, 33, 199–223.
- 13 Hofstadler, S.A., Griffey, R.H.: Analysis of noncovalent complexes of DNA and RNA by mass spectrometry. *Chem. Rev.* **2001**, 101, 377–390.
- 14 Swayze, E.E., Jefferson, E.A., Sannes-Lowery, K.A., Blyn, L.B., Risen, L.M., Arakawa, S., Osgood, S.A., Hofstadler, S.A., Griffey, R.H.: SAR by MS: a ligand based technique for drug lead discovery against structured RNA targets. *J. Med. Chem.* **2002**, 45, 3816–3819.
- 15 Ockey, D.A., Dotson, J.L., Struble, M.E., Stults, J.T., Bourell, J.H., Clark, K.R., Gadek, T.R.: Structure–activity relationships by mass spectrometry: identification of novel MMP-3 inhibitors. *Bioorg. Med. Chem.* **2004**, 12, 37–44.
- 16 Whitehouse, C.M., Dreyer, R.N., Yamashita, M., Fenn, J.B.: Electrospray interface for liquid

- chromatographs and mass spectrometers. *Anal. Chem.* **1985**, 57, 675–679.
- 17 Karas, M., Bachmann, D., Hillenkamp, F.: Influence of the wavelength in high-irradiance ultraviolet laser desorption mass spectrometry of organic molecules. *Anal. Chem.* **1985**, 57, 2935–2939.
  - 18 Annis, D.A., Nazef, N., Chuang, C.C., Scott, M.P., Nash, H.M.: A general technique to rank protein–ligand binding affinities and determine allosteric versus direct binding site competition in compound mixtures. *J. Am. Chem. Soc.* **2004**, 126, 15495–15503.
  - 19 Tethering is a registered service mark of Sunesis Pharmaceuticals, Inc., for its fragment-based drug discovery.
  - 20 Erlanson, D.A., Ballinger, M.D., Wells, J.A.: Tethering, in *Fragment-based Approaches in Drug Discovery*, ed. W. Jahnke, D.A. Erlanson, Wiley-VCH, Weinheim, **2006**, pp 285–310.
  - 21 Keire, D.A., Strauss, E., Guo, W., Noszál, B., Rabenstein, D.L.: Kinetics and equilibria of thiol/disulfide interchange reactions of selected biological thiols and related molecules with oxidized glutathione. *J. Org. Chem.* **1992**, 57, 123–127.
  - 22 McGovern, S.L., Caselli, E., Grigorieff, N., Shoichet, B.K.: A common mechanism underlying promiscuous inhibitors from virtual and high-throughput screening. *J. Med. Chem.* **2002**, 45, 1712–1722.
  - 23 Costi, M.P., Tondi, D., Rinaldi, M., Barlocco, D., Pecorari, P., Soragni, F., Venturelli, A., Stroud, R.M.: Structure-based studies on species-specific inhibition of thymidylate synthase. *Biochim. Biophys. Acta* **2002**, 1587, 206–214.
  - 24 Erlanson, D.A., Lam, J.W., Wiesmann, C., Luong, T.N., Simmons, R.L., DeLano, W.L., Choong, I.C., Burdett, M.T., Flanagan, W.M., Lee, D., Gordon, E.M., O'Brien, T.: In situ assembly of enzyme inhibitors using extended tethering. *Nat. Biotechnol.* **2003**, 21, 308–314.
  - 25 O'Brien, T., Lee, D.: Prospects for caspase inhibitors. *Mini Rev. Med. Chem.* **2004**, 4, 153–165.
  - 26 Choong, I.C., Lew, W., Lee, D., Pham, P., Burdett, M.T., Lam, J.W., Wiesmann, C., Luong, T.N., Fahr, B., DeLano, W.L., McDowell, R.S., Allen, D.A., Erlanson, D.A., Gordon, E.M., O'Brien, T.: Identification of potent and selective small-molecule inhibitors of caspase-3 through the use of extended tethering and structure-based drug design. *J. Med. Chem.* **2002**, 45, 5005–5022.
  - 27 Allen, D.A., Pham, P., Choong, I.C., Fahr, B., Burdett, M.T., Lew, W., DeLano, W.L., Gordon, E.M., Lam, J.W., O'Brien, T., Lee, D.: Identification of potent and novel small-molecule inhibitors of caspase-3. *Bioorg. Med. Chem. Lett.* **2003**, 13, 3651–3655.
  - 28 O'Brien, T., Fahr, B.T., Sopko, M., Lam, J.W., Waal, N.D., Raimundo, B.C., Purkey, H., Pham, P., Romanowski, M.J.: Structural analysis of caspase-1 inhibitors derived from Tethering. *Acta Crystallogr.* **2005**, F61, 451–458.
  - 29 Fahr, B.T., O'Brien, T., Pham, P., Waal, N.D., Baskaran, S., Raimundo, B.C., Lam, J.W., Sopko, M.M., Purkey, H.E., Romanowski, M.J.: Tethering identifies fragment that yields potent inhibitors of human caspase-1. *Bioorg. Med. Chem. Lett.* **2006**, 16, 559–562.
  - 30 Thornberry, N.A., Rano, T.A., Peterson, E.P., Rasper, D.M., Timkey, T., Garcia-Calvo, M., Houtzager, V., Nordstrom, P., Roy, S., Vaillancourt, J., Chapman, K., Nicholson, D.: A combinatorial approach defines specificities of members of the caspase family and Granzyme B. *J. Biol. Chem.* **1997**, 272, 17907–17911.
  - 31 Braisted, A.C., Oslob, J.D., Delano, W.L., Hyde, J., McDowell, R.S., Waal, N., Yu, C., Arkin, M.R., Raimundo, B.C.: Discovery of a potent small molecule IL-2 inhibitor through fragment assembly. *J. Am. Chem. Soc.* **2003**, 125, 3714–3715.



- 32 Arkin, M.R., Randal, M., DeLano, W.L., Hyde, J., Luong, T.N., Oslob, J.D., Raphael, D.R., Taylor, L., Wang, J., McDowell, R.S., Wells, J.A., Braisted, A.C.: Binding of small molecules to an adaptive protein–protein interface. *Proc. Natl Acad. Sci. USA* **2003**, 100, 1603–1608.
- 33 Raimundo, B.C., Oslob, J.D., Braisted, A.C., Hyde, J., McDowell, R.S., Randal, M., Waal, N.D., Wilkinson, J., Yu, C.H., Arkin, M.R.: Integrating fragment assembly and biophysical methods in the chemical advancement of small-molecule antagonists of IL-2: an approach for inhibiting protein–protein interactions. *J. Med. Chem.* **2004**, 47, 3111–3130.
- 34 Hardy, J.A., Lam, J., Nguyen, J.T., O'Brien, T., Wells, J.A.: Discovery of an allosteric site in the caspases. *Proc. Natl Acad. Sci. USA* **2004**, 101, 12461–12466.
- 35 Buck, E., Wells, J.A.: Disulfide trapping to localize small-molecule agonists and antagonists for a G protein-coupled receptor. *Proc. Natl Acad. Sci. USA* **2005**, 102, 2719–2724.
- 36 Buck, E., Bourne, H., Wells, J.A.: Site-specific disulfide capture of agonist and antagonist peptides on the C5a receptor. *J. Biol. Chem.* **2005**, 280, 4009–4012.

## 10

# Interrogation of Noncovalent Complexes by ESI-MS: A Powerful Platform for High Throughput Drug Discovery

*Steven A. Hofstadler and Kristin A. Sannes-Lowery*

### 10.1

#### Analysis of Noncovalent Complexes by ESI-MS

There are a number of operating parameters that must be carefully optimized and thoroughly understood if one is to analyze noncovalent complexes by mass spectrometry (MS). While it is always a good idea to have a known model system on which to optimize these parameters so that the “expected” complex is observed, it is equally important (if not more important) that the final operating parameters chosen are still able to distinguish specific complexation from non-specific aggregation [1–5]. A carefully chosen (and biologically relevant) model system, along with buffers, ionization parameters, and desolvation conditions which maintain specific noncovalent complexes, and which do not produce non-specific artifacts, is essential. As illustrated below, ion desolvation should be accomplished with minimal added energy to prevent unfolding and to minimize dissociation of the ligand from the complex ions. The choice of appropriate ionization mode is critical for both proteins and nucleic acids, since the location of charges is a function of solution and gas-phase  $pK_a$  values. For example, many proteins can be ionized in positive or negative mode, but the choice of negative or positive ionization for generation of the most “native” form depends on the solution isoelectric point of the protein. Understanding the effect various experimental variables will have on the results of a known system can provide valuable insight into the applicability of the experimental parameters as applied to unknown systems. This is particularly important in the area of high throughput drug discovery where one clearly can not know *a priori* whether or not a given substrate–ligand pair is “supposed” to bind.

#### 10.1.1

##### Solution Conditions

The solution conditions must be adjusted to ensure that the macromolecule of interest can adopt a native state and ligand–substrate complexes which are

formed in the electrospray ionization (ESI) buffer will be relevant under physiological conditions. While most buffers used in electrospray are highly dissimilar to true biological environments (blood, intracellular matrices, cell walls, etc.), electrospray-compatible buffer systems that maintain nondenatured macromolecular structures have been derived for several target classes.

### 10.1.2

#### Proteins

Buffer systems are generally neutral or mildly acidic/basic aqueous solutions; appropriate concentrations of buffer ( $\geq 10$  mM) are generally employed to avoid fluctuations in pH during the desolvation process; aqueous solutions at pH 6–8 with 10–100 mM buffer are typical [6, 7].

In many cases, organic solvent is co-mixed with the solution to aid gas-phase desolvation. Typical organic solvents such as methanol can alter the solution conformation of proteins dramatically [8]. The general rule of thumb for organic solvents with proteins is that a little (5–10%) can significantly improve desolvation, and therefore increase sensitivity, while a lot ( $>10\%$ ) will produce high signal-to-noise spectra of denatured proteins to which complexation (if any) has no biological significance.

These concepts are illustrated in Fig. 10.1 which shows the difference in appearance between myoglobin electrosprayed from denaturing and nondenaturing solutions. Myoglobin is comprised of a monomeric protein (MW = 16 951) which, under physiological conditions, binds a single heme cofactor (MW = 615.190). The spectrum in Fig. 10.1a was acquired from a solution containing 2  $\mu$ M myoglobin in 50% MeOH, 49% H<sub>2</sub>O, and 1% HOAc. It is comprised of a wide distribution of charge states representing apomyoglobin with charge states ranging from (M+23H)<sup>23+</sup> to (M+10H)<sup>10+</sup>. Also clearly evident in the spectrum is a peak at  $m/z$  616.192 corresponding to the unbound, protonated heme group. There are no peaks detected which correspond to the intact holomyoglobin species (MW = 17 566). The spectrum in Fig. 10.1b was acquired under the identical interface and source conditions (see figure caption) and the same myoglobin concentration. The only difference between the conditions used to acquire the two spectra in Fig. 10.1a, b is the composition of the buffer solution. The spectrum in Fig. 10.1b was acquired from a solution containing 2  $\mu$ M myoglobin in 10 mM NH<sub>4</sub>OAc (pH 7). In this spectrum only two primary charge states are observed, corresponding to the (M+9H)<sup>9+</sup> and (M+8H)<sup>8+</sup> charge states of the holomyoglobin species. Note also the absence of the free heme moiety at  $m/z$  616.192. Finally, it is worth making note of the disparate signal-to-noise ratios of the two spectra in Fig. 10.1a, b. While it may not be obvious in the normalized y-axis of the spectra in Fig. 10.1, the two primary peaks corresponding to the holomyoglobin in Fig. 10.1b are nearly 3-fold less intense than the peaks corresponding to the most abundant peaks, the (M+17H)<sup>17+</sup> and (M+18H)<sup>18+</sup> charge states of the apomyoglobin, in Fig. 10.1a. The more acidic environment and the presence of MeOH increases the overall ionization efficiency of the myoglobin in Fig. 10.1a.

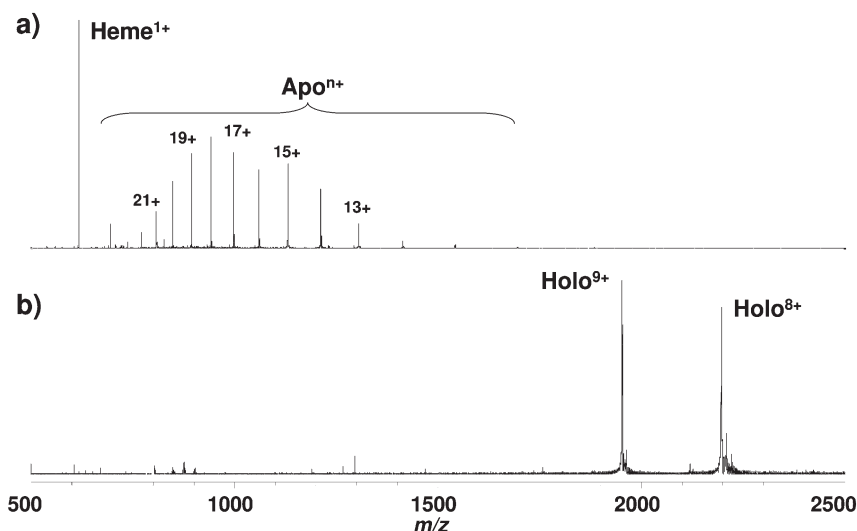


**Fig. 10.1** Effect of buffer composition on the ESI-FTICR-MS spectrum of myoglobin. The spectrum in (a) was acquired from a solution containing 2  $\mu$ M myoglobin in 50% MeOH, 49% H<sub>2</sub>O, and 1% HOAc. Peaks corresponding to apomyoglobin and free heme dominate the spectrum. The spectrum in (b) was acquired from a solution

containing 2  $\mu$ M myoglobin in 10 mM NH<sub>4</sub>OAc (pH 7) under otherwise identical instrument conditions. In this spectrum only two primary charge states are observed, corresponding to the (M+9H)<sup>9+</sup> and (M+8H)<sup>8+</sup> charges states of the holomyoglobin species.

The MeOH serves not only to denature the protein, exposing more charge-carrying residues to the solvent, it also aids desolvation by reducing the surface tension of the microdroplets. Thus, the addition of organic solvents for the analysis of proteins is a double-edged sword – the enhanced sensitivity is achieved by denaturing the protein to the extent that it can no longer bind the heme moiety. In many cases (including the myoglobin system) 5–10% MeOH does not induce a significant extent of denaturation but can enhance the ionization efficiency and produce a more stable electrospray plume.

### 10.1.3

#### Oligonucleotides

For nucleic acid targets, buffer systems which maintain pH 6–8 with relatively high concentrations of ammonium acetate (50–250 mM) and organic co-solvents (10–50%) are generally effective [9–11]. The concentration of buffer/salt must be high enough to allow proper base pairing of the strand(s) and to ensure that the melting transition temperature is well above ambient. The buffer used most widely in our laboratory for screening relatively small RNA motifs (18–50mers) against compound collections or natural product fractions is comprised of 150

mM  $\text{NH}_4\text{OAc}$ , 33% isopropyl alcohol, and no more than 1.5% DMSO [12–14]. A buffer system with the appropriate pH and ionic strength is equally important for native folding in nucleic acids as for proteins as binding to a denatured oligonucleotide, much like binding to a denatured protein, will not yield information representative of the same molecules *in vivo*. Similarly, denatured oligonucleotides generally exhibit a broad distribution of relatively high charge states, while nondenatured nucleic constructs most often produce mass spectra which are dominated by one or two distinct charge states at relatively high  $m/z$ . Denaturing solution conditions are ideal for obtaining accurate mass measurements of PCR products where it is desirable to thoroughly denature the duplex and obtain mass measurements for the forward and reverse strands of the amplicon independently, as opposed to a single mass measurement on a DNA duplex [15, 16]. Independent mass measurements of the forward and reverse strands allow one to unambiguously determine the base composition of a given amplicon [17, 18] (or mixture of amplicons) which has significant relevance in ESI-MS based microbial identification [16, 19], microbial forensics [20], and human forensic strategies [21]. Alternatively, nondenaturing solution conditions and gentle desolvation are important for maintaining natively folded macromolecular targets with which to form noncovalent complexes. The appearance and information content of the spectra can differ drastically depending on the solution conditions employed. For example, Fig. 10.2 illustrates mass spectra obtained from solutions containing the 27mer RNA construct which represents the 16S ribosomal A-site, an important target for bacterial drug discovery [22]. The spectrum in Fig. 10.2a was acquired from a solution comprised of 33% isopropyl alcohol with 25 mM piperidine/imidazole with an approximate pH of 8.5. The spectrum in Fig. 10.2b was acquired from a solution containing the same concentration of the 27mer RNA construct and the same concentration of isopropyl alcohol, but with 150  $\mu\text{M}$   $\text{NH}_4\text{OAc}$  with a pH of 7.0. The solution conditions employed in Fig. 10.2b allow the interrogation of specific interactions between the 27mer target and small molecule ligands, as the solution allows the target to maintain a native conformation amenable to the formation of specific noncovalent complexes (see below).

A number of larger RNA motifs, which have more complex high-order structures *in vivo*, rely on divalent metal ions (e.g.  $\text{Mg}^{2+}$ ) to adopt correct secondary and tertiary structures. One such construct that represents a potentially valuable antibiotic target is a 58-nucleotide domain of the 23S ribosomal subunit to which the L11 protein binds. This structural motif is highly conserved among prokaryotes and participates in GTP hydrolysis reactions involving several ribosomal factors. The crystal structure of the 58-nucleotide construct bound to the L11 protein was obtained by Draper and coworkers [23] and provides valuable insight into the functional operation of this part of the ribosome. A naturally occurring antibiotic, thiostrepton (MW = 1663 Da) is known to bind to this motif and to inhibit key interactions at the GTPase center. While thiostrepton has poor drug properties, owing to low solubility, poor oral bioavailability, and synthetically daunting

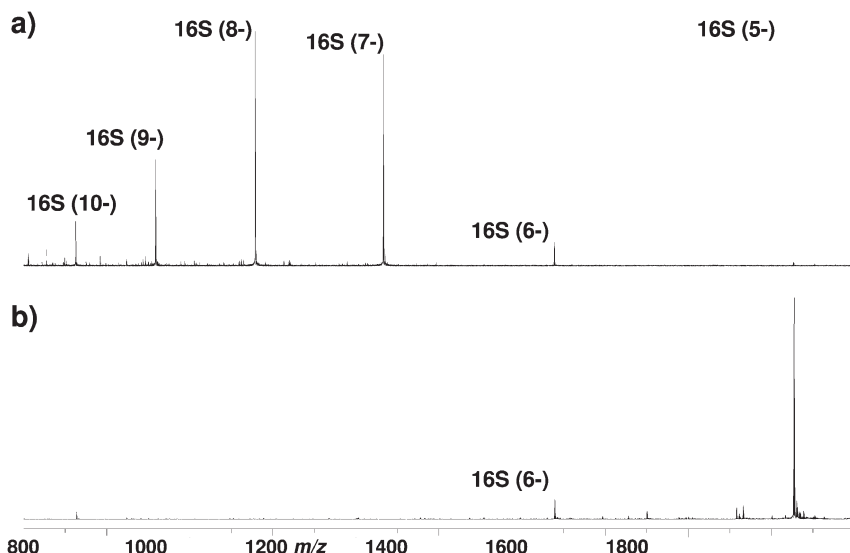


**Fig. 10.2** Effect of buffer composition on the ESI-FTICR-MS spectrum of a 27mer RNA construct representing the 16S A-site. The spectrum in (a) was acquired from a solution comprised of 33% isopropyl alcohol and 25 mM piperidine/imidazole with an approximate pH of 8.5. The spectrum in (b) was acquired from a solution containing the

same concentration of the 27mer RNA construct and the same concentration of isopropyl alcohol, but with 150 mM  $\text{NH}_4\text{OAc}$  at pH 7. These buffer conditions facilitate folding of the construct into a native structure that can serve as a drug binding substrate.

multi-ringed structure, it does serve as a proof-of-principle for what could be a very significant strategy for new classes of antimicrobial agents [24–26]. A mutant of this motif found in thermophiles (A1061) is particularly stable and thus an ideal substrate for ESI-MS based affinity screening. The A1061–thiostrepton complex was used to determine appropriate solution and interface conditions for the system.

This construct was initially evaluated with the same buffer system used for smaller RNA motifs and it was found that the ammonium acetate/isopropyl alcohol buffer provided only partial complexation of the thiostrepton and a relatively wide charge state distribution, indicative of a partially denatured conformation in solution. As  $\text{Mg}^{2+}$  was previously implicated as a key to proper folding *in vivo* [27, 28], a study was undertaken to characterize the magnesium-dependent folding of the A1061 construct in solution as measured by thiostrepton binding. Figure 10.3 shows the  $(\text{M}-8\text{H})^{8-}$  charge state of the A1061 construct, and the resulting A1061–thiostrepton complex that results when  $\text{Mg}^{2+}$  is added. In the absence of  $\text{Mg}^{2+}$ , only trace levels of the complex is observed and the spectrum is dominated by the 8– charge state of the unbound RNA. At increasing concentrations

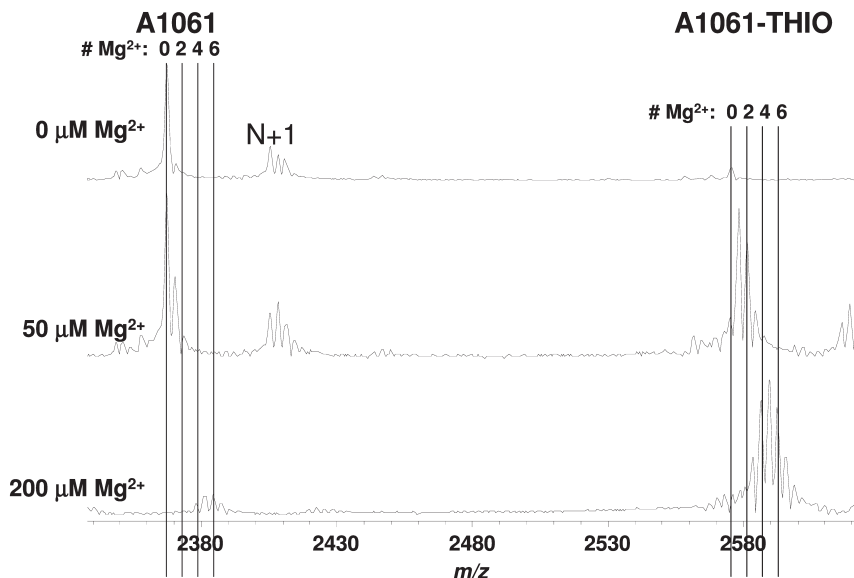


**Fig. 10.3** (M-8H)<sup>8-</sup> charge state of the 58mer A1061 RNA construct (see text) in the presence of an excess of thiostrepton. The buffer solution contains 20% MeOH and 25 mM NH<sub>4</sub>OAc. In the absence of adequate Mg<sup>2+</sup> ion, the A1061 construct is denatured and does not bind thiostrepton. At increasing Mg<sup>2+</sup> concentration, the A1061 adopts a

native conformation and binds a stoichiometric amount of thiostrepton. The peaks labeled “N+1” refer to a synthetic impurity arising from a nontemplated nucleotide. The even number of Mg<sup>2+</sup> ions bound to the RNA and complex is indicated by “#Mg<sup>2+</sup>: 0 2 4 6” above the corresponding lines in the spectrum.

of Mg<sup>2+</sup>, the abundance of the complex increases as does the amount and extent of Mg<sup>2+</sup> adducts. These Mg<sup>2+</sup> ions, while clearly assisting in the proper folding of the RNA construct have unwanted side-effects in the mass spectrum in the form of adducts. At 50 μM Mg<sup>2+</sup>, a significant portion of the A1061 is unbound while a nearly equal portion is complexed with thiostrepton. Interestingly, the signal from the unbound A1061 is dominated by the unadducted species, while the complex is dominated by the singly and doubly adducted species. Furthermore, with 200 μM Mg<sup>2+</sup>, the majority of the A1061 is in the form of the A1061–thiostrepton complex and the signal is dominated by species containing five Mg<sup>2+</sup> ions. While such solution conditions allow the detection of the complex, the relatively complex spectra and multiply adducted nature of the complexes limit the utility for screening applications in which multiple compounds with unknown binding properties are to be screened simultaneously.

In contrast, Draper and coworkers have shown that organic solvent such as methanol can actually help larger RNA constructs fold properly under salt conditions which would otherwise yield incompletely or improperly folded RNA con-

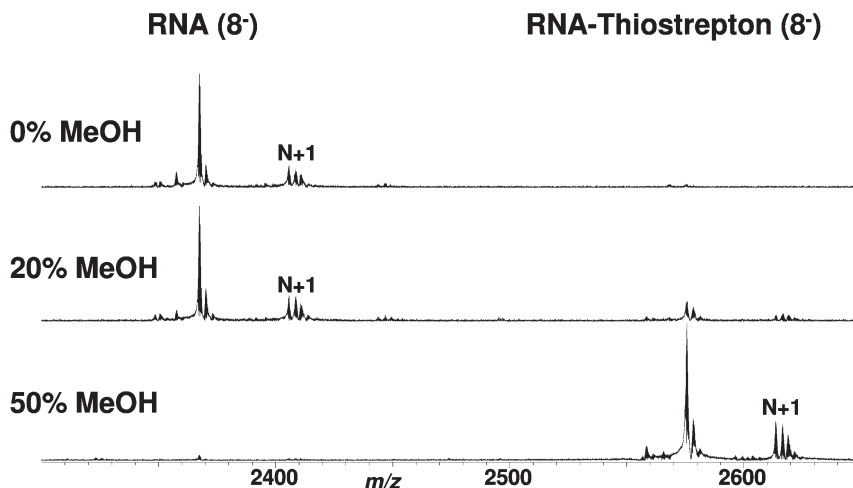


**Fig. 10.4** A1061 folding in the presence of MeOH. In a solution containing 25 mM  $\text{NH}_4\text{OAc}$  and a molar excess of thiostrepton, the A1061–thiostrepton complex is not observed at significant abundance with less than 25% MeOH. The spectrum acquired

from a solution containing 50% MeOH is dominated by the A1061–thiostrepton complex consistent with the properly folded conformation. The peaks labeled “N+1” refer to a synthetic impurity arising from a nontemplated nucleotide.

structs [29]. This is an important observation as solution conditions in which nonvolatile salts are employed to induce proper RNA folding (e.g.  $\text{Mg}^{2+}$ ) yield relatively complex mass spectra with poor signal to noise, as the peaks which represent the complexes of interest are spread over multiple states of adduction. As organic solvents are directly compatible with electrospray ionization and are completely removed during desolvation, an alternative buffer formulation lacking divalent metal cations but containing higher proportions of methanol was evaluated. Figures 10.4, 10.5 illustrate the effect of increasing methanol concentration on the A1061–thiostrepton complex in the absence of  $\text{Mg}^{2+}$ . In an aqueous solution containing 6  $\mu\text{M}$  A1061 with a slight stoichiometric excess of thiostrepton and 25 mM  $\text{NH}_4\text{OAc}$ , the complex is not detected above the chemical noise background. When 20% methanol is added, a relatively weak signal consistent with the complex is observed, while a solution containing 50% methanol produces a spectrum that is dominated by the A1061–thiostrepton complex. The titration profile in Fig. 10.5 suggests a relatively sharp transition in the A1061 structure between 30% and 40% methanol. Note also that, other than a synthetic impurity related to an additional nontemplated nucleotide (peak labeled N+1), the spectrum acquired with 50% methanol is relatively clean and readily interpretable – a situation much more amenable to screening of compounds with unknown binding properties.



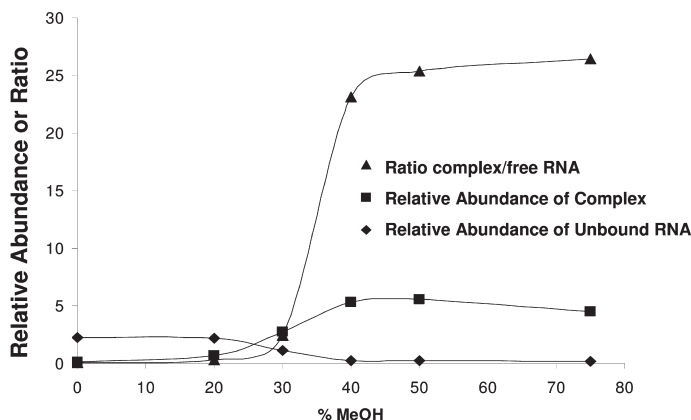


**Fig. 10.5** Proper folding of A1061 RNA construct (as measured by thiostrepton binding) as a function of MeOH composition of the buffer.

## 10.2

### Multitarget Affinity/Specificity Screening

We have integrated high throughput sampling robotics and a custom fluidics module to rapidly characterize noncovalent biological complexes in order to identify small molecules that bind RNA targets using ESI-FTICR [30]. The multitarget affinity/specificity screening (MASS) assay takes advantage of the “intrinsic mass” label of each compound and target RNA by obtaining high resolution, high precision mass measurements of intact RNA–ligand complexes [13, 31–33]. The identity of the small molecule(s) which bind, the RNA target to which it binds, and the compound-specific binding affinity can be determined in one set of rapid experiments. We have demonstrated the applicability of the MASS assay to screening natural product fractions for modified aminoglycosides that bind preferentially to the 16S A-site [34, 35].

At the core of the MASS approach is the premise that, in a solution containing multiple targets and multiple ligands, the molecular interaction between any given target–ligand pair is independent of the presence (or absence) of other ligands and targets in solution. While FTICR is by no means the first or the only platform on which noncovalent complexes have been detected, the performance attributes of the platform make it well suited to analyze complex mixtures. Thus multiple targets can be screened against multiple ligands simultaneously. This concept is illustrated in Fig. 10.6. In a nondenaturing buffer solution a macromolecular target (RNA construct, protein, or mixed complex) is allowed to interact with a molecule, or a collection of molecules, of interest. The compound collection might represent a “diversity” collection intended to explore a range of hydrophilic/hydrophobic moieties, charge-carrying groups, and electron donor/acceptor groups; it might represent a fraction from a natural product isolate for

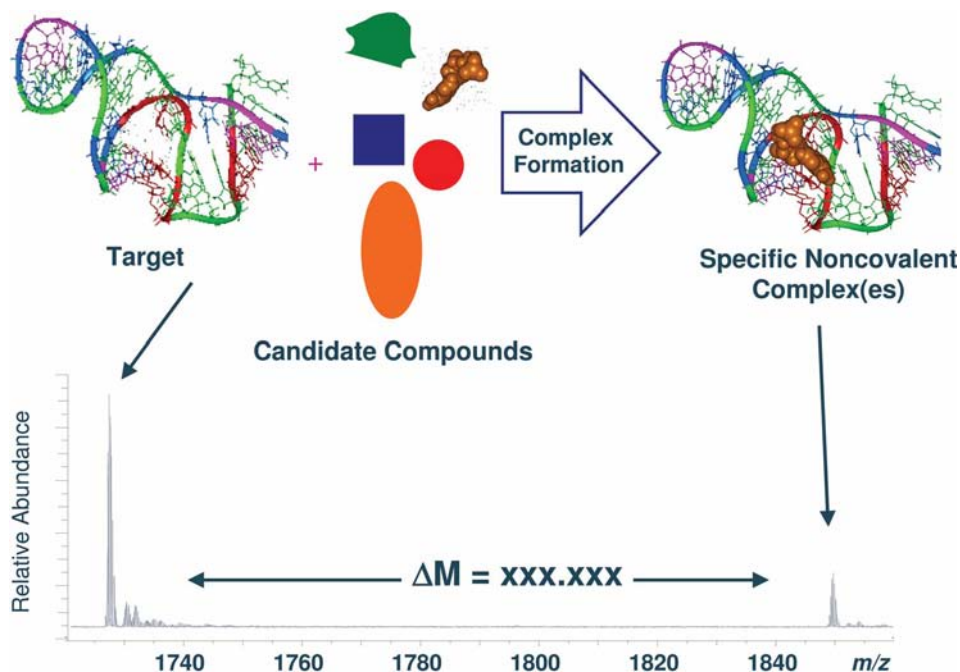


**Fig. 10.6** Concept of multitarget affinity specificity screening (MASS). Macromolecular targets (typically structured RNA constructs or proteins) in nondenaturing buffers are mixed in solution with a collection of potential ligands derived from natural product fractions, combinatorial libraries, or other diverse compound collections. The

mixture is analyzed by ESI-MS under gentle desolvation conditions that preserve noncovalent complexes; the exact molecular weight of compounds binding to targets (which can be used to derive an elemental composition), their relative (or absolute) affinity, and binding specificity of compounds are derived from the mass spectra.

which the complexity and range of functional groups is not known; it might represent a series of engineered compounds derived from carefully synthesized variants of known high affinity ligands; or it might represent a random combinatorial library or subset of a master compound collection. The target (or collection of targets) is allowed to interact in solution, under nondenaturing buffer conditions, with the compound library. Ligands which have an affinity for a given target will bind in solution with a compound-specific dissociation constant ( $K_d$ ) and specificity.

### 10.3

#### Multitarget Affinity/Specificity Screening in a High Throughput Format

Instrumentation for laboratory automation is increasingly becoming a “plug and play” operation. Many ancillary pieces of equipment, such as autosamplers, plate handlers, chromatographic instruments, and many classes of spectrometers, have

built-in communication ports and/or the ability to trigger (or be triggered by) other pieces of equipment. Thus, it is now commonplace in most industrial analytical laboratories to utilize various user-customized combinations of these devices to increase sample throughput and facilitate unattended sample analysis. It is often the case that, once an analytical protocol is in place and can be manually performed by a technician, it can be automated with standard (or customized) robotics and control software and subsequently be performed more rapidly and more reliably via an automated protocol. Thus, it is not surprising that, following the initial success of the MASS assay to interrogate RNA–ligand binding in a multiply-parallel format, a key push in our laboratory has been to fully automate the approach and thereby, improve both the sample throughput and robustness of the assay. There are two aspects of any analytical scheme which one must consider when attempting to “scale up” a protocol from a research method to a high throughput assay: data acquisition and data analysis. Both are essential to operate in a true high throughput format [30].

Our general screening approach involves the simultaneous screening of three RNA targets against 11 compounds, or 33 analyses per well. As each well requires only 39 s per analysis and the assay can be run around the clock in an unattended manner, a single ESI-FTICR mass spectrometer can perform in excess of 67 000 analyses per day. From the relative abundance of each noncovalent complex detected, a one-point  $K_d$  is calculated that gives a semi-quantitative indication of the binding for each ligand–substrate pair. For complexes that are not detected above a given threshold, a minimum value for the  $K_d$  is calculated based on the known concentration of the ligands and the targets – this is generally in the  $K_d \geq 2.5$  mM regime. As described in detail elsewhere, we have automated the entire protocol from plate preparation to spectral acquisition to data interpretation. It has also been shown that these and related methods can be used to directly measure dissociation constants [14, 36–39].

## 10.4

### Affinity/Specificity

When ESI-MS is used as a primary high throughput screening tool as in the MASS assay [13, 31–33], the goal is to identify ligands with  $K_d$  values less than 100  $\mu$ M and with some specificity relative to the other targets. These constraints ensure that the ligands bind to a unique structural feature of the target and are not just generic RNA binders. Although the ligands are screened only at a single concentration in the high throughput mode, it is possible to estimate a one-point  $K_d$  from the mass spectrometry data. A percent complex is calculated for each identified ligand–target combination by calculating the ratio of the integrated peak areas of the complexed and the free target and multiplying by 100. A one-point estimated  $K_d$  is then calculated by dividing 100 by the percent complex of the ligand and multiplying by the screening concentration. The one point estimated  $K_d$  values can be used to classify compounds as weak, medium, and strong

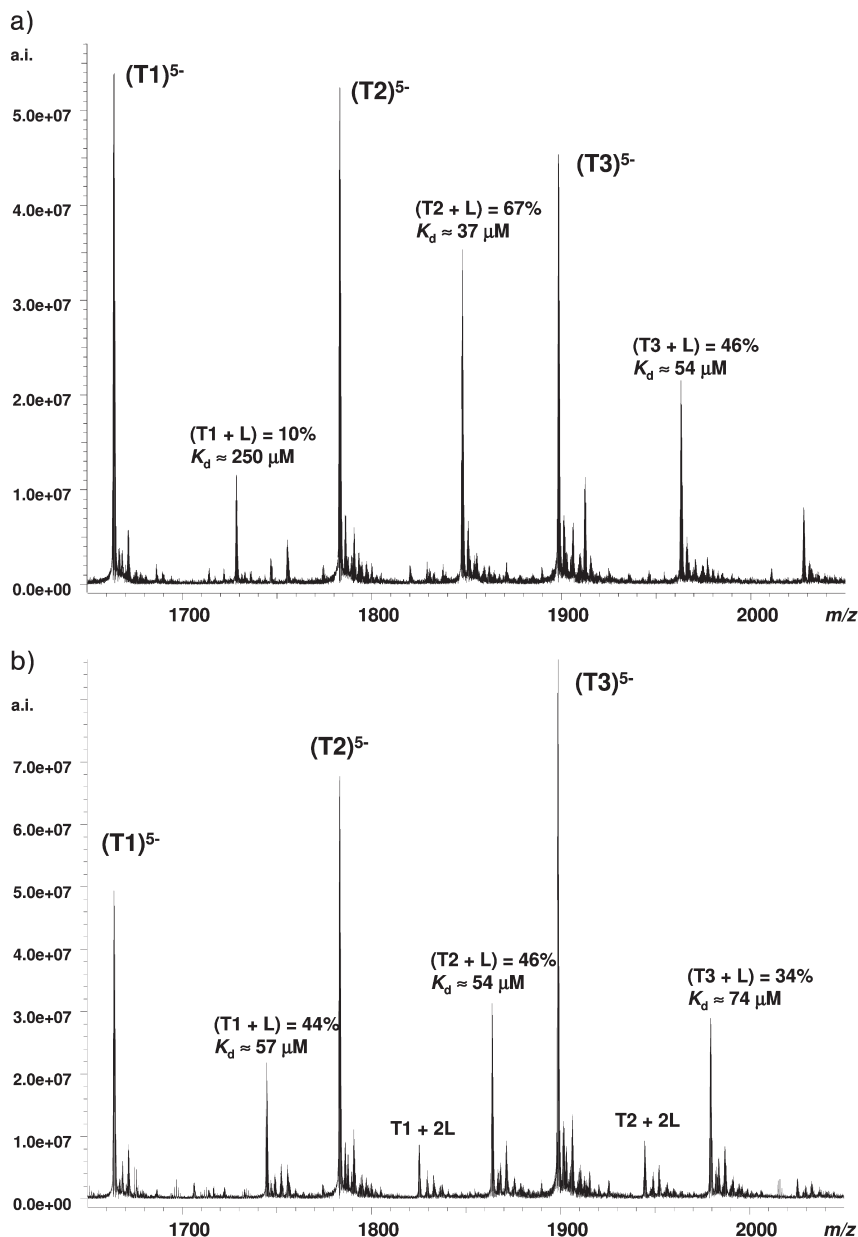


**Fig. 10.7** ESI-FTICR mass spectra of three RNA targets at 2.5  $\mu\text{M}$  each screened against 11 compounds at 25  $\mu\text{M}$  each. The percent complexes and one-point  $K_d$  values are shown for each ligand complex. (a) An example of a ligand that specifically binds target 2. (b) An example of a ligand that nonspecifically binds to all targets.

binders but cannot be used to accurately rank order compounds within the same classification. As illustrated in Fig. 10.7a, a ligand binds target 2 with a one-point estimated  $K_d$  of 37  $\mu\text{M}$  (i.e. estimated  $K_d = 100/67 * 25 \mu\text{M}$ ). The ligand binds target 2 with 3.4-fold greater specificity than target 1 and with 1.5-fold greater specificity than target 3. This ligand would be a candidate for further structure–activity relationship studies (SAR) by medicinal chemistry to improve both its binding affinity and specificity. An example of a generic RNA binder is shown in Fig. 10.7b. The ligand binds target 1 and target 2 equally well. In addition, complexes formed by binding two ligands to the target are observed for both target 1 and target 2. This result indicates that there are multiple weak binding sites with similar affinities for the ligand on the targets. It would likely be difficult to improve the affinity and specificity of this ligand, and therefore, it would probably not be pursued further as a drug candidate. Thus, MASS can be used to rapidly identify promising compounds and/or structural motifs from large chemical libraries and guide the medicinal chemistry efforts required to create high-value lead compounds [40–42].

## 10.5

### SAR by MS

Because MASS can detect ligands with a wide range of  $K_d$ s (10 nM to 1 mM) [12, 13, 30], we have developed a drug design approach utilizing the structure–activity relationships (SAR) of weak ligand–target interactions to build ligands that show increased binding affinity. We refer to this as SAR by MS [43]. In this approach, a panel of motifs (small, rigid molecules with molecular mass less than 300 Da) is initially screened against one or more targets. MASS identifies ligands that bind the target and, if two ligands bind the same target at different sites, a ternary complex is observed. Next, simple derivatives of the most interesting motifs are synthesized to provide information about the target-binding site; and these compounds are screened in another round of MASS to further probe the individual and collective affinities of the compounds. For example, if the addition of a chemical group changes a pair of ligands from concurrent to competitive binders, it implies that the additional moiety sterically hinders the binding of the other compound to the target and that the two compounds must share relatively close binding sites. Lastly, cumulative information is used to guide the linking of motifs into a single structure with higher affinity for the target.

The SAR by MS method was used to identify a new class of ligands that bind to the 1061 region of bacterial 23S rRNA which interacts with the L11 protein and is the binding site for the antibiotic thiostrepton [44]. Even though there is a crystal structure for the protein–RNA interaction [23], traditional structure-based rational drug design approaches are difficult to perform since the interaction between the protein and RNA is complex. Thus, it is an ideal target for the SAR by MS strategy.

A screen of compound libraries containing compounds from commercial sources and RNA-directed combinatorial libraries, revealed two classes of motifs that showed interesting SAR toward the 1061 region of bacterial 23S rRNA. The first class consists of D-amino acids (series A). A positively charged side-group improves binding relative to uncharged and unsubstituted side-chains. The second class consists of the quinoxaline-2,3-diones (series B). Substitutions of the carboxyl groups of the quinoxaline-2,3-dione are well tolerated, with large pendant groups being preferred. Because A and B are structurally different, it was hypothesized that the ligands bind at distinct sites on the target RNA. To further examine the spatial relationships between the different motifs that bind the RNA, MS competition experiments were conducted with the different ligand classes. Ligand A and Ligand B1 were shown to bind the RNA concurrently, as evidenced by the formation of a ternary complex between A, B1 and the RNA (Fig. 10.8). In contrast, Ligand A and Ligand B2 were shown to be competitive binders, as evidenced by the lack of binding of B2 in the presence of A and the lack of a ternary complex (Fig. 10.8).

Based on these competition experiments, it was postulated that the furan portion of A is separated from the carboxyl functional group of B1 by approximately three atoms. To test this hypothesis, several fused compounds were made with different linkages between the furan of A and the carboxyl functional group of B1. The compounds were tested for affinity to the RNA target as well as for their ability to inhibit bacterial transcription/translation in cell-free functional assay (Fig. 10.8b, c). The fused compounds all bound tighter to the target RNA than the parent motifs. The  $K_d$  measured by mass spectrometry for the fused compounds were in the range of 6–50  $\mu\text{M}$ , compared with  $>100 \mu\text{M}$  for the parent motifs. The rigid biaryl-linked compound AB in Fig. 10.8a shows 20-fold enhanced affinity for the RNA target relative to the motif ligands. More importantly, this compound shows similar activity in a functional assay ( $\text{IC}_{50} = 14 \mu\text{M}$ ) whereas the motifs are not active in the functional assay [45]. Thus, this compound may bind to the target RNA in a manner that interferes with ribosomal function. While still a relative newcomer to the drug discovery tool kit, SAR by MS appears to be a promising method for ligand-based lead discovery of specific, high affinity ligands which have the potential to have significant therapeutic activities. As with many newly emerging methodologies, time will tell which approaches have “staying power” in the drug discovery arena and provide the most value for lead identification and optimization.

## 10.6

### Future Directions

Early stages of drug discovery continue to move further and further away from biofunctional screening assays such as bacterial broths, cell cultures, and animal models, and closer towards functional assays where specific (and targeted) inter-

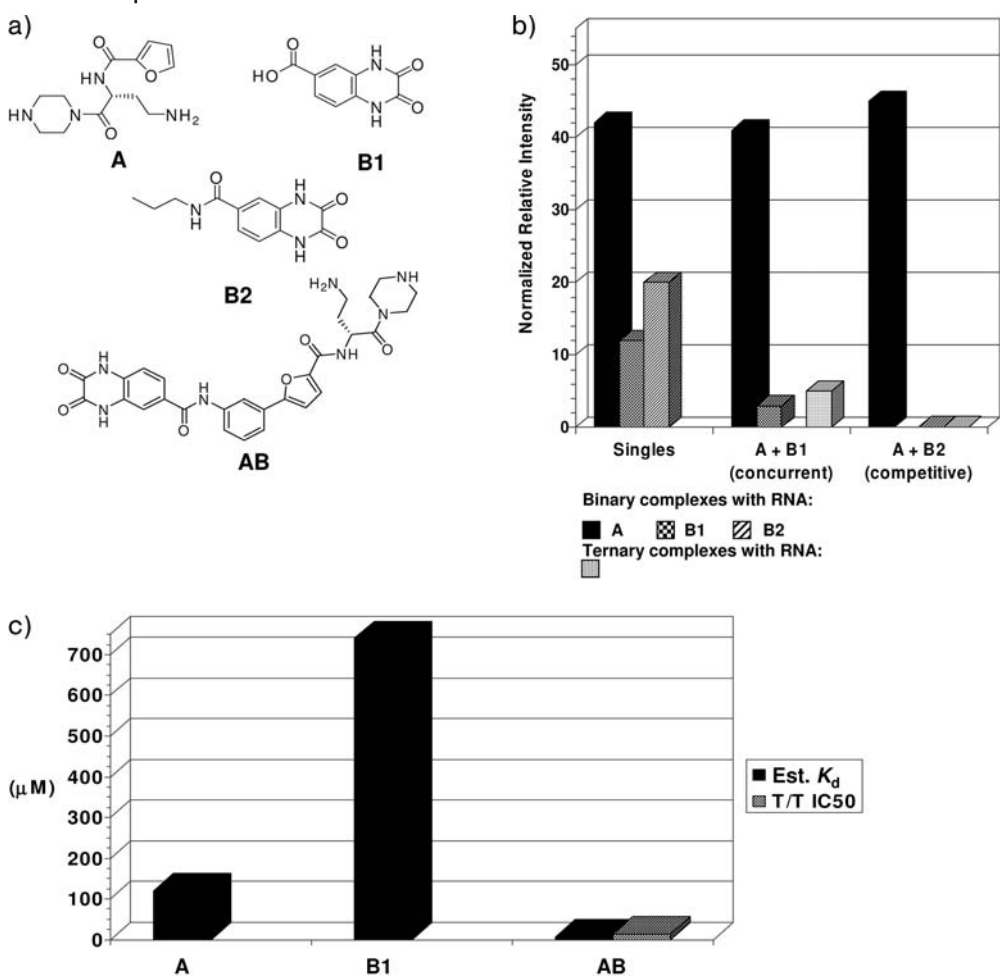


**Fig. 10.8** SAR by MS applied to the A1061 construct (see text). (a) Structures of key motifs screened against the RNA target. Compound A is a  $\alpha$ -amino acid. Compounds B1 and B2 are quinoxalin-2,3-diones. Compound AB is the rigid biaryl linked compound. (b) Binding affinity for the motifs when screened individually as well as binding affinity for motifs when screened in competition experiments are shown. Binding

is expressed as a normalized percent MS ion intensity of the RNA–ligand complex relative to the parent RNA such that a value of 100 indicates 50% of the ligand is bound to the target. A and B1 bind concurrently while A and B2 binding competitively. (c) MS determined  $K_d$  values for the RNA target and bacterial transcription/translation  $\text{IC}_{50}$  [T/T  $\text{IC}_{50}$ ] values for selected structures.

actions are interrogated at the molecular level. It is not surprising that mass spectrometry continues to play an expanding role in this area as gas-phase measurements, which can be both highly automated and highly informative, can be used to interrogate macromolecular interactions of many different target/ligand classes.

The increasing availability of high performance mass spectrometry systems based on a number of different platforms (hybrid FTICRs, ESI-(Q)-TOFs, and novel traps such as the linear ion trap and orbitrap) should increase the implementation and utilization of existing ESI-MS-based methods, such as those outlined above, but should also catalyze the development of novel approaches to high throughput screening. Furthermore, preliminary studies with ion mobility measurements of macromolecular complexes [46] suggest that such measurements may provide invaluable information to drug discovery researchers as the combination of experimentally derived collisional cross-sections and computationally derived structure models hold great promise as rapid methods to interrogate modes of binding and allosteric interactions among drug targets and drug candidates. Several researchers have demonstrated that extremely large noncovalent complexes can be ionized and measured as intact species; complexes comprising the components of molecular machines such as megadalton protein complexes [47], self assembling ring structures [48], even intact ribosomes [49, 50] and viruses [51–53] have been successfully characterized by ESI-MS. It is quite likely that mass spectrometric analysis of these molecular machines and the small molecules with which they interact will be the ligand–substrate systems researchers employ to find the next generation of antibacterial and antiviral compounds. Might it be possible to discover new aminoglycosides by analyzing complexes formed between drug candidates and intact ribosomes? Might next-generation antiviral compounds be discovered by analyzing intact viruses in the presence of compounds that selectively disrupt the viral capsids or selectively bind to structural elements of the intact viral genome? While only time will tell just how far the mass spectrometric analysis of noncovalent complexes can push the envelope of modern drug discovery methods, it is clear that, at the rate the underlying analytical methods are evolving, the future of such methods has never looked better.

## References

- 1 Benkestock, K., Edlund, P. O., Roeraade, J.: Electrospray ionization mass spectrometry as a tool for determination of drug binding sites to human serum albumin by noncovalent interaction. *Rapid Commun Mass Spectrom* **2005**, 19, 1637–1643.
- 2 Hardouin, J., Lange, C. M.: Biological noncovalent complexes by mass spectrometry. *Curr Org Chem* **2005**, 9, 317–324.
- 3 Benkestock, K., Sundqvist, G., Edlund, P. O., Roeraade, J.: Influence of droplet size, capillary–cone distance and selected instrumental parameters for the analysis of noncovalent protein-ligand complexes by nano-electrospray ionization mass spectrometry. *J Mass Spectrom* **2004**, 39, 1059–1067.
- 4 Jorgensen, T. J. D., Hvelplund, P., Andersen, J. U., Roepstorff, P.: Tandem mass spectrometry of specific vs. nonspecific noncovalent complexes of vancomycin antibiotics and peptide ligands. *Int J Mass Spectrom* **2002**, 219, 659–670.
- 5 Tahallah, N., Pinkse, M., Maier, C. S., Heck, A. J.: The effect of the source pressure on the abundance of ions of noncovalent protein assemblies in an electrospray ionization orthogonal time-of-flight instrument. *Rapid*



- Commun Mass Spectrom* **2001**, 15, 596–601.
- 6 Cheng, X., Hofstadler, S. A., Bruce, J. E., Harms, A. C., Chen, R., Smith, R. D., Terwilliger, T. C., Goudreau, P. N.: in *Tech Protein Chem VII* (9th Symposium of the Protein Society), ed. Marshak, D. R., Academic, San Diego, **1996**, pp 13–22.
  - 7 Bruce, J. E., Anderson, G. A., Chen, R., Cheng, X., Gale, D. C., Hofstadler, S. A., Schwartz, B. L., Smith, R. D.: Bio-affinity characterization mass spectrometry. *Rapid Commun Mass Spectrom* **1995**, 9, 644–650.
  - 8 Katta, V., Chait, B. T.: Conformational-changes in proteins probed by hydrogen-exchange electrospray-ionization mass-spectrometry. *Rapid Commun Mass Spectrom* **1991**, 5, 214–217.
  - 9 Hofstadler, S. A., Griffey, R. H.: Analysis of noncovalent complexes of DNA and RNA by mass spectrometry. *Chem Rev* **2001**, 101, 377–390.
  - 10 Griffey, R. H., Greig, M. J., Sasmor, H., Cummins, L. L., Manalili, S. L., Gaus, H. J.: Non-covalent complexes of oligonucleotides observed using electrospray ionization mass spectrometry. *NATO ASI Ser C* **1998**, 510, 117–133.
  - 11 Greig, M. J., Gaus, H.-J., Griffey, R. H.: Negative ionization micro electrospray mass spectrometry of oligodeoxyribonucleotides and their complexes. *Rapid Commun Mass Spectrom* **1996**, 10, 47–50.
  - 12 Griffey, R. H., Hofstadler, S. A., Sannes-Lowery, K. A., Ecker, D. J., Crooke, S. T.: Determinants of aminoglycoside-binding specificity for rRNA by using mass spectrometry. *Proc Natl Acad Sci USA* **1999**, 96, 10129–10133.
  - 13 Hofstadler, S. A., Sannes-Lowery, K. A., Crooke, S. T., Ecker, D. J., Sasmor, H., Manalili, S., Griffey, R. H.: Multiplexed screening of neutral mass-tagged RNA targets against ligand libraries with electrospray ionization FTICR MS: a paradigm for high-throughput affinity screening. *Anal Chem* **1999**, 71, 3436–3440.
  - 14 Sannes-Lowery, K. A., Griffey, R. H., Hofstadler, S. A.: Measuring dissociation constants of RNA and aminoglycoside antibiotics by electrospray ionization mass spectrometry. *Anal Biochem* **2000**, 280, 264–271.
  - 15 Greig, M., Griffey, R. H.: Utility of organic bases for improved electrospray mass spectrometry of oligonucleotides. *Rapid Commun Mass Spectrom* **1995**, 9, 97–102.
  - 16 Hofstadler, S. A., Sampath, R., Blyn, L. B., Eshoo, M. W., Hall, T. A., Jiang, Y., Drader, J. J., Hannis, J. C., Sannes-Lowery, K. A., Cummins, L. L., Libby, B., Walcott, D. J., Schink, A., Massire, C., Ranken, R., White, N., Samant, V., McNeil, J. A., Knize, D., Robbins, D., Rudnik, K., Desai, A., Moradi, E., Ecker, D. J.: TIGER: the universal biosensor. *Int J Mass Spectrom* **2005**, 242, 23–41.
  - 17 Muddiman, D. C., Anderson, G. A., Hofstadler, S. A., Smith, R. D.: Length and base composition of pcr-amplified nucleic acids using mass measurements from electrospray ionization mass spectrometry. *Anal Chem* **1997**, 69, 1543–1549.
  - 18 Aaserud, D. J., Kelleher, N. L., Little, D. P., McLafferty, F. W.: Accurate base composition of double-strand DNA by mass spectrometry. *J Am Soc Mass Spectrom* **1996**, 7, 1266–1269.
  - 19 Hofstadler, S. A., Hari, K. L., Sampath, R., Blyn, L. B., Eshoo, M. W., Ecker, D. J.: in *Encyclopedia of Rapid Microbiological Methods*, ed. Michael, J., Miller, P. D., Parenteral Drug Association, Bethesda, **2005**, 287–307.
  - 20 Van Ert, M., Hofstadler, S. A., Jiang, Y., Busch, J. D., Wagner, D. M., Drader, J. J., Ecker, D. E., Hannis, J. C., Huynh, L. Y., Schupp, J. M., Simonson, T., Keim, P.: Mass spectrometry provides accurate characterization of two genetic marker types in *Bacillus anthracis*. *Biotechniques* **2004**, 37, 642–651.

- 21 Hall, T. A., Budowle, B., Jiang, Y., Blyn, L., Eshoo, M., Sannes-Lowery, K. A., Sampath, R., Drader, J. J., Hannis, J. C., Harrell, P., Samant, V., White, N., Ecker, D. J., Hofstadler, S. A.: Base composition analysis of human mitochondrial DNA using electrospray ionization mass spectrometry: a novel tool for the identification and differentiation of humans. *Anal Biochem* **2005**, 344, 53–69.
- 22 Fourmy, D., Recht, M. I., Blanchard, S. C., Puglisi, J. D.: Structure of the A site of *Escherichia coli* 16S ribosomal RNA complexed with an aminoglycoside antibiotic. *Science* **1996**, 274, 1367–1371.
- 23 Conn, G. L., Draper, D. E., Lattman, E. E., Gittis, A. G.: Crystal structure of a conserved ribosomal protein–RNA complex. *Science* **1999**, 284, 1171–1174.
- 24 Xing, Y., Draper, D. E.: Cooperative interactions of RNA and thiostrepton antibiotic with two domains of ribosomal protein L11. *Biochemistry* **1996**, 35, 1581–1588.
- 25 Lu, M., Draper, D. E.: On the role of rRNA tertiary structure in recognition of ribosomal protein L11 and thiostrepton. *Nucleic Acids Res* **1995**, 23, 3426–3433.
- 26 Ryan, P. C., Lu, M., Draper, D. E.: Recognition of the highly conserved GTPase center of 23 S ribosomal RNA by ribosomal protein L11 and the antibiotic thiostrepton. *J Mol Biol* **1991**, 221, 1257–1268.
- 27 Blyn, L. B., Risen, L. M., Griffey, R. H., Draper, D. E.: The RNA-binding domain of ribosomal protein L11 recognizes an rRNA tertiary structure stabilized by both thiostrepton and magnesium ion. *Nucleic Acids Res* **2000**, 28, 1778–1784.
- 28 Blyn, L. B., Risen, L. M., Griffey, R. H., Draper, D. E.: Magnesium ion, thiostrepton, and ribosomal protein L11 all induce folding of the same rRNA tertiary structure. *RNA* **1999**.
- 29 Shiman, R., Draper, D. E.: Stabilization of RNA tertiary structure by monovalent cations. *J Mol Biol* **2000**, 302, 79–91.
- 30 Sannes-Lowery, K. A., Drader, J. J., Griffey, R. H., Hofstadler, S. A.: Fourier transform ion cyclotron resonance mass spectrometry as a high throughput affinity screen to identify RNA-binding ligands. *Trends Anal Chem* **2000**, 19, 481–491.
- 31 Griffey, R. H., Ding, Y., Lowery, K., Mohan, V., Swayze, E., Hofstadler, S. A.: Determinants of aminoglycoside binding specificity to RNA subdomains. *Abstr Pap Am Chem Soc* **2001**, 221, CARB-007.
- 32 Hofstadler, S. A., Drader, J., Sannes-Lowery, K. A., Swayze, E. E., Griffey, R. H.: High performance ESI-FTICR mass spectrometry as a high throughput screen to identify RNA-binding ligands. *Abstr Pap Am Chem Soc* **2001**, 221, ANYL-197.
- 33 Sannes-Lowery, K. A., Drader, J. J., Griffey, R. H., Hofstadler, S. A.: High-performance mass spectrometry as a drug discovery tool: a high-throughput screening assay to identify RNA-binding ligands. *Proc SPIE Int Soc Opt Eng* **2001**, 4264, 27–36.
- 34 Cummins, L. L., Shuo, C., Blyn, L. L., Sannes-Lowery, K. A., J. J., D., Griffey, R. H., Hofstadler, S. A.: Multitarget affinity/specificity screening of natural products: finding and characterizing high affinity ligands from complex mixtures by using high performance mass spectrometry. *J Nat Prod* **2003**, 66, 1186–1190.
- 35 Sannes-Lowery, K. A., Cummins, L., Chen, S., Drader, J. J., Hofstadler, S. A.: High throughput drug discovery with ESI-FTICR. *Int J Mass Spect* **2004**, 204, 197–206.
- 36 Zhang, S., Van Pelt, C. K., Wilson, W. D.: Quantitative determination of noncovalent binding interactions using automated nanoelectrospray mass spectrometry. *Anal Chem* **2003**, 75, 3010–3018.
- 37 Daniel, J. u. M., McCombie, G., Wendt, S., Zenobi, R.: Mass spectrometric determination of

- association constants of adenylate kinase with two noncovalent inhibitors. *J Am Soc Mass Spectrom* **2003**, 14, 442–448.
- 38 Daniel, J. M., Friess, S. D., Rajagopalan, S., Wendt, S., Zenobi, R.: Quantitative determination of noncovalent binding interactions using soft ionization mass spectrometry. *Int J Mass Spectrom* **2002**, 216, 1–27.
  - 39 Nesatyy, V. J.: Mass spectrometry evaluation of the solution and gas-phase binding properties of noncovalent protein complexes. *Int J Mass Spectrom* **2002**, 221, 147–161.
  - 40 Seeberger, P. H., Bauman, M., Zhang, G., Kanemitsu, T., Swayze, E. E., Hofstadler, S. A., Griffey, R. H.: Synthesis of neomycin analogs to investigate aminoglycoside–RNA interactions. *Synlett* **2003**, 9, 1323–1326.
  - 41 Ding, Y., Hofstadler, S. A., Swayze, E. E., Risen, L., Griffey, R. H.: Design and synthesis of paromomycin-related heterocycle-substituted aminoglycoside mimetics based on a mass spectrometry RNA-binding assay. *Angew Chem Intl Ed Engl* **2003**, 42, 3409–3412.
  - 42 He, Y., Yang, J., Wu, B., Robinson, D., Sprankle, K., Kung, P. P., Lowery, K., Mohan, V., Hofstadler, S., Swayze, E. E., Griffey, R.: Synthesis and evaluation of novel bacterial rRNA-binding benzimidazoles by mass spectrometry. *Bioorg Med Chem Lett* **2004**, 14, 695–699.
  - 43 Swayze, E. E., Jefferson, E. A., Sannes-Lowery, K. A., Blyn, L. B., Risen, L. M., Arakawa, S., Osgood, S. A., Hofstadler, S. A., Griffey, R. H.: SAR by MS: a ligand based technique for drug lead discovery against structured RNA targets. *J Med Chem* **2002**, 45, 3816–3819.
  - 44 Draper, D. E., Conn, G. L., Gittis, A. G., Guha Thakurta, D., Lattman, E. E., Reynaldo, L.: in *The Ribosome: Structure, Function, Antibiotics and Cellular Interactions*, ed. Garret, R., et al., ASM Press, Washington, D.C., **2000**, pp 105–114.
  - 45 Kung, P.-P., Casper, M. D., Cook, K. L., Wilson-Lingardo, L., Risen, L. M., Vickers, T. A., Ranken, R., Blyn, L. B., Wyatt, J. R., Cook, P. D., Ecker, D. J.: Structure–activity relationships of novel 2-substituted quinazoline antibacterial agents. *J Med Chem* **1999**, 42, 4705–4713.
  - 46 Gidden, J., Kemper, P. R., Shammel, E., Fee, D. P., Anderson, S., Bowers, M. T.: Application of ion mobility to the gas-phase conformational analysis of polyhedral oligomeric silsesquioxanes (POSS). *Int J Mass Spectrom* **2003**, 222, 63–73.
  - 47 Hanson, C. L., Robinson, C. V.: Protein–nucleic acid interactions and the expanding role of mass spectrometry. *J Biol Chem* **2004**, 279, 24907–24910.
  - 48 Shi, X., Mullaugh, K. M., Fetting, J. C., Jiang, Y., Hofstadler, S. A., Davis, J. T.: Lipophilic G-quadruplexes are self-assembled ion pair receptors, and the bound anion modulates the kinetic stability of these complexes. *J Am Chem Soc* **2003**, 125, 10830–10841.
  - 49 Benjamin, D. R., Robinson, C. V., Hendrick, J. P., Hartl, F. U., Dobson, C. M.: Mass spectrometry of ribosomes and ribosomal subunits. *Proc Natl Acad Sci USA* **1998**, 95, 7391–7395.
  - 50 Rostom, A. A., Fucini, P., Benjamin, D. R., Juenemann, R., Nierhaus, K. H., Hartl, F. U., Dobson, C. M., Robinson, C. V.: Detection and selective dissociation of intact ribosomes in a mass spectrometer. *Proc Natl Acad Sci USA* **2000**, 97, 5185–5190.
  - 51 Tito, M. A., Tars, K., Valegard, K., Hadju, J., Robinson, C. V.: Electrospray time-of-flight mass spectrometry of the intact MS2 virus capsid. *J Am Chem Soc* **2000**, 122, 3550–3551.
  - 52 Siuzdak, G., Bothner, B., Yeager, M., Brugkdou, C., Faquet, C. M., Hoey, K., Chang, C. M.: Mass spectrometry and viral analysis. *Chem Biol* **1996**, 3, 45–48.
  - 53 Siuzdak, G.: Probing viruses with mass spectrometry. *J Mass Spectrom* **1998**, 33, 203–211.

## **Part IV**

**Studying target-ligand interactions analyzing  
the target binding site by MS**



## 11

# Quantification of Protein–Ligand Interactions in Solution by Hydrogen/Deuterium Exchange (PLIMSTEX)

*Mei M. Zhu, David Hambly, and Michael L. Gross*

### 11.1

#### Introduction

Many important biological functions are mediated through protein–ligand interactions and the concomitant conformational change of the protein. The binding of therapeutic agents to the receptor sites of proteins is particularly important in drug design [1–3]. Recent trends in the discovery and development of new medicines demand new methods for rapidly screening protein–ligand binding properties in target selection and lead discovery, as well as for quantifying binding affinities and resolving subtle differences for lead optimization and further development [4]. Although computer modeling has been used to predict binding affinities [2, 5, 6], the strengths of these interactions are normally determined by experimental assays in which either equilibrium titrations, kinetic studies, or stability measurements are involved (e.g. [7–10]). Although success has been achieved in the determination of protein–ligand binding affinities by spectroscopic, calorimetric and other methods, limitations are often the large amounts of specifically labeled ligand or protein that are required. Often needed are additional spectroscopic or reaction probes, denaturants, or measurements of equilibrium concentrations following a separation, which may perturb the equilibrium. It remains of interest for biochemists and biophysicists to seek additional methods for quantification of protein–ligand binding that have general applicability, high accuracy, relative simplicity, and high throughput.

In the past decade, mass spectrometry has played an important role in the characterization of protein structure, differential expression, dynamics, and functions [11–14]. Several new mass spectrometry-based methods were reported for the characterization of protein–ligand binding [15–21]. Recently, we developed a novel method [22] to quantify protein–ligand interactions in solution by mass spectrometry, titration, and hydrogen/deuterium (H/D) exchange (PLIMSTEX). This strategy can determine the conformational change, binding stoichiometry and affinity in a variety of protein–ligand interactions including those involving small molecules, metal ions, peptides, and proteins [22, 23]. The detailed model-

ing procedures for the determination of binding constants using PLIMSTEX titration curves and the effect of model modifications on the precision and accuracy were also described [24]. Combined with kinetic measurements of H/D exchange, PLIMSTEX can provide insights on protein structure and protein–ligand interactions, the effect of media and ionic strength [25], species specificity, mutations on protein–ligand binding, and systematic changes in ligands [26]. The determination and interpretation of the titration curves will be described in this chapter. More perspectives of PLIMSTEX and the advantages of this approach over conventional methods and several other mass spectrometry-based methods will be illustrated using several examples.

A complementary approach to PLIMSTEX that we are developing is to compare the reactivity of hydroxyl radicals with a protein–ligand complex to that of the protein alone. If appropriate reagents are used, the change in solvent accessibility or conformation will alter the chemical reactivity of the target, typically the protein, enabling information regarding the location and affinity of the protein–ligand interaction to be determined. Chance and Brenowitz [27] pioneered the use of hydroxyl radicals for modifying Met, Cys or aromatic amino acid residues to determine sites of protein interactions and to follow RNA folding [28] and protein conformational changes [29]. We are developing a faster method that generates and quenches the hydroxyl radicals in less than a microsecond while allowing oxidation of more of the protein's solvent-exposed residues than can be achieved by other methods [30]. An example application shows that apomyoglobin has a conformationally flexible F-helix, as also indicated by nuclear magnetic resonance (NMR) [31] and that the porphyrin-binding pocket is closed in the absence of the ligand. Results from using this approach to the S-protein/S-peptide interaction suggest that this method should also be useful for studying binding of protein and ligands.

## 11.2

### The PLIMSTEX Method

#### 11.2.1

##### A General Protocol of H/D Exchange and LC/MS Analysis for PLIMSTEX

The general protocol for a PLIMSTEX experiment (Fig. 11.1) starts with equilibration of the protein of interest with different concentrations of ligand in aqueous buffer solutions. D<sub>2</sub>O containing the same concentrations of buffer and salts as in the starting solution is then added to initiate H/D exchange. The protocol utilizes a high D/H ratio in the forward and a high H/D ratio in the back exchange, and carries the added advantage of *in situ* desalting. When the system reaches a near steady state (1–3 h of exchange) where the fast exchangeable hydrogens reach steady state while the slow exchangers have not (as determined by a kinetic study conducted previously), the exchange is quenched by decreasing the pH to ~2.5. The solution is then loaded on a small C18 column (or C4 column for large

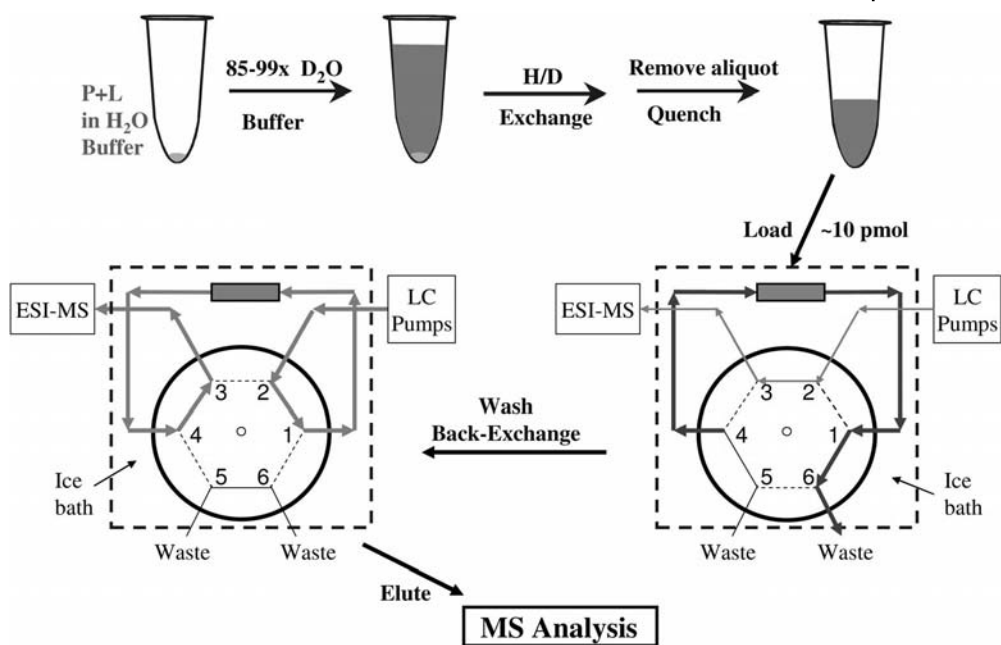


**Fig. 11.1** A general H/D exchange and LC/MS protocol for PLIMSTEX. P is protein, L is ligand.

protein), cooled to 0 °C, and the labile, non-amide sites of the immobilized protein are back-exchanged to the H form. The solution is desalted by washing with ice-cold, aqueous formic acid (pH ~ 2.5). The protein, which now bears an isotopic exchange “signature” in its amide linkages reflecting its state at the time of exchange, is introduced into a mass spectrometer, and its molecular weight is determined. Rapid elution (by an isocratic flow of solvent at 30–35  $\mu\text{L min}^{-1}$  with high organic composition or with a fast pH 2.5 gradient) delivers the protein to an electrospray ionization (ESI) source. Although the initial studies used ESI (ion trap or quadrupole/time-of-flight analyzers) in the positive-ion mode, matrix-assisted laser desorption ionization (MALDI)-MS may also be an appropriate method.

### 11.2.2

#### Determination and Interpretation of the Titration Curves

Quenching and desalting cause the ligand(s) to dissociate, liberating the protein for molecular mass measurements by mass spectrometry to afford the number of deuteriums taken up by solvent-accessible amides. A plot of the mass difference between the deuterated and nondeuterated protein (deuterium uptake) versus the total ligand concentration (or the ratio of total ligand concentration to the total protein concentration) gives the PLIMSTEX curve (Fig. 11.2). Usually, the deute-



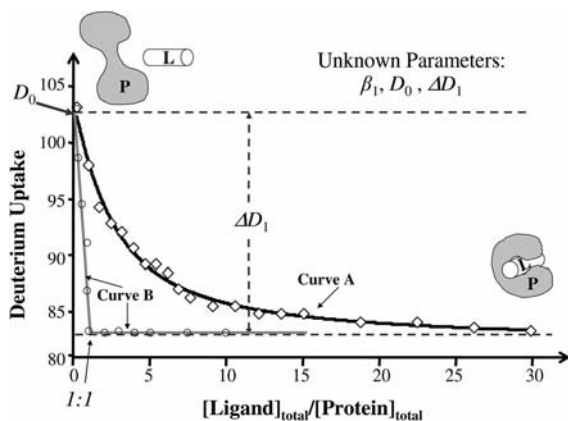


**Fig. 11.2** Schematic illustration of a PLIMSTEX curve for 1:1 protein:ligand binding. P is protein, L is ligand.  $\beta_1$  is the binding constant for binding one ligand;  $D_0$  is the deuterium level for apo-protein, and  $\Delta D_1$  is the difference between the average deuterium level of one-ligand-bound protein complex and that of the apo-protein.

rium uptake values decrease with an increase in the ligand concentration, and a decrease reflects increased hydrogen bonding (overall deuterium shift  $\Delta D$ ) of some backbone amide protons upon forming the complex. Intermediate states for multiple ligand binding may also be monitored when a species deuterium shift ( $\Delta D_i$ ) can be related to a specific binding species.

PLIMSTEX curves are sensitive to the total protein concentration. When the protein is titrated at high concentration ( $\sim 100$  times the  $1/K_a$  or  $K_d$ ), a “sharp-break” curve is obtained (see curve B in Fig. 11.2), and the ratio of  $[\text{ligand}]_{\text{total}}$  to  $[\text{protein}]_{\text{total}}$  at the break clearly indicates binding stoichiometry. To quantify affinity, PLIMSTEX requires that a change occurs in the extent of H/D exchange during a titration at a protein concentration comparable to the dissociation constant  $K_d$  (see curve A in Fig. 11.2). The change may be conformational and/or a stability difference between the apo- and ligand-bound proteins.

To extract the binding affinity, the titration data are fitted using a 1: $n$  protein:ligand sequential binding model, where  $n$  is the number of binding sites for the same ligand. There are two assumptions for the modeling: (1) the ligand binds the protein in a stepwise fashion, and (2) H/D exchange of each amide is independent (i.e., does not depend on exchange at any other site of the protein). A nonlinear least squares (NLLS) regression [32] is involved in a calculation of the extent of change in the H/D exchange during the titration ( $\Delta D$ ) as a function [Eq. (1)] of the total ligand concentration ( $[\text{Lig}_T]$ ), the overall binding constants ( $\beta_i$ , which is the product of the stepwise macroscopic binding constants  $K_i$ , where  $i = 1$  to  $n$ ), and the species deuterium shifts ( $D_0$  and  $\Delta D_i$ ,  $i = 1$  to  $n$ ).  $D_0$  is the shift in the molecular weight of the apo protein caused by H/D exchange (deuterium uptake). To minimize experimental errors, we do not accept the experiment

value of  $D_0$  (the deuterium uptake of the apo-protein) but rather take it as a variable or unknown parameter.  $\Delta D_i$  is the difference between the average deuterium level of each protein–ligand complex and that of the apo-form (Fig. 11.2). It is weighted by its binding fraction  $[\text{Prot-Lig}_i]/[\text{Prot}_T]$ , which is a function of  $[\text{Lig}_T]$  and  $\beta_i$  ( $i = 1 - n$ ), the latter of which is the product of all the stepwise equilibrium binding constants ( $\beta_i = K_1 K_2 \cdots K_i$ ). A positive  $\Delta D_i$  indicates that binding of  $i$  ligand(s) to the protein leads to more hydrogen bonding and less D uptake as compared to the apo-form. A negative  $\Delta D_i$  points to the formation of a more open structure with less hydrogen bonding relative to its apo form. When  $\Delta D_i$  is approximately zero, little conformational change apparently occurs upon binding although changes in one part of the protein may be compensated by changes in another. If no net change occurs, PLIMSTEX may not be appropriate for determining the corresponding equilibrium constant ( $\beta_i$ ).

$$\Delta D(\beta_1, \dots, \beta_n, D_0, \Delta D_1, \dots, \Delta D_n, [\text{Lig}_T]) = D_0 - \sum_{i=1}^n \Delta D_i \frac{[\text{Prot-Lig}_i]}{[\text{Prot}_T]} \quad (1)$$

The best fit is obtained by a search, which iterates through a sequence of trials to minimize the error between the calculated overall deuterium shift,  $\Delta D$ , and the experimentally measured shift by varying the unknown parameters ( $\beta_i, D_0, \Delta D_i$ ). The average data (at least two runs) are used for the curve fitting to give mean values for the unknown parameters ( $\beta_i, \Delta D_i, D_0$ ). The macroscopic  $K_i$  values are calculated from  $\beta_i$  values. Finally, a resampling statistical analysis is used to evaluate the precision for each parameter in the search.

We described previously the detailed modeling procedure for analyzing PLIMSTEX data [24]. For fitting the protein self-association data, we modified the modeling to acknowledge that both ligand and protein are the same, and these modifications were described at a recent conference [33]. All modeling procedures were implemented with Mathcad 2001 Professional (MathSoft, Cambridge, Mass.). This modeling process is not only a new tool for analyzing H/D exchange data acquired by electrospray ionization–mass spectrometry (ESI-MS), but also possesses some novel aspects in modeling experimental titration data to determine the affinity of ligand binding.

## 11.3

### Applications of PLIMSTEX

#### 11.3.1

#### Determination of Association Constant ( $K_a$ ), Stoichiometry ( $n$ ), and Protection ( $\Delta D_i$ )

To validate the method, we applied PLIMSTEX to determine the binding constants ( $K_a$ ), stoichiometry (1 protein to  $n$  ligands), and the protection against H/D exchange in various interactions. We chose as tests the binding of  $\text{Mg}^{2+}$  to guanosine diphosphate (GDP)-bound human ras protein, of  $\text{Ca}^{2+}$  to apo calmodulin

(CaM), of fatty acid carboxylate to intestinal fatty acid binding protein (IFABP), and of peptides (e.g., melittin) to  $\text{Ca}^{2+}$ -saturated calmodulin (holo CaM)]. We also extended PLIMSTEX to protein–protein interactions involving self-associations of various insulins [33]. These are widely studied systems, and their individual  $K$  values range from  $10^4 \text{ M}^{-1}$  to  $10^8 \text{ M}^{-1}$ .

Modeling the titration results for the test systems (Table 11.1) gives the binding stoichiometry from the best fit. The binding constants determined by PLIMSTEX for the tested system are within a factor of six of those reported previously using established methods (Table 11.1). The positive  $\Delta D_i$  values (Table 11.1) quantify the increased hydrogen bonding (more protection to H/D exchange). The  $\Delta D_i$  values in the case of insulin represent changes in the solvent accessibility of the

Table 11.1 Outcome of test systems for PLIMSTEX.

Protein ( $C_{\text{total}}$ ) + ligand (1 to $n$ )	$\Delta D_i$ <sup>[a]</sup>	PLIMSTEX $K_a$ ( $\text{M}^{-1}$ ) <sup>[a]</sup>	$\frac{K_a(\text{Literature})}{K_a(\text{PLIMSTEX})}$ <sup>[b]</sup>
Human Ras-GDP (1.5 $\mu\text{M}$ ) + $\text{Mg}^{2+}$ (1 to 1)	$25.6 \pm 0.6$ <sup>[c]</sup>	$K_1: (4.1 \pm 0.2) \times 10^4$	1.7 <sup>[d]</sup>
Porcine apo-CaM (15 $\mu\text{M}$ ) + $\text{Ca}^{2+}$ (1 to 4)	$12.6 \pm 0.3$ <sup>[e]</sup>	$K_3: (7 \pm 2) \times 10^4$ ; $K_4: (1.1 \pm 0.4) \times 10^5$ ; $K_3 K_4: (9 \pm 1) \times 10^9$	$K_3: 0.6$ <sup>[f]</sup> $K_4: 2.8$ <sup>[f]</sup> $K_3 K_4: 1.4$ <sup>[f]</sup>
Rat IFABP (0.3 $\mu\text{M}$ ) + Oleate (1 to 1)	$13.8 \pm 0.7$ <sup>[c]</sup>	$K_1: (2.6 \pm 0.6) \times 10^6$	1.2 <sup>[g]</sup>
Porcine holo-CaM (0.15 $\mu\text{M}$ ) + melittin (1 to 1)	$29.3 \pm 0.8$ <sup>[c]</sup>	$K_1: (5.4 \pm 0.9) \times 10^7$	6.1 <sup>[h]</sup> or 0.2 <sup>[i]</sup>
r-Human insulin + r-human insulin (mono- to di- to hexamer)	$14 \pm 2$ <sup>[j]</sup> $23 \pm 3$ <sup>[k]</sup>	$K_{12}: (7 \pm 1.2) \times 10^5$ $K_{26}: (2 \pm 0.7) \times 10^9$	$K_{12}: 0.2$ <sup>[l]</sup> $K_{26}: 0.2$ <sup>[l]</sup>

<sup>a</sup> Each protein–ligand titration was done in duplicate. Values were determined by fitting the average data at similar conditions. A subsampling method was used to evaluate the second order statistics of the parameters.

<sup>b</sup>  $K_i$  (literature data) determined under comparable experimental conditions (e.g., similar pH, ionic strength if available) were selected.

<sup>c</sup>  $\Delta D_1$ .

<sup>d</sup> From reference [41].

<sup>e</sup>  $\Delta D_4$ .

<sup>f</sup> From reference [47].

<sup>g</sup> From reference [51].

<sup>h</sup> From reference [58] for CaM from bovine brain.

<sup>i</sup> From reference [59] for CaM from wheat germ.

<sup>j</sup>  $\Delta D_{12}$ .

<sup>k</sup>  $\Delta D_{26}$ .

<sup>l</sup> From reference [72].

oligomer compared to that of monomer. Each system is now discussed in more detail.

### 11.3.2

#### Ras-GDP Interacting with $\text{Mg}^{2+}$ : A 1:1 Protein:Metal Ion Interaction

Human P21<sup>Ha-ras</sup>, a 21-kDa protein with 189 amino acid residues, plays a key role in controlling cellular growth and acts as a molecular switch in signal transduction pathways by cycling between its biologically active ras-GTP and inactive ras-GDP form [34]. The point mutations at several amino acid sites in ras account for 30% of human cancers.  $\text{Mg}^{2+}$  is an essential cofactor for the ras superfamily of small GTPases and is necessary for both guanine nucleotide binding and GTP-hydrolysis [35, 36]. We are interested in comparing the binding of apo-ras to GDP and GTP with and without  $\text{Mg}^{2+}$ . The C-terminal truncated P21<sup>Ha-ras</sup> (residues 1–166) preserves crucial kinetic and structural properties [37–39] and, thus, is a model for this study. We used PLIMSTEX to investigate the binding of  $\text{Mg}^{2+}$  to ras-GDP to form a ternary complex; that is, the ras-GDP binary complex was treated as the “apo” protein and  $\text{Mg}^{2+}$  was treated as the ligand.

##### 11.3.2.1 Kinetic Study of Forward H/D Exchange Ras-GDP with Different $[\text{Mg}^{2+}]$

To determine the appropriate H/D exchange time for the titration, we first determined the forward H/D exchange kinetics of ras-GDP (1.5  $\mu\text{M}$ ) as a function of  $[\text{Mg}^{2+}]$ . We chose this protein concentration for the kinetics of H/D exchange at different  $[\text{Mg}^{2+}]$  to [ras-GDP] ratios because we had a limited amount of protein and the initiation of H/D exchange by diluting the deuterated buffer would not cause significant dissociation of the ternary complex at this protein level [40]. Figure 11.3 shows the deuterium uptake versus the time of H/D exchange for three

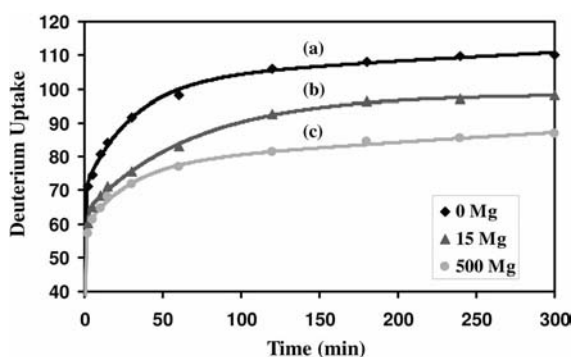


**Fig. 11.3** Forward H/D exchange kinetics for Ras-GDP with different  $[\text{Mg}^{2+}]$ . Line (a), diamonds:  $[\text{Mg}^{2+}]_{\text{free}}/[\text{Ras-GDP}]_{\text{total}} = 0$ . Line (b), triangles:  $[\text{Mg}^{2+}]_{\text{free}}/[\text{Ras-GDP}]_{\text{total}} = 15$ . Line (c), circles:  $[\text{Mg}^{2+}]_{\text{free}}/[\text{Ras-GDP}]_{\text{total}} = 500$ . Conditions: 1.5  $\mu\text{M}$  Ras-GDP, in 50 mM HEPES/100 mM KCl, apparent pH 7.4, 90%  $\text{D}_2\text{O}$ ,  $T = 21.5^\circ\text{C}$ . Waters CapLC and a Q-TOF Ultima were used for LC/ESI-MS analysis.

**Table 11.2** Average rate constants and number of amide hydrogens in each rate group for H/D exchange of ras-GDP under different Mg concentrations. Measurements were made in 100 mM KCl/50 mM HEPES, 90% D<sub>2</sub>O, apparent pH of 7.4, T = 21.5 ± 0.5 °C. The final [ras-GDP]<sub>tot</sub> in H/D exchange media was 1.5 μM. EDTA was used to control [Mg<sup>2+</sup>] in solution.

Rate constants and number of amides [Mg <sup>2+</sup> ]/[ras-GDP] <sub>tot</sub>	Fast		Intermediate		Slow	
	k <sub>1</sub> (min <sup>−1</sup> )	No. of H <sub>1</sub>	k <sub>2</sub> (min <sup>−1</sup> )	No. of H <sub>2</sub>	k <sub>3</sub> (min <sup>−1</sup> )	No. of H <sub>3</sub>
0	1.9	79	0.032	35	0.0007	48
15	1.4	70	0.014	39	<0.000001	53
500	1.5	65	0.027	21	0.0005	76
Average	1.6		0.03		0.004	

concentration ratios (0, 15, 500) which represent, for a titration with Mg<sup>2+</sup>: the initial (no ligand), an intermediate point, and the end. The data were fitted using a three-group, pseudo-first-order kinetics model [25] to give, for 162 amide hydrogens in C-terminal-truncated ras, the distribution of the fast-, intermediate-, and slow-exchanging amide hydrogens under these three [Mg<sup>2+</sup>]:[ras-GDP]<sub>tot</sub> ratios (Table 11.2). As the ratio of [Mg<sup>2+</sup>]:[ras-GDP]<sub>total</sub> increases, more binary ras-GDP complex is transformed to the ras-GDP-Mg<sup>2+</sup> ternary complex, and the number of fast-exchanging amide hydrogens decreases monotonically from 79 to 65, whereas the number of slow-exchanging hydrogens increases from 48 to 76. This distribution is a “signature” of ras protein’s conformation and should, in general, be a useful indicator for an unknown protein to guide theoretical calculations of folding. Fast-exchanging hydrogens are likely to be involved in minimal hydrogen bonding, whereas slow ones are protected by high-order structure and hydrogen bonding. That more hydrogens shift from fast to intermediate and slow groups upon Mg<sup>2+</sup>-binding is consistent with a global folding of ras into a more compact and stable, less solvent-accessible form. After 3 h of exchange, the deuterium uptake levels off for each of the three concentration ratios, indicating that the H/D exchange of the fast and intermediate amides had arrived at a near steady state. The small experimental errors in exchange time do not contribute significantly to the measurement of deuterium uptakes. Pointing to a successful application of PLIMSTEX are detectable differences between deuterium levels in ras-GDP (no Mg<sup>2+</sup>) and ras-GDP-Mg<sup>2+</sup> complex at this time. Therefore, we chose 3 h as the exchange time for the PLIMSTEX titration (i.e., the time of the quench in exchange).

### 11.3.2.2 PLIMSTEX Results for Ras-GDP Titrated with Mg<sup>2+</sup>

In the titration of 1.5 μM ras-GDP with Mg<sup>2+</sup>, as the [Mg]:[ras-GDP]<sub>tot</sub> ratio increases, the deuterium uptake decreases as the ternary complex is formed. Fit-

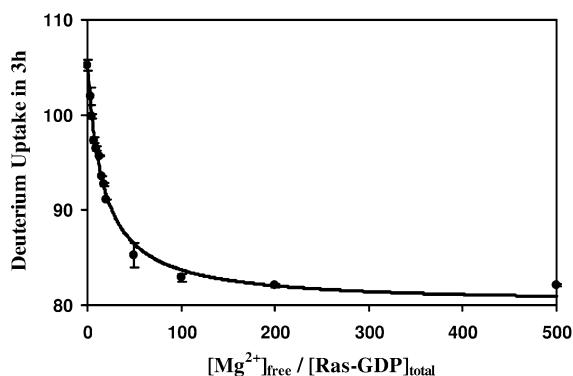


**Fig. 11.4** PLIMSTEX curve for 1.5  $\mu$ M Ras-GDP titrating with  $Mg^{2+}$ . Conditions: 90%  $D_2O$ , 50 mM HEPES buffer, 100 mM KCl, pH 7.4, H/D exchange time = 3 h. EDTA was used to control  $[Mg^{2+}]$  in solution. The error bars shown for each data point were based on the deviation from two independent runs.

$[Mg^{2+}]_{free}$  was calculated using the “Webmaxc Standard” program on the internet [43]. The solid line was the fitted PLIMSTEX curve for the average data using a 1:1 binding model and three-parameter ( $\beta_1, D_0, \Delta D_1$ ) fitting.

ting the PLIMSTEX curve (Fig. 11.4) gives  $K_a$ ,  $\Delta D_1$ , and  $D_0$  for ras-GDP as  $(4.1 \pm 0.2) \times 10^4 M^{-1}$ ,  $25.6 \pm 0.6$  and  $105.7 \pm 0.5$ , respectively. The root mean square (RMS) of the error between the predicted and the experimentally measured deuterium shifts is 0.7 Da. The results indicate a relatively weak 1/1 interaction between  $Mg^{2+}$  and ras-GDP, causing  $\sim 26$  backbone amide protons of the binary complex to become protected with the binding to  $Mg^{2+}$ . The binding constant agrees with the literature value ( $6.9 \times 10^4 M^{-1}$ ) obtained from an equilibrium unfolding stability study using circular dichroism [41]. The protection quantified by PLIMSTEX ( $\Delta D_1 = 26$ ) is also consistent with the difference between the number of the slow exchanging amide protons of ras in its ternary complex ras-GDP- $Mg^{2+}$  ( $\sim 76$ ) and that in the binary complex ras-GDP ( $\sim 48$ ).

### 11.3.2.3 Interpretation of PLIMSTEX Results with H/D Exchange Kinetics

The PLIMSTEX curve is directly related to the H/D exchange kinetics of the protein (e.g. ras-GDP) and its protein–ligand complex (e.g. ras-GDP- $Mg^{2+}$ ). Taking a certain sampling timepoint (e.g. 3 h) for the titration produces a view that is a weighted superposition of all protein conformation concentrations as a function of ligand concentration. If we were to choose a different time, we would obtain a view with a different weighting. For example, at 3 h, where the H/D exchange becomes nearly constant, the fast and intermediate hydrogens are nearly at equilibrium so their weight in the superposition is approximately zero, but those in the slow group are still exchanging so their weight is dominant. At the start of the titration, ras-GDP is the main species, and it has the smallest number of slow ex-

changing hydrogens. As a result, we see the highest extent of exchange. At the latter stages of the titration, the ternary complex ras-GDP-Mg<sup>2+</sup> is predominant and has the largest population of slow exchanging hydrogens. The middle part of the titration curve (Fig. 11.4) represents a superposition of various ras-GDP and ras-GDP-Mg<sup>2+</sup> species. Differences in kinetics give different uptakes of deuterium as a function of sampling time; indeed, if no change in H/D exchange kinetics were observed for different ligand-binding species, the titration curve would be a horizontal line. As mentioned previously, PLIMSTEX is applicable only if there is a change in the D uptake as the ligand is added. When the differences disappear at long time, methods such as pulsed labeling and rapid mixing are better choices because these methods sample fast exchanges ( $t_{0.5} < 1$  s).

#### 11.3.2.4 Application of PLIMSTEX to Relatively Weak Protein–Ligand Binding

The titration of ras-GDP with Mg<sup>2+</sup> also demonstrates that PLIMSTEX is applicable to those relatively weak noncovalent protein–ligand complexes that may be difficult to detect by direct electrospray. Although ESI-MS can detect the 20  $\mu$ M of ras-GDP binary complex and its nonspecific sodium adducts in 2 mM ammonium acetate, pH 5.2 [42], the ternary complex of ras-GDP-Mg<sup>2+</sup> does not survive under similar conditions because the constants ( $K_a$ ) for Mg<sup>2+</sup> binding are relatively small. Even with ras-GDP, a relatively strong complex, the solvent pH and electrospray source conditions are critical in a direct ESI-MS analysis. In the PLIMSTEX protocol, the ligands release upon quenching at low pH to form ras-GDP and allow an easy detection of apo-ras under normal ESI-MS conditions (47.5:47.5:5.0 of CH<sub>3</sub>CN:H<sub>2</sub>O:CH<sub>3</sub>COOH, pH 2.6). PLIMSTEX does not rely on the ability of MS to measure solution concentration from peak intensities but rather to measure  $m/z$ . The two complexes are distinguishable by their different H/D exchange kinetics, leading to different deuterium uptakes at certain exchange times.

#### 11.3.2.5 Experimental Issues Regarding Using Metal Chelators

In most PLIMSTEX experiments, the total ligand concentration is used in the curve fitting. The determination of free ligand concentration is not required because the relationship between the free and total ligand concentrations is resolved in the modeling procedure [24]. For the ras titration, however, we had no Mg<sup>2+</sup>-free ras-GDP stock but only a limited amount of ras-GDP-Mg<sup>2+</sup> stock solution (1.5 mM ras, 10 mM MgCl<sub>2</sub>, in 64 mM Tris-HCl, 10 mM MgCl<sub>2</sub>, 1 mM sodium azide, 1 mM DTT buffer, pH 7.6). After diluting by 100 times with 50 mM *N*-(2-hydroxyethyl)piperazine-*N'*-2-ethanesulfonic acid (HEPES) and 0.1 M KCl, pH 7.4 buffer, there was still excess of Mg<sup>2+</sup>. To conduct the Mg<sup>2+</sup> titration of free ras-GDP, we added EDTA to control free [Mg<sup>2+</sup>] in solution {free [Mg<sup>2+</sup>] was calculated using a WebChelators program (Webmaxc Standard) on the internet [43, 44]}.

## 11.3.3

**Apo-CaM Interacting with  $\text{Ca}^{2+}$ : A 1:4 Protein:Metal Ion Interaction**

With the success in studying 1:1 protein:metal ion binding, we applied PLIMSTEX to the more challenging 1:4 protein:metal ion binding of calmodulin and  $\text{Ca}^{2+}$  binding. Calmodulin, a small ( $\sim 17$  kDa), acidic, and highly conserved protein, is regulated by  $\text{Ca}^{2+}$  binding in most eukaryotic cells. When binding  $\text{Ca}^{2+}$ , calmodulin undergoes conformational changes that enable it to bind to and activate other target proteins, an action that is critical to various aspects of cell metabolism [45, 46]. We wished to learn whether PLIMSTEX can determine the conformational changes, binding stoichiometry, and binding constants for  $\text{Ca}^{2+}$  interactions with calmodulin (CaM) under varying conditions of electrolyte identity and ionic strength [25].

### 11.3.3.1 PLIMSTEX Results for CaM and Intermediate Protein–Ligand Binding Species

The PLIMSTEX titration curve shows that CaM becomes more stable (more hydrogen-bonded) upon Ca-binding (Fig. 11.5A). The formation of  $\text{CaM-4Ca}^{2+}$  species is the biggest contributor to the shape of the titration curve and accounts for the largest conformational change in the stepwise  $\text{Ca}^{2+}$  binding. The earlier

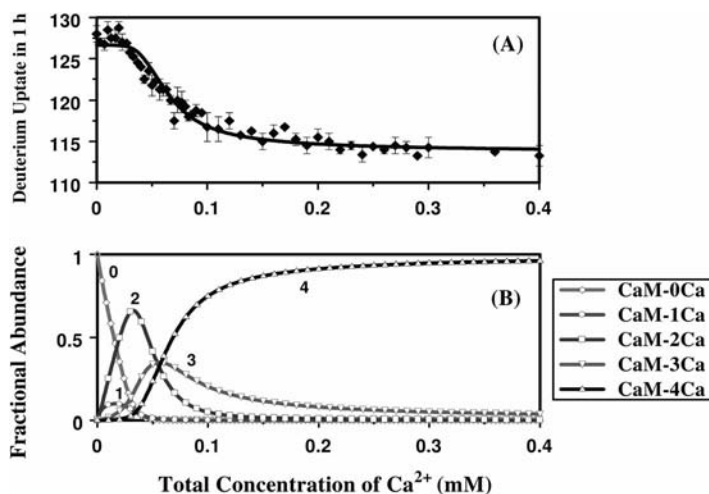


**Fig. 11.5** Ca titration of porcine calmodulin and fractional species calculation [25]. (A) Ca-titration for 15  $\mu\text{M}$  of porcine calmodulin in 50 mM HEPES (pH 7.4,  $T = 21.5^\circ\text{C}$ , 90%  $\text{D}_2\text{O}$ ). Error bars were based on the deviation from two sets of Q-TOF data. The solid curve was the best fit for the average data using the four-parameter model. (B) Fractional species as a function of  $[\text{Ca}^{2+}]$  for CaM interacting with four  $\text{Ca}^{2+}$ .



interactions with the first and second calcium ions do not perturb CaM's conformation in any significant way. Therefore, we cannot obtain  $K_1$  and  $K_2$  from the titration and took these constants from published fluorescence studies that were done under comparable pH and ionic strength [47]. Modeling the titration curve gave  $\beta_3$  and  $\beta_4$ , from which we could calculate  $K_3$  and  $K_4$ . The two literature sequential binding constants are:  $K_1 = 2.5 \times 10^5 \text{ M}^{-1}$ ,  $K_2 = 5.0 \times 10^6 \text{ M}^{-1}$  [47], whereas  $K_3 = 7.1 \times 10^4 \text{ M}^{-1}$ , and  $K_4 = 1.1 \times 10^5 \text{ M}^{-1}$  come from PLIMSTEX (Table 11.1); the latter agree with the literature  $K_3$  and  $K_4$  within a factor of 3. We then calculated the fractional-species of the Ca-bound CaM species, CaM- $x$ Ca ( $x = 0\text{--}4$ ) using the macroscopic binding constants  $K_3$  and  $K_4$  that come from the titration data and the literature values of  $K_1$  and  $K_2$  (Fig. 11.5B). The binding polynomial shows that apo-CaM (CaM-0Ca) disappears quickly with an increase of total  $[\text{Ca}^{2+}]$ . CaM-1Ca and CaM-3Ca never become abundant but give way quickly to CaM-2Ca and CaM-4Ca, respectively, substantiating cooperativity in the binding. The major changes in fractional species occur between the formation of CaM-2Ca and CaM-4Ca, which is mirrored by the titration curve, where the greatest difference in exchange also occurs as CaM-2Ca goes to CaM-4Ca. After the fourth  $\text{Ca}^{2+}$  is bound, the extent of exchange drops to its lowest level and becomes nearly constant. None of the nonspecific binding of more than four  $\text{Ca}^{2+}$  is registered in the titration, indicating that if further binding to  $\text{Ca}^{2+}$  occurs, it does not cause any significant conformational changes in the protein. This result demonstrates that PLIMSTEX can determine accurately the intermediate binding species and related binding constants, which are often difficult to obtain by most other mass spectrometry-based methods. It also bypasses any problems caused by nonspecific binding, which is often encountered by direct ESI measurements (complexes involving more than four  $\text{Ca}^{2+}$  can be seen by direct ESI).

#### 11.3.3.2 PLIMSTEX in Biologically Relevant Media and High Ionic Strength

Physiological conditions of cellular solutions often include relatively high ionic strength salt media with nonvolatile buffer and high concentrations of salt, which make difficult the detection of protein and protein–ligand complex by direct ESI or MALDI. Even with low ionic strength and a “mass spectrometry friendly” solvent, nonspecific adducts may arise, confusing the stoichiometry and affinity determinations. High sensitivity of mass measurements in PLIMSTEX can be achieved because the pH is decreased to quench the exchange, and metal cations and ligands normally dissociate and are removed by online chromatography prior to MS analysis. Further, all forms of the protein revert back to the apo state, giving minimal signal dispersion and good signal-to-noise ratio. The clean up improves the mass resolving power because metal-ion interference is removed. By maintaining a high D/H ratio in the forward exchange and a high H/D ratio in the back exchange, we find a narrow isotope distribution and concomitant improved mass resolving power. Therefore, PLIMSTEX allows one to explore  $\text{Ca}^{2+}$  binding to CaM in not only 15  $\mu\text{M}$  of CaM in low ionic strength media (2 mM  $\text{NH}_4\text{OAc}$ ) but also under conditions with buffer and high ionic strength (50 mM HEPES or 50 mM HEPES with 100 mM KCl; Fig. 11.6).

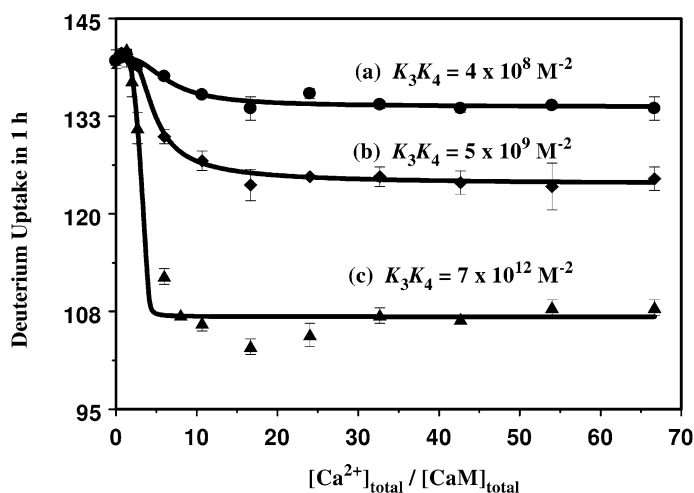


**Fig. 11.6** Ca titration of 15  $\mu\text{M}$  porcine CaM in three different media (99%  $\text{D}_2\text{O}$ ) [25]. Line (a): 50 mM HEPES/0.1 M KCl, apparent pH 7.4. Line (b) 50 mM HEPES, apparent pH 7.4. Line (c): 2 mM  $\text{NH}_4\text{OAc}$ , apparent pH 7.0. Error bars were based on two sets of LCQ titration data. Solid curves were taken from the four-parameter model and are the best fit for the average data.

The  $\Delta D_4$  decreases dramatically from low ionic-strength media (2 mM  $\text{NH}_4\text{OAc}$ ) to high ionic-strength media (50 mM HEPES with 100 mM KCl). The mid points of the curves shift from low  $[\text{Ca}^{2+}]_{\text{total}}$  to higher  $[\text{Ca}^{2+}]_{\text{total}}$ , indicating that the Ca-binding affinity decreases as ionic strength increases. The Ca-binding affinity ( $K_3K_4$ ) obtained from sequential ligand binding curve fitting, where the ratio of protein:ligand is 1:4, decreases by approximately four orders of magnitude with increases in ionic strength and  $[\text{K}^+]$ , in agreement with results from other methods [47, 48]. The binding is influenced by ionic strength and the presence of other cations, although many of these cations do not cause conformational changes in apo CaM. Both  $\text{Ca}^{2+}$  and  $\text{Mg}^{2+}$  bind to CaM with different affinities, causing different conformational changes.  $\text{K}^+$ , if it does bind, causes no detectable conformational change, and the interactions of  $\text{Ca}^{2+}$  with CaM in the presence of  $\text{Li}^+$ ,  $\text{Na}^+$ , and  $\text{K}^+$  occur with similar affinities and associated changes in solvent accessibility. These metal-ion effects point to nonspecific rather than competitive binding of alkali metal ions, as was discussed in a full research article [25].

#### 11.3.4

##### **Apo-IFABP and Oleate: A Protein–Small Organic Molecule Interaction**

Intestinal fatty acid-binding protein (IFABP) belongs to a family of  $\sim 15$  kDa, predominantly  $\beta$ -sheet proteins that bind a diverse group of polar lipids [49]. IFABP

consists of a helix-turn-helix motif and a  $\beta$ -clam topology surrounding a large cavity into which a single fatty acid binds, permitting intracellular trafficking and processing of dietary fatty acid in the intestine [50, 51]. A D34A-IFABP mutant with a single-site mutation by replacing Asp 34 with Ala is available, and the structure of its apo-form was solved by Ogbay and Cistola using NMR [52]. H/D exchange kinetics and PLIMSTEX applied to wild-type rat IFABP (WT-IFABP) and its D34A mutant (D34A-IFABP) add information on the differences in conformation and fatty acid-binding properties of this protein [53, 54].

The PLIMSTEX curve for 0.3  $\mu\text{M}$  WT-IFABP titrated with potassium oleate fits well with a 1:1 binding model [22, 24]. The  $K$  and  $\Delta D_1$  (difference between the average deuterium level of one-ligand-bound protein and that of apo protein) for WT-IFABP are  $(2.6 \pm 0.6) \times 10^6 \text{ M}^{-1}$  and  $13.8 \pm 0.7$  (Table 11.1), respectively, indicating that a strong interaction between oleate and WT-IFABP occurs with protection of  $\sim 14$  backbone amide hydrogens.

The titration curve for 3  $\mu\text{M}$  D34A-IFABP with oleate is more complicated and fits well a 1:3 protein:ligand sequential binding model [54]. The binding affinities of each oleate to D34A [ $K_{di}$  ( $i = 1 \sim 3$ )] are between 6  $\mu\text{M}$  and 140  $\mu\text{M}$  are lower than that of the single binding constant for WT-IFABP [0.38  $\mu\text{M}$ ]. Complexes with one and three oleates are more hydrogen-bonded than those of apo D34A-IFABP ( $\Delta D_1 = 25$ ;  $\Delta D_3 = 32$ ); however, the two-oleate bound D34A protein is less hydrogen-bonded than apo ( $\Delta D_2 = -9$ ). Mass profiles obtained in an FTMS experiment showed that multiple components form during oleate titration. For example, the pattern of peaks representing uptake of deuterium by D34A-IFABP when the ratio of oleate to D34A is 15:1 fits three binomial distributions.

These results demonstrate that the disruption of the D34-R126 ion pair in IFABP causes the D34A mutant to bind additional oleates (at least three) with lower binding constants than for WT-IFABP binding the first oleate.

### 11.3.5

#### **Holo-CaM and Melittin: A Protein–Peptide Interaction**

Most physiological relevant targets for CaM are proteins, but CaM also binds to a number of peptide hormones, toxins, and peptides, which represent CaM binding domains, as well as small drug-like molecules [55–57]. Melittin, a small hydrophobic peptide from bee venom consisting of 26 amino acid residues, is known to bind  $\text{Ca}^{2+}$ -saturated CaM (holo-CaM) in a 1:1 ratio with a range of  $K_d$  values between 3 nM [58] and 110 nM [59]. The low molecular weight of melittin (MW 2845), its  $\alpha$ -helical structure [60], and its high affinity for CaM make it a good candidate for detailed structural studies of CaM-target recognition. Although the melittin model has some drawbacks, there is phenomenological evidence [61, 62] that the binding of melittin to CaM resembles that of myosin light-chain kinase protein (MLCK) [63] and troponin I [64]. Binding the third and fourth  $\text{Ca}^{2+}$  becomes more endothermic, but the free energy coupling in the CaM- $\text{Ca}^{2+}$ -melittin system is entropically driven by hydrophobic interactions (i.e. by significant dehydration of nonpolar groups in the  $\text{Ca}^{2+}$ -binding sites and in the two surface-

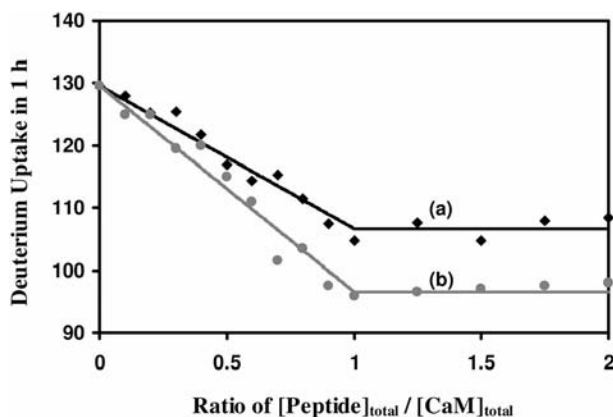


**Fig. 11.7** Sharp-break PLIMSTEX curves at high protein concentration [23]. Line (a): melittin (a 26-amino-acid peptide) titration. Line (b): mastoparan (a 16-amino-acid peptide) titration of 15  $\mu\text{M}$   $\text{Ca}^{2+}$ -saturated porcine calmodulin (CaM-4Ca) in 50 mM HEPES, 100 mM KCl, 0.49 mM  $\text{Ca}^{2+}$ , 99%  $\text{D}_2\text{O}$ , apparent pH 7.4. Data points are based on the average of two runs for each titration system, and the breaking point clearly indicates 1:1 protein–ligand binding stoichiometry.

accessible hydrophobic domains of CaM [62]). Melittin binding to  $\text{Ca}^{2+}$ -saturated CaM (holo-CaM) appears to be a good test for PLIMSTEX.

#### 11.3.5.1 PLIMSTEX Curves Under Different Holo-CaM Concentrations

As demonstrated earlier (Fig. 11.2), PLIMSTEX curves are sensitive to the total protein concentration and do not yield reliable  $K$  values when the protein is titrated at high concentrations ( $\sim 100$  times the  $1/K$  or  $K_d$ ). Nevertheless, when the concentration is too high, “sharp-break” curves (curve B in Fig. 11.2, curve b in Fig. 11.7) are obtained and can be used for stoichiometry determination. We found the binding stoichiometry for holo-CaM: melittin binding to be 1:1 by titrating a relatively high concentration of holo-CaM (15  $\mu\text{M}$ ) with melittin (Fig. 11.7, curve a). Interestingly, we found that the binding of mastoparan, which is a 14-amino-acid residue peptide from the wasp and is approximately half the size of melittin, is accompanied by a greater loss of solvent accessibility for CaM than that caused by binding of melittin (Fig. 11.7, curve b), ruling out a direct block of the surface amides, and indicating significant conformational change (additional H-bonding) with the binding. The PLIMSTEX result is in accord with the proposed structure of the holo-CaM:melittin complex [65] for which the holo-CaM changes from an open dumbbell shape to a closed globular shape with both domains interacting with the peptide. The conformational change induced by mastoparan binding may cause the small peptide to be surrounded by the two domains of CaM, whereas this full interaction may not be possible for the longer peptide melittin. These two examples show the opportunity for PLIMSTEX to suggest conformational changes associated with protein–ligand binding.

Owing to the high sensitivity of mass spectrometers and the chromatographic concentrating procedure in our protocol, we are able to measure a wide range of protein concentrations in PLIMSTEX by simply adjusting the injection for MS analysis. Small quantities (high picomolar) and low concentration (nanomolar) of proteins are sufficient for mass measurement for each point in a titration. To determine the binding affinity between the holo-CaM and melittin, we had to lower the protein concentration from 15.0  $\mu\text{M}$  to 0.15  $\mu\text{M}$  and redo the titration. The resulting  $K$  and  $\Delta D_1$  for holo-CaM are  $(5.4 \pm 0.9) \times 10^7 \text{ M}^{-1}$  and  $29.3 \pm 0.3$  (Table 11.1), respectively, indicating a strong interaction occurs in the binding of melittin and holo-CaM accompanied by protection of  $\sim 29$  backbone amide hydrogens. Although there is a wide range of binding constants  $[(0.93\text{--}33.0) \times 10^7 \text{ M}^{-1}]$  in the literature [58, 59], the latter constant, which is commonly cited, was determined by using an affinity column to separate free [ $^3\text{H}$ ] mono-acetyl-melittin from CaM-bound melittin and quantify it by liquid scintillation counting [58]. If the high affinity were correct, then the most appropriate protein concentration for the titration would not be 150 nM, but 3 nM, a concentration that challenges current MS.

### 11.3.6

#### Self-association of Insulin: A Protein–Protein Interaction

Protein–protein interactions mediate the majority of life processes. An understanding of these interactions is critical to understanding cell regulation [66] and to preventing human disease that can arise from errors in protein–protein interactions [67]. A clear understanding of these interactions points the way to developing new targets and discovering new drugs [68]. Insulin, a protein with 51 residues in two chains [69], is a good model system for testing whether a PLIMSTEX-like approach can determine protein self association. Oligomerization of insulin also has implications in the treatment of type I diabetes. The large size of the hexamer, which contains two  $\text{Zn}^{2+}$ , of insulin prevents its efficient absorption into the blood stream [70], whereas aggregation is prevented by using analogs of insulins that are stable in monomeric form [71]. PLIMSTEX can be used to study the self-association properties of various insulins [33] and may be a promising method for investigating protein–protein interactions.

#### 11.3.6.1 Modified Version of PLIMSTEX for Insulin Self-association

To obtain data similar to that from PLIMSTEX, the concentration of insulin in solution is varied and amide exchange is initiated, followed by quenching the exchange, and injecting the ice-cold solution into the ESI source of a mass spectrometer. After the quench, the oligomers dissociate into monomers, but the increase in mass of the monomer (compared to the control) gives a weighted average of the increase in mass of the various oligomers. These data can be used to obtain a species-specific deuterium number for each oligomer and to calculate the association constants for the oligomerization. For fitting the insulin self-association

data, the modeling is modified to acknowledge that both ligand and protein are the same [33].

The insulin amide exchange during the self-association shows that the number of exchangeable hydrogens decreases with increasing concentration of insulin, demonstrating that, as the self-association occurs, fewer amide hydrogens undergo exchange. The  $\Delta D$  values in the case of insulin represent changes in the solvent accessibility of the oligomer compared to that of the monomer. Assuming a monomer  $\rightleftharpoons$  dimer  $\rightleftharpoons$  hexamer model gives a good fit for the data. At convergence, the dimerization constant,  $K_{12}$ , is  $7 \times 10^5 \text{ M}^{-1}$  and the hexamerization constant,  $K_{26}$  (from dimer to hexamer), is  $2 \times 10^9 \text{ M}^{-1}$ , and these agree with the literature values ( $1.4 \times 10^5 \text{ M}^{-1}$  and  $4 \times 10^8 \text{ M}^{-1}$ ) [72] within a factor of 5. The corresponding  $\Delta D_{12}$  and  $\Delta D_{26}$  are 14 and 23, respectively (Table 11.1), quantifying the number of amide hydrogens in the dimer and hexamer (with respect to monomer) that lose solvent accessibility in the self-associations.

A similar approach is fruitful for investigating insulin mutants that may be under consideration as replacements for wild-type insulin in human therapy. For lispro insulin (in which positions P28 and K29 in human insulin are reversed), and for several other insulin mutants, PLIMSTEX clearly can distinguish the self-association properties and binding constants of lispro and r-human insulins [33].

## 11.4

### Features of PLIMSTEX

#### 11.4.1

##### Determines $K_i$ , Stoichiometry, and Protection ( $\Delta D_i$ )

PLIMSTEX can determine the association constant  $K_i$ , stoichiometry, and protection ( $\Delta D_i$ ) in protein–ligand interaction. It is a general mass spectrometry-based method that is applicable to a wide range of protein–ligand binding, including binding of metal ions, small organic molecules, peptides, and proteins. Combined with kinetic measurements of H/D exchange, PLIMSTEX also provides insights on protein structure and its changes with ligand interactions.

#### 11.4.2

##### Requires Low Quantities of Protein

NMR, X-ray crystallography, and calorimetry-based approaches typically require millimolar concentrations and milliliter volumes, hindering their use for proteins that are available only in low quantities and/or are difficult to purify. Furthermore, measuring affinity may require a concentration regime that is too low for determining the free energy of binding [51]. Spectroscopy-based approaches such as fluorescence or circular dichroism generally require less sample, but when the

binding is weak, these methods also require more sample [73]. Owing to the high sensitivity of mass spectrometers and the chromatographic desalting and concentrating procedure in the protocol, PLIMSTEX is applicable to a wide range of protein concentrations by simply adjusting the amount of solution injected into the mass spectrometer. Small quantities (high picomole) and low concentration (nanomolar) of proteins are sufficient to obtain each point in a titration or kinetic run. Other direct or indirect MS methods (e.g. SUPREX [74]) also need only small amounts of protein.

#### 11.4.3

##### **Relies Only on MS to Measure $m/z$ And Not Solution Concentration**

One asset of mass spectrometry in protein science is that ESI and MALDI [11, 75] can introduce noncovalent complexes to the gas phase [12, 76, 77]. If one can assume that the gas-phase ion abundances (peak intensities) for the complex, apo protein, and ligand are directly related to their equilibrium concentrations in solution, the relative and absolute binding affinities can be deduced [78–81]. Extended methods are now available that also make use of the intensity of the complex and the protein at high ligand concentration to determine binding constants [78, 82–84].

Unfortunately, ESI is discriminatory and peak intensities especially when measuring a system at equilibrium may not be reliable [85, 86]. Electrostatic forces in complexes are strengthened in the solvent-less environment of the mass spectrometer, making electrostatically bound protein–ligand complexes more stable in the gas phase than in solution. Binding that is largely governed by hydrophobic interactions in solution, however, weakens in the vacuum of a mass spectrometer, and complexes bound by hydrophobic forces break apart to an unpredictable extent, leading to incorrect affinities [76, 87, 88]. One may correct for fragmentation of a noncovalent complex in the gas phase by using response factors that relate the mass spectrometer signal to the concentration of the complex in solution and ultimately give the correct stability of the complex. A recently announced method [89] cleverly uses only the signal intensity of the complex and follows it in a titration, much the same way as PLIMSTEX takes only the changing mass of the protein during a titration. Modeling the changing intensity as a function of added ligand gives the response. Although use of response factors may avoid some of the problems of direct measurements, the ionization process must still bring detectable amounts of protein–ligand complex into gas phase, and this remains problematic for weakly bound systems. Furthermore, for systems having a small  $K_a$ , the titration must be performed at high concentration of ligand and protein, regions where the response of ESI may be nonlinear [90–94].

An additional problem for all direct methods is that they cannot use high ionic strength and nonvolatile buffers, which are needed to simulate physiological conditions, because ESI does not work under these conditions. Thus, nonspecific adducts may be produced, confusing the stoichiometry and affinity determinations.

Furthermore, if the affinity is to be measured in water, then ESI must be done with solutions that have high contents of water, which is difficult or impossible. Another problem is that different source configurations (e.g. normal vs nano ESI), desolvation conditions, and instruments may give different results in affinity determinations [95].

PLIMSTEX avoids these problems by following changes in H/D exchange by using the mass shifts accompanying exchange; the signal intensities for the complex are not required. As such, it takes advantage of the increasing ability of mass spectrometers to measure accurately  $m/z$ , a measurement that is not compromised by the discrimination in measuring signal intensities by ESI. The basis for PLIMSTEX is reactivity, similar to footprinting [96], but there is a strong analogy to titration monitoring by spectroscopic methods (e.g. absorbance or fluorescence). SUPREX, another method for measuring the free energies of binding from H/D exchange rates during unfolding (for some examples, see [20, 97]), also takes a single parameter from the mass spectrum (i.e. the  $m/z$ ) and avoids the complications of relying on ESI signal intensities.

#### 11.4.4

##### **Works in Biologically Relevant Media at High Ionic Strength**

The cleanup (desalting) and concentrating procedures allow one to use various proteins, buffer systems, salts, and pH in the exchange protocol and make PLIMSTEX able to measure protein–ligand binding in biologically relevant media at high ionic strength, which is not possible for direct ESI measurements. Moreover, desalting permits the high sensitivity in the mass measurements to be achieved by reducing interference from the ligand, buffer, and salt after quenching and desalting. The high resolving power arises because the desalting eschews formation of metal-ion adducts that disperse ionization. Furthermore, a high D/H in the forward exchange and a high H/D ratio in the back exchange afford a narrow isotope distribution. Desalting on the guard column and eluting into the mass spectrometer can be typically done in 1 min, minimizing back exchange.

#### 11.4.5

##### **Does Not Need Specially Labeled Protein or Ligand**

Many conventional methods, particularly NMR, require that the protein be specially labeled so that it can generate the signals that are a measure of concentration. Radio-labeled materials are essential when scintillation counting is used. For protein–ligand systems that do not contain chromophores or fluorophores, additional labels must be inserted into the molecules. Some affinity studies need special chemical reaction probes, and these probes may be expensive or difficult to obtain, thus hindering their application to a wide range of protein–ligand systems. PLIMSTEX, like other MS-based methods, relies on the hydrogen/



deuterium exchange of amide hydrogens that are present in all protein systems; therefore, no special labeling is necessary.

#### 11.4.6

##### **Avoids Perturbation of the Binding Equilibrium**

The use of D<sub>2</sub>O as an exchange reagent produces the least perturbation of any chemical method. No additional reagents are needed. No physical separations of the free ligand or protein from the protein–ligand binding system are required as in affinity chromatography, size exclusion chromatography, and ultra-filtration. Certain methods that track stability of protein–ligand interactions (e.g. circular dichroism and other spectroscopy methods [98–100] as well as SUPREX [20, 101]) require denaturants, and they may perturb the original binding equilibrium. ESI- or MALDI-based methods that attempt to measure directly the solution concentrations may also perturb the equilibrium during the ionization process, causing inaccuracies in the determination [76, 87, 88].

#### 11.4.7

##### **Has Potential for Peptide Resolution**

PLIMSTEX assays give H/D exchange profiles that provide a global view of the intact protein. One of the advantages of using MS to measure exchange is that the information can be extended to the peptide and even the amino-acid level by enzyme digestion and/or by MS/MS analysis [102–107]. Once the binding affinity and protection in the intact protein are determined by PLIMSTEX, the resolution of the information can be increased by digesting the protein with pepsin after the exchange is quenched (pepsin works at the low pH of the quench). The resulting peptides can be analyzed by MALDI-MS, or LC/ESI-MS and MS/MS. We compared different approaches for pepsin digestion [53] of IFABP, CaM, and ras protein. The online digestion on a custom-built immobilized pepsin column [53, 108] followed by LC-MS and MS/MS may give the best sequence coverage and experimental control. Compared to a solution approach, there is less pepsin interference in the mass spectrum, more complete digestion, more reproducible cleavage sites, and less digestion time (leading to less back exchange). We applied this online digestion to ligand binding of IFABP [53].

#### 11.4.8

##### **Current Challenges and Future Directions**

Present successes in PLIMSTEX rely on a measurable deuterium shift upon ligand binding accompanying a conformational change or detectable shielding induced by ligand binding region. PLIMSTEX procedures may be extended to proteins that do not significantly change conformation during ligand binding by using competition with a known protein that can serve as an indicator or by em-

ploying a pulsed-labeling strategy to shorten exchange times and allow focus on the fast exchanging amide hydrogens that may be affected by ligand binding but do not show difference in longer H/D exchange time that are currently used.

Metal ions, small organic molecules, peptides and small proteins are the ligands tested thus far. PLIMSTEX should be applicable to other ligands including nucleic acids and other proteins. PLIMSTEX should have utility for measuring affinities of proteins in complexes as well as alone, and if this works, it may be one of the few techniques that can probe interaction of a ligand with one protein that is interacting with others.

The current modeling procedure is implemented using Mathcad, which may not be efficient for more complicated protein–ligand binding systems than tested thus far. Other programs (e.g. C or C++) should increase the calculation speed and be more user-friendly. A kinetics factor may be built into the model to accommodate different exchange times used for the titration and to assist the evaluation of a best time-to-quench for a titration study. An example of a more complex system is the binding of two different ligands to one protein or two proteins competing for a single ligand.

A key future direction is expanding PLIMSTEX to provide a higher resolved view than the global view of the whole protein that is currently obtained. Digestion with pepsin followed by peptide analysis by MS and MS/MS should allow kinetics and titrations to be measured for portions of a protein, giving PLIMSTEX a view of the protein that currently emerges from NMR and X-ray methods.

Automation of sample handling and the LC/MS process may give PLIMSTEX a higher throughput character and make it useful for screening the binding of small libraries of drug candidates to target proteins.

## 11.5

### Fast Radical Footprinting for Protein–Ligand Interaction Analysis

Another approach, fast radical footprinting, uses reactions of a radical (e.g.  $\cdot\text{OH}$ ) with amino acid side-chains. It is complementary to PLIMSTEX because it exploits side-chain reactivity instead of exchange of backbone amides. It can be readily expanded to locating the amino acid residue that has reacted, because it introduces an irreversible modification (stable covalent bond) to the protein and can utilize any protease to locate reaction sites, taking advantage of *in silico* prediction of cleavage sites. Whereas PLIMSTEX must use pepsin to cleave the analyte under quenching conditions and necessitates rapid LC runs to minimize back exchange, any proteomic method can be used when probing protein interfaces that are determined by chemical reactions that make an irreversible change to the protein. A chemical reaction method such as hydroxyl radical footprinting probes specific functions (e.g. hydrophobic and sulfur-containing amino acid side-chains) whereas H/D exchange probes the exchange rate of every backbone amide hydrogen in the protein.

## 11.5.1

**Rationale for Hydroxyl Radicals as a Probe**

The hydroxyl radical is a small, highly reactive probe that is formed in water and primarily targets hydrophobic residues [109]. This may be an ideal probe for protein–protein interactions because tyrosine, tryptophan and phenylalanine are most likely to be found at an interface [110, 111]. Although protein–DNA interfaces are comprised of charged and hydrogen-bond donor side-chains, even these residues may be probed by hydroxyl radicals [112].

The hydroxyl radical reacts at nearly a diffusion limited rate ( $k \sim 1 \times 10^{10} \text{ M}^{-1} \text{ s}^{-1}$  to  $5 \times 10^9 \text{ M}^{-1} \text{ s}^{-1}$ ) with the aromatic amino acids, as well as with methionine, and cysteine [113]. Most other side chains are 10–100 times less reactive, making the hydroxyl radical specific for residues that are typically located at protein–protein interfaces yet sufficiently reactive to give a “snapshot” view of the protein. Hydroxyl radicals have been successfully used to study protein–DNA and protein–metal interactions [114–116].

## 11.5.2

**Methods for Generating Hydroxyl Radicals**

Hydroxyl radicals can be generated chemically by using the Fenton reagent [117]:  $\text{Fe}^{2+}$  reduces  $\text{H}_2\text{O}_2$  to hydroxide and hydroxyl radical, but this process is slow. The radicals can also be generated by radiation: for example, synchrotron radiation cleaves water into a proton, electron and a hydroxyl radical [118], whereas UV light homolytically cleaves  $\text{H}_2\text{O}_2$  into two hydroxyl radicals [119, 120]. As these methods require tens of milliseconds to minutes [121], we utilized a UV laser, which should have advantages for the fast photolysis of hydrogen peroxide into hydroxyl radicals [30]. No significant oxidation should occur prior to the laser pulse (traces of prior oxidation can easily be confirmed by performing a simple peroxide-plus-protein control; Fig. 11.8A). We expect the laser-produced hydroxyl radicals to react with the protein side-chains or recombine to reform  $\text{H}_2\text{O}_2$ . Owing to these two pathways, the radical concentration drops to below  $1 \mu\text{M}$  within approximately  $100 \mu\text{s}$  as determined by kinetic calculations using the known rate constant for hydroxyl–radical recombination [122]. The protein oxidation profile that is achieved in that timeframe shows considerable protein oxidation (note the peaks separated by  $16 \text{ Da}$  in Fig. 11.8B).

By adding excess chemical quencher to the system prior to irradiation, the radicals should react with the quencher according to first order kinetics. If  $20 \text{ mM}$  phenylalanine were added to the system, the radicals would be consumed within  $70 \text{ ns}$  of the laser pulse, and the use of  $20 \text{ mM}$  glutamine results in complete reaction of all radicals within  $1 \mu\text{s}$  of the laser pulse (Fig. 11.8C). Given that protein secondary structure packing does not unfold faster than  $10 \mu\text{s}$ , for even the fastest systems studied thus far [30, 123–125], a  $1\text{-}\mu\text{s}$  reaction timescale eliminates nearly all concerns about protein unfolding as a result of oxidation. The other way of mitigating this concern is to conduct the footprinting under “single hit”

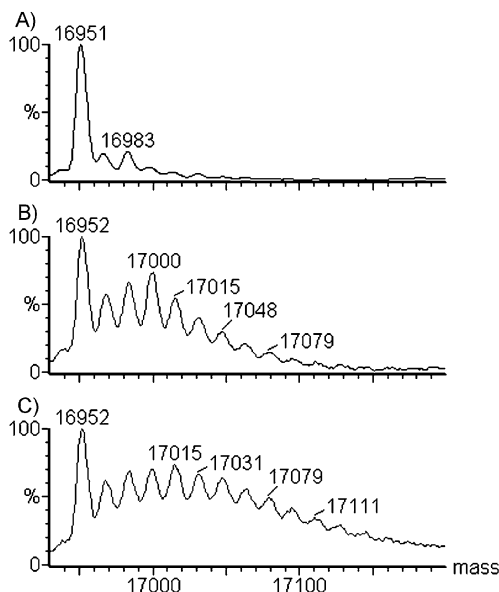


**Fig. 11.8** (A) Laser irradiation of 10  $\mu\text{M}$  apomyoglobin in 10 mM  $\text{NaH}_2\text{PO}_4$ , pH 7.8, and 20 mM phenylalanine as a scavenger. (B) Oxidation of 10  $\mu\text{M}$  apomyoglobin in 10 mM  $\text{NaH}_2\text{PO}_4$ , pH 7.8, 15 mM  $\text{H}_2\text{O}_2$ , and 20 mM glutamine as a scavenger, limiting the reaction to 1  $\mu\text{s}$ . (C) Oxidation of 10  $\mu\text{M}$  apomyoglobin in 10 mM  $\text{NaH}_2\text{PO}_4$ , pH 7.8, 15 mM  $\text{H}_2\text{O}_2$  with no scavenger, resulting in up to 100  $\mu\text{s}$  reaction duration.

conditions, where each protein molecule reacts only once with the radical. “Single hit” conditions, whereby each protein contains only one oxidation site, are difficult to achieve while still affording good coverage and sensitivity, however, and concerns linger when any method deviates from being fast and/or “single hit” [126].

### 11.5.3

#### Fast Photochemical Oxidation of Proteins

To ensure that there is sufficient sample of protein to be oxidized and then analyzed, we employed a flow system instead of firing a single laser shot into a small volume of protein [30]. In this fast photochemical oxidation of proteins (FPOP) setup, the protein, which is mixed with 15 mM  $\text{H}_2\text{O}_2$ , is passed through fused silica tubing, irradiated at a certain point, and collected. The laser pulse is introduced into a region of the tubing where the polyimide coating is removed to afford a UV transparent window. To ensure that no fraction of irradiated protein is oxidized a second time (receives a second pulse of light), the laser frequency can be carefully matched to the solvent flow rate and tubing diameter. Furthermore,

by designing the flow so that ~20% of the protein solution is not irradiated, one is confident that all oxidations are from the first pulse of light, leaving unreacted protein to serve as a reference point. This FPOP approach should allow one to capture a fast “snapshot” of the protein in solution. To observe the oxidations (Fig. 11.8) on the protein, one can load approximately 5 pmol (80 ng) of protein onto a small trap column and desalt the protein with water. The mixture of oxidized and unoxidized protein is then eluted into a mass spectrometer (e.g. QTOF), enabling analysis of the unmodified and modified protein as shown in Fig. 11.8.

#### 11.5.4

##### **Locating the Sites of Oxidation**

To determine the location of a protein–ligand interface, for example, it is necessary to probe separately the solvent-exposed side-chains of the protein alone and of the protein–ligand complex. Side-chains that are modified in the protein alone, and not in the complex, indicate areas of decreased solvent accessibility due to ligand binding. After the protein is modified, standard proteomic analytical methods can be applied to pinpoint the oxidized amino acids by comparing the product-ion spectra of the unmodified peptides with those of oxidized peptides. Most oxidations can be located by searching for peptides whose  $m/z$  values are +16, +32, +48, –22 or +5 Da compared to those of the parent ion. These mass shifts correspond to addition of one, two or three oxygens to any residue, except for histidine, which undergoes other side-reactions to afford mainly +5 and –22 end-products.

#### 11.5.5

##### **Application of FPOP to Apomyoglobin**

We tested FPOP by applying it to apomyoglobin [30], a protein that is well characterized in the holo form [127] and is often used as a model in the field of protein folding [128–130]. Radical footprinting by FPOP in the presence of 20 mM phenylalanine, a concentration that is 2000 times greater than that of the protein, should be complete in ~70 ns [30]. Indeed, virtually no protein oxidation occurs with this high concentration of scavenger (Fig. 11.8A). In the presence of 20 mM glutamine, a less reactive scavenger, the reaction duration lengthens from 70 ns to 1  $\mu$ s, and oxidation occurs (Fig. 11.8B). In the absence of scavenger, the reaction duration lengthens to >100  $\mu$ s, and now considerable oxidation occurs (Fig. 11.8C). These trends suggest that the kinetics of oxidation can be followed, at least roughly, by varying the nature and concentration of the scavenger.

The next step is to digest the protein and analyze the peptides for sites of oxidation. If the reactions indeed modify residues at the surface of the protein, one should find a correlation between reactive sites and those that are predicted to

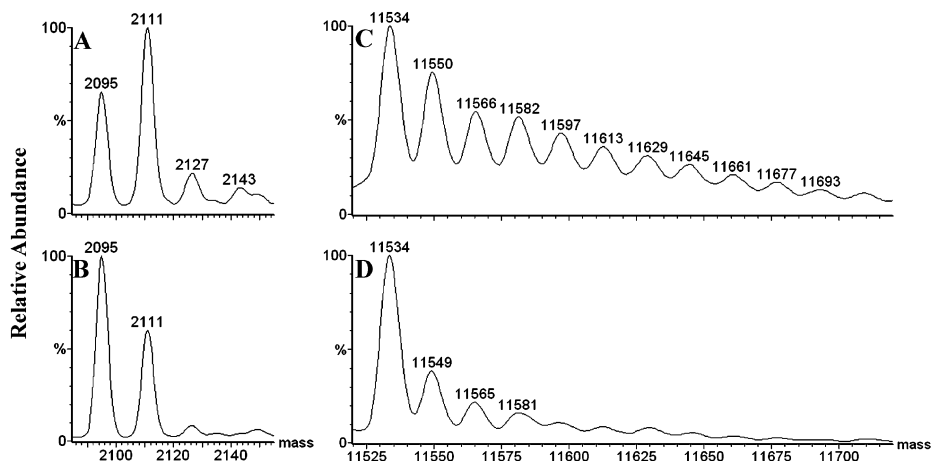


**Fig. 11.9** Deconvolved mass spectra [deconvolution by a maximum entropy algorithm (MaxEnt) supplied by instrument manufacturer] for S-peptide and S-protein, showing differences upon oxidation with 15 mM  $\text{H}_2\text{O}_2$  using 15 mM Gln as scavenger.

(A) S-peptide oxidized in absence of protein. (B) S-peptide oxidized while bound to RNase S protein, showing less oxidation. (C) RNase S protein oxidized in absence of peptide. (D) RNase S-protein oxidized while bound to S-peptide.

have significant solvent exposure. To test the hypothesis, one can calculate side-chain solvent accessibility using the X-ray structure and a 1.1-Å probe in the program GetArea 1.1, available on the web [131]. For apomyoglobin, the only protein tested thus far, the correlations are good [30].

The ability to measure the change in oxidation as a protein is titrated with its ligand may, like for PLIMSTEX, enable the characterization of the binding affinity. We know, for example, that hydroxyl radicals are suitable reagents for following the denaturation-induced unfolding of apomyoglobin [132]. Although fast radical footprinting has not yet been extended to affinity measurements, Fig. 11.9 shows one example where we can see large changes in the extent of oxidation of a peptide and protein when the protein is unligated and when it is interacting with the ligand (peptide). For S-peptide, Fig. 11.9A shows the extent of oxidation for the peptide in the absence of its binding partner, RNase S protein. In Fig. 11.9B, we see that the extent of oxidation of the peptide is attenuated because the peptide is now complexed with the S-protein. Similar changes are observed when the order of addition is reversed; that is, when S-protein is in solution in the absence of S-peptide, there is considerably more oxidation of the protein (Fig. 11.9C) than when the peptide is added to form the complex (Fig. 11.9D). Following the extent of oxidation as the protein is titrated with the peptide may afford the binding affinity of the complex, S-peptide/S-protein, as well as simultaneously reveal the residues involved in complex formation.

## 11.5.6

**Advantages of FPOP**

One of the major advantages of using an irreversible reagent to probe protein interactions is that the sites of reaction can be readily determined by standard proteomic procedures. When the method is fully developed, one may be able to determine the  $K_d$ , binding stoichiometry, and the residues involved in ligand binding. As with PLIMSTEX, the hydroxyl radical method measures a change in the  $m/z$  and, therefore, is not susceptible to variations in ESI efficiency. With the ability to use any enzyme for digestion of the protein, FPOP can be used under any solution conditions including high salt, with denaturants and at low concentrations (we successfully applied this method to 100 nM protein). Current technology permits minute sample amounts to be used. In our experiments, approximately 50 pmol (800 ng) of apomyoglobin is loaded onto a protein trap. The sequencing stage requires only a few picomoles; thus, these experiments can be carried out on less than 80 ng of protein, a quantity that is less than the amount that can be observed on an SDS-PAGE gel using Coomassie staining. Given that analytical proteomic methods are being utilized, this method can be carried out in heterogeneous solutions, although multiple proteins in solution would complicate data analysis. Additionally, no specially labeled proteins are required, and this method, like PLIMSTEX, enables significant information to be gleaned from wild-type proteins; that is, no mutants are needed. Finally, although PLIMSTEX and other H/D exchange methods certainly have no significant effect on the equilibrium of the system, this method has not yet undergone significant testing to confirm the same property. FPOP, however, when properly carried out with suitable chemical scavengers in solution, should produce oxidized proteins that are modified before the protein complex can change conformation owing to the changes caused by modifying the protein or its substrate.

Finally, it is likely that this method can be adapted for high throughput drug screening studies. This may be particularly relevant for systems where activity assays cannot be readily developed. Conceptually, the protein complex would be mixed with a compound designed to disrupt the interface, irradiated, and digested online with trypsin or other proteases. The resulting peptides would be collected on column and eluted with a fast gradient into the mass spectrometer. Having previously mapped the interface, one can predict those oxidations that indicate a disrupted interface and set up the instrument to monitor selected ions. When observed, data-dependent fragmentation would confirm that a particular residue was modified, confirming that the test compound disrupted the protein interaction.

Additional developmental milestones for FPOP include the demonstration of  $K_d$  determination and development of dose-dependent radical foot printing by using different scavengers and concentrations to vary and then quantify the loss of unmodified peptide signal and the increase of modified peptide. Further advances can be made by determining with certainty the reaction timescale. At the

present time, our calculations are worst case scenarios, so the reaction with 20 mM glutamine may be complete significantly before 1  $\mu$ s. Direct analysis of the reaction timescale may be performed using a tandem laser setup that records in time the signal of a probe molecule sensitive to hydroxyl radical attack, or by following the formation and reaction of various aromatic amino acid residues on the protein for a direct reading of the longest possible reaction duration. Finally, with significant resources now being directed towards locating inhibitors by using novel methodologies, FPOP may soon be used to identify new drugs and targets.

## 11.6

### Potential Applications in Drug Discovery

With the introduction of combinatorial chemistry, many high throughput screening technologies are being developed for discovering drugs, for screening the affinities of these many drug candidates with target proteins, and for determining protein–protein binding interactions. Associated analytical measurements include NMR, X-ray crystallography, mass spectrometry, chemical microarrays [133, 134] and protein microarrays [135, 136]. An automated approach for the analysis of protein structure by H/D exchange and MS was reported recently [137] (see also Chapter 12). A more recent publication utilizes a fully automated system to differentiate partial and full agonists of the ligand binding domain of the nuclear receptor PPAR $\gamma$  [138]. Other relatively new mass spectrometry-based methods are SUPREX [80, 139], frontal affinity chromatography with MS (FAC-MS) [19] (see also Chapter 6), MS-based diffusion measurements [18], “SpeedScreen” by size exclusion chromatography (SEC) and LC-MS [21], affinity capillary electrophoresis MS (ACE-MS) [140], and pulsed ultrafiltration–mass spectrometry (PUF-MS) [17] (see Chapter 4), and they have the potential for high throughput. High throughput is achieved by using automated sample preparation with robot systems and parallel LC/MS with autosampling and online desalting. These may be adapted for PLIMSTEX and FPOP.

Although PLIMSTEX and FPOP were originally developed using LC/ESI-MS, it does not eliminate the possibility of using MALDI for the protein–ligand titration. A different desalting procedure is needed, and the conditions for quench (PLIMSTEX) and analysis would be controlled differently than when using LC/ESI-MS. If successful, automated procedures for MALDI-MS could also be immediately adopted for PLIMSTEX and FPOP. Nevertheless, we are not recommending these approaches for *fast* screening of libraries containing thousands or millions of compounds as there are simpler assay methods available, including direct MS measurements of complexes. In the subsequent lead optimization phase of drug development, a cluster of related compounds may be selected. Their subtly different activities need to be quantified or defined more accurately, which may be a role for PLIMSTEX and FPOP.



## Acknowledgements

The research at Washington University was supported by the National Center for Research Resources of the National Institutes of Health, Grant P41RR00954, and by a supplemental grant from that resource. We acknowledge Don Rempel for his help in the development of modeling procedures for PLIMSTEX and we thank Dr. Zhaohui Du and Dr. Raghu Chitta for some of the kinetics and titrations. We acknowledge Ilan Vidavsky, Jim Walters, and Henry Rohrs for assistance with data collection and analysis involving fast radical footprinting development. We acknowledge donations of protein from collaborators Dr. B. Pramanik (Schering–Plough Research Institute), Prof. D. Cistola (Washington University) and Prof. M. Shea (University of Iowa).

## References

- 1 Böhm, H.-J.; Schneider, G.: *Protein–Ligand Interactions From Molecular Recognition to Drug Design*, Wiley–VCH, Weinheim, **2003**, 242 pp.
- 2 Klebe, G.; Bohm, M.; Dullweber, F.; Gradler, U.; Gohlke, H.; Hendlich, M.: Structural and energetic aspects of protein–ligand binding in drug design, in *Molecular Modeling and Prediction of Bioactivity* (Proceedings of the European Symposium on Quantitative Structure–Activity Relationships), Copenhagen, **1998**, 103–110.
- 3 Jackson, R.C.: Update on computer-aided drug design. *Curr. Opin. Biotechnol.* **1995**, 6, 646–651.
- 4 Geoghegan, K.F.; Kelly, M.A.: Biochemical applications of mass spectrometry in pharmaceutical drug discovery. *Mass Spectrom. Rev.* **2005**, 24, 347–366.
- 5 Gohlke, H.; Klebe, G.: Approaches to the description and prediction of the binding affinity of small-molecule ligands to macromolecular receptors. *Angew. Chem. Int. Ed.* **2002**, 41, 2644–2676.
- 6 Baker, B.M.; Murphy, K.P.: Prediction of binding energetics from structure using empirical parameterization. *Methods Enzymol.* **1998**, 295, 294–315.
- 7 Raffa, R.B.: Experimental approaches to determine the thermodynamics of protein–ligand interactions, in: *Methods and Principles in Medicinal Chemistry* vol. 19 (Protein–Ligand Interactions), ed. Böhm, H.-J.; Schneider, G., Wiley–VCH, Weinheim, **2003**, 51–71.
- 8 Wintor, D.J.; Sawyer, W.H.: *Quantitative Characterization of Ligand Binding*. John Wiley & Sons, New York, **1995**, 176 pp.
- 9 Sebillé, B.: Methods of drug protein binding determinations. *Fund. Clin. Pharmacol.* **1990**, 4[Suppl. 2], 151s–161s.
- 10 Cantor, C.R.; Schimmel, P.R.: Techniques for the study of biological structure and function, in *Biophysical Chemistry, Part 2*, W. H. Freeman, San Francisco, **1980**, 344–846.
- 11 Yates, J.R. III: Mass spectrometry and the age of the proteome. *J. Mass Spectrom.* **1998**, 33, 1–19.
- 12 Loo, J.A.: Studying noncovalent protein complexes by electrospray ionization mass spectrometry. *Mass Spectrom. Rev.* **1997**, 16, 1–23.
- 13 Kaltashov, I.A.; Eyles, S.J.: Studies of biomolecular conformations and conformational dynamics by mass spectrometry. *Mass Spectrom. Rev.* **2002**, 21, 37–71.
- 14 Engen, J.R.; Smith, D.L.: Investigating protein structure and dynamics by hydrogen exchange MS. *Anal. Chem.* **2001**, 73, 256A–265A.

- 15 Schermann, S.M.; Simmons, D.A.; Konermann, L.: Mass spectrometry-based approaches to protein ligand interactions. *Expert Rev. Proteomics* **2005**, 2, 475–485.
- 16 Breuker, K.: New mass spectrometric methods for the quantification of protein–ligand binding in solution. *Angew. Chem. Int. Ed.* **2004**, 43, 22–25.
- 17 Johnson, B.M.; Nikolic, D.; van Breemen, R.B.: Applications of pulsed ultrafiltration–mass spectrometry. *Mass Spectrom. Rev.* **2002**, 21, 76–86.
- 18 Clark, S.M.; Konermann, L.: Screening for noncovalent ligand–receptor interactions by electrospray ionization mass spectrometry-based diffusion measurements. *Anal. Chem.* **2004**, 76, 7077–7083.
- 19 Slon-Usakiewicz, J.J.; Ng, W.; Dai, J.-R.; Pasternak, A.; Redden, P.R.: Frontal affinity chromatography with MS detection (FAC-MS) in drug discovery. *Drug Discov. Today* **2005**, 10, 409–416.
- 20 Powell, K.D.; Ghaemmaghami, S.; Wang, M.Z.; Ma, L.; Oas, T.G.; Fitzgerald, M.C.: A general mass spectrometry-based assay for the quantitation of protein–ligand binding interactions in solution. *J. Am. Chem. Soc.* **2002**, 124, 10256–10257.
- 21 Muckenschnabel, I.; Falchetto, R.; Mayr, L.M.; Filipuzzi, I.: SpeedScreen: label-free liquid chromatography–mass spectrometry-based high-throughput screening for the discovery of orphan protein ligands. *Anal. Biochem.* **2004**, 324, 241–249.
- 22 Zhu, M.M.; Rempel, D.L.; Du, Z.; Gross, M.L.: Quantification of protein–ligand interactions by mass spectrometry, titration, and H/D exchange: PLIMSTEX. *J. Am. Chem. Soc.* **2003**, 125, 5252–5253.
- 23 Zhu, M.M.; Chitta, R.; Gross, M.L.: PLIMSTEX: a novel mass spectrometric method for the quantification of protein–ligand interactions in solution. *Int. J. Mass Spectrom.* **2005**, 240, 213–220.
- 24 Zhu, M.M.; Rempel, D.L.; Gross, M.L.: Modeling data from titration, amide H/D exchange and mass spectrometry to obtain protein–ligand binding constants. *J. Am. Soc. Mass Spectrom.* **2004**, 15, 388–397.
- 25 Zhu, M.M.; Rempel, D.L.; Zhao, J.; Giblin, D.E.; Gross, M.L.: Probing Ca<sup>2+</sup>-induced conformational changes in porcine calmodulin by H/D exchange and ESI-MS: effect of cations and ionic strength. *Biochemistry* **2003**, 42, 15388–15397.
- 26 Zhu, M.M.: (2004) *Determination of Protein–Ligand Interactions Using H/D Exchange and Mass Spectrometry*, PhD dissertation, Washington University, St. Louis, **2004**, 338 pp.
- 27 Guan, J.-Q.; Takamoto, K.; Almo, S.C.; Reisler, E.; Chance, M.R.: Structure and dynamics of the actin filament. *Biochemistry* **2005**, 44, 3166–3175.
- 28 Takamoto, K.; Das, R.; He, Q.; Doniach, S.; Brenowitz, M.; Herschlag, D.; Chance, M.R.: Principles of RNA compaction: insights from the equilibrium folding pathway of the P4-P6 RNA domain in monovalent cations. *J. Mol. Biol.* **2004**, 343, 1195–1206.
- 29 Liu, R.; Guan, J.-Q.; Zak, O.; Aisen, P.; Chance, M.R.: Structural reorganization of the transferrin C-lobe and transferrin receptor upon complex formation: the C-lobe binds to the receptor helical domain. *Biochemistry* **2003**, 42, 12447–12454.
- 30 Hambly, D.M.; Gross, M.L.: Laser flash photolysis of hydrogen peroxide to oxidize protein solvent-accessible residues on the microsecond timescale. *J. Am. Soc. Mass Spectrom.* **2005**, 16, 2057–2063.
- 31 Eliezer, D.; Wright, P.E.: Is apomyoglobin a molten globule? Structural characterization by NMR. *J. Mol. Biol.* **1996**, 263, 531–538.
- 32 Bates, D.M.; Watts, D.G.: *Nonlinear Regression Analysis and its Applications*, Wiley, New York, **1988**.
- 33 Raghu, K. Chitta, R.K.; Rempel, D.L.; Grayson, M.A.; Remsen, E.E.; Gross, M.L.: Application of SIMSTEX to

- oligomerization of insulin analogs and mutants, *J. Am. Soc. Mass Spectrom.* **2006**, 17, 1526–1534.
- 34 Wittinghofer, A.; Pai, E.F.: The structure of Ras protein: a model for a universal molecular switch. *Trends Biochem. Sci.* **1991**, 16, 382–387.
  - 35 Sprang, S.R.; Esch, C.D.: Invasion of the nucleotide snatchers: structural insights into the mechanism of G protein GEFs. *Cell* **1998**, 95, 155–158.
  - 36 Zhang, B.; Zhang, Y.; Wang, Z.; Zheng, Y.: The role of  $Mg^{2+}$  cofactor in the guanine nucleotide exchange and GTP hydrolysis reactions of Rho family GTP-binding proteins. *J. Biol. Chem.* **2000**, 275, 25299–25307.
  - 37 Pai, E.F.; Kabsch, W.; Krenkel, U.; Holmes, K.C.; John, J.; Wittinghofer, A.: Structure of the guanine-nucleotide-binding domain of the Ha-ras oncogene product p21 in the triphosphate conformation. *Nature* **1989**, 341, 209–214.
  - 38 de Vos, A.M.; Tong, L.; Milburn, M.V.; Matias, P.M.; Jancarik, J.; Noguchi, S.; Nishimura, S.; Miura, K.; Ohtsuka, E.; Kim, S.H.: Three-dimensional structure of an oncogene protein: catalytic domain of human c-H-ras p21. *Science* **1988**, 239, 888–893.
  - 39 John, J.; Schlichting, I.; Schiltz, E.; Rosch, P.; Wittinghofer, A.: C-terminal truncation of p21H preserves crucial kinetic and structural properties. *J. Biol. Chem.* **1989**, 264, 13086–13092.
  - 40 Du, Z.; Zhu, M.M.; Rempel, D.; Vidavsky, I.; Gross, L.M.; Pramanik, B.: The binding of  $Mg$  (II) to ras-GDP as determined by H/D exchange and HPLC/MS, in *Proceedings of 49th ASMS Conference on Mass Spectrometry and Allied Topics*, Chicago, **2002**.
  - 41 Zhang, J.; Matthews, C.R.: Ligand binding is the principal determinant of stability for the p21H-ras protein. *Biochemistry* **1998**, 37, 14881–14890.
  - 42 Pramanik, B.N.; Bartner, P.L.; Mirza, U.A.; Liu, Y.H.; Ganguly, A.K.: Electrospray ionization mass spectrometry for the study of non-covalent complexes: an emerging technology. *J. Mass Spectrom.* **1998**, 33, 911–920.
  - 43 Patton, C. *Webmaxc Standard*, available at: <http://www.stanford.edu/~cpatton/webmaxcS.htm>, **2003**.
  - 44 Patton, C.; Thompson, S.; Epel, D.: Some precautions in using chelators to buffer metals in biological solutions. *Cell Calcium* **2004**, 35, 427–431.
  - 45 Weinstein, H.; Mehler, E.:  $Ca^{2+}$ -binding and structural dynamics in the function of calmodulin. *Annu. Rev. Physiol.* **1994**, 56, 213–236.
  - 46 Klee, C.B.: Calmodulin, in *Molecular Aspects of Cellular Regulation*, Vol. 5: *Calmodulin*, ed. Cohen, P.; Klee, C.B., Elsevier, Amsterdam, **1988**, 371 pp.
  - 47 Linse, S.; Helmersson, A.; Forsén, S.: Calcium binding to calmodulin and its globular domains. *J. Biol. Chem.* **1991**, 266, 8050–8054.
  - 48 Haiech, J.; Klee, C.B.; Demaille, J.G.; Haiech, J.: Effects of cations on affinity of calmodulin for calcium: ordered binding of calcium ions allows the specific activation of calmodulin-stimulated enzymes. Theoretical approach to study of multiple ligand binding to a macromolecule. *Biochemistry* **1981**, 20, 3890–3897.
  - 49 Banaszak, L.; Winter, N.; Xu, Z.; Bernlohr, D.A.; Cowan, S.; Jones, T.A.: Lipid-binding proteins: a family of fatty acid and retinoid transport proteins. *Adv. Protein Chem.* **1994**, 45, 89–151.
  - 50 Cistola, D.P.; Kim, K.; Rogl, H.; Frieden, C.: Fatty acid interactions with a helix-less variant of intestinal fatty acid-binding protein. *Biochemistry* **1996**, 35, 7559–7565.
  - 51 Kurian, E.; Kirk, W.R.; Prendergast, F.G.: Affinity of fatty acid for rRat intestinal fatty acid binding protein: further examination. *Biochemistry* **1996**, 35, 3865–3874.
  - 52 Ogbay, B.: *Determinants of Stability and Stoichiometry in Intestinal Fatty Acid Binding Protein*, PhD Dissertation, Washington University, St. Louis, **2003**, 197 pp.

- 53 Zhu, M.M.; Rempel, D.L.; Vidavsky, I.; Gross, M.L.: Ligand binding to IFABP and D34A mutant revealed by H/D exchange, online pepsin digestion, and LC/MS, in *Proceedings of the 52nd ASMS Conference on Mass Spectrometry and Allied Topics*, Nashville, **2004**.
- 54 Zhu, M.; Rempel, D.; Du, Z.; Gross Michael, L.; Ogbay, B.; Cistola, D.P.: The influence of mutation on protein folding and ligand binding of IFABP as monitored by H/D exchange and HPLC/MS, in *Proceedings of 51st Annual Conference on Mass Spectrometry and Allied Topics*, Montréal, **2003**.
- 55 Malencik, D.A.; Anderson, S.R.: Binding of hormones and neuropeptides by calmodulin. *Biochemistry* **1983**, 22, 1995–2001.
- 56 Anderson, S.R.; Malencik, D.A.: Peptides recognizing calmodulin. *Calcium Cell Funct.* **1986**, 6, 1–42.
- 57 Osawa, M.; Swindells, M.B.; Tanikawa, J.; Tanaka, T.; Mase, T.; Furuya, T.; Ikura, M.: Solution structure of calmodulin-W-7 complex: the basis of diversity in molecular recognition. *J. Mol. Biol.* **1998**, 276, 165–176.
- 58 Comte, M.; Maulet, Y.; Cox, J.A.: Ca<sup>2+</sup>-dependent high-affinity complex formation between calmodulin and melittin. *Biochem. J.* **1983**, 209, 269–272.
- 59 Yao, Y.; Squier, T.C.: Variable conformation and dynamics of calmodulin complexed with peptides derived from the autoinhibitory domains of target proteins. *Biochemistry* **1996**, 35, 6815–6827.
- 60 Terwilliger, T.C.; Weissman, L.; Eisenberg, D.: The structure of melittin in the form I crystals and its implication for melittin's lytic and surface activities. *Biophys. J.* **1982**, 37, 353–361.
- 61 Maulet, Y.; Cox, J.A.: Structural changes in melittin and calmodulin upon complex formation and their modulation by calcium. *Biochemistry* **1983**, 22, 5680–5686.
- 62 Cox, J.A.: Interactive properties of calmodulin. *Biochem. J.* **1988**, 249, 621–629.
- 63 Mamar-Bachi, A.; Cox, J.A.: Quantitative analysis of the free energy coupling in the system calmodulin, calcium, smooth muscle myosin light chain kinase. *Cell Calcium* **1987**, 8, 473–482.
- 64 Keller, C.H.; Olwin, B.B.; LaPorte, D.C.; Storm, D.R.: Determination of the free-energy coupling for binding of calcium ion and troponin I to calmodulin. *Biochemistry* **1982**, 21, 156–162.
- 65 Scaloni, A.; Miraglia, N.; Orrù, S.; Amodeo, P.; Motta, A.; Marino, G.; Pucci, P.: Topology of the calmodulin-melittin complex. *J. Mol. Biol.* **1998**, 277, 945–958.
- 66 Scott, J.D.; Pawson, T.: Cell communication: the inside story. *Sci. Am.* **2000**, 282, 72–79.
- 67 Staub, O.; Dho, S.; Henry, P.C.; Correa, J.; Ishikawa, T.; McGlade, J.; Rotin, D.: WW domains of Nedd4 bind to the proline-rich PY motifs in the epithelial Na<sup>+</sup> channel deleted in Liddle's syndrome. *EMBO J.* **1996**, 15, 2371–2380.
- 68 Sidhu, S.S.; Fairbrother, W.J.; Deshayes, K.: Exploring protein–protein interactions with phage display. *ChemBioChem* **2003**, 4, 14–25.
- 69 Adams, M.J.; Blundell, T.L.; Dodson, E.J.; Dodson, G.G.; Vijayan, M.; Baker, E.N.; Harding, M.M.; Hodgkin, D.C.; Rimmer, B.; Sheats, S.: Structure of rhombohedral 2 zinc insulin crystals. *Nature* **1969**, 224, 491–495.
- 70 Brange, J.; Whittingham, J.; Edwards, D.; You-Shang, Z.; Wollmer, A.; Brandenburg, D.; Dodson, G.; Finch, J.: Insulin structure and diabetes treatment. *Curr. Sci.* **1997**, 72, 470–476.
- 71 Brange, J.; Volund, A.: Insulin analogs with improved pharmacokinetic profiles. *Adv. Drug Deliv. Rev.* **1999**, 35, 307–335.
- 72 Pocker, Y.; Biswas, S.B.: Self-association of insulin and the role of hydrophobic bonding: a thermodynamic model of insulin dimerization. *Biochemistry* **1981**, 20, 4354–4361.

- 73 Powell, K.D.; Fitzgerald, M.C.: Measurements of protein stability by H/D exchange and matrix-assisted laser desorption/ionization mass spectrometry using picomoles of material. *Anal. Chem.* **2001**, *73*, 3300–3304.
- 74 Powell, K.D.; Wales, T.E.; Fitzgerald, M.C.: Thermodynamic stability measurements on multimeric proteins using a new H/D exchange- and matrix-assisted laser desorption/ionization (MALDI) mass spectrometry-based method. *Protein Sci.* **2002**, *11*, 841–851.
- 75 Ferguson, P.L.; Smith, R.D.: Proteome analysis by mass spectrometry. *Annu. Rev. Biophys. Biomol. Struct.* **2003**, *32*, 399–424.
- 76 Loo, J.A.: Electrospray ionization mass spectrometry: a technology for studying noncovalent macromolecular complexes. *Int. J. Mass Spectrom.* **2000**, *200*, 175–186.
- 77 Hillenkamp, F.: Matrix-assisted laser desorption/ionization of non-covalent complexes. *NATO ASI Ser. C: Math. Phys. Sci.* **1998**, *510*, 181–191.
- 78 Sannes-Lowery, K.A.; Griffey, R.H.; Hofstadler, S.A.: Measuring dissociation constants of RNA and aminoglycoside antibiotics by electrospray ionization mass spectrometry. *Anal. Biochem.* **2000**, *280*, 264–271.
- 79 Rosu, F.; Gabelica, V.; Houssier, C.; De Pauw, E.: Determination of binding constants of oligonucleotide complexes with minor groove binders by electrospray ionization mass spectrometry. Comparison with fluorescence titration data. *Adv. Mass Spectrom.* **2001**, *15*, 795–796.
- 80 Zhang, S.; Van Pelt, C.K.; Wilson, D.B.: Quantitative determination of noncovalent binding interactions using automated nano-electrospray mass spectrometry. *Anal. Chem.* **2003**, *75*, 3010–3018.
- 81 Bligh, S.W.A.; Haley, T.; Lowe, P.N.: Measurement of dissociation constants of inhibitors binding to Src SH2 domain protein by non-covalent electrospray ionization mass spectrometry. *J. Mol. Recognit.* **2003**, *16*, 139–147.
- 82 Loo, J.A.; Hu, P.; McConnell, P.; Mueller, W.T.: A study of Src SH2 domain protein–phosphopeptide binding interactions by electrospray ionization mass spectrometry. *J. Am. Soc. Mass Spectrom.* **1997**, *8*, 234–243.
- 83 Lim, H.-K.; Hsieh, Y.L.; Ganem, B.; Henion, J.: Recognition of cell-wall peptide ligands by vancomycin group antibiotics: studies using ion spray mass spectrometry. *J. Mass Spectrom.* **1995**, *30*, 708–714.
- 84 Greig, M.J.; Gaus, H.; Cummins, L.L.; Sasmor, H.; Griffey, R.H.: Measurement of macromolecular binding using electrospray mass spectrometry. Determination of dissociation constants for oligonucleotide: serum albumin complexes. *J. Am. Chem. Soc.* **1995**, *117*, 10765–10766.
- 85 Sojo, L.E.; Lum, G.; Chee, P.: Internal standard signal suppression by co-eluting analyte in isotope dilution LC-ESI-MS. *Analyst* **2003**, *128*, 51–54.
- 86 Liang, H.R.; Foltz, R.L.; Meng, M.; Bennett, P.: Ionization enhancement in atmospheric pressure chemical ionization and suppression in electrospray ionization between target drugs and stable-isotope-labeled internal standards in quantitative liquid chromatography/tandem mass spectrometry. *Rapid Commun. Mass Spectrom.* **2003**, *17*, 2815–2821.
- 87 Robinson, C.V.; Chung, E.W.; Kragelund, B.B.; J., K.; Aplin, R.T.; Poulsen, F.M.; Dobson, C.M.: Probing the nature of non-covalent interactions by mass spectrometry: a study of protein–CoA ligand binding and assembly. *J. Am. Chem. Soc.* **1996**, *118*, 8646–8653.
- 88 Wu, Q.; Gao, J.; Joseph-McCarthy, D.; Sigal, G.B.; Bruce, J.E.; Whitesides, G.M.; Smith, R.D.: Carbonic anhydrase–inhibitor binding: from solution to the gas phase. *J. Am. Chem. Soc.* **1997**, *119*, 1157–1158.
- 89 Tjernberg, A.; Carnö, S.; Oliv, F.; Benkestock, K.; Edlund, P.-O.; Griffiths, W.J.; Hallén, D.:

- Determination of dissociation constants for protein–ligand complexes by electrospray ionization mass spectrometry. *Anal. Chem.* **2004**, 76, 4325–4331.
- 90 Tang, L.; Kebarle, P.: Dependence of ion intensity in electrospray mass spectrometry on the concentration of the analytes in the electrosprayed solution. *Anal. Chem.* **1993**, 65, 3654–3668.
  - 91 Zook, D.R.; Bruins, A.P.: On cluster ions, ion transmission, and linear dynamic range limitations in electrospray (ionspray) mass spectrometry. *Int. J. Mass Spectrom.* **1997**, 162, 129–147.
  - 92 Ikononou, M.G.; Blades, A.T.; Kebarle, P.: Investigations of the electrospray interface for liquid chromatography/mass spectrometry. *Anal. Chem.* **1990**, 62, 957–967.
  - 93 Cech, N.B.; Enke, C.G.: Practical implications of some recent studies in electrospray ionization fundamentals. *Mass Spectrom. Rev.* **2002**, 20, 362–387.
  - 94 Bruins, A.P.: ESI source design and dynamic range considerations. *Electrospray Ionization Mass Spectrom.* **1997**, 107–136.
  - 95 Zampronio, C.G.; Giannakopoulos, A.E.; Zeller, M.; Bitziou, E.; Macpherson, J.V.; Derrick, P.J.: Production and properties of nanoelectrospray emitters used in fourier transform ion cyclotron resonance mass spectrometry: implications for determination of association constants for noncovalent complexes. *Anal. Chem.* **2004**, 76, 5172–5179.
  - 96 Shea, M.A.; Sorensen, B.R.; Pedigo, S.; Verhoeven, A.S.: Proteolytic footprinting titrations for estimating ligand-binding constants and detecting pathways of conformational switching of calmodulin. *Methods Enzymol.* **2000**, 323, 254–301.
  - 97 Ma, L.; Fitzgerald, M.C.: A new H/D exchange- and mass spectrometry-based method for thermodynamic analysis of protein–DNA interactions. *Chem. Biol.* **2003**, 10, 1205–1213.
  - 98 McLaughlin, S.H.; Jackson, S.E.: Folding and stability of the ligand-binding domain of the glucocorticoid receptor. *Protein Sci.* **2002**, 11, 1926–1936.
  - 99 van Mierlo, C.P.M.; Steensma, E.: Protein folding and stability investigated by fluorescence, circular dichroism (CD), and nuclear magnetic resonance (NMR) spectroscopy: the flavodoxin story. *J. Biotech.* **2000**, 79, 281–298.
  - 100 Greenfield, N.J.: Circular dichroism analysis for protein–protein interactions. *Methods Mol. Biol.* **2004**, 261, 55–78.
  - 101 Powell, K.D.; Fitzgerald, M.C.: Accuracy and precision of a new H/D exchange- and mass spectrometry-based technique for measuring the thermodynamic properties of protein–peptide complexes. *Biochemistry* **2003**, 42, 4962–4970.
  - 102 Zhang, Z.; Smith, D.L.: Determination of amide hydrogen exchange by mass spectrometry: a new tool for protein structure elucidation. *Protein Sci.* **1993**, 2, 522–531.
  - 103 Smith, D.L.; Dharmasiri, K.: Protein–ligand binding studied by amide hydrogen exchange and mass spectrometry. *NATO ASI Ser. C* **1998**, 510, 45–58.
  - 104 Engen, J.R.; Gmeiner, W.H.; Smithgall, T.E.; Smith, D.L.: Hydrogen exchange shows peptide binding stabilizes motions in Hck SH2. *Biochemistry* **1999**, 38, 8926–8935.
  - 105 Wang, F.; Li, W.; Emmett, M.R.; Marshall, A.G.; Corson, D.; Sykes, B.D.: Fourier transform ion cyclotron resonance mass spectrometric detection of small Ca<sup>2+</sup>-induced conformational changes in the regulatory domain of human cardiac troponin C. *J. Am. Soc. Mass Spectrom.* **1999**, 10, 703–710.
  - 106 Woods, V.L. Jr.; Hamuro, Y.: High resolution, high-throughput amide deuterium exchange-mass spectrometry (DXMS) determination of protein binding site structure and

- dynamics: utility in pharmaceutical design. *Biochemistry* **2001**, 2001[Suppl. 37], 89–98.
- 107 Hamuro, Y.; Wong, L.; Shaffer, J.; Kim, J.S.; Stranz, D.D.; Jennings, P.A.; Woods, V.L. Jr.; Adams, J.A.: Phosphorylation driven motions in the COOH-terminal Src kinase, Csk, revealed through enhanced hydrogen–deuterium exchange and mass spectrometry (DXMS). *J. Mol. Biol.* **2002**, 323, 871–881.
  - 108 Wang, L.; Pan, H.; Smith, D.L.: Hydrogen exchange–mass spectrometry. Optimization of digestion conditions. *Mol. Cell. Proteomics* **2002**, 1, 132–138.
  - 109 Hawkins, C.L.; Davies, M.J.: Generation and propagation of radical reactions on proteins. *Biochim. Biophys. Acta* **2001**, 1504, 196–219.
  - 110 Ma, B.; Elkayam, T.; Wolfson, H.; Nussinov, R.: Protein–protein interactions: structurally conserved residues distinguish between binding sites and exposed protein surfaces. *Proc. Natl Acad. Sci. USA* **2003**, 100, 5772–5777.
  - 111 Bogan, A.A.; Thorn, K.S.: Anatomy of hot spots in protein interfaces. *J. Mol. Biol.* **1998**, 280, 1–9.
  - 112 Xu, G.; Chance, M.R.: Radiolytic modification and reactivity of amino acid residues serving as structural probes for protein footprinting. *Anal. Chem.* **2005**, 77, 4549–4555.
  - 113 M.J. Davies, R.T.D.: *Radical-Mediated Protein Oxidation: from Chemistry to Medicine*, Oxford University Press, Oxford, **1998**, 456 pp.
  - 114 Shcherbakova, I.; Gupta, S.; Chance, M.R.; Brenowitz, M.: Monovalent ion-mediated folding of the *Tetrahymena thermophila* ribozyme. *J. Mol. Biol.* **2004**, 342, 1431–1442.
  - 115 Dhavan, G.M.; Chance, M.R.; Brenowitz, M.: Kinetics analysis of DNA–protein interactions by time-resolved synchrotron X-ray footprinting. *Kinet. Anal. Macromol.* **2003**, 75–86.
  - 116 Kisellar, J.G.; Janmey, P.A.; Almo, S.C.; Chance, M.R.: Visualizing the  $\text{Ca}^{2+}$ -dependent activation of gelsolin by using synchrotron footprinting. *Proc. Natl Acad. Sci. USA* **2003**, 100, 3942–3947.
  - 117 Fenton, J.H.; Jackson, H.: The oxidation of polyhydric alcohols in presence of iron. *J. Chem. Soc. Trans.* **1899**, 75, 1.
  - 118 Guan, J.-Q.; Almo, S.C.; Chance, M.R.: Synchrotron radiolysis and mass spectrometry: a new approach to research on the actin cytoskeleton. *Acc. Chem. Res.* **2004**, 37, 221–229.
  - 119 Urey, H.C.; Dawsey, L.H.; Rice, F.O.: Absorption spectrum and decomposition of hydrogen peroxide by light. *J. Am. Chem. Soc.* **1929**, 51, 1371–1383.
  - 120 Schiffman, A.; Nelson, D.D. Jr.; Nesbitt, D.J.: Quantum yields for hydroxyl production from 193 and 248 nm photolysis of nitric acid and hydrogen peroxide. *J. Chem. Phys.* **1993**, 98, 6935–6946.
  - 121 Sharp, J.S.; Becker, J.M.; Hettich, R.L.: Protein surface mapping by chemical oxidation: structural analysis by mass spectrometry. *Anal. Biochem.* **2003**, 313, 216–225.
  - 122 Buxton, G.V.; Greenstock, C.L.; Helman, W.P.; Ross, A.B.: Critical review of rate constants for reactions of hydrated electrons, hydrogen atoms and hydroxyl radicals ( $\cdot\text{OH}/\cdot\text{O}^-$ ) in aqueous solution. *J. Phys. Chem. Ref. Data* **1988**, 17, 513–886.
  - 123 Vu, D.M.; Myers, J.K.; Oas, T.G.; Dyer, R.B.: Probing the folding and unfolding dynamics of secondary and tertiary structures in a three-helix bundle protein. *Biochemistry* **2004**, 43, 3582–3589.
  - 124 Gilmanshin, R.; Williams, S.; Callender, R.H.; Woodruff, W.H.; Dyer, R.B.: Fast events in protein folding: relaxation dynamics of secondary and tertiary structure in native apomyoglobin. *Proc. Natl Acad. Sci. USA* **1997**, 94, 3709–3713.
  - 125 Gulotta, M.; Gilmanshin, R.; Buscher, T.C.; Callender, R.H.; Dyer, R.B.: Core formation in apomyoglobin: probing the upper reaches of the folding

- energy landscape. *Biochemistry* **2001**, 40, 5137–5143.
- 126 Maleknia, S.D.; Wong, J.W.H.; Downard, K.M.: Photochemical and electrophysical production of radicals on millisecond timescales to probe the structure, dynamics and interactions of proteins. *Photochem. Photobiol. Sci.* **2004**, 3, 741–748.
  - 127 Evans, S.V.; Brayer, G.D.: High-resolution study of the three-dimensional structure of horse heart metmyoglobin. *J. Mol. Biol.* **1990**, 213, 885–897.
  - 128 Nishimura, C.; Dyson, H.J.; Wright, P.E.: Identification of native and non-native structure in kinetic folding intermediates of apomyoglobin. *J. Mol. Biol.* **2006**, 355, 139–156.
  - 129 Nishimura, C.; Lietzow, M.A.; Dyson, H.J.; Wright, P.E.: Sequence determinants of a protein folding pathway. *J. Mol. Biol.* **2005**, 351, 383–392.
  - 130 Dyson, H.J.; Wright, P.E.: Unfolded proteins and protein folding studied by NMR. *Chem. Rev.* **2004**, 104, 3607–3622.
  - 131 Fraczkiewicz, R.; Braun, W.: Exact and efficient analytical calculation of the accessible surface areas and their gradients for macromolecules. *J. Comput. Chem.* **1998**, 19, 319–333.
  - 132 Chance, M.R.; Sclavi, B.; Woodson, S.A.; Brenowitz, M.: Examining the conformational dynamics of macromolecules with time-resolved synchrotron X-ray ‘footprinting’. *Structure* **1997**, 5, 865–869.
  - 133 Lam, K.S.; Renil, M.: From combinatorial chemistry to chemical microarray. *Curr. Opin. Chem. Biol.* **2002**, 6, 353–358.
  - 134 Metz, G.; Otteleben, H.; Vetter, D.: Small molecule screening on chemical microarrays, in *Methods and Principles in Medicinal Chemistry*, Vol. 19: *Protein–Ligand Interactions*, ed. Böhm, H.-J.; Schneider, G., Wiley–VCH, Weinheim, **2003**, pp 213–236.
  - 135 Xu, Q.; Lam, K.S.: Protein and chemical microarrays – powerful tools for proteomics. *J. Biomed. Biotech.* **2003**, 5, 257–266.
  - 136 Kumble, K.D.: Protein microarrays: new tools for pharmaceutical development. *Anal. Bioanal. Chem.* **2003**, 377, 812–819.
  - 137 Hamuro, Y.; Coales, S.J.; Southern, M.R.; Nemeth-Cawley, J.F.; Stranz, D.D.; Rod, G.P.: Rapid analysis of protein structure and dynamics by hydrogen/deuterium exchange mass spectrometry. *J. Biomol. Tech.* **2003**, 14, 171–182.
  - 138 Chalmers, M.J.; Busby, S.A.; Pascal, B.D.; He, Y.; Hendrickson, C.L.; Marshall, A.G.; Griffin, P.R.: Probing protein ligand interactions by automated hydrogen/deuterium exchange mass spectrometry. *Anal. Chem.* **2006**.
  - 139 Powell, K.D.; Fitzgerald, M.C.: High-throughput screening assay for the tunable selection of protein ligands. *J. Combinat. Chem.* **2004**, 6, 262–269.
  - 140 Chu, Y.-H.; Dunayevskiy, Y.M.; Kirby, D.P.; Vouros, P.; Karger, B.L.: Affinity capillary electrophoresis-mass spectrometry for screening combinatorial libraries. *J. Am. Chem. Soc.* **1996**, 118, 7827–7835.





## 12

# Protein-targeting Drug Discovery Guided by Hydrogen/Deuterium Exchange Mass Spectrometry (DXMS)

*Yoshitomo Hamuro, Stephen J. Coales, and Virgil Woods*

### 12.1

#### Introduction

Most pharmaceuticals in clinical use target proteins and the number of potential protein targets has dramatically increased with the availability of the sequences of all human proteins. There is a large gap, bridged only with much investment in effort and time, between the discovery of a protein target for potential therapeutic intervention in a disease and the development of small molecules that can modulate the protein's activity in a clinically useful manner. A protein's high-resolution three-dimensional structure is typically determined by crystallographic means, its binding partners identified (other proteins/metabolites/signaling small molecules), and the precise manner in which these several entities bind to each other and modify each other's activity and conformation characterized. Small-molecule therapeutic candidates must then be produced and iteratively refined for their ability to interfere with or promote these activities.

While the well established protein structure determination methods of X-ray crystallography and nuclear magnetic resonance (NMR) are being pushed to meet the challenge, both technologies have limitations in their applicability and throughput. Crystallization is a major obstacle for X-ray analysis: most eukaryotic proteins are difficult to crystallize without lengthy experimentation, or may be inherently noncrystallizable. NMR has size limitations and sensitivity issues. X-ray crystallography can study a protein only in the solid state and NMR requires that the study protein be at high concentration. Both techniques require that the protein be highly purified.

Enhanced hydrogen/deuterium (H/D) exchange mass spectrometry (DXMS) has emerged as an effective tool free of these limitations, which promises to speed many of the steps from therapeutic target discovery to the development of drugs ready for clinical evaluation. In the early 1990s, Zhang and Smith described a methodology, in which H/D exchange reactions were followed by steps involving proteolysis, HPLC separation, and mass spectrometric (MS) analysis [1]. In this approach, medium-resolution information could be obtained by mea-

asuring the deuterium incorporation within each proteolytically generated peptide fragment. Since then, improvements to their fundamental method have been used to study protein structure/dynamics [1–15], protein–ligand interactions [16–19], and protein–protein interactions [20–29]. Reflecting the increased activity and advances in this field, several comprehensive reviews have been published [4, 30–33].

DXMS can now be used to dramatically improve the crystallizability of proteins for structure determination, characterize the binding interactions between the target protein and its binding partners, and rapidly determine the conformational changes that often accompany such binding events. Most importantly, DXMS has considerable potential to guide the development of clinically useful small-molecule therapeutics that can target protein–protein interaction surfaces – a notoriously difficult task. In this review, the experimental methodologies of enhanced DXMS technology are described, and examples given of its ability to speed the steps of the translational process.

## 12.2

### Theory of H/D Exchange

#### 12.2.1

##### Amide H/D Exchange

The exchange rate of a peptide amide hydrogen reflects its precise and unique environment within the protein's three-dimensional structure, and there is one such hydrogen for each amino acid in the protein, except for proline. A backbone amide hydrogen can exhibit highly variable exchange rates with solvent hydrogen, with rates ranging over eight orders of magnitude in folded proteins [4]. In contrast, amide hydrogen exchange rates in peptides lacking secondary and tertiary structure vary only about 100-fold, depending primarily on neighboring amino acid side-chains [34].

The exchange kinetics of amide hydrogens can be followed by deuterium or tritium isotope labeling with exchange times ranging from seconds to days. The exchange rates of hydrogens on  $-OH$ ,  $-SH$ ,  $-NH_2$ ,  $-COOH$ , and  $-CONH_2$  groups and the amino and carboxy termini are much faster. Carbon-centered hydrogens do not exchange under normal conditions, and undergo isotope substitution only following activation by chemical treatment, such as reaction with hydroxyl radicals [35].

#### 12.2.2

##### Protection Factor

Several features affect the rate of amide hydrogen exchange, which reflect the protein's structure and dynamic properties. These include an amide's participation in hydrogen bonding [36], its distance from the protein surface [3], and the

flexibility of the peptide chain [37]. The degree of retardation in amide hydrogen exchange rate that results from the amide's physical environment is termed its "protection factor ( $pf$ )":

$$pf = k_{ch}/k_{ex} \quad (1)$$

where  $k_{ex}$  is the observed exchange rate and  $k_{ch}$  is the "intrinsic" exchange rate calculated at a given pH and temperature in unstructured peptide chain [34].

### 12.2.3

#### Backbone Amide Hydrogens as Thermodynamic Sensors

Formalisms to relate the observed rates of amide hydrogen exchange to thermodynamic stabilization of proteins have been developed [38]. Amide hydrogens of proteins in the native, folded state are proposed to exchange according to the following equation:



$$k_{ex} = k_{op} \times k_{ch}/(k_{cl} + k_{ch}) \quad (3)$$

where  $k_{op}$  is the rate at which amide hydrogen converts from closed state to open state. Conversely,  $k_{cl}$  is the rate amide hydrogen converts from open state to closed state. For most proteins at or below neutral pH, amide H/D exchange occurs by an EX2 mechanism [39], where  $k_{cl} \gg k_{ch}$  and Eq. (3) becomes:

$$k_{ex} = k_{op} \times k_{ch}/k_{cl} = k_{ch}/K_{cl} \quad (4)$$

The closing equilibrium constant at each amide ( $K_{cl} = k_{cl}/k_{op}$ ) is equal to the protection factor ( $pf$ ) and can be translated into the stabilization free energy of closed state ( $\Delta G_{cl}$ ) by Eq. (5).

$$\Delta G_{cl} = -RT \ln(K_{cl}) = -RT \ln(pf) = -RT \ln(k_{ch}/k_{ex}) \quad (5)$$

The measured H/D exchange rates in the folded protein ( $k_{ex}$ ) can be compared with the calculated "intrinsic" rates ( $k_{ch}$ ) to probe the extent of tertiary structure and resulting dynamics. Frequently, the hydrogen exchange rates of two or more physical states of a protein, such as with and without ligand (here represented by  $k_{ex2}$  and  $k_{ex1}$ ), are measured to locate stabilization free energy changes upon the perturbation ( $\Delta\Delta G_{1-2}$ ):

$$\Delta\Delta G_{1-2} = \Delta G_2 - \Delta G_1 = -RT \ln(k_{ex1}/k_{ex2}) \quad (6)$$

Thus, the measurement of exchange rates of backbone amide hydrogen serves as a precise thermodynamic sensor of the local environment.

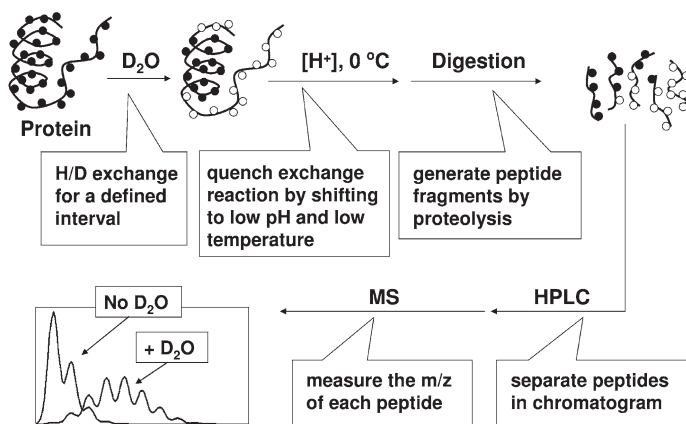


Fig. 12.1 Overall H/D exchange experiment.

### 12.3

#### Overview of H/D Exchange Technologies

Dramatic advances in mass spectrometry and improvements in the various steps within the experimental hydrogen exchange procedures have resulted in the development of automated systems for high-throughput, high-resolution H/D exchange analysis [6, 8, 40–44].

The system (Fig. 12.1), described in this section, incorporates the latest of these enhancements, including solid phase proteolysis, automated liquid handling and streamlined data reduction software [8].

##### 12.3.1

#### On Exchange Reaction

To initiate an H/D exchange reaction, a protein sample, initially in non-deuterated buffer, is incubated in a buffer with 50–90% mole fraction deuterated water. There are almost no restrictions on reaction conditions which allow exchange behavior to be studied as a function of protein and buffer composition, solution pH, and in the presence and absence of ligands. To follow the deuterium buildup of individual amide hydrogen or sets of hydrogens, several on exchange time points are sampled for each condition.

##### 12.3.2

#### Quench of Exchange Reaction

Following incubation in a deuterated environment for a defined interval, the exchange reaction is “exchange quenched” by diluting the protein sample with a cold, acidic solution (pH  $\sim 2.5$  and  $0\text{ }^\circ\text{C}$ ). The quench conditions significantly

slow the amide exchange reaction and limit undesirable back exchange. Subsequent experimental procedures are conducted near the quench conditions to minimize the loss of incorporated deuterium.

### 12.3.3

#### **Protein Fragmentation by Proteolysis**

To localize the rate of deuterium buildup to specific amides, the analyte protein is fragmented into a collection of peptides using combinations of endo- and exo-proteases. Due to the low pH of the quench conditions in which the protein and peptide samples are maintained after deuterium labeling, acid-reactive proteases such as pepsin must be employed. Studies with combinations of acid-reactive endoproteinases and carboxypeptidases have been employed to achieve greater sequence coverage and higher amide resolution [42, 45].

### 12.3.4

#### **Digestion Optimization**

The digestion conditions are optimized prior to conducting multiple H/D exchange experiments, to ensure high sequence coverage. Calculation of the differences in deuterium content between overlapping peptides is the preferred method to localize incorporated deuterium atoms [6, 22]. Variable digestion parameters include the type and bed volume of the protease columns, the transit time of the protein over the protease column, the type and concentration of denaturant [6], and inclusion of reducing reagents such as Tris(2-carboxyethyl)phosphine hydrochloride (TCEP) [46].

### 12.3.5

#### **HPLC Separation**

The peptides generated by proteolysis are separated using reverse-phase HPLC to minimize mass overlap and ionization suppression caused by ion competition in the electrospray source [40]. The optimized LC gradient parameters efficiently separate peptides while minimizing loss of deuterium through back exchange with solvent. Increased sensitivity can be achieved by using capillary HPLC columns and nanoelectrospray methods [47].

### 12.3.6

#### **Mass Analysis**

The majority of H/D studies that have been reported employ quadrupole ion trap (QIT) instruments due to their ease of use, excellent sensitivity, ability to perform MS/MS experiments, compact size, and low cost. Other reports discuss the use of instruments with higher mass-resolving power such as the hybrid QqTOF instruments [47]. A few groups have utilized FT-ICR mass spectrometry, which offers ultra-high mass-resolving power and improved mass accuracy [48, 49].

## 12.3.7

**Automation of H/D Exchange by MS**

A fully automated system for performing detailed studies has been developed to improve the reproducibility and throughput (Fig. 12.2) [8]. It consists of two functional components; a sample-deuteration device and a protein processing unit. The preparation operations (shown at the top of Fig. 12.2) are performed by two robotic arms equipped with low volume syringes and two temperature-controlled chambers, one held at 25 °C and the other held at 1 °C. To initiate the exchange experiment, a small amount of protein solution is mixed with a deuterated buffer and the mixture is then incubated for a programmed period of time in the temperature-controlled chamber. This on-exchanged sample is immediately transferred to the cold chamber where a quench solution is added to the mixture.

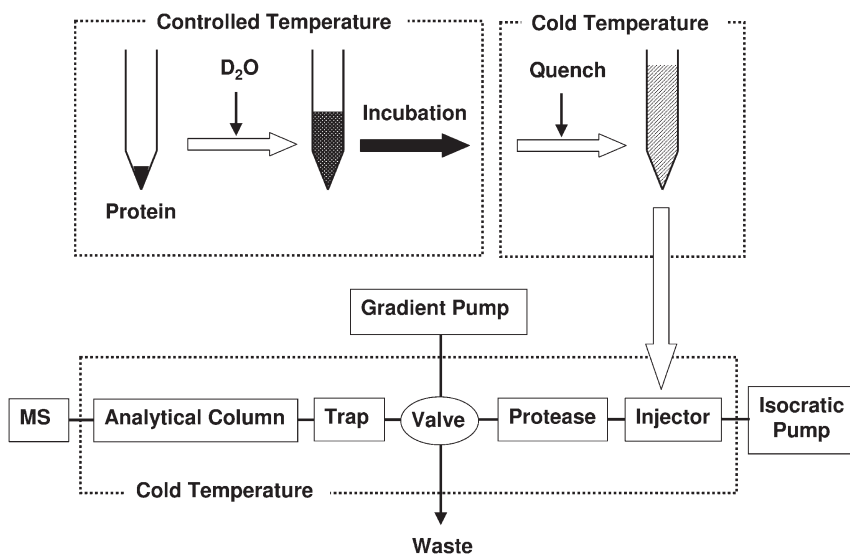


**Fig. 12.2** Diagram of a fully automated system for acquiring H/D exchange MS data starting with a stock solution of the nondeuterated protein. In this system [8], the liquid handler mixes a small amount of concentrated protein solution with a selected deuterated buffer and the mixture is incubated for a programmed period of time. The exchange reaction is conducted in a temperature-controlled chamber held at 25 °C. The mixture is then transferred to an acidic quench solution held at 1 °C. After quenching the exchange reaction, the entire sample is injected onto an LC-MS system

which includes injection loops, protease column(s), a trap, an analytical column, and isocratic and gradient pumps. The injector, columns, and electronically controlled valves reside in a low temperature chamber to minimize the loss of deuterium by back-exchange. The quenched protein solution is pumped in series over a column containing immobilized protease and a reverse-phase trap to capture the peptide fragments. The gradient pump is activated following the digestion and the peptides captured on the trap are eluted into the mass spectrometer after separation in the analytical column.

The exchange-quenched solution is then injected onto the protein processing system which includes injection loops, protease column(s), a trap column, an analytical column, electronically controlled valves, and isocratic and gradient pumps. The injector, columns and valves reside in a low temperature chamber to minimize the loss of deuterium by back exchange (Fig. 12.2). The quenched protein solution is pumped in series through a column containing an immobilized protease and a trap column to capture the peptide fragments. The gradient pump is activated following digestion and the peptides captured on the trap column are eluted and separated over an analytical reverse-phase HPLC column directly into the mass spectrometer.

#### 12.3.8

##### **Automated Data Analysis**

A software system capable of extracting and cataloging the large number of data points obtained during each experiment has been developed [8]. The automated system streamlines most data handling steps and reduces the potential for errors associated with manual manipulation of large data sets. In the first processing step, the centroid mass value is obtained for the isotopic envelope of each peptide ion observed in every LC-MS data file associated with the experiment. This step includes peak detection, selection of retention time window, selection of  $m/z$  range, and calculation of envelope centroid. The second step involves correction for deuterium losses subsequent to sample quench by reference to measured peptide-specific losses [1, 8]. After calculating the percent deuterium incorporation for each peptide at each time point, H/D exchange data is displayed in a number of formats, often as a stacked bar chart that is aligned with the protein primary sequence.

### 12.4

#### **DXMS-guided Design of Well Crystallizing Proteins**

##### 12.4.1

##### **Disordered Regions and Protein Crystallography**

Structure-based drug design is one of the most powerful strategies for current drug discovery. While this strategy requires a high-resolution structure of a target protein, most drug target proteins are not readily crystallizable. Many generally well structured proteins have disordered regions [50] that may inhibit crystallization and/or cause poor diffraction. The identification of disordered regions can help in designing new constructs that retain structure and biological function, but are depleted of disordered regions. While a number of approaches to identifying disordered regions are available, ranging from computational stability calculation to limited proteolysis, none of them have provided reliable identification of disordered regions at the pace required.



Since the exchange rates of backbone amide hydrogens are most influenced by their involvement in hydrogen bonding to other portions of the protein, measurement of exchange rates allows direct identification/localization of ordered/disordered regions in the protein. Amide hydrogens in disordered regions exchange very rapidly because the hydrogen bonds to amides in such regions are predominantly with solvent water most of the time. We have recently shown that suitably performed DXMS studies can rapidly localize such disordered regions, and guide the design of well crystallizing constructs selectively depleted of disorder [44].

#### 12.4.2

##### **Poorly Crystallizing Proteins Contain Substantial Disordered Regions**

To demonstrate the utility of DXMS analysis for crystallographic construct optimization, the exchange patterns of 21 different *Thermotoga maritima* proteins were measured in collaboration with the Joint Center for Structural Genomics (JCSG) [44]. Among the 21 proteins studied, 12 crystallized readily and the remaining nine crystallized poorly. While most of the crystallizable proteins contained no substantial disordered regions, four of the nine poorly crystallizing proteins contained 10% or more of their sequence in disordered regions. The exchange pattern of TM0160 is an example of disorder within a poorly crystallizing protein (Fig. 12.3a). The largest disordered region of this protein was seen to be at its C-terminus, suggesting a straightforward route to construct optimization by deletion of the disordered C-terminus.

#### 12.4.3

##### **Disorder-depleted Mutant Preserved Ordered Structure**

Four slightly differing deletion mutants of TM0160 devoid of the C-terminal disordered region were designed and prepared (Fig. 12.3a). It was important to determine if the truncated versions had the same folding patterns as the full-length protein in the regions with retained sequence. To answer the question, the exchange patterns of full-length TM0160 and its D3 deletion mutant were compared (Fig. 12.3b). Virtually identical exchange patterns of the two proteins in the retained regions indicated the preservation of native folded structure in the deletion mutant D3.

#### 12.4.4

##### **Disorder-depleted Mutant Improved Crystallization Efficiency and Produced High Resolution Structure**

Despite multiple screening attempts, the TM0160 full-length construct gave only three marginal hits from 2400 individual crystallization tests. In contrast, each of the four TM0160 mutants crystallized well. The TM0160 D3 mutant gave 78 hits

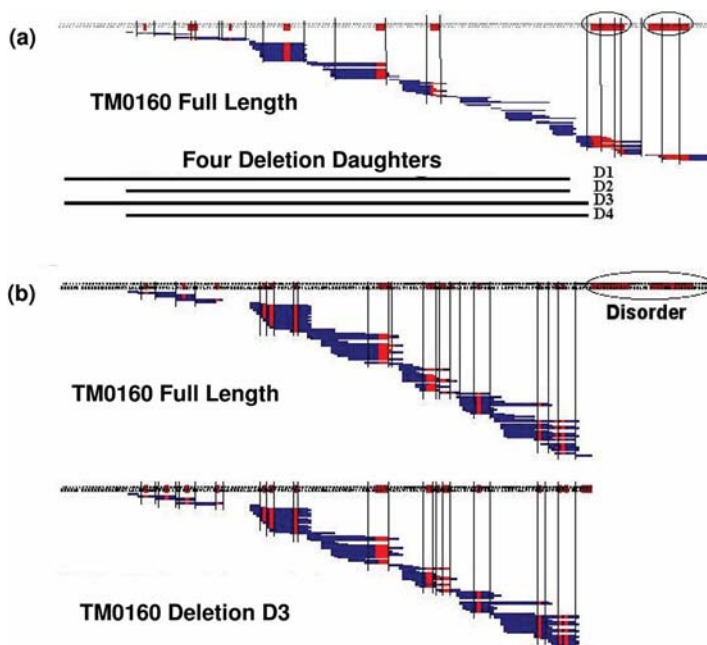


**Fig. 12.3** (a) The H/D exchange results of full length TM0160 after 10 s exchange reaction at 0 °C. Each line indicates a peptide fragment analyzed. Red is the region exchanged and blue is the region not exchanged. Long stretches of contiguous sequence (four or more residues) that are rapidly exchanging are indicative of disorder. There are substantial disordered regions at C-terminal of this full-length construct. Four

truncated constructs, D1–D4 were designed by eliminating the C-terminal disordered regions. (b) The repeat H/D exchange results of full-length TM0160 and D3 mutant after 10 s exchange reaction at 0 °C. They showed virtually identical patterns in retained sequence, but are depleted of the disordered regions at the C-terminus of the parental construct.

from 1920 individual tests, including numerous crystals of sufficient size and quality for diffraction studies. The crystallographic structure of TM0160 D3 was subsequently determined at a resolution of 1.9 Å [51]. This application of DXMS analysis was further validated by the successful crystallization and structure determination of other proteins in a similar manner [51, 52].

## 12.5

### Rapid Characterization of Protein Conformational Change with DXMS

DXMS can rapidly define the nature of protein conformational changes that result from small molecule binding, protein–protein interactions, and other perturbations [9–15, 19, 25–29, 44, 51]. Below we present an example in which

pH-induced alterations in protein structure were rapidly characterized at high resolution.

### 12.5.1

#### **Human Growth Hormone**

Human growth hormone (hGH) is a 191-amino-acid polypeptide that is released from anterior pituitary somatotrope cells. The hormone functions to promote linear growth during adolescence and modulate many physiological functions after completion of growth. Since 1984, somatropin (recombinant DNA-derived hGH) therapy has been applied in the treatment of growth hormone-deficient children. hGH is known to exhibit a distinct conformation at an acidic pH when compared to neutral pH [53]. Although the molecular conformations at acid and neutral pH share virtually identical extents of secondary structure, differences in the tertiary structure have been observed. The less stable acidic conformation is also implicated as the intermediate for undesirable aggregation [53].

### 12.5.2

#### **H/D Exchange of hGH**

The H/D exchange results of hGH at two different pHs are summarized in Fig. 12.4. There are four regions in hGH for which amide H/D exchange rates are very slow at both pH conditions tested. These regions include amino acids 15–35, 78–87, 113–124, and 159–182, corresponding to the four helix bundle, a structural fold frequently found in protein hormones and other signaling proteins. High levels of deuterium incorporation are observed for the loop regions of hGH so that, at the later time points, greater than 90% deuteration is observed at both pH 7.0 and pH 2.6. Overall the H/D-Ex results for hGH correlate with the existence of secondary structure, with the helical regions of high local secondary structure showing lower rates of exchange [36].

### 12.5.3

#### **Free Energy Change upon Folding of hGH**

The sampling of deuterium buildup at time points ranging from 30 s to 100,000 s allows estimation of the free energy change upon folding using Eq. (5). This analysis eliminates effects arising from differences in intrinsic amide hydrogen exchange rates by accurately modeling these rates and allowing for correction among different pH [34]. This becomes important considering the amide hydrogen exchange reaction is primarily base catalyzed near neutral pH. By correcting for these differences this approach is useful for the analysis of pH-dependent structural changes. Fig. 12.5a, b show the localized free energy changes upon folding at pH 7.0 and pH 2.6, respectively. The data clearly show that the overall

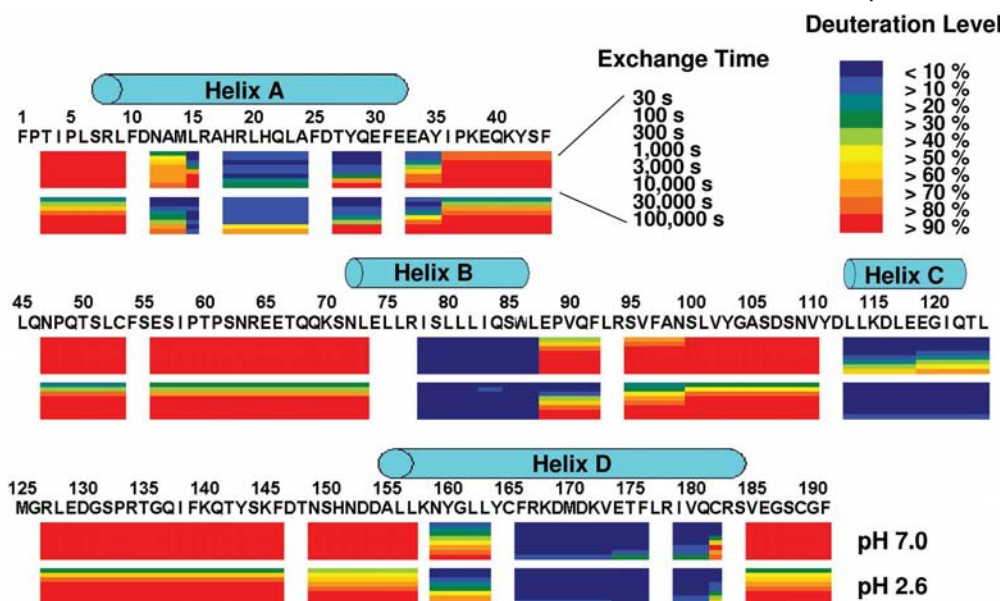


**Fig. 12.4** H/D exchange analysis of hGH at pH 7.0 and 2.6 [8]. Each block represents a pepsin-generated peptide. Each block consists of eight rows that represent eight distinct on-exchange time points, shown at the right. The level of deuteration in each peptide at each time point is represented by color according to the diagram displayed at the top right. Blocks representing on-exchange at pH 7.0 are on the top row, while blocks representing on-exchange at pH 2.6 are shown on the bottom. Light blue cylinders above the sequence indicate the

helices identified from the X-ray crystal structure of hGH (protein data bank ID: 1HGU). Peptides that contain mostly slow exchanging amide hydrogens are represented by blue bars, while red bars represent peptides that contain mostly rapidly exchanging amide hydrogens. Regions of the protein that contain amides that were not observed in the experiments are indicated in white. These gaps are primarily due to the fact that the first two residues of each peptide lose the deuterium during the analysis [34].

hGH structure is significantly more stable at neutral pH. At pH 7.0, interactions between helix B and the central portions of helices A and D were sufficiently stable that several peptide fragments derived from this region showed no deuterium incorporation, even after incubation for 100,000 s. It was estimated that free energy changes upon folding in these regions is greater than 7 kcal mol<sup>-1</sup> residue<sup>-1</sup> at pH 7.0. Overall, the loop regions are the least stable.

Regions of greatest stabilization in the helix bundle shift as a function of pH (Fig. 12.5a, b). At neutral pH, regions of high stability were located at the central portion of the helix bundle. At pH 2.6, the region of highest stability in the structure had markedly shifted so that most of the stabilizing interactions are located near the end of the bundle containing the N- and C-terminus. In contrast to the

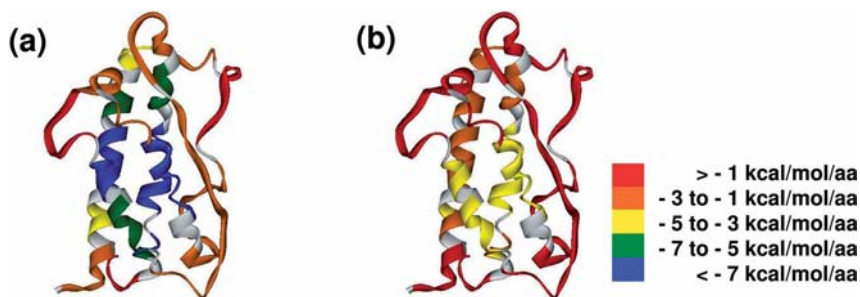


**Fig. 12.5** Free energy change (expressed in kcal mol<sup>-1</sup> per amino acid) upon folding of hGH: (a) at pH 7.0, and (b) at pH 2.6 [8]. Folding free energies are mapped on the X-ray structure (1HGU) by colored segments according to the key at the right. Gray indicates residues that were not analyzed [34].

stabilization energies of larger than 7 kcal mol<sup>-1</sup> residue<sup>-1</sup> at pH 7.0, stabilization energies approach only 5 kcal mol<sup>-1</sup> residue<sup>-1</sup> at pH 2.6.

## 12.6

### Application of H/D Exchange to Protein–Small Molecule Ligand Interactions

The ability to localize the physical interactions of proteins with candidate small molecule ligands plays a central role in current small molecule drug discovery efforts. Until recently, only X-ray crystallography and NMR could provide the submolecular details of such interactions. Unfortunately, both techniques have applicability limitations: NMR is applicable only for relatively small proteins at relatively high concentration and not all protein–ligand interactions can be co-crystallized. The hydrogen exchange perturbation of a target protein upon ligand binding can be measured with DXMS as long as over 90% of the protein is in ligand-bound form in solution. No crystallization is necessary and micromolar binding affinities for ligand are sufficient for study. As for sensitivity, a few nanomoles of a protein is usually enough to complete the analysis, and recent developments have decreased protein requirements 100-fold or more [47].

#### 12.6.1

##### p38 Mitogen-activated Protein Kinase

Protein kinases phosphorylate other proteins, and this action functions as a control switch for various cell activities. The switching functions make this family of proteins a very promising target for novel therapeutics. p38 mitogen-activated protein (MAP) kinase controls the production of growth factors and inflammatory cytokines, the molecules produced by the immune system that cause inflammation [54].

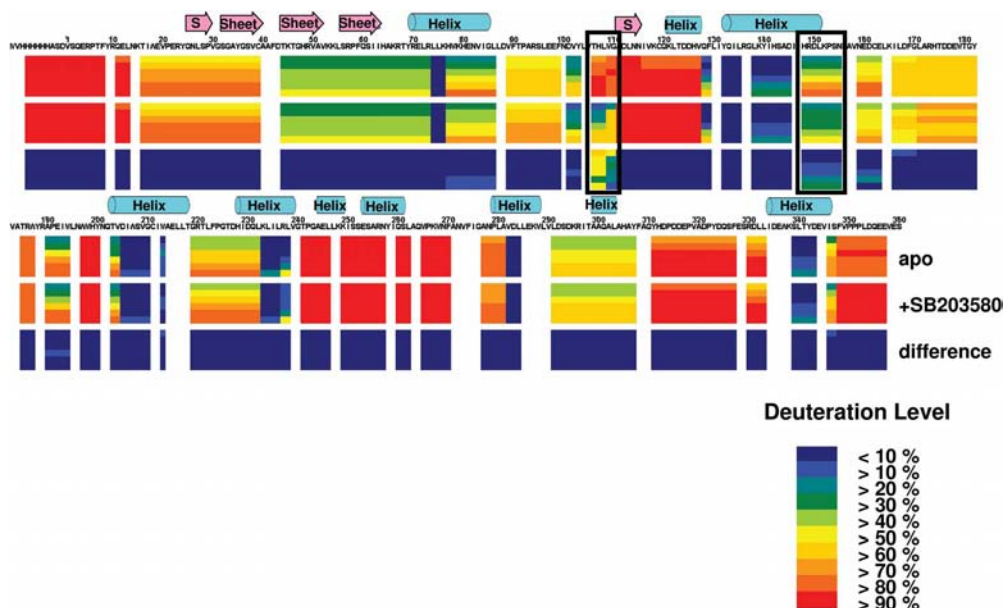


**Fig. 12.6** H/D-Ex results of p38 MAP kinase at pH 7.0 at 25 °C with or without SB203580 [56]. Each block represents a pepsin-generated peptide. Each block has six time points and the level of deuterium incorporation is indicated by colors that vary according to the legend at the bottom right. Upper and middle blocks show the results without and with SB203580, respectively.

Lower blocks are the difference of the two deuterium incorporations. Dark blue indicates no difference with or without the ligand. The regions showing the difference are highlighted by black rectangles. Regions of the protein that contain amides that were not observed in the experiments are indicated in white [34].

## 12.6.2

### H/D Exchange of p38 MAP Kinase

To determine how an inhibitor interacts with this target protein and changes its dynamics, H/D exchange of p38 MAP kinase was conducted with or without a small molecule inhibitor, SB203580 [55, 56]. The top row of Fig. 12.6 shows the H/D exchange pattern for unliganded p38 MAP kinase. p38 MAP kinase is organized about conformationally stable helices that include residues 74–86, 128–155, 203–213, 233–238, and 338–343. In contrast, residues 241–270 are especially mobile, even though they form a helix in the crystal structure [55, 57] (see also Fig. 12.7a).

A comparison of the exchange data for the unliganded (top row of Fig. 12.6) and liganded forms (middle row of Fig. 12.6) showed that in the SB203580 complex, two segments of p38 MAP kinase, residues 106–110 and 148–155, exhibited significant reductions in H/D exchange rates (bottom row of Fig. 12.6). The segments are separated in the amino acid sequence but adjacent in the folded struc-

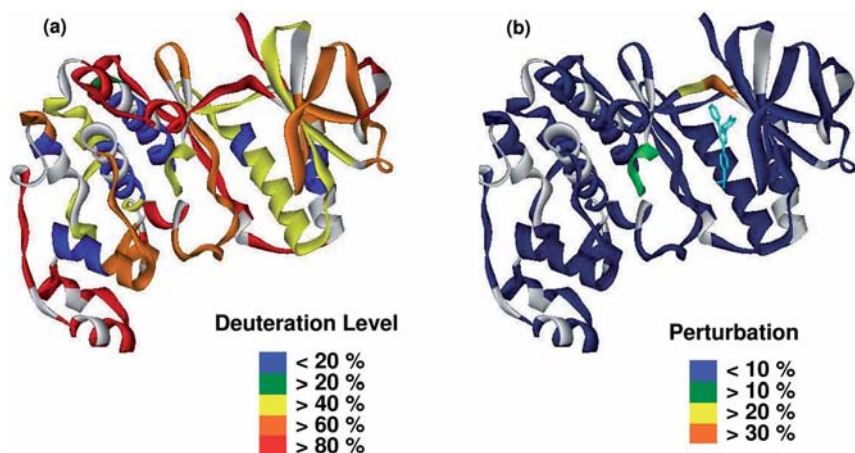


**Fig. 12.7** (a) Average deuteration level of each segment in apo p38 MAP kinase overlaid on the crystallographic structure (protein data bank ID: 1A9U) [56]. Blue indicates the region exchange slow and red the region exchange fast. (b) Ligand binding site identified by H/D exchange. Orange is the segment perturbed most. Dark blue is the regions that showed no H/D exchange perturbation. Light blue is SB203580. Gray indicates residues that were not analyzed [34].

ture, and encompass the ATP-binding residues and most of the activation loop (Fig. 12.7b). This kinase appears conformationally poised for this inhibitor, as no changes in dynamics were measured in other regions. The highly localized effects of SB203580 binding to p38 MAP kinase contrast with the global conformational changes induced by interactions with nucleotide substrates and protein partners that have been observed in other kinase systems [17, 22, 58].

### 12.6.3

#### Peroxisome Proliferator-activated Receptor $\gamma$

Peroxisome proliferator-activated receptor  $\gamma$  (PPAR $\gamma$ ) is a ligand-dependent transcription factor that is involved in glucose homeostasis and adipocyte differentiation, and is the molecular target of anti-diabetic agents, such as rosiglitazone. Many studies on this class of receptors indicate that the binding to agonists or antagonists induces different conformational changes in the ligand binding domain (LBD) [59–63]. These conformational changes induced by various biological modulators have been proposed to have key roles in the biological responses of nuclear receptors [62].

### 12.6.4

#### H/D Exchange of PPAR $\gamma$

The hydrogen exchange patterns of PPAR $\gamma$  LBD were measured with or without various biological modulators [64]. The presence of ligands significantly changes



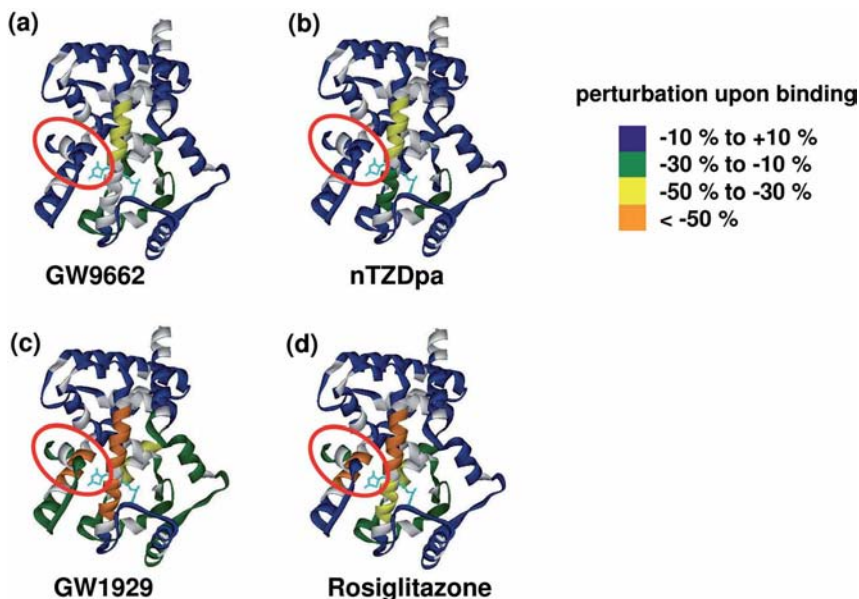


**Fig. 12.8** Average difference in deuteration levels of PPAR $\gamma$  LBD between ligand bound form and apo form [64]. Dark blue indicates the segment exchanges about the same rate with or without the ligand. Other colors indicate the segment exchanges slower with the ligand. Gray is the region not covered by the current experimental set [34].

the dynamics/conformation of PPAR $\gamma$  LBD and consequently perturbs hydrogen exchange in various regions of the protein (Fig. 12.8). The degree to which different kind of ligands perturb PPAR $\gamma$  LBD is distinguishable through H/D exchange. Three types of ligands were tested: (1) full agonists, rosiglitazone and GW1929; (2) partial agonist, nTZDpa; and (3) covalent antagonist, GW9662. Full agonists slowed exchange in wider regions and did it more strongly than either the partial agonist or the antagonist. This indicates the full agonist rigidifies the PPAR $\gamma$  LBD more extensively than the other two, and is consistent with the NMR cross-peak analysis [61]. One very interesting observation is that the two full agonists rigidified helix 12 significantly while the partial agonist and the antagonist did not perturb the H/D exchange of that region.

## 12.7

### DXMS-guided Design of Small Molecules that Target Protein–Protein Interaction Surfaces

Development of small molecule inhibitors of protein–protein binding interactions has been notoriously difficult. The tremendous investment that the pharmaceutical industry has made in the development and marketing of whole protein



therapeutics such as monoclonal antibodies and recombinant proteins is testament to the strength of the belief that small molecule replacements for these “expensive to produce and administer” biologics will not soon be forthcoming. Multiple noncovalent interactions between a protein and a ligand are required for sufficient affinity and specificity. Typical “druggable” proteins usually have identifiable cavities or crevices on their surfaces that allow direction of multiple interactions to a resident small molecule ligand, that is typically less than or equal to 500 Da in size. In protein–protein binding, these multiple interactions do not need to be focused to a single small area, but typically are spread across a broad, fairly flat binding surface that is devoid of identifiable “druggable” cavities [65].

Fortunately, it has been found that many protein–protein binding surfaces contain a small number of amino acid residues (binding surface “hot spots”) that predominantly contribute to the binding energy between partners. This was first demonstrated by Wells and collaborators in studies of the complex formed between hGH and its cellular receptor protein [66, 67]. Unfortunately, the methodology that demonstrated this phenomenon (site-directed mutagenesis-induced perturbation of binding affinity) has not proven to be a robust guide to small-molecule development to binding surfaces. One reason for this failure is suggested by the observation that small, but important, highly localized conformational changes are induced in apparently bland interaction surfaces when protein ligands bind to each other [65, 68]. Protein–protein binding may induce the formation of localized topography that focuses binding energy by way of induced crevices. Mutagenesis approaches may not allow these small conformational changes to be induced or localized with sufficient precision. These inducible crevices, if they could be reliably localized, might serve as targets for small molecule design efforts to protein binding surfaces. DXMS analysis can provide precisely the information required to identify protein–protein binding surface hot spots, and then guide the design of small molecules that precisely target such “hot spot” regions, all without the use of mutant proteins.

A United States patent describes how this can be accomplished [69]. First, DXMS analysis is performed on the interacting proteins, separately and complexed to each other. Measurement of the magnitude of exchange slowing (protection factor) in the complexed versus unbound state, for each of the amides participating in the protein–protein binding surface, allows direct identification of “hot spots”. The hot spots are the areas of the binding surface with the highest protection factors. Protein–protein binding surfaces are not rigid structures, but undergo continuous flexible movement, as does the entire protein. Protein–protein binding surfaces are bound together most tightly at their thermodynamic hot spots, and the bulk solvent has little opportunity to interact with the amides in such tightly bound regions. Indeed, the amide hydrogens in the hot spots serve as highly localized sensors of binding-induced free energy change, where binding free energy ( $\Delta G$ ) at such amides is related to specific measured amide protection factors according to Eq. (5).

Once binding hot spots are identified by DXMS analysis, combinatorial libraries can be generated, based in part on structural information available that may suggest the nature of the peptidic features of the interacting proteins that

are present at the exchange-localized hot spot. Libraries are screened against the protein target, not with conventional binding or activity assays, but by performing repeat high-throughput DXMS studies in which the target protein is functionally deuterated in the presence of an excess of each test compound. Small molecules that, by virtue of their protein binding, can induce exchange slowing selectively at the previously identified protein–protein binding surface hot spots are identified. These are then selected for further combinatorial perturbation, and repeat DXMS screening against the target protein. In this manner, DXMS analysis provides an almost real-time guide to the identification of library elements in each round of selection that are capable of binding to the protein–protein interaction-defined binding hot spots.

An analogy can be made to oil well drilling. Initial DXMS analysis of a clinically important protein–protein interaction provides the equivalent of a seismic map of an oilfield, showing where the oil may be located (hot spots). Further high-throughput DXMS analysis of protein–small molecule mixtures at each round of selection is analogous to having a sensor in the oil drilling rig that measures the proximity of the drill tip to the targeted oil deposit in real time. The numerous whole protein therapeutics that have proven to be great successes in the clinic make tempting targets for this small-molecule design strategy.

## 12.8

### Optimal Formulation and Quality Control of Whole Protein Therapeutics with DXMS

Whole proteins, including monoclonal antibodies, are the fastest-growing class of therapeutics. Compared with traditional small molecule drugs, much additional analysis is necessary for their development and production due to their large size and complex structure. The protein construct and its formulation have to be optimized during development, and its structural integrity must be closely monitored during production.

DXMS is the ideal analytical tool to monitor protein's structural integrity in the development and production of whole protein therapeutics. During development, DXMS data can rapidly determine the effects of mutation, chemical modification, and/or formulation change on protein folding/dynamics, and localize any changes at the submolecular level. During production, DXMS can be a rapid and sensitive method to identify batch-to-batch variation in protein folding. The foregoing studies of hGH exemplify the use of this technology for formulation optimization. In this case, the H/D exchange data allowed close monitoring of the changes induced by pH alteration.

Many blockbuster protein therapeutics will soon be coming off-patent. It is unclear how regulatory agencies might best evaluate and approve generic versions of these complex pharmaceuticals. Inventor companies assert that the production process must be precisely reproduced for biophysical and pharmaceutical equivalence, and argue that experimentally proving equivalence of their formulation versus potential generic whole protein therapeutics is impossible. From this perspective, generic protein therapeutics have to undergo costly clinical trials for

demonstration of efficacy and safety. Generic companies assert that experimentally demonstrating the equivalence between original and generic protein therapeutics by biophysical and biochemical measurements in the laboratory is possible as is now done with small molecule generics, a much less costly proposition. It is possible that DXMS will prove to be capable of establishing the structural equivalence (or lack thereof) between original and generic versions of these protein therapeutics.

## 12.9

### Conclusions

With the increased number of new protein sequences obtained by genomic and proteomic efforts, a high-throughput and widely applicable protein structure analysis technology such as DXMS is needed. Recent improvements of MS instrumentation, fluidics, automation, fragmentation chemistry, and data analysis software have made this technology sensitive, robust, high-throughput, and capable of achieving near single-amide resolution. Examples cited here demonstrate that DXMS has exceptional potential to facilitate many steps of the drug discovery process. First, DXMS can guide construct optimization to speed X-ray crystallographic structure determination. Second, the nature of binding sites and binding-induced conformational changes can be determined for the target protein with DXMS. Third, the unique high-resolution thermodynamic information provided by DXMS allows the focusing of discovery efforts to evolutionarily selected binding hot spots in what otherwise appear to be bland protein–protein binding surfaces. Finally, DXMS can be very useful in the characterization and quality control of whole protein therapeutics.

### Acknowledgements

We would like to sincerely thank Mark Fisher, Paul DeStefano, Robert Johnston, Kathleen Molnar, David Smith, and Walter Englander for their vision and support of this work, which would have not been possible without their efforts. This work was supported by NIH Grants CA099835 and CA118595 (V.L.W.). V.L.W. has equity interests in ExSAR Corporation.

### References

- 1 Zhang Z., Smith D.L.: Determination of amide hydrogen exchange by mass spectrometry: A new tool for protein structure elucidation. *Protein Sci.* **1993**, 2, 522–531.
- 2 Neubert T.A., Walsh K.A., Hurley J.B., Johnson R.S.: Monitoring calcium-induced conformational changes in recovering by electrospray mass spectrometry. *Protein Sci.* **1997**, 6, 843–850.
- 3 Resing K.A., Hoofnagle A.N., Ahn N.G.: Modeling deuterium exchange behavior of ERK2 using pepsin

- mapping to probe secondary structure. *J. Am. Soc. Mass Spectrom.* **1999**, 10, 685–702.
- 4 Engen J.R., Smith D.L.: Investigating protein structure and dynamics by hydrogen exchange MS. *Anal. Chem.* **2001**, 73, 256A–265A.
  - 5 Hoofnagle A.N., Resing K.A., Goldsmith E.J., Ahn N.G.: Changes in protein conformational mobility upon activation of extracellular regulated protein kinase-2 as detected by hydrogen exchange. *Proc. Natl Acad. Sci. USA* **2001**, 98, 956–961.
  - 6 Hamuro Y., Burns L.L., Canaves J.M., Hoffman R.C., Taylor S.S., Woods V.L. Jr: domain organization of D-AKAP2 revealed by enhanced deuterium exchange–mass spectrometry (DXMS). *J. Mol. Biol.* **2002**, 321, 703–714.
  - 7 Zawadzki K., Hamuro Y., Kim J., Garrod S., Stranz D., Taylor S., Woods V.L. Jr: Dissecting interdomain communication within cAPK regulatory subunit type I $\beta$  using enhanced amide hydrogen/deuterium exchange mass spectrometry (DXMS). *Protein Sci.* **2003**, 12, 1980–1990.
  - 8 Hamuro Y., Coales S.J., Southern M.R., Nemeth-Cawley J.F., Stranz D.D., Griffin P.R.: Rapid analysis of protein structure and dynamics by hydrogen/deuterium exchange mass spectrometry. *J. Biomol. Techn.* **2003**, 14, 171–182.
  - 9 Wong L., Lieser S., Chie-Leon B., Miyashita O., Aubol B., Shaffer J., Onuchic J.N., Jennings P., Woods V.L. Jr, Adams J.A.: Dynamic coupling between the SH2 domain and active site of the COOH terminal Src kinase, Csk. *J. Mol. Biol.* **2004**, 341, 93–106.
  - 10 Black B.E., Foltz D.R., Chakravarty S., Luger K., Woods V.L. Jr, Cleveland D.W.: Structural determinants for generating centromeric chromatin. *Nature* **2004**, 430, 578–582.
  - 11 Yang J., Garrod S.M., Deal M.S., Anand G.S., Woods V.L. Jr, Taylor S.: Allosteric network of cAMP-dependent protein kinase revealed by mutation of Tyr204 in the P+1 loop. *J. Mol. Biol.* **2005**, 346, 191–201.
  - 12 Wong L., Lieser S.A., Miyashita O., Miller M., Tasken K., Onuchic J.N., Adams J.A., Woods V.L. Jr, Jennings P.A.: Coupled motions in the SH2 and kinase domains of Csk control Src phosphorylation. *J. Mol. Biol.* **2005**, 351, 131–143.
  - 13 Derunes C., Briknarova K., Geng L., Li S., Gessner C.R., Hewitt K., Wu S., Huang S., Woods V.L. Jr, Ely K.R.: Characterization of the PR domain of RIZ1 histone methyltransferase. *Biochem. Biophys. Res. Commun.* **2005**, 333, 925–934.
  - 14 Iyer G.H., Garrod S., Woods V.L. Jr, Taylor S.S.: Catalytic independent functions of a protein kinase as revealed by a kinase-dead mutant: study of the Lys72His mutant of cAMP-dependent kinase. *J. Mol. Biol.* **2005**, 351, 1110–1122.
  - 15 Del Mar C., Greenbaum E.A., Mayne L., Englander S.W., Woods V.L. Jr: Structure and properties of  $\alpha$ -synuclein and other amyloids determined at the amino acid level. *Proc. Natl Acad. Sci. USA* **2005**, 102, 15477–15482.
  - 16 Engen J.R., Gmeiner W.H., Smithgall T.E., Smith D.L.: Hydrogen exchange shows peptide binding stabilizes motions in Hck SH2. *Biochemistry* **1999**, 38, 8926–8935.
  - 17 Andersen M.D., Shaffer J., Jennings P.A., Adams J.A.: Structural characterization of protein kinase A as a function of nucleotide binding. Hydrogen–deuterium exchange studies using matrix-assisted laser desorption ionization–time of flight mass spectrometry detection. *J. Biol. Chem.* **2001**, 276, 14204–14211.
  - 18 Davidson W., Frego L., Peet G.W., Kroe R.R., Labadia M.E., Lukas S.M., Snow R.J., Jakes S., Grygon C.A., Pargellis C., et al.: Discovery and characterization of a substrate selective p38 $\alpha$  inhibitor. *Biochemistry* **2004**, 43, 11658–11671.
  - 19 Garcia R.A., Pantazatos D.P., Gessner C.R., Go K.V., Woods V.L. Jr, Villarreal F.J.: Molecular interactions

- between matrilysin and the matrix metalloproteinase inhibitor doxycycline investigated by deuterium exchange mass spectrometry. *Mol. Pharmacol.* **2005**, 67, 1128–1136.
- 20 Mandell J.G., Falick A.M., Komives E.A.: Identification of protein–protein interfaces by decreased amide proton solvent accessibility. *Proc. Natl Acad. Sci. USA* **1998**, 95, 14705–14710.
  - 21 Ehring H.: Hydrogen exchange/electrospray ionization mass spectrometry studies of structural features of proteins and protein/protein interactions. *Anal. Biochem.* **1999**, 267, 252–259.
  - 22 Anand G.S., Hughes C.A., Jones J.M., Taylor S.S., Komives E.A.: Amide H/2H exchange reveals communication between the cAMP and catalytic subunit-binding sites in the RI $\alpha$  subunit of protein kinase A. *J. Mol. Biol.* **2002**, 323, 377–386.
  - 23 Wang Y., Gross M.L.: Application of hydrogen exchange and electrospray ionization mass spectrometry in studies of protein structure and dynamics, in *Applied Electrospray Mass Spectrometry (Practical Spectroscopy)*, ed. Pramanik BN, Ganguly AK, Gross ML **2002**, pp 389–410.
  - 24 Hamuro Y., Zawadzki K.M., Kim J.S., Stranz D., Taylor S.S., Woods V.L. Jr: Dynamics of cAPK type II $\beta$  activation revealed by enhanced amide H/2H exchange mass spectrometry (DXMS). *J. Mol. Biol.* **2003**, 327, 1065–1076.
  - 25 Hamuro Y., Anand G., Kim J., Juliano C., Stranz D., Taylor S., Woods V.L. Jr: Mapping intersubunit interactions of the regulatory subunit (RI $\alpha$ ) in the type I holoenzyme of protein kinase A by amide hydrogen/deuterium exchange mass spectrometry (DXMS). *J. Mol. Biol.* **2004**, 340, 1185–1196.
  - 26 Burns-Hamuro L., Hamuro Y., Kim J., Sigala P., Fayos R., Stranz D., Jennings P., Taylor S., Woods V.L. Jr: Distinct interaction modes of an AKAP bound to two regulatory subunit isoforms of protein kinase A revealed by amide hydrogen/deuterium exchange. *Protein Sci.* **2005**, 14, 2982–2992.
  - 27 Begley M.J., Taylor G.S., Brock M.A., Ghosh P., Woods V.L. Jr, Dixon J.E.: Molecular basis for substrate recognition by MTMR2, a myotubularin family phosphoinositide phosphatase. *Proc. Natl Acad. Sci. USA* **2006**, 103, 927–932.
  - 28 Derunes C., Burgess R., Iraheta E., Kellerer R., Becherer K., Gessner C.R., Li S., Hewitt K., Vuori K., Pasquale E.B., et al.: Molecular determinants for interaction of SHEP1 with Cas localize to a highly solvent-protected region in the complex. *FEBS Lett.* **2006**, 580, 175–178.
  - 29 Melnyk R.A., Hewitt K.M., Lacy D.B., Lin H.C., Gessner C.R., Li S., Woods V.L. Jr, Collier R.J.: Structural determinants for the binding of anthrax lethal factor to oligomeric protective antigen. *J. Biol. Chem.* **2006**, 281, 1630–1635.
  - 30 Hernandez H., Robinson C.V.: Dynamic protein complexes: insights from mass spectrometry. *J. Biol. Chem.* **2001**, 276, 46685–46688.
  - 31 Kaltashov I.A., Eyles S.J.: Crossing the phase boundary to study protein dynamics and function: combination of amide hydrogen exchange in solution and ion fragmentation in the gas phase. *J. Mass Spectrom.* **2002**, 37, 557–565.
  - 32 Hoofnagle A.N., Resing K.A., Ahn N.G.: Protein analysis by hydrogen exchange mass spectrometry. *Annu. Rev. Biophys. Biomol. Struct.* **2003**, 32, 1–25.
  - 33 Hamuro Y., Weber P.C., Griffin P.R.: High throughput analysis of protein structure by H/D exchange (H/D-Ex) mass spectrometry, in *Industrial Proteomics*, ed. Figey D., John Wiley & Sons, New York, **2005**.
  - 34 Bai Y., Milne J.S., Mayne L.C., Englander S.W.: Primary structure effects on peptide group hydrogen exchange. *Proteins Struct. Funct. Genet.* **1993**, 17, 75–86.
  - 35 Goshe M.B., Anderson V.E.: Hydroxyl radical-induced hydrogen/deuterium exchange in amino acid carbon-

- hydrogen bonds. *Radiat. Res.* **1999**, 151, 50–58.
- 36 Hilser V.J., Freire E.: Structure-based calculation of the equilibrium folding pathway of proteins. Correlation with hydrogen exchange protection factors. *J. Mol. Biol.* **1996**, 262, 756–772.
  - 37 Zhang Z., Post C.B., Smith D.L.: Amide hydrogen exchange determined by mass spectrometry: application to rabbit muscle aldolase. *Biochemistry* **1996**, 35, 779–791.
  - 38 Englander S.W., Kallenbach N.R.: Hydrogen exchange and structural dynamics of proteins and nucleic acids. *Q. Rev. Biophys.* **1984**, 16, 521–655.
  - 39 Sivaraman T., Arrington C.B., Robertson A.D.: Kinetics of unfolding and folding from amide hydrogen exchange in native ubiquitin. *Nat. Struct. Biol.* **2001**, 8, 331–333.
  - 40 Woods V.L. Jr: Method for characterization of the fine structure of protein binding sites employing amide hydrogen exchange. U.S. Patent 5 658 739, **1997**.
  - 41 Woods V.L. Jr: Method for characterization of the fine structure of protein binding sites using amide hydrogen exchange. U.S. Patent 6 331 400, **2001**.
  - 42 Woods V.L. Jr, Hamuro Y.: High resolution, high-throughput amide deuterium exchange-mass spectrometry (DXMS) determination of protein binding site structure and dynamics: utility in pharmaceutical design. *J. Cell. Biochem.* **2001**, S37, 89–98.
  - 43 Woods V.L. Jr: Methods for the high-resolution identification of solvent-accessible amide hydrogens in polypeptides or proteins and for the characterization of the fine structure of protein binding sites. U.S. Patent 6 291 189, **2001**.
  - 44 Pantazatos D., Kim J.S., Klock H.E., Stevens R.C., Wilson I.A., Lesley S.A., Woods V.L. Jr: Rapid refinement of crystallographic protein construct definition employing enhanced hydrogen/deuterium exchange MS. *Proc. Natl Acad. Sci. USA* **2004**, 101, 751–756.
  - 45 Englander J., Del Mar C., Li W., Englander S., Kim J., Stranz D., Hamuro Y., Woods Jr. V.: Protein structure change studied by hydrogen-deuterium exchange, functional labeling, and mass spectrometry. *Proc. Natl Acad. Sci. USA* **2003**, 100, 7057–7062.
  - 46 Yan X., Zhang H., Watson J., Schimerlik M.I., Deinzer M.L.: Hydrogen/deuterium exchange and mass spectrometric analysis of a protein containing multiple disulfide bonds: solution structure of recombinant macrophage colony stimulating factor-beta (rhM-CSFb). *Protein Sci.* **2002**, 11, 2113–2124.
  - 47 Wang L., Smith D.L.: Downsizing improves sensitivity 100-fold for hydrogen exchange-mass spectrometry. *Anal. Biochem.* **2003**, 314, 46–53.
  - 48 Lanman J., Lam T.T., Barnes S., Sakalian M., Emmett M.R., Marshall A.G., Prevelige P.E.: Identification of novel interactions in HIV-1 capsid protein assembly by high-resolution mass spectrometry. *J. Mol. Biol.* **2003**, 325, 759–772.
  - 49 Akashi S., Takio K.: Melittin-diacylphosphatidylcholine interaction examined by electrospray ionization fourier transform ion cyclotron resonance mass spectrometry. *J. Mass Spectrom. Soc. Jpn* **2002**, 50, 67–71.
  - 50 Wright P.E., Dyson H.J.: Intrinsically unstructured proteins: re-assessing the protein structure–function paradigm. *J. Mol. Biol.* **1999**, 293, 321–331.
  - 51 Spraggon G., Pantazatos D., Klock H.E., Wilson I.A., Woods V.L. Jr, Lesley S.A.: On the use of DXMS to produce more crystallizable proteins: structures of the *T. maritima* proteins TM0160 and TM1171. *Protein Sci.* **2004**, 13, 3187–3199.
  - 52 Yu B., Edstrom W.C., Benach J., Hamuro Y., Weber P.C., Gibney B.R., Hunt J.F.: Crystal structures of catalytic complexes of the oxidative DNA/RNA repair enzyme AlkB. *Nature* **2006**, 439, 879–884.

- 53 DeFelippis M.R., Kilcomons M.A., Lents M.P., Youngman K., Havel H.A.: Acid stabilization of human growth hormone equilibrium folding intermediates. *Biochim. Biophys. Acta* **1995**, 1247, 35–45.
- 54 Schieven G.L.: The biology of p38 kinase: a central role in inflammation. *Curr. Top. Med. Chem.* **2005**, 5, 921–928.
- 55 Wang Z., Canagarajah B.J., Boehm J.C., Kassisa S., Cobb M.H., Young P.R., Abdel-Meguid S., Adams J.L., Goldsmith E.J.: Structural basis of inhibitor selectivity in MAP kinases. *Structure* **1998**, 6, 1117–1128.
- 56 Hamuro Y., Coales S.J., Morrow J., Griffin P.R., Southern M.R., Weber P.C.: Application of hydrogen/deuterium-exchange to p38 mitogen-activated protein kinase. *Am. Biotechnol. Lab.* (in press).
- 57 Wilson K.P., Fitzgibbon M.J., Caron P.R., Griffith J.P., Chen W., McCaffrey P.G., Chambers S.P., Su M.S.-S.: Crystal structure of p38 mitogen-activated protein kinase. *J. Biol. Chem.* **1996**, 271, 29696–27700.
- 58 Hamuro Y., Wong L., Shaffer J., Kim J.S., Jennings P.A., Adams J.A., Woods V.L. Jr: Phosphorylation-driven motion in the COOH-terminal Src kinase, Csk, revealed through enhanced hydrogen–deuterium exchange and mass spectrometry (DXMS). *J. Mol. Biol.* **2002**, 323, 871–881.
- 59 Brzozowski A.M., Pike A.C., Dauter Z., Hubbard R.E., Bonn T., Engstrom O., Ohman L., Greene G.L., Gustafsson J.A., Carlquist M.: Molecular basis of agonism and antagonism in the oestrogen receptor. *Nature* **1997**, 389, 753–758.
- 60 Pike A.C., Brzozowski A.M., Hubbard R.E., Bonn T., Thorsell A.G., Engstrom O., Ljunggren J., Gustafsson J.A., Carlquist M.: Structure of the ligand-binding domain of oestrogen receptor beta in the presence of a partial agonist and a full antagonist. *EMBO J.* **1999**, 18, 4608–4618.
- 61 Johnson B.A., Wilson E.M., Li Y., Moller D.E., Smith R.G., Zhou G.: Ligand-induced stabilization of PPARgamma monitored by NMR spectroscopy: implications for nuclear receptor activation. *J. Mol. Biol.* **2000**, 298, 187–194.
- 62 Berger J.P., Petro A.E., Macnaul K.L., Kelly L.J., Zhang B.B., Richards K., Elbrecht A., Johnson B.A., Zhou G., Doebber T.W., et al.: Distinct properties and advantages of a novel peroxisome proliferator-activated protein [gamma] selective modulator. *Mol. Endocrinol.* **2003**, 17, 662–676.
- 63 Kallenberger B.C., Love J.D., Chatterjee V.K., Schwabe J.W.: A dynamic mechanism of nuclear receptor activation and its perturbation in a human disease. *Nat. Struct. Biol.* **2003**, 10, 136–140.
- 64 Hamuro Y., Coales S.J., Morrow J.A., Molnar K.S., Tuske S.J., Southern M.R., Griffin P.R.: Hydrogen/deuterium-exchange (H/D-Ex) of PPAR LBD in the presence of various modulators. *Protein Sci.* (submitted).
- 65 Whitty A., Kumaravel G.: Between a rock and a hard place? *Nat. Chem. Biol.* **2006**, 2, 112–118.
- 66 Clackson T., Wells J.A.: A hot spot of binding energy in a hormone–receptor interface. *Science* **1995**, 267, 383–386.
- 67 Arkin M.R., Wells J.A.: Small-molecule inhibitors of protein–protein interactions: progressing towards the dream. *Nat. Rev. Drug Discov.* **2004**, 3, 301–317.
- 68 Arkin M.R., Randal M., DeLano W.L., Hyde J., Luong T.N., Oslob J.D., Raphael D.R., Taylor L., Wang J., McDowell R.S., et al.: Binding of small molecules to an adaptive protein–protein interface. *Proc. Natl Acad. Sci. USA* **2003**, 100, 1603–1608.
- 69 Woods V.L. Jr: Methods for identifying hot-spot residues of binding proteins and small compounds that bind to the same. U.S. Patent 6 599 707, **2003**.

## **Part V**

### **MS in early pharmacokinetics**





## 13

### Mass Spectrometry in Early Pharmacokinetic Investigations

*Walter A. Korfmacher*

#### 13.1

##### Introduction

One of the challenges for the medicinal chemist in the new drug discovery process is the need to find a new chemical entity (NCE) that has the right combination of properties that satisfies the long list of requirements that is put on any molecule that is being brought forward as a compound that is suitable for development. In the past, if a compound showed pharmacological activity in the animal model, that was sufficient for progressing the NCE into development. Currently, lead optimization includes subjecting the current lead compounds to a series of drug metabolism and pharmacokinetic (DMPK) tests in order to improve the chances that the NCE selected for development will not fail for pharmacokinetic (PK) reasons when it gets into the clinic.

This newer strategy of testing the PK parameters as part of the lead optimization phase of new drug discovery has proven to be effective. As reported recently by Frank and Hargreaves [1], the reasons for attrition of new chemical entities (NCEs) during the clinical development phase changed between 1991 and 2000. In 1991, the major reason for failure of an NCE in clinical development was due to (human) PK issues, which accounted for 40% of the failures. In 2000, PK issues accounted for less than 10% of the failures in the clinical phase. This dramatic shift was due in large part to the fact that most major pharmaceutical companies added DMPK requirements to the lead optimization phase of new drug discovery, thereby improving the DMPK characteristics of the NCEs that were subsequently recommended for development.

One view of how to implement this newer strategy of adding DMPK requirements to the new drug discovery process is shown in Fig. 13.1. Figure 13.1 shows the stages of new drug discovery that lead up to the clinical phase. In this view, compounds must pass through a series of screens that sift out the problem compounds until a small number have been selected for more rigorous testing in the development phase. The series of screens is organized so that the earlier screens are higher throughput assays while the later screens are those that require significantly more resources to complete the study. One common feature that most of

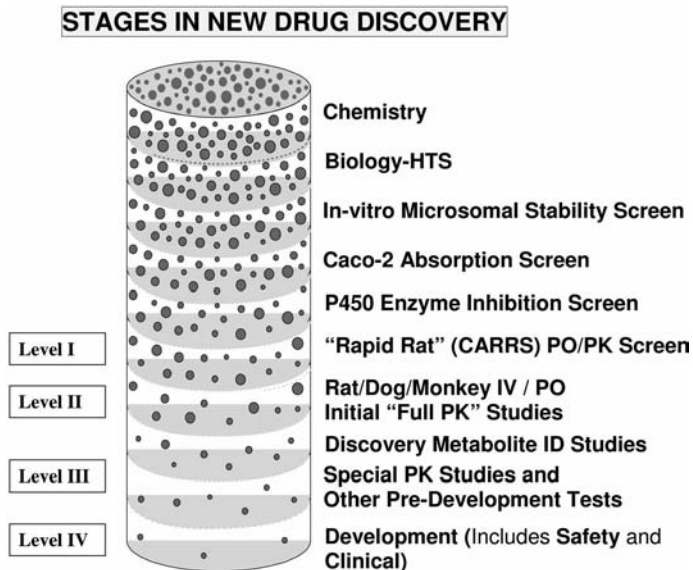


**Fig. 13.1** Stages of new drug discovery. This figure shows the various screens that could be used to select the compounds that proceed into development. At the top is Chemistry where many compounds are produced. After each screen, fewer compounds remain. Adapted from [6], used with permission from Taylor and Francis Group.

these screens share is that the analytical step in the screen is typically performed via high performance liquid chromatography–tandem mass spectrometry (HPLC-MS/MS) [2–11].

From a DMPK perspective, a common goal is to be able to compare multiple compounds based on their absorption, distribution, metabolism and excretion (ADME) properties as well their preclinical PK properties [8, 12–22]. Therefore, lead optimization typically is performed as an iterative process that uses the DMPK data to select structural modifications that are then tested to see whether the DMPK properties of the series have been improved. This iterative process is shown schematically in Fig. 13.2. Clearly an important element for the successful lead optimization of a series of NCEs is the ability to perform the DMPK assays in a higher throughput manner. The focus of this chapter will be to discuss ways that mass spectrometry (MS), particularly HPLC-MS/MS can be used to support the early PK studies for NCEs in a higher throughput manner.

## 13.2

### HPLC-MS/MS Overview

HPLC-MS/MS has been described as the premier analytical tool for drug metabolism participation in the new drug discovery process and has been applied to a

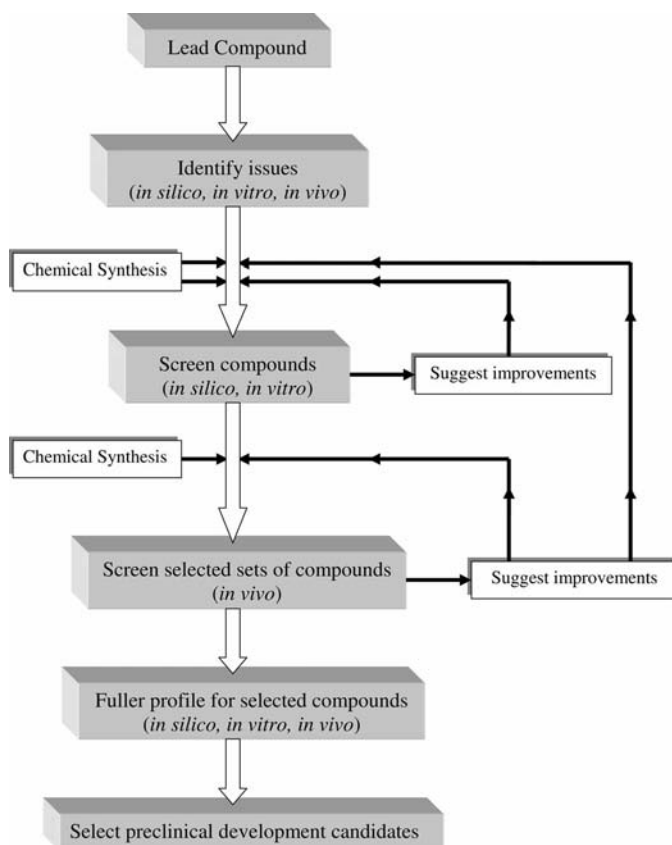


**Fig. 13.2** Schematic diagram showing the various stages and the iterative steps involved in the lead optimization process from a DMPK perspective. This schematic represents the iterative process that is an important part of the lead optimization process. The *in vitro* and *in vivo* screens refer to DMPK assays. Reprinted from [12], with permission from Taylor and Francis Group.

variety of DMPK samples [4, 6, 8, 9, 11, 23–27]. A description of HPLC-MS/MS principles and instrumentation can be found in Chapter 1 of this book as well as in some recent review articles and books [2, 3, 9, 11, 23, 26, 28–31]. Briefly, as shown in Fig. 13.3, HPLC-MS/MS systems combine an HPLC system with a mass spectrometer with the whole system under the control of a personal computer. While the most commonly used MS/MS system is the triple quadrupole mass spectrometer, there are now a variety of additional “hybrid” MS/MS systems that can be utilized for various drug discovery applications, including some DMPK applications. A discussion of various “hybrid” MS/MS systems can be found in Chapter 1 as well as in recent articles and other book chapters [9, 11, 32–38].

## Elements of an HPLC-MS/MS System

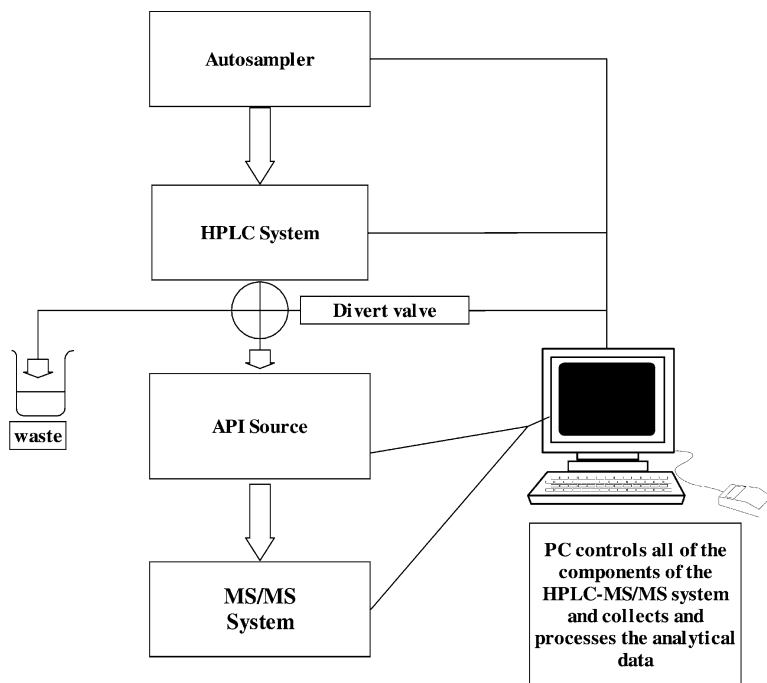


**Fig. 13.3** Elements of an HPLC-MS/MS system including the autosampler, the HPLC, a switching valve, the API ionization source and the MS/MS system. Typically, these are all controlled by a single PC that also serves as the data collection tool.

For the analysis of samples from discovery PK studies, the HPLC-MS/MS system will typically be based on a triple quadrupole mass spectrometer for the MS/MS part of the system [4, 6]. The reason that a triple quadrupole mass spectrometer is commonly used for bioanalytical assays is because it has the capability of operating in the selected reaction monitoring (SRM) mode. In SRM, analyte molecules are ionized by the atmospheric pressure ionization (API) source and the first quadrupole (Q1) is used to select the analyte ion (typically this will be the protonated molecule); the analyte ion is then fragmented in the collision cell (Q2) and the selected product ion is monitored via the third quadrupole (Q3). This mode of operation and its high degree of selectivity was first reported by Brotherton and Yost [39] in 1983; SRM has been used in conjunction with the separation capabilities of HPLC to produce an analytical tool that can be utilized to produce high quality data in a high throughput environment (see Chapter 1 for more on this topic).

### 13.3

#### **In Vitro Applications**

As shown in Fig. 13.1, part of the DMPK lead optimization process would include various *in vitro* assays used to screen out compounds before they would be considered for the (*in vivo*) PK studies [14, 40–42]. Kassel has provided an overview of strategies that can be used for increasing the throughput of these *in vitro* assays [16]. Typical *in vitro* screens would include microsomal stability, Caco-2 assay and p450 enzyme inhibition studies [14, 15, 18, 20, 22, 43–48]. Microsomal stability is used to give an indication of a compound's metabolic stability (this can also be done by using hepatocytes) [18, 22, 44, 49]. An early example of a higher throughput microsomal stability assay was described by Korfmacher et al. [50] in 1999; in this assay, the HPLC-MS analysis step was automated and the system was able to handle 75 compounds per week. A more recent example is described by Di et al. [51] who used robotic separation and a rapid HPLC-MS/MS system. A very high throughput highly automated microsomal stability assay has been reported by Xu et al. [52]; this assay had the capacity to handle up to 176 compounds per day. This system used a high throughput eight-channel parallel HPLC system along with intelligent software to process the data.

The Caco-2 cell monolayer permeability assay is one of the standard *in vitro* assays that are used to predict human absorption of NCEs [16, 22, 40, 43, 53–55]. The Caco-2 cell assay measures the permeability potential for a compound and can be used to help sort through large numbers of compounds. While various robotic procedures have been developed to perform the Caco-2 assay, it is now common to use HPLC-MS/MS to assay the samples that are produced in the procedure [53]. There have been several reports in the literature on various ways to use HPLC-MS/MS for Caco-2 assays [56–60]. For example, Fung et al. [57] described a procedure for higher throughput Caco-2 sample analysis that made use of the multiplexed electrospray interface (MUX) that can handle four parallel HPLC systems that are then monitored by a single MS/MS system. By using generic fast gradient HPLC conditions and special software for data processing, the one LC-MS/MS system could be used to assay the samples from 100 NCEs per week. In another example, Hakala et al. [58] discussed the possibility of performing Caco-2 assays on a mixture of compounds instead of the normal single compound studies. In addition, Hakala et al. [58] compared the utility of using electrospray ionization (ESI) to atmospheric pressure photoionization (APPI) for this application; the authors concluded that APPI provided a bigger linear quantitative range than was obtained from ESI (3–4 orders of magnitude vs 2–3 orders of magnitude, respectively).

Another higher throughput *in vitro* assay is the human cytochrome P450 enzyme inhibition assay. This assay is used to make sure that a compound does not have the potential for producing drug–drug interactions in a clinical setting due to the inhibition of one or more human P450 isozymes [61–66]. Often, these P450 assays are carried out in a higher throughput manner using 96-well plates

for sample preparation and combining multiple isozyme measurements into one-sample analysis. For example, Chu et al. [67] described an analysis based on HPLC-MS/MS that measured CYP2D6 and 3A4 using human liver microsomes. Bu et al. [68] reported that they were able to evaluate the inhibition potential for five P450 isozymes (CYP2D6, 3A4, 2A6, 2C9, 2E1) using a single assay based on human liver microsomes and five probe substrates. In another example, Testino and Patonay [69] validated an analysis for the high throughput inhibition screening of the five major P450 isozymes (CYP1A2, 2C9, 2C19, 2D6, 3A4) using human liver microsomes and HPLC-MS/MS for the assay [64]. Peng et al. [70] reported on the use of monolithic HPLC columns as part of an HPLC-MS/MS system that was used for high throughput screening of the same five major human cytochrome p450 isozymes; their HPLC-MS/MS assay was able to be completed in just 24 s, due to the higher flowrate capabilities of the monolithic column. Recently, Kim et al. [71] described a high throughput P450 enzyme inhibition assay based on HPLC-MS/MS that measures a compound's inhibition potential for nine p450 enzymes.

### 13.4

#### ***In Vivo* Applications**

While there are several high throughput *in vitro* screens as described above, there is still a significant need for *in vivo* assays as shown in Fig. 13.1. Several recent reports have discussed using HPLC-MS/MS for the bioanalytical step in discovery PK studies [5, 6, 8, 23, 72–74]. In the following sections, various aspects of the strategies that can be utilized in these *in vivo* studies are discussed. While the focus of this section will be on PK studies, another aspect of the lead optimization process is the understanding of the PK/pharmacodynamic (PD) relationships. While the topic of PK/PD is outside the scope of this chapter, the interested reader is directed to articles by Rohatigi or Chaikin et al. [75–77] for more information on this important topic. Finally, a discussion of metabolite identification methods and new technologies will also be included.

One of the issues that is still debated is whether or not to use cassette dosing as a way to increase the throughput for discovery PK studies. As shown in Fig. 13.4, cassette dosing (also called N-in-one dosing) is the practice of dosing multiple NCEs into one laboratory animal and then collecting blood samples from the animal and using HPLC-MS/MS for analysis of the samples [78]. It is the ability of HPLC-MS/MS to assay multiple compounds in one sample that has allowed this technique to be utilized. As discussed recently by Manitpisitkul and White [78], although cassette dosing is still used by about half of the major pharmaceutical companies, it does have problems that should be considered before implementing it as part of a drug discovery strategy. For example, drug–drug interactions between the multiple compounds dosed into one animal can lead to erroneous PK conclusions for one or more of the dosed compounds. Indeed, the possibility of drug–drug interactions from cassette dosing was proposed previously by White

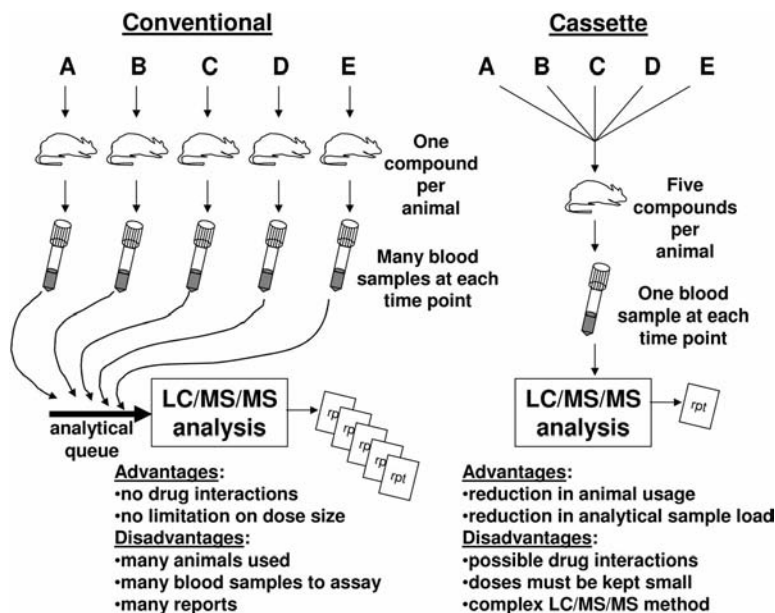


**Fig. 13.4** Conventional dosing vs cassette dosing. In conventional dosing, only one compound is dosed in each rat; in cassette dosing, multiple compounds are dosed in each rat. Adapted from [78], with permission from Elsevier.

and Manitpisitkul [79], who predicted that cassette dosing would lead to both false positive as well as false negative values for certain PK parameters. This prediction was confirmed recently by Smith et al. [80], who reported on problems with using cassette dosing to assess PK parameters for a group of compounds in mice. There are also practical issues with the cassette dosing approach. For example, it is important to make sure that the dosed compounds are not isomers that would likely be difficult to assay in a mixture. Some researchers also try to make sure that compounds are not within 14–16 Da from another dosed compound, so that +16 Da or –14 Da metabolites cannot interfere with the assay of a co-dosed compound [81]. There can also be formulation issues – often single compounds produce poor oral suspensions such that a mixture of these poorly soluble compounds might result in a formulation that is not suitable for dosing.

In spite of these concerns, there are still groups that find cassette dosing to be a useful strategy. For example, Ohkawa et al. [82] described using cassette dosing for 200 compounds in 50 cassettes. Zhang et al. [83] have reported the use of cassette dosing for measuring brain and plasma levels as part of new drug discovery. In their study, three or four compounds were grouped in a cassette and were dosed as a mixture to rats. Tamvakopoulos et al. [81] reported on the use of cassette dosing in rats in order to measure brain/plasma (B/P) ratios as part of a screening process; in their study, they found that the B/P ratios were largely un-



affected when using the cassette dosing method. More recently, Zhang et al. [83] discussed the use of cassette dosing in rats in order to get B/P ratios for a series of discovery compounds; in this work, they also described the use of a fast chromatographic separation as part of the HPLC-MS/MS assay. Another recent example of cassette dosing was provided by Sadagopan et al. [84]; in their work, rats were dosed with a mixture of compounds either by intravenous (IV) or oral (PO) routes.

An alternative to cassette dosing, Korfmacher et al. [85] described the use of the cassette accelerated rapid rat screen (CARRS). CARRS uses cassettes of six compounds as the basis for a systematic higher throughput rat oral PK screen. The six compounds in a given cassette are selected by the medicinal chemists from one drug discovery team. This is not cassette dosing; instead, each compound is dosed into two rats that are sampled at six timepoints (0.5, 1, 2, 3, 4, 6 h) by the serial-bleeding procedure. The plasma samples from the two rats are pooled at each timepoint, so that each dosed compound results in six plasma samples to be assayed by HPLC-MS/MS. As described by Korfmacher et al. [85], all the samples and standards that are needed for the assay for the six dosed compounds in one cassette can be placed in a single 96-well plate. With current fast HPLC-MS/MS methods, the methods can be developed and the 96-well plate can be assayed in no more than a few days. The CARRS system was set up to accept multiple (originally five and recently up to eight) cassettes of six compounds on a weekly basis [78]. Therefore, this system allows multiple (currently up to eight) drug discovery teams to be able to select six NCE's for testing in this rapid PK screen each week [78]. Each week, all of the selected compounds are dosed by the drug discovery dosing group and the resulting plasma samples are delivered to the discovery bioanalytical group for analysis during the following week. Within two weeks of the compound selection request, electronic PK summary reports are issued to the discovery teams that requested the compounds to be dosed. The PK report shows the individual plasma concentrations for the six timepoints as well as the calculated area under the curve (AUC) for each dosed compound in an Excel format. Because it is a discrete dosing procedure, it avoids the potential problems of cassette dosing (*vide supra*) while still providing a systematic process for testing multiple NCEs in an *in vivo* PK model. This higher throughput assay has continued to be very useful as a rat oral PK screen; in the first four years that it was in place, CARRS was used to screen over 7000 compounds [78].

### 13.5

#### Rapid Method Development

A stepwise procedure for rapid HPLC-MS/MS method development that was described recently by Xu et al. [10] is shown in Fig. 13.5. As shown in Fig. 13.5, there are three proposed checkpoints that are used to test the assay before it is used for the actual PK samples. If the assay (HPLC-MS/MS procedure) passes a

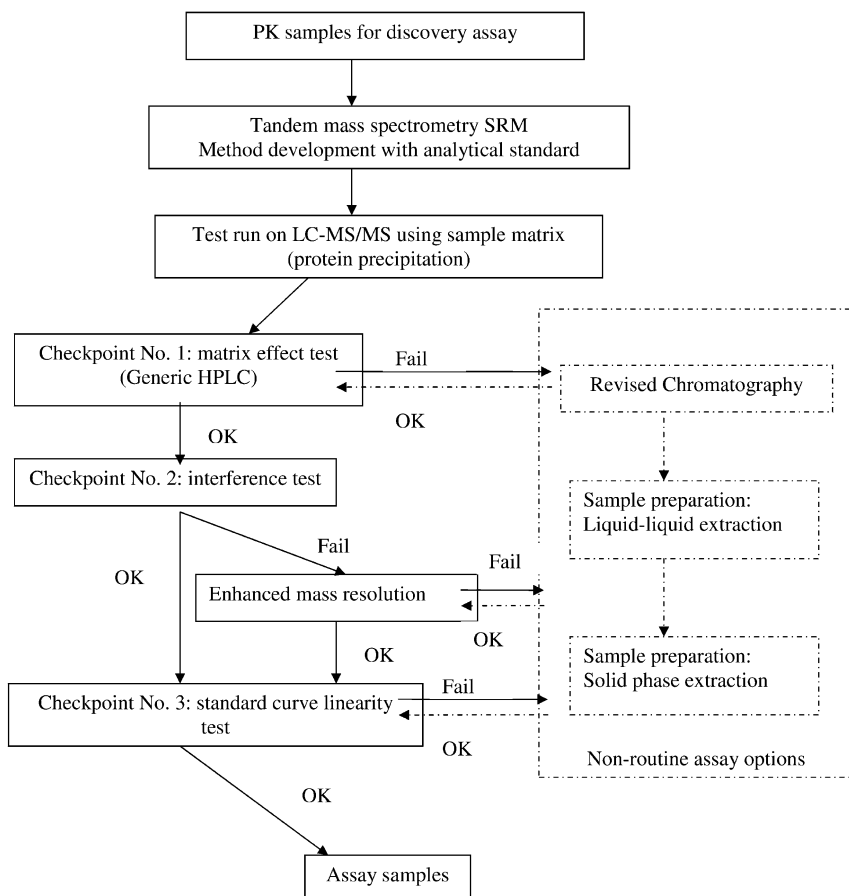


**Fig. 13.5** A schematic diagram showing the stepwise procedure for rapid method development of HPLC-MS/MS methods for discovery PK assays. Adapted from [10], with permission from the American Chemical Society.

checkpoint, then it moves to the next checkpoint; if it fails, then there are potential remedies to address the problem as shown in the schematic. The concept behind this schematic is that most discovery PK assays will pass all of the three checkpoints and can then be used for the sample analysis. When the method is used for sample analysis, then there needs to be additional rules to determine whether or not the assay is suitable, so that the results can be reported. While discovery PK assays are not bound by the rules of good laboratory practice (GLP), Korfmacher [6] has proposed a set of rules (*vide infra*) that can be used for various types of discovery PK assays.

### 13.6

#### Increasing Throughput in HPLC-MS/MS

Several reports have discussed the utility of increasing the speed of HPLC-MS/MS by using various techniques [6, 28, 72, 86–96]. Typical strategies make use of advances in chromatographic columns. For example, Hsieh et al. [97] describe the use of small HPLC columns and a fast HPLC gradient to provide a method for assaying a compound in a discovery PK study in about one minute per sample. In a report by Tiller and Romanyshyn [98], the authors stated that fast gradients were generally better than isocratic HPLC systems at keeping the HPLC column clean. Recently, Dunn-Meynell et al. [99] reported on the development of a fast generic HPLC method that could be used for discovery PK studies; the method was tested specifically for its ability to be used for CARRS samples. The method used a generic 1-min ballistic gradient and an optimized autosampler method that results in an 85-s cycle time (time from injection to injection). Using this methodology, one could assay a set of 96 samples in less than 2.5 h.

Another area of some interest has been the development of monolithic HPLC columns. These columns are unusual in that they can be used under higher flow rate conditions [86, 95, 100–107]. In some applications, these columns have been used for HPLC-MS/MS assays where the flow rate was set to 5–6 mL min<sup>-1</sup>. This higher flow rate allows one to get higher sample throughput by reducing the gradient time. For example, Hsieh et al. [86] demonstrated that HPLC gradients could be completed in 30 s by using monolithic columns. One disadvantage of these columns is that the high flow rates translate into a much higher use of mobile phase solvents and the need to dispose of them as waste solvents after they have been used.

Another approach for speeding up sample throughput has been the use of parallel HPLC columns. This was first explored by Korfmacher et al. [108], who demonstrated that the effluent from two HPLC systems could be combined and assayed by using the SRM capabilities of the MS/MS system. Jemal et al. [109] also demonstrated that two parallel HPLC systems could be combined for analysis using one MS/MS system. This parallel HPLC technology was further enhanced by the development of the MUX system, in which four HPLC columns could be assayed by a single triple quadrupole MS/MS system [52, 57, 110]. Another variation that has been used more recently is the staggered parallel analysis strategy. Using the staggered strategy, multiple HPLC columns (typically four) are used to assay samples, but the injection time is staggered so that the “analytical window” (the portion of the chromatographic procedure) can be selected sequentially in order to maximize the use of the MS/MS system and increase sample throughput [111, 112]. For example, King et al. [112] described a four column staggered HPLC-MS/MS system that was able to be validated to meet GLP standards for a bioanalytical assay. In this example, the assay throughput was increased almost four-fold while still maintaining good chromatographic resolution [112].

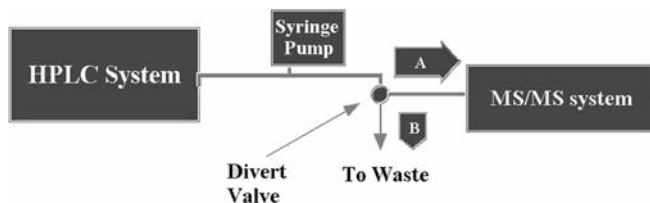
In addition to increasing throughput, researchers are finding ways to utilize the increased sensitivity of the new HPLC-MS/MS systems. For example, Xu et al. [113] recently described the development of a low sample volume assay for preclinical studies. In this assay, only a 10- $\mu$ L plasma sample volume is required for the analysis. The small volume is prepared by protein precipitation (1:6 = plasma:acetonitrile) using a special low volume 96-well plate. Only 5  $\mu$ L of the precipitated sample is injected onto the HPLC-MS/MS system. In spite of these low volumes, the example assay is reported to have a limit of quantitation (LOQ) of 0.1 ng mL<sup>-1</sup>. It can be predicted that there will be more reports of improved LOQs and reduced sample volumes as new LC-MS/MS instrumentation is introduced to more laboratories.

### 13.7

#### Matrix Effects

As scientists have shortened assay times by using shorter columns or higher mobile phase flow rates (*vide supra*), a new problem has become more apparent. This problem is often referred to as “matrix effects”. Matrix effects can be described as a component in the sample that is injected into the HPLC-MS/MS system that results in a reduction of the analyte signal (aka ion suppression) or an increase in analyte signal. There have been multiple papers written on various aspects of matrix effects in recent years [97, 114–124]. The problem that can be caused by matrix effects (if undetected) is that they can lead to erroneous results in a bio-analytical assay. One of the best ways to test a bioanalytical method for matrix effects is to use the post-column analyte infusion method as shown schematically in Fig. 13.6. The post-column infusion method was described by King et al. [121] in their report on ionization suppression and the possible causes and solutions of this problem. Briefly, in the post-column infusion method, one has a constant infusion of the analyte into the post-column eluant, this provides a steady signal of the analyte; the comparison is made by injecting either a mobile phase aliquot or a sample from control matrix that has been prepared using the sample preparation procedure [6, 97, 121, 124]. The resulting two chromatograms can be prepared and the difference is attributed to matrix effects. For example, as shown in Fig. 13.7, Dunn-Meynell et al. [99] used the post-column infusion technique to ensure that a generic ballistic gradient would be free from matrix effects in the part of the chromatogram where the analytes would be expected to elute; in this example, the generic HPLC-MS/MS method should be unaffected by matrix effects.

While matrix effects are generally attributed to sample constituents, sample preparation can also lead to matrix effects. Mei et al. [115, 124] demonstrated that matrix effects could be caused by the brand of sample tubes that are used in the sample storage step of the assay. In this example, the solution was to switch to a different supplier for the tubes. In addition, while it is generally reported that



#### Post-column Infusion Experiment:

1. Inject mobile phase or solvent blank while infusing analyte into the column eluant at a flow rate of 5 - 10  $\mu\text{L}/\text{min}$  and follow path A.
2. Inject control sample extract while infusing analyte into the column eluant at a flow rate of 5 - 10  $\mu\text{L}/\text{min}$  and follow path A.
3. Compare the mass chromatograms--differences are due to matrix effects.

#### Analysis of samples:

1. Inject sample (syringe pump off) and divert the flow to waste (path B) for the first 10-25% of the assay run time, then switch the divert valve to send the eluant into the MS/MS system (path A) for the analysis of the sample.

**Fig. 13.6** Post-column infusion technique as part of the HPLC-MS/MS system. Adapted from [9], with permission from Elsevier.

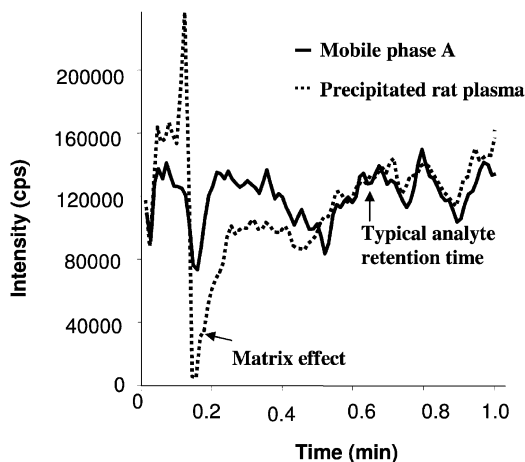


**Fig. 13.7** Post-column infusion study of a ballistic gradient. The matrix effects can be seen at the early part of the chromatogram, but the later part of the chromatogram where the analytes should elute did not show matrix effects. Adapted from [99], with permission from John Wiley and Sons.

ESI is more likely to exhibit matrix effects than is atmospheric pressure chemical ionization (APCI), Mei et al. [115, 124] reported that matrix effects could be seen in both APCI and ESI assays. In general, these matrix effects can be detected by using the post-column infusion technique as described above.

More recently, there have been reports of matrix effects that were caused by the formulation that was used in a preclinical PK study [6, 9, 119, 125–127]. For example, Shou and Naidong [125] used the post-column infusion technique to show that Tween 80 and PEG 400 (both commonly used as part of preclinical dosing formulations) could lead to significant matrix effects. As an example, they showed that if they used a fast HPLC-MS/MS method in a dog study where PEG 400 was used in the dosing formulation then a significant matrix ion suppression resulted and the analytical results were significantly in error for the plasma samples collected at timepoints up to 2 h. The authors reported that correct results could be obtained by extending the HPLC gradient so that the analyte and its internal standard eluted later and were outside of the matrix ion suppression “window”.

Xu et al. [119] discussed the problem of matrix effects caused by dosing formulation components in PK studies in a recent publication. Xu et al. [119] showed that using either Tween 80 or PEG 400 could lead to matrix effects for analytes that are very polar and elute early in a fast HPLC reversed phase method. In addition, Xu et al. [119] showed that these matrix effects were time-dependent; generally, early PK timepoints were more susceptible to these effects than were later PK timepoints. For example, as shown in Fig. 13.8, there was a time-dependent nature to the matrix effects caused by the Tween 80; the reason for this is that the amount of the Tween 80 in the plasma samples changed over the 24-h sampling time [119]. As shown in Fig. 13.8, the matrix effects were also dependent on the instrument vendor and the route of dosing the formulation. As discussed by Xu et al. [119], this problem could be avoided by not using Tween 80 or PEG 400 in formulations for PK studies. If these compounds have to be used in the formulation, then one should be careful when performing the HPLC-MS/MS assay on the samples that are obtained from the PK study. Generally, the matrix effect problem can be avoided by using a longer HPLC gradient or by doing a more extensive sample cleanup before performing the HPLC-MS/MS assay.

### 13.8

#### Discovery PK Assay Rules

While the rules that need to be followed when developing and using a bioanalytical assay in a GLP setting are well documented [128, 129], there is no standard set of rules to follow when one is developing or using a bioanalytical assay in a drug discovery setting. It is generally agreed that these nonGLP bioanalytical methods do not need to be validated before they can be used for the analysis of discovery (nonGLP) PK samples. This is important because the validation proce-

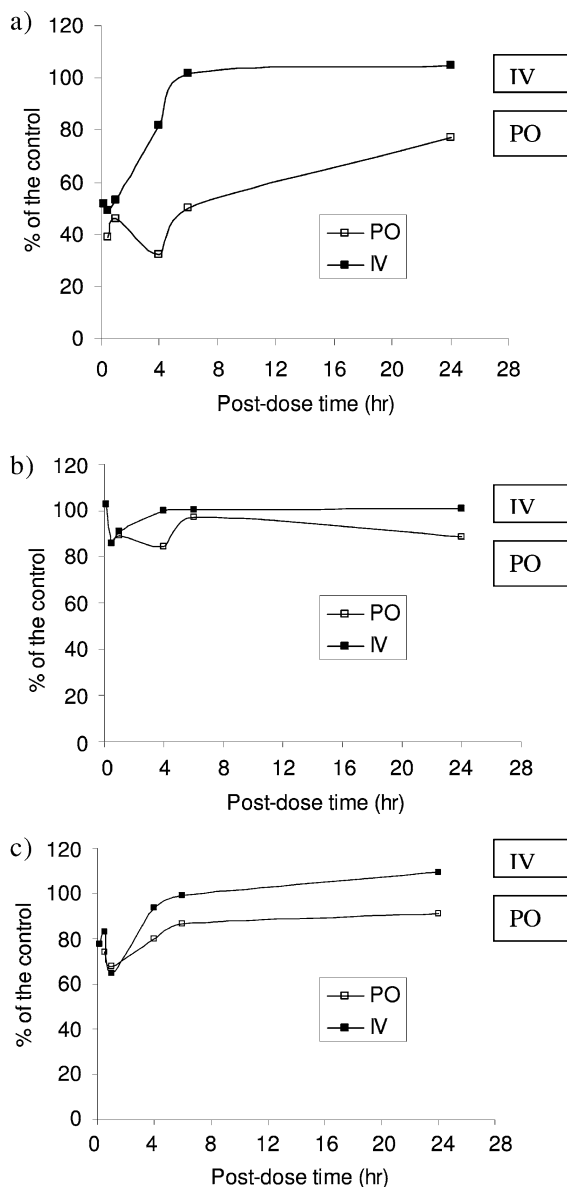


**Fig. 13.8** Time-dependent MS response for pseudoephedrine when 0.1% Tween 80 was used in the formulation that was dosed in the rats via either intravenous (IV) or *per os* (PO) routes. The HPLC-MS/MS assay was performed in the ESI mode using: (a) Thermo-Finnigan Quantum MS; (b) AB Sciex 3000 MS; (c) Waters-Micromass Quattro Ultima MS. The PK samples were spiked with

the pseudoephedrine after they were collected from the rats. The dip (below 100%) in the profiles shows the time-dependent nature of this type of matrix effect. It can be seen that the effect varied not only with time, but was also dependent on the instrument vendor and the dosing route. Adapted from [119], with permission from John Wiley and Sons.

ture can take 1–2 weeks to complete. Recently, Korfmacher [6] published a set of rules that can be followed for drug discovery PK assays. These rules are based on the concept of increasing the requirements that must be met depending upon the stage in the discovery process where the bioanalytical assay is to be utilized. Korfmacher [6] describes four stages in the drug discovery process (see Fig. 13.1): level I (compound screening), level II (lead optimization), level III (lead qualification) and level IV (development). When the compound is in the level IV development stage, GLP rules need to be followed in most cases (exceptions may be for certain exploratory studies or “bridging to development studies” where nonGLP assays can be used).

The rules for level I (screening) assays are shown in Table 13.1. An example of the type of samples where a level I assay could be used is the CARRS samples [85] that can be used for screening NCEs using a rat PK model (*vide supra*). The concept behind this assay is that it should use a small number of standards and a simple linear extrapolation. For level II assays (see Table 13.2) that might be used for discovery PK studies in preclinical species, a complete standard curve is required. In this case a complete standard curve is defined as 10–15 standards in duplicate assayed with at least five standards used in the final calibration curve. Neither level I nor level II assays require the use of quality control (QC) standards. When a compound is in the lead qualification stage, then a level III assay would be required. As shown in Table 13.3, the main distinction for level III assays is that they are required to include at least six QC standards. As described in Tables 13.1–13.3, these rules show the requirements for how an assay should be set up before the samples are assayed and then these rules describe the acceptance criteria for the assays after they have been performed.

## 13.9

### New Technology in LC-MS

As with any scientific endeavor, the field of LC-MS is continuing to evolve. New instrumentation and new technology provide new opportunities for increasing sample throughput or providing improved data quality. In this section, I will discuss some of these new technology advances and briefly state how they might be used for discovery DMPK applications. The types of advances that are described include those in either chromatography or mass spectrometry.

One of the more exciting new advances in the chromatography field is ultra-performance liquid chromatography (UPLC) [130, 131]. UPLC is a system where higher (than HPLC) pressure can be used, which allows one to use smaller (<2  $\mu\text{m}$ ) particles in the column with a resulting improvement in the chromatographic resolution. UPLC was introduced as a commercial product recently and was quickly adapted for use as part of the LC-MS field. Several recent reports on the utility of UPLC-MS/MS have been published [132–137] in the literature. For example, Castro-Perez et al. [136] describe the utility of UPLC-MS/MS for the analysis of *in vitro* drug metabolism samples; in their examples, it is clear that



**Table 13.1** Rules for discovery (nonGLP) “screen” assays (level I).  
Adapted from [6], with permission from Taylor and Francis Group.

- 
- 1 Samples should be assayed using HPLC-MS/MS technology.
  - 2 Sample preparation should consist of protein precipitation using an appropriate internal standard (IS).
  - 3 Samples should be assayed along with a standard curve in duplicate (at the beginning and end of the sample set).
  - 4 The zero standard is prepared and assayed, but is not included in the calibration curve regression.
  - 5 Standard curve stock solutions are prepared after correcting the standard for the salt factor.
  - 6 The standard curve should be three levels, typically ranging over 25–2500 ng mL<sup>-1</sup> (they can be lower or higher as needed for the program). Each standard is 10× the one below (thus, a typical set would be 25, 250, 2500 ng mL<sup>-1</sup>). The matrix of the calibration curve should be from the same animal species and matrix type as the samples.
  - 7 QC samples are not used and the assay is not validated.
  - 8 After the assay, the proper standard curve range for the samples is selected. This must include only two concentrations in the range that covers the samples. A single order of magnitude range is preferred, but two orders of magnitude is acceptable, if needed to cover the samples.
  - 9 Once the range is selected, at least three of the four assayed standards in the range must be included in the regression analysis. Regression is performed using unweighted linear regression (not forced through zero).
  - 10 All standards included in the regression set must be back-calculated to within 27.5% of their nominal values.
  - 11 The limit of quantitation (LOQ) may be set as either the lowest standard in the selected range or as 0.4× the lowest standard in the selected range, but the LOQ must be greater than three times the mean value for the back-calculated value of the two zero (0) standards.
  - 12 Samples below the LOQ are reported as zero (0).
  - 13 If the LOQ is 0.4× the lowest standard in the selected range, then samples with back-calculated values between the LOQ and the lowest standard in the selected range may be reported as their calculated value, provided the S/N for the analyte is at least three (3).
  - 14 Samples with back-calculated values between 1.0× and 2.0× the highest standard in the selected range are reportable by extending the calibration line up to 2× the high standard.
  - 15 Samples found to have analyte concentrations more than 2× the highest standard in the regression set are not reportable. These samples must be reassayed after dilution or along with a standard curve that has higher concentrations so that the sample is within 2× the highest standard.
-

**Table 13.2** Rules for discovery (nonGLP) “full PK” assays (level II).  
Adapted from [6], with permission from Taylor and Francis Group.

- 1 Samples should be assayed using HPLC-MS/MS technology.
- 2 Sample preparation should consist of protein precipitation using an appropriate internal standard (IS).
- 3 Samples should be assayed along with a standard curve in duplicate (at the beginning and end of the sample set).
- 4 The zero standard is prepared and assayed, but is not included in the calibration curve regression.
- 5 Standard curve stock solutions are prepared after correcting the standard for the salt factor.
- 6 The standard curve should be 10–15 levels, typically ranging from 1 to 5000 or 10 000 ng mL<sup>-1</sup> (or higher as needed). The matrix of the calibration curve should be from the same animal species and matrix type as the samples.
- 7 QC samples are not used.
- 8 After the assay, the proper standard curve range for the samples is selected; this must include at least five (consecutive) concentrations.
- 9 Once the range is selected, at least 75% of the assayed standards in the range must be included in the regression analysis.
- 10 Regression can be performed using weighted or unweighted linear or smooth curve fitting (e.g., power curve or quadratic), but is not forced through zero.
- 11 All standards included in the regression set must be back calculated to within 27.5% of their nominal values.
- 12 The regression  $r^2$  must be 0.94 or larger.
- 13 The limit of quantitation (LOQ) may be set as either the lowest standard in the selected range or as  $0.4\times$  the lowest standard in the selected range, but the LOQ must be greater than three times the mean value for the back-calculated value of the two zero (0) standards.
- 14 Samples below the LOQ are reported as zero (0).
- 15 If the LOQ is  $0.4\times$  the lowest standard in the selected range, then samples with back-calculated values between the LOQ and the lowest standard in the selected range may be reported as their calculated value provided the S/N for the analyte is at least three (3).
- 16 Samples with back-calculated values between  $1.0\times$  and  $2.0\times$  the highest standard in the selected range are reportable by extending the calibration curve up to  $2\times$  the high standard as long as the calibration curve regression was not performed using quadratic regression.
- 17 Samples found to have analyte concentrations more than  $2\times$  the highest standard in the regression set are not reportable. These samples must be reassayed after dilution or along with a standard curve that has higher concentrations so that the sample is within  $2\times$  the highest standard.

Table 13.2 (continued)

- 
- |    |   |
|----|---|
| 18 | The assay is not validated.   |
| 19 | The final data does not need to have quality assurance (QA) approval. This is an exploratory, nonGLP study. |
- 

the improved chromatographic resolution provided by the UPLC system allows the scientist to obtain better data from the sample analysis.

Another recent innovation is the QTrap mass spectrometer. The QTrap MS system combines the capabilities of a triple quadrupole mass spectrometer and a linear ion trap mass spectrometer into one MS system. Initially, the QTrap MS was used primarily as a tool for metabolite identification studies [34, 35, 38]. As reported by Li et al. [138], the QTrap MS can also be used as an excellent system for the quantitative analysis of discovery PK samples. The advantage of the QTrap MS system for quantitative analysis is that it can be used to look for plasma metabolites of the NCE and provide an easy way to monitor them while providing the quantitative data on the NCE.

Two more MS-related innovations are worth noting here: (1) higher mass resolution on a triple quadrupole mass spectrometer and (2) atmospheric pressure

Table 13.3 Additional rules for discovery (nonGLP) PK assays requiring QC samples (level III). Adapted from [6], with permission from Taylor and Francis Group.

- 
- |   |  |
|---|--|
| 1 | Use all the rules for “full PK – level II” assays (except rule 7) plus the following rules.  |
| 2 | Quality control (QC) standards are required and a minimum of six QCs at three concentrations (low, middle, high) are to be used. The QC standards should be frozen at the same freezer temperature as the samples to be assayed.   |
| 3 | The QC standards need to be traceable to a separate analyte weighing from the one used for the standard curve standards.   |
| 4 | The standard curve standards should be prepared on the same day the samples are prepared for assay – the standard curve solutions needed for this purpose may be stored in a refrigerator until needed for up to six months.   |
| 5 | At least two-thirds of the QC samples must be within 25% of their prepared (nominal) values.   |
| 6 | If dilution of one or more samples is required for this assay, then an additional QC at the higher level must be prepared, diluted and assayed along with the sample(s) needing dilution – this QC should be run in duplicate and at least one of the two assay results must meet the 25% criterion. |
-

photoionization (APPI). The higher mass resolution on a triple quadrupole mass spectrometer has been described in detail recently [88, 139, 140]. This new instrumentation provides an additional mass filtering capability that is not available on conventional triple quadrupole MS systems. It has been demonstrated that this enhanced mass resolution can be very helpful for discovery PK assays when one is approaching the limit of quantitation [88, 139, 140]. The APPI is a new ionization system that uses ultraviolet radiation as part of the ionization step [141–151]. The APPI source has the potential to provide improved sensitivity for those compounds that do not ionize well with either APCI or ESI. In a recent study by Cai et al. [143], the authors stated that APPI worked well for many non-polar compounds, including those that did not ionize well with either APCI or ESI sources.

### 13.10

#### Conclusion

The field of higher throughput discovery PK assays continues to evolve as new instrumentation and new challenges arise. It can be predicted that new technology will continue to improve the researcher's capabilities in this important step in the drug discovery process. Instrumentation will continue to get more sensitive and will be easier to automate in the future.

#### References

- 1 Frank, R.; Hargreaves, R.: Clinical biomarkers in drug discovery and development. *Nat Rev Drug Discov* **2003**, 2, 566–580.
- 2 Korfmacher, W.: *Using Mass Spectrometry for Drug Metabolism Studies*, CRC Press, Boca Raton, **2005**, 370 pp.
- 3 Lee, M. S.: *Integrated Strategies for Drug Discovery using Mass Spectrometry*, John Wiley & Sons, Hoboken, **2005**, 550 pp.
- 4 Korfmacher, W. A.; Cox, K. A.; Bryant, M. S.; Veals, J.; Ng, K.; et al.: HPLC-API/MS/MS: a powerful tool for integrating drug metabolism into the drug discovery process. *Drug Discov Today* **1997**, 2, 532–537.
- 5 Korfmacher, W. A.: Lead optimization strategies as part of a drug metabolism environment. *Curr Opin Drug Discov Dev* **2003**, 6, 481–485.
- 6 Korfmacher, W.: Bioanalytical assays in a drug discovery environment, in *Using Mass Spectrometry for Drug Metabolism Studies*, CRC Press, Boca Raton, **2005**, pp 1–34.
- 7 Olah, T. V.: The development and implementation of bioanalytical methods using LC-MS to support ADME studies in early drug discovery and candidate selection. *Ernst Schering Res Found Workshop* **2002**, 155–183.
- 8 Korfmacher, W.: New strategies for the implementation and support of bioanalysis in a drug metabolism environment, in *Integrated Strategies for Drug Discovery using Mass Spectrometry*, John Wiley & Sons, Hoboken, **2005**, pp 359–378.
- 9 Korfmacher, W. A.: Principles and applications of LC-MS in new drug

- discovery. *Drug Discov Today* **2005**, 10, 1357–1367.
- 10 Xu, X.; Lan, J.; Korfmacher, W.: Rapid LC/MS/MS method development for drug discovery. *Anal Chem* **2005**, 77, 389A–394A.
- 11 Lim, C. K.; Lord, G.: Current developments in LC-MS for pharmaceutical analysis. *Biol Pharm Bull* **2002**, 25, 547–557.
- 12 Roberts, S. A.: High-throughput screening approaches for investigating drug metabolism and pharmacokinetics. *Xenobiotica* **2001**, 31, 557–589.
- 13 Beresford, A. P.; Slick, H. E.; Tarbit, M. H.: The emerging importance of predictive ADME simulation in drug discovery. *Drug Discov Today* **2002**, 7, 109–116.
- 14 Eddershaw, P. J.; Beresford, A. P.; Bayliss, M. K.: ADME/PK as part of a rational approach to drug discovery. *Drug Discov Today* **2000**, 5, 409–414.
- 15 Jenkins, K. M.; Angeles, R.; Quintos, M. T.; Xu, R.; Kassel, D. B.; et al.: Automated high throughput ADME assays for metabolic stability and cytochrome P450 inhibition profiling of combinatorial libraries. *J Pharm Biomed Anal* **2004**, 34, 989–1004.
- 16 Kassel, D. B.: High throughput strategies for *in vitro* ADME assays: how fast can we go? in *Using Mass Spectrometry for Drug Metabolism Studies*, CRC Press, Boca Raton, **2005**.
- 17 O'Connor, D.: Automated sample preparation and LC-MS for high-throughput ADME quantification. *Curr Opin Drug Discov Dev* **2002**, 5, 52–58.
- 18 Thompson, T. N.: Early ADME in support of drug discovery: the role of metabolic stability studies. *Curr Drug Metab* **2000**, 1, 215–241.
- 19 Kumar, G. N.; Surapaneni, S.: Role of drug metabolism in drug discovery and development. *Med Res Rev* **2001**, 21, 397–411.
- 20 Riley, R. J.; Martin, I. J.; Cooper, A. E.: The influence of DMPK as an integrated partner in modern drug discovery. *Curr Drug Metab* **2002**, 3, 527–550.
- 21 Crowley, P. J.; Martini, L. G.: Enhancing oral absorption in animals. *Curr Opin Drug Discov Dev* **2004**, 4, 73–80.
- 22 Thompson, T. N.: Drug metabolism *in vitro* and *in vivo* results: how do these data support drug discovery, in *Using Mass Spectrometry for Drug Metabolism Studies*, CRC Press, Boca Raton, **2005**; pp 35–82.
- 23 Ackermann, B. L.; Berna, M. J.; Murphy, A. T.: Recent advances in use of LC/MS/MS for quantitative high-throughput bioanalytical support of drug discovery. *Curr Top Med Chem* **2002**, 2, 53–66.
- 24 Miller-Stein, C.; Bonfiglio, R.; Olah, T. V.; King, R. C.: Rapid method development of quantitative LC-MS/MS assays for drug discovery. *Am Pharm Rev* **2000**, 3, 54–61.
- 25 Oliveira, E. J.; Watson, D. G.: Liquid chromatography–mass spectrometry in the study of the metabolism of drugs and other xenobiotics. *Biomed Chromatogr* **2000**, 14, 351–372.
- 26 Rossi, D. T.; Sinz, M.: *Mass Spectrometry in Drug Discovery*, Marcel Dekker, New York, **2002**.
- 27 Kyranos, J. N.; Cai, H.; Wei, D.; Goetzinger, W. K.: High-throughput high-performance liquid chromatography/mass spectrometry for modern drug discovery. *Curr Opin Biotechnol* **2001**, 12, 105–111.
- 28 Hopfgartner, G.; Husser, C.; Zell, M.: High-throughput quantification of drugs and their metabolites in biosamples by LC-MS/MS and CE-MS/MS: possibilities and limitations. *Ther Drug Monit* **2002**, 24, 134–143.
- 29 Jemal, M.: High-throughput quantitative bioanalysis by LC/MS/MS. *Biomed Chromatogr* **2000**, 14, 422–429.
- 30 Lee, M. S.; Kerns, E. H.: LC/MS applications in drug development. *Mass Spectrom Rev* **1999**, 18, 187–279.
- 31 Siegel, M. M.: Early discovery drug screening using mass spectrometry. *Curr Top Med Chem* **2002**, 2, 13–33.
- 32 Fernandez-Metzler, C.; Subramanian, R.; King, R. C.: Application of technological advances in

- biotransformation studies, in *Integrated Strategies for Drug Discovery using Mass Spectrometry*, John Wiley & Sons, Hoboken, **2005**, pp 261–288.
- 33 Cox, K.: Special requirements for metabolite characterization, in *Using Mass Spectrometry for Drug Metabolism Studies*, CRC Press, Boca Raton, **2005**, pp 229–252.
  - 34 Hopfgartner, G.; Husser, C.; Zell, M.: Rapid screening and characterization of drug metabolites using a new quadrupole–linear ion trap mass spectrometer. *J Mass Spectrom* **2003**, 38, 138–150.
  - 35 Hopfgartner, G.; Varesio, E.; Tschappat, V.; Grivet, C.; Bourgoigne, E.; et al.: Triple quadrupole linear ion trap mass spectrometer for the analysis of small molecules and macromolecules. *J Mass Spectrom* **2004**, 39, 845–855.
  - 36 Leclercq, L.; Delatour, C.; Hoes, I.; Brunelle, F.; Labrique, X.; et al.: Use of a five-channel multiplexed electrospray quadrupole time-of-flight hybrid mass spectrometer for metabolite identification. *Rapid Commun Mass Spectrom* **2005**, 19, 1611–1618.
  - 37 Clarke, N. J.; Rindgen, D.; Korfmacher, W. A.; Cox, K. A.: Systematic LC/MS metabolite identification in drug discovery. *Anal Chem* **2001**, 73, 430A–439A.
  - 38 Hopfgartner, G.; Zell, M.: Q trap MS: a new tool for metabolite identification, in *Using Mass Spectrometry for Drug Metabolism Studies*, CRC Press, Boca Raton, **2005**.
  - 39 Brotherton, H. O.; Yost, R. A.: Determination of drugs in blood serum by mass spectrometry/mass spectrometry. *Anal Chem* **1983**, 55, 549–553.
  - 40 van De Waterbeemd, H.; Smith, D. A.; Beaumont, K.; Walker, D. K.: Property-based design: optimization of drug absorption and pharmacokinetics. *J Med Chem* **2001**, 44, 1313–1333.
  - 41 van de Waterbeemd, H.; Jones, B. C.: Predicting oral absorption and bioavailability. *Prog Med Chem* **2003**, 41, 1–59.
  - 42 Caldwell, G. W.; Ritchie, D. M.; Masucci, J. A.; Hageman, W.; Yan, Z.: The new pre-preclinical paradigm: compound optimization in early and late phase drug discovery. *Curr Top Med Chem* **2001**, 1, 353–366.
  - 43 van de Waterbeemd, H.: Which in vitro screens guide the prediction of oral absorption and volume of distribution? *Basic Clin Pharmacol Toxicol* **2005**, 96, 162–166.
  - 44 Thompson, T. N.: Optimization of metabolic stability as a goal of modern drug design. *Med Res Rev* **2001**, 21, 412–449.
  - 45 Bertrand, M.; Jackson, P.; Walther, B.: Rapid assessment of drug metabolism in the drug discovery process. *Eur J Pharm Sci* **2000**, 11 [Suppl 2], S61–S72.
  - 46 Chaturvedi, P. R.; Decker, C. J.; Odinecs, A.: Prediction of pharmacokinetic properties using experimental approaches during early drug discovery. *Curr Opin Chem Biol* **2001**, 5, 452–463.
  - 47 Kassel, D. B.: Applications of high-throughput ADME in drug discovery. *Curr Opin Chem Biol* **2004**, 8, 339–345.
  - 48 Naritomi, Y.; Terashita, S.; Kimura, S.; Suzuki, A.; Kagayama, A.; et al.: Prediction of human hepatic clearance from *in vivo* animal experiments and *in vitro* metabolic studies with liver microsomes from animals and humans. *Drug Metab Dispos* **2001**, 29, 1316–1324.
  - 49 Ansele, J. H.; Thakker, D. R.: High-throughput screening for stability and inhibitory activity of compounds toward cytochrome P450-mediated metabolism. *J Pharm Sci* **2004**, 93, 239–255.
  - 50 Korfmacher, W. A.; Palmer, C. A.; Nardo, C.; Dunn-Meynell, K.; Grotz, D.; et al.: Development of an automated mass spectrometry system for the quantitative analysis of liver microsomal incubation samples: a tool for rapid screening of new compounds for metabolic stability. *Rapid Commun Mass Spectrom* **1999**, 13, 901–907.

- 51 Di, L.; Kerns, E. H.; Hong, Y.; Kleintop, T. A.; McConnell, O. J.; et al.: Optimization of a higher throughput microsomal stability screening assay for profiling drug discovery candidates. *J Biomol Screen* **2003**, 8, 453–462.
- 52 Xu, R.; Nemes, C.; Jenkins, K. M.; Rourick, R. A.; Kassel, D. B.; et al.: Application of parallel liquid chromatography/mass spectrometry for high throughput microsomal stability screening of compound libraries. *J Am Soc Mass Spectrom* **2002**, 13, 155–165.
- 53 Li, Y.; Shin, Y. G.; Yu, C.; Kosmeder, J. W.; Hirschelman, W. H.; et al.: Increasing the throughput and productivity of Caco-2 cell permeability assays using liquid chromatography-mass spectrometry: application to resveratrol absorption and metabolism. *Comb Chem High Throughput Screen* **2003**, 6, 757–767.
- 54 Mandagere, A. K.; Thompson, T. N.; Hwang, K. K.: Graphical model for estimating oral bioavailability of drugs in humans and other species from their Caco-2 permeability and in vitro liver enzyme metabolic stability rates. *J Med Chem* **2002**, 45, 304–311.
- 55 Balimane, P. V.; Chong, S.: Cell culture-based models for intestinal permeability: a critique. *Drug Discov Today* **2005**, 10, 335–343.
- 56 Bu, H. Z.; Poglod, M.; Micetich, R. G.; Khan, J. K.: High-throughput caco-2 cell permeability screening by cassette dosing and sample pooling approaches using direct injection/on-line guard cartridge extraction/tandem mass spectrometry. *Rapid Commun Mass Spectrom* **2000**, 14, 523–528.
- 57 Fung, E. N.; Chu, I.; Li, C.; Liu, T.; Soares, A.; et al.: Higher-throughput screening for Caco-2 permeability utilizing a multiple sprayer liquid chromatography/tandem mass spectrometry system. *Rapid Commun Mass Spectrom* **2003**, 17, 2147–2152.
- 58 Hakala, K. S.; Laitinen, L.; Kaukonen, A. M.; Hirvonen, J.; Kostiainen, R.; et al.: Development of LC/MS/MS methods for cocktail dosed Caco-2 samples using atmospheric pressure photoionization and electrospray ionization. *Anal Chem* **2003**, 75, 5969–5977.
- 59 Larger, P.; Altamura, M.; Catalioto, R. M.; Giuliani, S.; Maggi, C. A.; et al.: Simultaneous LC-MS/MS determination of reference pharmaceuticals as a method for the characterization of the Caco-2 cell monolayer absorption properties. *Anal Chem* **2002**, 74, 5273–5281.
- 60 Wang, Z.; Hop, C. E.; Leung, K. H.; Pang, J.: Determination of in vitro permeability of drug candidates through a caco-2 cell monolayer by liquid chromatography/tandem mass spectrometry. *J Mass Spectrom* **2000**, 35, 71–76.
- 61 Kariv, I.; Rourick, R. A.; Kassel, D. B.; Chung, T. D.: Improvement of “hit-to-lead” optimization by integration of in vitro HTS experimental models for early determination of pharmacokinetic properties. *Comb Chem High Throughput Screen* **2002**, 5, 459–472.
- 62 White, R. E.: High-throughput screening in drug metabolism and pharmacokinetic support of drug discovery. *Annu Rev Pharmacol Toxicol* **2000**, 40, 133–157.
- 63 Yan, Z.; Caldwell, G. W.: Metabolism profiling, and cytochrome P450 inhibition & induction in drug discovery. *Curr Top Med Chem* **2001**, 1, 403–425.
- 64 Bjornsson, T. D.; Callaghan, J. T.; Einolf, H. J.; Fischer, V.; Gan, L.; et al.: The conduct of in vitro and in vivo drug-drug interaction studies: a Pharmaceutical Research and Manufacturers of America (PhRMA) perspective. *Drug Metab Dispos* **2003**, 31, 815–832.
- 65 Obach, R. S.: Drug–drug interactions: an important negative attribute in drugs. *Drugs Today* **2003**, 39, 301–338.
- 66 Obach, R. S.; Walsky, R. L.; Venkatakrishnan, K.; Gaman, E. A.; Houston, J. B.; et al.: The utility of *in vitro* cytochrome p450 inhibition data

- in the prediction of drug–drug interactions. *J Pharmacol Exp Ther* **2005**.
- 67 Chu, I.; Favreau, L.; Soares, T.; Lin, C.; Nomeir, A. A.: Validation of higher-throughput high-performance liquid chromatography/atmospheric pressure chemical ionization tandem mass spectrometry assays to conduct cytochrome P450s CYP2D6 and CYP3A4 enzyme inhibition studies in human liver microsomes. *Rapid Commun Mass Spectrom* **2000**, *14*, 207–214.
  - 68 Bu, H. Z.; Magis, L.; Knuth, K.; Teitelbaum, P.: High-throughput cytochrome P450 (CYP) inhibition screening via a cassette probe-dosing strategy. VI. Simultaneous evaluation of inhibition potential of drugs on human hepatic isozymes CYP2A6, 3A4, 2C9, 2D6 and 2E1. *Rapid Commun Mass Spectrom* **2001**, *15*, 741–748.
  - 69 Testino, S. A. Jr.; Patonay, G.: High-throughput inhibition screening of major human cytochrome P450 enzymes using an *in vitro* cocktail and liquid chromatography–tandem mass spectrometry. *J Pharm Biomed Anal* **2003**, *30*, 1459–1467.
  - 70 Peng, S. X.; Barbone, A. G.; Ritchie, D. M.: High-throughput cytochrome p450 inhibition assays by ultrafast gradient liquid chromatography with tandem mass spectrometry using monolithic columns. *Rapid Commun Mass Spectrom* **2003**, *17*, 509–518.
  - 71 Kim, M. J.; Kim, H.; Cha, I. J.; Park, J. S.; Shon, J. H.; et al.: High-throughput screening of inhibitory potential of nine cytochrome P450 enzymes *in vitro* using liquid chromatography/tandem mass spectrometry. *Rapid Commun Mass Spectrom* **2005**, *19*, 2651–2658.
  - 72 Cox, K. A.; White, R. E.; Korfmacher, W. A.: Rapid determination of pharmacokinetic properties of new chemical entities: *in vivo* approaches. *Comb Chem High Throughput Screen* **2002**, *5*, 29–37.
  - 73 Hopfgartner, G.; Bourgogne, E.: Quantitative high-throughput analysis of drugs in biological matrices by mass spectrometry. *Mass Spectrom Rev* **2003**, *22*, 195–214.
  - 74 Ong, V. S.; Cook, K. L.; Kosara, C. M.; Brubaker, W. F.: Quantitative bioanalysis: an integrated approach for drug discovery and development. *Int J Mass Spectrom* **2004**, *238*, 139–152.
  - 75 Chaikin, P.; Rhodes, G. R.; Bruno, R.; Rohatagi, S.; Natarajan, C.: Pharmacokinetics/pharmacodynamics in drug development: an industrial perspective. *J Clin Pharmacol* **2000**, *40*, 1428–1438.
  - 76 Derendorf, H.; Lesko, L. J.; Chaikin, P.; Colburn, W. A.; Lee, P.; et al.: Pharmacokinetic/pharmacodynamic modeling in drug research and development. *J Clin Pharmacol* **2000**, *40*, 1399–1418.
  - 77 Rohatagi, S.: A future in pharmacokinetic and pharmacodynamic modeling. *Curr Drug Discov* **2004**, *2004*, 25–29.
  - 78 Manitisitkul, P.; White, R. E.: Whatever happened to cassette-dosing pharmacokinetics? *Drug Discov Today* **2004**, *9*, 652–658.
  - 79 White, R. E.; Manitisitkul, P.: Pharmacokinetic theory of cassette dosing in drug discovery screening. *Drug Metab Dispos* **2001**, *29*, 957–966.
  - 80 Smith, N. F.; Hayes, A.; Nutley, B. P.; Raynaud, F. I.; Workman, P.: Evaluation of the cassette dosing approach for assessing the pharmacokinetics of geldanamycin analogues in mice. *Cancer Chemother Pharmacol* **2004**.
  - 81 Tamvakopoulos, C. S.; Colwell, L. F.; Barakat, K.; Fenyk-Melody, J.; Griffin, P. R.; et al.: Determination of brain and plasma drug concentrations by liquid chromatography/tandem mass spectrometry. *Rapid Commun Mass Spectrom* **2000**, *14*, 1729–1735.
  - 82 Ohkawa, T.; Ishida, Y.; Kanaoka, E.; Takahashi, K.; Okabe, H.; et al.: A new generic column switching system for quantitation in cassette dosing using LC/MS/MS. *J Pharm Biomed Anal* **2003**, *31*, 1089–1099.



- 83 Zhang, M. Y.; Kerns, E.; McConnell, O.; Sonnenberg-Reines, J.; Zaleska, M. M.; et al.: Brain and plasma exposure profiling in early drug discovery using cassette administration and fast liquid chromatography-tandem mass spectrometry. *J Pharm Biomed Anal* **2004**, 34, 359–368.
- 84 Sadagopan, N.; Pabst, B.; Cohen, L.: Evaluation of online extraction/mass spectrometry for in vivo cassette analysis. *J Chromatogr B Anal Technol Biomed Life Sci* **2005**, 820, 59–67.
- 85 Korfmacher, W. A.; Cox, K. A.; Ng, K. J.; Veals, J.; Hsieh, Y.; et al.: Cassette-accelerated rapid rat screen: a systematic procedure for the dosing and liquid chromatography/atmospheric pressure ionization tandem mass spectrometric analysis of new chemical entities as part of new drug discovery. *Rapid Commun Mass Spectrom* **2001**, 15, 335–340.
- 86 Hsieh, Y.; Wang, G.; Wang, Y.; Chackalamannil, S.; Brisson, J. M.; et al.: Simultaneous determination of a drug candidate and its metabolite in rat plasma samples using ultrafast monolithic column high-performance liquid chromatography/tandem mass spectrometry. *Rapid Commun Mass Spectrom* **2002**, 16, 944–950.
- 87 Hsieh, Y.; Brisson, J. M.; Wang, G.; Ng, K.; Korfmacher, W. A.: Simultaneous fast HPLC-MS/MS analysis of drug candidates and hydroxyl metabolites in plasma. *J Pharm Biomed Anal* **2003**, 33, 251–261.
- 88 Jemal, M.; Ouyang, Z.: Enhanced resolution triple-quadrupole mass spectrometry for fast quantitative bioanalysis using liquid chromatography/tandem mass spectrometry: investigations of parameters that affect ruggedness. *Rapid Commun Mass Spectrom* **2003**, 17, 24–38.
- 89 Hsieh, Y.; Brisson, J.-M.; Wang, G.: Fast HPLC-MS/MS for small molecules. *Am Pharm Rev* **2003**, 6, 14–20.
- 90 Romanyshyn, L.; Tiller, P. R.; Alvaro, R.; Pereira, A.; Hop, C. E.: Ultra-fast gradient vs fast isocratic chromatography in bioanalytical quantification by liquid chromatography/tandem mass spectrometry. *Rapid Commun Mass Spectrom* **2001**, 15, 313–319.
- 91 Romanyshyn, L. A.; Tiller, P. R.: Ultra-short columns and ballistic gradients: considerations for ultra-fast chromatographic liquid chromatographic–tandem mass spectrometric analysis. *J Chromatogr A* **2001**, 928, 41–51.
- 92 Shou, W. Z.; Chen, Y. L.; Eerkes, A.; Tang, Y. Q.; Magis, L.; et al.: Ultrafast liquid chromatography/tandem mass spectrometry bioanalysis of polar analytes using packed silica columns. *Rapid Commun Mass Spectrom* **2002**, 16, 1613–1621.
- 93 Smith, J. H.; McNair, H. M.: Fast HPLC with a Silica-Based Monolithic ODS Column. *J Chromatogr Sci* **2003**, 41, 209–214.
- 94 Tiller, P. R.; Romanyshyn, L. A.; Neue, U. D.: Fast LC/MS in the analysis of small molecules. *Anal Bioanal Chem* **2003**, 377, 788–802.
- 95 Zeng, H.; Deng, Y.; Wu, J. T.: Fast analysis using monolithic columns coupled with high-flow on-line extraction and electrospray mass spectrometric detection for the direct and simultaneous quantitation of multiple components in plasma. *J Chromatogr B Anal Technol Biomed Life Sci* **2003**, 788, 331–337.
- 96 Romanyshyn, L.; Tiller, P. R.; Hop, C. E.: Bioanalytical applications of ‘fast chromatography’ to high-throughput liquid chromatography/tandem mass spectrometric quantitation. *Rapid Commun Mass Spectrom* **2000**, 14, 1662–1668.
- 97 Hsieh, Y.; Chintala, M.; Mei, H.; Agans, J.; Brisson, J. M.; et al.: Quantitative screening and matrix effect studies of drug discovery compounds in monkey plasma using fast-gradient liquid chromatography/tandem mass spectrometry. *Rapid*

- Commun Mass Spectrom* **2001**, 15, 2481–2487.
- 98 Tiller, P. R.; Romanyshyn, L. A.: Implications of matrix effects in ultra-fast gradient or fast isocratic liquid chromatography with mass spectrometry in drug discovery. *Rapid Commun Mass Spectrom* **2002**, 16, 92–98.
  - 99 Dunn-Meynell, K. W.; Wainhaus, S.; Korfmacher, W. A.: Optimizing an ultrafast generic high-performance liquid chromatography/tandem mass spectrometry method for faster discovery pharmacokinetic sample throughput. *Rapid Commun Mass Spectrom* **2005**, 19, 2905–2910.
  - 100 Tanak, N.; Kobayashi, H.; Ishizuka, N.; Minakuchi, H.; Nakanishi, K.; et al.: Monolithic silica columns for high-efficiency chromatographic separations. *J Chromatogr A* **2002**, 965, 35–49.
  - 101 Tanaka, N.; Kobayashi, H.; Nakanishi, K.; Minakuchi, H.; Ishizuka, N.: Monolithic LC columns. *Anal Chem* **2001**, 73, 420A–429A.
  - 102 Tanaka, N.; Kobayashi, H.: Monolithic columns for liquid chromatography. *Anal Bioanal Chem* **2003**, 376, 298–301.
  - 103 Wu, J. T.; Zeng, H.; Deng, Y.; Unger, S. E.: High-speed liquid chromatography/tandem mass spectrometry using a monolithic column for high-throughput bioanalysis. *Rapid Commun Mass Spectrom* **2001**, 15, 1113–1119.
  - 104 van de Merbel, N. C.; Poelman, H.: Experiences with monolithic LC phases in quantitative bioanalysis. *J Pharm Biomed Anal* **2004**, in press.
  - 105 Hsieh, Y.; Wang, G.; Wang, Y.; Chackalamannil, S.; Korfmacher, W. A.: Direct plasma analysis of drug compounds using monolithic column liquid chromatography and tandem mass spectrometry. *Anal Chem* **2003**, 75, 1812–1818.
  - 106 Jarmalaviciene, R.; Kornysova, O.; Westerlund, D.; Maruska, A.: Non-particulate (continuous bed or monolithic) restricted-access reversed-phase media for sample clean-up and separation by capillary-format liquid chromatography. *Anal Bioanal Chem* **2003**, 377, 902–908.
  - 107 Barbarin, N.; Mawhinney, D. B.; Black, R.; Henion, J.: High-throughput selected reaction monitoring liquid chromatography-mass spectrometry determination of methylphenidate and its major metabolite, ritalinic acid, in rat plasma employing monolithic columns. *J Chromatogr B Anal Technol Biomed Life Sci* **2003**, 783, 73–83.
  - 108 Korfmacher, W. A.; Veals, J.; Dunn-Meynell, K.; Zhang, X.; Tucker, G.; et al.: Demonstration of the capabilities of a parallel high performance liquid chromatography tandem mass spectrometry system for use in the analysis of drug discovery plasma samples. *Rapid Commun Mass Spectrom* **1999**, 13, 1991–1998.
  - 109 Jemal, M.; Huang, M.; Mao, Y.; Whigan, D.; Powell, M. L.: Increased throughput in quantitative bioanalysis using parallel-column liquid chromatography with mass spectrometric detection. *Rapid Commun Mass Spectrom* **2001**, 15, 994–999.
  - 110 Deng, Y.; Wu, J. T.; Lloyd, T. L.; Chi, C. L.; Olah, T. V.; et al.: High-speed gradient parallel liquid chromatography/tandem mass spectrometry with fully automated sample preparation for bioanalysis: 30 seconds per sample from plasma. *Rapid Commun Mass Spectrom* **2002**, 16, 1116–1123.
  - 111 Wu, J. T.: The development of a staggered parallel separation liquid chromatography/tandem mass spectrometry system with on-line extraction for high-throughout screening of drug candidates in biological fluids. *Rapid Commun Mass Spectrom* **2001**, 15, 73–81.
  - 112 King, R. C.; Miller-Stein, C.; Magiera, D. J.; Brann, J.: Description and validation of a staggered parallel high performance liquid chromatography system for good laboratory practice level quantitative analysis by liquid chromatography/tandem mass

- spectrometry. *Rapid Commun Mass Spectrom* **2002**, 16, 43–52.
- 113 Xu, X.; Zhou, Q.; Korfmacher, W. A.: Development of a low volume plasma sample precipitation procedure for liquid chromatography/tandem mass spectrometry assays used for drug discovery applications. *Rapid Commun Mass Spectrom* **2005**, 19, 2131–2136.
  - 114 Liang, H. R.; Foltz, R. L.; Meng, M.; Bennett, P.: Ionization enhancement in atmospheric pressure chemical ionization and suppression in electrospray ionization between target drugs and stable-isotope-labeled internal standards in quantitative liquid chromatography/tandem mass spectrometry. *Rapid Commun Mass Spectrom* **2003**, 17, 2815–2821.
  - 115 Mei, H.; Hsieh, Y.; Nardo, C.; Xu, X.; Wang, S.; et al.: Investigation of matrix effects in bioanalytical high-performance liquid chromatography/tandem mass spectrometric assays: application to drug discovery. *Rapid Commun Mass Spectrom* **2003**, 17, 97–103.
  - 116 Schuhmacher, J.; Zimmer, D.; Tesche, F.; Pickard, V.: Matrix effects during analysis of plasma samples by electrospray and atmospheric pressure chemical ionization mass spectrometry: practical approaches to their elimination. *Rapid Commun Mass Spectrom* **2003**, 17, 1950–1957.
  - 117 Souverain, S.; Rudaz, S.; Veuthey, J. L.: Matrix effect in LC-ESI-MS and LC-APCI-MS with off-line and on-line extraction procedures. *J Chromatogr A* **2004**, 1058, 61–66.
  - 118 Taylor, P. J.: Matrix effects: the Achilles heel of quantitative high-performance liquid chromatography–electrospray–tandem mass spectrometry. *Clin Biochem* **2005**, 38, 328–334.
  - 119 Xu, X.; Mei, H.; Wang, S.; Zhou, Q.; Wang, G.; et al.: A study of common discovery dosing formulation components and their potential for causing time-dependent matrix effects in high-performance liquid chromatography tandem mass spectrometry assays. *Rapid Commun Mass Spectrom* **2005**, 19, 2643–2650.
  - 120 Zheng, J. J.; Lynch, E. D.; Unger, S. E.: Comparison of SPE and fast LC to eliminate mass spectrometric matrix effects from microsomal incubation products. *J Pharm Biomed Anal* **2002**, 28, 279–285.
  - 121 King, R.; Bonfiglio, R.; Fernandez-Metzler, C.; Miller-Stein, C.; Olah, T.: Mechanistic investigation of ionization suppression in electrospray ionization. *J Am Soc Mass Spectrom* **2000**, 11, 942–950.
  - 122 Matuszewski, B. K.; Constanzer, M. L.; Chavez-Eng, C. M.: Matrix effect in quantitative LC/MS/MS analyses of biological fluids: a method for determination of finasteride in human plasma at picogram per milliliter concentrations. *Anal Chem* **1998**, 70, 882–889.
  - 123 Matuszewski, B. K.; Constanzer, M. L.; Chavez-Eng, C. M.: Strategies for the assessment of matrix effect in quantitative bioanalytical methods based on HPLC-MS/MS. *Anal Chem* **2003**, 75, 3019–3030.
  - 124 Mei, H.: Matrix effects: causes and solutions, in *Using Mass Spectrometry for Drug Metabolism Studies*, CRC Press, Boca Raton, **2005**, pp 103–150.
  - 125 Shou, W. Z.; Naidong, W.: Post-column infusion study of the ‘dosing vehicle effect’ in the liquid chromatography/tandem mass spectrometric analysis of discovery pharmacokinetic samples. *Rapid Commun Mass Spectrom* **2003**, 17, 589–597.
  - 126 Tong, X. S.; Wang, J.; Zheng, S.; Pivnichny, J. V.; Griffin, P. R.; et al.: Effect of signal interference from dosing excipients on pharmacokinetic screening of drug candidates by liquid chromatography/mass spectrometry. *Anal Chem* **2002**, 74, 6305–6313.
  - 127 Larger, P. J.; Breda, M.; Fraier, D.; Hughes, H.; James, C. A.: Ion-suppression effects in liquid chromatography-tandem mass spectrometry due to a formulation

- agent, a case study in drug discovery bioanalysis. *J Pharm Biomed Anal* **2005**, 39, 206–216.
- 128 Bajpai, M.; Esmay, J. D.: In vitro studies in drug discovery and development: an analysis of study objectives and application of good laboratory practices (GLP). *Drug Metab Rev* **2002**, 34, 679–689.
  - 129 Shabir, G. A.: Validation of high-performance liquid chromatography methods for pharmaceutical analysis. Understanding the differences and similarities between validation requirements of the US Food and Drug Administration, the US Pharmacopeia and the International Conference on Harmonization. *J Chromatogr A* **2003**, 987, 57–66.
  - 130 Sherma, J.: UPLC: Ultra-performance liquid chromatography. *J AOAC Int* **2005**, 88, 63A–67A.
  - 131 Wren, S. A.: Peak capacity in gradient ultra performance liquid chromatography (UPLC). *J Pharm Biomed Anal* **2005**, 38, 337–343.
  - 132 Churchwell, M. I.; Twaddle, N. C.; Meeker, L. R.; Doerge, D. R.: Improving LC-MS sensitivity through increases in chromatographic performance: comparisons of UPLC-ES/MS/MS to HPLC-ES/MS/MS. *J Chromatogr B Anal Technol Biomed Life Sci* **2005**.
  - 133 Johnson, K. A.; Plumb, R.: Investigating the human metabolism of acetaminophen using UPLC and exact mass oa-TOF MS. *J Pharm Biomed Anal* **2005**.
  - 134 Plumb, R. S.; Granger, J. H.; Stumpf, C. L.; Johnson, K. A.; Smith, B. W.; et al.: A rapid screening approach to metabolomics using UPLC and oa-TOF mass spectrometry: application to age, gender and diurnal variation in normal/Zucker obese rats and black, white and nude mice. *Analyst* **2005**, 130, 844–849.
  - 135 Shen, J. X.; Wang, H.; Tadros, S.; Hayes, R. N.: Orthogonal extraction/ chromatography and UPLC, two powerful new techniques for bioanalytical quantitation of desloratadine and 3-hydroxydesloratadine at 25 pg/mL. *J Pharm Biomed Anal* **2005**.
  - 136 Castro-Perez, J.; Plumb, R.; Granger, J. H.; Beattie, I.; Joncour, K.; et al.: Increasing throughput and information content for in vitro drug metabolism experiments using ultra-performance liquid chromatography coupled to a quadrupole time-of-flight mass spectrometer. *Rapid Commun Mass Spectrom* **2005**, 19, 843–848.
  - 137 Plumb, R.; Castro-Perez, J.; Granger, J.; Beattie, I.; Joncour, K.; et al.: Ultra-performance liquid chromatography coupled to quadrupole-orthogonal time-of-flight mass spectrometry. *Rapid Commun Mass Spectrom* **2004**, 18, 2331–2337.
  - 138 Li, A. C.; Alton, D.; Bryant, M. S.; Shou, W. Z.: Simultaneously quantifying parent drugs and screening for metabolites in plasma pharmacokinetic samples using selected reaction monitoring information-dependent acquisition on a QTrap instrument. *Rapid Commun Mass Spectrom* **2005**, 19, 1943–1950.
  - 139 Xu, X.: Using higher mass resolution in quantitative assays, in *Using Mass Spectrometry for Drug Metabolism Studies*, CRC Press, Boca Raton, **2005**, pp 203–228.
  - 140 Xu, X.; Veals, J.; Korfmacher, W. A.: Comparison of conventional and enhanced mass resolution triple-quadrupole mass spectrometers for discovery bioanalytical applications. *Rapid Commun Mass Spectrom* **2003**, 17, 832–837.
  - 141 Hsieh, Y.; Wang, G.: Normal phase HPLC-APPI/MS/MS determination of stereoisomeric mixtures, in *Eastern Analytical Symposium*, Somerset, N.J., **2003**.
  - 142 Hsieh, Y.: APPI: a new ionization source for LC-MS/MS assays, in *Using Mass Spectrometry for Drug Metabolism Studies*, CRC Press, Boca Raton, **2005**, pp 253–276.
  - 143 Cai, Y.; Kingery, D.; McConnell, O.; Bach, A. C. 2nd: Advantages of atmospheric pressure photoionization mass spectrometry in support of drug

- discovery. *Rapid Commun Mass Spectrom* **2005**, 19, 1717–1724.
- 144 Hsieh, Y.; Wang, G.: Integration of atmospheric pressure photoionization interfaces to HPLC-MS/MS for pharmaceutical analysis. *Am Pharm Rev* **2004**, 7, 88–93.
- 145 Kauppila, T. J.; Kuuranne, T.; Meurer, E. C.; Eberlin, M. N.; Kotiaho, T.; et al.: Atmospheric pressure photoionization mass spectrometry. Ionization mechanism and the effect of solvent on the ionization of naphthalenes. *Anal Chem* **2002**, 74, 5470–5479.
- 146 Kauppila, T. J.; Kotiaho, T.; Kostiainen, R.; Bruins, A. P.: Negative ion–atmospheric pressure photoionization–mass spectrometry. *J Am Soc Mass Spectrom* **2004**, 15, 203–211.
- 147 McKenzie, D. E.; McDermott, L. L.: LC-MS investigation of atmospheric pressure photoionization versus electrospray ionization and atmospheric pressure chemical ionization using eleven test compounds, in *51st ASMS Conference on Mass Spectrometry and Allied Topics*, ASMS, Montreal, **2003**.
- 148 Raffaelli, A.; Saba, A.: Atmospheric pressure photoionization mass spectrometry. *Mass Spectrom Rev* **2003**, 22, 318–331.
- 149 Syage, J. A.; Evans, M. D.: Photoionization mass spectrometry. *Spectroscopy* **2001**, 16, 14–22.
- 150 Wang, G.; Hsieh, Y.; Korfmacher, W. A.: Comparison of atmospheric pressure chemical ionization, electrospray ionization, and atmospheric pressure photoionization for the determination of cyclosporin a in rat plasma. *Anal Chem* **2005**, 77, 541–548.
- 151 Yang, C.; Henion, J.: Atmospheric pressure photoionization liquid chromatographic–mass spectrometric determination of idoxifene and its metabolites in human plasma. *J Chromatogr A* **2002**, 970, 155–165.

## Index

### **a**

- absorption, distribution, metabolism and excretion (ADME) properties 402
- accurate mass 9, 35, 38, 45, 47, 55, 324
- 7-acetoxy-1-methyl quinolinium iodide (AMQI) 195 f.
- acetylcholine 292
- acetylcholinesterase (AChE) 191 ff., 292 ff.
- N-acetylglucosamine 297
- N-acetylglucosaminyltransferase V (GnT-V) 230 f.
- adipocyte differentiation 390
- affinity capture-MS 160
  - noncovalent 160
- affinity competition experiment
  - ACE<sub>50</sub> 140 ff., 150
  - – definition 140
- affinity ranking 134 f., 140 f.
- affinity screening 157, 162, 165, 325, 367
  - primary 164, 173
  - ultra-high throughput 163 ff.
- affinity selection 121, 174, 179
  - – MS (AS-MS) 123, 151, 162 ff., 176, 179, 254, 305
- affinity size exclusion 159
- agonist 391
- allele-specific expression 54
- Alzheimer's disease 194, 313
- D-amino acids 333
- $\gamma$ -amino butyric acid (GABA) 268 ff.
  - DL-3-amino-*n*-butyric acid 274
  - transporter (GAT) 269
  - – mGAT1 268 ff.
- trans-4-aminocrotonic acid (TACA) 273 f.
- aminoglycosides 328
- DL-4-amino-3-hydroxybutyric acid 273 f.
- (S)-4-amino-2-hydroxy butyric acid 273 f.
- 7-amino-4-methylcoumarin hydrochloride (AMC) 188 ff.
- (3-aminopropyl)triethoxysilane 237
- cAMP 188, 288
- antagonist 391
- anterior pituitary somatotrope cell 386
- anthrax lethal factor 298
- antibiotic drug 310
- antibody-antigen interaction 205
- antidigoxigenin FAb 209 f.
- antifungal drug 310
- anxiety 269
- apovinpocetin 46
- area under the curve (AUC) 408
- arterial hypertension 25
- atmospheric pressure
  - ionization (API) 11 ff., 34, 56, 404
  - – chemical (APCI) 12, 17 ff., 42 f., 57, 81 f., 89, 226, 413, 419
  - photoionization (APPI) 12, 19, 42, 57, 405, 419
- atomic mass 55
- ATP 137, 242, 390
- automated ligand identification system (ALIS) 121, 125 ff., 135 f., 141, 148 ff., 254
- automatic gain control (AGC) 27
- automation software 85 ff.
- average mass 55

### **b**

- background spectrum 85 f.
- background subtraction 85 f.
- bacterial transcription 333 f.
- base peak 56
- bicuculline 264
- binding
  - affinity 72, 97, 103, 274, 341, 357
  - – perturbation 392
  - – quantitative 130 f.
  - assay 200, 247 ff., 260 ff., 272 ff.
  - competition 134 f., 249 ff., 261, 272 ff.

binding (*cont.*)

- isotherm 218 ff., 227 f., 249
- site classification 136
- stoichiometry 341, 345

bioactivity screening 193 f., 204, 212

bioanalysis 41 ff., 285, 289, 292, 299

bioanalytical assay 404, 413

bioinformatics 41, 54

biological efficacy 121, 134, 142

biological media 352, 359

biological response 390

biomarker 48

biosensor

- acoustic 253
- optical 229

biotin 188, 201 ff.

- derivatives 204

blood 322

bosentan 9 f., 25 f., 29

bovine serum albumine (BSA) 76 ff., 294 f.

brain 407

breakthrough 233, 237 f., 241

- volume 221, 229, 241

buffer 74 ff., 160, 188, 194 f., 201 ff., 211,

224 f., 257 ff., 269, 343, 349

butaclamol 257 ff.

**c**C<sub>18</sub> column 218 f., 342*see also* restricted accessC<sub>4</sub> column 342

Caco-2 402, 405

Caenorhabditis elegans 52 f.

calabar bean

calcium 346 f., 351 ff.

calibration 43

calibration factor 132

calmodulin (CaM) 351, 360

- apo 345 f., 351 f.

- holo 346, 354 ff.

calorimetry 253, 357

cancer

- drug 310
- hepatocellular 231
- invasion 188
- mammary 231
- pancreatic 231

capillary electrophoresis 160, 185

- affinity (ACE) 367

tris(2-carboxyethyl)phosphine hydrochloride (TCEP) 381

carboxypeptidase 381

- A 287 f.

caspase-1 316 f.

caspase-3 312 ff.

caspase-5 316

cassette accelerated rapid rat screen (CARRS) 402, 408 ff.

cathepsin B 188 ff., 200

cell wall 322

central nervous system (CNS) disorder 95, 257

centrifugation 67 ff., 80 f., 259, 261, 268

channel electron multiplier (CEM) 39

charge residue (CR) model 16 f.

charge state 15

chelerythrine chloride 242

chemical etching 290

chemical ionization (CI) 10 ff.

- negative (NCI) 12, 56
- positive (PCI) 12, 56

chemical noise 76, 85

chemotypes 168

Cheng-Prusoff equation 272

chinese herbs 243

chlorpromazine 258 ff.

choline 292

CI 966 273 f.

circular dichroism 349, 357

collagenase 106

collision cell 24 f., 35, 404

collision energy 25

collision gas 35

collision-induced dissociation (CID) 13, 25, 29, 31, 37, 57

continuous-flow system 185 f., 200

- on-line 202 ff.

conversion dynode 40

Coomassie

- blue 50
- staining 366

corona discharge 18 f.

curtain gas 12 f.

 $\alpha$ -cyano-4-hydroxycinnamic acid 286

cyanuric chloride 294 f.

cyclohexane 5

cysteamine 306 ff.

cysteine 306 ff., 342, 362

cytochrome c 294

cytochrome P450 178, 405 f.

cytomegalovirus protease (CMVP) 67 f., 84, 99 ff., 108 ff.

**d**

daidzein 19 f.

DAMGO 266

DAPI 93

data analysis, automated 383

data dependent acquisition (DDA) 41, 46  
 data reduction 85  
 deconvolution 16, 167 f., 173 ff., 307, 365  
 dehydroisoandrosterone 229  
 deoxyuridine monophosphate (dUMP) 310  
 dependent scan 46  
 depression 269  
 desorption electrospray (DESI) 12, 20 f.  
 desorption/ionization on porous silicon (DIOS) 23, 116, 285, 289 ff., 299  
 detection 4 f.  
   – photo diode array 20  
 detection emitter plate 36  
 detector 38  
 detector dead time 35  
 diagnostic monitoring 54  
 dibromoquinazalone (DBQ) 99, 108 ff.  
 difluoromethyl ketone inhibitor (DFMK) 67 f., 84  
 digestion 360, 381  
   – enzymatic 50  
   – on-plate 294  
 digoxigenin 205 f.  
 digoxin 205 f., 209 ff.  
 dihydrofolate reductase (DHFR) 127 ff., 137, 237 f.  
 2,5-dihydroxy benzoic acid 286 ff.  
 direct analysis in real time (DART) 12, 20  
 direct current (DC) potential 23, 30  
 direct liquid interface (DLI) 3  
 discharge lamp 19  
 distamycin 93  
 disulfide linker 306 ff., 315  
 DMSO 75  
 DNA 90 f., 219, 324, 362, 386  
   – synthesis 310  
 doping control 41  
 dosing 407  
   – cassette 407  
 drug discovery 157 f., 185, 217, 289, 292, 298, 312, 321, 367, 377 ff., 401 f., 413 ff.  
   – fragment-based 305 ff.  
 drug metabolism 45 ff.  
   – pharmacokinetic tests (DMPK) 401 ff., 415  
 drug-protein  
   – complex 65 f.  
   – molar ratio 109 ff.  
 drug screening 65  
   – primary 89, 94 ff.  
   – – Amgen 98  
   – – Novartis 98  
   – report 86 f.

  – secondary 89  
   – – Amgen 94  
   – – Novartis 94

dual spray 35  
 dual endothelin receptor antagonist 25  
 dwell time 44  
 dynamic background subtraction (DBS) 46  
 dynamic range 33

## e

EC<sub>50</sub> 100  
   – MS EC<sub>50</sub> 111 ff.  
 EIC *see* extracted ion current  
 electron impact (EI) ionization 10 ff., 56  
 electrophoresis 50  
   – two-dimensional 50, 53  
 electrospray deposition (ESD) 291  
 electrospray ionization (ESI) 12 ff., 22, 38, 42 f., 49, 51, 56, 65 ff., 76 f., 81 ff., 89 ff., 106 ff., 123, 137, 161, 164, 186 ff., 200, 203 ff., 224 ff., 243, 254, 257 ff., 268, 272, 305 ff., 321 ff., 342, 360, 367, 413 f.  
   – electrophoretic cell 16  
   – multi-sprayer (MUX) technology 82 f., 98, 405, 410  
   – nanoelectrospray 14, 57  
   – nanospray 123  
   – – chip 47, 198 ff.  
   – negative mode 18, 91  
   – positive mode 16, 26, 91  
 electrostatic mirror *see* mass reflectron  
 elemental composition 9  
 ELISA 242 f.  
 ELSD 190  
 endoproteinase 381  
 enhanced multiply charged (EMC) 32  
 enhanced product ion (EPI) mode 32, 46 f.  
 enhanced Q3 single MS (EMS) 32, 46 f.  
 enhanced resolution Q3 single MS (ER) 32  
 enzymatic activity 103, 289  
 enzyme 46, 185 ff.  
   – inhibition assay 405 f.  
   – substrate complex 186, 296  
 EphB2 242 f.  
 epilepsy 269  
 esterase 292  
 $\beta$ -estradiol 89 f., 233  
 ethidium bromide 92 f.  
 ethylmethoxyacetate 287  
 exact mass 55  
 exact molecular weight (EMW) 130  
 exchange, H/D 342 f., 349  
   – amide 378  
   – automation 382



exchange, H/D (*cont.*)

– MS (DXMS) 377 ff.

excitation emitter plate 36

extender 310, 312 ff.

extracted ion current (XIC) 56, 129, 187,  
206, 230

## f

Faraday cup 38

fast atom bombardment (FAB) 4, 21, 205

fast photochemical oxidation of proteins  
(FPOP) 363 ff.

fast radical footprinting 361 ff.

fatty acid analysis 292

fatty acid carboxylate 346

Fenton reagent 362

fetal calf serum 170

flow-injection 67, 164, 199

fluorescein 201 ff.

fluorescence 186, 190, 194, 202 f., 223, 255,  
357

– correlation spectroscopy (FCS) 253

– labeling 122

– polarization (FP) 253

– resonance energy transfer (FRET) 253

– time-resolved (TRF) 253

5-fluorouracil 310

foreground spectrum 85 f.

forensic studies 41, 324

forgetfulness 194

Fourier transform

– mass spectrometry (FTMS) 37, 354

– ion cyclotron (FT-ICR) 5, 9, 30, 36 f.,  
47 f., 57, 213, 325, 328 ff., 381

fractionation range 74

fragmentation 11

free energy 388

– stabilization 379

free induction decay (FID) 37

frontal analysis (FA) 218 f.

frontal-affinity chromatography (FAC) 159,  
217 ff., 367

full-scan 41, 46, 209

## g

G alpha protein 94 ff.

Gabitril 269

$\beta$ -galactosidase 234 f.

$\beta$ -1,4-galactosyltransferase 297

galanthamine 194 ff.

gallamine 197

galvanostatic etching 290

gas chromatography mass spectrometry  
(GC-MS) 3 f., 41

gas phase affinity 123, 160

gel permeation chromatography (GPC)  
65 ff., 83 f., 89 ff., 108 ff.

– Gyros 116

gel type 74

genotyping 54

gluconolactone 287 f.

glucose 287 ff.

– homeostasis 390

glucose oxidase 287 f.

glucosidase 292

– mannosidase II 292

glucosone 289

glutamate 311

glutamine 362 f.

glycerol 286

glycopeptide antibiotics 254

gold 297 f.

good laboratory practice (GLP) 409, 413  
– non 413, 416 ff.

GSIB4 234 f.

GTP hydrolysis 324

GTPase 94 f., 324

guanosine diphosphate (GDP) 345 ff.

guanosine triphosphate (GTP) 347

Guvacine 273 f.

## h

haloperidol 258 ff.

haplotyping 54

$\alpha$ -helical structure 354

helix 386, 389 ff.

– F- 342

high throughput screening (HTS) 82, 114,  
124, 135, 157, 162, 168, 180, 185, 231, 244,  
294, 305 ff., 321, 402

hippuric acid 288

hippuryl-L-phenylalanine 287 f.

histidine 104 f.

(R)-homoproline 273 f.

HPLC 44, 51, 67, 75, 82 ff., 98, 113 ff., 185 ff.,  
208, 259 ff., 277, 309, 377, 381 ff., 402 ff.

human gamma interferon 16

human growth hormone (hGH) 386 f.,  
392 f.

human serum albumine (HSA) 133 ff.

human urine 45

Huntington's chorea 269

Huperzine A 194, 197

hydrophilic interaction chromatography  
(HILIC) 231, 241

hydroxyl radical 361 f., 367

7-hydroxy-1-methyl quinolinium iodide  
(HMQI) 194

8-hydroxyquinoline 109

4-hydroxypicolinic acid 286

3-hydroxyretinoic acid  
   – phase II metabolite 18  
 hyphenation 4

**i**

IC<sub>50</sub> 77, 88 f., 98 ff., 140, 149, 171, 197, 200,  
 227 f., 260 ff., 288, 334  
   – definition 111  
 identification 54, 263  
 immune system 388  
 in silico 403  
 in vitro 402 f., 405, 415  
 in vivo 403, 405 f.  
 incubation 259, 261, 271, 296 f.  
 indicator 232 ff., 242  
 inflammation 388  
 inhibition assay 185  
 inhibitor 143, 147 ff., 186, 190 ff., 242, 274,  
 288 f., 298, 305, 310, 313 ff.  
 insulin 346, 356 f.  
   – lispro 357  
   – r-human 357  
   – wild-type 357  
 insulin-like growth factor receptor (IGFr)  
   protein 74, 100 ff.  
 internal standard (IS) 43, 270, 416  
 intestinal fatty acid binding protein (IFABP)  
   346, 353 f., 360  
   – apo 353  
   – rat 346  
   – wild-type (WT) 354  
 intracellular matrix 322  
 intravenous 408  
 ion evaporation model (IEV) 16 f.  
 ion intensity 35  
 ion mobility (IM) 116  
   – high field asymmetric waveform ion  
     mobility spectrometry (FAIMS) 226  
 ion modulator 35  
 ion source 4 ff.  
 ionic strength 352  
 ionization gas, methane 12  
 isoelectric focusing (IEF) 51  
 isotope 56  
 isotopic abundance  
   – bromine 6, 9  
   – carbon 5 ff.  
   – chlorine 6 ff., 171  
   – hydrogen 6  
   – nitrogen 6, 9  
   – oxygen 6  
   – sulfur 6, 9  
 isotopical labeling 42, 122, 136, 288, 291,  
 299, 378  
 IUPAC 58

**k**

kinetic  
   – assay 250 f., 272 ff.  
   – first-order 70, 143  
   – Michaelis-Menten analysis 131  
   – pseudo-first order 348  
   – second-order 68  
   – study 341

**l**

lab-on-a-chip 151  
 Langmuir equation 241  
 lanthanide chelates 253  
 laser 285, 362 f.  
   – infrared 117  
   – Nd:YAG 21  
   – nitrogen 21  
   – ultraviolet 117  
 leupeptin 191 f.  
 library 89, 231, 308, 329  
   – NGL127A443 127 ff.  
   – Optiverse 235  
   – screening 157 ff., 169 f., 242, 263 ff.,  
     393  
 ligand binding domaine (LBD) 390 f.  
 limit of detection (LOD) 190, 200  
 limit of quantitation (LOQ) 416 f.  
 lipase 287, 292  
   – phospholipase A<sub>2</sub> 292 f.  
 Lipinski's rule 95  
 liposome 238  
 liquid chromatography 185 f.  
   – mass spectrometry (LC-MS) 3 f.,  
     12 ff., 22, 32, 41 ff., 54, 126, 166, 177,  
     207, 230, 255, 307 f.  
   – MS/MS 41 f., 52, 123, 257 ff., 268,  
     270 ff., 360, 402 ff.  
   – two-dimensional (2D-LC) 51 ff., 240  
 lock spray *see* dual spray  
 low reactive molecular mass (LRMM)  
   compounds 22 f.  
 lower limit of quantitation (LLOQ) 267 ff.  
 luciferase yeast pheromone 95  
 luteolin 243

**m**

magnesium 347 ff.  
 magnetic field strength 36  
 magnetic sector 5  
 p38 MAP kinase 388 f.  
 marker 248 ff., 263, 266 f.  
   – bound 255 f., 266, 273  
   – free 255  
 mass accuracy 381  
 mass analyzer 4 ff., 14, 23 ff., 57

- mass defect 55
- mass range 7, 28 f., 55
- mass reflectron 33 f.
- mass resolving power 56
  - ultra-high 381
- mass spectrum
  - negative mode 18, 173
- mastoparan 355
- matrix 21, 286, 296 f.
  - cobalt 21
  - $\alpha$ -cyano-4-hydroxycinnamic acid 295
  - glycerol 21
- matrix assisted laser desorption/ionization (MALDI) 12, 20 ff., 33 f., 49, 57, 116, 161, 224 ff., 239 f., 254, 285 ff., 342, 367
  - MALDI-TOF 50, 211 ff., 240, 285, 289
  - post source decay (PSD-MALDI) 51
  - principle 285 f.
- matrix effects 43, 411 f.
- Matthieu's equation 27
- maximum entropy algorithm (MaxEnt) 365
- melittin 346, 354 ff.
- 2-mercaptoethanol 307 f., 310 f.
- metabolic profiling 185
- metabolite identification 418
- metabolites 41, 45 ff., 178, 377
- metabolomics 54
- metalloproteinase-1 (MMP-1) 77, 79, 88, 106 f.
- metastable ion 56
- metastasis 188
- methadone 264 ff.
- methionine 342, 362
- 2-methoxy-N-[(1R)-1-phenylethyl]-acetamide 287
- methyl orange (MO) 76 ff.
- N-methyl scopolamine (NMS) 149 f.
- methylenetetrahydrofolate (mTHF) cofactor 311 f.
- microarrays, chemical 367
- microbial identification 324
- microbore column 222
- microcoil reactor 187, 208
- microfluidic compact disc (CD) 116 f.
- microfluidic system 116
- microosomal stability 402, 405
- microsome 178
- mitogen-activated protein (MAP) 388
- molecular mass
  - relative 15, 55
- molecular weight 66
- morphine 264 f.
- MRM 227, 240
- MS<sup>n</sup> 25, 28, 31 f., 37 f., 41, 47, 57, 198, 209, 240, 403
  - in space 28
- multi channel plate detector (MCP) 33, 40 f.
- multiple ionization source 19 f.
  - combined ESI-APCI (ESCI) 19 f.
- multitarget affinity/specificity screening (MASS) 328 ff.
- muscarinic acetylcholine receptor 134
- mutagenesis 307, 392
- mutant 384
- mutation 357
  - point 347
- myoglobin 322 f.
  - apo- 323, 363 ff.
- n**
- nafoxidine 229
- naloxone 264 ff.
- nebulization gas 15
- nefazodone 48
- neurotransmitter 269
- neutral loss (NL) 25 f., 32, 48, 57
- new chemical entity (NCE) 401 ff.
- nicotinic acid 286
- (R)-nipecotic acid 273 f.
- NO 711 269 ff.
- nominal mass 56
- nonlinear least squares (NLLS) regression 344
- norethindrone 229, 233
- nortryptiline 219
- nuclear magnetic resonance (NMR)
  - spectroscopy 45, 101, 105, 109, 122, 135, 171, 211, 253, 305, 342, 359 ff., 377, 388
  - – 2D <sup>1</sup>H-<sup>15</sup>N HSQC 95, 106
- nucleotide 327
- o**
- oleate 353 f.
- oligo(ethylene glycol) 296
- oligonucleotides 323 f.
- oligosaccharides 224, 231
- omeprazole 48
- oral 408
- orbitrap 5, 9, 30, 37, 47
- p**
- paromomycin 93
- Parkinson 269
  - Morbus 257
- particle beam (PB) 4
- pepsin 360, 387 ff.

- peptide 14, 35, 50, 53, 224, 285, 294 f., 341, 346, 355, 365, 378 f.  
 – mass finger print (PMF) 34, 50 f.
- per os 414
- peroxisome proliferator-activated receptor  $\gamma$  (PPAR $\gamma$ ) 390 f.
- pH shock 209 f.
- pharmaceutical compounds 41
- pharmacodynamic (PD) relationships 406
- pharmacokinetic (PK) investigations 401 ff., 413 f.
- phenotypic effect 157
- phenylalanine 288, 291, 293, 362 f.  
 – hydroxylase (PAH) 293
- phenylethylamine 287
- N-phenyl-sulfonamide fragment 310
- phospholipid 292  
 – lyso- 292 f.  
 – triacylglycerol 292 f.
- photodissociation 81 f.
- photographic plate 38
- photoluminescence 290
- photon multiplier detector 40
- physostigmine 194
- pig striatum 257, 260
- pimozide 258 ff.
- plasma 407  
 – human 43
- pleckstrin homology (PH) 138 f.
- PLIMSTEX 123, 341 ff.  
 – definition 161
- polyacrylamide 74 f.
- polyethylene glycol 292
- porcine 346, 353
- porphyrin-binding pocket 342
- post-source decay (PSD) 34, 57
- precursor 48  
 – ion scan (PC) 25 f., 32, 35 f., 57
- predictive fragmentation software 48
- product ion scan (PIS) 25 f., 32, 57
- proline 310, 378
- promiscuous compound filter (PCF) 168 ff.
- protection factor 378 f.
- protein 14, 22, 48 ff., 65 f., 285, 306 ff., 331, 341  
 – apo- 344 f., 347  
 – conformational change 385, 390  
 – denaturation 75, 164, 174  
 – fragmentation 381  
 – glyco- 231  
 – kinase A (PKA) 76 f., 80, 98  
 – kinase C- $\alpha$  288 f.  
 – light-chain kinase protein (MLCK) 354  
 – membrane 256, 317  
 – protein interaction 385  
 – ras 345 f., 347 ff., 360  
 – RNase S 365  
 –  $\beta$ -sheet 353  
 – targeting 377 ff.  
 – turnover, intercellular 188
- protein-ligand  
 – complex 70, 135, 143 ff., 201, 207, 344 f., 349 f.  
 – dissociation 142 ff., 207 ff.  
 – – simulation 145 ff.  
 – interaction 200
- proteolysis 381 ff.
- proteomics 51, 287
- pseudoephedrine 414
- pull-down assay 298 f.
- pumping  
 – differential stage 12, 14  
 – diffusion 13  
 – high vacuum cryogenic 13  
 – single stage 12 f.  
 – turbomolecular 13
- pyranose oxidase 288 f.
- pyridine 288
- pyrimethamine 238
- ## q
- quadrupole ion trap (QIT) 4 f., 27 ff., 57, 199, 208, 211 f., 342, 381, 418  
 – linear (LIT) 30 ff., 57, 335  
 – – LTQ-FTMS 37  
 – – LIT-orbitrap 48
- quadrupole mass spectrometer 4 f., 23 ff.  
 – QqTOF 35 f., 48, 57, 381  
 – triple (QqQ) 24 ff., 57, 403, 418  
 – QqQLIT 31 f., 57
- quality control (QC) 43, 415 ff.
- quantitative analysis 42 ff., 54
- quenching 146, 296 f., 348 ff., 360 ff., 380, 382
- quinoxalin-2,3-diones 333 f.
- ## r
- radiofrequency (RF) potential 23, 27 f., 30
- radiolabeling 45
- radioligand binding assay 247 ff., 260 ff., 270 ff.
- radionuclides 252
- rapid array informed structure evolution (RAISE<sup>TM</sup>) 160
- receptor 255  
 – benzodiazepine 255  
 – dopamine 256 ff.

- receptor (*cont.*)
  - estrogen 89
  - G protein-coupled (GPCRs) 125, 135, 149, 256 f.
  - nicotinic acetylcholine 255
  - opioid 263 ff.
- regression 417
- remikiren 48 f.
- resolution 7 ff., 24, 33, 35, 56, 418
- response 132
- restricted access (RA) column 207 ff.
- reversed phase chromatography (RPC) 51, 82 ff., 190, 259, 383
  - MS 123 ff., 133
- ribosome 324, 335
- Rivastigmine 194
- RNA 54, 67, 90 ff., 323 ff., 342
- robotic instrumentation 80 f.
- rosiglitazone 391
- s**
  - salicylic acid 314 ff.
  - salt bridge 105
  - sample introduction 4 f.
  - sample preparation 43
  - SARS-Coronavirus 243
  - saturation
    - assay 247, 268 ff.
    - binding 272
    - isotherm 271
  - scavenger 364 f.
  - SCH 23390 257 ff.
  - schizophrenia 257, 269
  - scintillation 252, 255
  - score 85 f.
  - screening assay 68, 415
  - selected reaction monitoring (SRM) 25 f., 29, 32, 44, 57, 404, 409
  - self-assembled monolayers (SAMs) 295 f., 299
  - self-assembled monolayers for MALDI-MS (SAMDI) 285, 295 ff.
    - principles 295 f.
  - sensitivity 35, 54, 74, 84, 116, 137, 198, 200
  - sephadex 74
  - sepsis 313
  - serine 104 f.
  - SGALDI 116
  - silicon 289 ff.
  - silver staining 50
  - sinapic acid 286
  - single ion monitoring (SIM) 26, 201, 204
  - single nucleotide polymorphism (SNP) 54
  - size exclusion
    - chromatography (SEC) 123 ff., 132 f., 367
  - see also* reversed phase chromatography
    - membrane 164
  - SKF 83566 258 ff., 273 f.
  - SNAP 5114 273 f.
  - sodium dodecyl sulfate polyacrylamide gel (SDS-PAGE) 51, 366
  - solid phase extraction (SPE) 43, 260 ff.
  - solvent 66
  - sorbitol dehydrogenase 228
  - spectra interpretation 48 f.
  - spermicides 292
  - spin column 65 ff., 73 f., 83 f., 89 ff., 108 ff., 159
  - spiperone 258, 261 ff.
  - staircase method 224 f.
  - staurosporine 76 f., 80, 133, 137 ff., 148
  - streptavidin 202 ff.
  - Streptococcus pneumoniae* 163
  - stroke 313
  - strong cation exchange column (SCX) 51
  - structure activity relationship (SAR) 158, 171, 311, 331 ff.
  - structure elucidation 11, 45
  - succinic acid 286
  - sulfamoyl fragment 317
  - sulpiride 258 ff.
  - SUPREX 123, 358 ff.
    - definition 161
  - surface enhanced laser desorption/ionization (SELDI) 23, 49
  - surface plasmon resonance (SPR) 122, 160, 219, 239, 253
  - survey scan 46
  - synaptic cleft 269
  - system monitoring compounds (SMC) 187, 191 f., 197 f.
- t**
  - tamoxifen 229
  - tandem chromatographic methods 114
  - tandem mass spectrometry 11, 409
    - MALDI-TOF/TOF 51
  - Tardive dyskinesia 269
  - target 248 ff., 268 ff., 313
    - ligand interactions 63 ff., 254
  - tethering 305 ff.
  - tetra-O-galloyl- $\beta$ -D-glucose 243
  - therapeutics 393
  - therapeutic monitoring 54
  - thermodynamic sensors 379

- thermospray (TSP) 4  
*Thermotoga maritima* 384  
 thioflavin T 197  
 thiol 306, 313  
 thiophene sulfone 314 f.  
 thiostrepton 324 ff.  
 thymidine monophosphate (dTMP) 310  
 thymidylate synthase (TS) 310 ff.  
 tiagabine 269, 273 f.  
 time delayed fragmentation (TDF) 32  
 time of flight (TOF) 5, 22, 30, 33 ff., 47,  
   69 ff., 90, 98, 195 ff., 203 ff., 243, 290, 307 f.,  
   343, 347, 364  
   – TOF-TOF 36, 57  
 titration 108 ff., 131 ff., 341, 342 f., 348 ff.  
 N-tosyl-D-proline 310 ff.  
 total ion current (TIC) 56, 190 ff., 309  
 toxicology 41  
 transferrin-binding protein B (TbpB)  
   240  
 transmission 24, 33  
 2,4,6-trichloro-1,3,5-triazine *see* cyanuric  
   chloride  
 trifluoromethylene ketone (TFMK) 99 ff.  
 trifluoperazine 258 ff.  
 trimethoprim 137  
 troponin I 354  
 trypsin 294 f.  
 tryptophan 362  
 tyrosine 291, 293, 362
- u**
- UDP-Mur-Nac-pentapeptide synthetase  
   enzyme (MurF) 163, 166, 169 ff.  
 ultrafiltration 157 ff.  
   – membrane 179  
   – pulsed (PUF) 159, 177 ff., 367  
 ultraperformance liquid chromatography  
   (UPLC) 115 f., 415, 418  
 UV detection 98, 122, 126, 190, 223
- v**
- vancomycin 254  
 Vero-E6 cells 243  
 virus 335
- w**
- warfarin 133 ff.
- x**
- X-ray crystallography 135, 171, 311, 357,  
   361, 365, 367, 377, 387 f., 394
- z**
- Zap-70 kinase 143, 147 ff.  
 Z-FR-AMC 188 ff.



## ***Methods and Principles in Medicinal Chemistry***

Edited by R. Mannhold, H. Kubinyi, G. Folkers

Editorial Board

H.-D. Höltje, H. Timmerman, J. Vacca, H. van de Waterbeemd, T. Wieland

### ***Previous Volumes of this Series:***

W. Bannwarth, B. Hinzen (eds.)

#### **Combinatorial Chemistry, 2nd Ed. Vol. 26**

2006, ISBN 3-527-30693-5

G. Cruciani (ed.)

#### **Molecular Interaction Fields Vol. 27**

2006, ISBN 3-527-31087-8

M. Hamacher, K. Marcus, K. Stühler, A. van Hall, B. Warscheid, H. E. Meyer (eds.)

#### **Proteomics in Drug Design Vol. 28**

2006, ISBN 3-527-31226-9

D. J. Triggle, M. Gopalakrishnan, D. Rampe, W. Zheng (eds.)

#### **Voltage-Gated Ion Channels as Drug Targets Vol. 29**

2006, ISBN 3-527-31258-7

D. Rognan (ed.)

#### **Ligand Design for G Protein-coupled Receptors Vol. 30**

2006, ISBN 3-527-31284-6

D. A. Smith, H. van de Waterbeemd, D. K. Walker

#### **Pharmacokinetics and Metabolism in Drug Design, 2nd Ed. Vol. 31**

2006, ISBN 3-527-31368-0

T. Langer, R. D. Hofmann (eds.)

#### **Pharmacophores and Pharmacophore Searches Vol. 32**

2006, ISBN 3-527-31250-1

E. R. Francotte, W. Lindner (eds.)

#### **Chirality in Drug Research Vol. 33**

2006, ISBN 3-527-31076-2

W. Jahnke, D. A. Erlanson (eds.)

#### **Fragment-based Approaches in Drug Discovery Vol. 34**

2006, ISBN 3-527-31291-9

J. Hüser (ed.)

#### **High Throughput-Screening in Drug Discovery Vol. 35**

2006, ISBN 3-527-31283-8